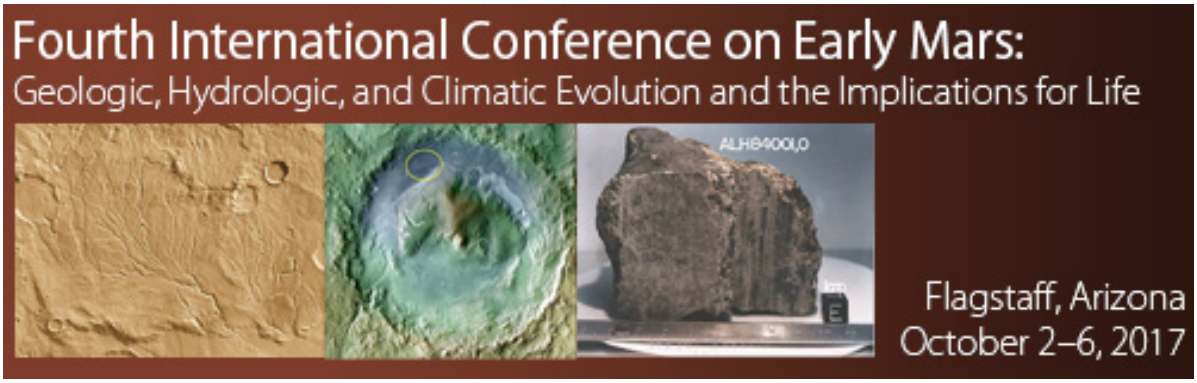


# Program and Abstract Volume

LPI Contribution No. 2014

LUNAR AND PLANETARY INSTITUTE

USRA

# Fourth International Conference on Early Mars:
## Geologic, Hydrologic, and Climatic Evolution and the Implications for Life

October 2–6, 2017 • Flagstaff, Arizona

## Sponsor

Lunar and Planetary Institute

Universities Space Research Association

National Aeronautics and Space Administration

## Conveners


Stephen Clifford
*Lunar and Planetary Institute*

Vic Baker
*University of Arizona*

David Beaty
*NASA Mars Program Office*

Alberto Fairen
*Centro de Astrobiologia*

Jack Farmer
*Arizona State University*

James Kasting
*Pennsylvania State University*



Lunar and Planetary Institute 3600 Bay Area Boulevard Houston TX 77058-1113

# Scientific Organizing Committee

Nadine Barlow, *Northern Arizona University*
Jean-Pierre Bibring, *Université Paris-Sud*
Janice Bishop, *SETI Institute*
Nathalie Cabrol, *SETI Institute*
Michael Carr, *U.S. Geological Survey*
Robert Craddock, *Smithsonian Institution*
Dave Des Marais, *NASA Ames Research Center*
Bethany Ehlmann, *Jet Propulsion Laboratory*
Jessica Flahaut, *University of Lyon*
Francois Forget, *Université Paris 6*
John Grant, *Center for Earth and Planetary Studies, Smithsonian Institution*
Virginia Gulick, *SETI Institute*
Robert Haberle, *NASA Ames Research Center*
Ernst Hauber, *German Aerospace Center (DLR)*
James Head, *Brown University*
Alan Howard, *University of Virginia*
Brian Hynek, *Laboratory for Atmospheric and Space Physics, University of Colorado*
Ralf Jaumann, *German Aerospace Center (DLR) Institute of Planetary Research*
Gerhard Kminek, *European Space Agency*
Alfred McEwen, *University of Arizona*
Jack Mustard, *Brown University*
Horton Newsom, *University of New Mexico*
Tullis Onstott, *Princeton University*
Gian Ori, *International Research School of Planetary Sciences*
Timothy Parker, *Jet Propulsion Laboratory*
Lisa Pratt, *Indiana University*
Susanne Schwenzer, *Open University*
Dirk Schulze-Makuch, *Washington State University*
Frances Westall, *Centre de Biophysique Moléculaire*
Robin Wordsworth, *Harvard University*

Abstracts for this conference are available via the conference website at

**www.hou.usra.edu/meetings/earlymars2017/**

Abstracts can be cited as

Author A. B. and Author C. D. (2016) Title of abstract. In *Fourth International Conference on Early Mars: Geologic, Hydrologic, and Climatic Evolution and the Implications for Life,* Abstract #XXXX. LPI Contribution No. 2014, Lunar and Planetary Institute, Houston.

**Monday, October 2, 2017**
**KEY SCIENCE QUESTIONS FROM THIRD EARLY MARS AND MEPAG**
**8:30 a.m. Coconino/Canyon Room**

8:30 a.m. *Welcome and Introductions*

8:35 a.m. Clifford S. M. *
*Key Science Questions from Third Early Mars Conference*

8:55 a.m. Diniega S. Banfield D. Johnson J. Hamilton V. E. Carrier B. Ashley J. W. Beaty D. W. Zurek R.
*Early Mars-Relevant Investigations Within the MEPAG Science Goals* **[#3055]**
We will identify Early Mars-relevant Objectives, Sub-objectives, and Investigations within the 2015 MEPAG Goals Document, as well as recent mission-generated inputs addressing those investigations.

**Monday, October 2, 2017**
**EARLY GEOLOGY, ATMOSPHERE, AND INVENTORY OF WATER I**
**9:15 a.m. Coconino/Canyon Room**

9:15 a.m. Andrews-Hanna J. C. * Bottke W. B.
*Mars During the Pre-Noachian* **[#3078]**
We use geophysical evidence to infer the prevailing surface conditions during the pre-Noachian. The emerging picture is a pre-Noachian Mars that was less dynamic than Noachian Mars in terms of impacts, geodynamics, and hydrology.

9:35 a.m. Lillis R. J. * Vervilidou F. Weiss B. P. Manga M. Frey H. V. Robbins S. J.
*Early MARS Chronology: When and How did the Dynamo Die?* **[#3024]**
Mars' dynamo is a key aspect of early Mars evolution. It likely started sometime after primordial crust formation and ceased before the Utopia impact. Its total duration depends on impactor flux following accretion and the timing of the LHB.

9:55 a.m. *Break*

10:10 a.m. Jakosky B. M. * MAVEN Science Team
*Loss of the Early Mars Atmosphere to Space Determined from MAVEN Observations of the Upper Atmosphere* **[#3004]**
The combination of loss rates inferred from MAVEN observations and loss derived from Ar isotopes indicates that loss to space was the major process responsible for changing Mars from its early, warm/wet environment to today's cold, dry climate.

10:40 a.m. Sakai S. * Seki K. Terada N. Shinagawa H. Tanaka T. Ebihara Y.
*Ion Escape Processes of Mars with a Weak Intrinsic Magnetic Field* **[#3034]**
The ion tailward flux increases by the magnetization of Mars. Ions escape through four channels in the magnetotail, which are related to the cusp region and the reconnection. This could result in the escape rate from the upper atmosphere enhanced.

11:00 a.m. Mayyasi M. * Clarke J. Bhattacharyya D. Deighan J. Jain S. Chaffin M. Schneider N. Jakosy B.
*The Seasonal Variability of Atmospheric Deuterium at Mars: Implications for Water Loss into Space* **[#3006]**
The variability of deuterium in the atmosphere of Mars is investigated to better understand the primordial water content at the planet.

11:20 a.m. Carr M. H. * Head J. W. [INVITED]
*Estimating the Hesperian Water Inventory from the Present Inventory: Where Did All the Water Go?* **[#3021]**
Elimination of an ocean-sized body of water in the Hesperian implies that the D/H fractionation factor and the hydrogen loss rates were much higher than at present as a result of more intense EUV output of the Sun.

11:50 a.m. Clifford S. M. * Costard F.
*Geomorphic Evidence for a Late Hesperian Northern Ocean and its Implications for the Noachian* **[#3083]**
We discuss the geomorphic evidence for the presence of a Late Hesperian ocean in the Martian northern plains and discuss its implications for the size of the planetary inventory of water and the size of the ocean during the Noachian.

12:10 p.m. *Lunch*

**Monday, October 2, 2017**
**EARLY GEOLOGY, ATMOSPHERE, AND INVENTORY OF WATER II**
**1:30 p.m. Coconino/Canyon Room**

1:30 p.m. Mustard J. F.. *
*Water in the Martian Crus Locked in Hydrated Minerals: A Significant Planetary Reservoir of Water* **[#3059]**
Calculations for a reservoir of water locked in hydrated minerals is estimated to range from a low of < 20 m global equivalent layer to approximately 1 km for the high end. This is sufficient to strongly impact surface geomorphic processes.

1:50 p.m. Baker L. L. *
*Basalt Weathering and the Volatile Budget of Early Mars* **[#3081]**
Basalt weathering on Earth consumes $CO_2$ and water and may have affected terrestrial climate. I apply a mass balance derived from terrestrial data to examine the effect surficial basalt weathering may have had on the $CO_2$ budget of early Mars.

2:10 p.m. 2-MINUTE POSTER SUMMARIES
Barlow N. G.
*The Noachian Impact Cratering Record Revisited* **[#3048]**

Lillis R. J. Deighan J. Fox J. L. Bougher S. W. Lee Y. Combi M. Leblanc F. Chaufray J.-Y. Cravens T. E. Rahmati A. Groller H. Yelle R. Jakosky B. M.
*Photochemical Escape of Oxygen from Mars: Consequences for Climate History* **[#3023]**

Slipski M. Jakosky B. M. Benna M. Mahaffy P. Elrod M. K.
*Atmospheric Argon Isotope Evolution Informed by MAVEN Results* **[#3027]**

Steele L. J. Kite E. S. Michaels T. I.
*Wind Erosion of Layered Sediments on Mars, and the Role of Terrain* **[#3052]**

**Monday, October 2, 2017**
**CLIMATIC AND HYDROLOGIC EVOLUTION I**
**2:20 p.m. Coconino/Canyon Room**

2:20 p.m. Craddock R. A. * Irwin R. P. III Howard A. D. Morgan A. M. [INVITED]
*The Geologic Evidence for a Warm and Wet Early Mars* **[#3056]**
The geologic evidence supporting a warm and wet climate on early Mars is presented. The case against an "icy highlands" scenario is also made. Climate models are converging to a solution, but any theoretical data must explain the empirical data.

2:50 p.m. Head J. W. III * Wordsworth R. Forget F. Turbet M. [INVITED]
*Deciphering the Noachian Geological and Climate History of Mars: Part 2: A Noachian Stratigraphic View of Major Geologic Processes and Their Climatic Consequences* **[#3047]**
We apply a stratigraphic approach to the major Noachian geological processes and observation, knowns and unknowns to provide insight into potential changes as a function of time, and to assess their climatic consequences.

3:20 p.m. *Break*

3:35 p.m. Forget F. Turbet M. Millour E. Kerber L. Wordsworth R. D. Head J. W. [INVITED]
*On the Challenge of Simulating the Early Mars Environment with Climate Models* **[#3061]**
We still do not understand which climate processes allowed water to flow on early Mars. Each proposed solution has its difficulties. Nevertheless, based on the new ideas that are regularly proposed, there is hope ahead.

4:05 p.m. Turbet M. * Forget F. Svetsov V. Tran H. Hartmann J.-M. Karatekin O. Gillmann C. Popova O. Head J.
*The Environmental Effect of Meteoritic Impacts on Early Mars with a Versatile 3-D Global Climate Model* **[#3062]**
We simulated the environmental effect of meteoritic impacts with a 3-D Global Climate Model to explore if they could trigger the warm conditions and the precipitation rates required to explain the formation of the Martian valley networks.

4:25 p.m. Steakley K. E. * Kahre M. A. Murphy J. R. Haberle R. M. Kling A.
*Revisiting the Impact Heating Hypothesis for Early Mars with a 3D GCM* **[#3074]**
We revisit the Segura et al. (2008) early Mars impact scenarios using the 3D Ames Mars GCM.

4:45 p.m. MODERATED DISCUSSION AND IDENTIFICATION OF KEY SCIENCE QUESTIONS

**Monday, October 2, 2017**
**POSTER SESSION I**
**6:30–8:00 p.m. Kaibab**

Anderson R. B. Williams R. M. E. Gullikson A. L.
*Alluvial Fan Morphology North of Hellas Indicates Multiple Stages of Deposition* **[#3050]**
Alluvial fans north of Hellas show three morphologies: channels/chutes, degraded surface, and inverted channels. These may represent different periods of deposition, with channels as the most recent and inverted channels as the most ancient.

Ashley J. W. Barlow N. G. Beaty D. W. Farmer J. Kring D. A. Parker W. G.
*Field Excursions to Terrestrial Analog Sites for the Fourth International Conference on Early Mars* **[#3054]**
Several field locations for terrestrial analog-based discussions of Early Mars are accessible from the conference venue, and will be addressed in two field-trips to be held mid- and post- conference.

Ashley J. W. Banfield D. Beaty D. W. Carrier B. L. Diniega S. Johnson J. R. Zurek R. W.
*Major Discoveries Related to Early Mars as Input to Hypothesis-driven Mission Responses — Preparing for the Next Decadal Survey* **[#3049]**
This abstract attempts to initiate a community-based discussion that brings together MEPAG Goals and recent Early Mars discoveries for anticipating mission/instrument responses to include in Planetary Science Decadal Survey white papers.

Barlow N. G.
*The Noachian Impact Cratering Record Revisited* **[#3048]**
New image and topographic data are being used to revised the author's Catalog of Large Martian Impact Craters. Additional craters have been identified, which adjusts the crater size-frequency distribution curves of Noachian terrains.

Baron F. Petit S. Gaudin A. Mangold N.
*Interpretation of Smectite VIS-NIR Spectra from Synthetic Smectites* **[#3019]**
The aim of this study was to contribute to the interpretation of VIS-NIR spectral features of smectites, based on synthetic smectites having a simple and a controlled crystal-chemistry.

Bruner R. B.
*Special Exhibit on Meteorites and Minerals Associated with the Origin of Life on Earth or Mars* **[#3001]**
This exhibit has been shown at eight conferences: 2014 Gordon Origin of Life, 2014 8th International Mars, 2015 2nd Mars2020 L S, 2016 Gordon Origin of Life, 2016 Biosignature, 2016 European Astrobiology, 2017 Exomars 2020 L S, 2017 AbSciCon.

Buhler P. B. Fassett C. I. Head J. W. Lamb M. P.
*Fluvial Volume, Timescales, and Intermittency in Milna Crater, Mars* **[#3053]**
We find that ~100 yr of total integrated fluvial sediment transport, spread over $10^5$–$10^6$ years, occurred in Milna Crater near the Noachian-Hesperian boundary. This quantifies fluvial intermittency/hiatus and constrains early climate scenarios.

Cardenas B. T. Goudge T. A. Hughes C. M. Levy J. S. Mohrig D.
*Justifying Martian Fluvial Sinuous Ridge Measurements Using Earth Analog Stratigraphy* **[#3060]**
Sinuous ridges/Testing interpretations/With analog work.

Cassanelli J. P. Head J. W.
*Formation of Valley Networks in a Cold and Icy Early Mars Climate: Predictions for Erosion Rates and Channel Morphology* **[#3020]**
Climate models suggest early Mars was cold and icy. To test this prediction we assess the influence of cold conditions and the presence of an ice-cemented substrate on the formation of the valley networks and compare results to morphometric data.

Di Achille G. Vaz D. A.
*Hydrological and Climatic Significance of Martian Deltas* **[#3041]**
We a) review the geomorphology, sedimentology, and mineralogy of the martian deltas record and b) present the results of a quantitative study of the hydrology and sedimentology of martian deltas using modified version of terrestrial model Sedflux.

Diniega S. Banfield D. Johnson J. Hamilton V. E. Carrier B. Ashley J. W. Beaty D. W. Zurek R.
*Early Mars-Relevant Investigations Within the MEPAG Science Goals* **[#3055]**
We will identify Early Mars-relevant Objectives, Sub-objectives, and Investigations within the 2015 MEPAG Goals Document, as well as recent mission-generated inputs addressing those investigations.

Fairén A. G. Mateo-Martí E. Gago-Duport L. Losa-Adams E. Chevrier V. Gil-Lozano C.
*Coeval Formation of Mineral Sequences on a Cold and Wet Early Mars* **[#3037]**
A Martian substrate associated with volcanogenic massive sulfide deposits can produce different mineralogical sequences under the same environmental conditions: a generally cold planet with transitional warm periods.

Forget F. Turbet M. Millour E. Kerber L. Wordsworth R. D. Head J. W.
*On the Challenge of Simulating the Early Mars Environment with Climate Models* **[#3061]**
We still do not understand which climate processes allowed water to flow on early Mars. Each proposed solution has its difficulties. Nevertheless, based on the new ideas that are regularly proposed, there is hope ahead.

Glines N. H. Gulick V. C.
*Evolution of Noachian Channels and Valleys in the Corozal Crater Region* **[#3080]**
We have mapped the channels in the region around Corozal Crater. The channel forms and distribution support a paleoshoreline for the Eridania NW subbasin proposed by Irwin et al., 2004.

Grau Galofre A. Jellinek A. M.
*Global Catalogue of the Martian Valley Networks: Evidences for Fluvial, Sapping and Subglacial Processes on Early Mars* **[#3011]**
We use erosion models and statistical morphometry schemes to show quantitative evidence for fluvial, glacial, groundwater sapping and subglacial erosion on the Noachian highlands, to then build a global map of valley network origin and distribution.

Haberle R. M. Zahnle K. Barlow N.
*Impact Delivery of Reduced Greenhouse Gases on Early Mars* **[#3022]**
Impacts may be a significant source of reduced greenhouse gases on Early Mars. A simple model suggests that during the Noachian they may raise surface temperatures near the melting point for a total of tens of millions of years.

Hartwick V. L. Toon O. B.
*Warming Ancient Mars with Water Clouds* **[#3028]**
High altitude clouds in the present day Mars atmosphere may form on interplanetary dust particles (IDPs). Paleo fluences of IDPs were likely higher, and similar clouds are expected to influence the Mars paleo-climate.

Head J. W. III Wordsworth R. Forget F. Turbet M.
*Deciphering the Noachian Geological and Climate History of Mars: A Stratigraphic, Geologic Process and Mineralogical Perspective — Part 1: Current Knowns and Unknowns* **[#3046]**
The Late Noachian climate, be it warm and wet or cold and icy, is inherited from events that occurred earlier in Mars history. We outline what is known and what remains unexplained about Noachian/Hesperian history and events.

Holo S. J. Kite E. S.
*Incision of the Jezero Crater Outflow Channel by Fluvial Sediment Transport* **[#3007]**
We developed a simple model of channel incision of the Jezero Crater outflow channel in which channel incision occurs contemporaneously with lake filling. The timescales required to erode the channel are comparable to the lake filling timescales.

**Monday, October 2, 2017**
**POSTER SESSION II**
**8:00–9:30 p.m. Kaibab**

Kahre M. A. Haberle R. M. Steakley K. E. Murphy J. R. Kling A.
*Atmospheric Collapse on Early Mars: The Role of $CO_2$ Clouds* **[#3066]**
We present a GCM investigation of the role of $CO_2$ clouds in atmospheric collapse on early Mars.

Kite E. S. Gao P. Mischna M. Mayer D. P. Goldblatt C. Yung Y.
*Methane-Burst Climate Scenarios for Early Mars Rivers and Lakes* **[#3073]**
We found physically self-consistent methane burst climate scenarios that can match Mars paleolake data. If these bursts truly occurred, >(1–10)% of the clathrate stability zone on past Mars must have been occupied by $CH_4$-clathrate. This is testable.

Lillis R. J. Deighan J. Fox J. L. Bougher S. W. Lee Y. Combi M. Leblanc F. Chaufray J.-Y.
Cravens T. E. Rahmati A. Groller H. Yelle R. Jakosky B. M.
*Photochemical Escape of Oxygen from Mars: Consequences for Climate History* **[#3023]**
Photochemical oxygen escape rates from Mars are derived from MAVEN in situ and remote data. Extrapolating back in time, several hundred millibars likely escaped this way.

Mitra K. Catalano J. G.
*Iron Oxidation By Chlorate: Implications for Akaganéite and Jarosite Formation on Mars* **[#3008]**
The present work tries to find out if chlorate and perchlorate can serve as active oxidants on Mars. We conclude that $ClO_4^-$ is not an oxidant in Martian conditions while $ClO_3^-$ is a potent oxidant forming akaganeite and jarosite in Cl and $SO_4$ fluids.

Miura Y.
*Formation of Ocean Sedimentary Rocks as Active Planets and Life-Like Systems* **[#3002]**
Wet shocked rocks are discarded globally and enriched elements in ocean-sedimentary rocks, which is strong indicator of ocean water of other planets. Ocean-sedimentary rocks are strong indicator of water planets and possible exo-life on planet Mars.

Palumbo A. M. Head J. W. Wordsworth R. D.
*Late Noachian Icy Highlands Climate Model: Exploring the Possibility of Transient Melting and Fluvial/Lacustrine Activity Through Peak Annual and Seasonal Temperatures* **[#3043]**
We use the LMD GCM to explore the role of seasonal and diurnal temperature variation on a “cold and icy” early Mars. In a cold climate with MAT ~243 K, peak summertime conditions permit ice melt, runoff, and possibly valley network formation.

Scanlon K. E. Head J. W. III Fastook J. L. Wordsworth R. D.
*The Dorsa Argentea Formation and the Noachian-Hesperian Transition: Climate and Glacial Flow Modeling* **[#3031]**
In MGCM simulations with a thick (≥ 600 mb) $CO_2$ atmosphere, an extensive south polar ice sheet forms, with DAF-like 0°W and 90°W lobes. With additional greenhouse warming, basal melting occurs, with melt maxima near observed eskers and channels.

Slipski M. Jakosky B. M. Benna M. Mahaffy P. Elrod M. K.
*Atmospheric Argon Isotope Evolution Informed by MAVEN Results* **[#3027]**
Mars’ atmosphere is enriched in heavy isotopes of its major species. We have modeled the evolution of Ar isotopes of 4 Gyr due to volcanic outgassing and loss to space, using MAVEN results to constrain how sputtering loss fractionates Ar isotopes.

Sneed J. W. Kite E. S. Mayer D. P.
*Constraining the Duration of Late Hesperian-Amazonian Habitability via Crater Interbedding with Alluvial Fans* **[#3075]**
Impact craters interbedded with alluvial fans are used to constrain the duration of liquid-water fluvial activity to a period of time not less than 44 Ma during the late Hesperian and early Amazonian.

Sneed J. W. Kite E. S. Mayer D. P.
*Searching for Indications of Snowmelt-Driven Erosion on Early Mars* **[#3079]**
We undertake a broad survey of slope orientations in the incised walls of craters containing large alluvial fans, in order to establish whether insolation angle was a major determinant of liquid water availability on early Mars.

Steele L. J. Kite E. S. Michaels T. I.
*Wind Erosion of Layered Sediments on Mars, and the Role of Terrain* **[#3052]**
Most sedimentary rocks on Mars exist as mounds in craters and canyons. To investigate the role of terrain in wind erosion, and the formation and evolution of these mounds, we combine mesoscale model output with a landscape evolution model.

Turbet M. Tran H. Hartmann J.-M. Forget F.
*Toward a more Accurate Spectroscopy of $CO_2$/$H_2O$-Rich Atmospheres: Implications for the Early Martian Atmosphere* **[#3063]**
We performed calculations, measurements and gathered existing data to construct a state-of-the-art spectroscopy for $CO_2$/$H_2O$-rich atmospheres, as expected after meteoritic impact events on early Mars.

Uceda E. R. Fairén A. G. Gil-Lozano C. Losa-Adams E. Gago-Duport L.
*Kinetic Modeling of Mineral Sequences on Early Mars Using Fully Open Systems* **[#3040]**
We model the formation of mineral sequences known to exist on Mars considering open system conditions both at the atmosphere-water and water-rock interfaces, and implementing a kinetic approach for the dissolution and precipitation of solid phases.

Wiseman S. M. Robertson K.
*Intercomparison of Martian Carbonate-Bearing Deposits* **[#3064]**
This work aims to identify and map the extent of specific carbonate mineral assemblage phases using Hapke radiative transfer modeling to provide more refined information on past environmental conditions/habitability on Mars.

**Tuesday, October 3, 2017**
**CLIMATIC AND HYDROLOGIC EVOLUTION II**
**8:30 a.m. Coconino/Canyon Room**

8:30 a.m. REVIEW OF DAY'S AGENDA

8:35 a.m. Wordsworth R. * Head J. III Wang H.
*Early Mars vs. LHS1140b and TRAPPIST-1f: How Comparative Planetology can Help Address Long-Standing Questions in Martian Climate Evolution* **[#3038]**
We propose that a systematic program of intercomparison with cool, rocky exoplanets will allow new insight into key questions in martian climate evolution.

8:55 a.m. Baker V. R. *
*Early Mars as an Evolving "Ocean World"* **[#3067]**
Mars has an immense hydrosphere that manifested itself very early as seas, lakes, and streams--all with immense consequences for the evolution of its surface. The earliest "ocean" phase probably occurred during the period of most intense bombardment.

9:15 a.m. Rodriguez J. A. P. * Zarroca M. Linares R. Komatsu G. Oehler D. Davila A. Baker V. Bernman D. Miyamoto H.
*Detecting Astrobiologically Significant Ocean Floor Sediments in the Tsunami-Battered Coasts of Early Mars* **[#3032]**
We document a potential tsunami deposit that was emplaced over a possible early Mars coastal cape. Unlike other deposits proposed to have been due to tsunamis extending far inland, its composition may be dominated by displaced ocean floor materials.

9:35 a.m. Ramirez R. M. * Craddock R. A.
*The Climatological and Geological Case for a Warmer and Wetter Early Mars* **[#3003]**
The climate of early Mars has been hotly debated for decades. We argue that a predominantly icy early Mars cannot be reconciled with either the geologic record or climate modeling simulations. Mars may have had a warm and semi-arid climate instead.

9:55 a.m. *Break*

10:10 a.m. Cang X. * Luo W.
*Frequency Distribution of Junction Angles of Valley Networks on Mars Consistent with an Early Warm Climate* **[#3072]**
The junction angles on Earth formed under different climatic conditions are different. Here, we investigated the junction angles on Mars. The results are consistent with a "warm" early Mars climate with precipitation.

10:30 a.m. Ruff S. W. *
*Investigating the Floor of Paleolake Jezero by Way of Gusev Crater* **[#3076]**
The similarities and differences between the volcanic floor units and associated features in Jezero and Gusev craters have implications for interpreting the stratigraphy and geologic history of Jezero crater.

10:50 a.m. Goudge T. A. * Fassett C. I.
*The Importance of Lake Overflow Floods for Early Martian Landscape Evolution: Insights from Licus Vallis* **[#3025]**
We study the geomorphology of Licus Vallis, a large paleolake outlet valley, and its tributary valleys. We conclude that overflow flooding outpaced tributary erosion, pointing to the importance of lake overflow floods in martian landscape evolution.

11:10 a.m. Haqq-Misra J. Batalha N. E. Kopparapu R. K. Kadoya S. Kasting J. F. *
*Limit Cycles Can Explain Fluvial Features on Early Mars* **[#3045]**
We argue that the presence of fluvial features on early Mars can be explained from limit cycles of global glaciation and deglaciation that occurred through modulation of $CO_2$ by the carbonate-silicate cycle under a faint young sun.

11:30 a.m. Di Achille G. Vaz D. A.
*Hydrological and Climatic Significance of Martian Deltas* **[#3041]**
We a) review the geomorphology, sedimentology, and mineralogy of the martian deltas record and b) present the results of a quantitative study of the hydrology and sedimentology of martian deltas using modified version of terrestrial model Sedflux.

11:50 a.m. *Lunch*

**Tuesday, October 3, 2017**
**CLIMATIC AND HYDROLOGIC EVOLUTION III**
**1:30 p.m. Coconino/Canyon Room**

1:30 p.m. Grau Galofre A. Jellinek A. M.
*Global Catalogue of the Martian Valley Networks: Evidences for Fluvial, Sapping and Subglacial Processes on Early Mars* **[#3011]**
We use erosion models and statistical morphometry schemes to show quantitative evidence for fluvial, glacial, groundwater sapping and subglacial erosion on the Noachian highlands, to then build a global map of valley network origin and distribution.

1:50 p.m. Kite E. S. *
*An Ice-and-Snow Hypothesis for Early Mars, and the Runoff-Production Test* **[#3044]**
Cold (snowmelt) models for Early Mars climate can be tested by measuring paleochannel widths and meander wavelengths for Early Mars watersheds with well-defined drainage area. I will review snowmelt models, and report results of these tests.

2:10 p.m. Kreslavsky M. A. * Head J. W.
*A Colder Early Mars: Insight from Crater Wall Slope Statistics* **[#3014]**
Statistics of crater wall slopes in the martian tropics indicates that fluvial erosion in the Late Noachian was minor and episodic. At lower elevations erosion lasted longer, into the Hesperian, which implies a thicker incondensable atmosphere.

2:30 p.m. 2-MINUTE POSTER SUMMARIES
Anderson R. B. Williams R. M. E. Gullikson A. L.
*Alluvial Fan Morphology North of Hellas Indicates Multiple Stages of Deposition* **[#3050]**

Buhler P. B. Fassett C. I. Head J. W. Lamb M. P.
*Fluvial Volume, Timescales, and Intermittency in Milna Crater, Mars* **[#3053]**

Cardenas B. T. Goudge T. A. Hughes C. M. Levy J. S. Mohrig D.
*Justifying Martian Fluvial Sinuous Ridge Measurements Using Earth Analog Stratigraphy* **[#3060]**

Cassanelli J. P. Head J. W.
*Formation of Valley Networks in a Cold and Icy Early Mars Climate: Predictions for Erosion Rates and Channel Morphology* **[#3020]**

Glines N. H. Gulick V. C.
*Evolution of Noachian Channels and Valleys in the Corozal Crater Region* **[#3080]**

Haberle R. M. Zahnle K. Barlow N.
*Impact Delivery of Reduced Greenhouse Gases on Early Mars* **[#3022]**

Hartwick V. L. Toon O. B.
*Warming Ancient Mars with Water Clouds* **[#3028]**

Head J. W. III Wordsworth R. Forget F. Turbet M.
*Deciphering the Noachian Geological and Climate History of Mars: A Stratigraphic, Geologic Process and Mineralogical Perspective — Part 1: Current Knowns and Unknowns* **[#3046]**

Holo S. J. Kite E. S.
*Incision of the Jezero Crater Outflow Channel by Fluvial Sediment Transport* **[#3007]**

Kahre M. A. Haberle R. M. Steakley K. E. Murphy J. R. Kling A.
*Atmospheric Collapse on Early Mars: The Role of $CO_2$ Clouds* **[#3066]**

Kite E. S. Gao P. Mischna M. Mayer D. P. Goldblatt C. Yung Y.
*Methane-Burst Climate Scenarios for Early Mars Rivers and Lakes* **[#3073]**

Palumbo A. M. Head J. W. Wordsworth R. D.
*Late Noachian Icy Highlands Climate Model: Exploring the Possibility of Transient Melting and Fluvial/Lacustrine Activity Through Peak Annual and Seasonal Temperatures* **[#3043]**

Scanlon K. E. Head J. W. III Fastook J. L. Wordsworth R. D.
*The Dorsa Argentea Formation and the Noachian-Hesperian Transition: Climate and Glacial Flow Modeling* **[#3031]**

Sneed J. W. Kite E. S. Mayer D. P.
*Constraining the Duration of Late Hesperian-Amazonian Habitability via Crater Interbedding with Alluvial Fans* **[#3075]**

Sneed J. W. Kite E. S. Mayer D. P.
*Searching for Indications of Snowmelt-Driven Erosion on Early Mars* **[#3079]**

Turbet M. Tran H. Hartmann J.-M. Forget F.
*Toward a more Accurate Spectroscopy of $CO_2$/$H_2O$-Rich Atmospheres: Implications for the Early Martian Atmosphere* **[#3063]**

3:10 p.m. *Break*

**Tuesday, October 3, 2017**
**GEOCHEMICAL AND MINERALOGICAL EVOLUTION I**
**3:25 p.m. Coconino/Canyon Room**

3:25 p.m. Bishop J. L. * Fairén A. G. Michalski J. R. Gago-Duport L. Baker L. L. Velbel M. A. Gross C. Rampe E. B. [INVITED]
*Diverse Early Aqueous Environments and Climate on Mars Revealed by the Phyllosilicate Record* **[#3030]**
We propose that short-term warmer and wetter environments, occurring sporadically in a generally cold early Mars, enabled formation of phyllosilicate-rich outcrops on the surface of Mars without requiring long-term warm and wet conditions.

3:55 p.m. Horgan B. * Baker L. Carter J. Chadwick O.
*Where is the Climate Signature in the Mineral Record of Early Mars?* **[#3077]**
We present a framework for interpreting weathering mineralogy based on terrestrial studies of climatic controls on surface weathering and identify outstanding knowledge gaps crtitical for Mars.

4:15 p.m. Palumbo A. M. * Head J. W.
*The Mineralogic Alteration History of Early Mars: The Role of Large Craters and Basins in Transient Regional High-Temperature Alteration* **[#3042]**
We explore a new formation hypothesis for the stratigraphic layers and associated alteration products in the Isidis region: the lowest layers were formed and altered contemporaneously with the impact event and do not require long-term warm conditions.

4:35 p.m. MODERATED DISCUSSION AND IDENTIFICATION OF KEY SCIENCE QUESTIONS

**Tuesday, October 3, 2017**
**SPECIAL EVENING SESSION: DISCUSSION AND IDENTIFICATION OF KEY SCIENCE QUESTIONS AND NEEDED OBSERVATIONS — TENTATIVE**
**7:00–9:00 p.m. Coconino/Canyon Room**

**Wednesday, October 4, 2017**
**MID-CONFERENCE ALL-DAY FIELD TRIPS**
**8:00 a.m. DoubleTree by Hilton**

***Due to logistical issues, we have decided to run both the Grand Canyon and Meteor Crater field trips concurrently on Wednesday. Participants will have a choice of going on either of these, but not both. One group will go to the South Rim of the Grand Canyon, then travel to Sunset Crater and the San Francisco Volcanic Field, before returning to the hotel; while the other group will go to Meteor Crater, the Petrified Forest, and then back to the hotel. Participation will be limited to one busload (approximately 50 people) for each field trip, so early enrollment is encouraged.***

**General information for all field trip participants:** Participants should bring the following: a small backpack (day pack), hiking boots are preferred but closed toe shoes suitable for hiking on rock are required, light jacket or other rain proof windbreaker or poncho, hat (with chin strap preferred), sunglasses, canteen and/or water bottles, personal first aid kit, an emergency blanket (suitable protection from sun), and a camera. You might also want to bring a pair of binoculars, if you have them (Note: water is not sold in the Grand Canyon Park, but there are springs and potable water is dispensed from a couple of filling stations near the Visitor's Center).

**What NOT to bring:** Rock hammer; it's a National Park and collecting samples is forbidden. A hand lens is ok for looking at rocks in-situ, but not for collecting samples.

**Field trip #1: South Rim of the Grand Canyon, Sunset Crater and San Francisco Volcanic Field**
This all-day field trip will be led by Jack Farmer (Arizona State University) and will include a geologically diverse series of stops relevant to Mars geology and habitability, including interpretation of the stratigraphic record, fluvial outcrops (red beds), and volcanic landforms. The tour bus will leave the hotel in Flagstaff and make its first stop at the Grand Canyon Visitor's Center, where we'll see an orientation film and exhibits, and then walk the Rim Trail (with excellent views of the Canyon) to the Geology Museum, with its excellent indoor exhibits. A field guide, based on a set of themes relevant to Mars, is being generated to guide discussions, starting with the basic concepts of habitability, the evolution of habitability over geologic timescales, and how these concepts have shaped Mars exploration, using the Canyon sequences as an example — particularly what the major unconformities exposed in the Canyon stratigraphy tell us about the nature of the geologic record (mostly missing due to erosion or a lack of deposition) and how Mars differs from a tectonically active, hydrologic-cycle-driven planet like Earth.
After visiting the south rim of the Grand Canyon, we will head east on Hwy 64 to Cameron and then take Hwy 89 south through the eastern part of the San Francisco volcanic field and on to Sunset Crater. Along our route, we will see many examples of the Triassic Moenkopi outcrops (red beds) which were formed by extensive coastal plain fluvial sedimentation during the early Triassic (some of which are good analogs for Gale Crater). Arriving at Sunset Crater, we will have an opportunity to take a 1.5 km trail hike through recent basaltic flows and pyroclastics erupted from along the western edge of Sunset Crater, almost 1100 yrs. ago. Following our hike at Sunset Crater, we will return to Flagstaff.

**Field Trip #2: Barringer Meteorite Crater and Petrified Forest National Park**
This field trip will explore geological processes of relevance to early Mars, including biosignature preservation and impact cratering, in two spectacular type localities on Earth. The insights from these analogs should provide useful input to Mars exploration and sample selection strategies. David Kring (Lunar and Planetary Institute) and William Parker (Petrified Forest National Park) will lead geological excursions at Barringer Meteorite Crater (aka Meteor Crater) and the Petrified Forest, respectively. At Meteor Crater, we will examine one of the freshest examples of an impact feature on Earth for evidence of post-impact processes that produced lake sediments, crater wall gullies, and potential niches for life. We will also explore the roles that impact breccias, impact ejecta, and overturned strata could play in the preservation of biosignatures on early Mars. Attendees may choose between a rare but physically challenging descent to the crater floor, or a less-strenuous traverse along the rim perimeter (to be led by Nadine Barlow of Northern Arizona University). The Petrified Forest will offer us a chance to observe/discuss the unique biosignature preservation attributes of the Upper Triassic Chinle Formation. We will visit the Painted Desert, jarosite-bearing organic horizons, Triassic fossils, petrified wood accumulations, and, of course, the giant logs.

**Thursday, October 5, 2017**
**GEOCHEMICAL AND MINERALOGICAL EVOLUTION II**
**8:30 a.m. Coconino/Canyon Room**

8:30 a.m. REVIEW OF DAY'S AGENDA

8:35 a.m. Rogers A. D. * Cowart J. C. Head J. W. Warner N. H. Palumbo A. Golombek M. P.
*Properties, Origins, and Preservation of Ancient Olivine-Bearing Bedrock: Implications for Noachian Processes on Mars* **[#3033]**
Olivine-bearing bedrock units are common and therefore significant surface units found in Noachian highlands, yet their origins are uncertain. We present new observations suggesting that some may have non-volcanic or non-effusive volcanic origins.

8:55 a.m. McCollom T. M. * Potter-McIntyre S. L.
*Jarosite and Alunite Cements in Jurassic Sandstones of Utah and Nevada, a Potential Analog for Stratified Sulfate Deposits on Early Mars* **[#3009]**
Jarosite and alunite in Jurassic sandstones are investigated to gain insights into occurrences of these minerals in stratified deposits on Mars. The deposits demonstrate that these minerals can persist for millions of years in aqueous environments.

9:15 a.m. Catalano J. G. * Nickerson R. D. Chemtob S. M. Morris R. V. Agresti D. G.
*Detrital Smectites as Potential Redox Indicators on Early Mars* **[#3010]**
Fe(II)-Mg smectites formed on early Mars via hydrothermal alteration convert to Fe(III)-phases if exposed to oxidants, such as during erosion and transport. Detrital smectites may be viable indicators of past redox conditions on the surface of Mars.

9:35 a.m. Salvatore M. R. * Goudge T. A. Bramble M. S. Edwards C. S. Bandfield J. L. Amador E. S. Mustard J. F. Christensen P. R.
*Bulk Mineralogy of the Northeast Syrtis and Jezero Crater Regions of Mars Derived Through Thermal Infrared Spectral Analyses* **[#3058]**
We derive quantitative estimates of bulk mineralogy throughout the Jezero crater, Jezero watershed, and NE Syrtis regions of Mars using TIR data. Results suggest the dominance of basaltic compositions and are compared to prior VNIR investigations.

9:55 a.m. Rutledge A. M. * Horgan B. Havig J. R. Rampe E. B. Scudder N. A. Hamilton T. L.
*Glacial Meltwater as a Source of Amorphous Silica on Early Mars* **[#3070]**
Cold-climate silica cycling on mafic volcanics due to glacial meltwater alteration is a significant terrestrial weathering process. Amorphous silica deposits on Mars could be interpreted as mineralogical evidence for past ice sheet melt.

10:15 a.m. 2-MINUTE POSTER SUMMARIES
Bruner R. B.
*Special Exhibit on Meteorites and Minerals Associated with the Origin of Life on Earth or Mars* **[#3001]**

Baron F. Petit S. Gaudin A. Mangold N.
*Interpretation of Smectite VIS-NIR Spectra from Synthetic Smectites* **[#3019]**

Fairén A. G. Mateo-Martí E. Gago-Duport L. Losa-Adams E. Chevrier V. Gil-Lozano C.
*Coeval Formation of Mineral Sequences on a Cold and Wet Early Mars* **[#3037]**

Mitra K. Catalano J. G.
*Iron Oxidation By Chlorate: Implications for Akaganéite and Jarosite Formation on Mars* **[#3008]**

Miura Y.
*Formation of Ocean Sedimentary Rocks as Active Planets and Life-Like Systems* **[#3002]**

Uceda E. R. Fairén A. G. Gil-Lozano C. Losa-Adams E. Gago-Duport L.
*Kinetic Modeling of Mineral Sequences on Early Mars Using Fully Open Systems* **[#3040]**

Wiseman S. M. Robertson K.
*Intercomparison of Martian Carbonate-Bearing Deposits* **[#3064]**

**Thursday, October 5, 2017**
**CURIOSITY AND GALE CRATER I**
**10:45 a.m. Coconino/Canyon Room**

10:45 a.m. Hurowitz J. A. * Grotzinger J. P. Fischer W. W. McLennan S. M. Milliken R. E. Stein N. Vasavada A. R. Blake D. F. DeHouck E. Eigenbrode J. L. Fairen A. G. Frydenvang J. Gellert R. Grant J. A. Gupta S. Herkenhoff K. E. Ming D. W. Rampe E. B. Schmidt M. E. Siebach K. L. Stack-Morgan K. Sumner D. Y. Wiens R. C. [INVITED]
*Redox Stratification of an Ancient Lake in Gale Crater, Mars* **[#3057]**
The geochemistry, mineralogy, and sedimentology of mudstones studied by MSL-Curiosity indicate redox stratification of the lake within Gale crater and place new constraints on the habitability of the ancient Martian surface.

11:15 a.m. Bedford C. C. * Bridges J. C. Schwenzer S. P. Wiens R. C. Rampe E. B. Frydenvang J. Gasda P. J.
*Geochemical Endmembers preserved in the Fluviolacustrine Sediments of Gale Crater* **[#3017]**
The source regions of Gale crater's sedimentary record leading up to sol 1482 are determined from ChemCam and CheMin analyses on fluviolacustrine sediments. We propose that 5 magmatic/volcanic endmembers have contributed to Gale's stratigraphy.

11:35 a.m. Tosca N. J. * Ahmed I. Ashpitel A. Hurowitz J. A.
*Magnetite Authigenesis and the Ancient Martian Atmosphere* **[#3015]**
Merging new experimental constraints with geological data from Gale Crater shows that magnetite authigenesis may have provided a short-term feedback for stabilizing liquid water once it was generated on early Mars.

11:55 a.m. L'Haridon J. * Mangold N. Rapin W. Forni O. Meslin P.-Y. Cousin A. Payré V. Johnson J. Dehouck E. Nachon M. Le Deit L. Gasnault O. Maurice S. Wiens R.
*Iron and Magnesium Enrichments in Ca-Sulfate Veins as Observed by ChemCam at Gale Crater, Mars* **[#3016]**
ChemCam observations of Fe and Mg enrichments in Ca-sulfate bearing veins attest of variations in the pH and redox conditions that prevailed in the parent fluid during the diagenesis of the sedimentary rocks of Gale Crater.

12:15 p.m. *Lunch*

**Thursday, October 5, 2017**
**CURIOSITY AND GALE CRATER II**
**1:30 p.m. Coconino/Canyon Room**

1:30 p.m. Horvath D. G. * Andrews-Hanna J. C.
*Reconstructing the Paleo-Climate and Hydrology of Gale Crater, Mars in the Late Noachian and Hesperian Epochs* **[#3069]**
Using indicators of paleo-lake levels and the observed extent of aqueous alteration, hydrological modeling is used to constrain the climate and hydrology at Gale crater during the Noachian and Hesperian.

1:50 p.m. Mangold N. * Dehouck E. Forni O. Fedo C. Achilles C. Bristow T. Frydevang J. Gasnault O. L'Haridon J. Le Deit L. Maurice S. McLennan S. M. Meslin P. Y. Morrison S. Newsom H. E. Rampe E. Rivera-Hernandez F. Salvatore M. Wiens R. C.
*Open-System Weathering at Gale Crater from the Chemistry of Mudstones Analyzed by the Curiosity Rover* **[#3013]**
Fine-grained sediments analyzed by ChemCam along the traverse of the Curiosity rover display increasing alteration identified by significantly high indices of alteration that are consistent with open system weathering .

**Thursday, October 5, 2017**
**LIFE AND POTENTIALLY HABITABLE ENVIRONMENTS**
**2:10 p.m. Coconino/Canyon Room**

2:10 p.m. Craig P. I. * Mickol R. L. Archer P. D. Jr. Kral T. A.
*Clay Minerals as Nutrient Sources for Life on Mars* **[#3036]**
Methanogens can draw nutrients from certain clay minerals. Potential biosignatures are left within these minerals and could be detected by future missions.

2:30 p.m. Tarnas J. D. * Mustard J. F. Sherwood Lollar B. Bramble M. S.
Cannon K. M. Palumbo A. M.
*Radiolytic $H_2$ Production on Noachian Mars: Implications for Subsurface Habitability* **[#3039]**
The amount of $H_2$ produced on Noachian Mars via radiolysis could support a subsurface biosphere. Geophysical models constrain depth of the longest-lived subsurface habitat, from which biosignature-hosting material can be excavated by later impacts.

2:50 p.m. Osinski G. R. * Caudill C. Cockell C. S. Pontefract A. Sapers H. M. Simpson S.
Svensson M. Tornabene L. L.
*The Role of Meteorite Impacts in Creating a Habitable Early Mars* **[#3071]**
Impact craters may have provided conditions suitable for the emergence of life on Mars through the production of substrates for prebiotic chemistry and through the production of habitats for the emergence and subsequent survival of microbial life.

3:10 p.m. *Break*

3:25 p.m. Caudill C. M. * Greenberger R. N. Tornabene L. L. Osinski G. R.
Flemming R. L. Ehlmann B. L.
*Relevance of Pitted Material and Impact Melt to Early Martian Hydrothermalism and Habitability; Ries Ejecta Deposits as a Martian Analogue* **[#3068]**
Hydrothermal features are investigated at the Ries impact structure as potentially analogous to crater-related pitted material in Martian ancient terrains, which may reveal shallow sub-surface hydrothermal environments and prime exploration targets.

3:45 p.m. Szynkiewicz A. * Mikucki J. Vaniman D.
*Understanding Hydrological and Climate Conditions on Early Mars Through Sulfate Cycling and Microbial Activity in Terrestrial Volcanic Systems* **[#3035]**
Our study is a type of Earth-based investigation in a Mars-analog environment that allows for determination of how changing wet and dry conditions in active volcanic/hydrothermal system affect sulfate fluxes into surface water and groundwater.

**Thursday, October 5, 2017**
**EARLY MARS: COLD, WARM, OR COLD AND EPISODICALLY WARM?**
**4:05 p.m. Coconino/Canyon Room**

*A Panel Discussion About the Nature of the Early Martian Climate Based on a Review of the Current Observational Evidence and Theoretical Modeling — Tentative*

4:45 p.m. MODERATED DISCUSSION AND IDENTIFICATION OF KEY SCIENCE QUESTIONS

**Thursday, October 5, 2017**
**CONFERENCE DINNER**
**6:30 p.m. Coconino/Canyon Room**

*Guest Speaker TBD*

**Friday, October 6, 2017**
**FUTURE EXPLORATION**
**8:30 a.m. Coconino/Canyon Room**

8:30 a.m. REVIEW OF THE DAY'S AGENDA

8:35 a.m. Michael Meyer * [INVITED]
*NASA's Future Planning for Mars*

8:55 a.m. Returned Sample Science Board * Carrier B. L. Beaty D. W. McSween H. Y. Czaja A. D. Goreva Y. S. Hausrath E. M. Herd C. D. K. Humayun M. McCubbin F. M. McLennan S. M. Pratt L. M. Sephton M. A. Steele A. Weiss B. P.
*Strategies for Investigation Early Mars Using Returned Samples* **[#3051]**
Here we will discuss scientific objectives related to our understanding of Early Mars that could be significantly advanced by Mars Sample Return.

9:15 a.m. Ashley J. W. Banfield D. Beaty D. W. Carrier B. L. Diniega S. Johnson J. R. Zurek R. W.
*Major Discoveries Related to Early Mars as Input to Hypothesis-driven Mission Responses — Preparing for the Next Decadal Survey* **[#3049]**
This abstract attempts to initiate a community-based discussion that brings together MEPAG Goals and recent Early Mars discoveries for anticipating mission/instrument responses to include in Planetary Science Decadal Survey white papers.

**Friday, October 6, 2017**
**NEW PERSPECTIVES**
**9:30 a.m. Coconino/Canyon Room**

*Panel of Selected Graduate Students and Recent Post-Docs,*
*Who will Discuss Their Ideas Regarding the Key Issues Raised at the Meeting — Tentative*

**Friday, October 6, 2017**
**KEY SCIENCE QUESTIONS AND NEEDED INVESTIGATIONS BY PRESENT AND FUTURE MISSION**
**10:25 a.m. Coconino/Canyon Room**

10:25 a.m. FINAL DISCUSSION

11:55 a.m. Clifford S. M. *
*Closing Remarks and Announcement of Conference Special Issue*

**PRINT ONLY**

Boatwright B. D. Head J. W.
*MARSSIM Landform Evolution Model: Hydrologic Constraints on the Noachian Early Dry Period* **[#3029]**
We propose to test several hydrologic parameters to constrain the nature of highland degradation on Noachian Mars. This early dry period is less well characterized than the terminal epoch of valley network formation.

Losa-Adams E. Gil-Lozano C. Bishop J. L. Hoser A. Davila A. F. Fairen A. G. Chevrier V. F. Gago-Duport L.
*Li-Isotope Fractionation into the Octahedral Framework of Clays: A Way to Understand the Weathering of Basalt in Early Mars Conditions* **[#3082]**
We track the use of lithium isotopes as a proxy to understand the degree and extent of basalt weathering in aqueous mediums, providing important information about the prevailing conditions during the formation of water bodies in the past of Mars.

Rosenberg E. N. Head J. W. III Cassanelli J. Palumbo A. Weiss D.
*Water Volume Required to Carve the Martian Valley Networks: Updated Sediment Volume* **[#3026]**
In order to gain insights into the climate of early Mars, we estimate the volume of water that was required to erode the valley networks (VNs). We update previous results with a new VN cavity volume measurement.

Schwenzer S. P. Bart G. Bridges J. C. Crowther S. A. Filiberto J. Gilmour J. D. Herrmann S. Hicks L. J. Kelley S. P. Miller M. A. Ott U. Steer E. D. Swindle T. D. Treiman A. H.
*Fractionated Noble Gases in Martian Meteorite ALH 84001 — An Indicator for Water-Rock Interaction, or a Sample of Ancient Atmosphere?* **[#3018]**
Noble gases in the nakhlite and ALH84001 Martian meteorites are still a mystery, but could tell us about either the history of the Martian atmosphere, Martian water rock interaction or - likely - both!

Vidmachenko A. P.
*Where Should Search Traces of Life, Which Could Appear on Mars in the First 300 Million Years* **[#3005]**
In its early years, Mars was like the ancient Earth. If life on Mars today there is, then, certainly, it is microbial. The proof of the presence of liquid water on Mars does not mean that there is life on Mars. But this gives some hope.

**ALLUVIAL FAN MORPHOLOGY NORTH OF HELLAS INDICATES MULTIPLE STAGES OF DEPOSITION.** R. B. Anderson[1], R.M.E. Williams[2], A.L. Gullikson[1], [1]United States Geological Survey Astrogeology Science Center, Flagstaff, AZ (rbanderson@usgs.gov), [2]Planetary Science Institute

**Introduction:** The cratered highlands north of Hellas are one of several locations on Mars where numerous large alluvial fans have been observed [1]. These fans have been interpreted as evidence of a late-stage period of fluvial activity on Mars [2], and recent work indicates that they may have formed over hundreds of Myr indicating persistent or recurrent habitability [3].

We have mapped sinuous ridges in the cratered highlands to the north and west of Hellas (-15°N to -45°N, 30°E to 75°E), using 6 m/pixel Context Camera (CTX) images [4]. We find that sinuous ridges in this region are primarily concentrated within intracrater alluvial fans and are interpreted as inverted distributary channels. Several of the most prominent examples are shown in **Figure 1**. We present initial observations and interpretations of the geomorphology of these fans and the morphometry of the inverted features.

**Results:** *Fan Morphology:* The craters highlighted in this study show three distinct morphological types of alluvial fans (**Figure 2**). Some fans exhibit negative relief channels or "chutes" while others are heavily eroded, resulting in extensive inversion of relief. The sinuous ridges exhibit slight sinuosity and distributary branching, consistent with channelized mud-rich flows [5], while the channels tend to be wider and more linear than the sinuous ridges. A third category of fans is "degraded", with a rough surface with few clear channels or sinuous ridges.

Figure 3 shows overviews of Saheki crater and Crater L, with sinuous ridges traced in yellow, and fan boundaries marked in green. The variations in fan morphology within the same crater may represent different periods of fan formation, with the oldest fans subject to extensive erosion and inversion of relief, younger fans exhibiting a degraded but not fully inverted surface, and the youngest fans retaining negative relief chutes or channels. If this is not the case and the fans are the same age, then the degree of induration would need to vary significantly to result in such different morphologies. This seems unlikely, particularly for fans that are sourced from adjacent catchments in the walls of the same crater (e.g. the two large fans in Saheki, **Figure 3**).


**Figure 1**: Craters of interest to the north of Hellas. Yellow markings are mapped sinuous ridges. Crater "L" is named based on [1], Crater "7" is the seventh unnamed crater in the broader mapping region containing sinuous ridges associated with alluvial fans or similar features.

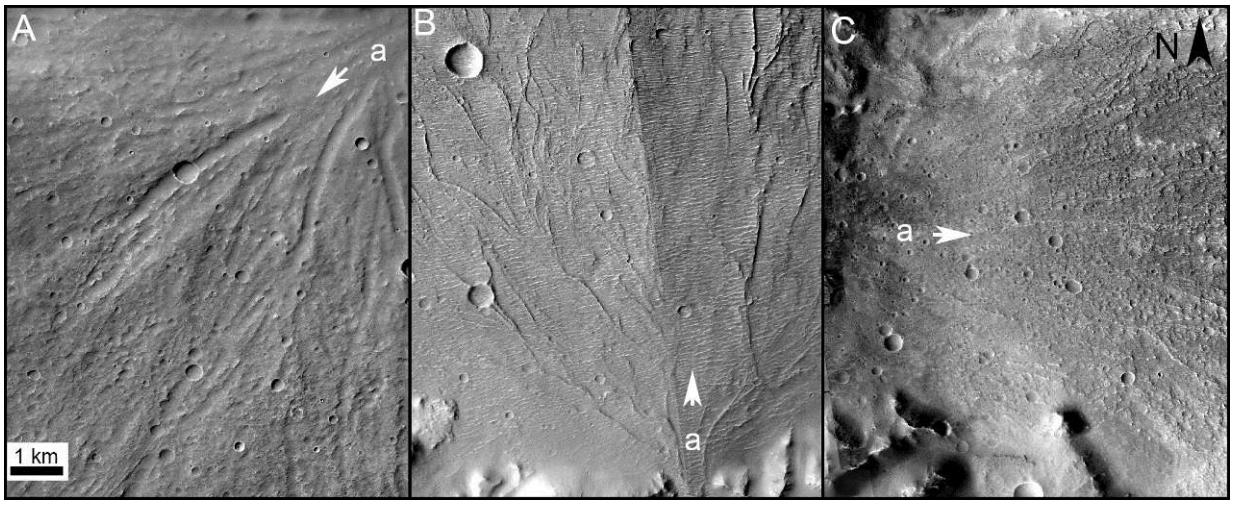


Figure 2: CTX images of fans in Crater L illustrating three distinct morphologies. Fan apices are marked with "a" and arrows indicate flow direction. (A) Negative relief "chute" morphology. (B) Inverted channel morphology. (C) Degraded morphology.

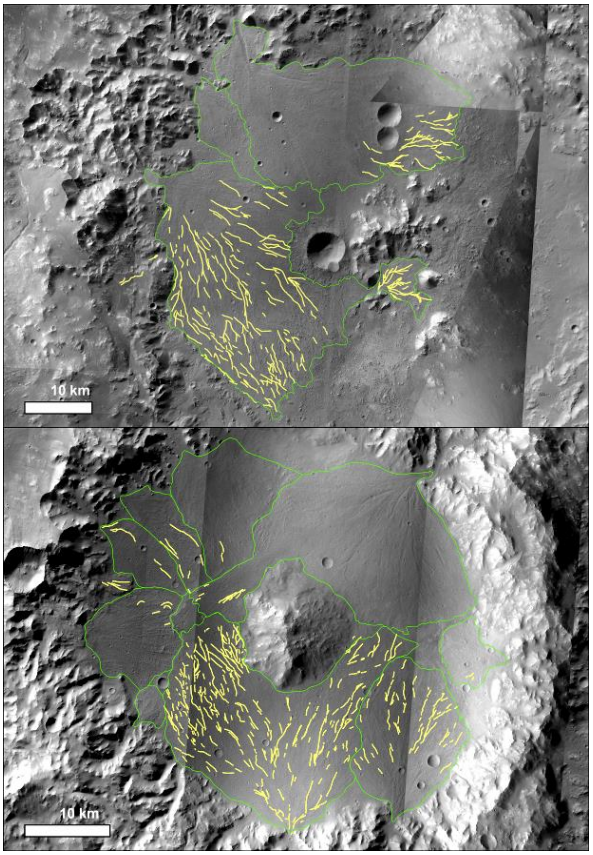


Figure 3: Fans (green outlines) and sinuous ridges (yellow) in Saheki (top), Crater L (bottom).

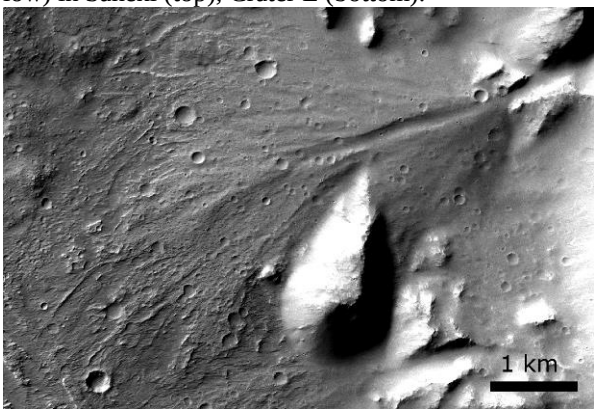


Figure 4: Small fan in Crater 7, showing transition from chute to inverted morphology.

In several cases, fans with channels transition to inverted relief at their distal ends. One explanation for this is that grain size sorting downfan during deposition led finer-grained and therefore more easily eroded distal deposits. Alternatively, this may fit with the interpretation above that the fan surfaces with channels represent a later stage of deposition that has partially buried the more proximal region of inverted relief. One possible example of this is shown in Figure 4.

Late stage deposition could also help to explain the apparent truncation of the small channel-bearing fans along the southern rim of Crater 7 by the larger, partially inverted fan sourced from the western wall. This is also consistent with the interpretation of the large alluvial fan in Harris crater as having formed in multiple discrete phases [6].

One challenge faced by the late-stage deposition hypothesis is that it does not appear to have occurred on all fans. For example, the southern fan in Crater L is almost entirely inverted, while the northern fan in the same crater is entirely chanellized (Figure 3). This may indicate that highly localized precipitation was responsible for at least the final stage of fan deposition

*Discharge Calculations*: We have also begun work on measuring the widths of the mapped sinuous ridges, to be used in estimating fluvial discharge. Width measurements are conducted using the highest resolution data available (HiRISE, 0.25-0.50 cm/pix), and when possible multiple measurements per ridge spaced every ~200 m are collected. Along with the average and standard deviation of the measured widths, each ridge is assigned a confidence ranking between 1 (very confident: well-defined flat-topped cap for the full length of the feature) and 4 (unmeasurable).

We find that the northern fan in Saheki crater has a median ridge width of 63 m, while the southern fan has a median ridge width of 34 m. Using width-discharge relationships from [7], these values yield a median discharge of ~170 $m^3/s$ for the northern large fan, and ~55 $m^3/s$ for the southern, more inverted fan. This latter value is in agreement with the 30-60 $m^3/s$ found by [5] for the southern fan. Although the uncertainties in empirical discharge calculations of this sort are large, and the number of measurable ridges in the northern fan is relatively small, the difference between the two results is consistent with the fans forming under different discharge conditions, and potentially at different times.

**Future Work:** Work is ongoing to understand the stratigraphic relationships between the fans in the craters discussed here, and to relate these to other ridge-bearing fans and fan-like features in the mapping area. We will also continue estimating discharge where possible to determine whether systematic changes in discharge can be related to the observed differences in fan morphology. These observations will lead to a better understanding of the history of fluvial activity on Mars.

**References:** [1] Moore, J.M., Howard, A.D. (2005) JGR, 110, E04005. [2] Howard, A.D., Moore, J.M., Irwin, R.P. (2005) JGR, 110, E12S14. [3] Kite, E.S. et al. (2017) GRL 44, 3991-3999. [4] Gullikson, A.L., Anderson, R.B., Williams, R.M.E. (2016) 47th LPSC, #2376. [5] Morgan, A.M. et al. (2014) Icarus, 229, 131-156. [6] Williams, R. M. E., et al. (2011) Icarus, 211 (1), 222-237. [7] Jacobsen, R.E. and Burr, D.M. (2016) GRL, 43, 8903-8911.

**MARS DURING THE PRE-NOACHIAN.** J. C. Andrews-Hanna[1] and W. B. Bottke[2], [1]Lunar and Planetary Laboratory, University of Arizona, Tucson, AZ 85721, jcahanna@lpl.arizona.edu, [2]Southwest Research Institute and NASA's SSERVI-ISET team, 1050 Walnut St., Suite 300, Boulder, CO 80302.

**Introduction:** The surface geology of Mars apparently dates back to the beginning of the Early Noachian, at ~4.1 Ga, leaving ~400 Myr of Mars' earliest evolution effectively unconstrained [1]. However, an enduring record of the earlier pre-Noachian conditions persists in geophysical and mineralogical data. We use geophysical evidence, primarily in the form of the preservation of the crustal dichotomy boundary, together with mineralogical evidence in order to infer the prevailing surface conditions during the pre-Noachian. The emerging picture is a pre-Noachian Mars that was less dynamic than Noachian Mars in terms of impacts, geodynamics, and hydrology.

**Pre-Noachian Impacts:** We define the pre-Noachian as the time period bounded by two impacts – the dichotomy-forming impact and the Hellas-forming impact. The latter has previously been used to define the boundary between the Noachian and pre-Noachian [1], and the former so profoundly changed the surface and interior of Mars as to make it a natural starting point for any study interested in early martian evolution. Isotopic and geochemical evidence supports the formation of the martian dichotomy by a giant impact at > 4.47-4.5 Ga [2], while the crater retention age of the Hellas basin is 3.97-4.06 Ga [3]. Based on the similar preservation state of the rim of the Borealis basin as expressed in the dichotomy boundary, and the rims of the Noachian-aged basins Hellas, Isidis, Utopia and Argyre (HUIA), a similar preservation state is expected for any crustal-scale basins formed during the intervening pre-Noachian. The lack of evidence for similarly well-preserved pre-Noachian basins of this scale and the lack of evidence for excavation of the dichotomy boundary by basins other than Isidis suggest that no other basins formed during this time [2].

The formation of at least three crustal-scale basins (Hellas, Isidis, and Argyre) during a span of ~200 Myr during the Noachian [3] and at most one crustal-scale basin (Utopia, whose age is poorly constrained) during a span of ~400 Myr during the pre-Noachian indicates that the average impact flux during the pre-Noachian was <17% of that during the Noachian. If Utopia is a Noachian-aged basin [4], the flux during the pre-Noachian would be lower still. At least one pre-Noachian basin, Ladon, has been confidently identified in the next size interval smaller than HUIA. The formation of one Ladon-sized basin during the 400 Myr pre-Noachian, and the four HUIA basins in the subsequent 200 Myr implies that the mean impact flux during the pre-Noachian was ~10% of that during the LHB. Consideration of the sawtooth-shaped exponentially declining impact fluxes both in the aftermath of planet formation and during the Late Heavy Bombardment [5] suggests that the impact flux during much of the pre-Noachian was even lower than indicated above. This bombardment history is consistent with a late heavy bombardment (LHB) of the inner Solar System [6] during which HUIA formed, which followed the planet formation era impacts during which the dichotomy formed.

**Pre-Noachian Tectonism and Volcanism:** The crust within each of the southern highlands and northern lowlands is remarkably uniform in thickness, aside from regions in which it has been thickened by volcanism (e.g., Tharsis, Elysium) or thinned by impacts (HUIA), both of which occurred dominantly in the Noachian. Furthermore, the path of the Borealis basin rim is within 1% of an ellipse, even where it has been buried beneath Tharsis [7], with no major deflections from this shape. These observations indicate that there were no large-scale changes to the crust of Mars during the pre-Noachian. This constraint effectively rules out a global plate tectonic cycle of lithosphere recycling akin to that currently operating on Earth. Similarly, no giant Tharsis-style volcanic rises formed during the pre-Noachian. In contrast, the incipient stages of Tharsis formation may have begun in the Early Noachian [8] with substantial construction continuing through the Hesperian [9]. However, smaller structures would be more easily destroyed during the LHB, and so neither localized rifting and tectonism, nor smaller shields and volcanic provinces can be ruled out during the pre-Noachian.

**Pre-Noachian Water and Climate:** Fluvial valley networks, lakes, and sedimentary deposits formed during the pre-Noachian would have been destroyed by impacts during the Noachian LHB. However, the preservation of the crustal dichotomy boundary does place some constraints on the pre-Noachian climate. The dichotomy boundary is a topographic step similar to that at the edges of many continents on the Earth (Fig. 1). Under a persistent Earth-like climate, such a step would be rapidly eroded to the local base level. On Earth the elevation of continents relative to sea level (the "freeboard") is reduced to a value slightly above zero by erosion on timescales of hundreds of millions of years. The Appalachian mountains of North America experienced long-term erosion rates of 10-50

m/Myr [10], which was likely limited by the uplift rate rather than erosion. This freeboard concept applied under cold climate conditions as well, resulting in the relatively uniform elevation of the edge of the continental shelves from erosion during ice ages when sea level was lower. The concept of freeboard is applicable whether the high-standing topography was generated by tectonism or by impact. On Mars, Earth-like erosion rates would have drastically reduced the elevation of the southern highlands and reduced the dichotomy boundary to a gradual slope leading down to the lowlands. At the rate of erosion experienced by the Appalachians, the 8 km topographic step across the dichotomy boundary could have been reduced by 4-20 km during the 400 Myr pre-Noachian. Although erosion would have been accompanied by flexural uplift [11], the dichotomy boundary scarp itself would have been largely erased under these conditions and a more gradual slope would be expected. As a caveat, it is difficult to completely rule out the other extreme end-member interpretation – that the near constant elevation of the southern highlands is the result of high erosion rates coupled with a pre-Noachian sea level close to the average southern highlands elevation. However, in this scenario one might expect higher elevations further from the putative shoreline, in conflict with the similar elevations within the southern highlands over distances of up to ~5000 km from the dichotomy boundary.

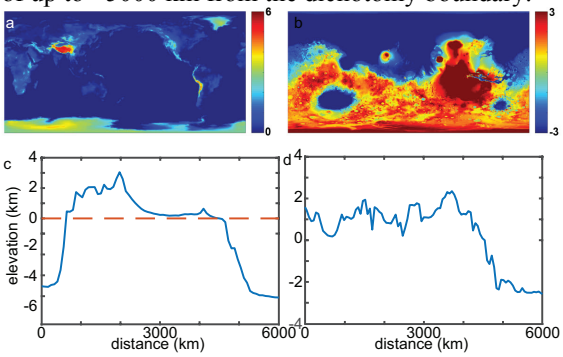


**Figure 1.** Maps of the elevation of Earth (a; relative to sea level) and Mars (b), and profiles across North America (at 45°N) and the Martian dichotomy (at 150°E). Earth's continents remain close to sea level (dashed red line in a) except in areas of active mountain building.

While the geophysical record effectively rules out Earth-like conditions being maintained throughout the pre-Noachian, the mineralogical record supports the presence of liquid water in the subsurface. Extensive Fe/Mg phyllosilicate deposits are found on Noachian surfaces, which may have formed at depth and later been exposed at the surface [12]. By this interpretation, these clays pre-date the Noachian surfaces in which they are found, and could have formed within surface-driven weathering sequences in the pre-Noachian. The pre-Noachian climate is thus inferred to be wet, but not persistently Earth-like, similar to some interpretations of the Noachian climate. Alternatively, if the Fe/Mg clays instead formed by hydrothermal processes [13] or from surface-driven weathering in the Noachian, combined with the lack of large-scale erosion of the dichotomy boundary, this leaves open the possibility of a cold and barren pre-Noachian with a stripped atmosphere waiting to be revived by Noachian-era impacts and volcanism.

**Conclusions and Implications:** The complete lack of a pre-Noachian geological record forces us to rely upon indirect inferences based on the geophysical and mineralogical records in an attempt to reconstruct the conditions during this substantial period of martian history. The preservation of the dichotomy boundary requires that there were no large-scale crustal rearrangements or modifications during the pre-Noachian. No basin-forming impacts occurred during this time period spanning between the Borealis and Hellas impacts. Impact rates during the pre-Noachian were <17% of those in the Noachian, and likely lower still. Neither plate tectonics nor regional volcanic rise construction were active during this time. Erosion of the newly formed dichotomy boundary scarp during the pre-Noachian occurred at rates substantially lower than is characteristic of recently generated high topography in terrestrial mountain belts, though widespread aqueous alteration of the crust suggests the presence of liquid water at shallow depths.

This interpretation of pre-Noachian conditions suggests that this epoch, spanning ~400 Myr of Mars' earliest history, was a quiescent time relative to the Noachian in every respect. For this reason, this period has been dubbed the martian "doldrums". However, the pre-Noachian may have had the greatest astrobiological potential of any time period on Mars. It was possibly wetter than the Hesperian and Amazonian epochs, but provided a more stable environment than the LHB-era Noachian.

**References:** [1] Carr M. H. and Head J. W. (2010) *EPSL 294*, 185–203. [2] Bottke W. F. and Andrews-Hanna J. C. (2017) *Nature Geosci., 10,* 344-348. [3] Robbins S. J. et al. (2013) *Icarus*, *225*, 173–184. [4] Werner, S. C. (2008), *Icarus*, *195*, 45–60. [5] Morbidelli, A. et al., (2012), *EPSL* 355, 144–151. [6] Gomes, R. et al., (2005), *Nature*, *435*, 466–469. [7] Andrews-Hanna, J. C. et al., (2008), *Nature, 453*, 1212–1215. [8] Karasözen, E. et al., (2016), *JGR, 121*, doi:10.1002/2015JE004936. [9] Bouley, S. et al., (2016), *Nature*, *531*, 344–347. [10] Reed J. S. et al. (2005), *Basin Research, 17*, 259-268. [11] Evans, A. J. et al., (2010), *JGR, 115*, doi: 10.1029/2009JE003469. [12] Carter, J. et al., (2013), *JGR, 118*, doi: 10.1029/2012JE004145. [13] Ehlmann, B. L. et al., (2011), *Nature, 479*, 53–60.

**Major Discoveries Related to Early Mars as Input to Hypothesis-driven Mission Responses — Preparing for the Next Decadal Survey**. J.W. Ashley[1], D. Banfield[2], D.W. Beaty[1], B.L. Carrier[1], S. Diniega[1], J.R. Johnson[3], R.W. Zurek[1] (james.w.ashley@jpl.nasa.gov); [1]Mars Program Office, Jet Propulsion Laboratory, California Institute of Technology, Pasadena, CA 91109; [2]Cornell University, 420 Space Sciences Building Ithaca, NY 14853; [3]John Hopkins University Applied Physics Laboratory, Laurel, MD 20723.

**Introduction:** In the charter of the United States National Research Council (NRC), the community-driven Planetary Science Decadal Survey (DS) [1] identifies planetary science goals and their relative priorities. Recommendations are also given in the DS for addressing these science objectives, primarily in the form of robotic missions. The report provides input for NASA's Science Mission Directorate (SMD), and is often called upon by Congress to inform policy and appropriations decisions. Each DS requires approximately two years to prepare. The current DS (covering the 2013-2022 period) has recently completed its mid-term review of progress by NRC.

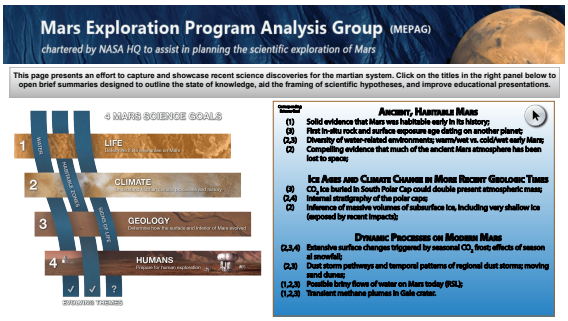


Figure 1. Work-in-progress example interface for Recent Discoveries Portal (soon to be released for community use).

Preparation for the next DS should begin with an assessment of what is known and what remains to be learned for each area of study in planetary science. For Mars, this assessment is attempted through the MEPAG Goals document [2,3], which serves the Mars Exploration Program in a similar, but more in-depth, capacity as the DS does the SMD.

New discoveries fuel hypothesis-driven science, and a thorough account of recent discoveries is useful for the purpose of conceiving and developing mission-based responses to those discoveries. Accordingly, MEPAG and the JPL Mars Program Office maintain a summary of discoveries on its public website. A new version of this will take the form of a portal that organizes discovery information in the context of both MEPAG Goals and the DS recommendations (An example for the work-in-progress interface is featured as Figure 1). The portal strives to capture and showcase recent science discoveries for the martian system. Brief summaries are designed to outline the state of knowledge, aid in framing scientific hypotheses, and improve educational presentations. The portal will be an on-going resource that is updated as new discoveries arise.

Excerpts of draft examples of discoveries, measurements, and observations that could apply specifically to Early Mars, are presented below.

***Ancient habitable environments preserved in the rock record:*** *The potential for habitable environments during a time window in Mars' ancient past (the Noachian-Hesperian transition) has been identified at Yellowknife Bay in Gale crater by the Mars Science Laboratory (MSL) science team. This consensus is based upon comprehensive sedimentological, mineralogical, and geochemical observations, and includes: 1) unambiguous evidence for fluvial transport of coarse-grained sediments, in concert with 2) deltaic deposits confirming the presence of a standing body of water together with laminated mudstones – also indicative of quiescent water deposition; 3) clay mineral detection and lack of chemical precipitates, confirming high water/rock ratio exposure in low-salinity water of near-neutral pH; 4) the presence of key chemical elements used by biology, including native carbon; and 5) the detection of nutrients such as nitrates and energy sources for microbial metabolism such as minerals in various oxidation states.*

***Compelling, quantitative evidence that much of the ancient Mars atmosphere has been lost to space:*** *MAVEN measurements of light gases and noble gas isotopes within the atmosphere, in concert with measurements taken in the well-mixed lower atmosphere, show that volatiles have been and continue to be lost to space by a variety of mechanisms. Observed gas distributions manifest as 1) an ion stream down the solar wind tail 2) another plume extending above the north pole (accounting for ~0.3-0.5 the total mass loss during the period of observation), and 3) an extended, planet-enveloping corona. Though measurements were made during a period of relatively quiet solar wind conditions, the few coronal mass ejections that have been observed at Mars can enhance loss by a factor of 10 or more, and so may have been one of the key drivers of loss historically during times when such outbursts were more frequent on the sun.*

***First in-situ rock and surface exposure age dating on another planet:*** *Recently, a technique for assessing radiogenic and cosmic ray exposure ages in-situ on Mars was developed using potassium-argon isotope systematics, and noble gas (3He, 21Ne, and 36Ar) isotope chemistry, respectively. Data was collected on mudstones drilled at Yellowknife Bay, Gale crater using the Sample Analysis at Mars (SAM) instrument on the Mars Science Laboratory (MSL) Curiosity rover. The resulting potassium-argon age of 4.21 ± 0.35 Ga (which dates the potassium-bearing phases in the rock) approximates the model age of the ancient crust around Gale crater estimated from crater counting. A surface exposure*

*age of 78 ± 30 Ma was determined by the noble gas measurements, reflecting recent exposure from aeolian scarp retreat. The authors of this dating technique note that while incomplete Ar extraction in some samples can complicate analyses, similar exposures may be among the best places to explore for biosignatures because they are likely to be relatively well-preserved, having been buried and shielded from cosmic radiation and surface-atmosphere chemistry.*

Additional recent discovery entries, spanning the full martian history, currently include the following titles: 1) Extensive surface change triggered by seasonal $CO_2$ frost; 2) Dust storm pathways and temporal patterns of regional dust storms; 3) Transient methane plume(s) in Gale Crater; 4) Recurring Slope Lineae: Evidence of liquid water on Mars today?; 5) Shallow ice extent further exposed by recent meteor impacts; 6) Seasonal snowfall on Mars; and 7) $CO_2$ ice buried in South Polar Cap could double present atmospheric mass.

In light of the breadth of recent discoveries which could be used to inform future priorities and recommendations for new Mars missions, we encourage the Early Mars community contribution of white papers to help inform the next decadal survey.

**References:** [1] NRC Space Studies Board (2011), *Visions and Voyages for Planetary Science in the Decade 2013-2022*. [2] MEPAG (2015) *Mars Scientific Goals, Objectives, Investigations, and Priorities: 2015*, 74 p. [3] Diniega et al. (2017; this conference), *Early Mars-relevant Investigations Within the MEPAG Science Goals*.

**Field Excursions to Terrestrial Analog Sites for the Fourth International Conference on Early Mars.** J. W. Ashley[1], N. G. Barlow[2], D. W. Beaty[1], J. Farmer[3], D. A. Kring[4], W. G. Parker[5] (james.w.ashley@jpl.nasa.gov); [1]Mars Program Office, Jet Propulsion Laboratory, California Institute of Technology, Pasadena, CA 91109; [2]Department of Physics and Astronomy, Northern Arizona University, Flagstaff, AZ 86011-6010; [3]School of Earth and Space Exploration, Arizona State University, Tempe, AZ 85287-3603; [4]USRA-Lunar and Planetary Institute, 3600 Bay Area Blvd., Houston, TX 77058; [5]Division of Resource Management, Petrified Forest National Park, Box 2217, Petrified Forest, AZ 86028.

**Introduction:** Several important terrestrial analog sites for different aspects of Early Mars occur within driving distance of the conference venue in Flagstaff AZ. Since Mars is first and foremost a field site, it is very important to take the opportunity to use these sites to discuss strategies for interrogating the outcrops to extract the crucial scientific messages we need.

Two field trips (one mid- and one post-conference) are scheduled as part of the Fourth International Conference on Early Mars. The excursions will explore major geological processes, including impact cratering, volcanism, habitability, and biosignature preservation.

- The mid-conference fieldtrip will focus on 1) the geology of the Grand Canyon and implications for how habitability changed over the billion-year history of the Colorado Plateau, and 2) the recent volcanic activity in the San Francisco Volcanic Field, near Flagstaff.
- The post-conference trip will begin with a visit to Meteor Crater, highly regarded as the best preserved impact crater in the world. We will consider the processes of impact cratering and how they shape planetary development, and effects of impacts on habitability. This will be followed by a visit to the Painted Desert and Petrified Forest to explore environments of successful biosignature preservation.

Insights gained from these sites should provide useful input to discussions about Mars landing sites, science goals, mission architectures, and sample selection strategies. Details of these excursions are presented below.

**Field Trip 1 (mid-conference):** This trip will include two major stops. The first location will be the south rim of the Grand Canyon, with opportunities to review the major events recorded within the nearly mile-thick sequence of strata exposed by erosion over the past ~5 million years. We will have opportunities to visit the famous Yavapai Geology Museum and review the major environmental changes recorded in the stunning exposures of the geological formations exposed in the canyon walls. These involve environments ranging from high grade metamorphic processes (Vishnu Schist) and plutonic igneous rocks (Zoroaster Granite) that record shallow magmatism and tectonic uplift, to erosion and deposition within habitable marine sedimentary environments [e.g., 1,2]. This early history is succeeded by major changes in sea level and climate changes, bounded by periods of erosion which produced the major erosion surfaces (unconformities) seen in the Canyon walls. Special emphasis will be on understanding the nature of environmental changes and how habitability changed over time. We will consider how the geological history recoded in the Grand Canyon differs from what we infer for early Mars and the changes that have occurred on that planet.


Figure 1. Anticipated route for Field Trip 1. North is up; Google Earth image width is approximately 178 kilometers.

Our experience on the South Rim of the Grand Canyon will be followed by a stop in the San Francisco Volcanic field near Flagstaff with field discussions at Sunset Crater, about the nature of recent basaltic volcanism over the region, and an invitation to consider how volcanism has varied over the million-year time frame recorded by the San Francisco volcanoes [3], and their impacts on habitability. We will also consider how these concepts can be applied to better understand early Mars. Outcrop exposures of the Moenkopi redbeds will be identified and discussed along the road during the drive from Grand Canyon to Flagstaff.

**Field Trip 2 (post-conference):** Martian impact craters are prime locations in the search for biosigna-

tures because they serve as catchment basins for materials deposited by other geologic processes (including fluvial activity), expose ancient stratigraphic layers and ice deposits from depth, and can initiate long-lived hydrothermal systems [4,5]. While only larger complex craters and basins can maintain active hydrothermal systems on time scales of thousands of years or more, the more numerous small simple craters provide important constraints on the spatial and temporal extent of processes and materials of astrobiological interest [6].

The 1.2-km-diameter Barringer Meteorite Crater ("Meteor Crater") east of Flagstaff will be examined for evidence of post-impact processes that produced lake sediments, crater wall gullies, and potential niches for life. The effect of ejecta emplacement and the atmospheric blast zone on the local environment when the crater formed 50,000 years ago will be discussed [7]. We will also explore the roles that impact breccias, impact ejecta, and overturned strata could play in the preservation of biosignatures on early Mars. Attendees may choose between a rare but physically challenging descent to the crater floor, or a less-strenuous traverse along the rim perimeter.

The lacustrine environment is a proxy for similar systems on early Mars. The floor of the crater harbored springs, ponds, and, at times, a fully-interconnected lake [7]. Water chemistry varied, depending on the proportion of groundwater contributions and precipitation, providing clement conditions for microscopic single-celled aquatic plants (diatoms) and single-celled protists (domain Eukarya). Water in the crater – or lack thereof as climate evolved – altered the flow of air in the crater, affecting temperatures in potential microniches and evaporation/condensation rates [8]. The modern environment hosts a complex set of flora and fauna. While that type of life is quite unlike that ever anticipated on Mars, microbial environments continue to persist. Colonies of cyanobacteria, for example, and integrated systems of lichens can be found throughout the crater. While our focus will be on conditions within the crater, tectonic joints in the bedrock outside the crater also host tiny reservoirs of water that flora utilize [9]. In arid environments, such as Mars, similar geologic features may be critical catchments for life.

The Petrified Forest will offer a chance to observe/discuss the unique biosignature preservation attributes of the Upper Triassic Chinle Formation. The spectral signal of the Petrified Forest area shows phyllosilicate and sulfate deposits that are considered to be analogous to deposits found on Mars [10]. These deposits in the Chinle Formation are associated with organic remains, mainly plant material, providing a potential analog for detecting organics in similar depositional and preservational systems. We will also discuss the potential association of the Manicouagan impact structure with a biotic turnover recorded in the Chinle Formation during the Late Triassic and preserved in the park [11]. Attendees will visit the Painted Desert, jarosite-bearing organic horizons, Triassic fossil exhibits, and petrified wood accumulations.

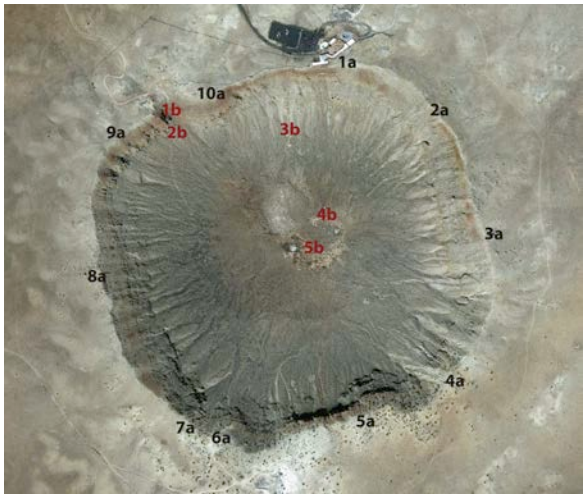


Figure 2. Field Trip 2 will include two excursion options for Barringer Meteorite Crater. Black numbers indicate points of interest along crater rim. Burgundy numbers highlight interior wall and floor discussion locations. North is up; crater diameter is ~1.2-km.

**References:** [1] Ranney, W. (2005) *Carving Grand Canyon: Evidence, Theories, and Mystery*; ISBN 0-938216-82-1. [2] Blakey, R. C., and Middleton, L. T. (2012) *GSA* Special Paper 489, p. 81-92. [3] Duffield, W. A. (1997) *Volcanoes of Northern Arizona: Sleeping Giants of the Grand Canyon Region*; ISBN 0-938216-58-2. [4] Beaty D. W. et al. (2006) *Astrobiology*, 6, 677-732. [5] Rummel J. D., et al. (2014), *Astrobiology*, 14, 887-968. [6] Barlow N. G. (2010) *GSA Bulletin*, 122, 644-657. [7] Kring D. A. (2007) *Guidebook to the Geology of Barringer Meteorite Crater*, LPI Contribution #1355, 150 pp. [8] Whiteman, C.D., Kring, D.A., and Hoch, S.W. (2008) *LPSC XXXIX*, Abs. #1405. [9] Kring, D.A. (2015) *LPSC XLVI*, Abs. #1036. [10] Noe Dobrea, E.Z et al., (2017) *AbSciCon* 2017, LPI Contrib. No. 1965, Abs. #3356. [11] Parker, W.G., and Martz, J.W. (2011). *Earth and Environmental Transactions of the Royal Society of Edinburgh* 101:231-260.

**BASALT WEATHERING AND THE VOLATILE BUDGET OF EARLY MARS.** Leslie L. Baker[1], [1]Dept. of Geological Sciences, University of Idaho, Moscow, ID 83844-3022, lbaker@uidaho.edu.

**Introduction:** Clay minerals are now known to be widespread in surficial and subsurface rocks of Mars [1, 2]. These minerals provide a geochemical record of aqueous weathering of the martian crust under past conditions that were warmer and wetter than the present day [3, 4] although specific conditions through time are not yet fully known. Although some of these clays are likely to have formed in the subsurface [5], it has been argued that many of them are pedogenic, and indicate surface weathering of basaltic rocks under broadly Earth-like conditions [4].

Weathering of fresh basalt, is a significant factor in fixation of atmospheric $CO_2$ on Earth [6-8] and in terrestrial climate cycling [9]. This process may also have affected the atmosphere of Mars, resulting in climate fluctuations controlled by competing rates of $CO_2$ production and consumption [10].

This study provides a quantitative mass balance estimate of martian $CO_2$ consumption by weathering of a given mass of basalt under surficial / pedogenic conditions. It also provides estimates of the mass of water fixed in pedogenic clay minerals and the dissolved salt yield per unit mass of basalt weathered.

**Terrestrial basalt weathering:** Flows of Columbia River Basalt (CRB) contain interbedded saprolites and paleosols formed by weathering during the intervals between eruptions. Weathering of CRB has been studied quantitatively in terms of mass loss from parent basalt through saprolite and paleosol formation [11-14] and mass loss has been linked to clay mineralogy [12].

Theoretically, as a result of the chemical reactions involved, basalt weathering should consume a molar amount of $CO_2$ that is two times the sum of dissolved base cations [15]. A global database of low-temperature basalt weathering [6] quantified dissolved ion release and $CO_2$ drawdown by examining the chemistry of freshwater runoff. This empirical database suggests that the proportion of $CO_2$ consumed to dissolved ions released is relatively constant across a wide range of weathering conditions, and that $CO_2$ consumption is equal to 1.89 times the sum of dissolved base cations, close to the theoretical value.

Weathering of Columbia River Basalts (CRB) has been studied quantitatively in terms of mass loss from parent basalt through saprolite and paleosol formation [11-14]. These studies provide estimates of mass loss at different stages of weathering and over different physical scales. Although individual study sites display variations, the geochemistry of basalt weathering in CRB has been found to be comparable to basalt weathering in other locations. By the weathering stage at which smectite clays are abundant, the majority of most soluble ions as well as considerable Si have been lost from a parent basalt, and the residue is dominated mainly by Al, Fe, and Ti oxides and silicates [12, 14, 16]. Here, CRB are used as Mars analogs because both their weathering chemistry and the clay mineralogy of the resulting saprolites and paleosols has been studied.

Estimated clay mineral abundances in the clay outcrops observed at Mawrth Valles and Nili Fossae on Mars range from 20 to 65% and spectral modeling suggests some relict primary minerals are present [17]. If these assemblages were formed by weathering, comparable CRB samples would include clay-rich saprolites that still contain relict primary igneous minerals [11, 12]. If the martian outcrops include clay soils, the comparable CRB samples would be smectite-bearing paleosols [13, 14].

**Methods:** The composition of the Gusev basalt Humphrey [18] was taken as a typical martian basalt. Mobility ratio ($\tau$ ) values for a CRB saprolite [12] and paleosol [14] were used to represent two possible weathering scenarios. For a fixed quantity of starting basalt, the mobility ratio may be used as a mass loss factor, and the mass of each element that is leached and that remains in the leached residue may be calculated. The mobility ratios for the saprolite and paleosol models were applied in this manner to the Humphrey composition. The mass of $CO_2$ consumed was calculated for each model using the factor of 1.89 tonnes $CO_2$ consumed per tonne of base cations produced.

The total mass remaining in the residue was assumed to have undergone 100% conversion to clay minerals. Because this is likely to be an overestimate for the saprolite model, , a calculation was also performed assuming 50% conversion to clay. This calculation yields a dry mass of clay; a water content of 20 wt % was added to this mass and its volume was calculated using an estimated density of 2000 kg/m$^3$.

These calculations mathematically relate the mass of basalt weathered to the mass of ions leached, mass of $CO_2$ consumed, and volume of clay produced. Given an observed volume of clay minerals, the masses of parent basalt weathered, dissolved ions released, and $CO_2$ consumed during the weathering reactions that produced the clay were back-calculated.

**$CO_2$ consumption by weathering:** Calculated values for $CO_2$ consumption show that in the paleosol model, 1 $m^3$ of clay would represent the weathered residue of approximately 2.0 $m^3$ of basalt, with consumption of 1534 kg of $CO_2$. Using the less extensively weathered saprolite model and assuming the residue is composed of 100% clay, the equivalent numbers would be 1.1 $m^3$ of parent basalt weathered, and 597 kg of $CO_2$ consumed. For a saprolite residue consisting of 50% clay and 50% relict basalt components, the equivalent numbers would be 1.4 $m^3$ of parent basalt and 1193 kg of $CO_2$ consumed.

A layer of pure clay 1 m deep, covering 10 % of the martian surface, would represent (in the paleosol model) weathering of 8 * $10^{13}$ tonnes of basalt and consumption of 2 * $10^{13}$ tonnes of $CO_2$. This is equivalent to drawdown of nearly the entire present-day mass of the martian atmosphere. The equivalent calculation using the saprolite model would represent weathering of 5 * $10^{13}$ tonnes of basalt and consumption of 9 * 1012 tonnes of $CO_2$. As most of the thick clay layers on Mars are observed outcropping from underneath younger materials, the total clay volume on the planet is not known, although the observed layers range from several meters thick to up to ~200 meters at Mawrth Valles [19] and extend laterally across an area ~1000 km wide [3]. Sufficiently thick, extensive, and continuous clay layers, if they exist, could represent the preserved record of consumption of a mass of $CO_2$ in the range of $10^{15}$ – $10^{16}$ tonnes.

Climate models suggest that warming on ancient Mars may have required up to several bars of $CO_2$ in order to maintain stable liquid water on the planet's surface [20]. The calculations presented here suggest that the observed clay outcrops on Mars may represent an amount of weathering that was sufficient to create a climate forcing by consuming atmospheric $CO_2$. On Mars, one bar of $CO_2$ is approximately 8.85 * $10^{19}$ moles [10], or 3.9 * $10^{15}$ tonnes. Under the paleosol weathering scenario, one bar of $CO_2$ would be consumed by the production of 2.5 * $10^{15}$ $m^3$ of clay. This quantity is equivalent to a layer of clay approximately 18 m thick over the entire surface of Mars.

**Water consumption and salt production:** The observed clay deposits represent a significant water reservoir. Terrestrial smectites such as nontronite contain ~20 wt% water. Under the paleosol weathering scenario and assuming consumption of 1 bar of CO2 the resulting clay layer would sequester 6.7 * $10^5$ $km^3$ of water, or the equivalent of a 4.6 m deep layer of water over the entire surface of the planet.

The calculations presented here suggest that basalt weathering adequate to draw down ~ 1 bar of $CO_2$ would have produced on the order of 7.8 * $10^{15}$ tonnes of dissolved basalt components, as well as 5.4 * $10^{15}$ tonnes of bicarbonate ions. This mass of material must have some ultimate sink. Documented occurrences of martian salts include the salts observed in martian dust, soils, and sediments [21-25] and rock outcroppings [1, 26-30], gypsum veins observed by Mars rovers [31], cements in sedimentary rocks [32, 33], and dissolved salts in subsurface brines [34]. The salts accounted for by each of these sinks are, at the present time, not easily quantifiable, but likely would not account for the entire salt budget produced by weathering [35].

**References: [**1] Murchie, S.L., et al. (2009) *J Geophys Res - Planets* 114, E00D06. [2] Bibring, J.-P., et al. (2006) *Science* 312, 400-404. [3] Bishop, J.L., et al. (2013) *Planet Space Sci* 86, 130-149. [4] Carter, J., et al. (2015) *Icarus* 248, 373-382. [5] Ehlmann, B.L., et al. (2011) *Nature* 479, 53-60. [6] Dessert, C., et al. (2003) *Chem Geol* 202, 257-273. [7] Berner, R.A. et al. (1983) *Am J Sci* 283, 641-683. [8] Louvat, P. and C.J. Allègre (1997) *Geochim Cosmochim Acta* 61, 3645-3669. [9] Cox, G.M., et al. (2016) *Earth Planet Sci Lett* 446, 89-99. [10] Batalha, N.E., et al. (2016) *Earth Planet Sci Lett* 455, 7-13. [11] Baker, L.L. (2017) *Amer Mineral* 102, 33. [12] Baker, L.L. and O.K. Neill (in press) *Amer Mineral* 102. [13] Hobbs, K.M. and J.T. Parrish (2016) *GSA Bulletin* 128, 1543-1554. [14] Thomson, B.J., et al. (2014) *Earth Planet Sci Lett* 400, 130-144. [15] Sheldon, N.D. (2006) *Precambrian Research* 147, 148-155. [16] Babechuk, M.G., M. Widdowson, and B.S. Kamber (2014) *Chem Geol* 363, 56-75. [17] Poulet, F., et al. (2008) *Astronomy and Astrophysics* 487, 41-44. [18] Greeley, R., et al. (2005) *J Geophys Res: Planets* 110. [19] Loizeau, D., et al. (2007) *J Geophys Res* 112, E08S08. [20] Ramirez, R.M., et al. (2014) *Nature Geosci* 7, 59-63. [21] Bandfield, J.L., et al. (2003) *Science* 301, 1084. [22] Boynton, W.V., et al. (2009) *Science* 325, 61. [23] Farrand, W.H., et al., (2016) *Amer Mineral* 101, 2005-2019. [24] Hecht, M.H., et al. (2009) *Science* 325, 64. [25] Langevin, Y., et al. (2005) *Science* 307, 1584. [26] Ehlmann, B.L., et al. (2008) *Science* 322, 1828. [27] Michalski, J.R. and P.B. Niles (2010) *Nature Geosci* 3, 751-755. [28] Morris, R.V., et al. (2010) *Science* 329, 421. [29] Osterloo, M.M., et al. (2008) *Science* 319, 1651. [30] Gendrin, A., et al. (2005) *Science* 307, 1587. [31] Nachon, M., et al. (2014) *J Geophys Res: Planets* 119, 1991-2016. [32] McLennan, S.M., et al. (2005) *Earth Planet Sci Lett* 240, 95-121. [33] Squyres, S.W. and A.H. Knoll (2005) *Earth Planet Sci Lett* 240, 1-10. [34] Ojha, L., et al. (2015) *Nature Geosci* 8, 829-832. [35] Milliken, R.E., et al. (2009) *Geophys Res Lett* 36.

**EARLY MARS AS AN EVOLVING "OCEAN WORLD."** V. R. Baker[1], [1]Department of Hydrology and Atmospheric Sciences, University of Arizona, Tucson, AZ, 85716-0011.

**Introduction:** For 35 years, beginning with the Mariner and Viking Missions, an immense wealth of geological evidence has strongly indicated that early Mars evolved as a "Water Planet" [1, p. 175]. Despite continued resistance over the intervening years [2], this long-standing inference has repeatedly been found to be consistent with the accelerating pace of new discoveries.

**The "Mars Ocean" Hypothesis:** The past presence of an immense water body on the northern plains of Mars was initially hypothesized on the basis of mapped sedimentary features [3,4], but its extent was more controversially delineated by what were interpreted to be shoreline landforms [5,6,7].

Naming it "Oceanus Borealis" Baker et al. [8] recognized the importance of a northern plains water body for driving the kind of dynamic hydrological cycle that would be necessary to explain widespread evidence for both fluvial and glacial features on the planet. Though, in retrospect, the surface expressions of Mars' "ocean" of water would have better been termed 'lakes' and 'seas,' the key point is that an immense planetary hydrosphere manifested itself for prolonged periods on the surface.

Multiple objections were marshaled against the "ocean" hypothesis, including the failure to confirm the shoreline features [9], the lack or correspondence of the hypothesized shoreline elevations with an equipotential surface [10], and claims that the required total planetary water endowment was too great relative to geochemical constraints and atmospheric escape considerations [11]. In contrast, other studies explained the shoreline deformation as a result of true polar wander [12]; documented the ice-rich character of sediments underlying northern plains [13]; showed that both valley networks and deltas [14] formed along the "ocean" boundaries; documented the subaqueous origin of the Olympus Mons aureole [15]; and presented alternative interpretations for planetary water volumes [16] and atmospheric escape.

Most recently it has been discovered that tsunami deposits have extensively modified the margins of one or more of the surface manifestations of the northern plains sea, thereby obscuring any shoreline landforms [17,18]. Whether generated by impacts or by immense mass movements from marine-based volcanic constructs, this discovery opens up a whole new aspect of Mars "ocean" research.

Although the Mars "ocean" may never have been an earthlike, land-encompassing global body of marine water, the immensity of the indicated hydrosphere and its episodic surficial expression as seas, lakes, rivers, and megafloods had huge consequences for the early evolution of the planetary surface.

**Hypothesized Timeline for Early Mars Hydro-Evolution:** Figure 1 is a timeline that summarizes data and inferences relevant to this early evolution of Mars as an "ocean planet." The stratigraphic units at the top of the diagram are shown as both the Mars geological time scale and the geochemical phases defined by Bibring et al. [19]. The latter are associated with phases of mineral evolution involving phyllosilicates and evaporite salts [20].

At the bottom of the diagram the timescale is also expressed relative to the exogenetic processes of impact cratering and the endogenetic processes associated with or emanating from the planetary interior. A key to the early impacting history is the nature of the heavy bombardment (HB) period prior to about 3.9 Ga, which culminated with the formation of the major impact basins Hellas, Isidis, and Argyre. A very early "Borealis Basin" event could have been key to developing the planetary dichotomy. Alternatively, an early phast of proto-plate tectonics may have had a role. Ultimately an event of critical planetary importance was the Noachian emplacement of an immense amount of volcanic rock at Tharsis. Subsequent volcanism seems to have been both episodic and of decreasing magnitude through a series of successive episodes.

The very earliest fluvial history, that occurred during the heavy bombardment phase (Pre- to Middle Noachian), is somewhat obscure. Cawley and Irwin [21] found that the ancient, southern Martian heavily cratered plains display inter-crater surfaces that are divided into escarpments, pediments, and plains. The pediments are relatively stable surfaces of moderate relief, and the plains are areas that have been filled with sediments. On Earth this kind of relief develops on exceptionally long time scales (millions of years) in relative dry climates, but with rainfall-generated fluvial action subject to stable base-level controls. Combined with the evidence for degradation of the crater morphologies [22] this suggests the long-term action of a global hydrological cycle that would require a large, planetary-scale area of evaporating surface water, such as the Borealis Sea.

The Late Noachian (LN), extending into the Early Hesperian (EH), involved the most prominent episode of valley network development [23], clearly as a result of rainfall [24,25]. This fluvial episode

seems to have persisted, probably episodically, with some valleys, such as Al-Qahira (A) being older than others, such as Warrego Vallis (W) and Parana Vallis (P), extending from about 3.8 to 3.4 Ga [26]. This most intensefluvial phase transitioned into a subsequent period of alluvial fan and delta formation, associated with lakes filling the floors of craters. Later phases of fluvial activity persisted into the Amazonian [27].

**References:** [1] Baker, V. R. (1982) The Channels of Mars (Univ. Texas Press, Austin). [2] Baker, V. R. (2015) *Geomorphology, 240*, 8-17. [3] Jöns, H. P. (1986) *LPS LVI,* 414-415. [4] Lucchitta, B. K. et al. [1986] *J. Geophys Res., 91, suppl.,* E166–E174. [5] Parker, T. J., et al. (1989) *Icarus, 82,* 111-145. [6] Parker, T. J., et al. (1993) J. Geophys. Res., 98, 11,061-11,078. [7] Clifford, S., and Parker, T. J. (2001) *Icarus, 154,* 40-79. [8] Baker, V.R., et al. (1991) *Nature, 352,* 589-594. [9] Malin, M. C., and Edgett, K. S. (1999) *Geophys. Res. Lett., 26,* 3049-3052. [10] Carr, M. H., and Head, J. W. (2003) *J. Goephys. Res., 108,* 5042. [11] Carr, M. H. (1996) Water on Mars (Oxford Univ. Press, Oxford). [12] Perron, T., et al. (2007) *Nature, 447,* 840-843. [13] Mouginot et al. (2012) *Geophys. Res. Lett., 39,* L02202. [14] DeAchille, G., and Hynek, B. M. (2010) Nat. Geosci., 3, 459-463. [15] De Blasio, F.V. (2011) [16] Luo, W. et al. (2017) *Nature Commun., 8,* 16766. [17] Rodriguez, J. A. P., et al. (2016) *Sci. Reports, 6,* 25106. [18] Costard, F., et al. (2017) *J. Geophys. Res. Planets, 122*, 633-649. [19] Bibring, J.-P. (2006) *Science, 312,* 400-404. [20] Ehlmann, B. L., and Edwards, C. S. (2014) *Ann. Rev. Earth Planet. Sci., 42,* 291-315. [21] Cawley, J. C., and Irwin, R. P. III (2017) *LPS XLVII*, abstract # 2271. [22] Mangold, N. et al. (2012) J. *Geophys. Res. 117,* E04003. [23] Howard, A. D., et al. (2005) *J. Geophys. Res. 110,* E12S14. [24] Hoke, M.R.T., et al. (2011) *Earth Planet. Sci. Lett., 312,* 1-12. [25] Matsubara, Y., et al. (2013) J. Geophys. Res. 118, 1365–1387. [26] Fassett, C. I. and Head, J. W. (2008*) Icarus, 195,* 61-89. [27] Wilson, S. A., et al. (2016) *Geophys. Res. Planets, 121*, 1667-169.

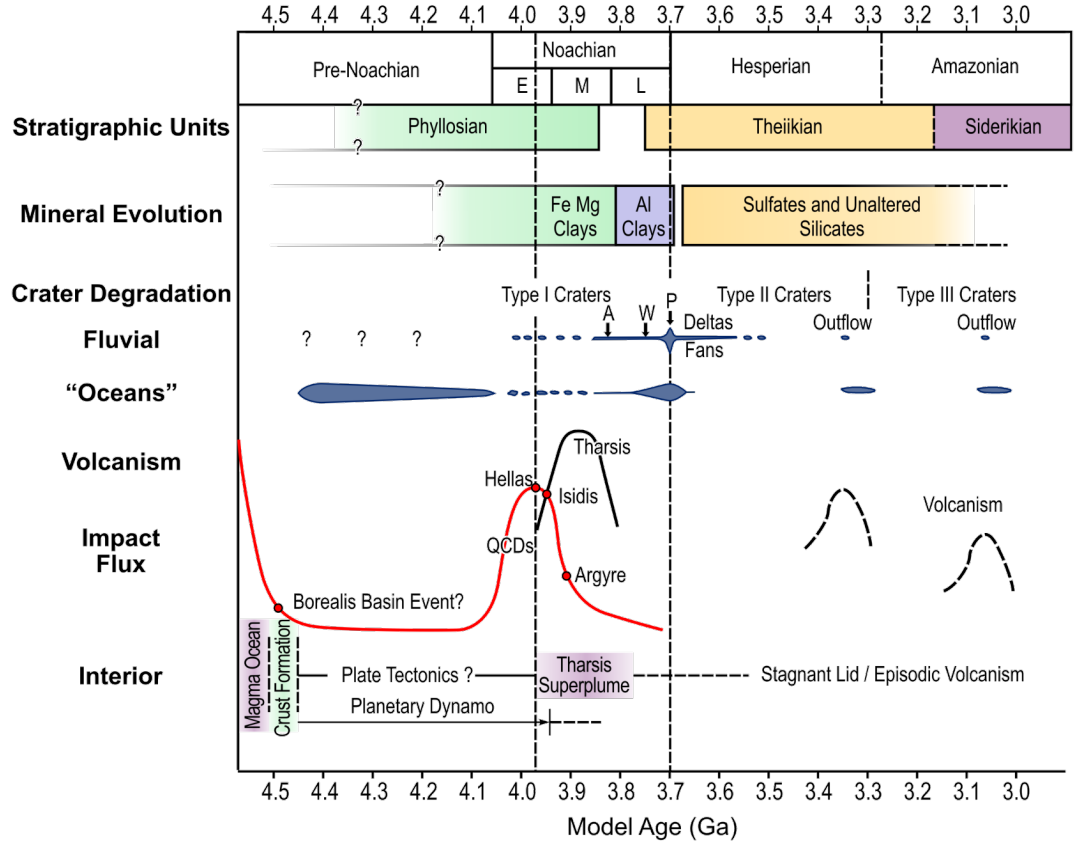


Figure 1. Timeline for early Mars hydro-evolution, showing major episodes of planetary-scale processes, related to phases of crater degradation [22] and other phenomena described above.

**THE NOACHIAN IMPACT CRATERING RECORD REVISITED.** N. G. Barlow, Dept. Physics and Astronomy, Northern Arizona University, Flagstaff AZ 86011-6010; Nadine.Barlow@nau.edu.

**Introduction:** Mars is the only body in the solar system which retains surface units formed throughout its 4.5 Ga history, as revealed by varying crater densities across its surface [1]. Initial crater databases were developed based solely on image data from the Mariner 9 [2] and Viking [1] orbiters. Improved image resolution along with topography data from recent missions have resulted in the creation of new, more complete crater databases from which we can investigate many questions about the geologic history of Mars [3, 4].

The revised crater datasets, combined with the detection of possible buried basins in MOLA topography [5], provide new insights into the intensity of cratering during the Noachian and pre-Noachian. This in turn provides new appreciation for the role of impacts in the early geologic and thermal history of the planet.

**Comparison of Inner Solar System Cratering Records:** Figure 1 shows the original comparison of crater size-frequency distribution (SFD) curves based on crater analysis by Strom and colleagues [6], using Lunar Orbiter, Viking, and Mariner 10 data analysis. The results show that the heavily cratered regions of the Moon, Mercury, and Mars all display a multi-sloped distribution function interpreted as reflecting the SFD of the late heavy bombardment population (LHB) of impactors. Strom et al. [7] have shown that this population is distinct from the current population of inner solar system crossing asteroids and comets, and likely reflects disruption of the main asteroid belt during the migration of the outer solar system planets.

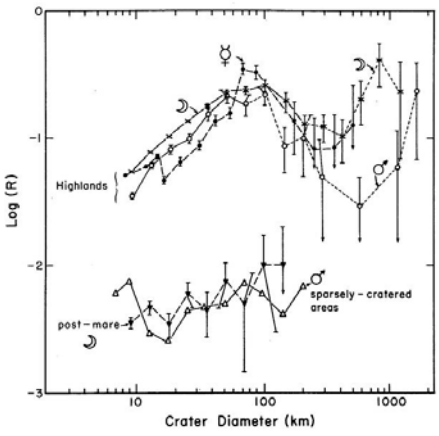


Figure 1: R-Plot Crater SFD curves for the Moon (☽), Mercury (☿ ), and Mars (♂ ). (From [6]).

The Martian highlands SFD curve is similar in shape and density to those for the Moon and Mercury. The downturn in crater density for craters smaller than about 70 km on all three bodies is primarily a reflection of the SFD of the LHB impacting population, with some contribution from erosion. Note that the Martian curve lies between those for the Moon and Mercury for craters <70 km, in spite of Mars having had a more active erosional environment during the Noachian. This is consistent with the interpretation that most of the downturn is due to a different SFD of the LHB impacting population rather than being entirely due to erosion.

New SFD curves for the inner solar system are being produced based on new crater databases for Mars (from THEMIS and CTX), Mercury (from MESSENGER), and the Moon (from Lunar Reconnaissance Orbiter) [8] and will be presented at the meeting. The lower density of large basins on Mars shown in Figure 1 is now remedied by inclusion of the buried basins revealed by MOLA. As a result, the Martian SFD curve for the Noachian period is consistent with those for the highlands of the Moon and Mercury.

**Implications for the Noachian Cratering Record:** Highly degraded craters have become easier to identify because of improved resolution and topography data. As a result, the data provide a better estimate of the cratering rate during the Noachian period. Comparison of the Viking-based *Catalog of Large Martian Impact Craters* ("Catalog 1.0") with our revised version based on THEMIS daytime IR and VIS images reveals an ~10% increase in the number of craters identified [4, 9]. Some of the topics my students, colleagues, and I are investigating with the new dataset include:

- Analysis of the amount of hydrothermal activitiy which may have occurred during the Noachian period. Complex impact craters (i.e., those larger than ~7 km diameter on Mars) can maintain hydrothermal systems for 1000's of years or more, depending on their size. The larger number of complex craters and basins now being recognized as forming during the Noachian increases the potential number and duration of hydrothermal sites during this early period of Mars. Hydrothermal systems on Earth are known to be prime locations for biologic activity and thus understanding the Noachian cratering record is directly relevant to

the question of where to search for biosignatures on early Mars.

- The early Mars paradox, where the geologic evidence indicating large amounts of liquid water on the planet's surface is in contrast to the lower luminosity of the early Sun, is a subject of considerable debate at the present time. One scenario argues that Mars was essentially a snowball world where occasional melting of a decameter's thick ice cover created the observed fluvial features [e.g., 10]. Impacts into such an ice-covered surface would result in observable differences within the Noachian cratering record. For example, excavation through an ice cover into the underlying surface and the subsequent removal of the ice cover would result in a shift in observed crater diameter to smaller values. We should therefore observe a shift to the left in the Martian SFD curve compared to those of the Moon and Mars. However, no such shift is observed. Comparing the predictions of the snowball Mars scenario, as well as the warm, wet early Mars model, with the observed Noachian-era cratering record can help test these alternative hypotheses for the early Mars climate.
- Segura et al. [11-13] proposed that one solution to the early Mars paradox was the release of reducing gases into the Martian atmosphere during impact events to create an enhanced greenhouse. New insights into the Noachian-era cratering record are allowing us to revisit this idea to determine whether it is a viable mechanism for the production of the observed fluvial landforms [14].
- SFD analysis of craters on Noachian-aged terrains without well-preserved ejecta deposits suggest they likely formed during the Noachian period [15]. Impact craters often serve as catchment basins for materials deposited by other geologic processes which no longer operate, such as fluvial and glacial processes. Conducting SFD analysis of craters containing fluvial and/or glacial deposits with younger craters without these deposits provides constraints on the timing of the climate episodes producing these deposits. Our analysis of craters in the Arabia Terra region reveals long-term water enhancement from both subsurface and surficial volatiles throughout this area, ranging from the Noachian up through the Amazonian [16, 17].

**Conclusions:** Improved image, topographic, and compositional datasets for Mars provide new insights into the role if impact cratering early in the planet's history. Analyses of these craters provide important constaraints on the climatic conditions existing during the Noachian and highlight locations where the search for biosignatures should be concentrated.

**Acknowledgements**: This work has been supported in part by the following NASA Mars Data Analysis Program awards to NGB: NAG5-12510, NAG50-12510, and NNX10AN82G

**References:** [1] Barlow N. G. (1988) *Icarus 75*, 285-305. [2] Mutch T. A. et al. (1976) T*he Geology of Mars*, Princeton Univ. Press, 400 pp. [3] Robbins S. J. and Hynek B. M. (2012) *JGR 117*, E05004. [4] Barlow N. G. (2017) *LPSC 48*, Abstract #1562. [5] Frey H. V. (2008) *GRL 35*, L13203. [6] Woronow A. et al. (1982) in *Satellites of Jupiter*, Univ. AZ Press, 237-276. [7] Strom R. G. et al. (2005) *Science 309*, 1847-1850. [8] Barlow, N. G. (2017) *3rd Planetary Data Workshop*, Abstract #7027. [9] Barlow N. G. (2015) *GSA Special Paper 518*, 31-63. [10] Weiss D. K. and Head J. W. (2016) *Icarus 280*, 205-233. [11] Segura T. L. et al. (2002) *Science 298*, 1977-1980. [12] Segura T. L. et al. (2008) *JGR 113*, E11007. [13] Segura T.L. et al. (2012) *Icarus 220*, 144-148. [14] Haberle R. M. et al. (2017) *4th Conf. on Early Mars*, this meeting. [15] Barlow N. G. (1990) JGR 95, 14191-14201. [16] Dohm J. M. et al. (2007) *Icarus 190*, 74-92. [17] Barlow N. G. et al. (2014) *LPSC 45*, Abstract #1221.

**INTERPRETATION OF SMECTITE VIS-NIR SPECTRA FROM SYNTHETIC SMECTITES.** F. Baron[1], S. Petit[2], A. Gaudin[1] and N. Mangold[1], [1]Laboratoire de Planétologie et Géodynamique, CNRS – Université de Nantes, 2 rue de la Houssinière, 44322 Nantes, France (fabien.baron@univ-nantes.fr), [2]Institut de Chimie des Milieux et des Matériaux de Poitiers, 4 rue Michel Brunet, 86073 Poitiers, France.

**Introduction:** Phyllosilicates, in particular Fe/Mg smectites have been evidenced in Noachian-aged terrains by orbital imagers and spectrometers, and exploration rovers, e.g., [1], [2], [3]. These hydrated minerals in their geological context serve as tracer of fluid/rock interactions and provided a unique view of the early environment on Mars. Smectites are currently formed during fluid/rock interactions in various conditions from weathering to deep subsurface hydrothermal alteration at the (sub-)surface of the Earth [4], [5] and Mars [2]. The abundant detection of smectites using orbital Visible-Near Infrared (VIS-NIR) spectroscopy placed these minerals at the center of attention.

Smectites are, however, very difficult to characterize unambiguously in terms of crystal-chemistry due to their small particle size and their wide range of chemical compositions. The determination of the precise crystal-chemistry of smectites from orbital NIR Martian data is still a challenge. Yet, the crystal-chemistry of smectite offers a unique marker of the conditions of formation of these minerals. Natural Earth smectites are currently, if not still, intimately associated with others minerals. This complex mineralogy and chemistry make the interpretation of natural smectite VIS-NIR spectra harder. To better interpret the VIS-NIR spectra of orbital and future rover Martian data, smectites syntheses are required to provide robust reference spectra.

The aim of this study was to contribute to the interpretation of VIS-NIR spectral features of smectites, based on synthetic smectites having a simple and a controlled crystal-chemistry.

**Experimental:** Pure $Mg^{2+}$- and $Fe^{3+}$-smectites were synthesized according to the procedure described in Baron et al. [6]. The crystal-chemistry and purity of synthetic smectites were checked using oriented and powder X-ray diffraction, mid-infrared spectroscopy, and for some of smectites using transmission electron microscopy equipped with an energy-dispersive X-ray spectrometer.

**Results and Discussion:** In NIR spectra of phyllosilicates (1000 – 2500 nm), an absorption band are characteristic of (i) a combination of vibrations of different or the same chemical bond, or (ii) a harmonic of a vibration of a chemical bond. Note that, a band is not still a diagnostic feature of a phyllosilicate, and several phyllosilicates could have the same absorption band if they are composed of the same chemical bonds. In particular, the 1350 – 1500 nm range is characteristic of overtones of stretching (ν) OH vibrations whereas the 2100 – 2500 nm range is characteristic of combinations between ν OH vibrations and (i) bending (δ) OH vibrations or (ii) lattice vibrations, e.g., [7]. Combinations and overtones of OH vibrations region provides many information on the crystal-chemistry of phyllosilicates, in particular on the cation chemistry of the octahedral sheet and the distribution of these cations. The VIS spectra of phyllosilicates (350 – 1000 nm) are essentially characteristic of the electronic transitions of some elements that composed these minerals. For example, the electronic transition of iron atoms ($Fe^{2+}$ and $Fe^{3+}$) induce several absorption bands depending to its location in the mineral structure [8]. Although not frequently used for diagnostic compared to the NIR spectra, the VIS spectra are of interest for the in-situ data from Curiosity rover, using multi-spectral Mastcam images and ChemCam passive spectra, both in these ranges of wavelengths.

The VIS spectra of synthetic $Fe^{3+}$-smectites having different value of tetrahedral $Fe^{3+}$ charges evidenced three broad complex feature due to electronic transition of $Fe^{3+}$ atoms around 450 – 550, 662, and 982 nm (Fig. 1). These last 662 and 982 nm absorption features are essentially attributed to octahedral $Fe^{3+}$ electronic transitions [8]. The complex feature around 450 – 550 nm is attributed to both octahedral and tetrahedral $Fe^{3+}$ electronic transitions. Indeed, the increase in the tetrahedral $Fe^{3+}$ charges is well correlated to the increase in in intensity of an absorption band at 462 nm. This band can be attributed to tetrahedral $Fe^{3+}$ electronic transitions. The tetrahedral $Fe^{3+}$ can, however, be only evidenced for nontronite samples having a high tetrahedral $Fe^{3+}$ content (> 0.6 per half unit-cell). The NIR spectra of synthetic $Fe^{3+}$-nontronite exhibited an absorption band at 1432 nm and a shoulder around 1470 nm. The 1432 nm band corresponds to the first overtone of the ν $Fe^{3+}{}_2OH$ vibration while the shoulder is attributed to first overtone of the ν OH vibrations of adsorbed and free water molecules e.g., [6]. The combination vibrations region of nontronite spectra evidenced a complex absorption feature between 1850 and 2100 nm, and two absorption bands at 2288 and 2399 nm e.g., [6], [9]. The complex feature is related to combinations of OH vibrations involving in parts OH vibrations of adsorbed and free water molecules. The 2288 nm band is attributed to the combination of the ν $Fe^{3+}{}_2OH$ vibration and the δ $Fe^{3+}{}_2OH$ vibration, while the 2399 nm corre-

sponds to the combination between the ν $Fe^{3+}{}_2OH$ vibration and the $^{[6]}Fe^{3+}$-$O_{apica}$-$Si^{4+}$ coupled lattice δ vibration [6]. Note that whatever the value of the tetrahedral charge, all the NIR absorption bands remain at the same position.

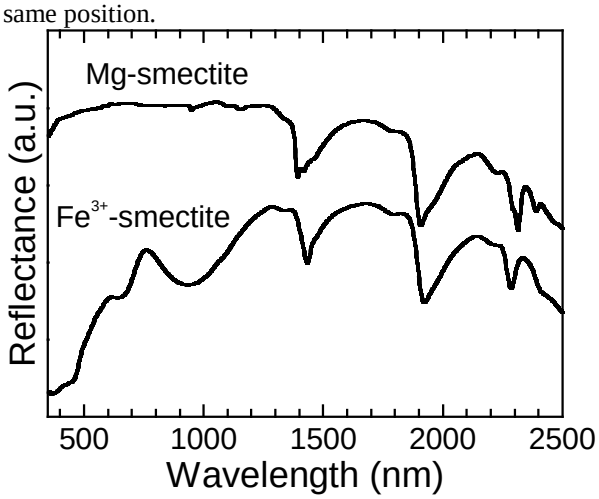


**Figure 1:** VIS-NIR spectra of synthetic smectites

The VIS spectra of synthetic $Mg^{2+}$-smectite exhibited three complex features at 948 - 961, 1095, and 1153 nm (Fig. 1). The 948 – 961 nm feature corresponds to the second overtones of the ν OH vibrations. The 1095 nm feature can be attribute to the combination between the first overtone of the OH vibrations (1350 – 1550 nm) and the skeleton (overtone) vibrations (around 5149 nm). The last feature at 1153 nm can correspond to the combination between the first overtone of the OH vibrations (1350 – 1550 nm) and the δ OH vibrations (6116 nm) linked to water molecules. The NIR spectra of synthetic $Mg^{2+}$-smectite showed an absorption band at 1392 nm with a shoulder at 1388 nm. These two bands correspond to the first overtone of the ν $Mg^{2+}{}_3OH$ vibrations of the hydrated state of $Mg^{2+}$-smectite layers (1388 nm) and the dehydrated state (1392 nm) [10]. The complex feature around 1400 – 1600 nm is attributed to first overtone of the ν OH vibrations of adsorbed and free water molecules. As for $Fe^{3+}$-smectite samples, the complex feature at 1850 – 2100 nm is related to combinations of OH vibrations involving in parts OH vibrations of adsorbed and free water molecules. The 2500 – 1600 nm range of the $Mg^{2+}$-smectite spectra is composed of lots of combination bands corresponding to the combination between ν $Mg^{2+}{}_3OH$ vibrations and the lattice vibrations or the δ $Mg^{2+}{}_3OH$ vibrations. In particular, the spectrum of pure $Mg^{2+}$-smectite exhibits three intense bands at 2290, 2312, and 2390 nm [11], which could correspond to the combination between the ν $Mg^{2+}{}_3OH$ vibrations and (i) the Si-O vibration, (ii) the δ $Mg^{2+}{}_3OH$ vibrations, and (iii) the lattice vibration involving OH group and Mg cations, respectively.

The VIS part of smectite spectra appear interesting regarding to distinguish between $Fe^{3+}$-smectite and $Mg^{2+}$-smectite, but the potential contributions of several minerals in the VIS part of a sample can reduce drastically the robustness of the diagnostic feature especially concerning electronic transitions. Note that in NIR smectites spectra, the 2288 nm bands commonly used to identify $Fe^{3+}$-smectites actually overlap the 2290 nm feature of pure $Mg^{2+}$-smectite. The identification of $Fe^{3+}$-smectites if mixed with $Mg^{2+}$-smectite should be performed on another part of the infrared spectra, in particular in the first overtone of the ν OH vibrations or the ν OH vibrations.

Further syntheses must be performed to enhance the spectral interpretation of VIS-NIR spectra and to potentially combine both the condition of formation and the crystal-chemistry of smectites. The crystal-chemistry evidencing using vibrational spectroscopy is a unique characteristic of smectites allowing to constrain the fluid/rock interactions that happened during early Mars. The spectral quality of the current orbital data do not always enable a diagnostic of spectral bands at this level of details. However, future in-situ IR data, such as from the SUperCam instrument on the 2020 rover would enable spectra with better signal-to-noise ratio than orbital data and would enhance the characterization of the crystal-chemistry of phyllosilicates. The development of the spectral interpretation of phyllosilicates on controlled crystal-chemistry samples appears as a key sector to better understand the orbital and future rover Martian data.

**References:** [1] Mangold N. et al. (2016) *Astron. Astrophys. Rev.*, 24 :15. [2] Carter J. et al. (2013) *J. Geophys. Res. Planets*, 118, 831–858. [3] Vaniman D. T. et al. (2014) *Science*, 343, 1243480. [4] Meunier A. (2005) *Clays*, Springer. [5] Michalski J. R. et al. (2015) *Earth Plan. Sci. Lett.*, 427, 215-225. [6] Baron F. et al. (2016) *Clay Clays Min.*, 64, 230-244. [7] Baron F. and Petit S. (2016) *Am. Min.*, 101, 423-430. [8] Sherman D. M. and Vergo N. (1988) *Am. Min.*, 73, 1346-1354. [9] Poulet F. et al. (2005) *Nature*, 438, 623-627. [10] Bukas V. J. et al. (2013) *Vib. Spectrosc.*, 68, 51-60. [11] Madejová J. et al. (2011) *Advances in the Characterization of Industrial Minerals*, EMU Notes in Mineralogy.

**GEOCHEMICAL ENDMEMBERS PRESERVED IN THE FLUVIOLACUSTRINE SEDIMENTS OF GALE CRATER.** C. C. Bedford[1], J. C. Bridges[2], S. P. Schwenzer[3], R. C. Wiens[4], E. B. Rampe[5], J. Frydenvang[6], P. J. Gasda[4]. [1]School of Physical Sciences, The Open University, Walton Hall, Milton Keynes, UK (candice.bedford@open.ac.uk), [2]Leicester Institute for Space and Earth Observation, University of Leicester, UK. [3]School of Environment, Earth and Ecosystem Sciences, The Open University, Milton Keynes, UK. [4]Los Alamos National Laboratory, Los Alamos, New Mexico, USA. [5]NASA Johnson Space Centre, Houston, TX, US. [6]Natural History Museum of Denmark, University of Copenhagen, Copenhagen, Denmark.

**Introduction:** Gale crater possesses a diverse stratigraphic record consisting of conglomerate, fine to coarse sandstone and mudstone units deposited after the crater's formation (~3.8 Ga) in an ancient fluviolacustrine system [1–3]. Since landing in August 2012, the NASA Mars Science Laboratory *Curiosity* rover has analysed the geochemistry and mineralogy of these sedimentary units using the Chemistry and Camera (ChemCam), Alpha Particle X-ray Spectrometer (APXS) and Chemistry and Mineralogy (CheMin XRD) onboard instrument suites. This has uncovered a largely unanticipated geochemical and mineralogical diversity across and within the Bradbury and Mt Sharp stratigraphic groups for sediments [4].

The Bradbury Group (sols 1–750) is dominantly fluvial conglomerate and sandstone with some lacustrine mudstone identified at Yellowknife Bay [1,2]. The Mt Sharp Group (Murray formation analysed from sols 750–1482, the latest sol used this study) consists of well laminated mudstone deposited in a lake environment with some interstratified fine sandstone [2].

Previous studies of CheMin derived mineralogy conducted on two drilled samples of sedimentary outcrop (Windjana, sol 610 [5] in the Bradbury Group and Buckskin, sol 1061 [6] in the Murray formation) have identified primary minerals indicative of evolved potassic [5] and silicic [6] igneous source regions. APXS and ChemCam analyses of identified igneous float and conglomerate clasts with aphanitic, porphyritic and leucocratic textures have also shown a wide range of igneous compositions [7,8] probably resulting from the fractionation of olivine from a subalkline basaltic parent melt [7]. This study uses the data obtained by ChemCam (over 1200 targets) for the stratigraphic record analysed from sols 1–1482 to determine the extent previously identified endmembers have contributed to Gale's sedimentary record as well as identify the source of compositional change between the Bradbury Group and studied Murray formation.

**Methods:** ChemCam acquires major, minor and trace element compositions through ablating a target host rock or soil between 2.2–7 m from the rover mast with its Laser-Induced Breakdown Spectroscopy instrument [9,10]. Between 30–50 spectral analyses are acquired per observation point and averaged to give the observation point compositions used in this study [9].

ChemCam observation point analyses were classified according to sample morphology, stratigraphic position and grain size [11]. This study focuses on points that have analysed *in situ* sedimentary outcrop in order to distinguish geochemical source characteristics. Observation points identified to have hit obvious diagenetic features (such as veins, nodules, raised ridges and haloes), soil targets, float, pebbles, drill tailings and dump piles have been removed from the refined database to acquire the best representation of whole rock compositions.

Due to ChemCam's small sample footprint (350–550 μm), point analyses are not fully representative of whole rock compositions. This is especially true for coarse-grained targets (>1 mm) where points are more representative of targeted mineral phases. In order to minimize this effect, individual point compositions are plotted on a series of scatter and density contour plots for their associated stratigraphic groups and units. This displays the compositional spread of the data population, highlighting average compositional foci and geochemical trends across the stratigraphy. This method should also minimize geochemical variation associated with closed system alteration within the stratigraphy.

Grainsize is shown to possess a strong influence on whole rock geochemistry for sedimentary deposits [12], particularly those associated with deposition in a distal, fluviolacustrine system [13,14]. Hence, endmember compositions are discussed in relation to grainsize dependent subgroups to reduce this effect on provenance analysis. Grainsize subgroups are classed as coarse (>1 mm), sandstone (0.063 mm – 1 mm) and mudstone (<0.063 mm) according to the literature [15].

**Results and Discussion:** On average, the Bradbury Group is more depleted in $SiO_2$, $Al_2O_3$ and $K_2O$ but enriched in CaO compared to the Mt Sharp Group (Murray formation). Bradbury density contours also show a distinct bimodality in MgO, $SiO_2$ and $Al_2O_3$ compositions. This bimodality is associated with grainsize as individual observation point analyses from the coarse units and coarser members of the sandstone group plot closer towards Gale crater felsic mineral compositions. On Earth, sediments coarser than 1 mm

are shown to maintain source rock characteristics [12] and as the Bradbury group high-aluminium subfocus also matches that of the Gale trachybasalt igneous group suggesting the same is true for Mars. The higher proportion of felsic minerals in sediments derived from this endmember may have increased its survivability in coarse grained units according to fluvial mineral sorting regimes of volcaniclastic material [13, 14].

Murray mudstone is unimodal and possesses a geochemistry indicative of a greater proportion of felsic minerals (rich in $Al_2O_3$, alkalis and depleted in MgO) compared to the mafic geochemistry of the Bradbury low-Al subgroup, defined by the majority of its fine sandstone and mudstone units. Elevated silica content is also a defining feature of the Murray formation compared to the Bradbury Group, especially in one area – Marias Pass (sols 995 – 1066), though here the extreme silica content (>75 wt%) is associated with the high abundance of tridymite and cristobalite detected in the Buckskin drill hole [6] which are not detected anywhere else in Gale's stratigraphy. Hence, with other Murray drilled samples showing a basaltic mineralogy, silica-rich diagenetic features [16] removed and minimal open system alteration inferred from secondary mineralogy [17], the source of the Murray studied here is hypothesized to be dominated by a silica-saturated tholeiitic provenance.

**Conclusions:** In total, five endmembers associated with unique igneous source regions have been identified (Fig. 1).

*Endmember 1:* A regional subalkaline basalt endmember which is similar in composition to the tholeiitic Adirondack Class basalts [18] of Gusev Crater and is the dominant composition observed in Bradbury Group sandstones and mudstones,

*Endmember 2:* A trachybasalt, mostly identified within Bradbury Group conglomerate and coarse-grained sandstone units, this endmember was initially observed in Gale igneous float and clasts [7] and is seen to dominate conglomerate geochemistry encountered before The Kimberley formation (sol 574).

*Endmember 3:* A potassium-rich volcanic source, identified by [5] in the Windjana drill hole analysed at The Kimberley, and a similar source in Shaler [19]. Associated with strong potassium-enrichment and a high abundance of sanidine, this endmember is present in fluvial sandstone identified near the top of the analysed Bradbury succession (from sol 574 to the base of Mt Sharp), and is also recognised throughout the lower Murray formation,

*Endmember 4:* A highly evolved silica-rich igneous source, identified by [6] in Murray formation Marias Pass mudstones sediments from this source possess extreme silica-enrichment associated with elevated amounts of tridymite and cristobalite.

*Endmember 5:* A fractionated Si-rich tholeiite seen to influence the majority of the Murray formation's geochemistry. This endmember is proposed as the cause of the marked geochemical difference between Bradbury and Mt Sharp group mudstones and the source of the low Ca and intermediate Fe/Mg pigeonite compositions identified by CheMin [20].

**References:** [1] Grotzinger J. P. et al. (2014) *Science, 343*, 1242777. [2] Grotzinger J. P. et al. (2015) *Science, 350*, aac7575. [3] Thomson B. J. et al. (2011) *Icarus, 2*, 413-432. [4] McSween H. Y. et al. (2009) *Science*, 5928, 736-739. [5] Treiman A. H. et al. (2016) *JGR: Planets*, *121*, 75 – 106. [6] Morris R. V. et al. (2016) *PNAS*, doi: 10.1073/pnas.1607098113. [7] Edwards P. H. et al. (in rev.) *MAPS*. [8] Cousin A. et al. (2017) *Icarus*, 288, 265-283. [9] Wiens R. C. et al. (2012) *Space Science Reviews*, *170*, 167-227. [10] Maurice S. et al. (2012) *Space Science Reviews*, *170*, 95-166. [11] Bedford C. C. et al. (subm.) *GCA*. [12] Bloemsma M. R. et al. (2012) *Sedimentary Geology*, *280*, 135-148. [13] Fedo C. M. et al. (2015) *EPSL, 423*, 67-77. [14] Siebach K. L. (2017) *JGR: Planets*, *122*, 295-328. [15] Mangold N. (2017) *Icarus*, *284*, 1-17. [16] Frydenvang J. (2017) *GRL*, *44*, 4716-4724. [17] Rampe E. B. et al. (2017) *EPSL, 471*, 172-185. [18] McSween H. S. et al. (2006) *JGR: Planets, 111*, 2156-2202. [19] Anderson R. et al. (2015) *Icarus, 249*, 2-21. [20] Morrison S. M. (in rev.) *American Min.*

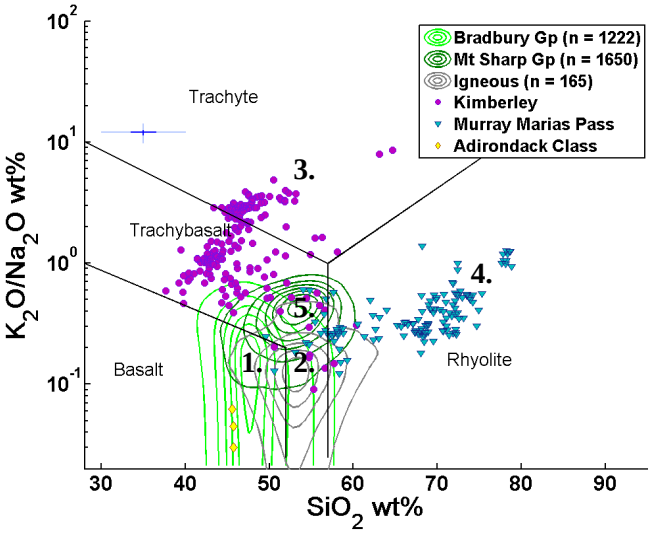


Figure 1. A $K_2O/Na_2O$ vs $SiO_2$ plot of stratigraphic units most influenced by unique end members. Compositionally unique endmembers are 1. A subalkaline basalt, 2. A trachybasalt, 3. A potassium-rich volcanic source, 4. A highly evolved, Si-rich volcanic source and 5. A Si-rich tholeiite. Adirondack MER APXS [NASA PDS, 18]

**DIVERSE EARLY AQUEOUS ENVIRONMENTS AND CLIMATE ON MARS REVEALED BY THE PHYLLOSILICATE RECORD.** J. L. Bishop[1,2], A. G. Fairén[3,4], J. R. Michalski[5], L. Gago-Duport[6], L. L. Baker[7], M. A. Velbel[8,9], C. Gross[10], and E. B. Rampe[11], [1]SETI Institute (Mountain View, CA; jbishop@seti.org), [2]NASA-Ames (Moffett Field, CA), [3]Centro de Astrobiologia (Madrid, Spain), [4]Cornell University (Ithaca, NY), [5]University of Hong Kong (Hong Kong, China), [6]University of Vigo (Vigo, Spain), [7]University of Idaho (Moscow, ID), [8]Michigan State University (East Lansing, MI), [9]Smithsonian Institution (Washington, DC), [10]Freie Universität Berlin (Germany), [11]NASA-JSC (Houston, TX).

**Hypothesis:** We propose that short-term warm and wet environments, occurring sporadically in a generally cold and dry early Mars, enabled formation of smectite-rich outcrops on the surface of Mars without requiring long-term warm and wet conditions. Other Mg-rich phyllosilicates occurring with lateral variations likely formed in subsurface hydrothermal environments. Our model is consistent with Martian surface features and mineralogy and current paleoclimate scenarios.

**Introduction:** One of the most perplexing questions on Mars is the nature of its early climate. Martian surface features such as alluvial fans, valley networks, and dendritic channels point towards running water and fluvial erosion on early Mars [e.g. 1, 2, 3, 4]. The martian surface also hosts abundant phyllosilicates and aqueous minerals requiring liquid water for formation nearly everywhere the ancient rocks are observed on that planet [e.g. 5, 6, 7]. However, climate modeling indicates that long-term warm and wet conditions are not sustainable [e.g. 8, 9, 10]. Periodic or seasonal melting of snow to produce icy conditions where liquid water could carve out the observed martian surface features has been proposed [11, 12]; however, these short-term icy conditions would be insufficient for formation of the observed phyllosilicates [13]. Some of these phyllosilicates could be formed in subsurface environments [7], but many phyllosilicate-rich outcrops exhibit layered morphologies and broad stratigraphies or horizonation [14] inconsistent with subsurface formation.


*Figure 1. View of light-toned phyllosilicate-rich material at Mawrth Vallis (HRSC stereo view towards S, 5x vertical).*

**Phyllosilicate Formation on Mars:** The goal of this project is to provide constraints on the early martian climate and the nature of aqueous surface environments through investigation of phyllosilicates. We have evaluated the nature and stratigraphy or horizonation of phyllosilicate-bearing surface units on Mars, in the context of phyllosilicate-forming environments on Earth, phyllosilicate reactions in the lab and modeling experiments involving phyllosilicates, other minerals and short-range ordered (SRO) materials.

Different phyllosilicates form in different alteration environments. We compare Martian outcrops dominated by smectite clays with those dominated by mixed layer smectite/chlorite and other clay assemblages. $Mg^{2+}$- or $Fe^{2+}$-rich smectites also require different formation conditions than $Al^{3+}$- or $Fe^{3+}$-rich smectites.

Mg-rich trioctahedral smectite mixtures are more consistent with formation under reducing conditions subsurface, in oceanic hydrothermal environments, or within alkaline lakes. Terrestrial smectite-bearing hydrothermally altered sea-floor sediments were used to classify interstratified smectite/ chlorite/ talc assemblages on Mars [15]. Zeolite mixed with nontronite is also an indicator of deep, subsurface alteration of Columbia River Basalt (CRB) [16]. Subsurface environments have been proposed for clay formation in regions such as Nili Fossae where several Mg-rich phyllosilicate assemblages (e.g. Fe/Mg-smectite, chlorite, prehnite, serpentine, talc) exist as lateral clusters in neighboring environments [17, 18]. This fits in the "crustal clays category" described by Ehlmann et al. [7]. These Mg-rich mixed clay assemblages can form in subsurface environments up to 400 °C and are not associated with the surface environment on Mars.

In contrast, clay profiles dominated by dioctahedral Al/Fe-smectites on Earth are typically formed in subaqueous or subaerial surface environments [19]. These temperate to warm climates with alternating wet (rainfall >50 cm/y) and dry (little or no rain) seasons support soil formation with high smectite abundances. Layered nontronite-bearing beds occurring over wide expanses on Mars within a common horizonation are consistent with formation in surface environments [20, 21]. For example, a 150-200 m thick Fe/Mg-smectite (nontronite) unit is the dominant aluminosilicate material observed at Mawrth Vallis (Figure 1). Often it is capped by sulfates and a 50 m thick Al-phyllosilicate/opal unit [22], that is covered by poorly crystalline aluminosilicates [23]. We propose models constraining how dioctahedral

smectite-rich outcrops and laterally extensive vertical profiles of Fe/Mg-smectites, sulfates, and Al-rich clay assemblages formed in surface environments.

SRO materials such as opal, nanophase aluminosilicates, ferrihydrite and akaganéite on the surface of Mars have been recognized recently through analysis of data from orbital [24, 25] and surface missions [26, 27]. In the Mawrth Vallis region, this poorly crystalline material is present at 20-30 vol.% for the light-toned regions where clay minerals are detected [23]. An X-ray amorphous component is also present at ~20-50 wt.% nearly everywhere the CheMin X-ray diffractomer has analyzed samples at Gale crater [27]. Nanophase aluminosilicates form preferentially over phyllosilicates in well-drained environments with low water/rock ratio systems [28, 29], and cold climates such as the Antarctic Dry Valleys [30]. Thus, the presence of abundant SRO materials without phyllosilicates could mark the end of the last warm and wet episode on Mars supporting smectite formation.

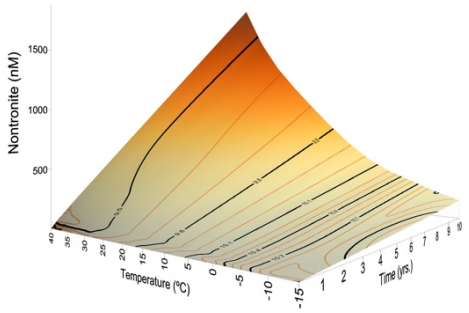


*Figure 2. Formation rates of nontronite on Mars based on crystallization kinetics of basalt dissolution. These vary greatly from near freezing to 20-40 °C.*

**Climate Implications:** *Cold and Wet Scenario: Long-term Presence of Liquid Water.* Clay formation reactions proceed extremely slowly at temperatures just above freezing [13, 31]. Previous models of nontronite formation found almost no production near freezing, but a significant increase in reaction rate at ~20 °C [13]. Thus, for liquid water temperatures ~10-20 °C, the ~200 m thick nontronite-rich beds at Mawrth Vallis would have required sustained periods of a high water/rock ratio environment on Mars to produce the observed smectite outcrops. This could represent standing water on Mars for hundreds of millions of years.

*Warm and Wet Scenario: Short-term Presence of Liquid Water.* Warmer temperatures could have enabled faster production of the observed Martian smectite beds. Low temperature modeling of phyllosilicate formation indicates that nontronite formation occurs much more rapidly near 30-40 °C than at lower temperatures (Figure 2). Nontronite synthesis experiments [32] and field observations [19] support formation of smectites below 100 °C, although warmer conditions are more common. Smectite-bearing CRB paleosols and nontronite-rich saprolites up to several meters thick formed at ambient temperatures on the Earth's surface over ~500,000 years or less [33].

**Conclusions:** *Climate Excursions.* We propose that many of the layered surface deposits of clay-rich materials formed on Mars during geologically brief climate excursions. Short-term warmer and wetter deviations from a generally cold climate could explain the water-derived geologic features and thick smectite beds. This model includes episodes of warmer environments supporting Fe/Mg-smectite formation for 10,000 to 100,000 years interspersed during the late Noachian period on Mars. Even short-lived climate excursions could have produced significant amounts of clay-rich alteration products from glass-rich volcanic or impact-generated basaltic material on Mars.

**Acknowledgments:** The authors are grateful to support from the NAI and MDAP (JLB), ERC-StG "icyMARS" (AGF), a Smithsonian Senior Fellowship (MAV), and the German Space Agency (DLR Bonn) Grant #50QM1702 (CG).

**References:** [1] Carr M. (1996) *Water on Mars*. Cambridge. [2] Craddock R. & Howard A. (2002) *JGR, 107,* 21-1-21-36. [3] Ansan V. et al. (2008) *JGR, 113,* doi:10.1029/2007JE002986. [4] Fassett C. & Head J. (2011) *Icarus, 211,* 1204-1214. [5] Murchie S. et al. (2009) *JGR, 114,* doi:10.1029/2009JE003342. [6] Carter J. et al. (2015) *Icarus, 248,* 373-382. [7] Ehlmann B. et al. (2011) *Nature, 479,* 53-60. [8] Sagan C. & Mullen G. (1972) *Science, 177,* 52-56. [9] Wordsworth R. etal.(2017)*GRL, 44,*665-671. [10] Ramirez R. (2017) *Icarus, 297,* 71-82. [11] Squyres S. & Kasting J. (1994) *Science, 265,* 744-749. [12] Wordsworth R. et al. (2015) *JGR, 120,* 1201-1219. [13] Fairén A. et al. (2011) *Nat.Geo., 4,* 667-670. [14] Bishop J. et al. (2008) *Science, 321,* 830-833. [15] Michalski J. et al. (2015) *EPSL, 427,* 215-225. [16] Benson L. & Teague L. (1982) *J.Sed.Res., 52,* 595-613. [17] Ehlmann B. et al. (2009) *JGR, 114,* doi:10.1029/2009JE003339. [18] Brown A. et al. (2010) *EPSL, 297,* 174-182, doi:10.1016/j.epsl. 2010.06.018. [19] Chamley H. (1989) *Clay Sedimentology*. Springer. [20] Bishop J. et al. (2013) *PSS, 86,* 130-149. [21] Noe Dobrea E. et al. (2010) *JGR, 115,* doi:10.1029/2009 JE003351. [22] Loizeau D. et al. (2010) *Icarus, 205,* 396-418. [23] Bishop J. & Rampe E. (2016) *EPSL, 448,* 42-48. [24] Rampe E. et al. (2012) *Geol., 40,* doi:10.1130/G33215.1. [25] Carter J. et al. (2015) Orbital detection and implications of akaganéite on Mars, *Icarus, 253,* 296-310. [26] Blake D. et al. (2013) Curiosity at Gale Crater, Mars: Characterization and analysis of the Rocknest sand shadow, *Science, 341,* doi:10.1126/science.1239505. [27] Vaniman D. et al. (2014) *Science, 343,* doi: 10.1126/science. 1243480. [28] Parfitt R. (2009) *Clay Miner., 44,* 135-155. [29] Rasmussen C. et al. (2010) *Geoderma, 154,* 473-485. [30] Bishop J. et al. (2014) *Phil. Trans. R. Soc. A, 372,* 20140198. [31] Kloprogge J. et al. (1999) *ClaysClayMiner., 47,* 529-554. [32] Decarreau A. et al. (2008) *ClaysClay Miner., 56,* 322-337. [33] Hobbs K. & Parrish J. (2016) *GSA Bulletin, 128,* 1543-1554.

**MARSSIM LANDFORM EVOLUTION MODEL: HYDROLOGIC CONSTRAINTS ON THE NOACHIAN EARLY DRY PERIOD.** B.D. Boatwright and J.W. Head, Department of Earth, Environmental and Planetary Sciences, Brown University, Providence, RI (benjamin_boatwright@brown.edu; james_head@brown.edu).

**Introduction:** The formation of valley networks, open- and closed-basin lakes, deltas and alluvial fans in the Noachian highlands of Mars has been constrained to a brief but intense episode of fluvial activity, known as the "terminal epoch," around the Noachian-Hesperian boundary [1]. Surveys of the valley networks have shown that they likely formed through the action of liquid water flowing at the surface [2-4]. However, climate modeling studies have failed to raise mean annual average temperatures (MAAT) above 273 K with an $H_2O$+$CO_2$ atmosphere at variable pressures [5-7]. This "cold and dry" model maintains a subfreezing, hyperarid environment during the Noachian with a global cryosphere more typical of present-day Mars [8]. Liquid water would have existed on the surface only during transient warming events caused by volcanism [9] or impact heating [10-11]. This is seemingly in contradiction to the geologic evidence, which suggests that the Noachian was instead "warm and wet," with a robust hydrologic cycle dominated by precipitation and surface runoff [12-14]. Recent work on an "icy highlands" model has attempted to reconcile some of these differences by allowing limited runoff from glaciers while maintaining MAAT below freezing [15-16].

Morphometric studies have shown that valley network profiles closely follow regional slopes and incise into previously reworked intercrater plains material [13-14,17]. This earlier, more extended period of highland degradation, herein referred to as the "early dry period," is significantly less well characterized than the terminal epoch. Discharges were too low to effectively transport sediment, drainage integration was localized, and valley networks, where they existed, generally did not form incised channels [17]. This led to a weathering- and infiltration-dominated regime that gradually filled crater floors and alluvial plains with hundreds of meters of permeable, loosely consolidated sediment [18-20]. The total volume of sediment removed during the early dry period was much greater than the amount eroded by the valley networks, but average erosion rates were comparable [21].

Beyond a qualitative idea of the climatic conditions that prevailed in the early dry period, little is known of the exact rates, amounts, and transport mechanisms that might have created the substrate that existed in the highlands before the valley networks formed. We propose a variety of tests using a landform evolution model [22] that can simulate fluvial and slope processes under accurate Martian conditions. In particular, we attempt to constrain hydrologic parameters to match the transport-limited regime of the early dry period.

**Previous estimates of erosion rates and sediment volumes:** A handful of studies in the 1990s and early 2000s [18-20] attempted to estimate how much material had been reworked by fluvial processes in the Noachian, mostly by comparing populations of degraded craters to modeled production functions. [19] and [20] used craters in and around Arabia Terra for their estimates, while [18] made a more comprehensive survey of all highland craters between 30 degrees north and south latitude. However, [18] also extended their age range to the end of the Hesperian, which given more recent evidence of the abrupt cessation of intense erosion shortly after the Noachian-Hesperian transition [1], is probably not accurate. Instead, each erosion estimate can be normalized to fall within either the Middle-Late Noachian or strictly the Late Noachian, with ages based on newer period boundaries than those used previously [23-24]. In such a scenario, erosion rates are on the order of $10^{-4}$ to $10^{-2}$ mm/yr [18-20].

**Proposed landform evolution modeling:** We use the MARSSIM landform evolution model first described by [22] and further explored in [27-33]. The model is written primarily with simulation of physical processes in mind, and therefore requires a fairly robust understanding of the underlying hydrologic and geologic conditions to produce accurate results. We propose to test several different parameters in order to constrain 1) the conditions under which the model produces transport-limited flow, as observed in the early dry period; 2) the erosion rates and sediment volumes typical of such a regime, and how they compare to previous estimates; and 3) how long the early dry period lasted. The solution is fundamentally dependent on the mechanisms of sediment transport, and to what extent sediment was reworked by fluvial, groundwater, and/or slope processes. The MARSSIM model is capable of simulating each of these in detail, and their characterization will serve as a starting point for future investigation [34].

Previous studies have relied on an inverse method by taking the largest "missing" crater diameter in an expected size distribution as a baseline for the amount of degradation that occurred [18]. Instead, MARSSIM implements a crater geometry model [35-37] that can

be used to quantify degradation with known initial conditions. By measuring elevation changes on crater floors between the input and output DEMs, the exact volume of infilled sediment can be obtained (Figure 1). Importantly, this same method can be applied to any material that remains outside of craters, since it is unlikely that the reworked sediment will be deposited exclusively within basins.

**References:** [1] Fassett C.I., Head J.W. (2008) *Icarus* 195, 61-89. [2] Carr M.H. (1995) *JGR* 100, 7479-7507. [3] Luo W., Stepinski T.F. (2009) *JGR* 114, E11010. [4] Hynek B.M. et al. (2010) *JGR* 115, E09008. [5] Kasting J.F. (1991) *Icarus* 94, 1-13. [6] Wordsworth R. et al. (2013) *Icarus* 222, 1-19. [7] Forget F. et al. (2013) *Icarus* 222, 81-99. [8] Clifford S.M., Parker T.J. (2001) *Icarus* 154, 40-79. [9] Halevy I., Head J.W. (2014) *Nature Geosci.* [10] Segura T.L. et al. (2008) *JGR* 113, E11007. [11] Toon O.B. et al. (2010) *Annu. Rev. EPS* 38, 303-322. [12] Craddock R.A., Howard A.D. (2002) *JGR* 107, E11, 5111. [13] Howard A.D. et al. (2005) *JGR* 110, E12S14. [14] Irwin R. P. et al. (2005) *JGR* 110, E12S15. [15] Head J.W., Marchant D.R. (2014) *Antarctic Sci.* 26, 774-800. [16] Fastook J.L., Head J.W. (2014) *Plan. Space Sci.* 106, 82-98. [17] Irwin R.P. et al. (2011) *JGR* 116, E02005. [18] Craddock R.P., Maxwell T.A. (1993) *JGR* 98, 3453-3468. [19] Craddock R.P. et al. (1997) *JGR* 102, 13321-13340. [20] Hynek B.M., Phillips R.J. (2001) *Geology* 29, 407-410. [21] Rosenberg E.N. et al. (in prep). [22] Howard A.D. (1994) *Water Resources Res.* 30, 2261-2285. [23] Hartmann W.K., Neukum G. (2001) *Mars Space Sci. Rev.* 96, 165-194. [24] Hartmann W.K. (2005) *Icarus* 174, 294-320. [25] Luo W. et al. (2017) *Nature Comms.* [26] Hoke M.R. et al. (2011) *EPSL* 312, 1-12. [27] Barnhart C.J. et al. (2009) *JGR* 114, E01003. [28] Forsberg-Taylor N.K. et al. (2004) *JGR* 109, E05002. [29] Howard A.D. (2007) *Geomorph.* 91, 332-363. [30] Luo W., Howard A.D. (2008) *JGR* 113, E05002. [31] Matsubara Y. et al. (2011) *JGR* 116, E04001. [32] Matsubara Y. et al. (2013) *JGR* 118, 1365-1387. [33] Boatwright B.D., Fassett C.I. (2014) *LPSC* 45, 2478. [34] Howard A.D. (2009) MARSSIM Release 3.0, http://erode.evsc.virginia.edu. [35] Garvin J.B. et al. (2000) *Icarus* 144, 329-352. [36] Garvin J.B. et al. (2002) *LPSC* 33, 1255. [37] Garvin J.B. et al. (2003) *Intl. Conf. on Mars* 6, 3277.

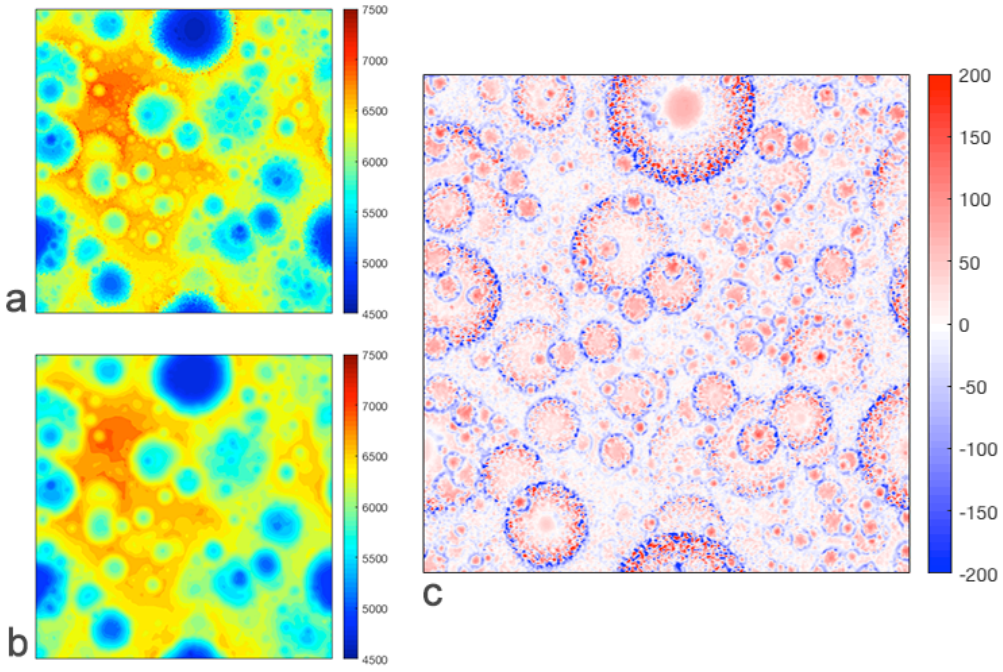


**Figure 1.** Topographic maps for a 10 million-year simulation (this study) using a 256x256 pixel DEM from the MARSSIM source code [34], scaled to 400 m/pixel with doubly periodic boundary conditions. Groundwater sapping and mass wasting were modeled over a pre-cratered surface. a) input elevation; b) output elevation; c) elevation change, all in meters. Note the infilling of crater floors and lowering of crater rims. This appears to be caused primarily by slope processes with small additions from seepage erosion.

**SPECIAL EXHIBIT ON METEORITES AND MINERALS ASSOCIATED WITH THE ORIGIN OF LIFE ON EARTH OR MARS.** R.B. Bruner1, 1Denver Museum of Nature and Science, 930 S Euclid Way, Denver, CO 80209; bobbruner40@hotmail.com.

**Black Smoker-type Hydrothermal Vent Theories**
- Pyrite to represent Wachtershauser's Iron-Sulfur world
- Saphalerite to represent Mulkidjanian's Zinc world

**Hydrothermal Pool Theories**
- Opaline Silica to represent Deamer and Damer

**Hydrothermal-Sedimentary Theories**
- Pumice to represent Westall et al

**Clay Theories**
- Montmorillonite to represent Ferris et al
- Kaolinite to represent Hashizume et al
- Muscovite to represent Hansma et al

**Lost City-type Serpentization Theories**
- Olivine, Pyroxene, Serpentine, Magnetite, Brucite, Molybdenum to represent Russell et al
- Serpentine proven by Nakhla meteorite - Bridges et al

**Conditions on Mars**
- Boron and molybdenum indicated by Wulfenite, Tourmaline, and Colemanite - Benner et al

**Conditions on Earth and Mars**
- Organic molecules proven by Murchison meteorite - Kvenvolden et al
- Organic molecules and CAI 's proven by Allende meteorite - Clarke et al
- Organic molecules proven by Tissint meteorite - Steele et al
- Organic molecules proven by Orgueil meteorite (cometary fragment) - Gardinier et al
- Other clay minerals (nontronite, saponite, halloysite, illite, chlorite) proving water - Ehlmann et al
- Water contribution from asteroids like Vesta (Camel Donga meteorite) - Alexander et al

P**hosphorus proven by**
- Apatite and Tambo Quemado meteorite - Pasek et al

**Life Materials Going from Mars to Earth - Dated by Zircon (CHNOPS)**
- Black Beauty Mars Meteorite NWA 7034 (and its cousins)

**FLUVIAL VOLUME, TIMESCALES, AND INTERMITTENCY IN MILNA CRATER, MARS.** P.B. Buhler[1], C.I. Fassett[2], J.W. Head[3], M P. Lamb[1], [1]California Institute of Technology, Department of Geological and Planetary Science, MC 170-25, Pasadena, CA, 91126, bpeter@caltech.edu, [2]Marshall Space Flight Center, Huntsville, AL, 35805, [3]Brown University, Department of Earth, Environmental and Planetary Sciences, Providence, RI, 02912

**Introduction:** Ancient lake deposits and valley networks on Mars provide strong evidence that its surface was once modified by liquid water [1,2,3,4,5], but the extent of that modification is still debated. Ancient lacustrine deposits in Milna Crater (23.4 S, 12.3 W; Fig. 1) provide insight into the timescale and fluid volume required to construct fluvially derived sedimentary deposits near the Noachian-Hesperian boundary. Placing the lacustrine deposits in their regional context in Paraná Valles provides a quantitative measurement of the intermittency of large, water-mediated sediment transport events in that region.

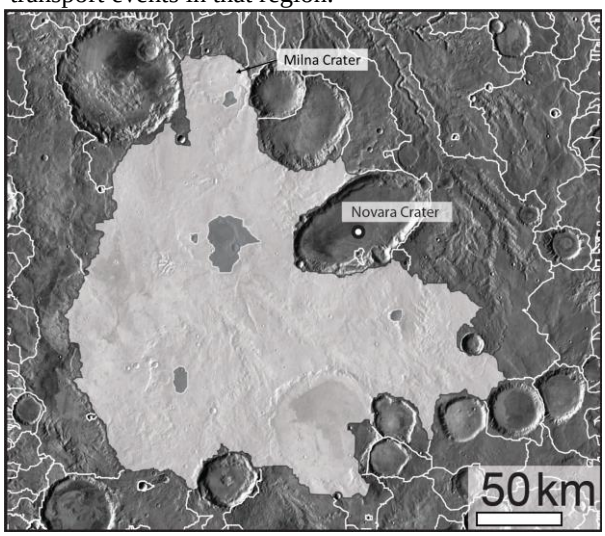


**Fig 1.** Context for Milna, with drainage divides (white lines). White area is drainage area source for Milna. North is up. THEMIS VIS image mosaic.

**Methods:** We use CTX, HiRISE, MOLA, and THEMIS data coregistered in ArcMap 10 for all measurements. Methods are more thoroughly described in [6]. We calculate the volume of the lacustrine deposits in Milna based on the current volume of the crater and the theoretical original volume of the crater [7]. We also take into account sediment porosity [8] and non-fluvially-sourced sediment by comparing the fill to that of an adjacent, similarly sized crater.

We then use a hydraulic model that takes into account bedload [9] and suspended sediment flux [10,11,12] to calculate the timescale and volume of water needed to transport the observed volume of lacustrine sediment through the inlet channel. We measure the ratio of inner channel dimensions to their host valley in the region surrounding Milna in order to constrain the dimensions of the inlet channel.We also consider a range of sediment sizes and model flow assuming various channel types (gravel, sand, and bedrock).

**Results:** Milna (Fig. 2) has a filled volume of 50 $km^3$, preserves many fans and sinuous valleys, and has an inlet and outlet valley, indicating that it was once filled with fluid. Under the assumption of continuous deposition, we find that the lacustrine fill in Milna was transported during 15-4700 terrestrial years, using the broadest possible range of model assumptions. Using the most reasonable model assumptions [see 6] we find that the range is likely to be 75-365 terrestrial years.

By placing the lacustrine deposits in Milna in regional and global context, we estimate the fraction of the time fluid flows capable of significantly transporting sediment operated (i.e. the intermittency, see [13]). Milna drains directly into the Paraná Valles system, which was fluvially active for $10^5$-$10^6$ years during the late Noachian [14,15,16,17]. By spreading the total flux duration in Milna (i.e. ~$10^2$ yr) over the total length of activity in Paraná Valles, we find that the intermittency of fluvial activity of ~0.01-0.1%. We also compare the erosion rate of the drainage area sourcing Milna (Fig. 1) to average Noachian erosion rates. The average thickness of the sedimentary erosion over the entire drainage area needed to produce the fill observed in Milna is 2.2 m. Since average Noachian erosion rates were on the order of $10^{-5}$-$10^{-6}$ m/yr [18], this again yields a ~0.01-0.1% fluvial intermittency factor.

**Discussion:** The hydrological activity in Milna can be compared to the predictions of different climate scenarios: (i) an arid climate capable of periodic flooding events sustained over ~$10^5$-$10^6$ years [e.g. 16,19], (ii) punctuated flooding events triggered by giant impacts [e.g. 20], and (iii) a pervasively glaciated southern highlands [e.g. 21,22].

Matsubara et al. [19] use a global hydrologic routing model to assess the the ratio of precipitation to evaporation (the "X-ratio") of a lake. Matsubara et al. [19] find an "X-ratio" under which lakes are sustained over long time periods, similar to the extent of lakes in the Great Basin region in the western United States during the Last Glacial Maximum. We apply this range of the "X-ratio" to the Milna system, under the assumption of one day-long storm per martian year delivering 0.5-5 cm of rainfall (the fluid flux required to create the sediment flux required by our preferred model [6]). Under this scenario we calculate evaporation rates of 0.16-17 m per terrestrial year, which is similar to typical terrestrial evaporation rates in a wide range of cli-

mates (~meters per year [21,22]), implying that a sustained arid climate capable of periodic flooding events is compatible with the observations we make at Milna.

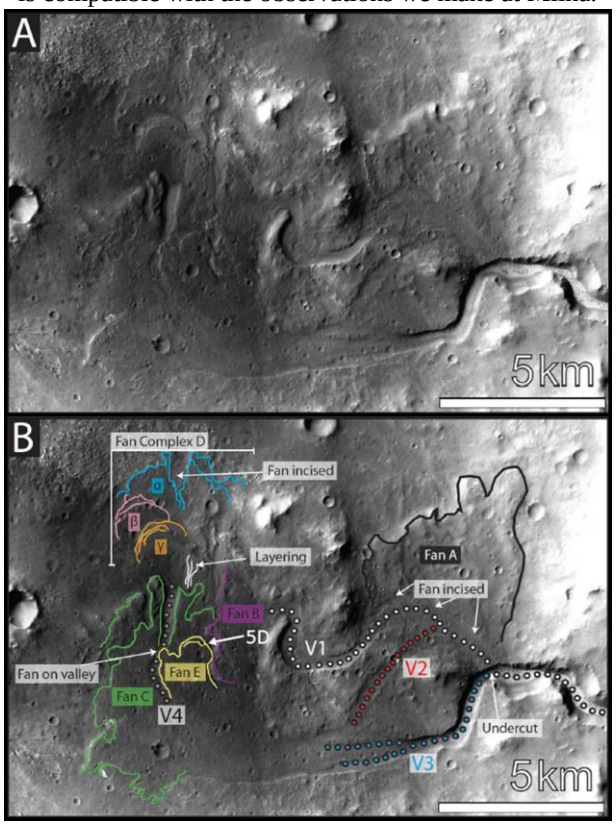


**Fig 2. A.** A large, multi-lobed fan that is incised by sinuous valleys in the southeast corner of Milna just below the inlet valley (lower left). **B.** Annotation. Solid lines denote scarps, dotted lines denote valleys. Note Fan E superposes a valley and that the valleys are sinuous and branched. Note also the stacked scarps visible at this (CTX) resolution in Fan Complex D, and Fans C & E. There is also layering not associated with a discrete lobe (white lines). CTX image.

Impacts may create transitory climates under which liquid water could be mobilized [20]. Using models from [20], assuming a ~100 km radius bolide under a 1 bar $CO_2$ atmosphere, ~$3 \times 10^{11}$ $m^3$ of water would be mobilized in the Milna drainage area. This is an order of magnitude less than the absolute minimum volume of water we calculate is required to transport the sediment observed in Milna (~$4 \times 10^{12}$ $m^3$, [6]). Thus, 10 bolides of this size would be required, which is unlikely since most of the giant impact basins were formed prior to formation of Paraná Valles [17,25]. Similar difficulties exist when considering smaller bolides [6]. Thus, flux generated by giant impacts alone is unlikely to be responsible for the morphology seen at Milna.

Periodic melting of an extensive southern ice sheet (e.g. by meteorite impacts, volcanism, or other temperature excursions [21,22,26]) may also provide a suitable water reservoir. Fastook and Head [22] suggest that top-down melting of such an ice sheet could produce 0.4 $Mkm^3$ of water across the southern highlands (enough to fill all open-basin paleolakes [27]) during an extended, moderately warm period or during a single, extremely warm summer. The observations at Milna indicate that an extended water release is more likely. We also emphasize that the required volume of water needs not only to fill the lakes, but also be capable of transporting the observed sedimentary fill.

**Conclusions:** We find that the total integrated fluvial activity in Milna took place over ~$10^2$ yr. Considering both the timescales of fluvial activity in the adjacent Paraná Valles and estimates for global Noachian erosion rates, we calculate an intermittency factor for fluvial activity of ~0.01-0.1% during $10^5$-$10^6$ yr near the Noachian-Hesperian boundary in the Paraná Valles region. These values are comparable to arid climates on Earth where the majority of fluvial sedimentary transport takes place during floods with multi-year to decadal recurrence intervals. Our calculations of intermittency help to quantitatively reconcile the divergent estimates of the short and long timescales of fluvial activity on Mars reported in the literature. Future investigations of additional paleolakes will increase the robustness of our result.

**References:** [1] Craddock, R.A. & Howard, A.D. (2002) *JGR 107*, 5111. [2] Gaidos, E. & Marion, G. (2003) *JGR 108*, 5055. [3] Moore, J.M. *et al.* (2003) *GRL 30*, 2292. [4] Burr, D.M. *et al.* (2009) *Icarus 200*, 52. [5] Carr, M.H (2012) *Phil Trans A 370*, 2193. [6] Buhler, P.B. *et al.* (2014) *Icarus 241*, 130. [7] Garvin, J.B. *et al.* (2002) *LPS XXXIII*, 1255. [8] Mavko, G. *et al.* (2009) *Cambridge UP* 450. [9] Fernandez Luque, R. & van Beek, R. (1976) *J Hyd Res 14*, 127. [10] Duck, R.W. & McManus, J. (1994) *J Hyd 159*, 365. [11] Pratt-Sitaula, B. *et al.* (2007) *Quat Res 68*, 11. [12] Turowski *et al.* (2010) *Sed 57*, 1126. [13] Wolman, M.G. & Miller, J.C. (1960) *J Geo 68*, 54. [14] Hynek, B.M. & Phillips, R.J. (2003) *Geo 31*, 757. [15] Irwin *et al.* (2007) *LPI 1353*, 3400. [16] Barnhart, C.J. *et al.* (2009) *JGR 114*, E01003. [17] Fassett & Head (2008) *Icarus 195*, 61. [18] Golombek *et al.* (2006) *JGR 111*, E12S10. [19] Matsubara *et al.* (2011) *JGR 116*, E04001. [20] Segura, T.L. *et al.* (2008) *JGR 113*, E11007. [21] Wordsworth *et al.* (2013) *Icarus 222*, 1. [22] Fastook & Head (2015) *PSS 106, 82*. [25] Farnsworth, R.K. & Thompson, E.S. (1983) *NOAA, NWS 34*. [24] Morton, F.I. (1983) *J Hyd 66*, 77. [25] Roberts, J.H. *et al*. (2009) *JGR 114*, E04009. [26] Head, J.W. & Marchant. D.R. (2014) *Antartctic Sci. 25*, 774. [27] Fassett and Head (2008), *Icarus 198, 37*.

We gratefully acknowledge Caltech SURF funding.

**FREQUENCY DISTRIBUTION OF JUNCTION ANGLES OF VALLEY NETWORKS ON MARS CONSISTENT WITH AN EARLY WARM CLIMATE.** X. Cang[1] and W. Luo[2], [1]Northern Illinois University (Department of Geography, Northern Illinois University, DeKalb, IL 60115 xcang@niu.edu), [2]Northern Illinois University (Department of Geography, Northern Illinois University, DeKalb, IL 60115 wluo@niu.edu).

**Introduction:** Valley networks (VNs) on Mars offer the evidence for its past water activities. Previous research empirically and theoretically suggested that the geometry properties of streams on Earth formed under different climatic conditions are different [1]. The frequency distribution of junction angles, as one of geometry properties, were influenced by the surface reforming processes, and can be accurately extracted from low resolution data. For this reason, the geometry properties of VNs are of significant importance for understanding the early Mars climatic conditions. Here, we calculated the VN junction angles of Mars, then utilized their frequency distributions to infer the dominant erosional process, and compared the dominant erosional process with the precipitation patterns from early Mars climate model [2] under different scenarios. The results are consistent with a "warm" early Mars climate with precipitation.

**Method:** Previous research showed that the frequency distribution of junction angles of streams follow a Gaussian distribution if the streams were formed in a long term climatically homogeneous area [1]. If the streams were formed by debris-dominated flow in arid areas, the mean of junction angle is around 45º [3]. If the streams were formed by fluvial regime flow in humid areas or by groundwater sapping, the mean of junction angles is around 75º [3-4].

Following this logic, one way to infer the climate of early Mars is to calculate the VN junction angles on Mars and to compare their frequency distribution to known terrestrial analogs. We extracted the junction angles from two VNs dataset [5-6] on the entire Mars surface, and applied the Gaussian Mixture Model (GMM) to decompose the junction angles' frequency distribution to 2 Gaussian distributions.

We divided the entire Mars surface to small tiles, each with size of 500 km by 500 km, which can beconsidered as a climatically homogenous area. We selected the tiles which contain more than fifty junction angles for analysis to avoid the problem caused by insufficient samples. Then, we applied the (GMM) to decompose the frequency distribution of junction angles within each tile to 2 Gaussian distributions. The weight for each Gaussian distribution is also derived. The erosional process with a higher weight is considered the dominant erosional process. The tiles with a lower average dominant frequency component (normally around 45º) indicate that VNs were formed predominately by surface runoff erosion, whereas tiles with a higher average dominant frequency component suggest that the VNs were formed predominately by groundwater sapping. Because the humid scenario on Earth was unlikely to happen on Mars, so we interpret that those VNs with high junction angles were formed via groundwater sapping.

We also compared the spatial distribution of dominant erosional process with ice accumulation/precipitation patterns predicted by climate models under "warm" or "cold" scenarios [2]. We selected the tiles which were dominated by surface runoff erosion and calculated the Pearson correlation between the mean of junction angles and precipitation/ice accumulation [2] within each tile. The scenario with higher coefficient is supported, because the spatial distribution of water under this scenario is in accordance with the measured landform results.

**Results:** The junction angles are extracted from two VN datasets: one derived from DEM automatically by Luo and Stepinski [5] and one manually digitized on image data by Hynek et al. [6]. The global averages for both datasets are between surface runoff (45º) and groundwater sapping (75º). It means that two processes worked together on Mars, therefore we need to decompose them by GMM. The frequency distributions of the global junction angles are shown in Fig. 1. The global Gaussian decomposition results are shown in Table 1.

Table 1. Gaussian decomposaion results of global VNs

| | Mean1 | Mean2 | Weight1 | Weight2 |
|---|---|---|---|---|
| Luo and stepinski | 36.52 | 72.48 | 0.40 | 0.60 |
| Hynek et al. | 44.55 | 101.64 | 0.59 | 0.41 |

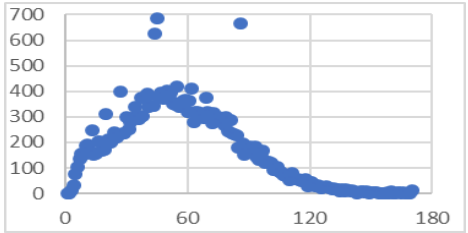


(A) VNs lines data are from Luo and stepinski [5]

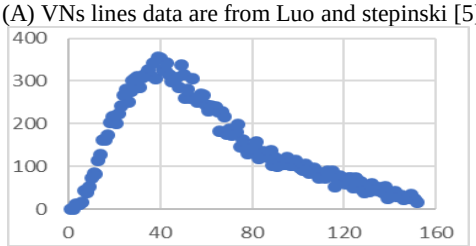


(B) VNs lines data are from Hynek et al. [6]

Fig. 1 Frequency distribution of global VNs

Fig. 2 shows the spatial distribution of dominate erosional process with MOLA topography in the background. The red grids represent that the dominant erosional process is groundwater sapping, and the blue ones represent that the dominant erosional process is surface runoff. The hallow grids indicate that there are less than 50 junction angles within each grid, so they did not participate calculation. It is clear from Fig. 2 that the dominant erosion process in most areas is surface runoff.

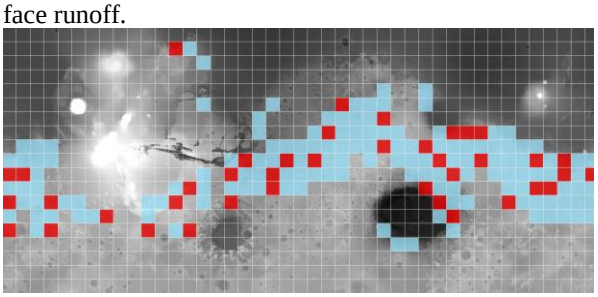

(A)

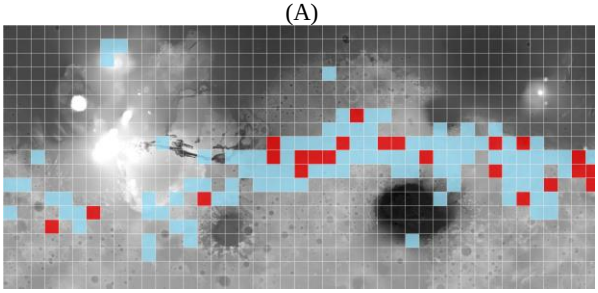

(B)

Fig.2 Spatial distribion of dominant erosional process (A) Luo and stepinski (B) Hynek et al.

To compare the precipitation/ice accumulation under different climatic scenarios, we calculated the coefficient and p-value of Pearson correlation between the mean of junction angles and precipitation/ice accumulation [2] within each tile. The results are shown in Table 2.

Table 2 Correlations Under Different Climate Scenarios

| Data | warm scenario | | ice scenario | |
|---|---|---|---|---|
| | coefficient | p-value | coefficient | p-value |
| Luo | 0.22 | 0.01 | 0.10 | 0.20 |
| Hynek | -0.30 | 0.00 | -0.12 | 0.22 |

**Discussion:** On the global scale, the junction angles extracted from both versions of VN data [5-6] showed that the VNs on Mars were formed by at least two types of erosional processes. The weights are inconsistent between two VNs data, however the surface runoff erosion are important in both of them. The means of two components from Hynek et al. data are larger than the means from Luo and stepinski data. The reason may be that the Hynek et al. VNs included more direction uncertainties as the VNs were manually drawn on images and they may not always follow topography and may have erroneous directions. The junction angle extraction utilized the VNs' topology information and cannot extract the junction angles with wrong topology information. For this reason, we suggest decomposition results from Luo and Stepinki VNs are more credible. This results showed that Mars' VNs are formed by surface runoff and groundwater sapping. The mean of VNs eroded by surface runoff is 36º which is lower than the mean in the relative arid area of contiguous U.S. This result is consistent with previous research which suggests that the early Mars had fluvial processes, even though the climate was much drier than Earth today[7].

The spatial distribution of dominate erosional process showed that most areas with dense VNs are mainly formed by surface runoff process. The ground sapping dominated areas are mostly located at the edge of dense VNs areas. The wide distribution of surface runoff-dominated areas suggests that liquid water could globally flow on the early Mars. Fig. 2 also showed that the surface runoff dominated tiles from Luo and Stepinski data are more widely distributed than those from Hynek et al. data

The correlations showed that the junction angles formed via surface runoff are significantly correlated with the precipitation distribution under warm scenario, but have non-significant correlation with ice accumulation under ice scenario. The significant but negative correlation between Hynek et al.'s junction angles and estimated precipitation is interpreted to be unreliable due to the uncertainties in VN direction.

**Conclusion:** This paper compared the frequency distribution of junction angles of VNs on Mars to terrestrial research results and climate model predicted precipitation pattern. The global junction angles frequency distribution supports that the surface runoff was an important erosional process on Early Mars; the spatial distribution of dominant erosion process suggests that water could widely flow on early Mars; the correlation with climate model results suggestes that erosional agent is likely water from precipitation under a warm climatic scenario, not melting water from cold scenario.

**References:** [1] Seybold, H. (2017) *GRL*, 44, 2272-2280. [2] Wordsworth, RD. (2015) *JGR*, 120 1201-1219. [3] Hooshyar, M. et al. (2017) *WRR*, [4] Devauchelle, O. et al. (2012) *PNAS*, 109. [5] Luo, W. and Stepinski T. (2009) *JGR*. 114. [6] Hynek, BM. et al.(2009) *JGR* 115. [7] Matsubara, Y. et al. (2011) *JGR*. 116

**JUSTIFYING MARTIAN FLUVIAL SINUOUS RIDGE MEASUREMENTS USING EARTH ANALOG STRATIGRAPHY.** B. T. Cardenas[1], T. A. Goudge[1], C. M. Hughes[1], J. S. Levy[2], and D. Mohrig[1], [1]Jackson School of Geosciences, University of Texas at Austin, Austin, TX, [2]Department of Geology, Colgate University, Hamilton, NY (Contact: benjamin.cardenas@utexas.edu)

**Introduction:** Topographically-inverted channel-filling deposits exist across the surface of Mars as sinuous ridges. Though the origin of these features is genrally agreed to have occurred via fluvial sedimentation, widely varying interpretations of their stratigraphy have led to a variety of interpreted depositional settings [1-9].

We present results of field work on topographically-inverted fluvial channel deposits in the Cretaceous Cedar Mountain Formation located 13-km south of Green River, Utah, USA [10-11]. Stratigraphic measurements were related to high-resolution images and DEMs of a scale similar to that of HiRISE data. Our results provide a framework for further study of sinuous ridges on Mars.

**Methods:** UAV photosurveys were used to create high-resolution photomosaics and DEMs of two portions of a discontinuous sinuous ridge in the Cedar Mountain Fm., which contains 3 bends (Fig. 1). The aerial extent of dune cross-strata sets were mapped in the field, and measurements of foreset dip directions were collected as measures of local paleo-transport direction (Fig. 2). Laterally persistent stratigraphic surfaces were also mapped in the field.

**Results:** *Stacked channel-fills:* Channel-filling sandstones and conglomerates are separated by laterally-continuous mudstone layers of variable thickness (cm-m scale). Today, these exposed mudstone layers are relatively erodible and recessive, and are often associated with topographic breaks on ridge surfaces (Fig. 2). We interpret these mudstones as representing sedimentation during periods of inactivity within a channel due to flow diversion by an upstream avulsion. With time, the inactive channel transferred to a floodplain setting with associated overbank sedimentation and pedogenic processes [12-14]. At some later time this low area on the floodplain was re-occupied by a younger active channel, removing some mudstone thickness via channel-bottom erosion and depositing coarser-grained channel-filling deposits on top of this erosional surface (Fig. 2). We have identified a total of 3 stacked channel-fills within this ridge.

*Preservation of channel-bottom topography:* The upper-most channel-filling deposit on the ridge top preserves topography similar to a mid-channel bar [15] (Fig. 1). This topographic element is constructed of stacked sets of cross beds climbing up and then down topography in the downstream direction. The spread in paleo-transport direction measured from these cross-beds increases with local elevation on this element, which we interpret as recording the dispersion of flow and sediment around the highest portions of the bar (Fig. 3A). Preservation of a bar form requires the rapid cessation of sediment transport within the channel, likely associated with an upstream avulsion and subsequent burial in a floodplain setting.

*Centerline preservation:* To test the degree of preservation of the original channel centerline in these deposits, paleo-transport directions were compared to the local trend of a calculated ridge centerline (Fig. 4) with the value $\Delta_{AZ}$ (local centerline azimuth – local paleo-transport azimuth). The normal distribution of $\Delta_{AZ}$ around a near-zero mean of -12 degrees and a 35 degree standard deviation is within the range of an active river, and indicates the ridge centerline represents the centerline of the channel reasonably well. The non-zero mean may represent the lateral migration that is recorded, or the control of differential erosion of the ridge on centerline placement.

**Discussion:** The vertical stacking and lateral migration recorded by the ridge in the Cedar Mountain Fm. represents an integration of channel-fills associated with a succession of separate river channels. The dimensions of a single sinuous ridge thus do not represent the dimensions of the formative channel. However, based on our results, the centerline shape of re-occupied channels are preserved well enough for centerline analyses (Fig. 4) [1].

Topographic breaks have been shown to occur along channel-fill contacts, and such breaks can be observed as steps on the tops of martian sinuous ridges, distinguishing separate channel-fill deposits [e.g., 1].

The preservation of channel-bar topography (Fig. 1) supports the interpretation of a depositional environment characterized by avulsing river channels. This observation also indicates that channel-fill thickness may reasonably be equated to the thickness of a bar, a common proxy for channel depth [12]. Ongoing work is contrasting these results to nearby, exhumed channel-filling deposits in the Jurassic Morrison Fm., which seems dominated by lateral, rather than vertical, channel amalgamation.

**References:** [1] Cardenas B. T. et al. (accepted) *GSAB* [2] Kite E. S. et al. (2015) *Icarus, 253*, 223-242. [3] DiBiase R. A. et al. (2013) *JGR: Planets, 118*, 1285-1302. [4] Burr D. M. (2009) *Icarus, 200*, 52-76. [5] Williams R. M. E. et al. (2013)

*Icarus, 225*, 308-324. [6] Davis J. M. et al. (2016) *Geology, 44*, 847-850. [7] Lefort A. et al. (2012) *JGR: Planets, 117*, E3. [8] Lefort A. et al. (2015) *Geomorphology, 240*, 232-136. [9] Matsubara Y. et al. (2015) *Geomorphology, 240*, 102-120. [10] Williams R. M. E. et al. (2011) *GSA Special Papers, 483*, 483-505. [11] Nuse B. R. (2015) *MS Thesis, Colorado School of Mines.* [12] Mohrig D. et al. (2000) *GSAB, 112*, 1787-1803. [13] Cuevas Martínez J. L. et al. (2010) *Sedimentology, 57*, 162-189. [14] Chamberlin E. P. and Hajek E. A. (2015) *JSR, 85*, 82-94. [15] Hooke J. M. and Yorke L. (2011) *ESPL, 36*, 1910-1928.

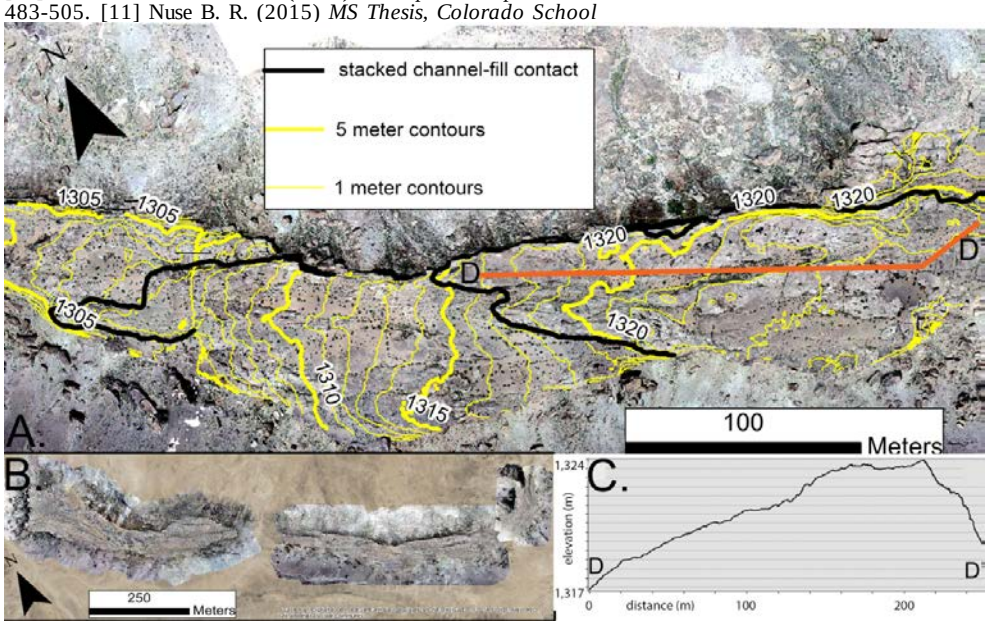


Figure 1 – A: Contoured photomosaic of part of a Cedar Mountain Fm. ridge. D-D' along the orange line shows the location of the topographic profile in C. B: Complete study area at the Cedar Mountain Fm., with photomosaics superimposed on Google Earth images. C: Topographic profile from D-D' is similar to bar stoss and lee slopes.

Figure 2 – Thin, recessive, laterally-continuous mudstone separating two, coarser channel-filling deposits in the Cedar Mtn Fm. Top of the mudstone is marked by the bottom of the notebook.

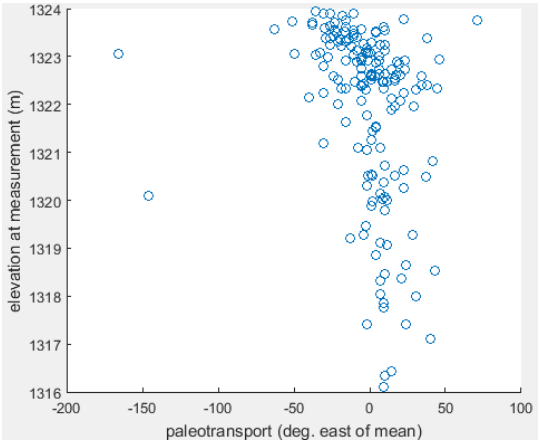


Figure 3 – Paleo-transport direction vs. elevation in the bar-like topographic feature (Fig. 1).

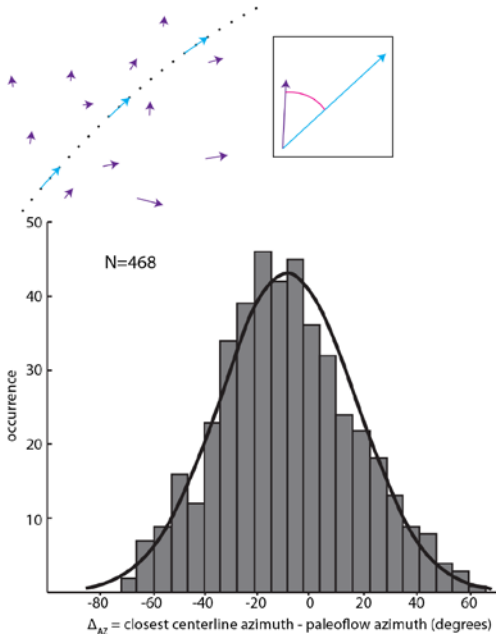


Figure 4 – Top: Schematic of the $\Delta_{AZ}$ measurement, and the distribution of $\Delta_{AZ}$ with the fitted normal curve. Purple arrows represent the locations and azimuths of paleo-transport measurements. The black dots and blue arrows represent the centerline and its local tangent azimuth. Inside the inset, the pink angle between the centerline azimuth nearest a paleo-transport measurement is $\Delta_{AZ}$. Bottom: Normal distribution of $\Delta_{AZ}$ around a mean of -12 degrees with a standard deviation of 35 degrees.

**ESTIMATING THE HESPERIAN WATER INVENTORY FROM THE PRESENT INVENTORY: WHERE DID ALL THE WATER GO?** Michael H. Carr[1] and James W. Head[2], [1]U. S. Geological Survey, Menlo Park, CA 94025 USA (mhcarr265@gmail.com), [2]Department of Geological Sciences, Brown University, Providence RI 02912 USA (james_head@brown.edu).

**Introduction:** Large bodies of water must have been left behind on the martian surface in the Hesperian after formation of the large outflow channels. The youngest and best defined of proposed shorelines (Deuteronilus ) [1] around these bodies of water would have enclosed roughly 130 m GEL of water. Approximately 30 m GEL of water is estimated to be at the surface today [2,3], of which some fraction must be water that has outgassed since the Hesperian. Thus, if the Deuteronilus shoreline is real, over a 100 m GEL has been lost from the surface to space and/or by infiltration into and chemical reaction with the surface. Here we examine where the water might have gone in light of recent measurements of D/H in Hesperian sediments [4], recent estimates of the past heat flows [5] and early MAVEN results [6]. We conclude that while infiltration into the surface may have been significant in the Noachian, it is unlikely to have been significant in post-Noachian times and that most of the losses were from the upper atmosphere during the Hesperian and early Amazonian when the Sun's irradiance in the EUV was 6-10 times higher than at present [7].

**Outgassing.** The fraction of the present near-surface water inherited from the Hesperian depends on how much has outgassed since that time. The total volume of Hesperian and Amazonian volcanic rocks erupted to the surface (2.5e07 $km^3$) was estimated from the areas of the volcanic units depicted on the global geologic map [8] and from thicknesses derived from burial of impact craters. Assuming 1 wt.percent water, we conclude that roughly 4 m GEL of water has outgassed since the end of the Noachian, a significantly smaller volume than estimated by Greeley and Scheid [9]. Most of the present surface inventory of water was probably inherited from the Hesperian.

**Implications of D/H.** The present D/H ratio in the martian atmosphere, and by implication the entire near-surface water inventory is 6 times SMOW. In contrast, the D/H ratio in smectites from mudstones from the floor of Gale crater, with an age estimated to be 3.0 to 3.8 billion years, is 3.0 SMOW [4]. So the D/H ratio of surface water has doubled in the last 3-3.8 b.y. If the near surface reservoir has been isolated from the rest of the planet and experienced losses only to space then the Hesperian inventory can be estimated directly from the present day exchangeable reservoir, and the present and Hesperian D/H values as follows: $I_H = I_P\ (R_P/R_H)^{(1/1-f)}$ , where $I_H$ and $I_P$ are the Hesperian and present inventories, $R_H$ and $R_P$ are the present and Hesperian D/H ratios and f is the D/H fractionation factor for upper atmosphere losses [10]. Calculated values are shown in Figure 1. The values of f reported in the literature range widely from a highly fractionating 0.02 for the present [11] to a less fractionating 0.4 [12]. With a fractionation factor of 0.02, almost no deuterium is lost and an increase in the D/H by a factor of 2 implies the Hesperian inventory was twice the present or roughly 60 m GEL, well short of that required by the Deuteronilus shoreline. To account for the an Hesperian inventory of 130 m by this mechanism alone would require, for example, a present inventory of 40 m and a fractionation factor of 0.4, so the lower estimates of the fractionation factor fall well short of that required to explain the large losses needed. The estimates of Hesperian inventories are almost unchanged by including the effects of outgassing because the outgassing rates are low and because of offsetting effects of introducing unfractionated water onto the surface and reducing the present inventory that has been inherited from the Hesperian.

Figure 1. Hesperian inventories as a function of the D/H fractionation factor and different present-day near-surface inventories.

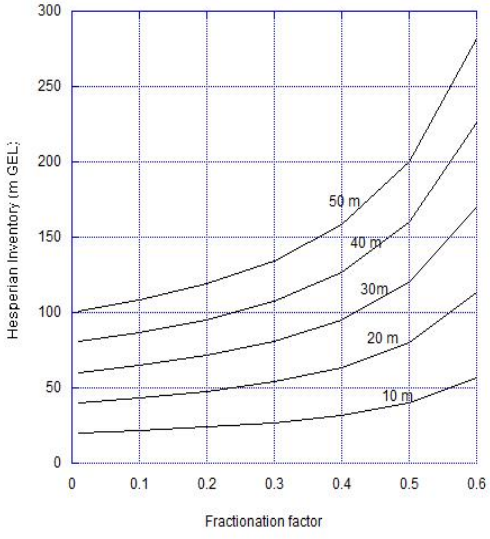


**Infiltration into the surface.** Clifford [17] has suggested that water could be lost from the surface by infiltration into the subsurface as a result of basal melting of the polar layered deposits. The mechanism is sensi-

tive to the internal heat flow. With estimates of the sent heat flow close to 15 mW $m^{-2}$ [5] and a the conductivity k= 2 W $m^{-1}K^{-1}$, the layered deposits w have to be 16 km thick for melting at their base to But heat flows in the past would have been larger. [5], integrating a large number of geophysical and chemical measurements, estimates that 3.5 b.y. ago heat flow was 45 mW $m^{-2}$, which would require the p terrains to be 5.3 km thick for basal melting with k= $m^{-1}K^{-1}$. At 2.5 b.y. with a heat flow of 37 mW $m^{-2}$, a km thickness would be required for basal melting. present layered terrains range up to 3 km in thickn well short of the Hesperian estimates. It appears that for basal melting to occur in the Amazonian and late Hesperian the polar layered deposits would have to have been significantly thicker than at present. We conclude therefore that basal melting, while it may have been an important recharge mechanism in the Noachian, is unlikely to have been a major factor in removal of surface water after the mid-Hesperian.

**Speculation.** Despite convincing geologic evidence for the presence of large bodies of water on Mars during the Hesperian 3 to 3.8 b.y. ago, the mechanisms whereby the water was eliminated have proven elusive. At present loss rates of hydrogen, as measured by MAVEN [6], only 1-15 m GEL of water would have been lost over the last 4 b.y. With the present D/H fractionation factor of 0.2 [12], no more than 30 m of water would have been been lost since the mudstones in Gale crater were deposited. In addition, estimates of heat flow suggest that significant losses of surface water to the ground through polar basal melting are unlikely. A possible answer lies in the history of the Sun. Between 3.5 and 3.9 b.y. ago solar EUV radiation was 6-10 times the present [7], which would lead to higher hydrogen loss rates than at present. But this alone is insufficient to explain the water losses because estimates of the Hesperian inventory from D/H depend only on the present inventory and the fractionation factor and not on the loss rates. In addition to the loss rates the fractionation factor must change with time if losses to space are to account for the water loss. This is not unreasonable since interactions between solar radiation and the upper atmosphere in the past would have been more energetic and less fractionating than at present. As indicated above, 130 m would have been lost if the present exchangeable surface inventory is in the 40 m range and the effective fractionation factor was 0.4. Most of the losses and fractionation would have occurred in the Hesperian and early Amazonian.


- **References. [1]** Clifford, S. M. and Parker, T. J., *Icarus***. 154**, 40-79 (2001). [2] Carr M. H., and Head, *J. Geophys. Res. Lett.* , **42**, 626-732 doi:1002/2014 GL062464 (2015). [3] Lasue, J., et al., *Space Sci. Rev.*,**174,** 155-212 (2013). [4]. Mahaffy et al., *Science* DOI: 10.1126/ science.1260291 (2014). [5] Ruiz, J. *Scientific Reports* **4**, 4338, doi:10.1038/srep04338 (2014). [6] Jakosky, B. M. *AGU Annual Mtg. San Francisco* (2016). [7]. Gudel, M., and Kasting, J. , *Origin and evolution of life,* **6,** 167-182 (2011). [8] Tanaka, K. L. et al., *USGS Sci. Inv. Map2888* (2005). [9] Greeley, R and Schneid, B. D., *Science*, **254,** 996-998. [10] Kurokawa, H. et al., *Earth Planet. Sci. Lett.*, **394,** 179-185, (2014). [11]. Krasnapolsky, V. , *Icarus,* **148,** 597-602. [12] Yung, Y. L. et al., *Icarus,* **76,** 146-159 (1988). [13] Clifford, S. M., *J. Geophys. Res.,* **92,** 9135-9152 (1987).

**FORMATION OF VALLEY NETWORKS IN A COLD AND ICY EARLY MARS CLIMATE: PREDICTIONS FOR EROSION RATES AND CHANNEL MORPHOLOGY.** J. P. Cassanelli[1] and J. W. Head[1], [1]Department of Earth, Environmental, and Planetary Science, Brown University, Providence, RI 02912 USA (James_Cassanelli@Brown.edu)

**Introduction:** The ancient Noachian highlands of Mars host an extensive population of valley networks [*e.g.* 1]. The valley networks are systems of branching linear-to-sinuous depressions which have been interpreted to have formed by fluvial erosion [*e.g.* 2,3]. Geological characteristics of the valley networks have been cited as evidence of an origin by precipitation in a relatively warm and wet climate during the Noachian period [*e.g.* 2,3], requiring a vertically integrated hydrologic system [4].

However, these interpretations conflict with the predictions of climate modeling studies [5-7], which suggest that early Mars was characterized by a cold and icy climate exhibiting adiabatic cooling and an icy highlands, with mean annual surface temperatures almost 50 °C below the melting point of water (~225 K). Precipitation-derived valley network formation is therefore generally inconsistent with the background cold and icy climate. Several mechanisms, invoking episodic melting of ice deposits in the highland terrains, have been proposed to account for valley network formation under these cold and icy climate conditions including: transient warming from volcanic greenhouse gas emissions [8], melting of ice under peak daily and seasonal temperatures [9], and ice melting through glaciovolcanic interactions [10].

How might the nature of fluvial processes and the formation of valley networks have been influenced by such cold and icy conditions? Head and Cassanelli [11] proposed a conceptual model for channel incision and evolution under cold and icy conditions with a substrate characterized by the presence of an ice-free dry active layer and subjacent ice-cemented regolith, similar to that found in the Antarctic McMurdo Dry Valleys [4] (Fig. 1). In this scenario, the structure of the cold and icy substrate is predicted [11] to cause a dichotomy in erosional efficiency during channel incision, leading to preferential lateral erosion when the channel reaches the more coherent ice-cemented material (Fig. 1). Here we explore this conceptual framework through a quantitative assessment of the influence of cold and icy climate conditions, and the associated substrate structure, on the formation of valley networks. We outline predictions for: 1) the nature and structure of the substrate, 2) mechanical erosion and incision rates, 3) thermal erosion rates of the ice-cemented substrate, and 4) the resulting geomorphic channel characteristics.

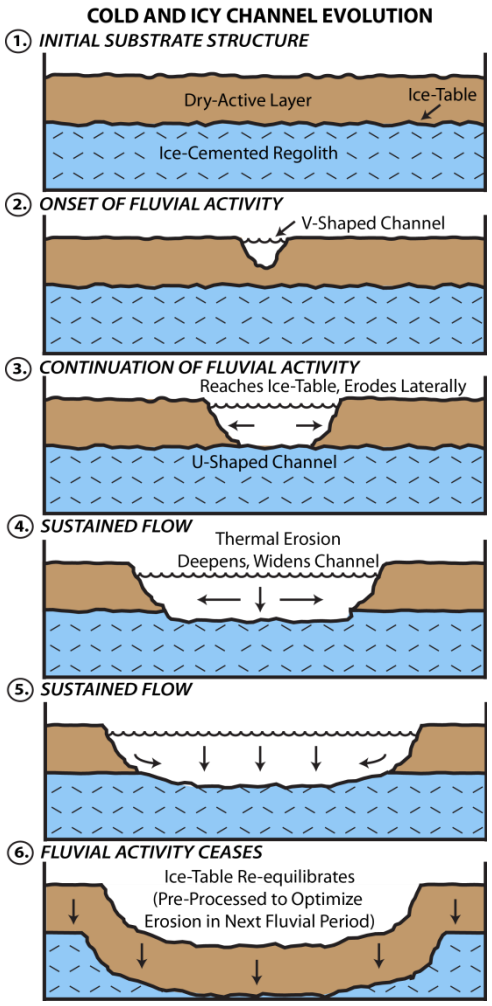


**Figure 1.** Conceptual model for channel evolution and valley network formation under cold and icy conditions (adapted from [11]). The fluvial substrate is comprised of an ice-free dry active layer and ice-cemented regolith, with the interface between them being the ice-table [4].

**Substrate Nature:** The primary factor predicted to affect valley network channel evolution under cold and icy conditions is the presence of an erosionally resistant ice-cemented regolith within the substrate [11]. The depth at which the substrate becomes ice-cemented (the ice-table) is governed by the diffusive equilibrium of water vapor with the atmosphere. We estimate equilibrium ice-table depths (following Mellon et al. [12]) under typical predicted Late Noachian climate conditions (1 bar $CO_2$ atmosphere and

45° obliquity; [6-9]) using temperature and atmospheric water abundance data from recent global circulation model studies [9]. Results of this analysis predict that the valley networks occur in areas with equilibrium ice-table depths of ~50-100 m, averaging ~80 m. This suggests that the infiltration capacity of the martian regolith would not be reduced by a shallow impermeable ice-table, thereby requiring a minimum threshold of surface water input to generate runoff.

**Mechanical Erosion:** The rate of channel growth in the ice-free substrate will be governed by the mechanical erosion rate produced by the fluvial flow. In order to estimate the mechanical fluvial incision rates, we implement a simple stream power based estimate [13] (following Hurwitz et al. [14]), with the vertical erosion rate given by:

$$\frac{\partial z}{\partial t} = K\rho g Q sin(\alpha) \quad (1)$$

where $K$ ($Pa^{-1}$) is a substrate erodibility factor expressing the efficiency of the incision process, and the remaining terms define the stream power [13,14]. Estimates of the mechanical erosion rate produced by equation (1) are sensitive to the value of the erodibility factor $K$ [14], which is a poorly constrained parameter aggregating the effects of many factors [13] (e.g. substrate strength, sediment supply, grain size, incision mechanism and others). We adopt tentative erodibility factor values of $10^{-7}$ (for the ice-free substrate) and $10^{-8}$ (for the ice-cemented substrate) based on approximate values utilized by Hurwitz et al. [14]. The remaining parameters related to the stream power are calculated using estimated valley network flow data from Hoke et al. [15] and therefore the results presented here are representative only for large valley network systems (with lengths of several $10^3$ km and interior channel widths greater than 1 km). We find mechanical incision rates of ~5 x $10^{-6}$ m/s in the ice-free substrate and ~5 x $10^{-7}$ m/s in the ice-cemented substrate.

**Thermal Erosion:** Once the incising channel has reached the ice-table, vertical mechanical erosion will become more difficult as a result of the increased strength of the underlying material. However, at this point, the underlying ice-cemented substrate is subjected to both mechanical and thermal erosion. If thermal erosion rates are lower than the mechanical erosion rates, vertical erosion may be less efficient than lateral erosion, causing preferential channel widening (Fig. 1(3)). In contrast, if thermal erosion rates are higher than the mechanical erosion rates, the ice-cemented regolith will have little influence on channel incision and evolution.

The rate of thermal erosion is governed by the flux of heat transferred into the substrate by the overlying fluid flow. In a turbulent flow regime (representative of the valley networks considered here), this heat flux is given by [16]:

$$q = h(T_w - T_m) \quad (2)$$

where $h$ is a heat transfer coefficient dependent upon the Nusselt number, which is calculated with an empirical relation [16]. Thermal erosion rates are assessed through the implementation of a simple 1-D finite difference heat conduction model (with the phase-change of the pore-ice accounted for by the heat integration method; [17]). A constant heat flux, equal to that given by equation (2) is applied at one end of the model with an insulating boundary condition at the other, and any thawed material is assumed to be instantaneously removed from the system.

We find that after the flow initially reaches the ice-table, melting is delayed for ~0.02 yr (~7 days) as the pore-ice is warmed to the melting point. After melting begins, thermal erosion proceeds at an average rate of ~2 x $10^{-5}$ m/s, with a total long-term average (including the transient warming period) of ~9 x $10^{-6}$ m/s.

**Conclusions:** Initial results suggest: 1) Ice-table depths in the valley network forming regions are on the order of ~50-100 m, averaging ~80 m. Therefore, only valley networks which have incised beyond these depths should have been influenced by the presence of the ice-cemented substrate. 2) Thermal erosion rates predicted using channel dimension data for large valley network systems [15] are comparable to the rates of mechanical incision in the ice-free substrate, and are greater than the rate of mechanical incision in the ice-cemented substrate (though results are subject to uncertainties in the erodibility factor expressing incision efficiency). 3) Given the rates determined by these preliminary analyses, channel incision is not predicted to be limited by thermal erosion, and therefore channel evolution and incision into the ice-cemented substrate are predicted to proceed without any major influence.

**References:** [1] Hynek et al. (2010) *JGR Planets*, 115. [2] Craddock and Howard (2002) *JGR Planets*, 107, 5111. [3] Barnhart et al. (2009) *JGR Planets*, 114. [4] Head and Marchant (2014) *Antarc. Sci.*, 26, 774. [5] Forget et al. (2013) *Icarus*, 222, 81. [6] Wordsworth et al. (2013) *Icarus*, 222, 1. [7] Wordsworth et al. (2015) *JGR Planets*, 120. [8] Halevy and Head (2014) *Nature Geo.*, 7, 865. [9] Horan and Head (2016) *LPSC 47*, 2394. [10] Cassanelli and Head (2016) *Icarus*, 271, 237. [11] Head and Cassanelli (2014) *LPSC 45*, 1413. [12] Mellon et al. (1997) *JGR*, 112, 19357. [13] Sklar and Dietrich (1998) *Rivers over Rock*, 237. [14] Hurwitz et al. (2010) *Icarus*, 210, 626. [15] Hoke et al. (2011) *EPSL*, 312, 1. [16] Costard et al. (2003) *Earth Surf. Process. Landforms*, 28, 1349. [17] Hu and Argyropoulos (1996) *Model. Simul. Mater. Sci. Eng.* 4, 371.

**DETRITAL SMECTITES AS POTENTIAL REDOX INDICATORS ON EARLY MARS.** J.G. Catalano[1], R.D. Nickerson[1], S.M. Chemtob[2], R.V. Morris[3], D.G. Agresti[4], [1]Washington U., St. Louis, MO (catalano@wustl.edu), [2]Temple U., Philadelphia, PA, [3]Johnson Space Center, Houston, TX, [4]U. Alabama at Birmingham, Birmingham, AL.

**Introduction:** Clay minerals, most notably smectites, are widely distributed products of water-rock reactions on early Mars [1]. While aluminous smectites appear to be primarily associated with near-surface weathering or leaching zones, Fe- and Mg-rich phases occur in multiple geological settings, often in thick exposures that appear to have undergone largely isochemical alteration, suggesting a subsurface origin. Some occurrences of Fe-Mg smectites show clear associations with phases indicating hydrothermal alteration, and such alteration as warm fluids moved through the subsurface may be a key formation process for many smectites on Mars.

Hydrothermal alteration weakens rock [2] in addition to forming smectites and other secondary phases, and this makes such units susceptible to physical erosion and detrital transport, including inside basins associated with impact craters. Smectites formed via subsurface hydrothermal alteration are expected to contain iron in the ferrous, Fe(II), oxidation state [3]. These materials are redox-sensitive [4] and may convert to ferric phases if exposed to oxidants during transport or deposition. Hydrothermal smectites may thus be potential indicators of redox conditions on early Mars, when detrital transport was most likely to occur. However, the nature of clays that form via basalt alteration, their susceptibility to oxidation by Mars-relevant oxidants, and the extent and products of such oxidation are currently poorly understood. Terrestrial occurrences of such phases are largely limited to the deep subsurface [3] and these materials oxidize upon exposure to Earth's $O_2$-rich atmosphere [4]. The present work seeks to address these knowledge gaps through a series of alteration and oxidation experiments coupled to mineralogical characterization of clays and accessory phases.

**Smectite Formation during Hydrothermal Basalt Alteration:** To investigate the composition and properties of smectites that form under hydrothermal conditions, USGS basalt standards DNC-1a and BIR-1a were heated under an $O_2$-free nitrogen atmosphere at 200°C for 21 days in PTFE-lined hydrothermal vessels at a water:rock ratio of 2.5. Recovered solids were dried in an anoxic glovebox [$O_2$(g) < 1 ppm]. Secondary electron imaging identifies smectites occurring as rinds on primary olivine grains (Fig. 1). XRD identifies clear basal and turbostratic features consistent with a smectite structure, with the (060) d-spacing of 1.54 Å indicating a trioctahedral phase (Fig. 1). A composition of $K_{0.01}Na_{0.03}Ca_{0.26}(Fe_{1.09}Mg_{1.26}Al_{0.40}Mn_{0.02})^{VI}(Si_{3.46}Al_{0.54})^{IV}O_{10}(OH)_2$ was obtained by EMPA consistent with a trioctahedral saponite. XANES spectroscopy confirms that Fe remained in the ferrous oxidation state during alteration. Rietveld determination of phase abundance from XRD data along with XANES quantification of Fe distribution among mineral hosts indicates that substantial olivine alteration is coupled to formation of up to 48 wt.% smectite, along with a slight increase in magnetite abundance. The (02l) reflections of the Fe(II)-Mg smectite produced during alteration occur at a similar d-spacing to (02l) reflections from smectites in the Bradbury Formation at Gale Crater, Mars (Fig. 2). Hydrothermal basalt alteration under anoxic conditions thus produces a mixed Fe(II)-Mg saponite potentially similar to the trioctahedral smectites observed in Gale Crater mudstones containing detrital basalt grains [5].

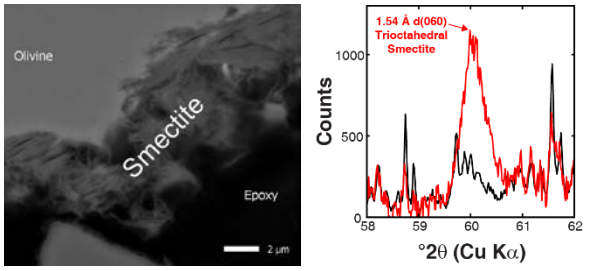


***Figure 1.*** *(left) Secondary electron image of a cross-section of an altered olivine grain in DNC-1a. (right) XRD pattern of unaltered (black) and altered (red) basalt DNC-1a in the (060) region.*

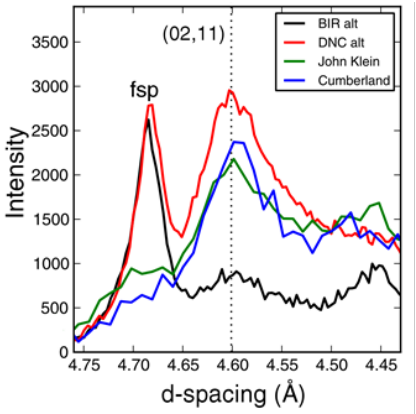


***Figure 2.*** *(02l) XRD features in the altered basalts compared to the those obtained by ChemMin for the John Klein and Cumberland drill holes in the Bradbury Formation at Gale Crater [5]; fsp = feldspar.*

**Properties of Fe(II)-Bearing Smectites:** Trioctahedral Fe(II)-Mg smectites were synthesized using a hydrothermal sol-gel procedure [6] to assess their chemical, structural, and spectral properties. These smectites show XRD features [(02l) and (060) positions] and VNIR spectra that systematically vary with composition

(**Fig. 3**). Notably, Fe(II)-rich smectites show diffraction features with longer d-spacings and weaker metal-OH bands between 2.1 and 2.5 μm compared to more Mg-rich clays. Synthetic smectites with octahedral Fe:Mg:Al ratios of 58:34:7 and 30:60:10 are closest compositional and structural matches to those produced by hydrothermal basalt alteration. Notably, the VNIR spectra of these phases are dominated by features typically associated with Mg-saponites, suggesting that Fe(II)-bearing smectite compositions may be overlooked in remote sensing of clay-bearing units on Mars.

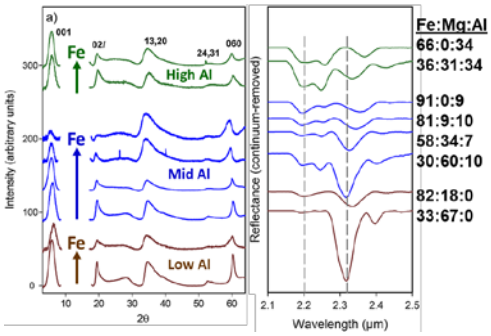


***Figure 3.*** *XRD patterns (left) and VNIR spectra (right) of smectites with varying octahedral cation ratios [6].*

**Oxidation Products of Fe(II)-Smectites:** Synthetic smectites in the mid-Al series (7-10% octahedral Al; Fig. 3) were exposed to $O_2$ and $H_2O_2$ to assess their susceptibility to oxidation and the resulting mineral products. The smectites were suspended in an air-saturated (dissolved $O_2$ as the oxidant) $CaCl_2$ solution for 1 week followed by hydrothermal recrystallization to allow the structure to relax. These were then oxidized in an air-saturated fluid a second time. In parallel experiments the smectites were oxidized by hydrogen peroxide and then hydrothermally recrystallized. The clays undergo gradual, partial oxidation of Fe(II) to Fe(III) in air-saturated fluids (Fig. 4), producing a mixed-valent tri- or di-trioctahedral smectite. Peroxide causes complete oxidation coupled to partial ejection of structural Fe, forming ferrihydrite or hematite nanoparticles. VNIR spectral bands (Fig. 4) progressively shift with iron oxidation, producing a strong band near 2.30 μm for the mixed-Fe(II)-Mg smectites most similar to those formed from basalt alteration. It has been noted that the prevalence of a ~2.30 μm VNIR reflectance band on Mars indicates clays with high Fe:Mg ratio [7], requiring chemical processes that fractionate Fe from Mg during basalt alteration. The present work shows that alteration of basalt followed by oxidation yields smectites with similar spectral features but subequal Fe:Mg ratios. Many Fe-Mg smectite occurrences on Mars, most of which date to early in the planet's evolution, may thus simply represent the oxidized remnants of initially ferrous iron-bearing clays formed via basalt alteration.

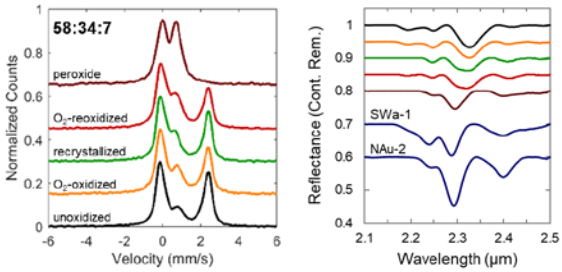


***Figure 4.*** *Mössbauer (left) and VNIR spectra (right) of a mixed Fe(II)-Mg smectite during progressive oxidation by $O_2$ and after complete oxidation by $H_2O_2$.*

**Implications for Smectites as Paleoredox Indicators:** The abundance of Fe-Mg smectite detections on Mars [1] indicates widespread alteration of the basaltic crust. The present work demonstrates that such clays will consist primarily of trioctahedral Fe(II)-Mg smectites. Such clays are susceptible to relatively rapid, partial to complete oxidation when exposed to photochemically-generated oxidants ($O_2$, $H_2O_2$) observed on Mars today. Fe-Mg smectites would have been similarly susceptible to oxidation during detrital transport on early Mars if oxidant-forming processes operated at the time. The redox state of Fe-Mg smectites in sedimentary settings on Mars may thus serve as viable paleoredox indicators if these phases lithify in units that are protected from later oxidation.

The use of Fe(II)-Mg smectites as redox indicator phases may be complemented by also examining co-existing redox-active mineral, such as iron sulfides and magnetite. Both phases have been detected in the Bradbury Formation in Gale Crater, along with a possibly mixed-valent trioctahedral smectite [5]. The specific presence of pyrrhotite indicates a detrital origin for sulfides, and while magnetite and smectite have been interpreted to be authigenic [8], this study shows that a detrital origin is also plausible. Other phases in the Bradbury Formation, such as hematite and akaganéite, do indicate that the sediments experienced oxidizing conditions. However, the mineral assemblages present are not equilibrated and the ferric minerals, along with non-stoichiometric magnetite, may indicate later, localized oxidation. Resolving the timing of deposition, diagenesis, and oxidation is critical to evaluating the redox evolution of early Mars using sedimentary deposits.

**References:** [1] Ehlmann B.L. and Edwards C.S. (2014) *AREPS*, *42*, 291-315. [2] Julia F. et al. (2014) *Eng. Geol.*, *183*, 80-95. [3] Alt J.C. et al. (1986) *JGR*, *91*, 309-335. [4] Andrews A.J. et al. (1983) *Init. Rep. DSDP*, *69*, 585-588. [5] Vaniman D.T. et al. (2014) *Science*, *343*, 1243480. [6] Chemtob et al. (2015) *JGR*, *120*, 1119-1140. [7] Michalski et al. (2015) *EPSL*, *427*, 215-225. [8] Hurowitz J.A. et al. (2017) *Science*, *356*, eaah6849.

**RELEVANCE OF PITTED MATERIAL AND IMPACT MELT TO EARLY MARTIAN HYDROTHERMALISM AND HABITABILITY; RIES EJECTA DEPOSITS AS A MARTIAN ANALOGUE.**

C. M. Caudill[1], R. N. Greenberger[2], L. L. Tornabene[1], G. R. Osinski[1,3], R. L. Flemming[1], B. L. Ehlmann[2,4]. [1]Centre for Planetary Science and Exploration / Dept. Earth Sciences, University of Western Ontario, Canada, [2]Jet Propulsion Laboratory, California Institute of Technology, Pasadena, California, USA, [3]Dept. Physics and Astronomy, University of Western Ontario, Canada, [4]California Institute of Technology, Pasadena, California, USA.

**Introduction:** Impact structures and their ejecta deposits act as windows into the mineral, lithologic, and volatile composition of planetary crusts. The Ries impact structure (~24 km-diameter, Germany) has arguably the best preserved and best studied ejecta deposits on Earth. The two main deposit types described are a melt-poor/free ballistically-emplaced impact breccia [1, 2] overlain by a discontinuous impact melt-bearing breccia (e.g., [3]). The top-most, melt-bearing breccia deposits at the Ries impact structure host evidence of post-impact hydrothermal alteration [e.g., 4, 5]. One style is found as disseminated, ephemeral systems in the impact melt-bearing ejecta unit associated with vertical degassing pipe structures [6, 7]. As melt-rich ejecta deposits are emplaced over volatile-bearing material, a degassing of the underlying layer is proposed to have occurred [6, 8]; this is also the preferred interpretation of pitted material observed in Martian crater fill and ejecta deposits [9, 10, 11].

As Earth and Mars both have volatiles, the Ries impact structure can provide ground-truth field data relevant to understanding impactite deposits on other planetary bodies due to excellent exposures and preservation states. The Ries site allows examination of the effect of volatiles on materials during and after impact cratering [12]. The melt-bearing unit at Ries has been altered through various processes [13, 14] and is dominated by phyllosilicate minerals, both in the fine-grained matrix and infilling fractures and vesicles. Here, we report on hyperspectral mineral mapping of the degassing pipes specifically, supported by lab-based mineralogical studies. We discuss their relevance to: 1) Martian crater-related pitted material, 2) the origin of some phyllosilicates in the early Martian crust, and 3) early habitability potential on Mars.

**Methods:** Hyperspectral imaging of degassing pipe-bearing outcrops at the Aumühle quarry, Germany, were acquired in situ with a Headwall Photonics Inc. co-boresighted system custom built for the California Institute of Technology. The shortwave infrared (SWIR) sensor used in this study covers 1.0-2.6 µm with 640 spatial pixels, 283 spectral bands, and 6 nm spectral resolution, with spatial resolution on the order of several cm's in the field. The spectral characteristics were analyzed by calculating spectral parameters [e.g., 15] to map minerals and phases.

*Lab-based analysis:* Spot-size analyses of hand samples from Aumühle quarry exposures and degassing pipes observed in Wörnitzostheim 1965 and Otting drill cores were analyzed in the lab via SWIR spectroscopy and X-ray diffractometry. The ASD Inc. TerraSpec Halo spectroradiometer provided SWIR (1.0-2.5 µm) reflectance spectra at 8 – 9 nm resolution. The µXRD Bruker D8 Discover microdiffractometer [see 16], with a 100-500 µm beam diameter and Vantec-500 2D detector and general area detector diffraction system (GADDS) software, was also used. This yielded determinations of mineralogy and crystallinity (including texture and microstructural information) of 300 µm spot-size integrated areas of the hand samples.

**Results:** Preliminary results from our spectral analyses indicate the presence of hydrated and hydroxylated mineral phases. Figure 1 shows a map of the spatial distribution of representative clay mineral phases in the melt-bearing unit as they relate to degassing pipe features. The shapes and positions of absorption features indicate montmorillonite, nontronite, and calcite.

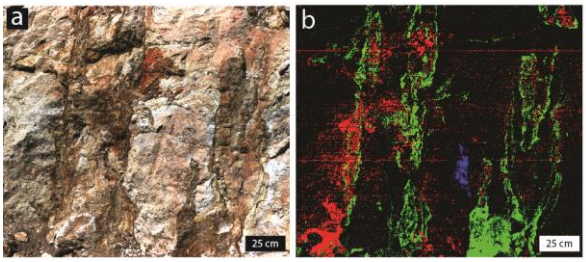


Fig. 1. Images of an outcrop at Aumühle quarry. a) Approximate true color composite of vertical degassing pipes within the Ries melt-bearing unit and b) corresponding mineral indicator map. Red: BD2200 parameter, showing common absorptions of Al-OH bearing minerals, as in montmorillonites; Green: BD2300 showing common features of Fe/Mg smectites; Blue: BD2340, having an absorption indicative of calcite. The melt-bearing lithology in the background was not highlighted, although it exhibits a 2.2 µm feature, weaker than the mapped BD2200 parameter which highlights the degassing pipes.

The bulk melt-bearing breccia unit is characterized spectrally by a mix of a weaker 2.2 µm feature (representing Si-OH and/or Al-OH bearing minerals), and the degassing pipes show a strong 2.30 µm feature (representative of Fe/Mg-OH bearing minerals [17], consistent with nontronite) shown as green. The interior of some degassing pipes shown in Fig. 1 appears to be

dominated by montmorillonite, while rimmed by nontronite. A shift from 2.2 to 2.3 μm results from an increased Fe/Al ratio in the dioctohedral site of the smectite, with a continuum of smectite compositions possible [18]. Calcite is present within the altered zone of the degassing pipes and is finely disseminated through the degassing pipes. Iron oxides are also abundant.

Laboratory SWIR data supports the field analysis, with the bulk unit being dominated by a 2.2 μm feature (consistent with montmorillonite) and the degassing pipes dominated by 2.30 – 2.32 μm features (consistent with Fe/Mg smectites nontronite and saponite). An enrichment of zeolites and minor chlorites are also associated with the degassing pipes.

Subtle differences in the 1D μXRD diffraction patterns show multiple clay phases with mixed-layer smectites. Superstructure composite peaks are present, which are common in montmorillonite interlayered with other clays, hydroxyls, and water molecules. The broad asymmetry of the peaks indicates turbostractic stacking. An asymmetric shoulder in peaks is indicative of an illitic component. When the 1D patterns are overlain on the correlating 2D GADDS image, these clay phases correlate to complete, broad rings indicating polycrystalline material and very fine grained crystallites [19]. These polycrystalline phases correlate to Fe-bearing oxides and hydroxides (goethite and hematite) as well as clays.

**Discussion:** This work suggests that multiple distinct clay mineral phases comprise the alteration mineralogy of the degassing pipes of the Ries. The degassing pipes have an Fe-oxide alteration within the pipes and as halos surrounding the pipes; the alteration halos also record multiple generations of clays with perhaps varying degrees and timing of hydrothermal alteration. Furthermore, the turbostratic stacking observed in the highly stratified clays indicates that they have not been subject to drying-wetting cycles, as would be expected of clays formed as the result of ambient surficial weathering [20], and thus strongly indicates a representative sampling of the original hydrothermal alteration. This is at odds with previous work on these deposits at the Ries: Newsom et al. [6] found an Fe-rich oxide or hydroxide coating on the degassing pipes and an absence of clay phase alteration; Muttik et al. [21] suggested that the smectite mineralogy is due to surficial alteration at ambient temperatures. We suggest that degassing pipes were formed in higher-temperature, water-saturated environments and were potentially longer-lived hydrothermal environments than has been previously thought.

More broadly, we seek to use the findings from Ries to investigate ties to Martian crater-related pitted material and the mineralogy of post-impact alteration as a potential source of hydrated silicates in the Noachian crust [e.g., 22]. The pitted materials are significant in regions where impact deposits from ancient Mars are relatively well-preserved. If indeed pitted materials are analogous to the degassing pipes at the Ries impact structure, they represent hydrothermal environments which are present in the shallow subsurface. It has been suggested that hydrothermally-altered melt-bearing impactites provided environments conducive to microbial colonization, providing water, thermal energy, and essential macro and micronutrients that are present in natural impact glass [e.g., 23, 24, 25]. Clays and zeolites produced as secondary impact-hydrothermal minerals are known to act as mineral structure templates and are catalysts for prebiotic synthesis [26]. Impact craters therefore may be prime astrobiological targets. Investigation of potential ancient impact-hydrothermal systems and associated secondary clay substrates, expressed as impact-related pitted deposits in the shallow subsurface, may yield a best-case scenario for preservation and exploration of biologic signatures. Furthermore, elucidating the mineral provenance and thus past processes of the ancient terrains of Mars through such analogous studies are essential in understanding early environments and habitability potential.

**References:**

[1] Morrison, R.H. and Oberbeck, V.R. (1978) 9th LPSC, #3763-3785. [2] Hörz (1982) Geol. Soc. Am. 190, 39–55. [3] Osinski et al. (2011) Earth Planet. Sci. Lett. 310, 167–181. [4] Osinski, G. R. (2005) Geofluids 5: 202-220. [5] Sapers, H.M. et al. (2017) MAPS 52, 2, 351-371. [6] Newsom, H. E., et al., (1986) J. Geophys. Res. Solid., 91, E239-E251. [7] Sturm, S. et al. (2013) Geology 41: 531-534. [8] Wittmann, A. and Kenmann, T. (2007) Bridging the Gap Between Nature and Modeling II, Montreal. [9] Tornabene, L.L. et al. (2007) 7th Mars Conference. #3288. [10] Tornabene, LL. et al. (2012) Icarus. 220, 348-368. [11] Boyce, J.M. et al. (2012) Icarus 221: 262-275. [12] Kenkmann, T. and Schonian, F. (2006) Meteoritics & Planetary Science 41: 1587–1603. [13] Muttik, N. et al. 2010. Earth and Planetary Science Letters 299:190–195. [14] Osinski, G. R. 2005. Geofluids 5:202–220. [15] Viviano-Beck et al. (2014) JGR, v. 199, 1403-1431. [16] Flemming, R.L. et al. (2007) Canadian Journal of Earth Sciences, 44: 1333-1346. [17] Clark, R. N. et al. (2009) JGR. 95, 12653-12. [18] Ehlmann et al. (2009) JGR, v114, E2. [19] Klug, H.P. and Alexander, L. (1956) Wiley, New York, doi:10.1016/0001-6160. [20] Mamy, J. and Gaultier, J.P. (1976) Applied Publishing Co., Wilmette, Illinois, 149-155. [21] Muttik, N. et al. (2008) EPSL, 299, 190–195. [22] Tornabene et al. (2013) JGR. 118, 994-1012. [23] Saper, H.M. et al. (2014) Geology, 42, 6. [24] Banerjee, N. R. and Muehlenbachs, K. (2003) Geochemistry, Geophysics, Geosystems, 4, 1037-1059. [25] Osinski et al. (2017) *this conf.* [26] Cockell, C.S. (2006) Philos Trans R Soc Lond B Biol Sci., 361, 1845–1856.

**GEOMORPHIC EVIDENCE FOR A LATE HESPERIAN NORTHERN OCEAN AND ITS IMPLICATIONS FOR THE NOACHIAN.** S. M. Clifford[1] and F. Costard[2], [1]Lunar and Planetary Institute, 3600 Bay Area Blvd, Houston, TX, 77058 USA (clifford@lpi.usra.edu); [2]GEOPS, Université Paris-Sud, CNRS, Orsay, France.

**Introduction:** Rodriguez et al. [1] and Costard et al. [2] identified and mapped the distribution of lobate flow deposits that appear to have emanated from within the Martian northern plains and propagated from lower to higher elevations along the dichotomy boundary [Fig. 1]. The distribution of these deposits is consistent with the location of the possible paleoshoreline of a northern ocean (Contact 2, at an elevation of approximately -3760 m), previously identified by Parker et al. [3] and Clifford and Parker [4].

The lobate flows extend up to 150 km beyond the location of the proposed paleoshoreline, climbing local slopes and reaching elevations of over ~100 m. Backwash channels are also found in association with these deposits [Fig. 1]. Such features are strikingly similar to those associated with terrestrial tsunamis – suggesting that the Martian examples may have originated from one or more marine impacts.

Costard et al. [2] investigated the potential occurrence of impact-generated tsunamis in a northern ocean using a two-pronged approach: first, by analyzing the propagation of possible tsunamis originating from several potential source craters (~30–50 km in diameter), using numerical simulations based on well-validated terrestrial models, scaled to Mar and, second, by comparing these predictions with the actual geographic distribution of lobate deposits and backwash channels, mapped at high resolution, in northern Arabia Terra.

During an ocean impact, two successive waves are formed: the first one is produced by the expulsion of ocean water in the formation of the crater's transient cavity at the moment of the impact. The second is produced by the sudden inflow of ocean water which refills the transient cavity, rebounds at the crater's center, and then flows outward. For the three candidate source craters identified by Costard et al. [2], the predicted wave heights (above sea level) at the rim of the transient cavity are over 150 m, traveling at a speed of ~60 m/s. In the simulation, their predicted progagation through the plateaus and up the flat-floored valleys along the dichotomy boundary is virtually identical to the observed distribution of lobate flow deposits and backwash channels.

In addition, the predicted sedimentation patterns caused by the interference of the late-arriving second wave with the outgoing waves associated with the reflection and refraction of the initial tsunami wave by the dichotomoy boundary, are consistent with the distribution of the troughs and ridges which characterize

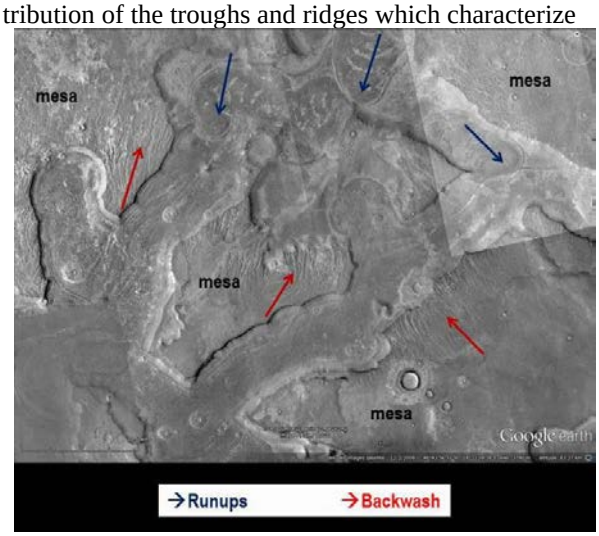


Figure 1. Examples of lobate debris flows (propogating upslope) and backwash channels along the dichotomy boundary in norther Arabia Terra, the likely product of one or more impacts into a northern ocean during the Late Hesperian [1, 2].

the enigmatic "thumbprint terrain" found along the plains boundary in northern Arabia Terra [5, 6].

The strong similarities between the geomorphic characteristics of the Martian lobate deposits and terrestrial tsunami deposits, as well as the close agreement between the observed and predicted distribution of impact-generated deposits and backwash channels along the dichotomy boundary [Figure 2], provides new and compelling evidence of the existence of a Martian northern ocean as recently as the Late Hesperian (LH, ~3 Ga).

The volume of water necessary to fill the northern plains to the elevation of Contact 2 (-3760 m) is ~100 m GEL [7]. But this is only a portion of the planetary inventor of water that must have existed at this time. Given geologically reasonable estimates of the mean permeability of the top ~25 km of the Martian crust (i.e., $\geq 10^{-15}$ m$^2$) and the likely depth of hydraulic continuity (~10-26 km), virtually all of the interconnected crustal porosity, lying beneath the absolute elevation of the northern ocean sea level, must have been saturated with groundwater – representing a total volume of ~225 m GEL [4].

A susbstantial quantity of water must have also been cold-trapped in the cryosphere as ground ice. With temperatures that extend well below the freezing

point of water, the Martian cryosphere represents the dominant thermodynamic sink for for both crustal and atmospheric $H_2O$ on Mars. With regard to the subsurface, a geothermal gradient as small as 15 K/km can induce a thermal vapor flux between a subpermafrost reservoir of groundwater and the base of the cryosphere of up to ~1 km GEL of $H_2O$ every ~$10^7$ years, insuring that the pore volume of the cryosphere has remained saturated with ice throughout its evolution, for as long as a reservoir of subpermafrost groundwater survived [1]. The estimated pore volume of the cryosphere at the end of the LH suggests that it may have stored ~300 m GEL of $H_2O$ as ground ice [4].

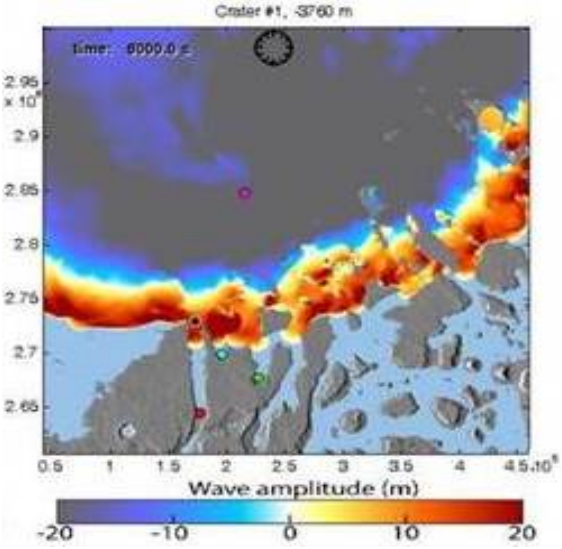


Figure 2. A simulation of a Late Hesperian impact into a northern ocean with a sea level of -3760 m for one of three candidate impact craters [2]. The predicted distribution of lobate debris flows and backwash channels associated with the resulting tsunami is an excellent match to their observed distribution along the dichotomy boundary.

Finally, there is evidence that the south polar layered deposits (SPLD) were far more extensive in the Late Hesperian than they are at present. Based on an analysis of the original extent and thickness of the Dorsa Argentia Formation (which is thought to be an eroded remnant of the Late Hesperian SPLD), Ghatan and Head [8] estimate a water total ice volume of ~30 m GEL.

This analysis suggests that the total planetary inventory of water on Mars at the end of of the Hesperian was ~655 m GEL. But what was the size of the planetary inventory during the Noachian? And how might this have affected the existence of a northern ocean?

Estimates of the the amount of water added to the planetary inventory between 4 and 3 Ga ago fall in the range of ~5-10 m GEL by extrusive volcanism -- which is roughly the same amount that is believed to have been lost by exospheric escape. Assuming the polar inventory was the same or smaller (due to the expected warmer temperatures that are thought to have characterized the Noachian [9-11]), that means that the total inventory of water on Mars 4 Ga was likely similar to that at the end of the LH. The most significant difference between these two eras is that the ~33% higher heat flow during the Noachian [12] means that the cryosphere would have been significantly thinner, thus the inventory of liquid $H_2O$ during the Noachian (i.e., the sum total stored as groundwater, in a northern ocean, and as lakes and seas), would have been ~100 m GEL greater [Figure 3]. This implies that the Noachian northern ocean was at least ~10% more areally extensive than the one that existed at the end of the LH – a conclusin that has important implications for understanding the evolution of the Martian hydrosphere and the potential for the origin and survival of life.

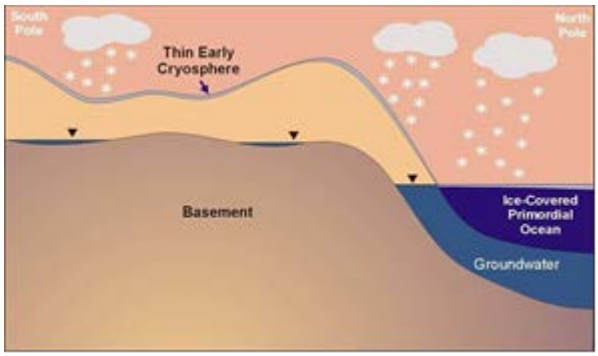


Figure 3. The relationship between the various reservoirs of surface and subsurface water on Mars during the Noachian and Late Hesperian, including a northern ocean, groundwater, the south polar layered deposits and ground ice in the cryosphere [4]. The principal difference in the amount and distribution of water between these two eras is that the higher heat flow of the Noachian would have reduced the amount of $H_2O$ cold-trapped in the cryosphere, resulting in another ~100 m GEL of liquid water that would have been available as groundwater and as surface water in a northern ocean.

**References:** [1] Rodríguez, J. A. P., et al. (2016), Nat. Scie. Rep., 6, 25106, doi:10.1038/srep25106. [2] Costard, F. et al. (2017), JGR-Planets, 122(3), 633-649. [3] Parker et al. (1993), JGR, 98, 11,061–11,078, doi:10.1029/93JE00618. [4] Clifford, S. M., & Parker, T. J. (2001). Icarus, 154(1), 40-79. [5] Schaefer, M. W. (1990), Icarus, 83(1), 244-247. [6] Lockwood et al. (1992), LPSC Abstracts, vol. 23, p. 795. [7] Head, J. W. et al. (1999), Science, 286(5447), 2134-2137. [8] Ghatan, G. J., & Head, J. W. (2002), JGR-Planets, 107(E7). [9] Forget, F. et al. (2013), Icarus, 222(1), 81-99, doi:10.1016/j.icarus.2012.10.019. [10] Wordsworth, R.. F. et al. (2013), Icarus, 222(1), 1-19, doi:10.1016/j.icarus. 2012.09.036. [11] Wordsworth, R.D. et al. (2015), JGR-Planets, 120(6), pp.1201-1219. [12] McGovern, P. et al. (2004), J. Geophys. Res, 109, E07007.

**THE GEOLOGIC EVIDENCE FOR A WARM AND WET EARLY MARS.** R. A. Craddock[1], R. P. Irwin, III[1], A. D. Howard[2], and A. M. Morgan[1,2], [1]Smithsonian Institution, Center for Earth and Planetary Studies, National Air and Space Musem, MRC-315, Washington, DC 20560, craddockb@si.edu, [2]University of Virginia, Department of Environmental Sciences, 205 Clark Hall, 291 McCormick Road, Charlottesville, VA 22904.

**Introduction:** After decades of exploration the climatic history of Mars remains a contentious issue, primarily because climate models have failed to reconcile the faint young sun problem [e.g., 1]. Arguments that early Mars was cold and dry continue to persist, but the geologic evidence for a warmer and wetter early Mars is unequivocal.

**The Geologic Evidence:** There are two suites of geologic features that attest to a warmer, wetter climate during the Noachian. The oldest features are modified impact craters, which typically lack crater rims, are steep sided, and have a flat floors (Figure 1). However, there are varying degrees of crater modification that are preserved at a range of crater diameters [2, 3]. This variation in modification that is independent of crater diameter indicates that crater erosion operated continuously (if not episodically) throughout the Noachian as new craters were forming [2, 3]. Analysis of the preserved crater morphology indicates that a combination of linear diffusional creep and advective processes were responsible, which is best explained by rainfall and surface runoff [3, 4]. While other processes have been suggested to explain one or both of the observed processes, such as liquefaction induced by subsequent impact cratering to explain the observed diffusional component in crater morphology [e.g., 5], the efficiency in such processes would scale poorly to crater diameter and would be areally limited to areas near fresh impact craters, which is not observed [e.g., 4]. Modified impact craters attest to an arid climate during the early and middle Noachian where precipitation occurred, but the resulting runoff was limited to do low intensity precipitation events, high evaporation rates, or high transmission losses.

Although valley networks are most commonly cited as evidence that liquid water was once stable on the Martian surface [10], it is now apparent that their formation was restricted to the end of the Noachian and the beginning of the Hesperian when climatic conditions become ideal [e.g., 5]. This is suggested by the fact that valley networks have lower preserved drainage densities, shorter lengths, relatively constant widths, and low sinuosity [5, 6]. Sharp divides between tributaries are rare, and most intervalley surfaces are poorly dissected, so that the valley networks are not well integrated with the surrounding cratered landscape, [5, 6]. Simulations modeling shows that if the more humid conditions that supported valley network formation persisted, drainage density would have improved and the martian highlands would have become more dissected [e.g., 7]. Nevertheless, the scale of erosion represented by many valley network systems is immense and can often rival the Grand Canyon (Figure 2), and the volume of water necessary to erode them would have been massive [8]. Quantitative evaluation of their paleohydrology also indicates that their formation took place over a prolonged period (i.e., hundreds of thousands of years at least) [9]. Conditions for alluvial fan formation also became favorable [e.g., 10]. In addition, the Hesperian supported the formation of outflow channels through the catastrophic release of liquid water [11]. There is also compelling evidence for an ocean in the northern hemisphere, too [12, 13]. Thus, the Hesperian represents a brief period in which the climate became more humid, precipitation intensity increased, or transmission losses were reduced due to changes in the surface lithology (e.g., formation of a duricrust). Rainfall intensity and climatic conditions may have been influenced by waning atmospheric pressures through time [14]. Collectively, the entire suite of geologic features attest to the fact that Mars experienced periodic if not sustained precipitation during the Noachian and through the Hesperian [e.g., 4].

**The Case Against The "Icy Highlands" Scenario:** In the absence of a model supporting a warm and wet early Mars, many alternative scenarios for interpreting the geology have been presented over the years. The current is the "icy highland" model [e.g., 15]. However, there are many weaknesses with this scenario. (1) There is no physical evidence for extensive snow or ice sheets in the equatorial highlands. While this have been explained as a result of cold-based glaciation, cold-based glaciers move and deform resulting in significant modification of the underlying landscape [e.g., 16]. In fact, even in Antarctica there is evidence that cold-based glaciers entrain, slide and abrade their beds [17]. (2) Aggradation of snow or ice simply does not explain the morphology of modified impact craters [3, 4, 5]. (3) Valley networks follow the local topography, initiate at topographic divides, are often deep (100s of meters), steep sided, and v-shaped. None of these characteristics are common of streams formed in glacial environments [e.g., 18]. Valley networks are also found to intersect impact craters, fill them with water, and overflow downslope, which re-

quires a hydrologic cycle that is not explained by the icy highlands scenario [5, 6, 7, 8, 9].

**Future Work:** We are currently looking at the record of modified impact craters to understand the history of water at least through the Noachian. We are also analyzing several different valley network systems to identify possible variations in the types of geologic processes that operated and their intensity. Ultimately, if climate models cannot reconcile the astronomy, geology, and meteorology, then climate modelers need to explore other possibilities. However, any model needs to be based in the geology. The implications are not only for understanding the history of water on Mars, but the origin of life on Earth as well as the habitable zones of extrasolar planets.

**Figure 1.** Examples of modified impact craters. These are located at high latitude (56.93° S, 24.75° E). The crater at the bottom is ~30-km in diameter. Note the absence of valley networks and the varied degree of crater modification. Craters such as these suggest that modification processes were ubiquitous in the early Noachian and that the climate conditions supporting erosion was global.

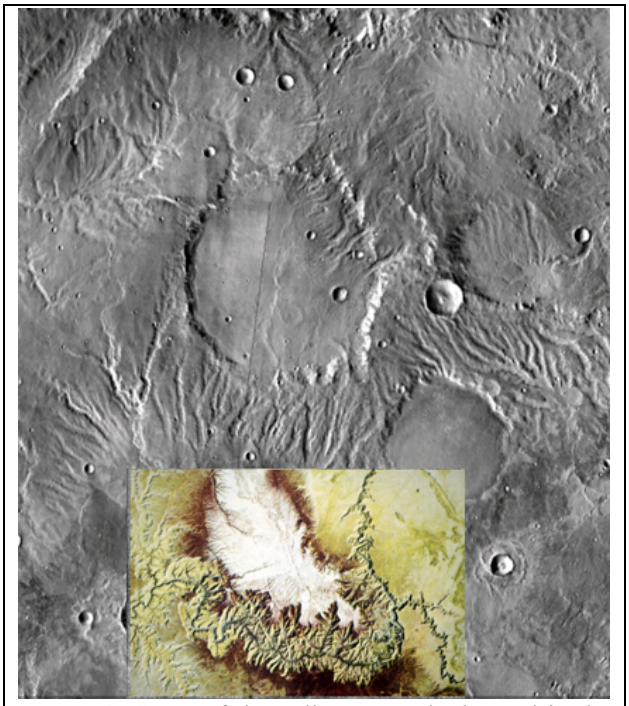

**Figure 2.** Some of the valley networks located in the Iapygia region of Mars (5.97° S, 56.22° E). The modified impact crater located in the center of the image is ~58-km in diameter. The colored insert at the bottom shows the Grand Canyon at the same scale.

**References:** [1] Wordsworth, R. et al. (2013) *Icarus*, *222*, 1-19. [2] Craddock, R. A. and T. A. Maxwell (1993) *JGR*, 98, 3453–3468. [3] Craddock, R. A. et al., (1997) *JGR*, *102*, 13321-13340. [4] Craddock, R. A. and A. D. Howard (2002) *JGR*, *107(E11)*, 10.1029/2001JE001505. [5] Irwin, R. P., III et al. (2005) *JGR, 110*, E12S15, [6] Fasset, C. I. and J.W. Head, III (2008) *Icarus, 198,* 37-56, [7] Matsubara, Y. et al. (2013) *JGR*, *118*, 1-23, doi:10.1002/jgre.20081. [8] Luo, W. et al. (2017) *Nature Comm.*, *8*, 15766. [9] Irwin, R. P., III et al. (2005) *Geology, 33(6),* 489–492. [10] Morgan, A. M. et al. (2014) *Icarus*, *229*, 131-156. [11] Baker, V. R. (2001) *Nature, 412,* 228-236. [12] Parker, T. J. et al. (1989) *Icarus, 82*, 111-145. [13] Head, J. W., III et al. (1999) *Science*, *286*, 2134-2137. [14] Craddock, R. A. and R. Lorenz (2017) *Icarus*, *293*, 172-179. [15] Fastook, J. L. and J. W. Head (2015) *PSS*, *106*, 82-98. [16] Hall, A. M. and N. F. Glasser (2003) *Boreas*, 32, 191– 207. [17] Cuffey, K. M. et al. (2000) *Geology*, *28*, 351-354. [18] Livers, B. and E. Wohl (2015) *Geomorphology*, *231*, 72-82.

**Clay Minerals as Nutrient Sources for Life on Mars.** P. I. Craig[1], R. L. Mickol[2], P. D. Archer[3], T. A. Kral[2,4], [1]Lunar and Planetary Institute, 3600 Bay Area Blvd, Houston TX 77058 (craig@lpi.usra.edu), [2]Arkansas Center for Space and Planetary Sciences, University of Arkansas, Fayetteville, AR 72701, [3]Jacobs at NASA Johnson Space Center, Houston, TX 77058, [4]Dept. of Biological Sciences, University of Arkansas, Fayetteville, AR, 72701.

**Introduction:** Clay minerals have been identified on Mars' oldest (Noachian) terrain and their presence suggests long-term water-rock interactions. The most commonly identified clay minerals on Mars to date are nontronite (Fe-smectite) and montmorillonite (Al-smectite) [1], both of which contain variable amounts of water both adsorbed on their surface and within their structural layers. Over Mars' history, these clay mineral-water assemblages may have served as nutrient sources for microbial life.

**Methods:** Two methanogen species, *Methanobacterium formicicum* and *Methanosarcina barkeri*, were tested for their ability to grow in the presence of nontronite, montmorillonite, or a mixture of both, without the use of additional nutrients. In the first batch of experiments, two grams of each mineral were added to each of five test tubes. In the second set, test tubes consisted of a mixture of one gram of each mineral. The tubes were placed into a Coy Anaerobic Chamber to deoxygenate overnight. Ten milliliters of bicarbonate buffer were added to each tube. The tubes were sealed with crimps, then sterilized via autoclave. Before being inoculated into the sterilized clay solutions, methanogens were aerobically washed [2]. Next, 0.5 mL cells+buffer were added to each tube. The tubes were pressurized with 2 bar $H_2$, incubated at 37°C, and monitored over time for methane production. Each set also included negative controls (clay mineral only, no microbes) that underwent identical experimental conditions as those tubes with microbes.

After 70 days, the minerals were removed from the tubes and analyzed for the presence of possible biosignatures in the form of mineralogical changes using X-ray diffraction (XRD), chemical changes using scanning electron microscopy with energy dispersive spectroscopy (SEM/EDS), and volatile and organic content with evolved gas analysis (EGA).

**Results:** *M. barkeri* failed to produce significant methane in any of the 2 g nontronite or 2 g montmorillonite sets but did show slight growth after ~30 days in the mixture set. *M. formicicum* produced the most methane on montmorillonite, but was unsuccessful with nontronite (Fig. 1).

No mineralogical changes were observed via XRD in any of the reacted clay minerals [3]. However, SEM/EDS analysis showed micro-scale textural changes in montmorillonite with *M. formicicum* and elemental depletions in the new textures. Figure 2 shows a sample of montmorillonite after being altered by *M. formicicum*. The bright, "fluffy" texture is chemically similar to the montmorillonite from the negative control group. However, there is also a darker, smoother texture that is depleted in Fe, Na, Mg, and Al relative to the control.

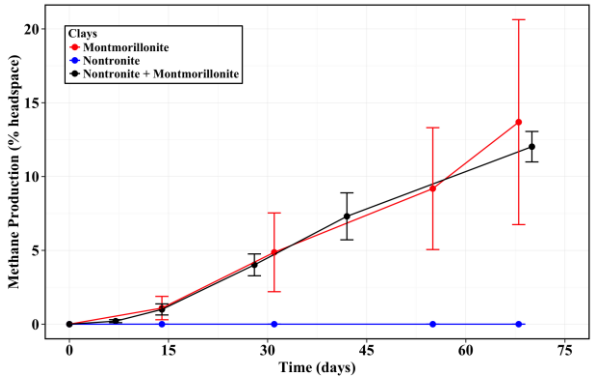


Figure 1. Methane production by *M. formicicum* in media containing solely bicarbonate buffer and clay mineral.

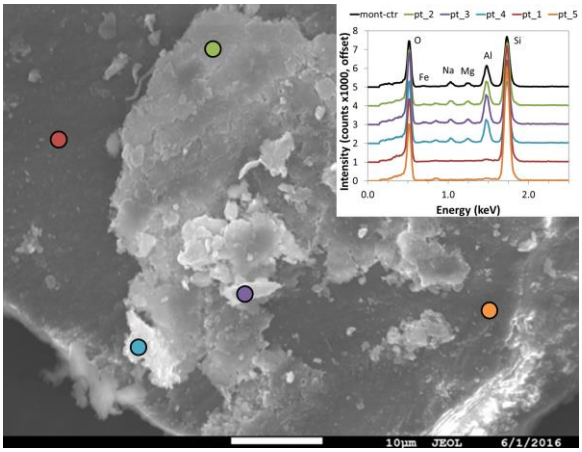


Figure 2. SEM/EDS analysis showing new texture and elemental depletion of montmorillonite with *M. formicicum*.

Montmorillonite altered by *M. formicicum* showed another textural difference from the control sample of montmorillonite. This texture is depleted in Fe and Mg but appears enriched in Na relative to the control montmorillonite sample. This could be a relative enhancement of Na due to a depletion of other elements.

Samples of *M. formicicum* in montmorillonite and mixed montmorillonite/nontronite that showed the highest production of methane were subjected to EGA on instruments that have been configured to reproduce

the instrument operating conditions of the Sample Analysis at Mars (SAM) instrument on the Mars Science Laboratory (MSL) *Curiosity* rover [4]. Samples were heated to ~1000°C at 35°C/minute in a 30 mbar atmosphere using He as a carrier gas at a flow rate of ~0.8 sccm.

Samples incubated with microbes show clear differences from control samples, particularly for m/z (mass/charge) 44, which is likely $CO_2$ evolution (Fig. 3). Additional work is needed to determine if this increased $CO_2$ released around 150°C is the result of the decomposition of the microbial biomass itself or due to biologically-mediated changes to the original clay minerals. Other masses, such as m/z 18 ($H_2O$), also show differences between the control samples and samples with microbes.

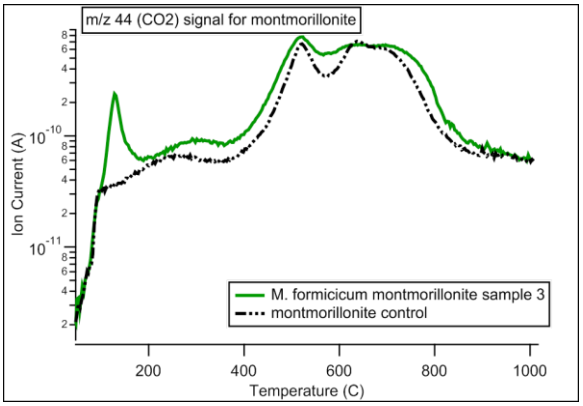


Figure 3: EGA curves for the control montmorillonite and montmorillonite with *M. formicicum.*

**Discussion:** Our experiments were specifically designed so that the methanogens would be deprived of the supplements they use to thrive and force them to utilize nutrients from the clay mineral substrate. Of the two species and three substrates tested, *M. formicicum* fared the best on montmorillonite. Although no mineralogical changes were detected via XRD, SEM analysis showed two new textures different from the control montmorillonite sample. Not only were new textures created as a result of biological alteration, these new textures were of a different chemical composition from the control montmorillonite. We view this as proof that the methanogens were forced to draw their nutrients from the clay minerals substrate. This suggests that this sort of nutrient utilization could have taken place, or could still be taking place, on Mars.

**Implications for Mars:** An Al-phyllosilicate akin to montmorillonite is among the most commonly identified clay minerals in the martian Noachian terrain. The presence of clay minerals suggests eras of long-standing, near-neutral, liquid water on the surface. These conditions create a setting for the development and sustainability of microbial life.

If methanogens did once occupy the surface or subsurface of Mars, they would have relied on their surroundings for nutrients. We have shown that at least one species of methanogen can indeed survive using only montmorillonite as a source of nutrients.

If methanogens do occupy the current martian subsurface (it has been theorized that the radiation environment would not support methanogens on the surface), the microbes could still be utilizing nutrients from clay mineral substrates. The results of this utilization is the production of methane, which could be the source of recently observed methane plumes on Mars. Short-lived increases of atmospheric methane have been detected both from orbiters over Nili Fossae [5] and in Gale Crater by the SAM instrument on the MSL *Curiosity* rover [6].

**Conclusions:** We have shown that methanogens can utilize nutrients from montmorillonite without supplemental media. Not only can methanogens utilize montmorillonite for their nutrients, we have identified potential biosignatures in the form of textural and chemical changes in the minerals. Although mineralogical changes were not identified, given more time or increasing the ratio of methanogens to minerals could increase the amount of altered clay minerals above the detection limits of XRD. We will compare our laboratory data to observations of Mars in order to identify potential biosignatures on Mars.

**Future Work:** Based on the promising results of our 70-day experiment, we have conducted a second set of experiments lasting 195 days. The idea is to allow the methanogens more time to alter the clay mineral substrate such that the volume of altered material would be detectable using instruments akin to those on a Mars rover or orbiter. In this set, we used montmorillonite, nontronite, kaolinite, and mixtures of these. Initial results show that the methanogens still produce methane after 195 days, indicating growth without the use of supplemental media, and we will show results of the mineralogical analyses of the altered clay mineral substrate.

**References:** [1] Carter, J., et al., (2015) *Icarus* 248, 373-382. [2] McAllister, S.A., and Kral, T.A., (2006) *Astrobio* 6, 819-823. [3] Mickol et al., (2016) *Biosig. Workshop*, #2035. [4] Archer, P.D. Jr, et al., (2014) *JGR* 119, 237-254. [5] Mumma, M., et al., (2009) *Science* 323, 1041-1045. [6] Webster, C., et al., (2015) *Science* 347, 415-417.

**HYDROLOGICAL AND CLIMATIC SIGNIFICANCE OF MARTIAN DELTAS.** G. Di Achille and D. A. Vaz, INAF, Istituto Nazionale di Astrofisica, Osservatorio Astronomico di Teramo, Italy, diachille@inaf.it.

**Introduction:** During the last years, the availability of high resolution topography, imagery, and hyperspectral datasets of the martian surface led to the discovery and detailed geological studies of tens of possible ancient fluvio-lacustrine deposits. Among the latter deposits, deltaic systems are considered to be the most prominent evidence suggesting the existence of bodies of standing water during the Early Mars [e.g. 1-8]. Furthermore, deltas might be key to understanding potentially habitable periods in Mars history.

However, despite their potential as paleoclimatic indicators, the open questions about the formation and evolution of martian deltas often make their hydrological/climatic interpretations uncertain. In fact, it is unclear whether martian fluvio-deltaic deposits formed during extended epochs of clement climatic conditions (and thus if they are unequivocal indicators of favorable conditions for life) or during limited and episodic events produced by regional factors, like for example impact craters, volcanism, or tectonics [e.g. 9, 10] and resultant hydrothermal activities and/or under more cold/dry conditions by alternative depositional mechanisms (e.g. lava flows? High viscosity/density mass-wasting? lahar/mud flows?) to fluvio-lacustrine deposition (and thus if they could have been formed also under climatic conditions not necessarily different from present Mars thus likely prohibitive for life).

Here, we a) review the geomorphology, sedimentology, and mineralogy of the martian deltas record and b) present the results of a quantitative study of the hydrology and sedimentology of martian deltas using modified version of state of the art terrestrial model Sedflux [11] whose concepts have been vetted in several different terrestrial settings and also for Mars [12].

**Geomorphology and sedimentology:** Among the known martian deltas only a few (Eberswalde [1], Jezero [2], Sabrina and Hypanis [6], Moa Valles [4]) show well-developed stratigraphy with evidence of avulsing channels and multilobate depositional patterns; they are the largest deposits (in terms of surface area and volume) and are found exclusively at the mouth of relatively large valleys with tributaries and alluvial plains that were presumably formed by sustained and persistent surface runoff discharges [13, 14]. The latter deposits might be strictly interpreted as river-deltas and are typically found as highly eroded deposits without original depositional surfaces. Whereas, the majority of Martian deltaic deposits are small (a few km wide and long) single-lobe with deep (and often steep) delta front resembling terrestrial Gilbert-type fan-deltas. These deposits are tipically found at the mouth of short (often theather-headed) valleys lacking tributaries and alluvial plains [13, 14]. The latter deltas do not show evident signs of avulsion and multilobate depositional patterns and are typically well preserved showing relatively pristine morphology.

Therefore, from the geomorphological/sedimentologic point of view, Martian deltas can be divided into two main categories [13, 14]: a few highly eroded (older? Noachian?), sedimentologically complex/mature, multilobate, and relatively large deposits fed by regionally integrated valley networks (hereinafter referred to as “river-like deltas”) and many small, well-preserved (younger? Post-Noachian?), sedimentologically simple/immature, single-lobe fan-deltas fed by isolated valleys (hereinafter referred to as “fan-deltas”).

**Mineralogy:** The mineralogy of martian deltas has been investigated with CRISM data during the last years [e.g. 15, 16]. Clear evidence for spatially diffuse phyllosilicates have been identified only in few deltaic sites (always associated to river-like deltas) [15] while the majority of deposits are characterized by either the absence of unambiguous evidence for aqueous alteration or only minor phyllosilicate detections [16]. Therefore, the abovementioned morphological duality of martian deltas seems to be visible also from the mineralogic point of view, with river-like deltas showing convincing evidence for clay minerals and fan-deltas lacking of significant mineralogical evidence for a sustained aqueous activity.

**Numerical modeling:** Using the Sedflux model [11, 12] we completed hundreds of parametric simulations to estimate the minimum formation time for deltas as a function of river width and depth and resulting water and sediment discharges. Particularly, we used channel depths ranging from 3 to 25 meters and channel width from 5 to 5000 meters while sediment and water discharges were derived form the river morphometric paramenters using Darcy-Weisbach formulations and sediment transport predictors described in [12]. In parallel with parametric simulations we tried to reproduce actual martian deltas deriving input parameters, like for example the bathymetry of the receiving basin and the channel width and depth and thus water and sediments discharges at the mouth of the river, from remote sensing imagery and topography, i.e. high resolution digital elevation models (DEMs) from CTX and HiRISE stereopairs. With respect to previous analog studies [e.g. 17, 18] our approach is more repre-

sentative of actual deltaic deposition since the model simulates several depositional/erosional processes, such as surface plumes, bedload transport, sediment slope failure, turbidity currents, debris flows, subsidence, compaction, water base level changes, sediment remobilization due to waves and currents, and subaerial erosion and deposition by river on the delta plain. Moreover we believe that input parameters used by previous studies [17, 18], and particularly river depth, which is one of the most important parameter affecting the sediment transport processes, are highly unrealistic likely as a result of wrong geologic/hydrological assumptions. As an example, in [17, 18] the authors used 'delta forming' river depths down to 100 meters deep for determining water and sediment discharges with the wrong assumption that the maximum depth of the tens of kilometers long feeder valleys would be representative of the deltaic depositional process. On the contrary, we used a range of typical terrestrial river width and depths for parametric simulations while we derived the latter parameters from HiRISE DEMs of channels visible on delta plains for the simulation of actual deposits. Finally, output files include three dimensional grids of sediment property, bathymetric slope, water depth, grain size distribution, etc.

Results from both the parametric simulations and the sedimentary characterization of a significant portion of the known martian deltas, obtained by using different assumptions and combinations of water discharges and sediment load, point to minimum formation timescales in the order of $10^2$-$10^3$ years for fan-deltas while $10^4$ years figures are obtained for the largest river-like deltas. These latter results confirm again the already mentioned morphological and mineralogical duality, suggesting that fan-deltas, in particular, might have not been exclusively formed during extended epochs of clement climatic conditions. In fact, this time range could be compatible with a formation by alternative mechanisms even under relatively cold/dry environmental conditions.

**Summary and discussion:** Morphology, sedimentology, mineralogy and minimum formation timescales of martian deltaic deposits show a noticeable duality, which raises many questions about their formation and evolution. This shall suggest to the martian scientific community to open a thoughtful discussion on the hydrological and climatic interpretations of these deposits. Indeed, the right interpretation and understanding of martian deltas is fundamental to answer many questions about Early Mars, its amount of water (and its sources: rain? ice melting?) and for how long water was stable at surface and its fate. From these latter answers we might infer the climate of Early Mars and its modifications with time.

Our results suggest that the majority of martian deltas (i.e. the fan-deltas) might have not been exclusively formed during extended epochs of clement climatic conditions and that episodic events, like impacts and volcanism, could have produced them likely even without necessarily influencing the planet's climate on a global scale. Therefore martian fan-deltas do not necessarily imply the occurrence of favorable and durable conditions for life, also raising the question on whether paleolakes with fan-deltas shall be considered as ideal landing sites for future in situ exploration of Mars.

Finally, reconsidering the geologic evidence about martian deltas to comply with results from climate modeling is crucial. Indeed, our results are in agreement with recent overviews about early Mars climate, suggesting that Mars climate was more variable and transient through time than thought before and forced mainly by a combination of orbital and external factors [19] and/or that lacustrine environments might have formed by processes that allowed for confined hydrological activity under cold conditions [20].

**References:** [1] Malin, M. C., and Edgett, K. S. (2003), Science, 302, 1931-1934. [2] Fassett C. I. and Head J. W. (2005), GRL, 32, L14201. [3] Irwin, R. P. et al., (2005). JGR (1991–2012), 110(E12). [4] Salese et al (2016), J. Geophys. Res., 121, 194-232. [5] Di Achille et al, (2006), J. Geophys. Res., 111, E04003. [6] Di Achille, G., G. G. Ori, and D. Reiss (2007), J. Geophys. Res., 112, E07007. [7] Hauber, E. et al. (2009), Planet. Space Sc., 57(8), 944-957. [8] Di Achille G. and Hynek B.M. (2010), Nature Geo., 3, 459-463. [9] Brackenridge G. R. et al. (1985), Geology, 13, 859-862. [10] Halevy I., and Head, J. W. (2014), Nature Geo., 7, 865-868E. [11] W. H. Hutton and J. P. M. Syvitski (2008), Computers & Geosciences 34, 1319–1337 [12] Hoke, M.R.T. et al. (2014), Icarus, 228, 1-12. [13] Di Achille and Salese (2015), 46th LPSC, Abstract #2609. [14] Goudge et al. (2016), Geology, 44, 419-422. [15] Ehlmann B. et al (2008), Nature, Nat. Geoscience, 1(6), 355-358. [16] Osterloo M. and Kierein-Young K (2017), EGU Gen. Assembly, Abstract #2017-9389. [17] Kleinhans M. G. (2005), JGR, 110, 12003. [18] Kleinhans M. G. et al (2010), Earth a nd Plan. Sc. Lett, 294, 294, 3-4, 378-392. [19] Wordsworth R. D. (2016), Annu. Rev. Earth Planet. Sci., 44, 381-408 [20]. Bristow T. F. et al. (2017), PNAS, 114(9), 2166-2170.

**Early Mars-relevant Investigations Within the MEPAG Science Goals.** S. Diniega[1], D. Banfield[2], J. Johnson[3], V.E. Hamilton[4], B. Carrier[1], J.W. Ashley[1], D.W. Beaty[1], R. Zurek[1]. [1]Mars Program Office, Jet Propulsion Laboratory, California Institute of Technology, Pasadena, CA 91109 (serina.diniega@jpl.nasa.gov); [2]Cornell University; [3]John Hopkins University, Applied Physics Laboratory; [4]Southwest Research Institute.

**Introduction:** At the 8th International Conference on Mars (held in 2014 in Pasadena, CA, USA [1]), an important debate focused on the environmental conditions early in martian history – on whether Early Mars had been warm and wet or cold and icy (possibly with transient warm and wet periods). At that time, orbital and surface composition data did not seem to align with geomorphology-based hypotheses about the nature, distribution, and volume of water present on Mars, early in its history. This debate fed into the 2015 revision of the MEPAG Goals Document [2].

Since 2015, data received from the ongoing Mars missions – and in particular the MAVEN orbiter and NASA's Curiosity Rover, coupled with early climate modeling, has yielded new inputs and perspectives for questions about the first billion years of martian history. This debate continues and discussion on this topic is anticipated for the present conference.

In this presentation, we will identify Early Mars-relevant Objectives, Sub-objectives, and Investigations within the 2015 MEPAG Goals Document [2]. We also will outline recent mission-generated inputs addressing those investigations. Our hope is that discussion at this conference will further elucidate progress made in the last few years and clarify the direction of near-term updates to the MEPAG Goals.

**Early Mars-relevant Entries:** Early Mars-relevant items are found within all three Science Goals (Life, Climate, and Geology).

In the first two Goals, questions about the environmental conditions on Early Mars are highlighted within a specific objective (emphasis has been added here; sub-objectives are listed in Table 1):

- GOAL I: Determine if Mars ever supported life; Objective A: Determine if environments having high potential for prior habitability and preservation of biosignatures contain evidence of **past** life.
- GOAL II: Understand the processes and history of climate on Mars; Objective C: Characterize Mars' **ancient** climate and underlying processes.

Because Goal III focuses on geologic history and interpretation – which can involve investigations of states/features and processes that occur over a range of timescales and spatial scales (and sometimes via interactions between the different scales), Early Mars-relevant questions appear in all 3 Objectives (Table 2):

- Goal III: Understand the origin and evolution of Mars as a geological system; Objective A: Document the geologic record preserved in the crust and interpret the processes that have created that record; Objective B: Determine the structure, composition, and dynamics of the Martian interior and how it has evolved; Objective C: Determine the manifestations of Mars' evolution as recorded by its moons.

**References:** [1] Ehlmann, Beaty, & Meyer (2014) **EOS Earth & Space Science News**, Meeting Report, 30 Sept. 2014. [2] MEPAG (2015) *Mars Scientific Goals, Objectives, Investigations, and Priorities: 2015*, 74 p., http://mepag.nasa.gov/reports.cfm.

***Table 1.*** *Goal I & II Objectives and Sub-objectives that have direct relevance for studies of Early Mars, since they focus on conditions within the early martian environment.*

| Objectives | Sub-objectives |
|---|---|
| **GOAL I: Determine if Mars ever supported life.** | |
| **A. Determine if environments having high potential for prior habitability and preservation of biosignatures contain evidence of past life.** | **A1.** Identify environments that were habitable in the past, and characterize conditions and processes that may have influenced the degree or nature of habitability therein. |
| | **A2.** Assess the potential of conditions and processes to have influenced preservation or degradation of biosignatures and evidence of habitability, from the time of formation to the time of observation. Identify specific deposits and subsequent geological conditions that have high potential to have preserved individual or multiple types of biosignatures. |
| | **A3.** Determine if biosignatures of a prior ecosystem are present. |
| **GOAL II: Understand the processes and history of climate on Mars.** | |
| **C. Characterize Mars' ancient climate and underlying processes.** | **C1.** Determine how the chemical composition and mass of the atmosphere have evolved from the ancient past to the present. |
| | **C2.** Find and interpret physical and chemical records of past climates and factors that affect climate. |
| | **C3.** Determine present escape rates of key species and constrain the processes that control them. |

**About the MEPAG Goals Document:** Since 2001, the Mars Exploration Program Analysis Group (MEPAG) has maintained a document outlining community consensus priorities for scientific goals, objectives, and investigations for the robotic and human exploration of Mars [2]. This "Goals Document" is a living document that is revised regularly (~every 2yrs) in light of new results from Mars and changes in NASA's strategic direction. It is organized into a hierarchy of goals, objectives, and investigations. The four Goals are not prioritized and are organized around major areas of scientific knowledge: "Life", "Climate", "Geology", and "Preparation for Human Exploration". Vicky Hamilton led the 2015 revision, and Don Banfield is the current MEPAG Goals Committee Chair.

***Table 2.*** *Goal III Objectives, Sub-objectives, and Investigations that have relevance for studies of Early Mars. The Early Mars environment and history can be explored via identification of landforms/surfaces from that time period (and "separation" of alterations since), with bounds imposed by an understanding of the early martian heat flux, magnetic, impactor, and atmospheric conditions.*

| Objectives | Sub-objectives | Investigations |
|---|---|---|
| **GOAL III: Understand the origin and evolution of Mars as a geological system.** | | |
| **A. Document the geologic record preserved in the crust and interpret the processes that have created that record.** | **A1.** Identify and characterize past and present geologic environments and processes relevant to the crust. | 1. Determine the role of water and other processes in the sediment cycle. |
| | | 2. Identify the geochemical and mineralogic constituents of crustal materials and the processes that have altered them. |
| | | 3. Characterize the textural and morphologic features of rocks and outcrops. |
| | | 4. Identify ice-related processes and characterize when and how they have modified the Martian surface. |
| | | 5. Document the surface manifestations of igneous processes and their evolution through time. |
| | | 6. Evaluate the effect of large- and small-scale impacts on the nature and evolution of the Martian crust and establish their production rates. |
| | **A2.** Determine the absolute and relative ages of geologic units and events through Martian history. | 1. Quantitatively constrain the absolute ages of the surface and accessible crustal layers. |
| | | 2. Assess the characteristics of Martian craters and document their distribution. |
| | | 3. Identify and characterize the distribution, nature, and age relationships of rocks, faults, strata, and other geologic features, via comprehensive and topical geologic mapping. |
| | **A3.** Constrain the magnitude, nature, timing, and origin of past planet-wide climate change. | 1. Identify paleoclimate indicators in the geologic record and estimate the climate timing and duration. |
| | | 2. Characterize surface-atmosphere interactions as recorded by aeolian, glacial/periglacial, fluvial, lacustrine, chemical and mechanical erosion, cratering and other processes. |
| | | 3. Determine the present state, 3-dimensional distribution, and cycling of water on Mars including the cryosphere and possible deep aquifers. |
| **B. Determine the structure, composition, and dynamics of the Martian interior and how it has evolved.** | **B1.** Identify and evaluate manifestations of crust-mantle interactions. | 1. Determine the types, nature, abundance and interaction of volatiles in the mantle and crust. |
| | | 2. Seek evidence of plate tectonics-style activity and metamorphic activity, and measure modern tectonic activity. |
| | **B2.** Quantitatively constrain the age and processes of accretion, differentiation, and thermal evolution of Mars. | 1. Characterize the structure and dynamics of the interior. |
| | | 2. Measure the thermal state and heat flow of the Martian interior. |
| | | 3. Determine the origin and history of the magnetic field. |
| | **C2.** Determine the material and impactor flux within the Mars neighborhood, throughout Mars' history, as recorded on the Mars moons. | 2. Understand the flux of impactors in the Martian system, as observed outside the Martian atmosphere. |

**COEVAL FORMATION OF MINERAL SEQUENCES ON A *COLD AND WET* EARLY MARS.**
A. G. Fairén[1,2], E. Mateo-Martí[1], L. Gago-Duport[3], E. Losa-Adams[3], V. Chevrier[4] and C. Gil-Lozano[1]. [1]Centro de Astrobiologia (CSIC-INTA), Madrid, Spain. [2]Department of Astronomy, Cornell University, Ithaca, New York, USA. [3]Departamento de Geociencias Marinas, Universidad de Vigo, Vigo, Spain. [4]Arkansas Center for Space and Planetary Science, University of Arkansas, Fayetteville, USA.

**Introduction:** The presence of Mg-Fe-phyllosilicate, carbonate and sulfate bearing rocks on Mars is consistent with a wide variety of aqueous environments - from alkaline-neutral to acidic waters - existing in the past, which are usually explained assuming a drastic climate change early on Mars' history. Here we present the results of our aqueous alteration experiments on different olivine and pyrite powdered mixtures, to analyze their weathering products under early Mars conditions: a $CO_2$ atmosphere ($PCO_2$ = 0.5 bar), low fluid-to-rock ratio (~10), and UV irradiation. Our experiments recreate the geological setting of surface ponded water, to discuss the effect that the host-rock composition has on the resulting mineral assemblage [1]. We used mechanically activated pyrite as the source of sulfur because of its ability to produce both acidic and oxidizing conditions through aqueous alteration without the addition of an external oxidizing agent. As a semiconductor, the role of pyrite versus UV exposition is particularly interesting because (1) iron is an effective absorber of UV light; and (2) the surficial electronic structure of pyrite promotes redox reactions forming Oxygen Reactive Species (ROS) by photo-oxidation, which could catalyze the formation-decomposition of some secondary products.

**Experimental procedure:** Powdered samples were washed in ethanol, HCl and deoxygenated water by sequential cycles of sonication and centrifugation. After the cleaning process mineral mixtures were prepared by weight and exposed to deoxygenated water during 42 days + 5 days of evaporation under a $CO_2$ atmosphere. UV radiation experiments were performed inside the Planetary Atmospheres Simulation Chamber (PASC) at CAB [2] (Figure 1). The simulated Martian atmospheric composition was 99% $CO_2$ and 0.6% $H_2O$ at a pressure of 7 mbar. The weathered sample with the highest $FeS_2$ content (60%wt) was placed in a gold sample holder inside the PASC and it was UV irradiated during 75 hours. The lamp is a polychromatic source with a continuous spectrum in a wavelength range from 200-400 nm, with a dose emission of 2.3 $W/m^2$.

**Results:** *XPS:* We studied the stability of the surface products after UV irradiation by using X-ray Photoelectron Spectroscopy (XPS). Overall, the spectra show a significant increase to higher binding energies which are associated with an increase of the oxidation

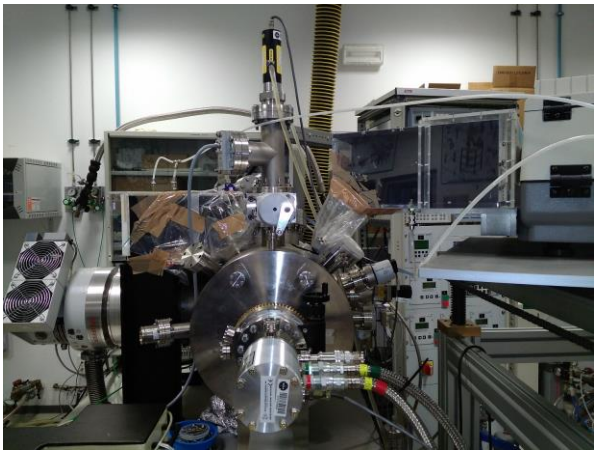

**Figure 1.** The Planetary Atmospheres Simulation Chamber (PASC) at CAB.

state of the corresponding species (Figure 2). The most noticeable changes appeared in Fe2p and S2p orbitals that indicate a decrease of iron disulfide species in favor of iron sulfates and iron oxides formation. These results confirms that photo-Fenton reaction between adsorbed water and iron surface species of pyrite can occur under Mars-like conditions.

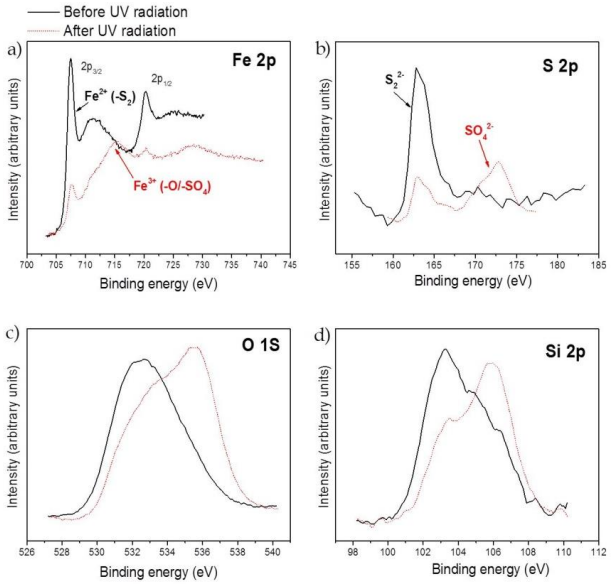


**Figure 2.** XPS spectra before and after UV radiation. Orbital lines: a) Fe2p, b) S2p, c) O1s and d) Si2p.

*FTIR:* We measured the IR spectra of the mineral samples using the diffuse reflection method (DRIFT). Due to the high iron content of the samples, we firstly analyzed the pristine and the weathered samples by comparing the spectra in the MIR region (figure 3a). We observed a decrease of the disulfide (S-S) stretching vibration at 430 $cm^{-1}$, and an increase of a wide and split band around 1100 and 1145 $cm^{-1}$, tentatively attributed to the stretching vibration of sulfate (S-O). As in the XPS analysis, the spectrum after UV exposition showed the highest increment of the S-O vibration band. We used the ν3 asymmetric stretching mode of $CO_3^{2-}$ as a diagnostic band to detected carbonates, because it does not overlap with the sulfate and silicate vibration modes (figure 3b). Initial samples showed some $CO_3^{2-}$ contribution (probably formed during the cleaning process) characterized by a wide band split into three peaks at 1400, 1430 and 1470 $cm^{-1}$. After the reaction process the band evolved, and the peak centered at 1430 $cm^{-1}$, almost becoming the only contribution, indicating an increment of the crystallinity of the carbonate compound. This peak could be related to calcite. However, after UV radiation the band was split once again (Figure 3b). The presenc of shoulders around the ν3 band after the UV exposition could indicate the coexistence of various carbonate species.

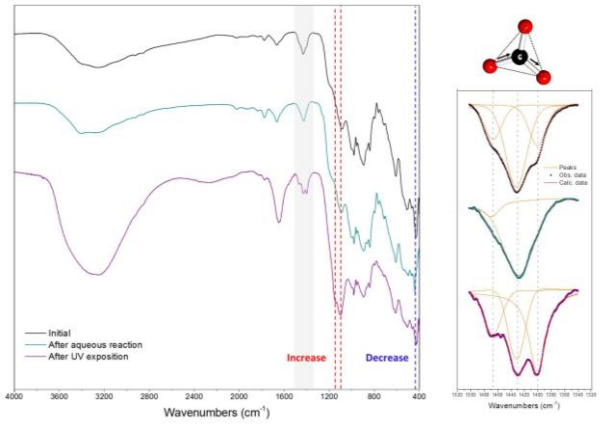


**Figure 3.** Left) Comparing IR spectra of the sample with 60%wt of pyrite in the MIR region. Right) Detailed ν3 asymmetric stretching mode of $CO_3^{2-}$.

*SEM:* To characterize the element distribution (Figure 4) and to identify secondary phases after the reaction process (Figure 5), samples were analyzed with scanning electron microscope (SEM). Combination maps of the main elements show that iron and sulfur species are the most mobile species covering some forsterite grains, which is reflected in the apparent increment of these elements after the weathering process (Figure 4).

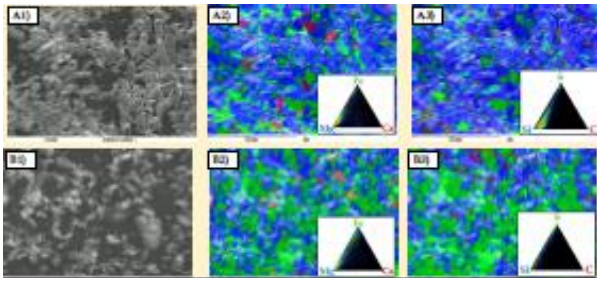

**Figure 4.** Combination maps obtained with X-Ray mapping of samples containing 30% wt of $FeS_2$. A) before and B) after reaction.

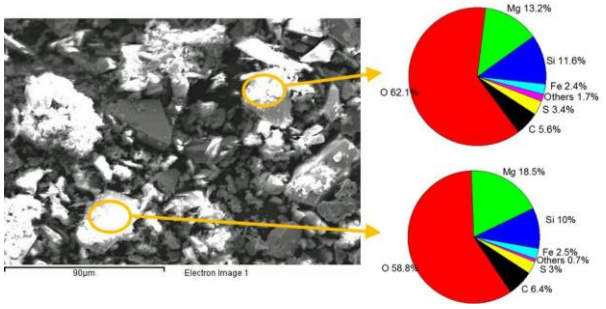


**Figure 5.** a) SEM image of the UV irradiated sample showing a mineral coating over forsterite grains. b) Energy dispersed X-ray Spectroscopy (EDS) analyses show that the secondary material is enriched in oxygen, iron and sulfur. Note that EDS analyses are partially masked by the bulk contribution of forsterite grains.

**Conclusions:** Mineral mixtures composed by pyrite and forsterite powders can form sulfates and carbonates in aqueous conditions and in short periods under anoxic conditions. The influence of UV radiation over mineral samples containing pyrite catalyzed sulfide oxidation by photo-Fenton reaction under Mars-like conditions. The instability of iron disulfide under Mars-like conditions can explain the lack of this mineral on Mars surface. Therefore, a Martian substrate associated with volcanogenic massive sulfide deposits can lead to different mineralogical sequences under the same environmental conditions: a generally cold planet with transitional warm periods.

**References:** [1] Dehouck, E., et al. (2012) Geochim. Cosmochim. Acta, 90: 47-63. [2] Mateo-Marti, E., et al. (2006) Meas. Sci. Technol., 17: 1-7.

**Acknowledgements:** The research leading to these results is a contribution from the Project "icyMARS", funded by the European Research Council, Starting Grant no 307496.

**ON THE CHALLENGE OF SIMULATING THE EARLY MARS ENVIRONMENT WITH CLIMATE MODELS.** F. Forget[1], M. Turbet[1], E. Millour[1], L. Kerber[2], R. D. Wordsworth[3], J. W. Head[4], [1]Laboratoire de Météorologie Dynamique, IPSL, CNRS, Université Paris 6, Paris, France (forget@lmd.jussieu.fr), [2]Jet Propulsion Laboratory, Caltech, CA, USA, [3]Harvard University, Cambridge MA, USA, [4]Brown Univ., Providence, RI, USA.

**Introduction.** Yes, there is compelling evidence and widespread agreement that water flowed on the surface on early Mars, at least episodically. But we still do not know which climate processes operated. Each proposed solution has its difficulties. Nevertheless, based on the new ideas that are regularly proposed, and the constant improvement of the climate models, there is hope ahead.

At the 4th Conference, we wish to review some of the climate modelling studies recently conducted (notably using the LMD 3D climate model). We shall describe the work performed in the recent years, notably since the 3rd Early Mars conference, but will focus on the most recent advances and new ideas (It can be noted here that excellent reviews on the subject, covering studies published until 1 to 2 years ago, have recently been published [1,2]).

**The $CO_2$-$H_2O$ atmosphere solution.**

A pure $CO_2$-$H_2O$ atmosphere under early Mars conditions cannot easily warm the planet to explain the geological record. Yet, 3D simulations of early Mars with a $CO_2$ atmosphere thicker than today have simulated an interesting environment, different than today.

*Icy highland*. The key difference is related to the fact that, if the surface pressure is high enough, the elevated regions are colder than the low lying plains [3], providing a cold trap where water tends to accumulate as snow and ice in high altitude [4,19], and a process to constantly replenish these reservoirs. Interestingly, the resulting distribution of glaciers is in somewhat good agreement with the observed valley networks [4,5,18].

*Icy highlands before Mars "true polar wander"*. An interesting twist in the icy highland-valley network correlation is the possibility of a late "polar wander" of Mars [6]. If one assume that the growth of Tharsis induced a reorientation of the planet with respect to its spin axis, and that this took place after the incision of the valley network, then the distribution of the valleys along a small circle tilted with respect to the equator is found to correspond to a southern-hemisphere latitudinal band in the pre-TPW geographical frame. Even more than with the current Mars map, this points to a climate origin to explain the Valley Network distribution [6].

*Icy highlands and the preservation of early Noachian phyllosilicates*. Furthermore, if one explores the location of the possible ice reservoir on a "pre-Noachian Mars" with a simple topography, it is interesting to find that ice tends to accumulate where the major phyllosilicate deposits are now found. This have been suggested to provide a means to protect the deposits throughout Noachian, and explain their current location [10].

*$CO_2$ ice clouds.* Once assumed to provide an attractive solution to the early Mars climate enigma thanks to their scatterring greenhouse effect [7], $CO_2$ ice clouds are now considered to provide a limited surface warming because of their limited coverage [3] and detailed optical properties [8]. Yet they warrant further study with more detailed models.

*Water ice clouds.* High altitude water ice clouds could, in theory, provide a very strong greenhouse effect. The interesting findings by Urata and Toon [9] on this subject cannot easily be reproduced in other models [4,11]. However this also warrants further studies with a high resolution model including an extended domain. We will present new results on this subject at the conference.

.

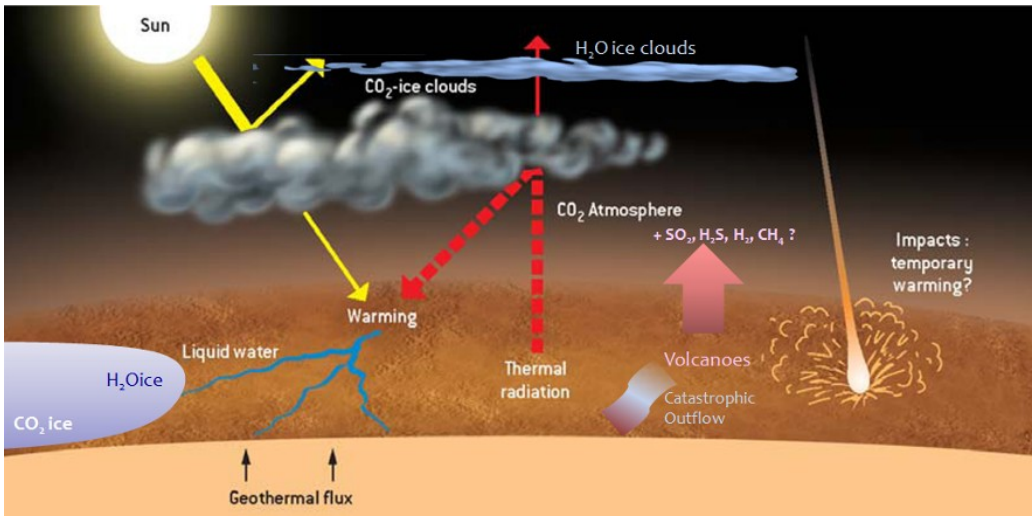


Fig. 1. Key climate processes on Early Mars. Adapted from [17]

*$CO_2$ ice cap and glaciers.* Mars with a $CO_2$ atmosphere thicker than today is a place where $CO_2$ condensation can form spectacular $CO_2$ ice glaciers [3, 12] that may have played a role in Mars geology and past climate [20]. This is interesting to study and detail.

*Obliquity variations.* The large martian orbital variations must have played a role in the early Mars climate system. However, while summertime diurnal mean surface temperatures above 0°C (a condition which could have allowed rivers and lakes to form) are predicted for obliquity larger than 40° at high latitudes, they are not in locations where most valley networks or layered sedimentary units are observed. Nothing in the climate record suggests a link between high obliquity excursions and flowing water [3,4, 15]

*Spectroscopic issues.* Interestingly, the spectroscopy of a $CO_2$ atmosphere thicker than a few hundreds of millibars atmosphere remains an active field of research (see Turbet et al., abstract 1, this issue), with several remaining issues

**Volcanoes, Impacts, catastrophic outflow and episodic warming.**

If a thick Mars $CO_2$ atmosphere only yields a cold and icy planet, one has to take into account additional processes to warm it and melt significant amounts of water to explain the geological record.

*The climatic impact of impacts* is, within that context, a key process to study. This is discussed in the companion paper by Turbet et al. (This issue, abstract 2).

*The consequence of catastrophic outflows.* It has been speculated that the catastrophic flooding that formed the Hesperian outflow channel events could have induced significant rainfall and caused the formation of late-stage valley networks. However, 3-D Global Climate Model simulations [16] designed to reproduce the impact of a wide range of outflow channel formation scenarios suggest that these events have a limited effect, and that they cannot trigger long-term greenhouse global warming.

*Volcanic activity* could have supplemented such an early atmosphere with additional greenhouse gases such as $SO_2$, $H_2S$, $CH_4$, $NH_3$, and $H_2$ and boost the greenhouse effect for some time if their concentration could be raised to an adequate level and for a sufficient duration.

*Volcanic $SO_2$.* Following many modeling studies, Kerber et al. [13] recently used the LMD GCM to explore the possible climates induced by releases of $SO_2$. $SO_2$ was found to be incapable of creating a sustained greenhouse on early Mars. Even in the absence of aerosols, local and daily temperatures rise above 273 K only for limited periods with favorable background $CO_2$ pressures. In the presence of even small amounts of aerosols, the surface is dramatically cooled for realistic aerosol sizes. Brief, mildly warm conditions were found to require the co-occurrence of many improbable factors, while cooling is achieved for a wide range of model parameters.

*The $H_2$-$CH_4$ seducing solution.*

Ramirez et al. [14] argued that $H_2$ emitted from volcanoes into a thick $CO_2$-dominated atmosphere could have significantly warmed the planet assuming a very reducing mantle and a very high rate of volcanism. This scenario was thus not easy to prove right. However, Wordsworth et al. [15] recently showed that in this study the strength of the greenhouse effect induced by the $CO_2$–$H_2$ collision-induced absorption could have been significantly underestimated (by using the available spectroscopic properties, originally derived for an $N_2$ atmosphere instead of $CO_2$). Furthermore, they reported that methane could also have acted as a powerful greenhouse gas on early Mars due to $CO_2$–$CH_4$ Collision Induced Adsorption in the critical 250–500 $cm^{-1}$ spectral window region. The required outgassing fluxes become more realistic, and the scenario is very interesting. At the conference, we will present new simulations performed with atmospheres including $H_2$ and $CO_2$

**References:** [1] Haberle, R. M., D. Catling, M. Carr and K. Zahnler, The Early Mars Climate System, in "*The atmosphere and climate of Mars*", Cambrige University Press, 2017.[2] Wordsworth, R. D. Annu. Rev. Earth Planet. Sci. 2016. 44:381–408 (2016) [3] Forget, F., Wordsworth, R., Millour, E., et al. (2013) *Icarus*, 222, 81– 89 (2013) [4] Wordsworth R, Forget F, Millour E, Head JW, Madeleine JB, Charnay B. 2013.. Icarus 222:1–19 [5] Wordsworth R, Kerber L, Pierrehumbert R, Forget F, Head JW III. J. Geophys. Res. Planets 120:1201–19 (2015) [6] Bouley et al., *Nature*, 531:344-347, 2016. [7] Forget, F., and Pierrehumbert, R. T. (1997) Science,278, 1273– 1276.[8] Kitzmann D, Patzer ABC, Rauer H., 2013., Astron. Astrophys.557:A6 [9] Urata R.A, Toon O.B. 2013. *Icarus* 226:229–50 [10] Bibring, J.-P.; Forget, F., 44th Lunar and Planetary Science Conference, No. 1719, p.2161 (2013) [11] Ramirez and Kasting Icarus 281 (2017) 248–261 [12] Soto A, Mischna M, Schneider T, Lee C, Richardson M. 2015.. Icarus 250:553–69. [13] Kerber L, Forget F, Wordsworth RD. 2015. Icarus 261:133–48. [14] Ramirez RM, Kopparapu R, Zugger ME, Robinson TD, Freedman R, Kasting JF. 2014.. Nat. Geosci. 7:59–63 [15] Wordsworth et al., Geophys. Res. Lett., 44, 665–671 (2017) [15] Mischna MA, Baker V, Milliken R, Richardson M, Lee C.. Effects of obliquity and water vapor/trace gas greenhouses in the early martian climate. *J. Geophys. Res. Planets* 118:560–76 (2013) [16] M. Turbet, F. Forget, J. W. Head, and R. Wordsworth. 3D modelling of the climatic impact of outflow channel formation events on early Mars. Icarus, 288:10-36, 2017.[17] Forget, Costard and Lognonne. *Planet Mars, story of another world*, Springer, 2008. [18] Head J. and Marchant, D., Antarctic Science, 26, 774-800,, 2014 [19] Fastook J, and Head J.. Planet. Space Sci., 106, 82-98, 2015.
, 2015, [20] Kreslavsky, M and Head, J. *Icarus, 216,* 111-115, 2011.

# EVOLUTION OF NOACHIAN CHANNELS AND VALLEYS IN THE COROZAL CRATER REGION

N. H. Glines[1] and V. C. Gulick[1], [1]SETI Institute/NASA Ames Research Center (MS 239-20, NASA Ames, Moffett Field 94035, natalie.glines@nasa.gov, virginia.c.gulick@nasa.gov)

**Introduction:** The Southern Highlands of Mars experienced extensive erosion during the Late Noachian and Hesperian, by the formation of numerous channels and valley networks. One such location is a ~80 km diameter unnamed crater within Terra Cimmeria, that is surrounded by channels and valley networks. This region may have been completely covered by the Eridania paleolake through the Noachian to Early Hesperian [1,2], at a water surface elevation of approximately 1100 m [1].

Within this crater are 5 smaller craters, the largest of which is the ~8km diameter gullied Corozal Crater [3]. Three of the four other unnamed craters also contain gullies, and range in diameter from 2.6 to 8km.

These interior craters formed much more recently than this previous period of fluvial and lacustrine activity. This region of Terra Cimmeria has experienced a long history of water activity, that may have preserved evidence for past microbial activity.

To better understand the fluvial history in this region, we have mapped the channels at CTX resolution. There are at minimum 3,000 km of channels within this study region of almost 28,000km$^2$ , including gullies, valleys, and crater wall valleys.

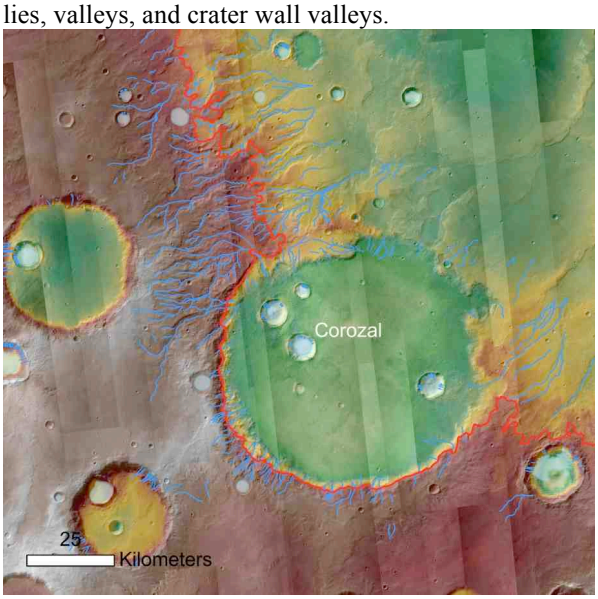


***Figure 1****: Study region map of channelized features (blue: channels, valleys, gullies, and wall valleys), 1100m paleolakeshoreline (red), and late-stage ice-rich or previously liquid water or ice-rich deposits (light blue). North is up, high elevation (2109m) is left, low is -214m, and flow direction is ~left to right.*

The majority of ice-rich or previously liquid water/ice-rich deposits are within craters. Some of these deposits have channels emanating away from them, suggesting melt water flows. These are located in the crater west of Corozal and on the larger crater rim.

The highest concentration of channels eroded through early-to-mid Noachian terrain units. Two major basins drain into the larger crater to the northwest, and would have flooded the crater floor. There is no remaining evidence of lacustrine deposits, although any evidence may have long since been removed or buried by subsequent processes. However, there is geomorphologic evidence of ice-rich material having been removed from the crater floor, and spectra suggesting sustained water presence.

***Figure 2****: Corozal Crater perspective false-color view of layers with likely clay-rich material, and a gully undercutting that layer. The viewing direction is southwest. HiRISE image: MIRB color, over HiRISE DTM: DTEEC_013948_1410_013236_1410.*

Ehlmann et al., [4], report the presence of hydrated minerals (in CRISM data) on the surface beside Corozal Crater (2011). Clays formed near the surface and provide evidence for a warm and wet conditions in this region compared to the present-day.

**Discussion**:

The original surface laid down is Noachian in origin [5], and most channels on the plains north of Corozal have many craters superposing them, suggesting that the channels formed soon after. Channels formed as slope material was removed, however there are no clear deposits in which the channels terminate. It is possible that these channels terminate in the Eridania paleolake basin. Crater counting will more definitively reveal the timing of these events.

While atmospheric precipitation and runoff may have formed many of the original channel depressions, subsequent melting of ice deposits has modified them more recently. The bedrock unit just east of this study region is reported to have been resurfaced by liquid water in the Early Amazonian [6], and there are many features indicative of ice loss in the near subsurface of this region, which may have been from a combination of sublimation and melt. The "brain terrain" floor morphology of Corozal crater and surrounding craters indicates sublimation of icy floor fill material, with flow direction lines from the northeastern walls of the crater. Possible ring-mold craters suggest ice as well. While icy crater floor fill has been previously proposed to have originated from atmospherically-emplaced glacial ice deposits [e.g. 7], ground water or frozen ponded water in the crater may play a role as well. During a changing climate, the ground water, which infiltrated this region during the Noachian, may have frozen when reaching the surface, although ground water remained liquid due to higher subsurface pressures. As water escaped through exposed layers, it may have filled the crater with icy lobes. Atmospheric water would play a role as well as it accumulates over time on crater walls and floors. Alternatively, water which became frozen in the crater walls may have provided the source layers from which the gullies have more recently developed. Sublimating ice in the crater walls may have removed support for overlying rocks and sediment and may have helped form the initial gully alcove. The pitted floor texture indicates significant loss of water ice, and may suggest that the crater floor was higher in the past.

It is likely that water shaped the surface of this region over a long period of time. If this region's surface was covered in water over a significant period, as the extensive channel networks, previously proposed lake basin extent, and CRISM data suggest, significant water volumes pooling on the surface would have infiltrated into the subsurface, and incorporated in the ground-water system. The degree to which ground water played a role in shaping the surface remains uncertain. Due to a lack of major tributaries flowing into the basin, the paleolake may have been filled by ground-water springs, with the addition of some overland flow [8], in the channels that we mapped. It is possible that the region's gullies, which originate at distinct stratigraphic layers, may be linked to ground-water flow. If the channels that we have mapped in this region source most recently from ice melt in the Amazonian, and not the Noachian, then the gullies are more closely linked to the channels than previously thought, with the potential of both being influenced by ice or snowpack melting. Although talus slopes are not ideal surfaces on which to perform crater counts; however, Berman et al., [9] measured western Corozal Crater using MOC image E11-01445 for a crater retention age of the order of some tens of millions of years, which we suggest to be an absolute minimum.

It is likely that recent Amazonian channel modification exploited the existing channel depressions from the Noachian, which may explain the lack of finer branching channels even at CTX-resolution. Instead the less degraded channels visible today have formed along the thalweg, where ice melt may have occurred beneath debris cover in the recent past.

**Conclusions:**

We hypothesize that Noachian channels that were later modified by ice fill and subsequent melting would be broader or deeper than more pristine Noachian channels unaffected by late-stage ice depositions. When studying the geomorphology of assumedly Noachian channels in the mid-latitudes, it is important not to assume the full width and depth were carved in the ancient past. These channels and valleys likely were enlarged by subsequent ice melting or sublimation throughout Mars paleohistory. Such assumptions may affect water flow modeling of velocity and discharge estimates. Further study comparing crater counting and channel dimension mapping on Noachian terrains in the mid-latitudes and closer to the equator, for example, less affected by atmospheric ice emplacements during higher obliquity, may support this. A similar effect may occur in Amazonian gullies, where ice may have carved out an original alcove only to be later modified by finer channels.

**Acknowledgements:**

Support was provided by the SETI Institute's NAI grant NNX15BB01A, and MRO HiRISE Co-I funds to Gulick.

**References:**

[1] Irwin et al 2004. JGR-Planet, v. 109, DOI 10.1029/2004JE002287. [2] Pajola et al., 2016, Icarus, 275, 163-182, doi: 10.1016/j.icarus.2016.03.029. [3] Gulick et al., 2014 Abstract "New insights to gully formation using HiRISE Digital Terrain Models", 8th Int. Conf. on Mars, [4] Ehlmann et al., 2011, Nature, v.479, p. 53-60. [5] Tanaka et al., 2014, Planet. And Space Sci., 95, 11-24. [6] Adeli et al., 2016, Icarus, 277, 286-299. [7] Dickeon et al., 2010, E.P.S.Letters, 294, 332-342. [8] Andrews-Hanna et al., 2007. [9] Berman et al., 2005. Icarus 178, 465-486, doi: 10.1016/j.icarus.2005.05.011.

**THE IMPORTANCE OF LAKE OVERFLOW FLOODS FOR EARLY MARTIAN LANDSCAPE EVOLUTION: INSIGHTS FROM LICUS VALLIS.** T. A. Goudge[1] and C. I. Fassett[2], [1]Jackson School of Geosciences, UT Austin, [2]NASA Marshall Space Flight Center. (Contact: tgoudge@jsg.utexas.edu)

**Introduction:** Open-basin lake outlet valleys are incised when water breaches the basin-confining topography and overflows. Outlet valleys record this flooding event and provide insight into how the lake and surrounding terrain evolved over time [1–5]. Here we present a study of the paleolake outlet Licus Vallis, a >350 km long, >2 km wide, >100 m deep valley that heads at the outlet breach of an ~30 km diameter impact crater (**Fig. 1**). Multiple geomorphic features of this valley system suggest it records a more complex evolution than formation from a single lake overflow flood. This provides unique insight into the paleohydrology of lakes on early Mars, as we can make inferences beyond the most recent phase of activity.

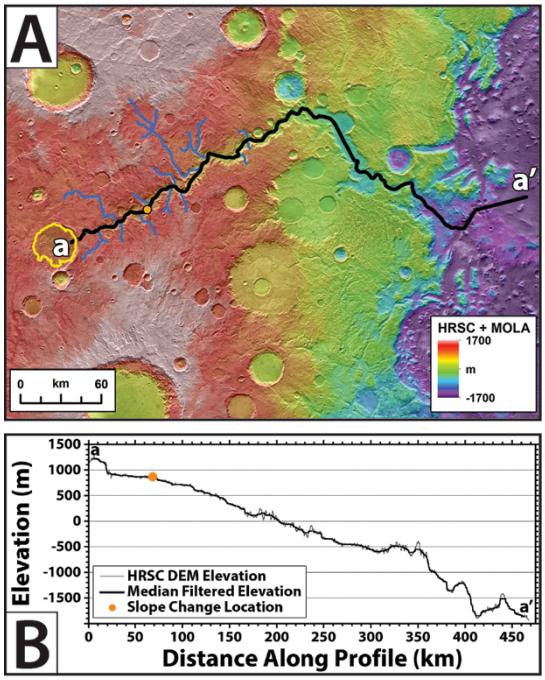


**Fig. 1.** ***(A)*** *Overview of the Licus Vallis system. Main valley shown in black and tributary valleys shown in blue. Outline of open-basin lake at the head of the valley shown in yellow. Orange circle shows location of major slope change. HRSC DEM mosaic and MOLA gridded topography overlain on the ~100 m/pixel THEMIS global daytime infrared mosaic. North is right.* ***(B)*** *Profile a–a' along Licus Vallis. Note the change in valley slope at ~70 km (orange circle). Profile location shown in (A). Moving window of 10 km used for median filter. Elevation data are from HRSC DEM mosaic.*

**Methods:** We studied the topography and geomorphology of the Licus Vallis system using: CTX images [6]; the THEMIS ~100 m/pixel global daytime infrared mosaic [7,8]; a 75 m/pixel mosaic of six HRSC DEMs [9,10]; MOLA gridded topography [11]; and a CTX-derived DEM produced using the NASA Ames Stereo Pipeline [12–14]. Centerlines of Licus Vallis and contributing tributary valleys were mapped, and longitudinal profiles extracted from HRSC and/or CTX DEMs.

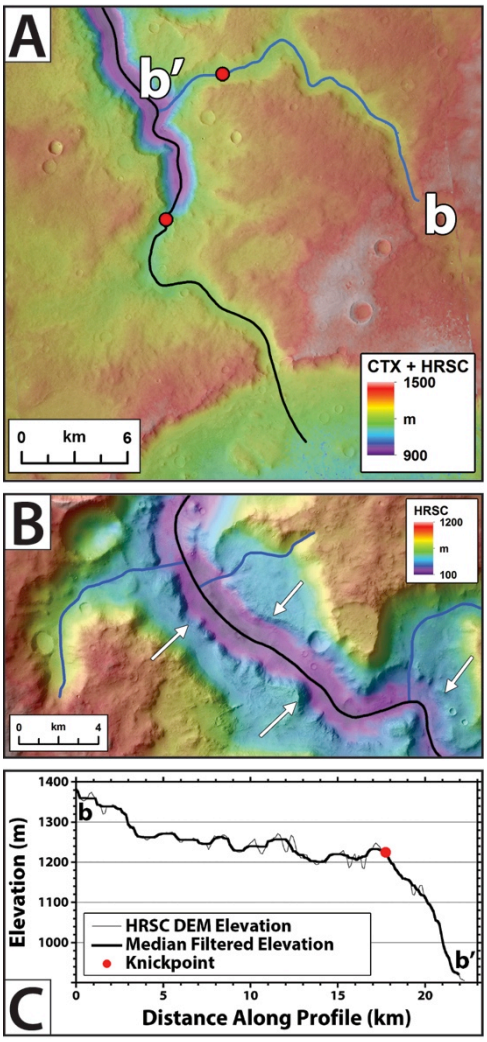


**Fig. 2.** ***(A)*** *Major knickpoint (red circle) in Licus Vallis near the head of the valley. HRSC DEM mosaic and CTX DEM overlain on a CTX mosaic.* ***(B)*** *Paired terraces (white arrows) within Licus Vallis. HRSC DEM mosaic overlain on CTX.* ***(C)*** *Profile b–b' along an upstream tributary to Licus Vallis. Profile location shown in part (A). Moving window of 1 km used for median filter. Elevation data are from HRSC DEM mosaic.*

**Results:** The Licus Vallis longitudinal profile has an abrupt change in slope at ~70 km that separates two

reaches with approximately constant slopes of ~$1.4x10^{-3}$ (upstream) and ~$6.4x10^{-3}$ (downstream; **Fig. 1**). At ~20 km along the profile there is a major knickpoint where the valley drops ~200 m in elevation over ~2 km (**Fig. 2A**). Downstream of approximately the slope change location, Licus Vallis has paired interior terraces that can be continuously mapped for tens of km (**Fig. 2B**).

Licus Vallis has 13 main tributary valleys, which start just downstream of the major knickpoint (**Fig. 2A**). Longitudinal profiles show that the 10 most upstream tributary valleys have knickpoints along their length, near the topographic level of the Licus Vallis rim (**Fig. 2C**). We estimated the total retreat distance of each knickpoint from the Licus Vallis centerline along the tributary valley centerline. Knickpoint retreat distances are positively correlated with the position of the tributary junction, with the largest retreat distances for downstream tributary valleys (**Fig. 3**).

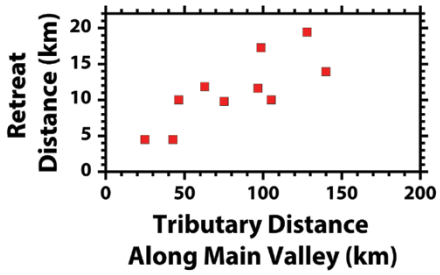


**Fig. 3.** *Licus Vallis tributary valley knickpoint retreat versus tributary junction distance along main valley.*

**Evolution of Licus Vallis:** The topography and geomorphology of Licus Vallis show several signs of disequilibrium that suggest the system did not adjust to stable fluvial boundary conditions. Taken together, we interpret these features as recording two discrete episodes of valley incision – one to form the steeper downstream portion of the valley, and one to form the shallower upstream portion as well as the interior valley bounded by the paired terraces.

Given the large size of the valley, we hypothesize that the first episode of incision was driven by overflow flooding of a large paleolake contained within a now degraded inter-crater basin (**Fig. 4**). This is supported by the observation that valley networks upstream of Licus Vallis do not extend below approximately the 1400 m MOLA contour (**Fig. 4**, white arrows), consistent with the presence of a standing body of water in this region. The 1400 m contour above Licus Vallis is not closed, but the topography responsible for enclosing the basin to the north would likely have been significantly eroded/obscured during the overflow flooding.

Subsequently, overflow flooding from the lake currently at the head of the valley pirated the pre-existing Licus Vallis, forming a major knickpoint, establishing the upstream section of the valley at a lower slope, and incising an interior valley bounded by paired terraces.

**Overflow Floods vs. Background Activity:** Given our hypothesized scenario for the evolution of Licus Vallis, the regional tributary valleys can offer insight into how background fluvial incision compared to incision from lake overflow flooding. We note that knickpoints in downstream tributary valleys have retreated more than knickpoints in upstream tributary valleys (**Fig. 3**). This is consistent with the tributary valley knickpoints forming from a wave of incision [15–17] that incompletely swept up Licus Vallis as incision rates from overflow flooding outpaced rates from background surface runoff. Comparing retreat distances between the upstream tributary valley knickpoints and the knickpoint in the main valley suggests retreat rates at least 4x larger in the main valley. This is likely to be a significant underestimate as the tributaries were likely active longer than the catastrophic lake overflow flood [4,5]. This conclusion points to the importance of lake overflow floods in setting the pace of landscape evolution on early Mars and in shaping the martian surface [e.g., 2,3].

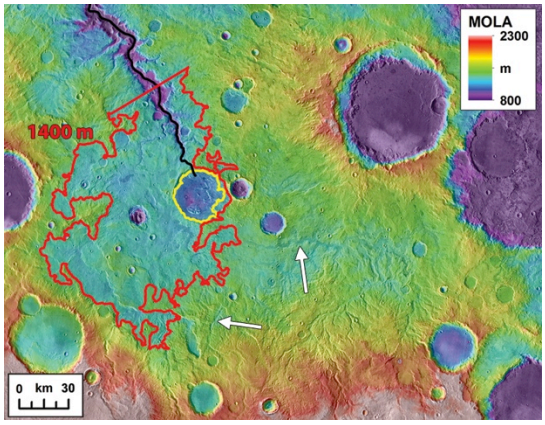


**Fig. 4.** *Potential inter-crater basin that sourced overflow flooding responsible for incision of downstream portion of Licus Vallis. Main valley shown in black, open-basin lake at the head of the valley shown in yellow, and MOLA contour at 1400 m shown in red. MOLA gridded topography overlain on the ~100 m/pixel THEMIS global daytime infrared mosaic. North is up*

**References:** [1] Fassett, C., J. Head (2008), *Icarus,* **198**:37–56. [2] Irwin, R., et al. (2002), *Science,* **296**:2209–2212. [3] Irwin, R., et al. (2004), *JGR,* **109**:E12009. [4] Coleman, N. (2013), *JGR*, **118**:263–277. [5] Coleman, N. (2015), *Geomorph.,* **236**:90–108. [6] Malin, M., et al. (2007), *JGR,* **112**:E05S04. [7] Christensen, P., et al. (2004), *Space Sci. Rev.*, **110**:85–130. [8] Edwards, C., et al. (2011), *JGR*, **116**:E10008. [9] Neukum, G., et al. (2004), *ESA SP-1240*, 17–35. [10] Gwinner, K., et al. (2010), *EPSL*, **294**:506–519. [11] Smith, D., et al. (2001), *JGR*, **106**:23,689–23,722. [12] Broxton, M., L. Edwards (2008), *LPSC 39,* #2419. [13] Moratto, Z., et al. (2010), *LPSC 41,* #2364. [14] Shean, D., et al. (2016), *ISPRS J. Phot. Rem. Sens.,* **116**:101–117. [15] Crosby, B., K. Whipple (2006), *Geomorph.,* **82**:16–38. [16] Berlin, M., R. Anderson (2007), *JGR,* **112**:F03S06. [17] Crosby, B., et al. (2007), *JGR*, **112**:F03S10.

**Global Catalogue of the Martian Valley Networks: Evidences for Fluvial, Sapping and Subglacial Processes on Early Mars.** A. Grau Galofre[1] and A. M. Jellinek[1], [1]Department of Earth, Ocean and Atmospheric Science, University of British Columbia (agraugal@eoas.ubc.ca)

**Introduction:** The southern highlands of Mars, and in particular the regions along the dichotomy line between 30ºN and 30ºS are covered in ancient networks of valleys that extend for hundreds of kilometers and present a striking variety of morphologies. These valley networks are one of the few keys to understand Mars' surface conditions and climate of a past dating back to 3.8Byr ago.

Based on their morphology and on their resemblance to terrestrial analogues, numerous hypothesis have been suggested for their origin: (1) extensive fluvial runoff incision, triggered by rainfall, requiring warm and wet climate conditions and an active hydrological cycle [1], [2]; (2) groundwater sapping and episodic surface runoff, requiring a climate that allows for surface water stability for short periods of time and near surface groundwater [3]; (3) valleys incised by glacial erosion, implying a cold and wet climate with snowfall rather than rainfall [4], [5]; and (4) valleys as an ancient drainage system below ice sheets and ice caps, indicating a cold, dry climate with a surface hydrological cycle limited to snow precipitation and sublimation [6].

Using Principal Component Analysis (PCA) statistics, modeling efforts and analogy with terrestrial valley networks [7], we demonstrate the presence of all the above mentioned styles of erosion on Mars. We accordingly build the first large scale characterization and classification of Martian valley networks, and present a global map of Mars displaying the areas where the different types of erosion are dominant. Our results show: (1) A difference in erosion style between valley networks along the dichotomy boundary and those between the Noachian highlands and Arabia Terra, (2) A heterogeneous distribution of valley networks within the Noachian highlands, and therefore (3) the need to consider local and severe changes in surface climate conditions over short timescales.

**Methodology**: We apply the methodology developed and tested in [7] to characterize and classify a suite of 65 Martian valley networks into different groups. This method consists on measuring 5 parameters: stream order, length to width aspect ratio, minimum channel width, fractal dimension and junction angle, to characterize the style of erosion underlying the channel formation. To this parameters, we add the presence of significant undulations in the valley network longitudinal profile as a sign of subglacial erosion by pressurized water.

For each valley network, we measure length along the longest flow path and valley network stream order from the dataset in [8]. We use the High Resolution Stereo Camera (HRSC) digital elevation maps with resolution ranging between 12 and 75m/pixel when available, complemented with the MOLA digital elevation map (256m/pixel at the equator) to measure channel width and undulations in the longitudinal profile. We complement the small scale analysis of minimum channel width with images from the CTX camera, at a resolution of 2m/pixel. We finally measure fractal dimension using a MATLAB box counting algorithm, and the junction angle between a tributary and the stem channel with the stream lines in [8].

To build understanding, we use a Principal Component Analysis to classify the suite of 65 valley networks into different statistical clusters. We then identify the style of erosion better representative of each cluster by comparing the channels that are part of it with suitable predictions of each metric drawn from models of landscape evolution and erosion [7].

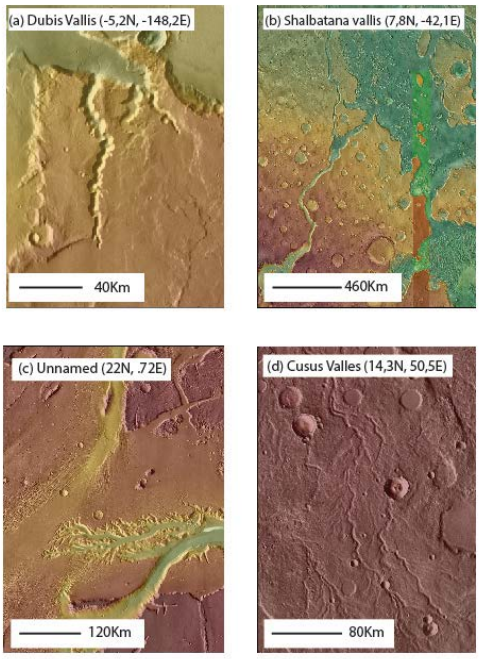


**Fig 1.** Examples of valley networks characterized according to the methodology as (a) a sapping valley, (b) a subglacial channel, (c) a glacier valley and (d) a fluvial valley

**Results:** Values of small minimum channel width, little or zero undulations in the longitudinal profile,

large length to width ratios and high stream orders are indicative of surface liquid water flows. The presence of significant undulations in the longitudinal profile, however, is indicative of subglacial erosion and requires overlying ice thickness of a few hundred meters. Low stream orders, no undulations, small length to width ratios and junction angles around 72 degrees indicate groundwater sapping originating the valley network [7]. Large (~1-2Km) minimum channel widths, small length to width ratios and low stream orders are indicative of glacial erosion. Figure 1 shows examples of four valley networks that fit each of these descriptions.

The findings of both techniques are consistent for the majority of valley networks, allowing for the construction of a reliable catalogue of valley networks. According to the results, we built global probability maps of Mars that highlight the areas where the different styles of erosion are dominant (figure 2).

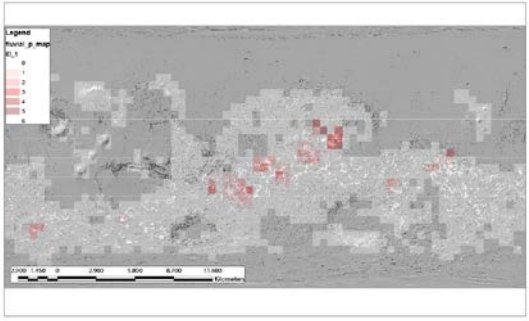

**Fig.2** Example of a probability map showing the areas of dominant fluvial erosion, evaluated from the results of the technique presented in [7] and considering a total of 65 valley networks. Areas in white indicate the presence of channels according to [8]. Solid red indicates high presence o fluvial erosion and faint red the presence of a reduced number of fluvial channels. Bins are 5x5º.

The maps show that subglacial erosion is dominant along the dichotomy boundary leading to the Martian lowlands, with undulating longitudinal profiles with uphill sections up to 300m high. The corridor linking Arabia Terra with the Noachian highlands, however, is dominated with overland fluvial erosion, with evidence of surface water incision. Sapping valleys nucleate around large canyon systems, such as Valles Marineris, according with previous descriptions of sapping morphologies on Mars [3]. Finally, we also identify wet based glaciations in areas below 55-60S, also according to previous studies [5].

**Discussion:** The existence of subglacially incised channels on the Martian Noachian surface has important implications for the climate of Early Mars. The formation of subglacial drainage systems on Earth requires the existence of a thick, ~100m layer of overlying ice and the accumulation of a large amount of meltwater underneath [9]. Subglacial channels open and close periodically driven by increased summer rates of rainfall, volcanic eruptions, pressurized groundwater subglacial aquifers, etc, and typically concentrate at the terminal areas of the ice sheet, where meltwater is more abundant. The highly pressurized meltwater they carry can cut into bedrock or regolith at fast rates, sometimes during the course of a meltwater season (spring and summer) [9]. When these formation mechanisms are considered on Mars, the presence of subglacial channels supports the existence of a highlands extensive Noachian ice sheet, potentially a few hundreds of meters thick, extending towards and possibly terminating at the dichotomy line.

We also show, however, the presence of valley networks which morphology requires surface water incision. Such channels are concentrated around the topographic drop between the Noachian highlands and Arabia Terra. The spatial proximity of fluvial and subglacial channels suggests dramatic climate changes during the Noachian period, with advance and retreat of large ice masses in the Martian highlands.

**References:** [1] Craddock R.A. and Howard A.D. (2002) *JGR Planets, 107*(E11). [2] Baker V.R. and Strom R.G. (1991) *Nature, 352*(6336), 589. [3] Laity J.E. and Malin M. C. (1985) *GSA Bulletin, 96*(2), 203-217. [4] Fairen, A. G. (2010) *Icarus, 208*(1), 165-175. [5] Banks M.E. et al. (2008) *JGR Planets, 113*(E12). [6] Lee, P. et al. (1999) *LPSC XXX* [7] Grau Galofre A. and Jellinek A.M. (2017) *JGR Earth Surface 122*(4), 1037-1059. [8] Hynek B.M. et al. (2010) *JGR Planets, 115*(E9). [9] Kehew et al. (2012) *Earth Science Reviews, 113*(1), 33-58.

**IMPACT DELIVERY OF REDUCED GREENHOUSE GASES ON EARLY MARS** R.M. Haberle[1], K. Zahnle[1], and N. Barlow[2] , [1]Space Science and Astrobiology Division, NASA/Ames Research Center, Moffett Field, CA 94086, [2] Dept. Physics and Astonomy, Northern Arizona University, Flagstaff, AZ 86011.

**Introduction**. Reducing greenhouse gases are once again the latest trend in finding solutions to the early Mars climate dilemma. In its current form - as proposed by Ramirez et al. [1], later refined by Wordsworth et al. [2], and confirmed by Ramirez [3] - collision induced absorptions between $CO_2$-$H_2$ or $CO_2$-$CH_4$ provide enough extra greenhouse power to raise global mean surface temperatures to the melting point of water provided the atmosphere is thick enough and the reduced gases are abundant enough. To raise surface temperatures significantly by this mechanism, surface pressures must be at least 500 mb and $H_2$ and/or $CH_4$ concentrations must be at or above the several percent level. Both Wordsworth et al. [2] and Ramirez [3] show that the melting point can be reached in atmospheres with 1-2 bars of $CO_2$ and 2-10% $H_2$; smaller concentrations of $H_2$ will suffice if $CH_4$ is also present.

If thick weakly reducing atmospheres are the solution to the faint young Sun paradox, then plausible mechanisms must be found to generate and sustain the gases. Possible sources of reducing gases include volcanic outgassing, serpentinization, and impact delivery; sinks include photolyis, oxidation, and escape to space. The viability of the reduced greenhouse hypothesis depends, therefore, on the strength of these sources and sinks.

**Sources.** Volcanic outgassing of reduced gases is possible given that the Martian mantle appears to be more reducing than Earth's [4,5]. Oxygen fugacities in Martian meteorites range from Iron-Wüstite (IW) all the way up to the Quartz-Fayalite-Magnetite (QFM) buffer [4]. If the early Martian mantle was at the low end of this range then a greater fraction of $H_2$, $CH_4$, and CO would have been included in the outgassed materials. However, a reducing mantle will outgas less $CO_2$.

Serpentinization is a mechanism in which ultramafic minerals (e.g., olivine) are hydrothermally altered to produce serpentine and magnetite, liberating $H_2$ in the process. If $CO_2$ is present in the water it can react with $H_2$ to produce $CH_4$. Thus, serpentinization can produce both $H_2$ and $CH_4$. Serpentine deposits have been identified on the surface [6] and extensive crustal serpentinization may have taken place early in the planet's history [7] though evidence for this is not seen in the canyon walls of Vallis Marineris [8].

Impact degassing of asteroids and comets is a third source of reduced gases. The intense heat and rapid chemistry following an impact will produce $H_2$ and can produce $CH_4$ depending on the composition, size, and entry velocity of the impactor, as well as the composition and strength of the target material [9,10,11].

**Sinks.** Sinks for reduced gases are more easily quantifiable. $H_2$ escapes while $CH_4$ is photolyzed and/or oxidized. If $H_2$ escapes at the diffusion limit, a simple analytical expression can be used to calculate escape rates as a function of the volume mixing ratio (VMR) and exobase temperature. However if the $H_2$ VMR is high enough, escape becomes energy-limited; this too can be calculated from a simple expression [see, for example, ref 12]. The sink for methane can be expressed by its photochemical lifetime.

**A Simple Model**. In this work we focus on the production of reduced gases by impacts. Impact production is the least well understood source and the model we construct is meant to assess its potential. We employ a stochastic cratering model that reproduces the observed crater size frequency distribution of Noachian surfaces (Fig. 1).

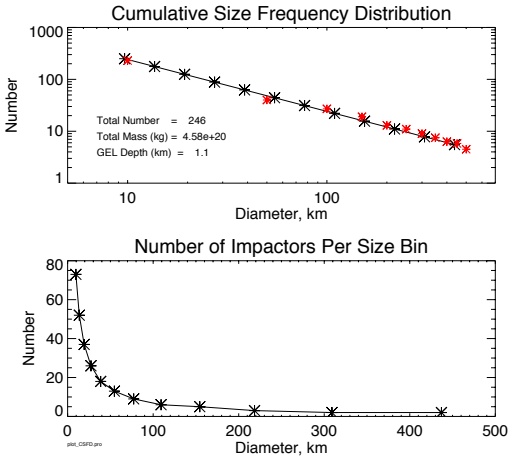


Fig. 1. Top: Cumulative size frequency distribution: modeled (black) observed (red, from Segura et al. [13]). Bottom: Number per size bin. There are 12 size bins.

For each simulation impactors are randomly assigned to the 100 model time bins which are chosen to emphasize early delivery. The model then marches through 400 My of time from 4.1-3.7 Ga keeping track of the reduced gases released into a 1 bar $CO_2$ atmosphere after each impact.

At present we focus on $H_2$ and simply specify that a fraction of the impactor mass, $f_{H2}$, is converted to $H_2$ with $f_{H2}$ ranging from 0.04-0.4%.This is the range of values we estimate from the gas equilibrium calcula-

tions of [9] and [11] for several classes of asteroids, and from our own work for comets.

Escape of $H_2$ in the model, shown in Fig. 2, occurs at the rapid diffusion limit for low $H_2$ VMR's and at the slower energy limit for high $H_2$ VMR's. The transition between these two regimes, which depends on the Sun's XUV flux, occurs for a $H_2$ VMR ~1 at 4.1 Ga. VMR's this high can be achieved by volatile-rich cometary impactors, such as our $f_{H2}$=0.4% case, greater than 300 km in diameter. There are 4 such impacts in our model suggesting that $H_2$ escape may be throttled by energy limitations following such impacts.

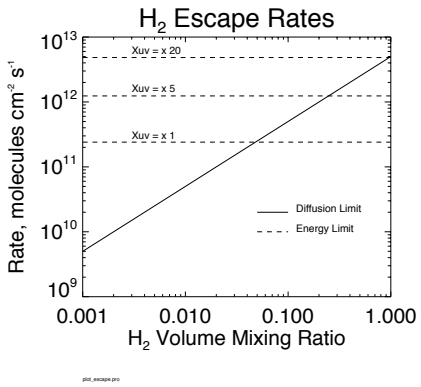


Fig 2. Hydrogen escape rates. Diffusion limit = ($H_2$ VMR) x b/H where b/H=$10^{13}$ molecules $cm^{-1}$ $s^{-1}$. Energy limited escape is shown for several values of the Xuv flux. For a given VMR, the model uses the minimum rate.

**Results.** Fig 3 shows a typical result for a single simulation with $f_{H2}$=0.04%, which is our estimate for the H-chondrites in ref [9] and is our least favorable case for $H_2$ production. $H_2$ VMR's are generally less than $10^{-3}$ throughout this simulation which is not high enough to significantly raise global mean surface temperatures. However, $H_2$ VMR's do spike following large impacts and in some cases exceed the 10% concentration level (horizontal dashed line in bottom panel of Fig. 3) required to raise global mean surface temperatures to the melting point – at least according to the models of [2] and [3]. For this particular simulation atmospheric VMR's > 0.1 (i.e., 10% concentration) are sustained for a total of 24 My. For cometary like impactors, where we estimate $f_{H2}$=0.4%, post-impact atmospheric VMR's > 0.1 are more frequent and the amount of time spent near the melting point can be doubled. Thus, the total time spent near the melting point from this simple model assuming a range of impactor types is in the 10s of millions of year range, which is an interesting result.

**Discussion**. There are, of course, many issues we have swept under the rug. The main ones are our assumed crater size distribution, the timing of delivery, the size of the early atmosphere, the mix of impactor types, and the details of $H_2$ escape.

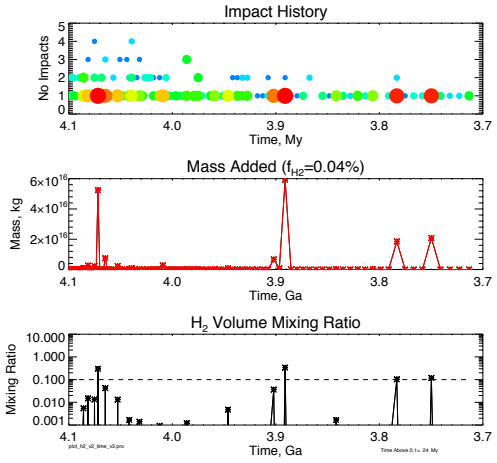


Fig 3. Top: Number of impacts vs time. Each filled circle is an impact event. Circle size and color are proportional to impactor diameter. Middle: Mass added after each event. Bottom: $H_2$ volume mixing ratio.

These are complicated, potentially show-stopping subjects, that need further study. Between now and the meeting, we plan to improve each of these aspects of the model. For example, to improve the impact size distribution information, we are utilizing Barlow's revised *Catalog of Large Martian Impact Craters* [14] to identify all impactors ≥10-km-diameter. For the moment, however, these simple calculations suggest that impact delivery of reduced greenhouse gases is a potentially important part of the early Mars story and may be part of the solution to the early Mars paradox.

**References:** [1] Ramirez et al. (2014), Nature Geo. 7, 59-63. [2] Wordsworth, et al., (2017), Geophys. Res. Lett., 44, 665-671. [3] Ramirez (2017), Icaurs, 297, 71-82. [4] Wadhwa, M. (2008), Rev. Mineral. and Geochem. 68,493-510. [5] Hirschmann et al. (2008), Earth and Planet. Sci. Lett. 270, 147–155. [6] Ehlmann et al. (2010), Geophys. Res. Lett. 37, 6. [7] Chassefière et al. (2013), J. Geophys. Res., 118, 1123-1134. [8] Edwards et al. (2008), J. Geophys Res., 113(E11003), doi: 10.1029/2008JE00309. [9] Schaefer and Fegley (2007), Icarus, 186, 462–483. [10] Schaefer and Fegley (2010), Icarus, 208, 438–448. [11] Hashimoto et al. (2007), J. Geophys. Res., 112, E05010. [12] Tian et al. (2005) Science, 308, 1014-1017. [13] Segura et al. (2008), J. Geophys. Res., 113, E11007. [14] Barlow N. G. (2017), LPS XLVIII, Abstract #1562.

**LIMIT CYCLES CAN EXPLAIN FLUVIAL FEATURES ON EARLY MARS.** J. Haqq-Misra[1], N. E. Batalha[2], R. K. Kopparapu[3], S. Kadoya[4], and J. F. Kasting[2], [1]Blue Marble Space Institute of Science (jacob@bmsis.org), [2]The Pennsylvania State University, [3]NASA Goddard/University of Maryland, [4]University of Tokyo.

**Summary:** For decades, scientists have tried to explain the evidence for fluvial activity on early Mars, but a consensus has yet to emerge regarding the mechanism for producing it. One hypothesis suggests early Mars was warmed by a thick greenhouse atmosphere. Others suggest that early Mars was generally cold but was warmed occasionally by impacts or by episodes of enhanced volcanism. These latter hypotheses struggle to produce the amounts of rainfall needed to form the martian valleys, but are consistent with inferred low rates of weathering compared to Earth.

Here, we provide a geophysical mechanism that could have induced cycles of glaciation and deglaciation on early Mars. Our energy balance climate model calculations show the conditions under which early Mars [1], as well as other planets in the outer regions of the habitable zone [2], should oscillate between long, globally glaciated states and shorter periods of climatic warmth, known as 'limit cycles'.

**Modeling the Outer Edge of the Habitable Zone:** The carbonate-silicate cycle regulates atmospheric $CO_2$ on geologic timescales through the weathering of silicate rocks into carbonate rocks, balanced by outgassing of $CO_2$ from volcanoes. Silicate weathering slows down as temperature decreases, which allows an Earth-like planet to accumulate a dense $CO_2$ atmosphere at lower levels of instellation, such as toward the outer edge of the HZ. But silicate weathering is also enhanced in the presence of a dense $CO_2$ atmosphere, which can cause the rapid draw-down of $CO_2$ and loss of greenhouse warming. This suggests that some planets, including early Mars, may actually be caught in such a cycle where warm conditions come only briefly between long episodes of global glaciation.

We develop a model that allows us to determine the limit cycle boundaries relative to the conventional liquid water HZ for different stellar spectral types [2]. Our energy balance model (EBM) calculations improve upon previous work by Menou [3] and Kadoya & Tajika [4,5] by implementing an updated parameterization of radiative transfer as well as including the effect of $CO_2$ condensation and the impact of seafloor weathering.

**Warming Early Mars:** Our model produces dramatic climate limit cycles with extended periods of glaciation punctuated by warm periods lasting up to 10 Myr, much longer than those generated in other episodic warming models [1]. The cycles occur because solar insolation was low, and because $CO_2$ outgassing is not able to keep pace with $CO_2$ consumption by silicate weathering followed by deposition of carbonates. While $CO_2$ by itself is not able to deglaciate early Mars in our model, we assume that the greenhouse effect is enhanced by modest to substantial amounts of $H_2$ and/or $CH_4$ outgassed from Mars' reduced crust and mantle.

We argue that the presence of fluvial features on early Mars can be explained, at least in part, from limit cycles that occurred through modulation of $CO_2$ by the carbonate-silicate cycle under a faint young sun. Recent calculations [6] indicate that collision induced absorption in a $CO_2$-$H_2$ atmosphere is even more effective than previously thought, and thus aids in maintaining habitable surface conditions. This reduces the amounts of required $CO_2$ and $H_2$ compared to those calculated by [1], thereby lowering the volcanic outgassing rates needed to make this mechanism work. We are currently exploring this with our EBM.

Recently, Ramirez [7] has argued that, given the uncertainties in the $pCO_2$ dependence of weathering, limit cycling should *not* have occurred on early Mars and that the climate should have been maintained in a stable, warm state. We acknowledge that our weathering rate parameterizations are uncertain. However, limit cycling is predicted to occur whenever low stellar flux and low volcanic outgassing rates combine to generate such unstable conditions. Thus, as Mars' interior cooled and the rate of volcanism slowed, it seems inevitable that the planet would have passed through the limit cycling regime, had it ever been warm in the first place.

The limit cycle hypothesis for early Mars remains consistent with available geological proxies, suggesting that liquid water flowed on Mars for long enough to carve fluvial features--but still in punctuated episodes of warmth between longer periods of time. Our hypothesis can be tested by future Mars exploration that better establishes the time scale for valley formation.

**References:** [1] Batalha N. E. et al. (2016) *Earth. Planet. Sci. Lett., 455*, 7–13. [2] Haqq-Misra J. et al. (2016) *ApJ, 827*, 120. [3] Menou K. (2015) *Earth. Planet. Sci. Lett., 429*, 20. [4] Kadoya, S. & Tajika, E. (2014) *ApJ, 790*, 107. [5] Kadoya, S. & Tajika, E. (2015) *ApJL, 815*, L7. [6] Wordsworth R. et al. (2017) *Geohys. Res. Lett. 44*, 665-671. [7] Ramirez, R. M., *Icarus*, in press.

**Warming Ancient Mars with Water Clouds.** V. L. Hartwick[1] and O. B. Toon[1], [1] Department of Atmospheric and Ocean Sciences, Laboratory of Atmospheric and Space Physics, University of Colorado at Boulder, Boulder, CO, USA (viha1825@colorado.edu)

**Introduction:** High clouds in the present day Mars atmosphere nucleate on interplanetary dust particles (IDPs) that burn up on entry into the Mars atmosphere. Clouds form when superstaturated water vapor condenses on suspended aerosols. The classic view of cloud nucleation on Mars considers mineral dust lofted from surface deposits as the sole source of ice nuclei. However, it is difficult to mix these aerosols to high altitudes where clouds are observed. We consider smoke particles formed from the ablation of micrometeoroids a reasonable high altitude source of ice nuclei.

Water ice clouds above 30-40 km are extremely common and are observed year round. Clouds are optically thin but can have large radiative impacts. Radiatively active water ice clouds may play a crucial role in warming the early Mars climate. Urata and Toon [1] simulate a stable warm paleo-climate for Mars if clouds form high in the atmosphere and if particles are sufficiently large (r > 10um).

The annual fluence of micrometeors at Mars was larger early on in the evolution of our solar system [2]. Additionally, the water vapor budget throughout the middle and high atmosphere was likely heightened [1]. Both factors should contribute to enhanced nucleation and growth of water ice cloud particles at high altitudes. Here, we examine the radiative impact of high altitude water ice clouds on the early Mars climate and as a possible solution to the faint young sun problem for Mars.

**Model Description:** MarsCAM-CARMA is a three-dimensional general circulation model adapted for Mars from the NCAR Community Atmosphere Model (CAM3.1) in 2013 [4] .The Mars hydrological and dust cycles are extremely tightly coupled; we therefore choose to incorporate physically based, fully interactive representations for both dust lifting and advection [5] as well as cloud nucleation, growth and precipitation. Aerosol microphysics are treated in a bin-resolved sectional model (CARMA).

We consider a constant fluence of interplanetary dust particles distributed evenly at the model top. The observed altitude of peak ablation (approximately 90 km) is above our highest simulated atmospheric level; we therefore assume total ablation and recoagulation into 0.01 um smoke particles. IDP and surface dust particles are treated as compositionally identical in simulations.

Detections by the IUVS instrument on MAVEN place a lower limit for the present day global IDP flux of 2-3 tonnes per sol [6]. For paleo-mars simulations we vary fluences from 10 to 1000 tonnes per sol.

**Results:** The addition of IDP smoke particles to the Martian high atmosphere enhances cloud formation at pressures below 100 Pa in simulations of the present day Mars climate. Figure 1 shows the zonal average ice extinction [$km^{-1}$] at the northern hemisphere spring equinox for SPICAM wavelengths (approximately 1.38 μm). Cloud layers are stretched vertically at all latitudes and in particular over the southern polar cap. High altitude cloud layers in simulations with IDPs are particularly notable in the northern midlatitudes near 50N.

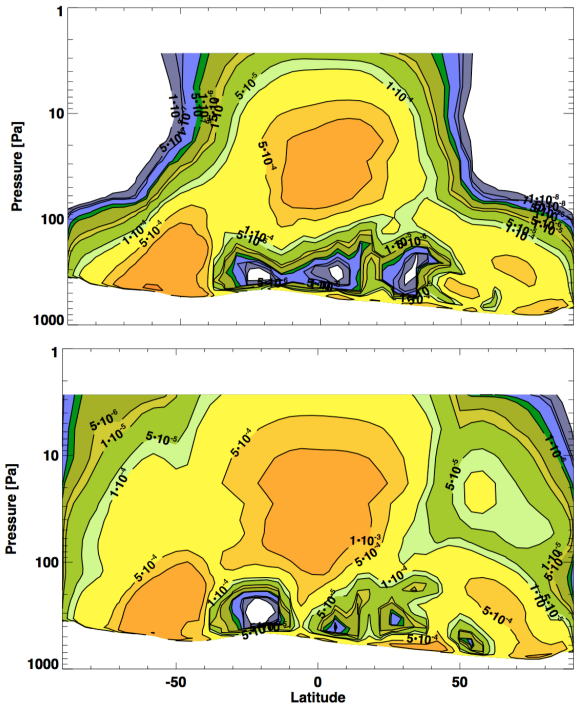


*Figure 1: Simulated zonal average ice extinction ($km^{-1}$) at 1.25 μm versus pressure [Pa] for simulations with (bottom) and without (top) IDPs. Data is averaged over 2 days near Ls=180. Contour levels cover the range of $1x10^{-8}$ to $5x10^{-2}$ with half an order of magnitude intervals.*

Clouds at high altitudes impact the average atmospheric thermal structure. At the same season, the addition of IDPs leads to a 3K warming at tropical high altitudes (Figure 2). Clouds can additionally indirectly impact climate by influencing large scale circulation patterns and through complex feedbacks with the global dust cycle. Similar enhancements in cloud formation

are anticipated at high altitudes in paleoclimate simulations. These new cloud features should play an important role in the atmospheric thermal structure and may enhance surface warming. We will discuss simulations similar to those of Urata and Toon [1] exploring the ability of these clouds to solve the fain young sun problem for Mars.

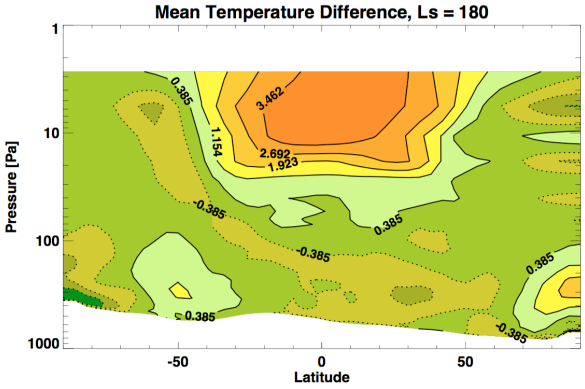


*Figure 2: Simulated difference in the mean temperature versus pressure for simulations with IDPs minus simulations without IDPs. Data is zonally averaged over 10 days near Ls=180. Dashed contours indicate cooling, solid contours, warming.*

**References:**

[1] Urata R. A. and Toon O. B. (2013a) *Icarus, 226, 1,* 229-250. [2] Maurette M. et al. (2006) *Adv. Space Res., 38,* 701-708. [3] Mischna M. A. et al. (2013) *J. Geophys. Res. Planets, 118,* 560-576. [4] Urata R. A. and Toon O. B. (2013a) *Icarus, 226, 1,* 336-354. [5] Kahren M. A. et al. (2006) *J. Geophys Res. 111*, E06008. [6] Crismani, M. M. J. et al. (2017) *Nat. Geosc. 10,* 401-404.

**DECIPHERING THE NOACHIAN GEOLOGICAL AND CLIMATE HISTORY OF MARS: A STRATIGRAPHIC, GEOLOGIC PROCESS AND MINERALOGICAL PERSPECTIVE – PART 1: CURRENT KNOWNS AND UNKNOWNS.** J. Head[1], R. Wordsworth[2], F. Forget[3], and M. Turbet[3], [1]Brown Univ., Providence, RI 02912 USA (james_head@brown.edu), [2]Harvard University, Cambridge MA 02138 USA, [3]Lab. de Météorolog Dynamique du CNRS, Université Paris 6, Paris, France.

**Introduction:** The Late Noachian (LN) climate, be it warm and wet or cold and icy, is inherited from events that occurred earlier in Mars history [1]. We first outline what is known and what remains unexplained about Noachian/Hesperian history and events, and then examine the full range of geological processes known to precede and immediately follow the Late Noachian period of fluvial and lacustrine activity. We conclude that this new geologic/stratigraphic framework provides an important perspective in which to view the climate history of early Mars which we develop separately [2].

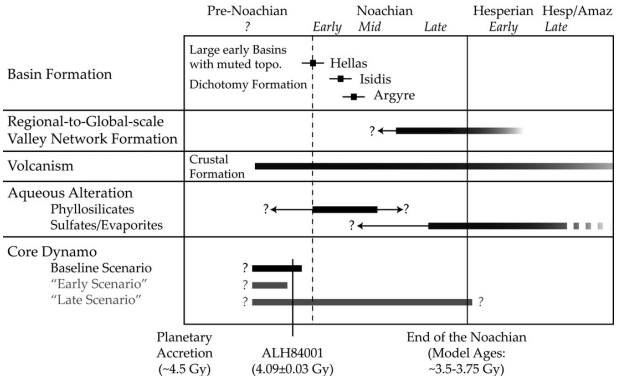


Fig. 1. Early Mars history and key events/processes [3].

**Knowns and Unknowns:** Fassett and Head [3; see references therein for the following points] reviewed the sequence and timing of conditions on early Mars (Fig. 1), and we use this as a baseline for identifying key knowns and unknowns, focusing on the Noachian. 1) Mars was characterized by the existence of an *active magnetic dynamo*; unknown is whether this persisted into the Noachian, and the influence of its decay and demise on the retention of the atmosphere. 2) Early Mars was characterized by a *much higher impactor flux* and a more significant role for impact cratering at all scales; unknown is the flux size-frequency distribution, whether its decay was monotonic [4], and how much of the volatile inventory and atmosphere were provided by this exogenous mechanism. 3) *Multiple large impact basins*, the largest being the Borealis Basin, formed during this period, including, in the Noachian, Hellas, Isidis and Argyre; unknown in detail are the effects of these individual basin-scale events on the atmosphere, surface, and interior. 4) *Magmatic processes* (plutonism/intrusion and volcanism/extrusion) were of critical importance in building the crust, resurfacing the evolving cratered surface, and providing exsolved (endogenous) volatiles to build the atmosphere; unknown is the time of transition from pre-Noachian early crust to the dominance of mantle-derived magmatism and volcanic resurfacing, the volcanic flux and resurfacing rate, the ratio of effusive to explosive eruptions, the nature of mantle petrogenesis and implications for the surface mineralogy, and endogenous volatile contributions to the atmosphere. 5) A significant part of the *Tharsis rise/volcanic province* had been constructed by the end of the Noachian; unknown is the mechanism for its formation, the detailed volcanic flux and implications for endogenous atmospheric input, and even whether Tharsis could have been constructed *after* LN valley network (VN) formation [5]. 6) Formation of the Tharsis rise stabilized Mars from *true polar wander* (TPW); unknown is whether Tharsis emplacement caused TPW, and whether TPW ever occurred. 7) The emplacement of *widespread flood lavas* occurred in the Late Noachian and Early Hesperian, resurfacing at least 30% of Mars and played a huge role in endogenous atmospheric input, potentially significantly warming and altering the climate episodically; explosive volcanic activity, forming paterae and ash deposits, also occurred; unknown is the petrogenesis, magmatic volatile content and flux, and the influence of emplacement on the climate. 8) Impact craters underwent significant degradation during the Noachian, erasing craters <~10-20 km; larger craters lost sharp rim crests and ejecta and underwent significant infilling and shallowing; unknown is the exact mechanism(s) of degradation and infilling, the relation to warm and wet [6] or cold and icy [7-9] climates (Fig. 2) and the implications for climate history. 9) Crustal rocks underwent *widespread aqueous alteration and phyllosilicate formation* during the Noachian, requiring environments above 273K for a range of times (Figs. 2, 3); unknown are the required ranges of elevated temperatures and times, and the exact environments of formation (subsurface hydrothermal, surface climate environmental?). 10) *Minerals readily altered by the presence of liquid water*, apparently dating from the Noachian (e.g., olivine), *are often preserved* to the present, in apparent contradiction to the extensive development of phyllosilicates and related alteration minerals. 11) *Weathering/erosion rates were orders of magnitude higher* in the Noachian than immediately thereafter, although still much lower than those on Earth; unknown are the process(es) responsible and the cause of the radical decrease. 12) An *assemblage of liquid water-related features* (VN, hundreds of open and closed-basin lakes, and perhaps oceans), provides extensive geologic evidence for aqueous precipitation (rainfall), regional overland flow and drainage, lake formation and perhaps oceans; unknown are the specific climatic condition that

led to this assemblage of features, and whether they formed contemporaneously, continuously or episodically. 13) Estimates of the initial *global water budget* range over several orders of magnitude; the surface/near-surface water budget at the end of the Noachiam has been estimated at ~ 24 GEL [10]; unknown are the original global abundances, additions and losses with time, and evolution of the total water budget, its partitioning to the surface/near surface inventory, and its state. 14) Noachian Mars was characterized by a much *higher atmospheric pressure than today*, perhaps even as much as several bars; unknown are the sources and relative proportions of the gases contributing to the atmosphere, their accumulation and loss rates, fluctuations during the Noachian, and the nature of the transition to Hesperian/Amazonian atmosphere and climate. 14) The *Noachian transition to the Hesperian period* involved major changes in cratering (decreased flux, no major basins), volcanism (flood basalts decrease after Early Hesperian), mineralogy (phyllosilicates to sulfates), fluvial processes (VN to LH outflow channels), atmospheric pressure, and erosion rates; unknown are the rates of these changes, their possible relationships, and their influence on climate history. 15) The *Noachian climate* has been interpreted to be characterized over some period by warm and wet conditions [6] (Figs. 2, 3) required by pervasive phyllosilicate alteration, extensive crater degradation and infilling, and the presence of valley networks and related pluvial, fluvial and lacustrine features; unknown is the nature of the ambient background climate (e.g., was it "*warm and wet*", "*warm and arid*" (both with MAT >273 K) (Fig. 3) or "*cold and icy*" (MAT ~225 K) (7-9) (Fig. 4) with episodic, periodic punctuated excursions to 273 K (Fig. 3).

**Summary:** On the basis of these Noachian knowns and unknowns, we apply a stratigraphic approach to the major geological processes and observations [2] to provide insight into potential changes as a function of time.

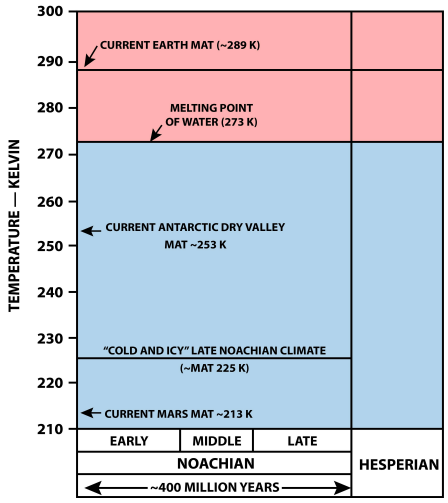


Fig. 2. Temperature-time framework for Noachian climate history illustrating key MAT (mean annual temperatures).

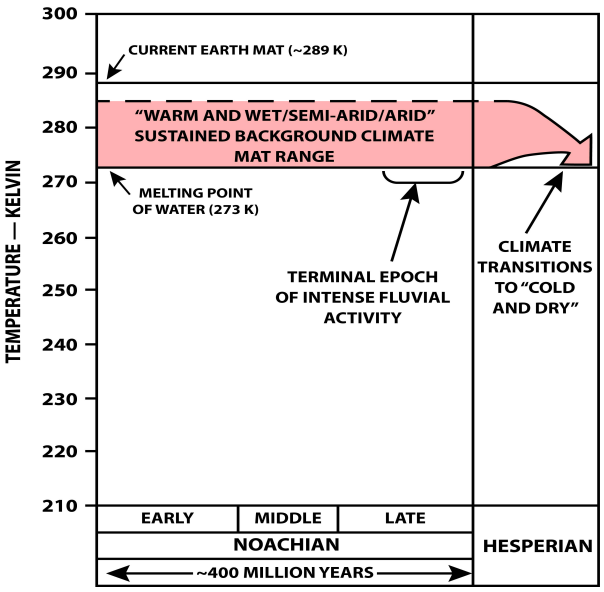


Fig. 3. Baseline "warm and arid/wet" climate conditions.

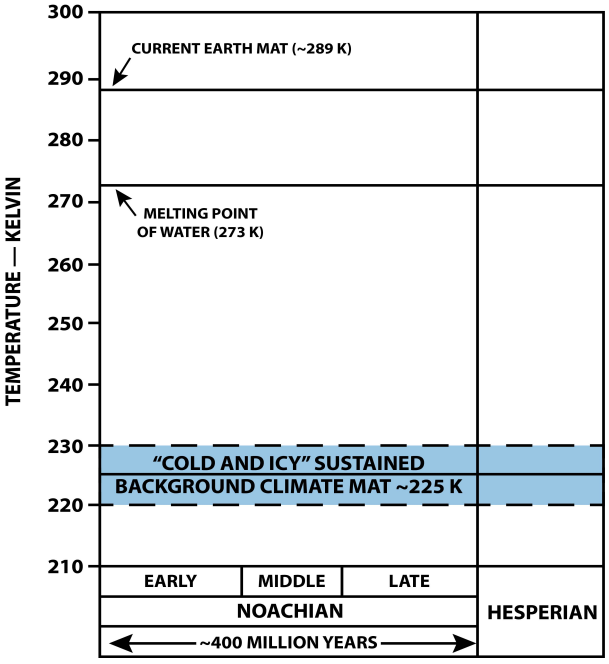


Fig. 4. Baseline "cold and icy" climate conditions.

**References:** 1. Head et al., 2015, LPSC 46, #2176; 2. Head et al., 2017, 4th EMC; 3. Fassett and Head, 2011, Icarus 211, 1204; 4. Bottke and Andrews-Hanna, 2017, Nat. Geosci.; 5. Bouley et al., Nature 531, 344; 6. Craddock and Howard, 2002, JGR 107, 5111; 7. Forget et al. 2013, Icarus 222, 81; 8. Wordsworth et al., 2013, Icarus 222, 1; 9. Head and Marchant, 2014, Ant. Sci. 26, 774; 10. Carr and Head, 2015, GRL 42, 1.

**DECIPHERING THE NOACHIAN GEOLOGICAL AND CLIMATE HISTORY OF MARS: PART 2 - A NOACHIAN STRATIGRAPHIC VIEW OF MAJOR GEOLOGIC PROCESSES AND THEIR CLIMATIC CONSEQUENCES.** J. Head[1], R. Wordsworth[2], F. Forget[3], and M. Turbet[3], [1]Brown Univ., Providence, RI 02912 USA (james_head@brown.edu), [2]Harvard University, Cambridge MA 02138 USA, [3]Lab. de Météorolog Dynamique du CNRS, Université Paris 6, Paris, France.

**Introduction:** We apply a stratigraphic approach to the major Noachian geological processes and observation, knowns and unknowns [1-3] to provide insight into potential changes as a function of time, and to assess their climatic consequences.

**Early Noachian:** This is the era of large impact basins, with Hellas Basin defining the base of the Noachian, followed by formation of Isidis and Argyre. Impacts are known to have size-dependent effects in terms of ejecta and influence on the atmosphere, ranging from blowing off a significant part of the atmosphere, through global distribution of silicate vapor that results in precipitation of silicate vapor cloud condensate, and significant but short-lived very hot rainfall [4-6]. Recent research has underlined the size-dependent effects, finding that large basins could form global effects while those below ~50 km would have only local effects [7]. Could the global effects form a global stratigraphic marker horizon for the major Noachian basin analogous to the Imbrium basin on the Moon?

**The Noachian Mineralogical Alteration Paradox:** Ever since OMEGA [8] documented the dominance of phyllosilicates (clays) in the Noachian, a solution has been sought to provide the three necessary ingredients to account for their formation: 1) abundant liquid water, 2) temperatures >273K, and 3) prolonged exposure [9], while at the same time accounting for other observed minerals (e.g., olivine) that are unstable under these conditions. A "warm and wet" climate has often been cited as the solution [10], but the phyllosilicates do not clearly coincide in time or space with the Late Noachian VN/CBL/OBL assemblage [3], leading many to consider that at least some of the phyllosilicates formed deeper in the crust under hydrothermal conditions [11]. A solution to this paradox might be found in the formation of impact basins earlier in the Noachian: In an update [6] of the global effects of impact basin formation [4-5], the immediate aftermath of the vapor cloud condensation is shown to be characterized by the global precipitation of sustained hot rains (considerably above 273K), and lasting for several centuries. This mechanism (Fig. 1) [6] provides widespread, extremely hot water interacting with the surface and near-surface substrate for centuries, a duration sufficient to provide leaching of decameters of substrate. Support for this hypothesis [6] comes from extensive the association of many of the phyllosilicates with the Noachian basins Hellas, Isidis and Argyre [9, 12-13] and other extensive deposits dated to this period [14]. These deposits may provide stratigraphic time-markers for the specific impact basins [6, 15].

**Middle-Late Noachian:** This is the post-Argyre basin period; impact cratering at the sub-large basin scale continues with declining flux. In the "warm and wet/arid" climate scenario [10], the dominant process of crater degradation (loss of small craters; erosion of larger crater rim/ejecta, infilling of crater interior) is rainfall-related diffusional processes that are intermittent and at sufficiently low rates that water infiltration dominates over surface runoff and VN systems do not form. In this scenario, although the climate is arid, MAT is required to be >273 K [10], implying a vertically integrated hydrologic system in the equatorial/mid latitudes. This ambient "warm and arid" climate is envisioned to persist for several hundred million years [10] (Fig. 1). The Late Noachian dominance of the VN-CBL-OBL geomorphic assemblage is envisioned as representing a "climatic optimum" [16], producing "warm and wet" conditions characterized by sufficient rainfall precipitation to overcome infiltration, and cause widespread fluvial and lacustrine activity. Here we separate out the "crater loss/degradation" component of the "warm and arid/wet geomorphic assemblage" and treat separately the remaining "pluvial/fluvial/lacustrine" component (VN/CBL/OBL).

***"Crater Loss/Degradation" Component:*** Are there alternatives to the "warm and arid crater loss/degradation" [10] scenario? Could the formation of the earlier Noachian impact basins have played a role? Following [4-5], [6] have proposed that global deluge-scale rainfall phases that immediately follow basin formation could obliterate small craters and cause extensive planation and infilling of pre-existing distal craters. Furthermore, [7] have shown that smaller basins and large craters may also produce regional erosion and degradation effects. Detailed stratigraphic analyses are required to assess this option further [6]. A second alternative, involving the "cold and icy" climate scenario [17-19]; [20] explores the effects of a regional ice sheet predicted by this model in masking the sub-ice surface from smaller impacts, and facilitating the observed rim degradation and infilling of Noachian craters. Neither of these two options requires MAT in the >273 K range. We conclude that the "crater loss/degradation" component of the "warm and arid/wet geomorphic assemblage" may also be consistent with other climate scenarios

***Volcanism and Volcanic Resurfacing:*** The beginning of the LN-EH volcanism phase; resurfacing of Arabia Terra and other Noachian plains formation, potential explosive volcanism, and peak eruptive phases could potentially cause decades to centuries of warming [22].

**Late Noachian "Climate Optimum":** This is the known period of dominance of the VN-CBL-OBL geomorphic assemblage envisioned as representing a "climatic optimum" [16] (Fig. 1), transitioning from "warm and arid" to produce "warm and wet" conditions charac-

terized by sufficient rainfall precipitation to overcome infiltration, and cause widespread fluvial and lacustrine activity. Because of the alternative explanations for the "crater loss/degradation" component [6, 20], not involving MAT in the 273 K range, here we focus only on the "pluvial/fluvial/lacustrine" component (VN/CBL/OBL) of the "warm and arid/wet geomorphic assemblage" and assess the climate implications (Fig. 1). Key questions are: Nature of ambient climate [10, 18], source of water [21], volume of water [21], continuous or discontinuous conditions [21], intermittency [23], total duration [23], and presence of oceans [24]?

**The Late Noachian Climate Paradox (LNCP):** The Late Noachian climate paradox [1] can be stated as follows: 1) Robust LN Mars climate and general circulation models [17-18] predict MAT ~225 K, and an altitude-dependent stability of snow and ice, such that the surface water inventory is deposited preferentially above an ELA of ~+1 km (southern uplands and south circumpolar regions), the "icy highlands" model [18-19]. In this ambient atmosphere, no combination of spin-axis/orbital parameters can produce significant melting of this snow and ice anywhere on the planet [25]. 2) The well-documented, "pluvial/fluvial/lacustrine (VN/CBL/OBL)" component of the "warm and wet geomorphic assemblage" [10, 16], in contrast, shows unequivocally that liquid water flowed extensively across the surface, ponded, and overflowed, creating fluvial networks systems as long as 1000 km [3]. Clearly, these two aspects are incompatible and represent a paradox. On the one hand, climate modelers find great difficulty in achieving MAT >273 K (no combination of sustained greenhouse gas sources have been able to achieve MAT >273 K for the duration of M-L Noachian), and geologists have not found an alternate explanation to widespread flowing liquid water for the VN/CBL/OBL fluvial assemblage.

**A Candidate Solution to the Late Noachian Climate Paradox:** We propose that a solution to the LNCP lies in a "cold and icy" ambient background climate (MAT ~225K) [17-19] that undergoes multiple episodic/periodic regional to global warming perturbations, that either individually or collectively are sufficient to account for the observed "warm and wet geomorphic fluvial assemblage". Among the candidates for such perturbations are: 1) periods of abbreviated greenhouse gas release sufficient to raise MAT 10-15 K so that peak seasonal (PST) seasonal or peak daytime melting (PDT) can melt snowpack to form the observed VN/CBL/OBL [19, 25]; 2) Effusive/explosive volcanic eruptions at high enough fluxes that $SO_2$ release causes equatorial/mid-latitude atmospheric heating for decades to centuries to form the VN before global cooling [22]; 3) Post-Argyre large crater/small basin formation sufficient to perturb the atmosphere regionally to form the VN [7].

**Conclusions:** A stratigraphic approach to understanding the climate of Noachian Mars [1-3] indicates that: 1) The Early Noachian is dominated by the formation of Hellas, Isidis and Argyre basins; associated with each basin is the collapse of a global vapor plume, condensation of silicate vapor and a hundreds of year long phase of torrential hot rains, potentially accounting for significant alteration of surface materials to phyllosilicates [15]. The formation of each basin emplaced a global meters-thick isochronous silicate condensate time marker accompanied by significant associated alteration to phyllosilicates [15]. The Early Noachian ambient background climate was profoundly perturbed by each impact event, with exact recovery pathways and times uncertain [7]. On the basis of the difficulty of sustaining a "warm and wet/arid" climate [10] for several hundred million years (Fig. 1), we adopt the "cold and icy" post-basin period (MN-LN) climate to be the ambient background climate. The LN "climatic optimum", during which the VN/CBL/OBL systems formed, is interpreted to be due to one or more climatic perturbations operating to perturb MAT, PST, and/or PDT on the "icy highlands" climate model. These ideas can be tested with further analyses of the critical stages as described above. The transition from the Late Noachian to Early Hesperian sulfate formation is interpreted to be related to EH basaltic flood volcanism resurfacing at least 30% of the planet [26]; the subsequent waning global volcanic flux [21], together with losses to space [27], transitioned the global atmosphere toward decreased atmospheric pressure [28], an end to the "icy highlands", the reduction of south polar cap (DAF) area/volume [29], the beginning of a bi-polar Mars, and reduction to even lower weathering/erosion rates.

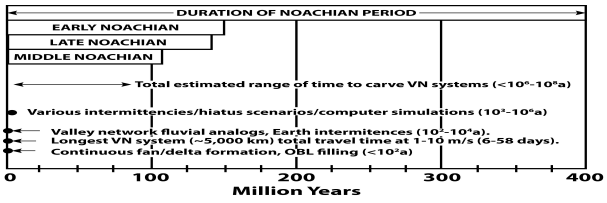


**Fig. 1. Estimates for VN formation duration (from [23]).**

**References:** 1. Head et al., 2017, 4th EMC; 2. Head et al., 2015, LPSC 46, #2176; 3. Fassett & Head, 2011, Icarus 211, 1204; 4. Segura et al., 2008, JGR, 113, E11; 5. Toon et al., 2010, AREPS 38, 303; 6. Palumbo et al., 2017, 6th MAMO; 7. Turbet et al., 2017, 6th MAMO; 8. Bibring et al., 2006, Science 312, 400; 9. Bishop et al., 2017, LPSC 48 1804; 10. Craddock & Howard, 2002, JGR 107, 5111; 11. Ehlmann et al., 2011, HNature 479. 53; 12. Murchie et al., 2009, JGR 114; 13. Mustard et al., 2006, JGR 112; 14. Bishop & Rampe, 2016, EPSL 448, 42; 15. Palumbo & Head, 2017, 8th Moscow S3; 16. Irwin et al., 2005, JGR 110, E12515; 17. Forget et al. 2013, Icarus 222, 5111; 18. Wordsworth et al., 2013, Icarus 222, 1; 19. Head & Marchant, 2014, Ant. Sci. 26, 774; 20. Weiss and Head, 2015, Planet. Space Sci. 117, 401; 21. Carr & Head, 2015, GRL 42, 1; 22. Halevy & Head, 2014, Nat. Geosci.1-4; 23. Buhler et al., 2014, Icarus 241, 130; 24. Clifford & Parker, 2001, Icarus 154, 40; 25. Palumbo et al, 2017, LPSC 48 2107; 26. Head et al., 2002, JGR 107, E1; 27. Jakosky et al., 2017, LPSC 45 1114; 28. Halevy & Head 2017, LPSC 48 2519; 29. Scanlon et al., 2016, LPSC 47 1315.

**INCISION OF THE JEZERO CRATER OUTFLOW CHANNEL BY FLUVIAL SEDIMENT TRANSPORT**

Samuel J. Holo and Edwin S. Kite, University of Chicago, Chicago, IL, 60637. (holo@uchicago.edu)

**Introduction:** Jezero crater, the top candidate landing site for the Mars 2020 rover, once possessed a lake that overspilled and eroded a large outflow channel into the Eastern rim [1]. The Western deltaic sediments that would be the primary science target of the rover record a history of lake level, which is modulated by the inflow and outflow channels. While formative discharges for the Western delta exist (~500 $m^3/s$) [2], little work has been done to see if these flows are the same responsible for outflow channel incision [3].

Previous models (e.g. [3]) of the Jezero outflow channel incision assume that a single flood, with unknown initial hydraulic head and no discharge into the lake (e.g. from the inflow channels or the subsurface), incised an open channel with discharge modulated by flow over a weir.

We present an alternate model, where the incision of the outflow channel occurs in concert with lake filling due to an instability at the threshold of sediment motion. We identify controls on incision of the outflow channel and estimate the time scale of outflow channel formation through a simple dynamical model.

We find that the observed 300m of channel erosion [3] can be reproduced in decades to centuries of progressive bed load as the delta forming flows fill the lake. This corresponds to time scales on the order of or smaller than the time scale required for the delta forming flows to fill the crater.

**Model Description:** We assume that the outflow channel is hydraulically connected to the crater lake and that pressure gradients between the lake and channel equilibrate on a time scale smaller than the erosion time scale (Fig. 1A). The channel is assumed to have a rectangular cross section, a planar slope, and banks that fail at the angle of repose (Fig. 1B).

The lake rises and falls at a rate proportional to the net discharge rate and inversely proportional to its cross sectional area. Mean flow through the channel is modeled using Manning's equation and Manning's n is assumed to scale with channel roughness and median grain size [4,5].

The model assumes capacity sediment transport using the Meyer-Peter and Mueller relation [6], that the slope is uniform in the channel at all times during the simulation, that the channel has a fixed elevation boundary at its distal edge, and that mass is conserved.

This model does not resolve backwater effects or concavity in the alluvial system, but it does capture the non-linear feedbacks between lake draining, erosion rate, channel flow rate, and slope relaxation.

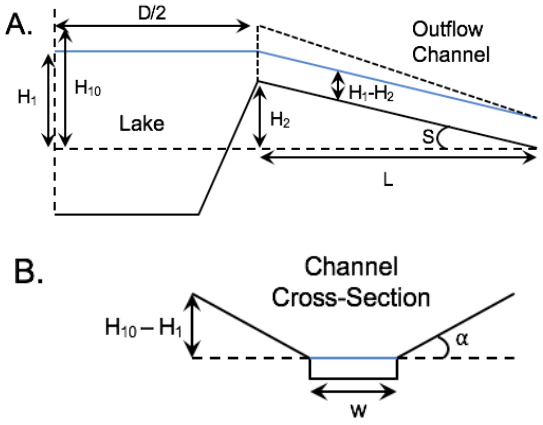


**Figure 1.** Schematic of model geometry (A = long section, B = cross section). Blue lines represent the water level. Finely dashed line in A. shows the initial topography.

**Model Results:** Each simulation is initialized by choosing the channel slope, width, and length scale, as well as the crater diameter, grain size, and inflow rate. In all simulations, the angle of repose is taken to be 30° and the critical Shields number for incipient motion is taken to be 0.045.

At the threshold for incipient sediment motion, there is a unique inflow rate that allows the lake level to stay steady without eroding the channel. For lower inflow rates, the lake level drops and erosion is impossible. For higher inflow rates and nearly fixed channel width, the lake level rises, initiating erosion.

In the cases where erosion occurs, the lake level rises until enough of the underlying material has been excavated for the outflow discharge to exceed the inflow rates (recall discharge scales super-linearly with flow depth). When the lake level starts to fall, it initiates a large erosion pulse that is rapidly shut down due to increased contribution by the channel banks to the sediment flux. The channel then enters a longer term period of convergence to negligible erosion.

A representative simulation using Jezero-relevant length and slope parameters is shown in Figure 2. For 6 cm gravels and inflow rate of 500 $m^3/s$, the observed ~300 m of channel incision can be obtained within ~100 years of initiating sediment transport. To compare this with the time required for the chosen inflow rate to fill the lake, we set $T \sim (0.1/q_{in})(D/2)^3$ where T is the time scale of lake filling and D is the crater diameter. In this case, we find that the time scale of erosion is equal to the lake filling timescale.

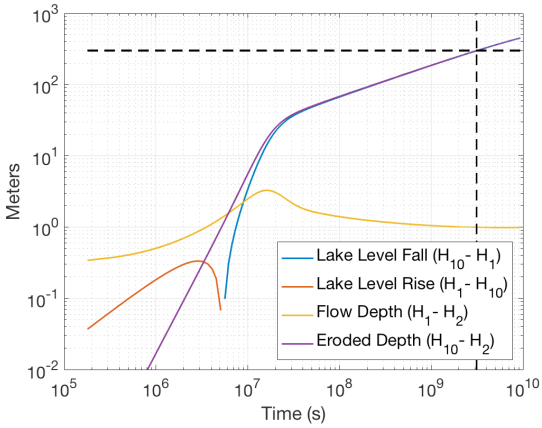


**Figure 2.** Representative Jezero simulation with an assumed grain size of 6 cm and assumed inflow rate of 500 $m^3/s$. Dashed lines show observed Jezero incision depth and independently inferred filling time scale.

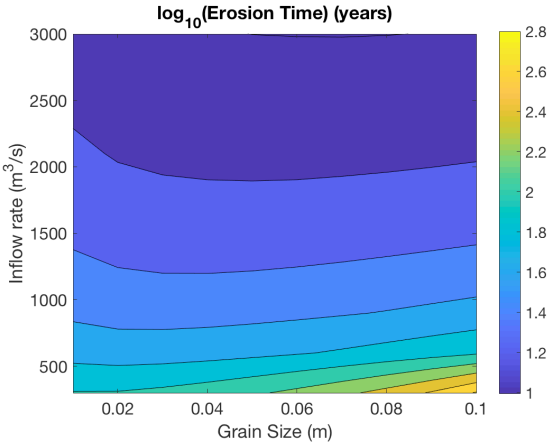


**Figure 3.** Effect of grain size and inflow rate on time to erode 300m starting from brim-full.

The model is sensitive to both choice of grain size and inflow rate (as well as length and slope parameters that are measurable from orbit). For increased inflow rate, the amount of time needed to erode 300m decreases (Fig. 3). The behavior is non-monotonic in grain size due to competing effects of increased grain size on flow roughness and on resistance to sediment transport (Fig. 3). For a wide range of parameters, the erosion can be achieved on a time scale within one order of magnitude of the filling time scale.

**Discussion of Model Assumptions:** This model framework relies on the assumptions that the flow in the channel is hydraulically connected to the lake, that channel width is constant, and that erosion of the outflow channel is largely transport limited. The transport limited approach is appropriate because the channel has relaxed its slope relative to the terrain around it with a fixed elevation at a distance L downstream, which is inconsistent with the conditions induced in detachment-limited models [7,8].

The hydraulic connectivity assumption contrasts with previous work done in [3] where increased elevation at the breach relative to the main channel was interpreted as some erosionally resistant portion of the rim that is modeled as a weir. We suggest alternate explanations for this observation. One, that this is the result of initial concavity near the rim not modeled here. Or two, that it is partial infilling of the valley after shutdown of the whole crater-lake system.

We assumed a constant channel width of 100m even though we cannot directly observe it due to post-fluvial infill. Variations in the flow depth are small relative to this assumed width in all simulations, suggesting that the contribution of changing channel width with lake level is also small.

**Conclusions:** We presented a simple model of incision of the Jezero outflow channel in which open channel flow and sediment transport modulate the crater lake level over century timescales.

We made simplifying assumptions about the geometry of the system to study the effect of feedbacks between lake level rising/falling, open channel flow, and sediment transport on outflow channel formation. Because we fully modeled these feedbacks, the results are not dependent on "bank full" theories. Further, the results support a progressive incision of the channel at low transport stages, consistent with other estimates for large outflow floods on both Earth and Mars [4,5].

While we present no direct evidence that the outflow channel incision occurred contemporaneously with lake-filling, our model does not require that the lake filling process shut down completely prior to channel incision (like in [3]). Comparison with the outflow channel dimensions from other craters on Mars provides the potential to both test our hypothesis of contemporaneous lake filling/channel incision and also constrain the hydrologic sources responsible for filling crater lakes.

**Acknowledgements:** We thank Caleb Fassett for a helpful discussion. We acknowledge funding from NASA (NNX16AG55G and NNX16AJ38G).

**References:** [1] Goudge, T. A. et al. (2016), *EPSL*, *458*, 357–365. [2] Fassett, C. I., Head, J.W. (2005), *GRL*, *32*, L14201. [3] Fassett, C.I. and Goudge, T.A. (2017) *LPSC* 48, 1145. [4] Lapotre, M.G.A. et al. (2016), *JGR – Planets,* 121(7), 1232-1263. [5] Larsen, I.J. and Lamb, M.P. (2016), *Nature*, 538(7624), 229-232. [6] Meyer-Peter, E. and Mueller, R. (1948) *Proc. Int. Assoc. Hydraulic Struct. Research*, 2, 39-64. [7] Perron, J.T. et al. (2008), *JGR*, 113. [8] Black, B.A. et al. (2012) *JGR*, 11.

**WHERE IS THE CLIMATE SIGNATURE IN THE MINERAL RECORD OF EARLY MARS?** B. Horgan[1], L. Baker[2], J. Carter[3], and O. Chadwick[4], [1]Purdue University (briony@purdue.edu), [2]University of Idaho, [3]Institut d'Astrophysique Spatiale, Université Paris-Sud, [4]University of California – Santa Barbara.

**Introduction:** Ancient surfaces on Mars exhibit a variety of secondary minerals that suggest the presence of liquid water [e.g., 1]; however, the implications of these minerals for surface environments and climates has not been resolved. Here we present a framework for interpreting weathering mineralogy based on terrestrial studies of climatic controls on surface weathering and identify outstanding knowledge gaps crtitical for Mars. Based on this framework, we propose that while most secondary minerals on early Mars likely formed in environments not directly linked to climate, a subset may have climatic implications.

**Weathering mineralogy under various climates:**

*Cold and perennially wet climates:* Cold climates here are defined as climates where precipitation is dominated by snow, and weathering occurs due to seasonal melt of snow and glaciers. On Earth, this occurs in arctic and alpine environments, and soils in these locations are dominated by poorly crystalline phases like allophane, which mature into more crystalline kaolins like halloysite and kaolinite [2,3]. Melt-driven weathering under alpine glaciers and above permafrost also produces poorly crystalline aluminosilicates [4,5], and on mafic terrains, glaciers also liberate significant silica that is precipitated as rock coatings [6]. These environments are dominated by poorly crystalline phases due to the high instantaneous leaching rates induced by melt events, which result in mineral deposition driven by kinetics instead of thermodynamics [7]. Under these constraints, the first minerals to precipitate will be dominated by the fastest minerals to precipitate, primarily poorly crystalline phases.

*Warm and perennially wet climates:* Warm climates here are defined as climates where precipitation mostly falls as rain, and in perennially wet climates, precipitation falls regularly either throughout the year or seasonally. This describes most soils on Earth. Under arid to semi-arid climates (typically <1m mean annual precipitation), terrestrial soils are dominated by smectite clays produced as the thermodynamically stable product of slower instantaneous weathering rates [2,8-10]. Over long time periods (typically My+), these soils mature to kaolinite. Under more humid climates (typically >1 meter mean annual precipitation), high instantaneous leaching rates lead to precipitation of poorly crystalline aluminosilicates which mature to kaolin clays on timescales of 100k+ years [11,12].

*Punctuated climates:* Punctuated climates here are defined as having precipitation dominated by rare but strong rainfalls or melt events. Weathering in these climates is similar to melt-dominated climates, where mineral deposition is controlled by kinetics, and poorly crystalline phases dominate [7]. Volcanic soils in humid climates produce large abundances of poorly crystalline phases due to rapid weathering of glass [13]. Over time, these phases mature into more crystalline halloysite and then kaolinite. This type of weathering has been observed on the dry side of Hawaii, where a few large storms deliver all of the precipitation in a given year [7]. In this area, the timescale for kaolin formation is millions of years [14].

**Weathering indicators applied to Mars:**

*Deep weathering profiles:* While the weathering profiles that produce most soils are typically on the meter scale or less, weathering over long timescales, at sustained high weathering rates, or on highly porous parent materials (e.g., tephra) can produce much deeper weathering profiles, ten meters or more in depth, which are thick enough to be observable from orbit. These weathering profiles are typically topped by kaolinite or other advanced weathering minerals (e.g., gibbsite, iron oxides) [15]. On Mars, kaolinite has been observed throughout Noachian terrains as a thin layer (meter-scale) above much thicker Fe/Mg-clays, and these occurences have been interpreted as leaching profiles indicating long-term rain-dominated weathering [16]. At Mawrth Vallis, a thick 40m+ sequence of kaolinite and Al-smectites over several hundred meters of Fe/Mg-smectites has been proposed to be a leaching profile [e.g., 17], but given the exceptional thickness, may be more consistent with an Al-smectite paleosol sequence topped by a thinner leaching profile [18].

*The importance of Al-smectites:* Smectite clays have a variety of compositions, which are related to the fluid chemistry in their formation environment. Fe-smectites require reduced Fe-rich fluids, typically related to hydrothermal or groundwater activity [19]. Mg-rich smectites require specific conditions typically only found in subaqueous environments [20]. Al-rich smectites can form in a variety of environments, but are notable as the most common soil mineral, even in basaltic terrains on Earth. In mafic soils, Fe-substitution within Al-smectites produces spectrally intermediate clays that have not yet been observed in other environments [21]. Other smectite compositions are rare in soils, and require extreme parent material compositions (e.g., serpentine can transform to Mg-smectites in soils).

Thus, on Mars, Al- and Al/Fe-smectites may be an indicator of pedogenic processes, especially when found in extensive units outside of basins. Al-smectites have been identified in extensive Noachian units at Mawrth Vallis [e.g., 17] as well as in many smaller exposures throughout Noachian terrains [16]. Al/Fe-smectites have been tentatively identified at Mawrth [17], and may be present in Gale Crater [22]. However, this framework also suggests that the most common smectites on Mars - Fe/Mg-smectites - may not be related to surface weathering and instead formed by subsurface hydrothermal or groundwater processes [23].

*Poorly crystalline phases on Mars:* Poorly crystalline phases can form in abundance in soils when instantaneous weathering rates are high, such as during melt events or strong rainstorms. On Mars, we hypothesize that these phases may be indicators of a cold and/or rarely wet climate regime, so determining the climate reigime will require additional context. In models of thermal IR spectra, a large portion of the surface of Mars includes a significant high-silica, poorly crystalline component, and this component is heavily concentrated in the Amazonian northern plains [24,25]. Poorly crystalline phases of unknown composition have been identified as a major component of sediments at Gale and Gusev craters [26,27]. So far, these detections correspond to Hesperian and Amazonian terrains, perhaps suggesting that poorly crystalline phases may be less common in Noachian terrains, especially compared to the large number of detections of crystalline clays. The presence or absence of poorly crystalline phases in Noachian terrains could be tested *in situ* by the upcoming Mars 2020 rover.

**Critical knowledge gaps:** The weathering mineralogy framework presented here is based on proceses observed in typical terrains on Earth, and thus may not account for exceptional circumstances that could have been prevalent on Mars. For example, in one proposed scenario for Noachian Mars, large, mostly cold-based ice sheets dominated the southern highlands, and liquid water was produced during rare melting events [28]. The framework presented here would suggest that poorly crystalline phases should be a major product of snowpacks and localized wet margins of the ice sheet, perhaps with more advanced weathering to kaolinite near the snowline if melting was frequent [29]; however, the geochemistry and mineralogy of long term weathering under a large ice sheet is poorly understood. New results from Antarctica suggest that pockets of melt within the ice sheet could produce crystalline clays, but further work is needed [30]. Outside of these melt pockets, whether or not chemical weathering occurs under the cold-based portions of an ice sheet or glacier is poorly understood.

In addition, the full range of climate regimes and environmental conditions under which deep weathering profiles form is unclear. Deep leaching profiles have not been observed in locations with My+ duration punctuated climates like the dry side of Hawaii, but it is unclear whether or not they could form over exceptionally long timescales. While no deep profiles have been documented in cold and icy climates, it is unclear whether or not long-term melt-driven alteration on an ice free and stable surface could produce deep leaching profiles. This process may be limited by the formation of permafrost layers or erosion by glaciers. Furthermore, it has been proposed that weathering profiles on Mars were enhanced by acidic (as opposed to circumneutral) top down alteration; however, this also has not been documented on Earth, so the mineralogy that would be produced by this process is unclear.

**Conclusions:** Based on a terrestrial framework, Al-clays dating from Noachian Mars (kaolinite-topped leaching profiles and regionally extensive Al-smectite alteration) are consistent with an arid to semi-arid rain-dominated climate, most likely with persistent or seasonal rainfall. Based on terrestrial analogs, these climatic conditions must have persisted over geologic timescales, consistent with geomorphic evidence for a surface hydrological cycle on the scale of millions of years or more. However, this interpretation is limited by major knowledge gaps that still exist in both our understanding of terrestrial weathering mineralogy and its expression on Mars, and additional work is needed to rule out exceptional weathering mechanisms.

**References:** [1] Ehlmann & Edwards (2014) *An Rev Earth Planet Sci, 42,* 291-315. [2] Graham & O'Geen (2010) *Geoderma 154*, 418-437. [3] Rasmussen et al (2010) *Geoderma 154*, 473-485. [4] Rampe et al (2017) LPSC *48*, #2437. [5] Ming et al (2015) AGUFM 2015, #P24A-02. [6] Rutledge et al (2017) this volume. [7] Ziegler et al (2003) *Chem Geol 202*, 461-478. [8] Singer (1980) *Earth Sci Rev 15*, 303-326. [9] Alexander & Mallory (1993) *Catena* 20, 113-128. [10] Dere et al (2016) Soil Sci Soc Am J 80, 623. [11] Tsai et al (2010) *Geoderma 156*, 48–59. [12] Fisher & Ryan (2006) *Clays Clay Min 54*, 571-586. [13] Ugolini & Dahlgren (2002) *Global Env Res 6*, 69-81. [14] Vitousek et al (1997) *GSA Today*, *7*, 1-40. [15] Gaudin et al (2011) *Icarus 216*, 257-268. [16] Carter et al (2015) *Icarus 248*, 373–382. [17] Bishop et al (2013) *Planet Space Sci 86*, 130-149. [18] Horgan et al (2017) Mars 2020 3rd LSW. [19] Baker (2017) *Am Min*. [20] Michalski et al (2017) *Nature 8*, doi:10.1038/ncomms15978. [21] Horgan et al (2017) GSA Cordilleran, #5-6. [22] Milliken et al (2010) *Geophys Res Lett 37*, L04201. [23] Ehlmann et al (2011) *479*, 53–60. [24] Rampe et al (2012) *Geol 40*, 995–998. [25] Bandfield et al (2000) *Science 287*, 1626–1630. [26] Ruff & Hamilton (2017) *Am Min 102*, 235–251. [27] Dehouck et al (2015) *J Geophys Res 119*, 2640–2657. [28] Fastook & Head (2014) *Planet Space Sci 106,* 1–46. [29] Mavris et al (2011) *Geoderma 105*, 106-117. [30] Graly et al (2017) *Goldschmidt.*

**RECONSTRUCTING THE PALEO-CLIMATE AND HYDROLOGY OF GALE CRATER, MARS IN THE LATE NOACHIAN AND HESPERIAN EPOCHS.** D. G. Horvath[1] and J. C. Andrews-Hanna[2], [1]Southwest Research Institute, Boulder, CO. [2]Lunar and Planetary Laboratory, University of Arizona, Tucson, AZ.

**Introduction:** The central sedimentary deposit in Gale crater, Aeolis Mons, may preserve one of the best records of the early Martian climate during the late Noachian and early Hesperian, and the transition from wetter conditions when fluvial valleys and lakes were active [1, 2, 3] to drier conditions when most of the thick accumulations of sediments were forming [4]. Following these drier conditions, late stage hydrology, after the formation of Aeolis Mons, has been identified from fluvial dissection of Aeolis Mons and fan deposits on the Gale crater floor [5].

Here we used numerical models of the surface and subsurface hydrology of Gale crater and its surroundings, constrained by the sedimentary record preserved in Aeolis Mons (Fig. 1a) and late-stage lake levels, inferred from fan deposits in Gale (Fig. 2a), to reconstruct the climate history of Gale crater.

**Model:** In this study, we used the hydrological model of [8] with parameters appropriate for Mars over Gale crater. This model combines a finite-difference approximation of the groundwater flow equation to simulate subsurface hydrology with an analytical surface runoff model. The model was forced using evaporation potential ($E_p$) and precipitation ($P$) rates from Earth-based observations of analog climates provided by the North American Land Data Assimilation Systems (NLDAS). We focused on a semi-arid Great Plains and an arid Arizona climate. The model results are most sensitive to the mean annual ratio of $E_p$ to $P$, referred to as the aridity index ($\phi$). The evaporation potential and precipitation rates were then scaled to investigate a range of aridity indices from 1.5 to 33, representing climates on Earth ranging from sub-humid to hyper-arid. While a range of annual precipitation was investigated, models shown here use an annual precipitation of 160 mm/yr.

The total annual aquifer recharge and surface runoff were determined from the precipitation and evaporation potential using an Earth-based empirical relationship [9], which uses the aridity index to determine the fraction of precipitation that contributes to the surface and subsurface hydrology rather than evaporating immediately back into the atmosphere.

This model assumed a megaregolith aquifer model adapted from [10], which has a vertically averaged aquifer permeability from the surface to 10 km depth of $3\times10^{-13}$ m$^2$.

**Late Noachian climate at Gale crater:** Lake and fluvial deposits observed by the Mars Science Laboratory (MSL) making up the lowest stratigraphic unit of Aeolis Mons suggest persistent long-lived lakes following the formation of Gale crater near the end of the Noachian [1]. By removing Aeolis Mons and reconstructing the pre-Aeolis Mons topography at Gale, lake conditions during the deposition of the basal units (Murray mudstones) of Aeolis Mons was modeled. Using the upper contact of the Murray lake bed mudstones as an indicator for lake level, we find that an aridity index less than 6 is required (Fig. 1b), at the transition between arid and semi-arid climates. Although the climate could have been wetter than the semi-arid conditions suggested by this model, drier conditions cannot account for the extent and elevation of the lake bed deposits. This indicates that wet conditions, and specifically a semi-arid or wetter climate, were required to form the Murray mudstone lake deposits at the base of Aeolis Mons. A semi-arid climate is consistent with previous estimates of the Noachian climate using the geomorphology of fluvial networks [2].

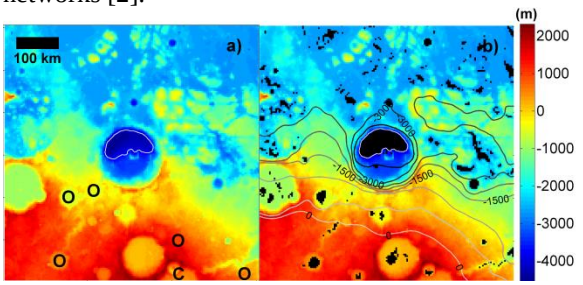


**Fig 1. a)** Reconstructed topography at Gale crater prior to the formation of Aeolis Mons (color map) showing the elevation contour (white outline) at the upper contact of the Murray lake bed mudstone [1] and identified open and closed-basin lakes outside of Gale ("O" and "C" respectively; [6, 7]). **b)** A lake (black) and hydraulic head (contour) map for an aridity index of 6 corresponding to the highest elevation of the Murray mudstone.

**Early Hesperian climate at Gale crater:** The majority of the thickness and volume of Aeolis Mons is comprised of the sulfate-cemented lower formation [4]. Although MSL has yet to explore this unit in Gale, similarities to the deposits in Meridiani Planum [11] suggest a formation mechanism via groundwater-mediated cementation and alteration of aeolian sediments. The transition in deposits from mudstones to cemented aeolian material cannot be explained solely as a result of the infilling of the crater, and requires a climate change. Global and regional groundwater models have been successfully used to reproduce the distribution and thickness of ground-

water cemented sediments in both Meridiani and Gale, and have shown that the elevation of the top of the hydrated lower formation matches the predicted rise height of the water table during the infilling of the crater with sediments [12]. Thus, even if the anhydrous upper formation were deposited in the same climate and hydrological environment as the lower formation, it would not be expected to be similarly cemented and altered.

An origin for the Aeolis Mons lower formation by groundwater-mediated alteration and cementation implies that the crater was once filled with sediments to at least the top of the lower formation. A massive erosion event is then required to explain the present-day mound shape, similar to the widespread erosion of sedimentary deposits in Arabia Terra [13]. Aeolian erosion of the sediments likely required a drop in the water table to the level of the present-day crater floor or lower [14], and thus requires a change to a hyper-arid climate.

**Gale crater lakes during the Early Hesperian:** Continued hydrology and lake formation during the Hesperian, after the erosion of the crater deposits to their current mound shape, is evidenced by fluvial erosion of Aeolis Mons and well preserved fan deposits on the floor of Gale [5]. Based on lake level estimates from these fan deposits (Fig 1a), an aridity index of 3.5 matches the highest observed lake stand assuming a shape parameter of 1.6 and an annual precipitation of 160 mm/yr (Fig. 2c). Climates in the sub-humid ($\phi$=1.5) and arid ($\phi$=9) regimes, predict lake levels that exceed the highest lake stand and fall short of the lowest observed lake stand in Gale crater respectively (Fig. 2b, d). Depending on the assumed annual precipitation and amount of water that reaches the surface and subsurface hydrology, an aridity index range between 3 and 6, in the semi-arid climate regime, matches the range of observed lake stands in Gale crater during the Hesperian. At the assumed annual precipitation of 160 mm/yr, this range of aridity indices is comparable to high latitude, cold deserts and steppe climates on Earth. These climates are much wetter than is thought to characterize much of the Hesperian, requiring wetter interludes after the transition to arid conditions in the Hesperian.

**Conclusions:** Using indicators of paleo-lake levels and the observed extent aqueous alteration we have used hydrological models to provide constraints on the past climate at Gale crater. These results favor a persistent semi-arid climate ($\phi$<6) during the Late Noachian to account for the lake bed mudstones at the base of Aeolis Mons, a transition to arid conditions during the Early Hesperian and persistent groundwater flow to Gale crater accounting for the aqueously altered aeolian deposits in Aeolis Mons, a transition to hyper-arid conditions to allow erosion of the deposits to their current mound shape, and periodic returns to semi-arid conditions during the Hesperian to reproduce the observed late-stage lake stands [5]. These results indicate drastic climate changes over the lifetime of the hydrological system at Gale, suggesting a return to semi-arid conditions similar to the Noachian climate at some point during the Hesperian in order to produce lakes that correspond to the observed late-stage lake stands. Furthermore, this work has shown that with continued observation of lake bed deposits on Mars, hydrological modeling can be used to further constrain the past climate and hydrology on Mars.

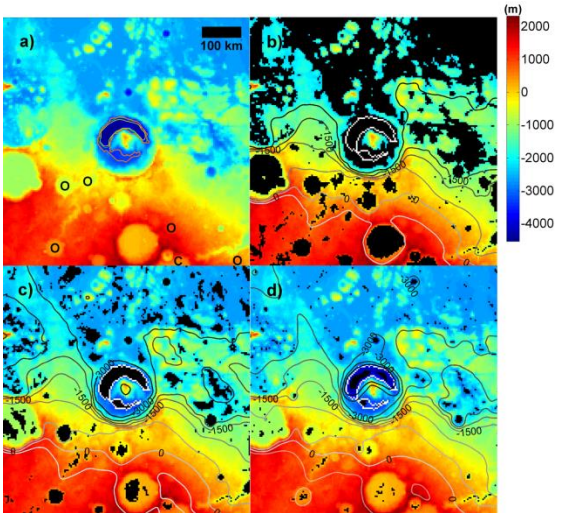


**Fig. 2. a)** MOLA topography at Gale crater (color-map) showing the inferred post-Aeolis Mons lake stands in Gale (colored contours; [5]) and identified open and closed-basin lakes outside of Gale ("O" and "C" respectively; [6, 7]). Lakes (shown in black) and hydraulic head maps (contours) are shown for different aridity indices of **b)** 1.5 **c)** 3.5 and **d)** 9, and compared to the highest lake stand inferred in Gale [5].

**References:** [1] Grotzinger, J. P. et al. (2015) *Science*, 350, 6257. [2] Hynek, B. M. et al. (2010) *JGRP*, 115, E09008. [3] Bibring, J. P. et al. (2006) *Science*, 312, 400-404. [4] Thomson, B. J. et al. (2011) *Icarus*, 214, 413-432. [5] Palucis, M. C. et al. (2016) *JGRP*, 121, 472-496. [6] Goudge, T. A. et al. (2012) *Icarus*, 219, 211-229. [7] Goudge, T. A. et al. (2015) *Icarus*, 260, 346-367. [8] Horvath, D. G. et al. (2016) *Icarus*, 277, 103-124. [9] Budyko, M. I. (1974) *Climate and life*, Academic Press., New York, 508. [10] Hanna, J. C. & Phillips, R. (2005) *JGR*, 110, E01004. [11] McLennan, S. M. et al. (2005) *Nature*, 438, 1129-1131. [12] Andrews-Hanna, J. C. et al. (2012) *3rd Early Mars Conf.*, id. 7038. [13] Zabrusky, K. et al. (2012) *Icarus*, 220, 311-330. [14] Andrews-Hanna, J. C. et al. (2010) *JGR*, 115, E06002.

**REDOX STRATIFICATION OF AN ANCIENT LAKE IN GALE CRATER, MARS.** J. A. Hurowitz[1], J. P. Grotzinger[2], W. W., Fischer[2], S. M. McLennan[1], R. E. Milliken[3], N. Stein[2], A.R. Vasavada[4], D. F. Blake[5], E. Dehouck[6], J. L. Eigenbrode[7], A.G. Fairén[8, 9], J. Frydenvang[10,11], R. Gellert[12], J.A. Grant[13], S. Gupta[14], K. E. Herkenhoff[15], D. W. Ming[16], E. B. Rampe[16], M. E. Schmidt[17], K. L. Siebach[1,2], K. Stack-Morgan[4], D. Y. Sumner[18] and R. C. Wiens[10], [1]Department of Geosciences, Stony Brook University, Stony Brook, NY. [2]California Institute of Technology, Pasadena, CA. [3]Brown University, Providence, RI. [4]Jet Propulsion Laboratory, Pasadena, CA. [5]NASA Ames Research Center, Moffett Field, CA. [6]University Paul Sabatier, Toulouse, France. [7]NASA Goddard Space Flight Center, Greenbelt, MD. [8]Centro de Astrobiología, Madrid, Spain. [9]Cornell University, Ithaca, NY. [10]Los Alamos National Laboratory, Los Alamos, NM. [11]University of Copenhagen, Copenhagen, Denmark. [12]University of Guelph, Guelph, Ontario, Canada. [13]National Air and Space Museum, Smithsonian Institution, Washington, DC. [14]Imperial College London, London, UK. [15]U.S. Geological Survey, Flagstaff, AZ. [16]NASA Johnson Space Center, Houston, TX. [17]Brock University, St. Catharines, Ontario, Canada. [18]University of California–Davis, Davis, CA.

**Introduction:** Fine-grained sedimentary rocks deposited in lakes and oceans provide valuable proxy records of changes in the Earth's dynamic surface environment. These rocks have been used to deduce the nature and extent of variations in global climate [1], the evolution of the composition of the Earth's crust [2], and biologically-driven changes in the redox state of the Earth's atmosphere [3]. Such rocks contain detrital components that carry information about sediment provenance and weathering, and secondary minerals that carry information about the environment of deposition and lithification. In cases where post-depositional diagenesis has partly modified primary signals, it is often possible to decipher those changes to reconstruct past events [4]. Given their importance to understanding Earth history, locales containing layered sedimentary rocks linked to depositional processes in rivers and lakes on Mars have also become a focal point for paleo-environmental studies. Indeed, a primary motivation behind the selection of Gale crater as the landing site for the Mars Science Laboratory (MSL) *Curiosity* rover mission was the presence of a ~5km tall mountain of layered sedimentary rock, hypothesized to contain a long-duration record of secular changes in Martian surface environments [5-8].

As it traversed towards Aeolis Mons (informally known as Mt. Sharp) *Curiosity* studied mudstones, sandstones, and conglomerates of the Bradbury group, and younger mudstones and sandstones of the Murray formation (fm.) at the base of Mt. Sharp [9, 10]. The lacustrine mudstones of these two genetically-related units are separated by ~60m of stratigraphic thickness but are related by a common depositional setting, allowing comparison of their chemical and mineralogical properties. This enables an evaluation of the geochemical and environmental history of the ancient lake system in Gale crater, placing constraints on its habitability and paleoclimate [11].

**Data Sources:** We use X-ray diffraction data obtained by the CheMin instrument between sols 1-1300 from six mudstone samples [12-14]. We also make extensive use of geochemical data [15] collected with the Alpha-Particle X-ray Spectrometer and images from *Curiosity's* camera payload.

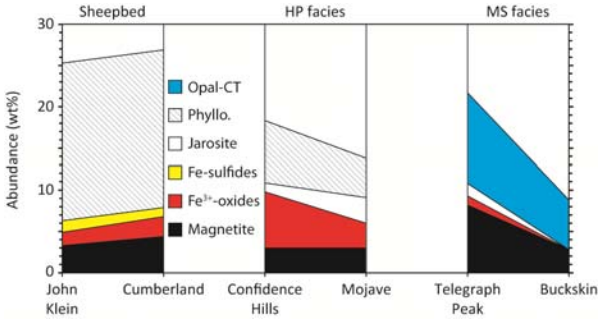


**Fig. 1:** Wt. % abundance of secondary phases and redox sensitive minerals in Gale crater mudstones.

**Results:** Two lacustrine mudstone units have been recognized: the Sheepbed member of the Yellowknife Bay formation, an older set of strata defining the base of the stratigraphic section, and the Murray formation, of relatively younger age and positioned higher in the stratigraphic section. On the basis of mineralogy, geochemistry, textural properties, and stratigraphic relationships, the Murray formation can be subdivided into two sedimentary associations, or facies: the Hematite-Phyllosilicate (HP) facies, and the Magnetite-Silica (MS) facies, shown on **Fig. 1**. The HP facies is characterized by abundant $Fe^{3+}$-oxides accompanied by phyllosilicates, as well as indications of Mn-oxidation and trace metal concentration. These properties are consistent with deposition in an oxidizing environment. The MS facies is recognized by a near-complete absence of pure $Fe^{3+}$-minerals, and high concentrations of silica accompanied by magnetite, consistent with deposition in an anoxic environment. The Sheepbed mudstones contain sulfide minerals of probable detrital origin and magnetite of probable authigenic origin, also consistent with anoxia during deposition [16-18].

As shown on **Fig. 2**, the Chemical Index of Alteration (CIA) paleoclimate proxy [1] increases by up to ~10-20 CIA units (expressed in %) from the Sheepbed member to the Murray formation. Geochemical enrichments in MgO, CaO, and $SO_3$, often associated with late diagenetic features (red symbols), indicate that the Murray fm. was affected by a saline overprint after burial and lithification. Discrete Ca-sulfate filled veins are also a prominent diagenetic feature.

**Discussion:** The observed variations in CIA are consistent with fluctuations in the ancient climate between cold, dry conditions and relatively warmer, wetter conditions. The distinct properties of the two Murray facies were developed as a result of: (i) fractionation of river-borne detritus into coarser, denser materials in shallow water close to shore, and finer, lower density materials offshore in deeper water due to deceleration of river-flow as it entered the lake; (ii) redox stratification of the lake water body, caused by depth-dependent variations in the concentration of atmospheric oxidants and dissolved, groundwater-derived solutes, resulting in oxidizing conditions in shallow water, and anoxia in deeper water, as shown on **Fig. 3**. The addition of saline minerals during a later phase of brine migration through the section records longer-term changes in Martian climate at Gale crater, perhaps driven by global atmospheric escape processes. The recognition of a stable redox-stratified water body adds important detail to our understanding of the potential for microbial autotrophy on Mars at ~3.5 Ga.

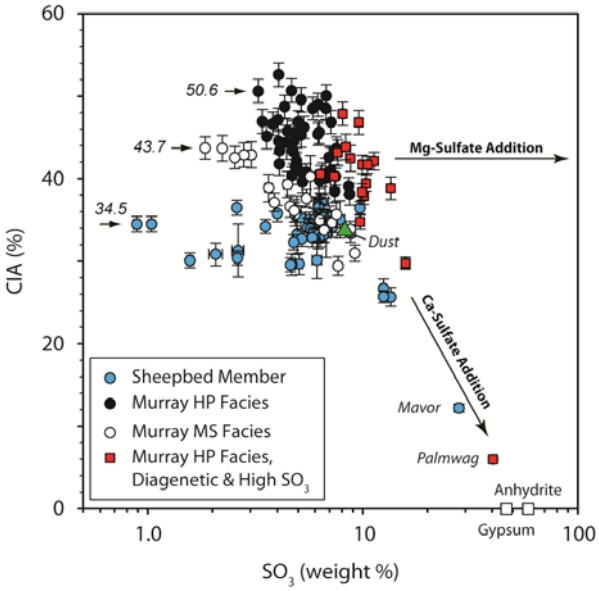


**Fig. 2**: CIA (%) versus $SO_3$ (wt. %) with vectors for the addition of Mg- and Ca-sulfate to mudstones. Arrowheads and italicized CIA values reference the lowest $SO_3$ samples from each mudstone suite, which display a maximum difference of 16.1 %. Airfall dust from [19].

**References:** [1] Nesbitt, H.W. and G.M. Young (1982), *Nature*, 299, 715-717. [2] Taylor, S.R. and S.M. McLennan (1985) *The Continental Crust*, Blackwell Scientific Publications. [3] Klein, C. (2005) *Amer. Min.*, 90, 1473-1499. [4] Fischer, W.W. and A.H. Knoll (2009) *GSA Bull.*, 121, 222-235. [5] Anderson, R. and J.F. Bell (2010) *Mars*, 5, 76-128. [6] Grotzinger, J.P., et al. (2010) *Space Sci. Rev.*, 170, 5-56. [7] Milliken, R.E., et al. (2010) *GRL*, 37. [8] Thomson, B.J., et al. (2011) *Icarus*, 214, 413-432. [9] Grotzinger, J.P., et al. (2015) *Science*, 350. [10] Grotzinger, J.P., et al. (2014) *Science*, 343. [11] Hurowitz, J.A., et al. (2017) *Science*, 356. [12] Vaniman, D. (2012) *MSL CheMin RDR Data V1.0, NASA Planetary Data System*. [13] Morris, R.V., et al. (2016) *PNAS*, 113, 7071-7076. [14] Rampe, E.B., et al. (2017) *EPSL*, 471, 172-185. [15] Gellert, R. (2013) *MSL APXS RDR Data V1.0, NASA Planetary Data System*. [16] Bristow, T.F., et al. (2015) Amer. Min., 100, 824-836. [17] Vaniman, D.T., et al. (2014) *Science*, 343. [18] Tosca, N.J., et al. (2017) in *4th International Conference on Early Mars*. [19] Berger, J.A., et al. (2016) *GRL*, 43, 67-75.

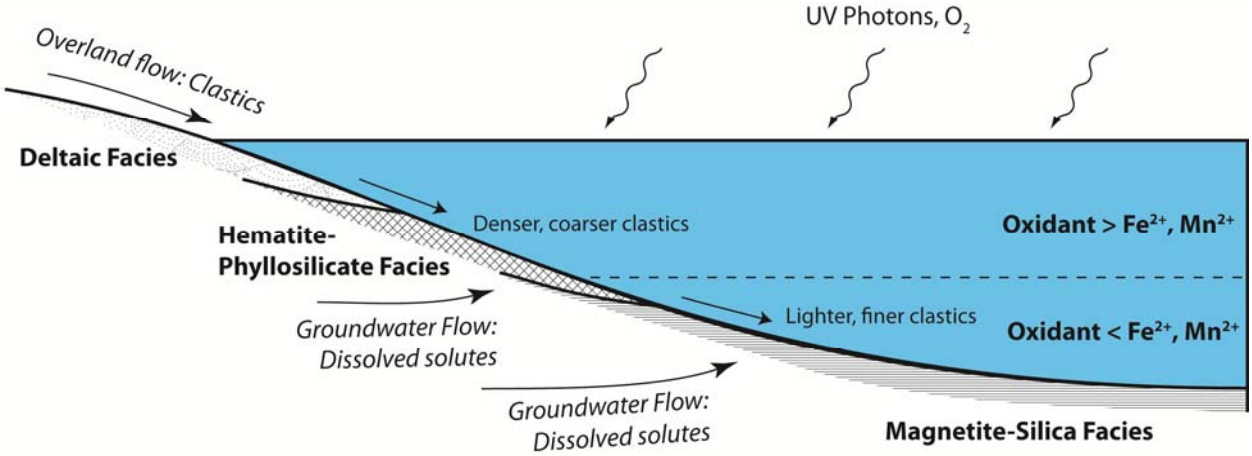


**Fig. 3:** Model of physical transport and geochemical processes occurring during deposition of the Murray fm [11].

**LOSS OF THE EARLY MARS ATMOSPHERE TO SPACE DETERMINED FROM MAVEN OBSERVATIONS OF THE UPPER ATMOSPHERE.** B. M. Jakosky[1] and the MAVEN Science Team, [1]Laboratory for Atmospheric and Space Physics, University of Colorado at Boulder, USA (bruce.jakosky@lasp.colorado.edu).

**Introduction:** There is compelling evidence that liquid water was abundant on early Mars, despite Mars being too cold today to sustain significant amounts of liquid water. The most likely explanation, especially in the face of the Sun having been dimmer early in its history, is that early Mars had a more-effective greenhouse atmosphere. Measurements from spacecraft and from the surface over the last several decades indicate that there are insufficient carbonate deposits to hold enough $CO_2$ from this early, thicker atmosphere to provide significant warming, however. In that context, the *Mars Atmosphere and Volatile Evolution* (*MAVEN*) mission was designed to explore in detail the loss of gas to space occurring at the present epoch; this would allow determination of the integrated loss to space through time and the ability of loss to space to explain the changes inferred for the Martian climate. We report here the loss rates derived through a full Mars year of *MAVEN* observations, and use these loss rates to extrapolate back in time to get the time-integrated loss to space. These will allow us to determine the role that loss to space played in the changes in climate inferred from the surface morphology and mineralogy.

MAVEN has been observing the Mars upper atmosphere, ionosphere, and magnetosphere, along with the solar and solar-wind energetic inputs into the system. The goals are to determine the composition, structure, and behavior of the system and how they are controlled by the energetic drivers, the current rates of loss to space and how they are controlled by the energetic drivers, and properties that allow us to determine the integrated loss to space through time. *MAVEN* has been making science observations for more than a full Mars year.

**Results:** *MAVEN* observations have been used to derive the rates of loss of gas to space, as follows:

*Hydrogen loss.* Hydrogen is created in the upper atmosphere from the photodissociation of $H_2O$ in the lower and middle atmosphere and the transport of the H upward. The H atom is light enough that those atoms in the high-energy tail on the Boltzmann distribution and residing above the nominal exobase will have enough energy to escape to space. This thermal (or Jeans) escape is likely to be the main mechanism by which H is lost to space. The combination of escaping atoms and atoms having sufficient energy to travel ballistically to high altitudes but not to escape creates an extended corona of H atoms surrounding Mars; this corona can extend out past 10 $R_M$ or greater.

For the range in observed column abundance and temperature of H in the corona, the loss rate is inferred to vary with season during the Mars year between ~ 1-11 x $10^{26}$ H $s^{-1}$. This is equivalent to a loss rate of ~ 160-1800 g H $s^{-1}$. At this rate, the entire column of atmospheric water at present (nominally, about 10 precipitable micrometers, or $10^{-3}$ g/$cm^2$) would be removed in between ~ 3000 - 30,000 years. Over 4 b.y., loss at this rate would be able to remove a global layer of water between ~ 3-24 m thick.

*Oxygen ion loss.* Ion loss occurs via the acceleration of ions in an electric field. The electric field can be generated by the moving magnetic field of the impinging solar wind or by the motion of ions around the magnetic field in magnetic cusp regions associated with the crust.

The integrated escape is obtained by summing up the loss across the planet, breaking the loss into separate $O^+$ and $O_2^+$ rates. The net global loss rate for O is 5 x $10^{24}$ $s^{-1}$, equivalent to a loss rate of ~130 g O $s^{-1}$. If loss occurred at this constant rate, the entire column of atmospheric O (present mainly as $CO_2$) would be removed in 3 b.y.

*Photochemical loss.* Photodissociation can ionize $O_2$ or $N_2$. When the electrons and ions recombine, the energy is released via one of multiple pathways. In some of the recombinations, the energy is sufficient both to break the $O_2$ bond and to give each of the resulting O atoms an amount of energy (as kinetic energy) greater than the escape energy from Mars; when recombination occurs above the exobase, such that the upward-moving atom will not hit anything, it will escape to space.

*MAVEN* does not measure the escaping neutral O atoms. But it does measure the upper-atmospheric ion composition and electron properties, allowing the photodissociation and recombination rates and the resulting escape rate to be calculated. The loss rate can be calculated for each orbit. The derived loss rate varies dramatically through the mission due to the precession of the orbit, with geographic location, solar zenith angle, and local time all varying. Values calculated where measurements are made on the night side of the planet, for example, are extremely low due to the extremely tenuous ionosphere there. Loss rates on the

day side, where the ionosphere is significant, are greater.

The average O loss rate inferred from these observations is 5 x $10^{25}$ O $s^{-1}$, equivalent to 1300 g O $s^{-1}$. At this rate, the O present as $CO_2$ in today's atmosphere would be lost in 300 m.y.

*Sputtering loss.* The electric field generated by the solar wind will accelerate ions in one hemisphere (relative to the magnetic field) away from the planet causing them to escape, and from the other hemisphere into the planet where they collide with molecules in the upper atmosphere. When these ions collide at high velocities (up to twice the solar-wind velocity, or nearly 1000 km/s), they can physically knock upper-atmospheric constituents out of the atmosphere. This sputtering process can be very effective in removing neutral atoms (and is the only significant mechanism for removing species such as argon, which is a noble gas). *MAVEN* does not measure escaping neutrals. However, we can measure the properties of the incoming ions (composition and speed) and the composition of the upper-atmospheric target onto which they impinge. From these, we can calculate the sputtering loss yield based on well-developed theories of sputtering.

For the coverage obtained during the year of observations, the average loss rate is ~3 x $10^{24}$ O $s^{-1}$, equivalent to ~80 g O $s^{-1}$. At this loss rate, it would take more than 4 b.y. to remove the atmospheric column of O.

*Integrated loss rates.* We can sum up the loss as observed or inferred during this one Mars year. The loss of H, over 4 b.y., would result in loss of an equivalent of a global layer of $H_2O$ between 3 – 24 m thick.

The total loss rate of O at present is 6 x $10^{25}$ O $s^{-1}$. At this rate, the present column of atmospheric O would be lost in about 250 m.y.; equivalently this would remove a total of ~75 mbar of $CO_2$ over 4 billion years.

*Extrapolation back in time.* These rates are not expected to have been constant in time. The major factors that were different early in Mars history were the EUV flux from the Sun and the nature of the solar wind. These were recognized as being important drivers of the escape rate by each of the above processes by Luhmann et al. (1992), and the extrapolations to early times indicated that loss rates could have been orders of magnitude greater than they are today. These models have been updated as our understanding of the evolution of sun-like stars and of the escape processes themselves have improved. We use the most recent integrated model, that of Chassefiere and Leblanc (2013), to extrapolate back in time.

When integrated through time, the integrated loss of O is equivalent to loss of greater than 0.5 bar of $CO_2$, 15 m global equivalent layer of water, or some combination of the two depending on the source of the O. Our extrapolation makes these numbers a conservative estimate, with the actual loss possibly being considerably larger.

Loss of H is more difficult to extrapolate into the past. One issue is that we do not as yet fully understand what drives the seasonal behavior of the abundance of H in the corona and of the escape rate. While the suggestion of dust allowing $H_2O$ to rise higher during southern summer and be photodissociated closer to the exobase is plausible, it has not been cleanly demonstrated. Even if it is correct, we do not as yet understand the seasonal variability in either the dust cycle or the lower-atmosphere water cycle well enough to determine whether the year observed by *MAVEN* is representative of the current epoch, or even whether the extreme high or low values of H escape rate might be representative.

Even if we understood the present-day H loss rate, it would be difficult to extrapolate to ancient times. On the one hand, loss could have been greater in ancient times than it is today based on the increased solar EUV flux. The EUV would have provided additional heating of the upper atmosphere, increasing the H escape rate. On the other hand, loss of H could have been less in ancient times if, by having a more-Earth-like atmosphere, the Martian middle atmosphere had a more-efficient cold trap that kept the $H_2O$ from getting as high in the atmosphere.

**Conclusions:** Combined with the previous results on loss derived from the Ar isotopes (Jakosky et al., 2017), these results provide a direct indication that the bulk of the early Martian atmosphere has been lost to space. The timing of this loss as determined from the history of the Sun is consistent with that inferred from the geology of the surface. Combined with the lack of evidence for a substantial $CO_2$ reservoir on the surface or in the subsurface, we conclude that loss to space was the major process by which the Mars atmosphere evolved from an early, warmer and wetter climate to the cold, dry climate that we see today.

**ATMOSPHERIC COLLAPSE ON EARLY MARS: THE ROLE OF $CO_2$ CLOUDS.** M. A. Kahre[1], R. M. Haberle[1], K. E. Steakley[2], J. R. Murphy[2], and A. Kling[3,1], [1]NASA Ames Research Center, [2]New Mexico State University, [3]Bay Area Environmental Research Institute.

**Introduction:** The abundance of evidence that liquid water flowed on the surface early in Mars' history strongly implies that the early Martian atmosphere was significantly more massive than it is today [1]. While it seems clear that the total $CO_2$ inventory was likely substantially larger in the past, the fundamental question about the physical state of that $CO_2$ is not completely understood. Because the temperature at which $CO_2$ condenses increases with surface pressure, surface $CO_2$ ice is more likely to form and persist as the atmospheric mass increases. For the atmosphere to remain stable against collapse, there must be enough energy, distributed planet wide, to stave off the formation of permanent $CO_2$ caps that leads to atmospheric collapse. The presence of a "faint young sun" that was likely about 25% less luminous 3.8 billion years ago than the sun today makes this even more difficult.

Several physical processes play a role in the ultimate stability of a $CO_2$ atmosphere. The system is regulated by the energy balance between solar insolation, the radiative effects of the atmosphere and its constituents, atmospheric heat transport, heat exchange between the surface and the atmosphere, and latent heating/cooling [2,3]. Specific considerations in this balance for a given orbital obliquity/eccentricity and atmospheric mass are the albedo of the caps, the dust content of the atmosphere, and the presence of water and/or $CO_2$ clouds.

Forget et al [4] show that, for Mars' current obliquity (in a circular orbit), $CO_2$ atmospheres ranging in surface pressure from 500 hPa to 3000 hPa would have been stable against collapsing into permanent surface ice reservoirs. Soto et al [5] examined a similar range in initial surface pressure to investigate atmospheric collapse and to compute collapse rates. $CO_2$ clouds and their radiative effects were included in [4] but they were not included in [5]. Here we focus on how $CO_2$ clouds affect the stability of the atmosphere against collapse.

**Model Description:** We use a version of the NASA Ames Mars GCM that has recently been modified for early Mars simulations. We have upgraded our two-stream, correlated-k radiative transfer scheme to incorporate the effects of $CO_2$ collision-induced absorption (CIA; [6,7,8]) and to include the $CO_2$ far line absorption assuming sublorenztian line shapes [9]. We have added a simple $CO_2$ cloud microphysics that is similar to the one described in [4], whereby atmospheric $CO_2$ condenses onto a specified spatially and temporally constant number of ice nuclei. The nominal number mixing ratio of ice nuclei is $10^5$ #/kg, but we vary this number to understand its sensitivity since it is not well constrained. The $CO_2$ clouds are radiatively active. We have also included processes appropriate for a water cycle (see Steakley et al., this conference), but these are not utilized here.

**Simulations.** Two 1000 hPa simulations are presented to demonstrate the importance of $CO_2$ clouds in maintaining the atmosphere against collapse on early Mars. The first simulation includes $CO_2$ cloud formation as described above. The second simulation does not explicitly include $CO_2$ clouds. Instead, any condensed atmospheric mass that would form clouds when the temperature drops below the saturation temperature is instantaneously deposited onto the surface. In the first case, atmospheric condensation only leads to surface ice accumulation when the cloud particles reach the surface through gravitional sedimentation, while in the second, all atmospheric condensation leads to surface ice accumulation. Once $CO_2$ ice reaches the surface via either method, the surface albedo is reset to 0.5.

**Results:** The two end member simulations show very different behavior: the simulation that explicitly includes $CO_2$ clouds is stable, while the simulation without $CO_2$ clouds collapses into permanent surface $CO_2$ reservoirs.

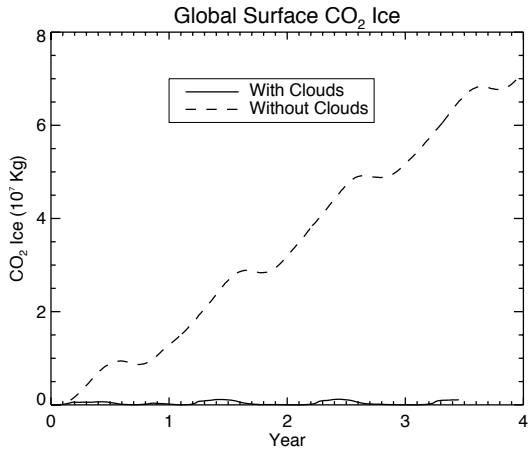


Figure 1: Global surface $CO_2$ ice inventories as a function of simulated year for the simulations with (solid line) and without (dashed line) $CO_2$ clouds.

Figure 1 shows the global surface $CO_2$ inventory for the two simulations. The amount of surface $CO_2$

ice grows and shrinks seasonally when $CO_2$ clouds are included but increases almost monotonically when $CO_2$ clouds are not included. The total amount of $CO_2$ ice on the surface is significantly less in the simulation with clouds than the simulation without.

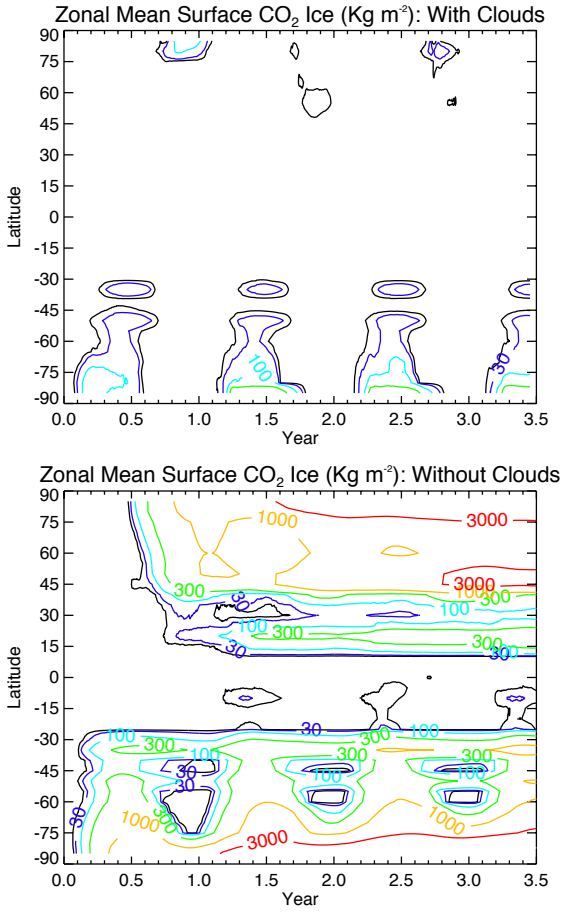


Figure 2: Zonal mean surface $CO_2$ ice inventories as a function of simulated year for the simulations with (top panel) and without (bottom panel) $CO_2$ clouds.

Figure 2 shows the latitudinal variation in surface $CO_2$ ice as a function of time for the two simulations. When clouds are included, seasonal $CO_2$ ice caps grow and recede at high latitudes. When clouds are not included, permanent reservoirs of surface ice accumulated at high *and* middle latitudes.

**Discussion:** The striking difference between these two cases illustrates the important role of $CO_2$ cloud microphysical processses. In both cases, significant atmospheric condensation is occurring in the atmosphere throughout the year. This condensation occurs at nearly all latitudes, particularly in the regions of large topographic features (e.g., Olympus Mons). In most cases, the condensing region is disconnected from the surface. In the case without $CO_2$ clouds, all atmospheric condensation (even if it occurs at altitude) leads directly to the accumulation of surface ice, whereas in the case with $CO_2$ clouds, there is a finite settling timescale for the cloud particles. Depending on this timescale and the local conditions, the cloud particles could stay aloft or sublimate as they fall toward the surface. In the case with $CO_2$ cloud formation, thick $CO_2$ clouds cover a good portion of the planet in the middle of the atmosphere (Figure 3).

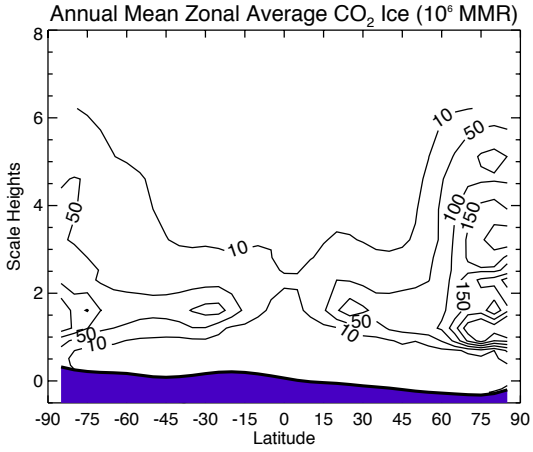


Figure 3: Annual and zonal mean cross-section of $CO_2$ cloud mass mixing ratio for the $CO_2$ cloud case.

**Conclusions and Future Work:** Cloud microphysical processes appear to be of vital importance to the question of atmospheric collapse on early Mars. We have shown that assumptions made regarding how atmospheric condensation and $CO_2$ clouds are handled in the model have a significant impact on the predicted atmospheric stability against collapse. In particular, the settling timescale controls how much of the condensation that occurs in the atmosphere will lead to surface ice accumulation, which is an important part of determining whether the atmosphere will collapse or not. The settling timescale depends, in turn, on cloud particle size, which will be sensitive to microphysical assumptions such as the number of available ice nuclei, etc. We plan to conduct further detailed studies on the sensitivity of these processes to microphysical parameters in order to better understand the nature of atmospheric collapse on early Mars.

**References:** [1] Haberle et al (2017), in *The Atmosphere and Climate of Mars*, Cambridge Univ. Press. [2] Haberle et al (1994) *Icarus, 109*, 102-120. [3] Nakamura and Tajika (2002) *JGR, 107*. [4] Forget et al (2013) *Icarus, 222*, 81-99. [5] Soto et al (2015) *Icarus, 250*, 553-569. [6] Wordsworth et al. (2010) *Icarus, 210*, 992-997. [7] Baranov et al. (2004) *JMS, 228*, 432-440. [8] Gruszka and Borysow (1998) *Mol. Phys, 93*,1007-1016. [9] Perrin and Harmann (1989) *JSRT, 42*, 311-317.

**AN ICE-AND-SNOW HYPOTHESIS FOR EARLY MARS, AND THE RUNOFF-PRODUCTION TEST.**
Edwin S. Kite – University of Chicago (kite@uchicago.edu).

**The problem:** How can Early Mars climate data and models be reconciled [1,2]? Early Mars had precipitation-fed lakes which individually persisted for $>10^{(3\text{-}4)}$ yr (plausibly $>10^5$ yr), with strong evidence for intermittency [e.g., 3]. Textural and mineralogic evidence requires groundwater flow and exchange with surface waters [e.g., 4]. However, climate models struggle to achieve mean annual temperatures above the freezing point [5], and mineralogy indicates $<10^8$ yr exposure to water [6]. One hypothesis for reconciling these findings - previously adumbrated by many authors [e.g. 7-9] - is seasonal melting of ice and snow. In this presentation, I review possible tests of this hypothesis, and zero in on one prediction: modest (energy-limited) runoff production.

**An ice-and-snow hypothesis:** *During the middle Noachian through early Amazonian, Mars experienced individually prolonged, but increasingly infrequent excursions to temperatures as warm as the floors of the Antarctic Dry Valleys (ADV) today – perhaps as warm as the Putorana Plateau. During these relatively-warm excursions, perennial lakes existed beneath ice cover* [10]. *Taliks beneath these lakes, and narrow conduits through permafrost that were maintained maintained either by high solute concentration or by advection, permitted surface-interior hydrologic circulation* [11]. *Warmer-than-Central-Siberia temperatures occurred only in the immediate aftermath ($<10^2$ yr) of basin-forming impacts – these warm conditions were too brief to permit interior-to-surface groundwater flow.* I call this specific ice-and-snow climate hypothesis for Early Mars the vanilla hypothesis (VH).

The vanilla hypothesis is acceptable to many palates: many climate models can achieve ADV-like conditions [12-13], and the VH can also reproduce the best-understood geologic data. Because of the key role of sub-lake 'through taliks,' the VH also permits both vertical segregation and vertical integration of the Early Mars hydrosphere [e.g., 14]. On the other hand, many climate models predict climates that were intermittently (or stably) warmer than the ADV [15,16]; conversely, some climate models predict that lake-enabling conditions were very brief [17]. Thus, the VH is not a consensus statement. It is controversial.

What is the most efficient and decisive way to test the VH?

**How can the ice-and-snow hypothesis be falsified?:** *Paleo-temperature proxies.* ~3.9 Ga Mars-meteorite $\Delta_{47}$ indicates near-surface formation at (291 ± 4) K [18]. This is the strongest extant challenge to the VH, but so long as we have only one near-surface Noachian $\Delta_{47}$ data point, it cannot be decisive.

If the Al-clays required clement temperatures to form, then the VH is false [19]. But Al-clays can also be produced under cold low-pH conditions [20], so this test awaits better constraints on Al-clay origins.

The lack of evidence for icy conditions along the MSL traverse hints at ice-free lakes [21]. This will be a weak argument until facies models for ice-covered lakes are more developed [22].

Meridianiite (or ikaite) psuedomorphs constrain past temperature [e.g. 23]. In principle, reaction-transport codes combined with mineralogy can also constrain temperature. However, the kinetics of low-temperature soil weathering are incompletely understood. It is unclear whether the amorphous component of Mars materials records low temperatures, low pH, water limitation, or protolith effects [e.g. 24].

*Paleo-pressure proxies.* Mars atmospheric pressure was likely $\lesssim$1 bar around the time rivers formed [e.g. 25], generally favoring colder climate solutions such as the VH [26].

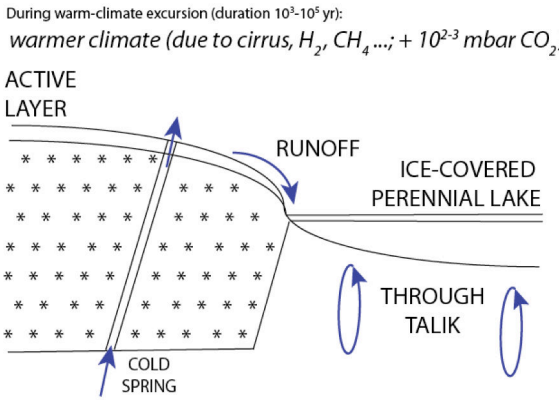


**Fig. 1.** Sketch of the vanilla hypothesis (VH).

*Paleo-hydrology proxies.* Seas (Eridania) and oceans (Borealis?) are consistent with the VH because thin ice cover can be sustained by latent heat transport via drainage of seasonal lakes. For example, drainage of 10 cm of melted sea-ice every warm season – and the associated advection of latent heat – can sustain ice cover <100 m thick. But much thinner ice would require warmer (non-VH) temperatures.

Rainfall would strongly disfavor the VH. Softened crater rims have been proposed as evidence for rainsplash erosion [27]. However, many non-rainsplash processes can soften crater rims, and rainsplash erosion is ineffective on Earth. High drainage density has been proposed as evidence for rainfall [28]. However, snowmelt landscapes can have high drainage density.

Rainfall can be tested more directly using runoff production. Runoff production cannot exceed snowmelt rate

in a cold climate, or precipitation minus infiltration rate in a rainy climate. High runoff production precludes snowmelt. Rainfall suggests a warm climate. How can runoff production be reliably measured?

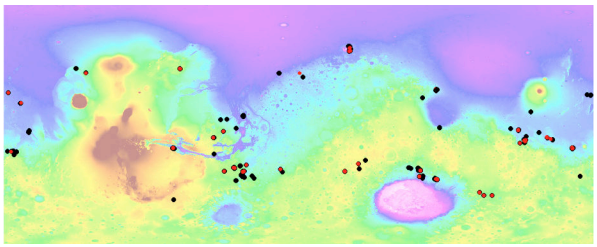

**Fig. 2.** Locations of measurement sites for Early Mars channel width (black) and meander wavelength (red).

**The runoff-production test:** I am measuring paleochannel widths and meander wavelengths for Early Mars watersheds with well-defined drainage area. The measurement method is the same as in ref. [29]. >250 channel-width measurements and 89 meander wavelength measurements are included, representing 158 drainage areas (Fig. 2). The catalog emphasizes better-preserved (post-Noachian) paleochannels, but includes a re-survey of the early sites listed in ref. [34].

Channel widths and wavelengths are a proxy for paleodischarge [30-33]. Discharge ($m^3/s$) can be divided by drainage area ($m^2$) to obtain a lower bound on runoff-production (mm/hr). If runoff production >(1-3) mm/hr, then a seasonal melting snow-and-ice climate is strongly disfavored [8]. However, high runoff production is consistent with rainfall.

**The main surprise so far:** Channels are frequently too big (relative to their drainage area) to be easily reconciled with a seasonal-snowmelt climate. Here are several possible reasons for big channels:

- Limited image resolution veils smaller channels (Unlikely to be a severe bias for HiRISE).
- Postfluvial modification has enlarged paleochannels. (Cannot explain wide inverted channels, nor large meander wavelengths).
- Reentry heating from distal impact ejecta turned the sky into a griddle, which flash-melted snow and ice [35]. (Possible for Lyot. Cannot transport enough sediment to form alluvial fans).
- Discharges reflect dam-overtopping, not climate-driven runoff. (Plausible, but only for some sites).
- We see strath terraces or channel amalgamations, not paleochannels [36]. (Plausible for some sites).
- Karst-like modification of paleochannels [37]. (Cannot explain large meander wavelengths).
- Steeper "channels" are debris-flow chutes. (Plausible).
- Published terrestrial width-discharge scalings do not fully account for gravity, steep-slope, and/or permafrost effects. (Plausible).
- Rainfall on Early Mars. (Plausible).

At the conference, I will present the catalog, and discuss the preferred interpretation(s).

**Acknowledgements:** David P. Mayer produced the GIS and stereo DTMs for this study. Sharon Wilson, Caleb Fassett, and Marisa Palucis shared unpublished work. Grants: NASA (NNX15AM49G, NNX16AG55G).

**References:** [1] Vasavada, A. (2017), *Physics Today*, 70, 34-41 [2] Hynek, B. (2016) *Geology*, 44, 879-880 [3] Palucis, M., et al. (2016), *JGR-E*, doi: 10.1002/2015JE004905 [4] Frydenvang, J., et al. (2017) *GRL*, in press [5] Wordsworth, R.D. (2016) *AREPS* 44, 381-408 [6] Dehouck, E. (2014) *JGR-E* 119, 2640-2657 [7] Fairén, A.G. (2010) *Icarus,* 208, 165-175 [8] Kite, E.S. (2013) *Icarus*, 223, 181-210 [9] Head, J.W (2017) *EGU 2017*, p.17735. [10]. Lee, P.; McKay, C. P. (2003) *LPSC*, abs. #2127 [11]. Scheidegger, J. M.; Bense, V. F. (2014) *JGR-F* 119, 758-778 [12] Wordsworth, R., et al. (2017) *GRL* 44, 665-671 [13] Kite, E.S., et al., this conf. [14] Head, J. W. (2012) *3rd Conf. on Early Mars*, id.7056 [15] Urata, R.A. & Toon, O.B. (2013) Icarus, 226, 1, p. 229-250 [16] Batalha, N.E., et al. (2016) *EPSL*, 455, 7-13 [17]. Segura, T. L., et al. (2013), in *Comparative Climatology of Terrestrial Planets*, S.J. Mackwell, et al. (eds.), U. Arizona Press, Tucson, p.417-437 [18] Halevy, I.; et al. (2011) *PNAS* 108, 41, 16895-16899 [19] Carter, J., et al. (2015); Icarus, 248, p. 373-382. [20] Zolotov, M.Y. & Mironenko, M. (2016), *Icarus,* 275, 203-220 [21] Grotzinger, J. P., et al. (2015) *Science*, 350, 6257 [22] Sumner, D. Y. et al. (2016), *AGU Fall Meet.* #P21C-2112 [23] Peterson, R.C., et al. (2007), *Am. Mineral.*, 92, 1756-1759 [24] Bandfield, J. (2017) *Am. Mineral*., 102, 233-234 [25] Kite, E.S., et al. (2014), *Nature Geosci.*, 7, 335-339 [26]. Ozak, N., et al. (2016), *JGR-E*, 121, 965-985 [27], Craddock, R.A.; Lorenz, R.D. (2017), *Icarus,* 293, 172-179 [28] Malin, M.; et al. (2010) *Mars Journal* 4, 1-60 [29] Kite, E.S. (2015), *EPSL* 420, 55-65. [30] Parker, G., et al., 2007. *JGR-F* 112. CiteID F04005. [31] Dietrich, W. E., et al. (2017), Fluvial gravels on Mars, in *Gravel-Bed Rivers*, D. Tsutsumi & J. Laronne (eds.), 755–784, John Wiley [32] Eaton, B.C., 2013. Chapter 9.18: Hydraulic geometry. In: Wohl, E.E. (Ed.), *Treatise on Geomorphology*, Elsevier [33] Jacobsen, R.; Burr, D. (2016), *GRL*, 42, 8903-8911 [34] Irwin, R.P., et al. (2005), *Geology,* 33, p.489 [35] Goldin, T. J.; Melosh, H. J. (2009), *Geology*, 37, 1135-1138 [36] Hayden, A.; et al. (2017) *48th LPSC*, id.2488 [37] Williams, R., et al. (2017) *GRL* 44, 1669-1678.

**METHANE-BURST CLIMATE SCENARIOS FOR EARLY MARS RIVERS AND LAKES.**

Edwin S. Kite[1], Peter Gao[2,3], Michael Mischna[4], David P. Mayer[1,5], Colin Goldblatt[6], Yuk Yung[7]. [1]University of Chicago (kite@uchicago.edu) [2]NASA Ames. [3]U.C. Berkeley. [4]JPL. [5]USGS Astrogeology. [6]U. Victoria. [7]Caltech

**Motivation:** Early Mars climate models using $CO_{2(g)}$ + $H_2O_{(g)}$ greenhouse forcing yield temperatures too cold to match geologic data [1,2]. A promising candidate for the extra warming is $CH_4(\pm H_2)$ [3,4]. Reducing gases are expected products of water-rock reactions early in Mars history [5,6]. However, $CH_4$ is rapidly lost from the atmosphere due to photolysis. Therefore, in order to outgas $CH_4$ late enough to match geology data and swiftly enough to overwhelm the loss processes, we need a trap-and-release mechanism. A plausible trap is $CH_4$-clathrate formation. A possible release mechanism for the Late Hesperian - Amazonian lake-forming climate(s) [7] is chaotic transitions in mean obliquity. A possible release mechanism for the Late Noachian / Early Hesperian climate optimum [8] is atmospheric collapse-and-reinflation. We are investigating both mechanisms.

**Summary of results:** We found physically self-consistent methane burst climate scenarios that can match the geologic constraints. Our models draw on an ensemble of integrations of Mars' obliquity history [9], grids of GCMs [2], recent $CH_4$-$CO_2$ Collision-Induced Absorption (CIA) results [4], and full photochemistry codes. Strengths of these scenarios are: climate optima of duration $10^4$-$10^6$ yr, consistent with data; intermittent lakes permitting olivine preservation; and potent self-sustaining feedbacks (Fig. 1). The key requirement of our models is that the $CH_4$ clathrate stability zone (CSZ) on past Mars had an occupancy fraction >(1-10)%. If these high past CSZ occupancy fractions actually occurred, then this would imply nonzero present-day CSZ degassing. This prediction can be tested by tracking the source of (putative) $CH_{4(g)}$ on modern Mars.

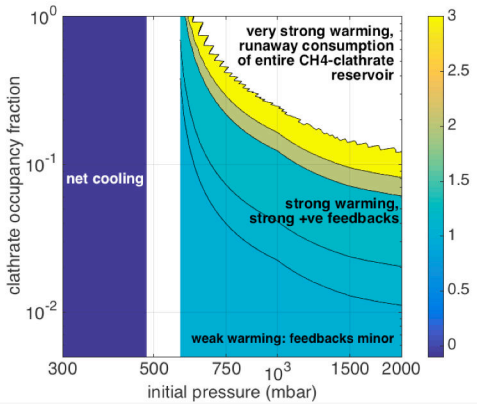


**Fig. 1.** *Gain due to $CH_4$-warming-induced $CH_4$-release (colors). Gain = 1 implies no net feedback. White corresponds to runaway (∞ gain). Results are for a single regolith column at initial (pre-burst) surface temperature of 240K. Results for 3D simulations with realistic topography and surface temperature variations are qualitatively similar.*

**Late Hesperian - Amazonian lake-forming climates triggered by transitions in mean obliquity** [10]**:** Build-up of relatively young (<3.6 Ga) deltas and alluvial fans on Mars required lakes to persist for >3 Kyr (assuming dilute flow), and the watersheds' little-weathered soils indicate a climate history that was >99% dry. However, the post-Noachian lake-forming climates' trigger mechanism remains unknown. In our $CH_4$-burst scenario, chaotic transitions in mean obliquity drive latitudinal shifts in temperature and ice loading that destabilize $CH_4$ clathrate. Outgassed $CH_4$ builds up to levels whose radiative forcing is sufficient to modulate lake-forming climates for past clathrate hydrate stability zone occupancy fractions >0.04. Such occupancy fractions are consistent with $CH_4$ production by >3 Ga water-rock reactions. Individual lake-forming climates are curtailed to $<10^6$ yr duration (matching data) by UV-limited $CH_4$ photolysis.

**Collapse-and-reinflation trigger for the Late Noachian – Early Hesperian fluvial optimum** [11]**:** The progressive drying-out of Mars' surface was punctuated by a dramatic transient increase in fluvial erosion around the Noachian-Hesperian boundary [8]. Standard explanations of this climate optimum appeal to volcano- or impact-triggered climates and imply that individual runoff episodes were brief, apparently inconsistent with evidence for persistent runoff. We have examined a scenario in which the duration, intensity and uniqueness of the Noachian-Hesperian climate optimum result from degassing of $CH_4$-clathrate consequent to Mars' first prolonged atmospheric collapse (Fig. 2). Atmospheric collapse causes low-latitude surface $H_2O$-ice to sublimate, depressurizing and destabilizing $CH_4$ clathrate in subglacial pore space. Subsequent atmospheric re-inflation leads to further warming and further destabilizes $CH_4$-clathrate. $CH_4$-induced warming is efficient, permitting strong positive feedbacks, and possibly raising Mars into a climate optimum. The optimum is brought to a close by photolysis of $CH_4$, and drawdown of the clathrate reservoir prevents recurrence. This scenario predicts a $10^5$-$10^6$ yr climate optimum, transient connections between the deep hydrosphere and the surface, and strong surface weathering, all of which are consistent with recent observations. Crustal hydrothermal circulation very early in Mars history could yield $CH_4$ that would be incorporated into clathrate on approach to the cold surface. The scenario explains why regional watershed integration on Mars occurred relatively late and only once, and suggests that the contrasts between Noachian versus Hesperian climate-sensitive deposits on Mars correspond to a transition from a never-collapsed atmosphere to a collapse-prone climate, ultimately driven by slow loss of $CO_2$ to space.

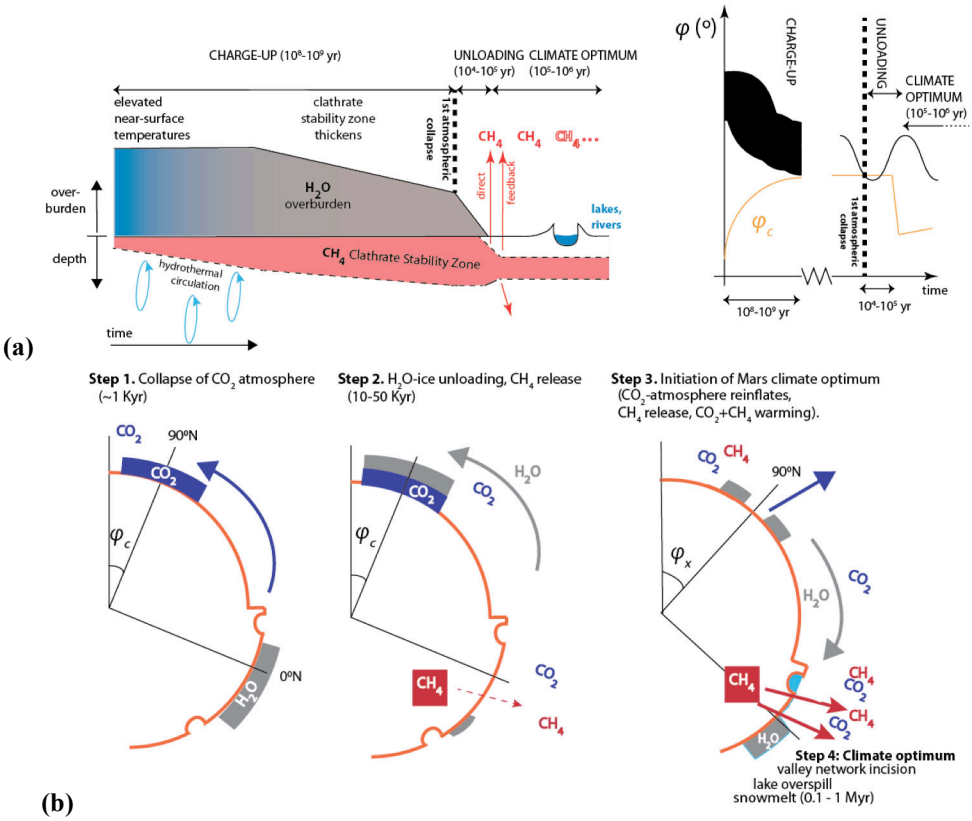


**Figure 2.** *Overview of proposed scenario for the Late Noachian / Early Hesperian climate optimum. (a) Left: schematic of the long-term evolution of a column of the Mars highlands. Right: obliquity diffusion and slow $CO_2$ loss lead to polar temperatures dropping below a pressure-dependent critical value for atmospheric collapse initiation, $\varphi_c$. (b) Below $\varphi_c$, >90% of the atmosphere will condense in 1-10 Kyr (step 1). This unloads high ground (step 2), releasing $CH_4$ from sub-ice clathrate. (GCM simulations indicate that ice unloading can take $>10^6$ yr, but conclusions are unaffected.) Reinflation of the atmosphere leads to climate optimum (steps 3-4).*

**Discussion:** The methane burst hypothesis is an attractive explanation for lake-forming climate optimate in Early Mars history. Formation of $CH_4$-clathrate at relatively shallow (<300 m) depths in the Mars subsurface requires that temperatures were warm at these shallow depths at the time of clathrate formation. This might occur due to insulation from a Late Noachian Icy Highlands ice sheet, or due to a very early (pre-Noachian?) warm climate. The $CH_4$-burst hypothesis cannot explain all aspects of the Early Mars sedimentary record. For example, thick packages of light-toned, layered sedimentary rock required many Myr to form, too long to be explained by methane bursts. Modest amounts of snowmelt may be sufficient to form these features [12].

**Tests:** The collapse-and-reinflation $CH_4$-burst scenario for the climate optimum makes novel, testable predictions. Perchlorates and <50m-diameter craters should be absent before the climate optimum, because both require a thin atmosphere to form. The $CH_4/CO_2$ ratio during the climate optimum can be high, permitting abiotic soots to be incorporated into the geologic record. Present-day $CH_4$ degassing should occur and may be detectable with NOMAD.

**Acknowledgements.** Thanks to R. Wordsworth, F. Forget, A. Howard, R. Irwin, and A. Soto. Grants: NASA (NNX16AG55G, NNX15AM49G).

**References.** (Many excellent references omitted due to space constraints). [1] Forget, F., et al. (2013), *Icarus* 222, 81-99 [2] Mischna, M.A., et al. (2013), *JGR-E* 118, 560-576. [3] Ramirez, R., et al. (2014), Nature Geosci. 7, 59-63.[4] Wordsworth, R.; et al. (2017), *GRL* 44, 665-671. [5] Chassefière, E., et al. (2016), *M&PS*, doi:10.1111/maps.12784. [6] Etiope, G., Sherwood Lollar, B. (*2013). Rev. Geophys.* 51, 276-299. [7] Grant, J.A., Wilson, S.A. (2011) *GRL* 38, L08201. [8] Irwin, R. P., et al. (2005), *JGR-E* 110, E12S15. [9] Kite, E.S., et al. (2015), *Icarus* 253, 223-242 [10] Kite, E.S., et al., *Nature Geosci.,* accepted in principle [11] Kite, E.S., et al. (2017), *LPSC.* [12] Kite, E. S., et al. (2013), *Icarus,* 223, 181–210.

**A COLDER EARLY MARS: INSIGHT FROM CRATER WALL SLOPE STATISTICS.** *M. A. Kreslavsky*[1] and *J. W. Head*[2], [1]Earth and Planetary Sciences, University of California – Santa Cruz, 1156 High, Santa Cruz, CA, 95064, USA, mkreslav@ucsc.edu, [2]Earth, Environmental and Planetary Sciences, Brown University, Providence RI 02912 USA).

**Introduction:** Steep slopes on Mars effectively record the history of fluvial erosion, and therefore, climate conditions in the past. We have found [1] a strong latitudinal zonality of steep slope occurrence on Mars: steep (>25-30°) slopes are almost absent in high latitudes; pole-facing steep slopes are also absent in midlatitudes, which produces a distinctive zone of slope asymmetry. We have interpreted this [1] as a result of intensive slope degradation, when the summer day-average surface temperature exceeds the melting point of ice, which, under the Late Amazonian thin atmosphere conditions is only possible at high latitudes and pole-facing midlatitude slopes, and only when the spin-axis obliquity and the orbit eccentricity are high; this occurred episodically throughout the Late Amazonian. Thus, intensive degradation of steep slopes is a good indicator of warm conditions. Here we analyze slopes of *crater* walls in the *tropical zone* of Mars: in the *tropics* the signature of early erosion was not erased in the Amazonian, while *craters* enable characterization of ages in a statistical way.

**Crater wall slope data:** We used the global catalog of impact craters on Mars by S. Robbins [2] and measured the steepness of the northern and southern crater walls with individual topographic profiles from Mars Orbiter Laser Altimeter MOLA onboard MGS. We limited our analysis to craters in the 4 km – 32 km diameter ($D$) range. The lower boundary of this range is defined by the density of MOLA profiles: the majority of $D$>4 km craters have at least one profile crossing them close to their center, while for smaller $D$ the percentage of measured craters steeply decreases. Craters larger than a few tens of km have a complex floor topography (e.g., peak rings, etc.) and a chance of superposed younger craters distorting the walls, making automated slope retrieval less reliable. Since the total number of $D$>32 km craters is small, their exclusion does not worsen the statistics.

The total number of 4 – 32 km craters is ~$5.3\times10^4$, which makes manual slope retrieval impossible. We implemented an automated algorithm that extracted all individual MOLA profiles crossing each crater within 0.25$D$ from its center and found the steepest center-facing segment of each profile within the expected range of wall distances from the center. For robustness of this heuristic algorithm, we excluded non-circular craters with ellipticity [2] greater than 1.15. Typically, each crater had 2 – 3 profiles or more, and the median number of slope measurements per crater is 10. The slopes are measured at a 300 m baseline (the distance between sequential MOLA shots). The measured along-profile slopes were recalculated into wall slopes assuming their radial orientation.

In summary, we obtained a rich data set for quantitative statistical analysis of crater geometry and degradation, especially north-south slope asymmetry. In this study we focused on ancient terrains in the tropics and we only used the median of all measured wall slopes (both north- and south-facing) in each crater as a single measure of wall steepness, which we refer to hereafter as "slope".

**Age estimates:** Overall, we successfully obtained slopes for ~$4.3\times10^4$ craters, ~81% of the total number of craters in the selected size range. Of the missing 19%, one half was missed because of the gaps in MOLA coverage that can be assumed independent of crater age and degradation state. The other half was filtered out due to their irregular shape (ellipticity), which may correlate with degradation. We ignored this correlation in the present analysis and admitted a bias in absolute crater densities at a few % level: we compensate for the missing craters by adding flat 19% to all spatial crater densities. We formally applied the Neukum production function from [4] and period boundaries from [5] to convert the spatial rater density $N$(4 km)-$N$(32 km) into chronostratigraphic periods.

**Analysis and interpretation:** For analysis of crater degradation on Early Mars, we used the tropical zone between 35°S and 35°N, where Amazonian-age obliquity-driven climate variations are minimal, and no crater wall asymmetry is observed either in morphology or in statistics. We compared slope-frequency distributions for craters superposed on geomorphologic units of different age; we took the unit identification from the digital version of the recent global 1:20M geologic map of Mars [3]. Fig. 1A compares wall slopes for Early Hesperian terrains (curve eH, combined units eHv and eHh from [3] dominated by volcanic plains in Hesperia Planum) and Noachian highlands (curve Nh, combined units eNh, eNhm, mNh, mNhm, lNh from [3]). For comparison, Fig. 1A also shows the distributions for circumpolar zones (curve $P$, 60°S – 80°S and 60°N – 80°N combined). The distributions in Fig. 1 are normalized by surface area; therefore, the area below each curve is proportional to the mean spatial crater density, a proxy of the surface age. The mean crater density of the combined polar zone $P$ is almost the same as for the eH and close to the Hes-

perian/Noachian boundary. We formally separated the area below the Nh curve according to the expected crater density above the Noachian boundary (A+H), in the late Noachian (lN) and earlier (mN)

Comparison of curves eH and Nh in Fig.1A illustrates the lack of wall degradation since the Early Hesperian (the absence of gentle slopes in eH) and noticeable wall degradation in the Noachian (the presence of moderate and gentle slopes in Nh). This is consistent with the other morphological indications of fluvial erosion in the Noachian. On the other hand, comparison with curve *P* shows that the total amount of erosion in the Late Noachian is tiny in comparison to the circumpolar regions in the Late Amazonian (a large number of slopes as steep as 15 – 25° survived the Late Noachian in the tropics, but was erased in the circumpolar zones in the Late Amazonian, curve *P*). Thus, the crater wall slope distribution in the tropical Noachian highlands is not consistent with persisting warm wet conditions in the Late Noachian.

The presence of Noachian-age craters with gentle (<10°) walls does not necessarily mean abundant fluvial erosion in the Middle Noachian: for those ages wall degradation was (at least partly) caused by impacts.

There is a dependence of wall slopes on elevation in the Noachian highlands. While Early Hesperian terrains in the tropics occupy only high elevations, Noachian terrains span a wider range from lower Arabia Terra to higher typical highlands. In Fig.1B the Nh curve from Fig. 1A is replaced with 2 curves for craters and terrains below -1 km and above +1 km elevation with respect to the areoid, as defined in the MOLA data set. The observed difference (fewer steep slopes at lower elevations) well exceeds the formal statistical uncertainty. This means more effective slope degradation at low elevations.

Two curves in Fig. 1C are obtained from the same distributions by subtracting the eH curve. If crater emplacement and wall degradation occurred exactly in the same way both on highlands and Hesperian plains since the Early Hesperian, then the subtraction result would be non-negative and reflect only Noachian-age craters. We interpret the small (but statistically significant) negative values for the high-elevation subpopulation to be due to the difference in the target mechanical properties: it is likely that craters newly formed in the megaregolith of the highlands have somewhat shallower pristine wall slopes than craters formed in consolidated volcanic material of the Hesperian plains. This effect, however, should not depend on elevation. Therefore, the greater negative values for the low-elevation subpopulation (Fig. 1C) should be explained by some slope degradation that occurred at low elevations in the Hesperian (after emplacement of the Early Hesperian terrains), but did not occur at higher elevations. The presence of elevational zonality in surface temperatures indicates a thicker atmosphere.

**Interpretation:** Our analysis of wall slope distribution indicates that: (1) Warm climate conditions occurred in the Late Noachian, however, the total duration of warm episodes was tiny; (2) The latest warm episodes at low elevations (in Arabia Terra) occurred later than at higher elevations, in the Hesperian; (3) The atmosphere was thicker in the Hesperian. These inferences are consistent with the "icy highlands" scenario [6,7]: early Mars was cold with a thicker incondensable ($N_2$, Ar, ?) atmosphere; condensable volatiles ($H_2O$, $CO_2$) were stored in ice sheets at high elevations; there were a number of short warm episodes, when greenhouse gases ($CO_2$, $H_2S$, $SO_2$, $CH_4$, ?) were ejected into the atmosphere from the surface or subsurface by impacts, volcanic eruptions, outflow events, etc.; due to the elevational zonality, at lower elevations the erosion episodes occurred more often, and the last such episodes occurred later.

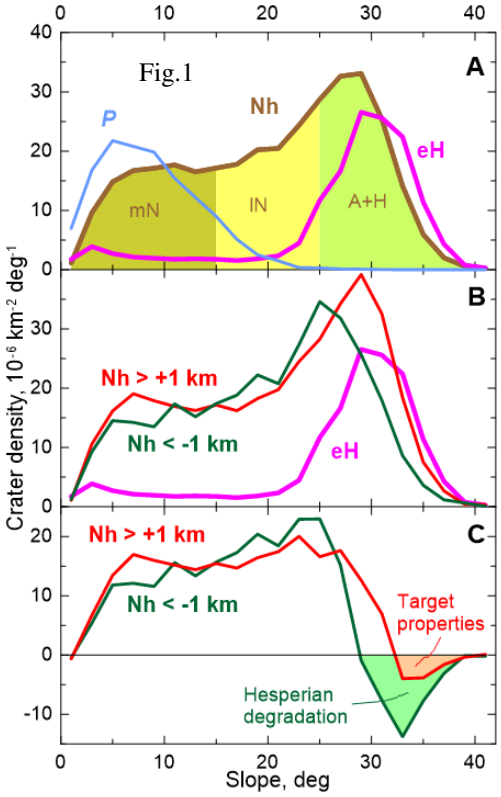


**References:** [1] Kreslavsky M. & Head J. (2003) *GRL 30*, doi:10.1029/2003GL017795. [2] Robbins S. & Hynek B. (2011) *JGR 117*, E05004. [3] Tanaka K. et al. (2014) USGS Scientific Investigations Map 3292. [4] Ivanov B. (2001) *Space Sci. Rev. 96*, 87-104. [5] Werner S. & Tanaka K. (2011) *Icarus 215*, 603 – 607. [6] Wordsworth et al., 2013, *Icarus 222*, 1. [7] Weiss D. & Head J. (2015) *Planetary Space Sci. 117*, 401-420.

# IRON AND MAGNESIUM ENRICHMENTS IN CA-SULFATE VEINS AS OBSERVED BY CHEMCAM AT GALE CRATER, MARS.

J. L'Haridon [1] (jonas.lharidon@univ-nantes.fr), N. Mangold [1], W. Rapin [2], O. Forni [2], P.-Y. Meslin [2], A. Cousin [2], V. Payré [3], J. Johnson [4], E. Dehouck [2], M. Nachon [5], L. Le Deit [1], O. Gasnault [2], S. Maurice [2], R. Wiens [6], others?
[1] LPGN, Nantes, France, [2] IRAP, UPS-OMP, Toulouse, France, [3] GeoRessources, Nancy, France, [4] Johns Hopkins University Applied Physics Laboratory, Laurel, Maryland, USA, [5] UC Davis Earth and Planetary Science, Davis, California, USA, [6] Los Alamos National Laboratory, Los Alamos, New Mexico, US.

**Introduction:** Diagenetic mineralized veins have been consistently observed along the Curiosity rover traverse [1,2,3], starting at Yellowknife Bay shortly after landing. Among these features, light-toned veins – primarily composed of Ca-sulfate [1,4] – are pervasive to all units and cross-cut other diagenetic features [5], thus hinting at a regional late-stage episode of fluid circulation.

The chemistry and mineralogy of these veins are instrumental in determining the nature of the diagenetic fluids at the time of formation. Such veins therefore provide insights into the diagenetic processes of the sedimentary deposits of Gale crater, on Mars. In particular, ChemCam-derived elemental compositions from light-toned veins have shown on occasions FeOT and MgO detections associated with low-to-no SiO2 abundance, alongside the expected high CaO abundance and S emission peaks in LIBS spectra. Here we report on these observations.

**Data processing:** All data used in this study were collected between sols 0 and 1700 by Chemcam [6], the Mars Science Labora-tory (MSL) Laser Induced Breakdown Spectroscopy instrument, and the associated Remote Micro-Imager (RMI). Chemical quantifications for major elements are obtained using an updated multivariate analysis technique [7].

**Methods:** Observations of mixed composition between the surrounding host rock and diagenetic features are not uncommon with ChemCam, because the surface ablated by the laser covers 300-600 µm in diameter. Thus it frequently simultaneously samples material from distinct lithologies (such as bulk rock silicate minerals and calcium sulfate in veins) if the LIBS point is located at the interface.

Quantification of major elements in these diagenetic facies come however with some uncertainties, as such marginal chemical compositions are not necessarily represented in the ChemCam calibration dataset. So in order to highlight Fe and Mg enrichments in light-toned veins, we propose to evaluate the Fe/Si and Mg/Si ratios based on the Fe (260.02 nm), Mg (285.3 nm) and for Si (288.24 nm) emission peaks, which present little convolution with other elements. ChemCam targets with ratios 3-σ above local host rock mean are considered enriched in Fe and/or Mg compared to Si. This method allows us to distinguish specific enrichments in these these elements from mixed composition with the surrounding host rock.

**Results and Interpretations:** We have identified two sets of light-toned veins showing Fe and Fe+Mg enrichment trends (Figure 1). Passive reflectance observations of Fe rich light-toned veins indicates the presence of $Fe^{3+}$ mineral phase(s) such as ferric oxide (hematite) or ferric sulfate. Conversely, Fe+Mg rich light-toned veins are observed in association with dark-toned material (either as inclusions in the veins or layers in close proximity) that show similar enrichment in Fe ± Mg compared to Si, as well as elevated Mn and detection of P [8]. They are also associated with ferrous ($Fe^{2+}$) spectral features on passive spectra.

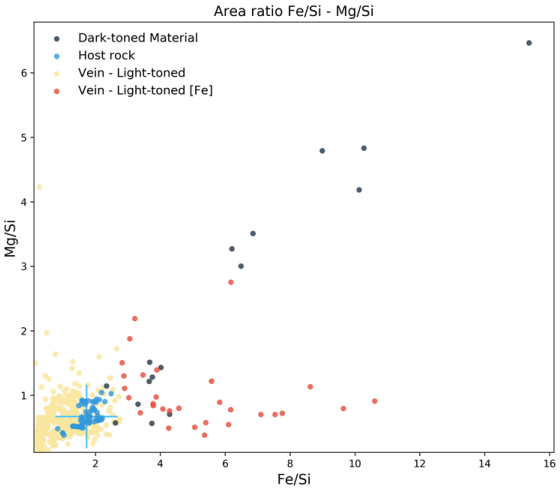


Figure 1: Peak area intensity ratios for Fe/Si and Mg/Si illustrating the trends towards Fe and Fe+Mg enriched composition in subsets of light-toned veins.

Fe and Mg abundances in these features are not correlated with elevated contents in other major (Al, K, Na & Ti) and minor (Ba, Cr, Li, Rb, Sr, Ni, Zn) elements apart from occasional observations of elevated Al/Si ratios in Fe rich light-toned veins. Furthermore, the two trends are clearly identified on a CaO - $FeO_T$ - $SiO_2$ ternary diagram (Figure 2) as they plot along Ca-sulfate mixing lines with Fe-oxide/sulfate and dark-

toned material respectively, which deviates significantly from a mixed composition with the surrounding host rock.

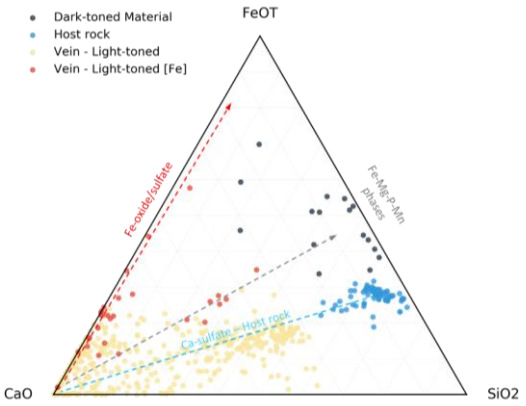


Figure 2: CaO - $FeO_T$ - $SiO_2$ ternary diagram (wt%), illustrating the mixing line between Ca-sulfate and Host rock (blue), Dark-toned Features (grey) and Fe-oxide / Fe-sulfate (red).

These two subsets of light-toned veins were both encountered within the fluvio-lacustrine sedimentary rocks of the Murray formation but at distinct stratigraphic levels and localities along the rover traverse (Figure 3). Fe rich light-toned veins were mostly found below the unconformable contact with the overlying eolian sandstones of the Stimson formation near the *Naukluft Plateau* whereas the Fe+Mg rich light-toned veins were analysed near *Precipice* in association with these dark-toned features.

**Discussion:** Interpretation of mineralolgy with ChemCam is limited in these features, as no cross-analysis were performed by CheMin (X-ray diffraction) on board *Curiosity*. In addition, a number of diagnostic elements such as P and S are difficult to observe with ChemCam and do not allow for the discrimination of minor phosphate and/or sulfate phases from oxides, especially if present in association with Ca-sulfate. Nevertheless, the absence of correlation with Ti indicates that these enrichments are likely authigenic and thus reflect changes in pH and/or redox state in the parent fluid at the time of formation.

$Fe^{3+}$ mineral phases would indicate more oxidizing conditions, consistent with detection of hematite in the surrounding host rock from Naukluft Plateau up to the hematite ridge [9]. Fe-sulfates if present would also reflect more acidic conditions consistent with the emplacement Si rich fracture halos in the overlying Stimson formation [10] as well as chemical trends observed in the Murray formation [11], and would account for the elevated Al/Si ratios encountered in a few Fe rich features.

On the other hand, the association of Fe+Mg rich light-toned veins with dark-toned features showing enrichments in Mn and P near Precipice would indicate near-neutral pH (no dissolution of P) and possibly more reducing conditions ($Fe^{2+}$). P could be present either as phosphate or adsorbed onto Fe/Mn-oxides. Further observations of Fe-Mg-Mn/P rich features upsection will likely further contrain the mineralogy of these features and help in the reconstruction of the diagenetic history of the sedimentary deposits of Gale crater.

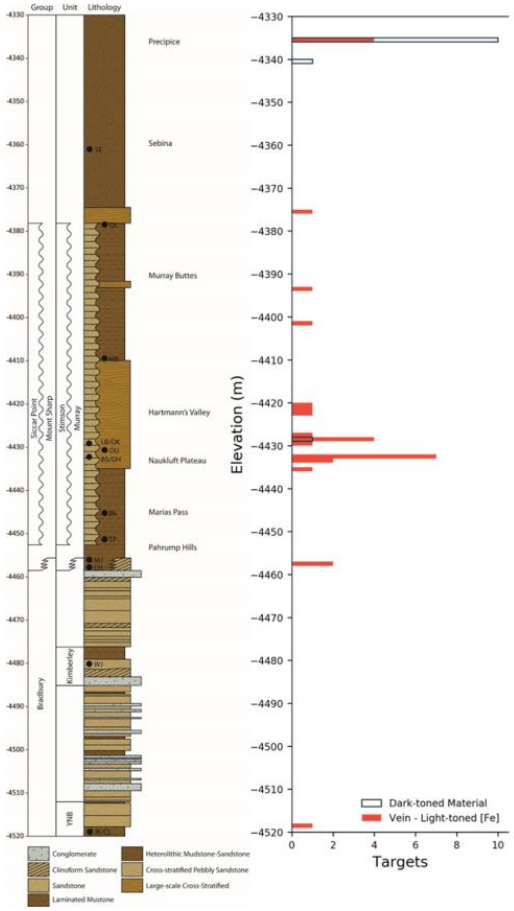


Figure 3: Distribution of Fe rich light-toned veins in the stratigraphy, highlighting the concentration of these targets at specific elevations within the Murray formation.

References: [1] Nachon, M. et al. (2014), JGR Planets, 119, 1991–2016. [2] Nachon, M. et al. (2017), Icarus, 281, 121. [3] Léveillé, R. J., et al. (2014), JGR Planets, 119, 2398–2415. [4] Rapin, W. et al. (2016), EPSL, 452, 197-205. [5] Kronyak, R. et al. (2015), AGU abstract. [6] Wiens, R.C., et al. & Maurice, S. et al. (2012), Space Sci. Rev., 170. [7] Clegg et al. (2017) SCAB, accepted. [8] Forni, O. et al. (2017), LPSC. [9] Fraeman, A. et al. (2016), Fall AGU, San Francisco. [10] Yen et al. 2017, EPSL, 471, 186–198. [11] Rampe et al. 2017, EPSL, 471, 172–185.

**PHOTOCHEMICAL ESCAPE OF OXYGEN FROM MARS: CONSEQUENCES FOR CLIMATE HISTORY.**

R. J. Lillis[1], J. Deighan[2], J. L. Fox[3], S.W. Bougher[4], Y. Lee[4], M. Combi[4], F. Leblanc[5], T. E. Cravens[6], A. Rahmati[6], H. Gröller[7], B. M. Jakosky[2] [1]UC Berkeley Space Sciences Laboratory (rlillis@ssl.berkeley.edu), [2]Laboratory for Atmospheric and Space Physics, University of Colorado Boulder, [3]Department of Physics, Wright State University, [4]Department of Atmospheric, Oceanic and Space Sciences, University of Michigan, [5]Laboratoire de Météorologie Dynamique, Jussieu, Paris [6]Department of Physics and Astronomy, University of Kansas. [7]Lunar and planetary laboratory, University of Arizona.

**Introduction:** One of the primary goals of the MAVEN mission is to characterize rates of atmospheric escape at the present epoch and relate those escape rates to solar drivers. One of the major escape processes is known as photochemical escape, which is broadly defined as a process by which a) an exothermic reaction in the atmosphere results in an upward-traveling neutral particle whose velocity exceeds planetary escape velocity and b) the particle is not prevented from escaping through any subsequent collisions. At Mars, photochemical escape of oxygen is expected to be a significant channel for atmospheric escape, particularly in the early solar system when extreme ultraviolet (EUV) fluxes were much higher. Thus characterizing this escape process and its variability with solar drivers is central to understanding the role escape to space has played in Mars' climate evolution [1, 2].

**Dataset**: we use near-periapsis (<400 km altitude) data from three MAVEN instruments: the Langmuir Probe and Waves (LPW) instrument measures electron density and temperature [3], the Suprathermal And Thermal Ion Composition (STATIC) experiment measures ion temperature [4] and the Neutral Gas and Ion Mass Spectrometer (NGIMS) measures neutral and ion densities [5]. We use data from the MAVEN primary mission: February 1, 2015 to July 31, 2016 comprising ~78% of a Mars year.

**Calculating instantaneous escape fluxes.** For each profile of in situ measurements, we make several calculations, each as a function of altitude. The first uses electron and ion temperatures and simulates the dissociative recombination of $O_2^+$ to calculate the probability distribution for the initial energies of the resulting hot oxygen atoms. The second is a Monte Carlo hot atom transport model that takes that distribution of initial O energies and the measured neutral density profiles and calculates the probability that a hot atom born at that altitude will escape. The third takes the measured electron and ion densities and electron temperatures and calculates the production rate of hot O atoms. We then multiply together the profiles of hot atom production and escape probability to get profiles of the production rate of escaping atoms. This is integrated with respect to altitude to give us the escape flux of hot oxygen atoms for that periapsis pass. Figure 1 shows how we calculate hot oxygen escape fluxes for each MAVEN periapsis pass, using a combination of measured quantities, experimental laboratory data and models.

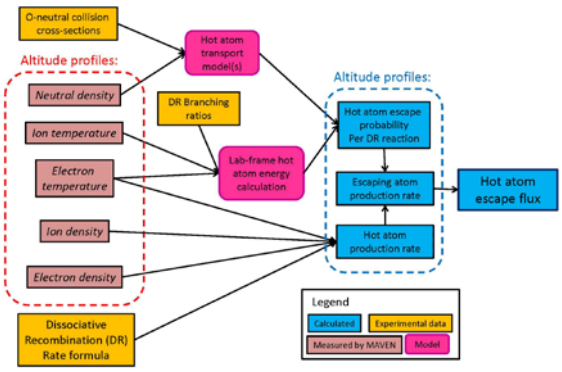


**Figure 1: Flowchart explaining calculation of hot oxygen escape from measured altitude profiles of neutral densities and ion and electron densities & temperatures.**

**Hot Oxygen total escape fluxes**. Figure 2 shows CO2 ionization frequency (calculate from from solar EUV irradiance) and calculated escape fluxes as a function of Mars season (abscissa) for Mars years 33 and 34.

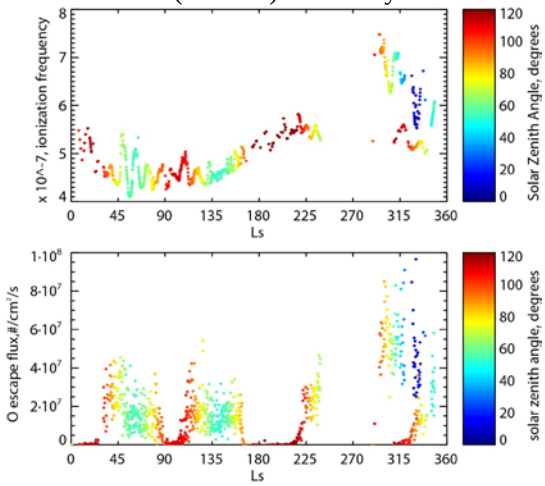


**Figure 2: total derived photochemical O escape fluxes are shown as a function of solar zenith angle and season.**

We see that escape fluxes are substantially higher in early 2015, when Mars is comparatively close to the sun and the sun is reasonably active (approximately solar moderate), ranging 4 to 8 x 107 /cm2/s. As Mars recedes and solar activity diminishes, photoionization frequency drops and average escape fluxes drop correspondingly during the same period. By the time MAVEN's periapsis is on the dayside again in October 2015, ionization frequencies have dropped by ~40% from their highest values and derived escape fluxes have dropped by a factor of two or more. From then

until mid-2016, both ionization frequencies and dayside escape fluxes stay generally low.
Factors of ~2-3 variability within a short time span arises from both natural variability in the physical system and our sampling of that system. Relative neutral density changes due to gravity waves and atmospheric tides cause variability in escape probabilities and $O_2^+$ densities[6,7]. In addition, plasma transport and ionospheric currents are another source of variability [8,9].

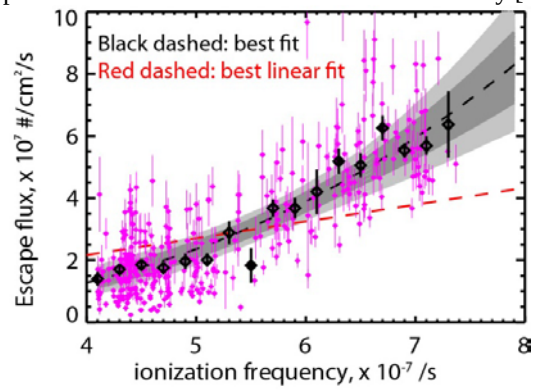


**Figure 3:All 594 individual dayside derived escape flux values (small pink dots) and binned values (black diamonds) with standard errors. All power law fits to these binned averages that fall within the 1-sigma and 3-sigma error ellipsoid are shown as dark and light gray lines respectively. The best fit (power law index of 2.64) is shown in black.**

**Dependence on EUV flux.** Figure 3 shows how photochemical escape of oxygen depends on photoionization frequency over the range of values that have been measured by MAVEN. Despite a substantial spread in values, it is clear that a positive correlation exists. Best-fit power laws are larger than 2, with a linear dependence [10] providing a possible but unlikely fit to the data.

**Consequences for Mars climate history.** If we extrapolate this power law dependence of photochemical escape flux on photoionization frequency, we can estimate photochemical escape rates in the past when the sun was much brighter in the EUV [11]. Figure 4 shows, as a function of time in the past, photoionization frequency, extrapolated photochemical oxygen escape rates and cumulative atmospheric loss, under our best fit conditions (including 1-sigma and 3-sigma uncertainties), the linear assumption and no EUV dependence.

These extrapolations show that photochemical escape of oxygen could easily account for several hundred millibars of oxygen escape over the last 3.5 billion years. This, combined with the other escape processes MAVEN is probing (thermal hydrogen escape, pick up ion escape and sputtering escape) makes it clear that atmospheric escape is indeed the primary explanation for the drastic reduction in Mars' surface pressure and therefore the lack of stability of liquid water on Mars' surface since that time.

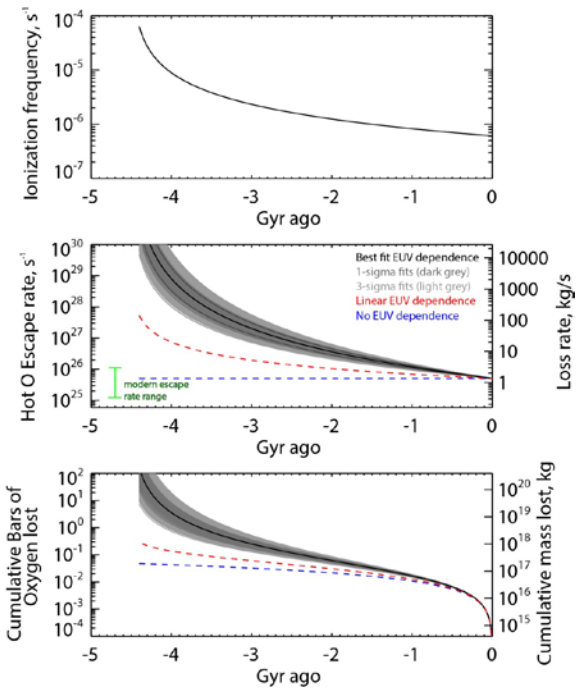


**Figure 4: Extrapolation of photochemical O escape rates over Martian history. Panel a) shows the assumed history of ionization frequency [11] b) and c) shows the resulting escape rates and cumulative oxygen lost respectively, assuming the best power law fit (2.64) to ionization frequency dependence (thick black), the range of 1- and 3-sigma power law fits, a linear dependence (red dashed) [10] and no EUV dependence (blue dashed).**

**Conclusions and next steps:** As well as this effort using in situ data, MAVEN can also constrain photochemical escape using remote sensing of the oxygen corona with the Imaging Ultraviolet Spectrograph (IUVS) [12, 13], the Solar Energetic Particle (SEP) instrument and the Solar Wind Ion Analyzer [14]. These multiple methods will eventually allow validation of photochemical escape from Mars and its dependence on solar and planetary conditions, enabling confident extrapolation back into the past.

**References:** [1] McElroy et al., *JGR*, 1977, [2] Fox and Hac, *Icarus*, 2009, [3] Andersson et al, SSR, 2015, [4] McFadden et al., SSR, 2015, [5] Mahaffy et al., SSR, 2015, [6] Yigit and Medvedev, JGR, 2012, [7] England et al., JGR, 2016, [8] Morgan et al., JGR, 2008], [9] Riousset et al., JGR, 2013, [10] Cravens et al., JGR, 2016. [11] Ribas et al., ApJ, 2005, [12] Lee at al, GRL, 2015, [13] Deighan et al., GRL, 2015, [14] Rahmati et al., JGR, 2016.

**EARLY MARS CHRONOLOGY: WHEN AND HOW DID THE DYNAMO DIE?**

Robert Lillis[1], Foteini Vervelidou[2], Benjamin P. Weiss[3], Michael Manga[4], Herb Frey[5], Stuart Robbins[6]. [1]Space Sciences Laboratory, University of California, Berkeley, [2]German Research Center for Geosciences, Potsdam, [3]Massachusetts Institute of Technology, Cambridge, MA, [4]Department of Earth and Planetary Sciences, University of California Berkeley, [5]NASA Goddard Space Flight Center, [6]Southwest Research Institute, Boulder, Colorado.

**Introduction:** Mars does not currently possess a global dynamo magnetic field but evidence of strong crustal magnetization and remanent magnetization in the 4.1 Ga year old Martian meteorite ALH 84001 implies that such a field is certain to have existed in the early Noachian [1, 2]. The dynamo may have started immediately following differentiation [3] or alternatively may have been inhibited past initial crust formation by thermal stratification of the core resulting from collisions with large planetary embryos [4]. We are concerned with constraining the time at which and manner in which Mars' global magnetic field disappeared, for two primary reasons a) it places constraints on Mars' interior evolution and b) a global magnetic field has major implications for atmospheric escape from Mars, particularly ion escape and ion-driven sputtering escape [5].

We can place constraints on the history of the martian global magnetic field by studying the natural remanent magnetism (NRM) of Martian rocks of known age. When cooled below the Curie point, deposited as sedimentary materials, crystalized, aqueously altered, or shocked magnetic minerals within these rocks acquire a magnetization that scales with the strength and direction of the ambient magnetic field. These studies of NRM and age are ideally done by examining such rocks directly in the laboratory, but can also be approximated using spacecraft measurmenets of crustal magnetic fields above age-dated features on the Martian surface. We will examine these two approaches in turn.

**Constraints from Martian meteorites**. Paleomagnetic and thermochronometric laboratory studies can constrain the magnetic history of samples. The oldest Martian meteorite, NWA 7034, has U-Pb ages ranging up to 4.4 Ga and but its magnetization was reset on Earth by collectors' hand magnets [6]. The only other known pre-Amazonian Martian meteorite is the 4.1 Ga ALH 84001, which has been found to have a significant primary NRM that originated on Mars [7, 8, 9]. Its NRM resides mostly in single domain magnetite, acquired at 4.1 Ga, and pyrrhotite-bearing carbonate, acquired likely at 4.1 Ga but possibly as late as 3.9 Ga [10, 11, 12, 13, 14]. The paleomagnetic field intensity at this time was was ~50 μT [15]. Because this field could have been either that of a dynamo or nearby crustal magnetization, the 4.1 Ga age of the magnetization only sets a minimum age for the origin of the dynamo and does not require that the dynamo was still active at 4.1 Ga. The next youngest Martian meteorites that have been analyzed are the 1.3 Ga nakhlites, which have been found to carry no stable NRM [16]. Thus, the meteorite record indicates that the Martian dynamo had initiated by 4.1 Ga and ceased sometime before ~1.3 Ga.

**Volcanic features** and magnetic fields thereabove have been used to imply the dynamo history may have lasted into the Hesperian epoch [17]. In our view such features are ill-suited because they are typically constructed over many episodes of magma intrusion and lava emplacement, implying a tenuous link between the age of the youngest visible lava flow and the age of the magnetization in the full depth of crust beneath.

**Large craters as magnetic markers.** Notwithstanding that crater retention ages are subject to substantial uncertainties [18], impact basins > 300 km in diameter are the most reliable dynamo markers as their cratering age and magnetization (down to the Curie isotherm depth) were reset simultaneously. Post-impact demagnetization within the crater is therefore a proxy for the absence of ancient magnetic field at that time.

From orbital magnetic field data, the degree of demagnetization of a given crater with respect to its surroundings can only be determined probabilistically, with increasing confidence for larger diameters [19]. Figure 1 shows magnetization probability distributions for four example craters with ages determined via carefully analyzing crater size frequency distributions [20]. Figure 2 shows the application of this principle to a set of 38 ancient Martian craters/basins.

**Mars Dynamo Timelines.** Figure 2a shows a timeline for only the basins >1000 km with their ages determined by over-printed craters 300 km and larger [19]. The basins quite clearly fall into 2 groups: 1) 4 basins with essentially zero probability of containing any substantial magnetization: Argyre, Hellas, Utopia and North Polar all likely formed when no substantial global magnetic field existed and 2) the remainder of the craters, all with probability distributions implying that they are at least partially magnetized and therefore likely having formed in the presence of a global magnetic field. These 2 basin populations do not overlap in age by more than a small fraction of the typical age uncertainty. Together they imply that the cessation of the Martian dynamo may have occurred at a cratering density N(300) = ~2.8 (absolute model age of ~4.1 Ga [18]).

The timeline constructed using the cratering densities and age estimates of Robbins et al. 2013 [8] (figure 2b) allow us to examine smaller and in many cases younger craters compared to Frey, 2008 [9]. All 6 basins with model ages greater than 4.05 Ga (Cassini, "epsilon", "iota", Tikhonravov, "eta" and Ladon) have zero probability of being completely demagnetized, whereas all basins with model ages younger than 4.05 Ga have their probability maxima at zero magnetization. However, Prometheus, Hellas, Isidis and Argyre, in the same model age range, have basically zero probability of being magnetized. Considering these 13 basins together argues strongly for a single dynamo cessation sometime after the oldest 6 basins and before the youngest 7. In terms of absolute model age this dynamo cessation would have occurred 4.0 and 4.1 Ga [18].

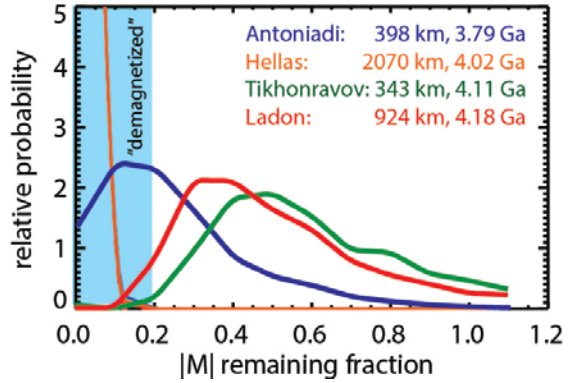


**Figure 1: probability distributions as a function of remaining magnetization fraction are plotted for four craters formed on early Mars. Ages shown are absolute model ages [19].**

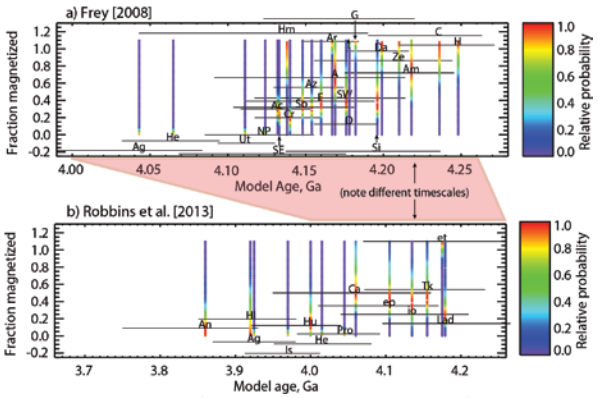


**Figure 2: Timelines of magnetization probability of large craters formed on early Mars, from [18] and [19]. Magnetization probability distribution curves for each crater are shown as colored vertical lines. Note the different time scales.**

**Problems with early Mars chronology: when did the dynamo really die?** The cratering chronology used to arrive at the absolute model ages mentioned above [18] assumes a monotonically, exponentially decreasing impactor flux with time. However, the largest craters naturally divide into two morphologically very different groups, as shown in figure 3. The four youngest basins Utopia, Hellas, Isidis, and Argyre, show much more pronounced crustal thickness variations than the older basins, suggesting that a substantial amount of time passed between the formation of the oldest basins and the four youngest, i.e. the crust had substantial time to cool and become less ductile before these impacts.

These youngest basins also contain extremely weak or nonexistent crustal magnetic fields, implying that they were formed in the post-dynamo era. In contrast, the older basins all contain substantial crustal magnetic fields, implying formation while the dynamo was active. Taken together, the topographic pronouncement and magnetization differences between these two populations suggest that there may have been a substantial 'lull' (perhaps up to 300 Ma) in the rate of large impactors and that the dynamo may have ceased at any time during this lull up to and including the time of the first 'young' mega impact Utopia.

**Climate implications**: The dynamo's strength as a function of time and when its ultimate cessation occurred, are key ingredients in the puzzle of early climate change on Mars, due to the very different solar wind interaction and atmospheric escape regimes for terrestrial planets with and without global fields [5].

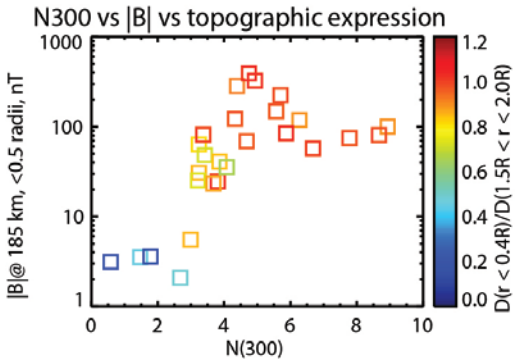


**Figure 3: Basin magnetization vs. N(300) crater retention age for megabasins on Mars (D>1000 km). Colors are coded for crustal thickness ratio (inside basin/outside basin). The youngest four basins (Isidis, Argyre, Hellas, and Utopia) show both greater variation in topography and lower magnetization than the other basins.**

**References:** [1] Acuña et al., 1999, *Science*. [2] Weiss et al, 2002, EPSL, [3] Williams and Nimmo, 2000, *Geology*. [4] Arkani-Hamed, 2012. [5] Chassefiere et al, 2007, *PSS*, [6] Gattaceca et al., 2014; [7] Lapen et al., 2010; [8] Cassata et al., 2010; [9] Bouvier et al., 2009; [10] Antretter et al., 2003; [11] Rochette et al., 2005; [12] Weiss et al., 2002; [13] Weiss et al., 2004; [14] Shuster and Weiss, 2005; [15] Weiss et al., 2008; [16] Funaki et al., 2009, MPS; [17] Milbury et al., 2012, JGR; [18] Hartmann and Neukum, 2001, SSR [19] Lillis et al, 2013, *JGR*. [20] Robbins et al., 2013, *JGR*

**LI-ISOTOPE FRACTIONATION INTO THE OCTAHEDRAL FRAMEWORK OF CLAYS: A WAY TO UNDERSTAND THE WEATHERING OF BASALT UNDER EARLY MARS CONDITIONS.** E. Losa.-Adams[1], C. Gil-Lozano[2], J.L. Bishop[3], A. Hoser[4], A.F. Davila[3], A. G. Fairén[2], V.F. Chevrier[5], L .Gago-Duport[1] .[1]Universidad de Vigo. 36200 Vigo, Spain. (elosa@uvigo.es). [2]Centro de Astrobiología, 28850 Spain.[3]NASA Ames, CA 94043, USA. HZB.14109, Berlin. [5]Arkansas Center for Space and Planetary Sciences. Fayetteville, AR, USA.

**Introduction:** Geochemistry of Lithium (Li) isotopes provide important information about the weathering of primary silicates in aqueous environments. Li can be found, in the range of ppm, in almost all of the basalt bearing minerals, because of its small ionic radius, similar to Mg. The two stable isotopes of Lithium, $^{7}$Li and $^{6}$Li, have a large relative mass difference (~15%) that results in significant fractionation between water and secondary minerals phases, mostly clays, the main weathering product of basalt dissolution. Clay minerals preferentially incorporate the light isotope in their structural lattice, thus leaving the remaining water with a heavier isotopic signature. This behaviour open interesting possibilities for the use of lithium isotopes as a proxy to understand the degree and extent of basalt weathering in aqueous mediums, providing important information about the Earth's Early Ocean and helping to determine the prevailing conditions during the formation of water bodies in the past of Mars. [1], [2], [3], [4].

The substitutions of Li in two crystallographic sites of clay minerals may complicate the interpretations of bulk Li-isotope ratios. It has been suggested that the magnitude of the isotopic fractionation of Li between water and clay may be different at the interlayers than in the octahedral sites of clay minerals.

Actually it is unclear whether Li-isotopic fractioning only occur during the process of clay nucleation and growth (i.e., in trioctahedral hectorite), or by Li migration from the interlayer to either an octahedral position or to the ditrigonal cavities (i.e., in dioctahedral montmorillonites and beidellites), depending on the charge of the layer.

In this study, we performed high resolution neutron scattering experiments to evaluate whether is possible to discrimitate by neutron diffraction the isotopic ratio of lithium isotopes entring in the octahedral framework of clay minerals after contact with solutions containing both Li isotopes. The determination of lithium isotopic signature with this technique is based on the very different Scattering Length Densities (SCL) of both isotopes, that can selectively affect the intensisity of various reflections, in the neutron scattering diagrams.

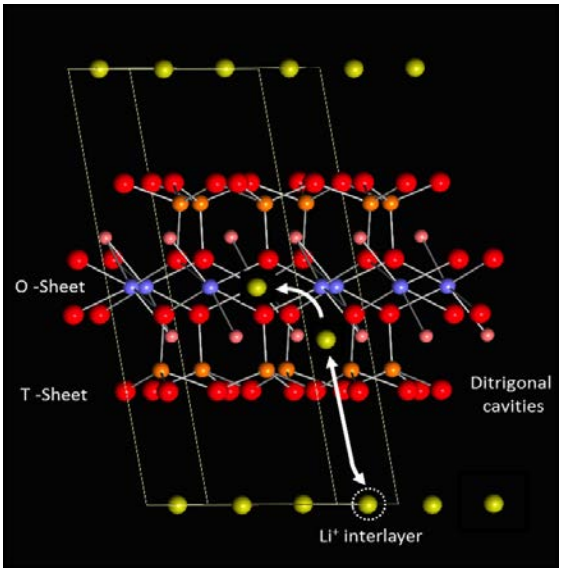


*Figure 1. Possible sites for lithium uptake by smectites. Li can be incorporated to the octahedral sheets or migrate from the interlayer. It is assumed that only the Li atoms placed in the structural framework, undegoes isotope fractionation.*

To this end, we are analyzing the neutron scattering spectra of various clays before and after lithium adsorption using the Rietveld method by including the different scattering lengths of, $^{6}$Li and $^{7}$Li in the calculation of the intensities.

**2. Experimental set-up:** We are using dioctahedral and trioctahedral smectites. In the diocthedral case, it is expected that lithium migration from the interlayer occurs to compensate the differences on layer charge. In order to analyze this process, Li-exchanged sample were prepared by using the Gene Kelly procedure (GK) i.e.: washing clays with LiCl and heating overnight at 300 ºC. The GK test was used to determine whether $Li^{+}$ ions remain at the interlayers- in smectites with tetrahedral charges- or are attracted to the vacant octahedral sites in dioctehedral smectites. Octahedral charged clays (montmorillonites) become non-expandable after GK test due to the incorporation of $Li^{+}$ to octahedral sites, while regularly interstratified smetites (i.e.montmorillonite-beidellite) have particular distribu-

tions of negative layer charges, inducing the incorporation of $Li^+$ to both positions and previsibly in diferent $^6Li$ /$^7Li$ isotope ratios. The experiments were performed in the High Resolution Neutron Powder Diffractometer (E9) of the HZB in Berlin.[5].

**3. Structural Analysis and Preliminary results:** The Rietveld structure-refinements are being done with the program FULLPROF [6].

In order to track the effect lithium isotopes on the diffraction profile, preliminary spectra were calculated by using the Neutron Scattering Lengths of both lithium isotopes (figure 1). Data were taken from the NIST database. As is show in Figure 1, there are appreciable changes on the intensities of various reflections, following the relative occupancies

Consequently, each isotope was considered separately in the structural model. Refinement of the various smectites employed in the experiments, was done according this procedure. The diffraction profiles were modelled using the (TCH) pseudo-Voigt profile-function. The background was determined using a refinable fifth-order polynomial or a cubic spline of 30 selected points. An example of refinement for the case of beidellite/montmorillonite is shown in figure 2. The upper plot (a) show the Rietveld refinement of the mineral sample "as received", i.e.: prior to adsorption of $Li^+$ by thermal treatment at 300ºC.

The observation of two basal reflections (001) clearly suggest the presence of a regularly interstratified beidellite/montmorillonite structure. In this case the refinement was donne by using two similar phases but with different c-parameters. Results of quantitative phase analysis show similar wt% amounts for both mixed phases. In addition, accessory quartz (14%) was included in the refinement.Figure 2(b) corresponds to the same phase after Li adsorption and thermal treatment at 300ºC. In spite of lithium incorporation to the octahedral framework, the two (001) swelling refections are still observed, although the reflection at ≈ 27Å is weaker. This suggest that the incorporation of $Li^+$ to the octahedral set was not enough to provide a complete compensation of charges and that some tetrahedral charge is still present in the interstatified structure. The later is probably due to the substitution of tetrahedral Si by Al in beidellite. Consequently, refinement of atomic positions involving $Li^+$ was done by including both lithium isotopes at the octahedral position (0,0,1/2) and at interlayer position (0,1/2,0). Relative occupancy at every position of each isotope was refined employing atomic constrains. Preliminary calculations of $\delta^7Li$ normalized to L-SVEC were obtained from the Rietveld occupation factors. Resulting fractionation values were $\delta^7Li \approx -0.63$ for the octahedral position and $\delta^7Li \approx 0.02$, for the swelling position.

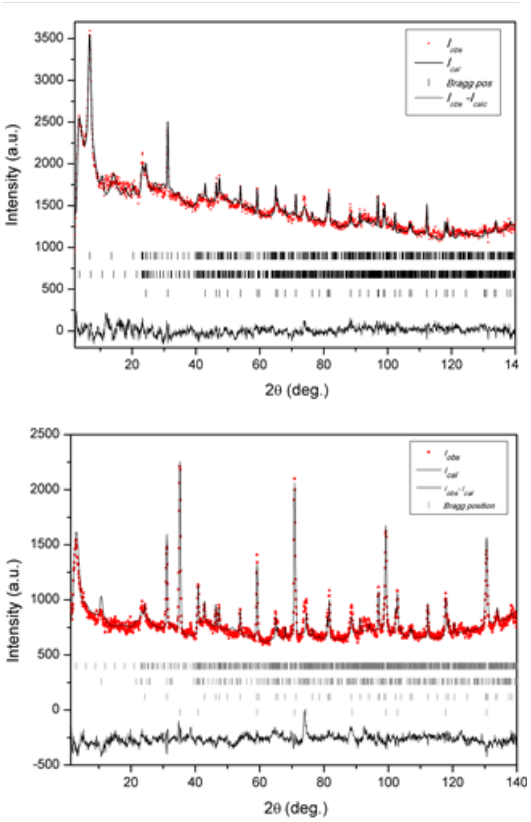


*Figure 2. Rietveld plots of (a): mixed-layer beidellite/montmorillonite at 25 ºC before Li adsorption. (b): after GK treatment with LiCl at 300 ºC. Refinements were done by including the ratio $^7Li/^6Li$ at (0,0,1/2) and (0,1/2,0) positions.*

These results are consistent with a selective incorporation of the light isotope to the octahedral sites. Comparison of the isotopic signatures determined from experiments based on this technique, with the Li - isotopic ratios in clays obtained from meteorite samples, may provide important insights regarding the weathering processes and the persistence of water on Mars.

**References:** [1] Losa-Adams et al (2014), *LPS VL*, Abstract #1777. [2] Fairen et al.(2015) *Geochem. Geophys. Geosyst.* ,16(4):1172-1197. [3] Magna. T.B. (2015), *Geochim Cosmochim Acta* 162:46–6. [4] Tomascak P.B. et al. (2015) *Advances in Lithium Isotope Geochemistry* [5] D. M.Többens et al (2001) *Materials Science Forum* 378-381, 288-293 [6] J. Rodriguez-Carvajal (1993), *Physica B*, 192, 55.

**OPEN-SYSTEM WEATHERING AT GALE CRATER FROM THE CHEMISTRY OF MUDSTONES ANALYZED BY THE CURIOSITY ROVER.**

N. Mangold[1], E. Dehouck[2], C. Fedo[3], O. Forni[2], C. Achilles[4], T. Bristow[5], J. Frydenvang[6], O. Gasnault[2], J. L'Haridon[2], L. Le Deit[1], S. Maurice[2], S.M. McLennan[7], P.-Y. Meslin[2], S. Morrison[4], H.E. Newsom[8], E. Rampe[9], F. Rivera-Hernandez[10], M. Salvatore[11], R.C. Wiens[6]. [1]Laboratoire de Planétologie et Géophysique de Nantes, Université de Nantes, Nantes, France, nicolas.mangold@univ-nantes.fr. [2]IRAP, UPS-OMP, Université de Toulouse, Toulouse, France, [3]Dept Earth Planetary Sci., University of Tennessee, Knoxville, USA, [4]University of Arizona, Tucson, USA, [5]NASA Ames Research Center, Moffett Field, USA, [6]Los Alamos National Laboratory, Los Alamos, New Mexico, USA, [7]Stony Brook Univ, Stony Brook, New York, USA, USA, [8]U. New Mexico, Albuquerque, NM 87131, USA [9]Aerodyne Industries, JETS at NASA JSC, Houston, [10]UC Davis Earth and Planetary Science, Davis, California, [11]Dept Physics Astronomy, NAU, Flagstaff, USA.

**Introduction:** Since its landing, the Curiosity rover has traversed 17 km towards the layered rocks at Mt. Sharp (also named Aeolis Mons), spending >1700 sols (Martian days) at the surface of Mars. On sol 750, the rover entered into continuous light-toned layers named the Murray Formation marking the base of Mt. Sharp [1] . This study focuses on the Chemical Index of Alteration (CIA) within the Murray Formation.

**Stratigraphy:** The Murray formation was divided into four areas from their facies [2]. The base of the Murray was analyzed by ChemCam at the location named Pahrump Hills (named Murray-PH hereafter) and is composed of various facies including laminated mudstones and fine- to coarse-grained sandstones [1]. From there, the Murray formation includes two areas at similar elevation separated by the Naukluft plateau. Referred as Murray-HV (for Hartmann's Valley) hereafter, this second area of Murray consists of silt to very fine-sand [2]. The third area is named Murray Buttes and is composed of more regular laminated mudstones. The fourth area, informally named the Upper Murray, displays more heterolithic mudstones and sandstones [1]. The facies is interpreted as having been deposited in lacustrine and lacustrine-margin environments [1,2] with evidence in the form of desiccation cracks to indicate at least partial drying out [3].

**Method:** ChemCam determines the chemistry of rocks over series of points with diameters close to the laser beam, ca. 0.3-0.5 mm. Bulk chemistry for each target can be established only by averaging several points, especially for coarse-grained targets that display strong point-to-point variations. Each target is assigned a bulk composition that is the result of the average of >5 points. Although 5 points are not sufficient for good statistics on coarse-grained rocks, mudstones and fine-grained sandstones have grain sizes smaller than the laser beam ensuring good statistics. In addition, all points corresponding to obvious diagenetic features such as light-toned veins [4, 5] are removed to obtain a composition devoid of obvious post-depositional modifications.

Indications of alteration from chemistry can be evaluated using various indexes such as the Chemical Index of Alteration (CIA), which is defined as $CIA=100*Al_2O_3/(Al_2O_3+CaO^*+Na_2O+K_2O)$ (molar). The CIA index starts to reflect the influence of chemical weathering when CIA>50 for felsic rocks, and 40-45 for mafic rocks [8]. CaO* is the CaO abundance limited to silicate minerals. While carbonates have never been observed at Gale, apatite or anhydrite could be significant contributors to the total CaO. As we have systematically avoided points with evidence of Ca-sulfates to limit the effect of this ubiquitous diagenetic episode, the calculation of the CIA becomes closer to the actual CIA*, although it still remains a lower bound.

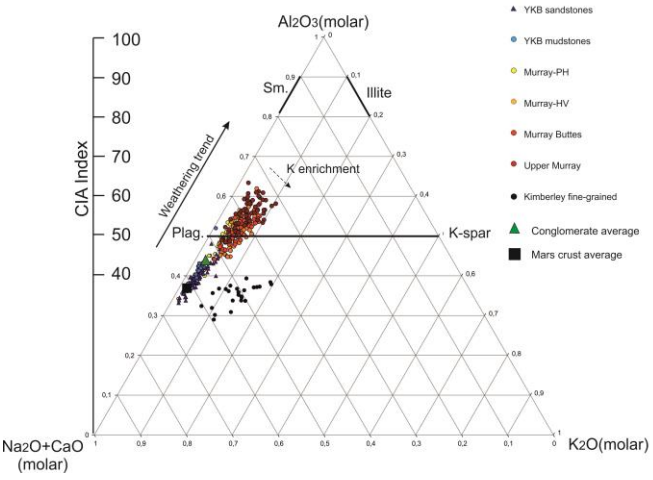


**Figure 1**: A-CN-K ternary diagrams (top) Diagram with total CaO reported (lower bound of CIA). (bottom) Similar diagram with an upper bound of CIA.

**Results:** The CIA index has been below 50 for all aqueous sediments studied before Pahrump Hills, including the Sheepbed mudstones where phyllosilicates were detected [6]. Starting at Pahrump Hills, and then

through the entire Murray Formation so far, values >50 are frequent, especially in the Murray Buttes and Upper Murray for which the CIA index reaches 60 (Figures 1 and 2, red and dark red), a value usually suggesting significant weathering [7]. The A-CN-K ternary diagram (Figure 1) shows that the two upper areas plot above the plagioclase/K-spar line that bound any mixing of primary silicate minerals. This diagram therefore shows that no mixing of primary minerals is able to explain the high CIA observed here linking to open system weathering. This observation may be related to the presence of phyllosilicates at the 20-25% level in the Murray formation at the three drill sites analyzed at Murray Buttes and Upper Murray [8].

Chemical variations along the stratigraphy show that the increase in CIA is correlated with a decrease in CaO abundance, which becomes <2% in many targets or Upper Murray outcrops. This negative correlation is not found for $Na_2O$ or $K_2O$. Leaching of calcium is a reasonable explanation for the low CaO abundances and high CIA from alteration of Ca-pyroxene and/or plagioclase. While both minerals were present in many rocks analyzed so far, CheMin analyses on recent Murray rocks show only low amounts of mafic crystalline phases (<5%) [8].

**Interpretations**:

The origin of the alteration identified from high CIA is not always obvious to determine, with three main candidates possible: weathering at the source, weathering during deposition, or alteration by diagenesis. The drift from the CN-A join towards higher K abundance is usually due to the potassium metasomatism in association with the formation of illite (Figure 1). This trend cannot explain the high CIA and corresponding alteration. Indeed, higher potassium tends to decrease the CIA toward lower values, not increase it. The calculation of the CIA on terrestrial rocks is usually corrected from effects of potassium [10]. The presence of potassium feldspars has also a similar effect: for instance, potassium feldspars were observed at Kimberley [11], but Kimberley sedimentary rocks plot far beneath the alteration lines as a distinct trend (black dots, Figure 1). Diagenesis cannot explain the high CIA, but the observed trend suggests that diagenetic effects were able to start potassium metasomatism.

Numerous terrestrial studies have shown the link between climate and variations in CIA values. Conditions producing a CIA of 60 vary from semi-arid to temperate humid conditions, but a cold and dry climate is not able to generate such alteration indices, as shown from studies in Arctic [12]. Previous results from the Curiosity mission indicated the presence of substantial fluvial and lacustrine sedimentation, in what appeared to be a relatively cold and dry location according to geochemical markers, but lacking obvious glacial/periglacial landforms [1]. The finding of significant weathering from chemical variations fills a gap in this history, showing that the lacustrine activity was coupled, at least for some time during its existence, with substantial open-system weathering indicative of more temperate surface conditions.

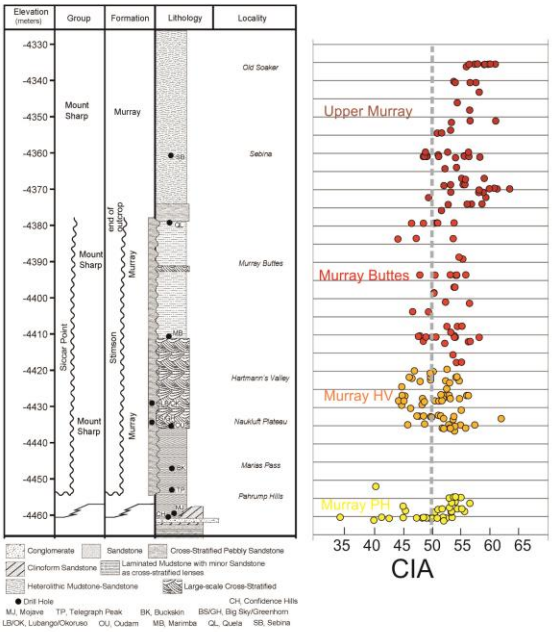


**Figure 2:** (Left) Stratigraphic section of the Murray formation (from [2]), (Right) Corresponding plot of CIA for all targets of the four areas of the Murray formation considered.

**References:** [1] Grotzinger et al. (2015), *Science*, 350, 6257. [2] Fedo et al. (2017) LPSC abstract #XXXX. [3] Stein et al., (2017) LPSC abstract #XXXX [4] Nachon et al. (2014) *JGR-Planets*, *119*, 1991-2016. [5] Nachon et al. (2017) *Icarus*, 2814, 121-136. [6] McLennan et al. (2014) *Science*, 343, 6169. [7] Nesbitt and Young (1982) *Nature*, 299, 715-717. [8] Bristow et al. (2017) LPSC abstract XXXX [9] Newsom et al. (2017) LPSC. [10] Fedo et al., (1995) Geology, 23, 921-924. [11] Le Deit et al (2016) *JGR-Planets*, 121, 784-804. [12] Nesbitt and Young, (1996), Sedimentary Geology, 43, 341.

**THE SEASONAL VARIABILITY OF ATMOSPHERIC DEUTERIUM AT MARS: IMPLICATIONS FOR WATER LOSS INTO SPACE.** M. Mayyasi[1], J. Clarke[1], D. Bhattacharyya[1], J. Deighan[2], S. Jain[2], M. Chaffin[2], N. Schneider[2] and B. Jakosky[2], [1]Boston University, Boston, MA (majdm@bu.edu), [2]LASP, University of Colorado, Boulder, CO.

## Introduction

Mars is thought to have held a large body of liquid water that escaped over the planet's history. At present, the martian water reservoir is found in the form of subsurface ice, surface ice, ice in atmospheric clouds, and atmospheric vapor. The water cycle at Mars includes: sublimation of polar ice, atmospheric mixing and circulation, condensation, photo-dissociation by sunlight, chemical reactions, transport to higher altitudes, and ultimately, loss into outer space. By quantifying the current escape rate, and understanding the variability of this escape with time, we are able to estimate Mars' ancient water reservoirs and to explain how these reservoirs were lost. The relative abundance of atomic deuterium to hydrogen (the D/H ratio) has been widely used to quantify the water escape rate by analyzing the preferential escape of the lighter species with respect to its heavier isotope.

The D/H ratio in water molecules at the surface of Mars has previously been measured [1, 2]. Ground- and space-based infrared spectra have been used to obtain an HDO/$H_2O$ ratio in the lower atmosphere (surface to 100 km) [3, 4, 5, 6, 7]. Space-based UV spectra are used to determine the atomic D/H ratio in the upper atmosphere [8, 9, 10]. The resulting ratios are different due to the various altitude-dependent chemical and physical interactions that water isotopologues undergo throughout the hydrological cycle. Furthermore, measurements of the Martian D/H ratio at the same altitude region have been found to vary by a factor of ~3 on diverse timescales due to seasonal, and topological factors [11, 12, 13, 14, 15, 16]. Understanding the temporal variability of deuterium and hydrogen UV brightness will be useful for tracking the variation in the properties and dynamical processes controlling both emissions in the upper atmosphere of Mars where water components can escape the planet.

The Mars Atmosphere and Volatile Evolution (MAVEN) orbiter includes a remote-sensing Imaging Ultraviolet Spectrograph (IUVS) instrument that can operate in echelle mode [17, 18]. IUVS is capable of resolving the separate contributions of D and H Lyman-α emissions at 121.534 nm and 121.567 nm, respectively. Data observed by the MAVEN IUVS echelle channel are used to determine the brightness of deuterium as observed at the limb of Mars. The D emission is found to be highly variable, with a peak in brightness just after southern summer solstice. The trends in D brightness are examined against extrinsic as well as intrinsic sources. It is found that the fluctuations in deuterium brightness in the upper atmosphere of Mars (up to 400 km), corrected for periodic solar variations, vary on timescales that are similar to those of water vapor fluctuations lower in the atmosphere (20-80 km). The observed variability in deuterium may be attributed to seasonal factors such as regional dust storm activity and subsequent circulation in the lower to middle atmosphere that introduce D and H into the thermosphere (Figure 1).

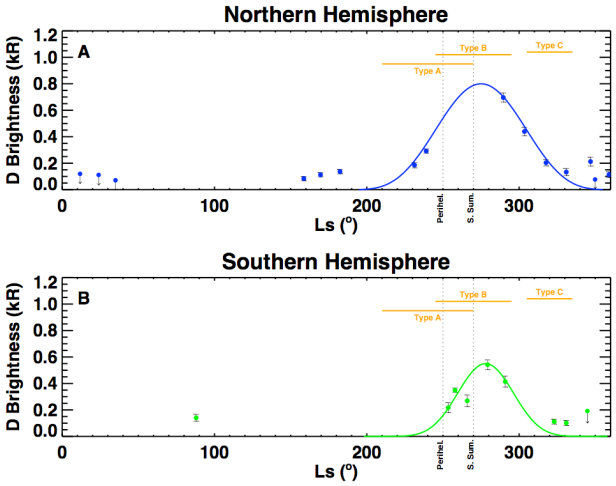


**Figure 1:** *The brightness of deuterium Lyman-α observed at the limb, over 15 Mars months, at different latitude regions. The observations are averaged to remove the effects of solar rotation, and corrected for solar activity variations. The line of sight tangent point latitude was used to separate observations made over the (A) Northern Hemisphere (blue circles), and (B) Southern Hemisphere (green circles). Uncertainties are shown as vertical bars. Brightness values within three-sigma of the noise level are considered upper limits and their uncertainties are denoted by downward pointing arrows. The times of perihelion and southern summer solstice are shown as dotted vertical lines at 250° and 270° subsolar longitude ($L_s$), respectively. Solid curves in Panels A (blue) and B (green) are best fits to the observations in each latitude region. Markers for regional storms of three types are shown for reference (horizontal orange lines).*

The hydrogen content of the upper atmosphere is now known to also be highly variable [10, 19, 20]. The variation in deuterium content, shown here, reflects the dynamical nature of the upper atmosphere of Mars. The observed variations in D Lyman-α emission brightness are due to a combination of variations in the temperature and density of the atmospheric deuterium atoms. Atmospheric temperatures are constrained using the empirically determined values in the Mars Global Ionosphere-Thermosphere Model (MGITM) [21]. Simulations using a radiative transfer code are then used to model the abundances of deuterium at the observed altitudes.

Determining the drivers of seasonal variability of the deuterium content of the upper atmosphere will complement the understanding of what drives the variability of the escape rate of water from Mars. Using data analysis and models, the optically thin D and optically thick H Lyman-α brightness measurements can be simulated to determine abundances of D and H (the quantities needed to obtain the D/H ratio) in the upper atmosphere of Mars [22, 23].

**References**

[1] Webster C. et al. (2013), *Science*, 341, 260-263
[2] Mahaffy P. et al. (2015), *Science*, 347, 6220, 412-414
[3] Owen, T., J. P. Maillard, C. de Bergh, and B. Lutz (1988), *Science*, 240,1767–1770
[4] Bertaux, J. L., and F. Montmessin (2001), *J. Geophys. Res.*, 106(E12), 32,879–32,994,
[5] Novak, R., M. Mumma and G. Villanueva (2011), *Planet. Space Sci.*, 59, 163–168
[6] Villanueva, G. et al (2012), *J. Quant. Spec. Rad. Tran.*; 113, 202-220
[7] Krasnopolsky, V. A. (2015), *Icarus*, 257, 377–386.
[8] Clarke, J. T. et al., (2006), *Bull. Amer. Astr. Soc.*, 38, 600.
[9] Clarke, J. T., et al. (2017), , *J. Geophys. Res. Space Physics*, 122.
[10] Clarke, J. T. et al. (2014), *Geophys. Res. Lett.*, 41, 8013–8020..
[11] Montmessin, F., T. Fouchet, and F. Forget (2005), *J. Geophys. Res.*, 110, E03006.
[12] Aoki, S. et al. (2015), *Icarus*, 260, 7-22
[13] Villanueva, G. et al. (2015), *Science*, 348(6231), 218–221.
[14] Trokhimovskiy, A. et al (2015), *Icarus*, 251, p. 50 – 64
[15] Fedorova, A. et al. (2017), *Icarus*, *under revie*
[16] Mayyasi et al., 2017, *submitted to JGR*?
[17] McClintock, W., et al. (2015), *Space Sci. Rev.*
[18] Jakosky, B. (2015), *Science*, 360, 6261.
[19] Bhattacharyya, D., J. T. Clarke, J.-L. Bertaux, J.-Y. Chaufray, and M. Mayyasi (2015), *Geophys. Res. Lett.*, 42
[20] Bhattacharyya, D. et al. (2017), *submitted to JGR*
[21] Bougher, S. W. et al. (2015), *J. Geo- phys. Res. Planets*, *120*, 311–342.
[22] Chaufray, J. Y., J. L. Bertaux, F. LeBlanc, E. Quemerais (2008), *Icarus, 195,* p. 598-613
[23] Chaffin, M. et al. (2014), *Geophys. Res. Lett.*, *41.*

**JAROSITE AND ALUNITE CEMENTS IN JURRASIC SANDSTONES OF UTAH AND NEVADA, A POTENTIAL ANALOG FOR STRATIFIED SULFATE DEPOSITS ON EARLY MARS.** T. M. McCollom[1] and S. L. Potter-McIntyre[2], [1]LASP, University of Colorado, Boulder (mccollom@lasp.colorado.edu), [2]Department of Geology, Southern Illinois University.

**Introduction:** Sulfate minerals of the alunite-jarosite family have been identified in stratified deposits at numerous locations across Mars, including two of the rover landing sites [e.g., 1-4]. Because these minerals precipitate from acidic aqueous solutions, there has been considerable interest in studying their occurrence in martian settings as indicators of depositional and diagenetic conditions on early Mars. In many martian deposits, the occurrence on minerals from the alunite-jarosite family within stratified formations suggests that the minerals may have been deposited during emplacement of the strata as sediments, or during diagenetic alteration of the strata. However, occurrences of jarosite and alunite in sedimentary settings have received only limited study as martian analogs, with most attention focused on weathering of sulfide minerals or volcanic hydrothermal environments [e.g., 5-7].

In southern Utah, Jurassic sandstones at Mollies Nipple (MN) contain abundant jarosite and alunite cements [8,9] whose depositional characteristics and sedimentary setting may be analogous to stratified deposits on Mars. Similar occurrences are also found in sandstone of the same age in western Nevada [10]. We are currently investigating the formation and persistence of these deposits in an effort to provide insight into occurrences of jarosite and alunite on Mars.

**Figure 1.** Overview of Mollies Nipple. Red line delineates the approximate base of caprocks cemented by jarosite or alunite plus kaolinite. Jarosite- and alunite-bearing float rocks eroded from the caprock cover much of the lower slopes of the butte. White exposed areas are bleached Navajo Sandstone.

**Geologic setting:** Mollies Nipple is a prominent butte located in southern Utah that rises ~200 m above the surrounding landscape (Fig. 1). The base of the butte is composed of eolian Navajo Sandstone, a fine-grained quartz arenite. The butte persists because the sandstone caprock is resistant to erosion owing to the presence of cements dominated by jarosite, alunite, and kaolinite (Fig. 2). Curiously, most of the cemented

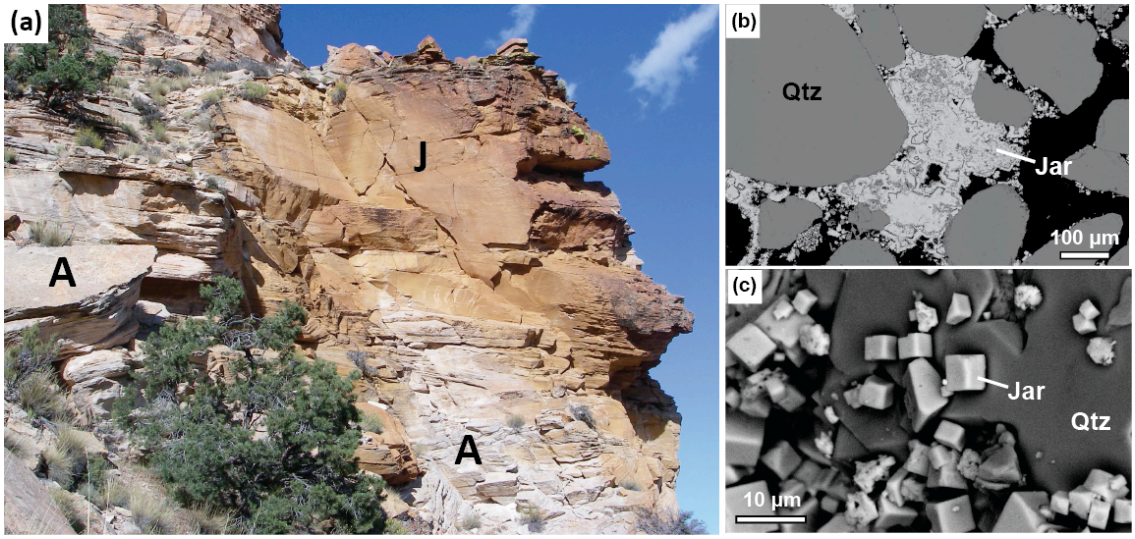


**Figure 2.** (a) Jarosite- and alunite/kaolinite-cemented sandstones near the top of Mollies Nipple. Yellow-toned rocks labeled "J" have cement dominated by jarosite while the white-toned rocks labeled "A" have cements dominated by alunite plus kaolinite. (b,c) Back-scattered electron images of jarosite-cemented sandstone. Bright, psuedocubic crystals are jarosite (Jar). Qtz = quartz.

rocks contain either jarosite or alunite plus kaolinite, but not both (Fig. 2a). The sulfates occur as pseudocubic crystals up to 20 μm in diameter (Fig. 2b,c). Although the cements constitute only a few percent of the sandstone, the visible-near infrared spectra of the rocks are dominated by jarosite or alunite plus kaolinite since the quartz matrix has no spectral signal [5,6].

**Origin of the jarosite/alunite:** The origin of the sulfate-rich cements is the subject of ongoing investigation. Preliminary analysis indicates that the sandstones are matrix-supported, indicating the cements formed after original deposition of the sediments. Two of the most likely scenarios for precipitation of the sulfate-rich cements are illustrated in Fig. 3. Although the Navajo Sandstone is an eolian erg deposit, the overlying Carmel and Page Formations were deposited on the margins of an inland sea that formed to the west of MN after the Navajo Sandstone was emplaced. One possibility, therefore, is that the sulfate cements precipitated during early diagenesis in an interdune, sabhka-like environment on the margin of the inland sea, contemporaneous with deposition of the overlying Carmel/Page Formations (left panel, Fig. 3). Another possibility is that the sulfates are a burial diagenetic feature formed by interaction of migrating acidic, sulfate-rich groundwaters with K-feldspar and hematite present in the original sandstone (right panel, Fig. 3). We are currently testing these and other alternatives through fieldwork and geochemical models.

If the first scenario is correct, it would imply that the Fe- and Al-sulfates precipitated in the middle Jurassic (~170 Ma), while the second scenario would allow a younger age that would most likely postdate the Laramide orogeny (~50Ma) but is older than recent uplift and exposure (>10Ma). In either case, the sulfates have likely persisted in the sandstones for many millions of years.

**Implications for Mars:** Because jarosite is found to dissolve fairly rapidly in laboratory experiments, it has been suggested that sites where it occurs on Mars were not in contact with neutral aqueous fluids for more than a few thousand years after the jarosite formed [11-13]. Yet, the jarosite at MN has persisted in highly porous sandstones with an active aquifer for for probably several million years or longer. The persistence of jarosite and alunite in these rocks indicates that they can persist for much longer periods than indicated by laboratory dissolution experiments.

We anticipate that continued study of the jarosite/alunite cements at MN and resolution of their origin will provide additional insights that will be useful for assessing depositional environments and persistence of these minerals in stratified deposits on Mars.

**References:** [1] Klingelhöfer G. et al. (2004) *Science* **306**, 1740. [2] Thollot P. et al. (2012) *JGR* **117**, E00J06. [3] Ehlmann B. et al. (2016) *Am. Mineral.* **101**, 1527. [4] Johnson J.R. et al. (2016) *Am. Mineral.* **101**, 1501. [5] Morris R.V. et al. (1996) in *Mineral Spectroscopy: A Tribute to Roger G. Burns*, pp. 327-336. [6] Fernández-Remolar D. C., et al. (2010) *EPSL* **240**, 149. [7] Papike J.J., et al. (2006) *Geochimica Cosmochimica Acta,* **70**, 1309. [8] Bell J. H. et al. (2010) *Remote Sens. Environ.* **114**, 2259. [9] Bell J. H. and Bowen B. B. (2014) *Geofluids* **14**, 251. [10] Eichhubl P. et al. (2004) *GSA Bull.* **116**, 1120. [11] Elwood Madden M. E. et al. (2004) *Nature* **431**, 821. [12] Elwood Madden M. E. et al. (2009) *Geology* **37**, 635. [13] Miller J. L. et al. (2016) *Geochim. Cosmochim. Acta* **172**, 93.

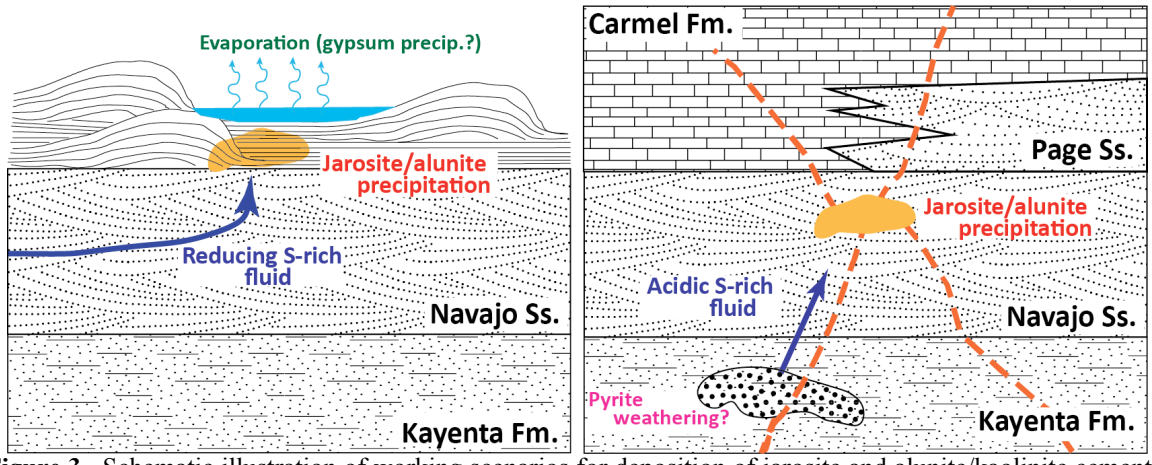


**Figure 3.** Schematic illustration of working scenarios for deposition of jarosite and alunite/kaolinite cements at Mollies Nipple. (left) Deposition as shallow pore-filling cements from upwardly migrating reducing fluids beneath sabkha environment on margin of inland seaway. (right) Deposition from acidic, sulfur-rich fluids migrating along fractures (dashed organic lines) in deeper subsurface.

**IRON OXIDATION BY CHLORATE: IMPLICATIONS FOR AKAGANÉITE AND JAROSITE FORMATION ON MARS.** K. Mitra and J. G. Catalano, Department of Earth & Planetary Sciences, Washington University, Saint Louis, MO 63130 USA (k.mitra@wustl.edu)

**Introduction:** Perchlorate and chlorate are the most common oxychlorine species on Mars [1]. These oxidants are produced continuously on the Martian surface and often have concentrations as high as 0.5 to 1.0 wt.% in soil [2]. Oxychlorine species have wide implications for both past and present Martian environments, affecting preservation of organic compounds, forming metastable brines and possibly flowing water in recurring slope linea, contributing to the oxidizing nature of the regolith, and serving as a potential electron donor, as occurs in microbial metabolisms on Earth [3, 4]. One role of oxychlorine species on Mars that has been largely overlooked to date is their potential to serve as oxidants of reduced iron. While perchlorate is chemically unreactive with $Fe^{2+}$ despite the favorable thermodynamics of such reactions, chlorate is kinetically more reactive [5] and thus may be a major oxidant on the surface of Mars. However, the rates and mineral products of Fe(II) oxidation by these oxychlorine species is currently unclear. The kinetics of oxidation of dissolved Fe(II) by perchlorate and chlorate at pH 3, 5 and 7 have been studied in Mars-relevant fluids. The mineralogy of the solids generated during oxidation was then determined for different initial fluid compositions.

**Methods:**

*Kinetic Experiments:* 40 ml solutions were prepared that contained 10 mM $FeCl_2$ along with equimolar $NaClO_3$ or $NaClO_4$. All studies were conducted in a 0.1M $MgCl_2$ or $MgSO_4$ electrolyte to buffer the ionic strength and to provide anions with different ability to complex dissolved iron. An oxychlorine-free control experiment was set up with 1 mM $FeCl_2$ in 0.1 M $MgCl_2$ with no chlorate or perchlorate. All reactions were carried out in an anaerobic chamber ($N_2$ = 97%, $H_2$ = 3%) with <1 ppmv $O_2$ concentration. The experimental solutions were prepared in 50 mL centrifuge tubes wrapped in aluminum foil to prevent photochemical $Fe^{+2}$ oxidation. These were continuously mixed on an end-over-end rotator. Experiments were conducted with initial pH values of 3, 5 and 7 in both chloride- and sulfate-rich fluids. The pH was allowed to drift with reaction. The pH and $Fe^{+2}$ concentration were measured at regular time intervals, the latter via spectrophotometry following complexation by ferrozine [6].

*Mineral Precipitation Studies:* Select kinetic experiments were repeated with a solution volume of 150 mL to generate larger amounts of mineral solids needed for characterization. Additional experiments were also conducted using higher concentrations of dissolved Fe(II) and chlorate (100 mM each) to explore the effect of concentration on the type(s) of mineral precipitated; lower initial pH was also investigated. The solutions were stored in polypropylene bottles wrapped with aluminum foil and continuously stirred for approximately 4 weeks. The resultant solution was allowed to settle and the fluid separated from the solids via either centrifugation or filtration using 0.22 µm pore size MCE membrane. The resulting solid samples were dried in the anaerobic chamber in a vacuum desiccator for 3-4 days. The mineralogy of the dried solids were then characterized using powder X-ray diffraction (XRD), extended X-ray absorption fine structure (EXAFS) spectroscopy, and visible and near infrared (VNIR) spectroscopy.

**Results:**

*Kinetics of $Fe^{2+}$ Oxidation:* Perchlorate was found to induce negligible oxidation of $Fe^{2+}$ in $MgSO_4$ solution (Fig. 1). In contrast, chlorate caused near-complete $Fe^{2+}$ oxidation within 30 days for all fluid compositions examined. The rate of oxidation differed for the two fluid types: for sulfate, pH 5 > pH 3 > pH 7, for sulfate, pH 7 > pH 3 > pH 5. No oxidation was detected in the oxychlorine-free control experiment. $Fe^{2+}$ oxidation was coupled with a drop in pH for all chlorate experiments, while little pH changes were observed for the oxychlorine-free control and perchlorate studies.

*Mineral Products:* The mineralogy of the solids produced during $Fe^{2+}$ oxidation by chlorate varied with

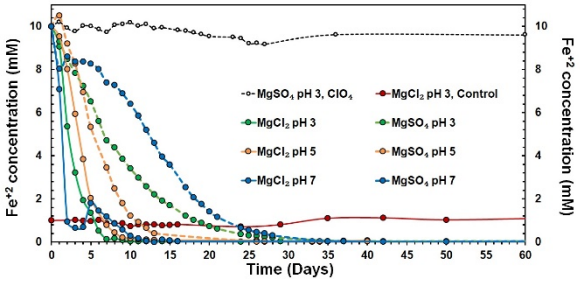


*Figure 1:* Fe(II) concentrations as function of reaction time for different initial fluid compositions. Solid lines represent chloride fluids and dashed lines sulfate fluids.

fluid composition. At pH 7, lepidocrocite [γ-FeOOH] formed at low (10 mM) $Fe^{+2}$ concentration in both chloride and sulfate fluids along with minor magnetite and goethite, respectively. At higher $Fe^{+2}$ concentration

(i.e., 100 mM) at all pH values akaganéite [β-FeO(OH,Cl)] formed in chloride fluids and mixed natro- and hydronium-jarosite [$XFe_3(OH)_6(SO_4)_2$, X= $Na^+$ or $H_3O^+$] formed in sulfate fluids. EXAFS and VNIR spectroscopy confirm the XRD results.

**Discussion:**

*Lack of $Fe^{2+}$ Oxidation by Perchlorate:* These studies show that perchlorate does not cause detectable $Fe^{2+}$ oxidation in both chloride and sulfate fluids, in agreement with prior work [5]. The results support the consensus that perchlorate is a kinetically inert oxidant at temperatures relevant to the surfaces of Earth and Mars despite such reactions being thermodynamically favorable. Perchlorate thus likely induces little to no oxidation of iron on the surface of Mars.

*Extensive $Fe^{2+}$ Oxidation by Chlorate:* In contrast, all experiments that contained chlorate displayed a substantial decline in dissolved $Fe^{+2}$ with time and the formation of ferric iron-bearing solids. The rate of reaction depended on the initial pH and the dominant anion in the solution, i.e., chloride or sulfate. The rate of $Fe^{2+}$ oxidation by chlorate is faster in chloride fluids than in those containing sulfate because of substantially

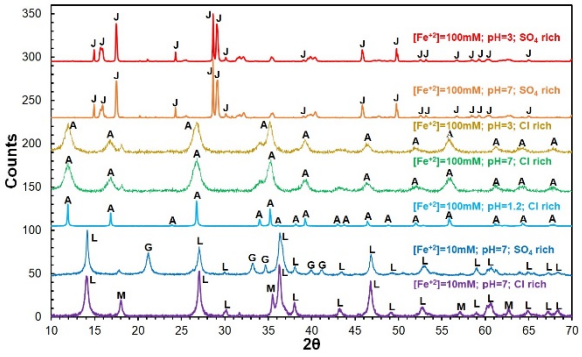


*Figure 2:* XRD patterns of solids produced during $Fe^{2+}$ oxidation by chlorate. Diagnostic peaks are marked as follows: J=Jarosite, A=Akaganéite, L=Lepidocrocite, G=Goethite, M=Magnetite

stronger complexation of $Fe^{2+}$ by $SO_4^{2-}$. The complex pH-dependence of the observed oxidation rates likely reflect the oxidation mechanisms, which are known to vary with pH [7], the differing aqueous complexation of $Fe^{3+}$ by chloride and sulfate, and the mineral products that form. The increase in oxidation rate in many systems after an initial period of slow oxidation appears to be an autocatalytic phenomenon. The increase in acidity associated with hydrolysis and precipitation of $Fe^{3+}$ produced during oxidation acts to increase the kinetics. This suggests that oxidation of $Fe^{2+}$ by chlorate on Mars may drive local microenvironments into the stability fields of minerals associated with highly acidic condition even when the initial systems began at, and the broader mineral assemblages, indicate circumneutral pH.

*Mineral Products of Iron Oxidation by Chlorate:* An array of Fe(III) minerals form when chlorate oxidizes dissolved Fe(II). Dilute Fe(II) solutions lack the concentration needed to produce highly acidic fluids and produce lepidocrocite with minor additional goethite or magnetite, depending on the anion present. The mineralogy of the systems differs when more concentrated solutions are used, even when the initial pH is 7. In chloride fluids, akaganéite forms for initial pH values ranging from 7 to 1.2. The most acidic initial solution (pH 1.2) produced highly crystalline akaganéite but in low overall abundance because of the high solubility of $Fe^{3+}$ at very low pH. At higher initial pH values (3 to 7), the XRD patterns show that the akaganéite produced is nanocrystalline in nature. Jarosite formed in concentrated solutions containing sulfate. This occurred as a mixture of natro- and hydronium-jarosite, with the sodium contributed by the initial $NaClO_3$ salt; $Mg(ClO_3)_2$ is not commercially available. Hydronium jarosite likely would be the sole phase formed if sodium was absent. Similar amounts of jarosite and akaganéite formed at pH 7 and 3, but in the presence of sulfate no solids were produced at pH 1.2, with $Fe^{3+}$ staying in solution due to the acidity and complexation by sulfate. The formation of akaganéite and jarosite by chlorate indicates the potential importance of this oxychlorine species as an active oxidant on Mars.

**Conclusion:** Both akaganéite and jarosite are rare in natural terrestrial settings but have been reported at various locations on Mars [8, 9]. Despite being a minor component in the Martian regolith, these minerals are key indicators phases. Both require acidic and highly saline conditions to form [10]. Oxidation of dissolved Fe(II) by concentrated chlorate fluids, such as brines, may represent key formation mechanisms for both akaganéite and jarosite on Mars, including in Gale Crater. The potential formation of oxychlorine species on early Mars needs to be further evaluated as these species may have provided substantial additional oxidizing capacity as the planet evolved.

**References:** [1] Sutter et al. (2016) *Int. J. Astrobiol., 16,* 203-217. [2] Hecht et al. (2009) *Science, 325*, 64-67. [3] Ojha et al. (2015) *Nat. Geosci., 8,* 829-832. [4] Kounaves et al. (2010) *Env. Sci. Tech., 44,* 2360-2364. [5] Urbansky et al. (1998). *Bioremediation J., 2***,** 81-95. [6] Viollier et al. (2000). *Appl. Geochem., 15*, 785–790. [7] Madlo et al. (1982) *Collect. Czech. Chem. Comm., 46*, 1069-1077. [8] Bhattacharya et al. (2016) *JGR, 121,* 402-411. [9] Carter et al. (2015) *Icarus, 253,* 296-310. [10] Papike et al. (2006) *Geochim. Cosmochim. Acta, 70,* 1309-1321.

**FORMATION OF OCEAN SEDIMENTARY ROCKS AS ACTVE PLANETS AND LIFE-LIKE SYSTEMS.**

Y. Miura, Yamaguchi University (Chuou 4123, Yamaguchi, Yamaguchi, 753-0074, Japan; yasmiura50@gmail.com)

**Introduction:** Active planets and mini-planet-type life are formed under significant global ocean water system between atmosphere and rock systems, where air system is easily discarded for circulated active process but solid system of ocean sedimentary rocks are remained as evidences of active process of planetary system and mini-planet-like system with life-like system which are remained as solidified and replaced fossil rocks observed on water-Earth [1-5]. The present paper is to elucidate wide ocean-water sediments of carbonate rocks as significant solid evidences of related sea-sediments on active planets (including Mars) and life-like system formed on water-planets based on remained database of water-planet Earth [1-5].

**Primordial surface of ocean water planet Earth:** Figure 1 shows estimated ocean on old Earth (ca.650Ma) published the Paleomap [6], where higher lands are very small on global Earth with major ocean water system. This means that present continents (ca.29.2 volume %) contained remnants of ocean sedimentary rocks of carbonates (limestone etc.) and present ocean floor on active planet Earth [5].

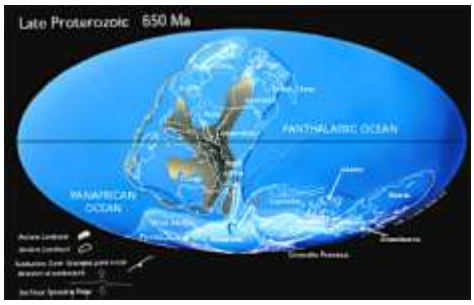


Fig.1. Estimated old Earth surface (Late Proterozoic, ca.650Ma) suggested significant global ocean water surface on active Earth and evolution for life activity [6].

**Driving force process on ocean impact:** Ocean impact signatures on global water-planet are considered to be 1) discarded sea-bottom impact-blocks near oceanic islands moved ocean-floors widely, 2) buried impact-structure broken partly by moved crust plates locally, and 3) elemental enrichments of Earth and meteoritic metals formed by impact mixing as ocean-related indicators which are obtained in recent formed Japanese islands and old continental crust supplied by ocean plates [4-5]. This shock type is based on solid-liquid-air process during short fluid reaction followed quenching, which is similar with magmatic melting process for elemental and mineral assemblage largely at volcanic crusts.

**Laboratory experiment at sedimentary rocks in wet liquid condition:** Microscopic elements-bearing quenched grains from sea-sedimentary rock used by the laser beam in our laboratory. The volatile (carbon)-bearing quenched grains which is assumed to be ocean impact indicators can be obtained in possible ocean-impacts on water-Earth [4-5]

**Water produced experiment from meteorites:** Author has produced fluid-water from dry meteorite in our laboratory. Dry rocks of waterless planets and asteroids can be applied the shocked rocks of dry rocks on Earth, where minor evaporated volatiles are remained partly to form crystalline minerals globally and largely. Water effects on mixed extraterrestrial and terrestrials rocks are clearly different with local formation and global ocean water, respectively. Fluid-contribution of extraterrestrial surfaces are clearly different with dry terrestrial rocks with well crystallized minerals. This indicates that existence of global water on extraterrestrial bodies can be explained not by simple water elements, but by wide ocean sedimentary rocks on unknown bodies in next explorations [4-5].

**Indicator of Earth-like planets and exo-life observation:** Ocean-water sedimentary rocks are only direct formation of global ocean-water on planet, which are considered to be strong indicator of water Earth-like planet and possible exo-life on extraterrestrial planets for future remote-sensing observation from our planets of the Solar System [4-5].

**Summary:** The present study is summarized as follows: 1) Wet shocked rocks of Earth's ocean surface are discarded largely from original shocked rocks and structures globally, but enriched elements during surface melting with the continental drift with ocean-sedimentary rocks and carbon-bearing grains, which is considered to be strong indicator of global ocean water by asteroids. 2) Ocean-sedimentary rocks are only direct formation of global ocean water on planet as strong indicator of water Earth-like planet and possible exo-life on extraterrestrial planets (including Mars).

**References:** [1] French B. (1998): Traces of catastrophe (LPI), 120 pp. [2] Miura Y. et al.(1999): J. Materials Proc. Tech., 85, 192-193.. [3] Miura Y. et al. (2000): LPS XXXI, abstract#2096. [4] Miura Y. et al. (2017): Planet. Science Vision 2050Workshop 2017, #8101. [5] Miura Y. (2017): SPS-2017 (Sendai), No. 22. pp.4 (in press). [6] Paleomap Project (2017): Texas 76012 USA. http://www.scotese.com/earth.htm.

**WATER IN THE MARTIAN CRUST LOCKED IN HYDRATED MINERALS: A SIGNIFICANT PLANETARY RESERVOIR OF WATER** J.F. Mustard[1], [1]Dept. of Earth, Environmental and Planetary Sciences, Box 1846, Brown University, Providence, RI 02912 (Contact: John_Mustard@brown.edu)

**Introduction and Science Objectives:** Where and in what form water currently resides in reservoirs on Mars is important for understanding modern processes and the evolution of water on the planet. Estimates of water stored in reservoirs on Mars are expressed as the equivalent thickness of water spread over the planet in meters (Global Equivalent Layer (GEL)). Geological and geomorphological estimates for the total amount of water that may have been present on or passed over the Martian surface, or that resides in the crust range from a minimum of 600 m to upwards of 3000 m GEL [1, 2] while accretion models suggest a total water inventory of 600-2600 m GEL[3,4]. While these estimates of the GEL of water throughout Martian history are intriguing, in many ways quantitative observations that provide constraints on these estimates are lacking.

A recent synthesis of current reservoirs and an analysis of how those reservoirs may have changed going back in Mars geologic time provided an excellent assessment of water in the form of liquid, ice, and estimates of additions through volcanic processes and loses through escape and other mechanisms [1]. [5] also provide an updated assessment of GEL of water based on geomorphic and radar sounding data. The starting point for analysis was based on an inventory of present water that existed in six reservoirs: (1) surface ice such as the exposed polar deposits; (2) shallow sequestered ice buried beneath regolith cover; (3) the global permafrost layer [6, 7] (4) hypothesized groundwater beneath the base of the cryosphere [8], (5) water vapor, and (6) water sequestered in hydrated mineral phases or consumed through alteration reactions and radiolysis [9, 10, 11].

Currently defined water reservoirs are insufficient to account for the estimated water inventory for the planet over its history based on geologic estimates and and planetary evolution models. Water has likely been lost through processes such as impact erosion or solar wind sputtering [8] with substantial but not defined amounts of water proposed via the MAVEN mission [12]. Observations of globally distributed hydrated minerals (e.g., clays and sulfates) [9, 15] now make it possible to derive a first order estimate of the amount of water that may be stored in the martian crust in the form of hydrous minerals.

My approach is to estimate the water content of surface soils, characterize the distribution of hydrated minerals across the surface and with depth, and estimate the abundance of hydrated minerals. I then calculate the global average water content of martian rocks and soils to arrive at an estimate of the total amount of water sequestered in hydrated phases.

**Water in surface soils:** Every near infrared spectrum of Mars acquired since the first telescopic IR observations [14] shows clear evidence for the presence of water in a key absorption near 3 μm due to fundamental OH and $H_2O$ stretching vibrations. [19] showed that the absolute water content of many hydrous phases can be estimated within ±1 wt. % using this absorption. The strength of this absorption was mapped across Mars with OMEGA data led to estimates of 2-4 wt. % $H_20$ at equatorial and mid-latitudes [20, 21]. Specific exposures of high concentraitons of hydrous minerals (e.g., Mawrth Vallis and Nili Fossae) were enriched in water by 2-3x this amount. The global estimates from spectroscopy are broadly consistent with the determination of water equivalent hydrogen (WEH) in the upper ~1 m generated from Mars Odyssey Gamma Ray Spectrometer data [6], which show ~1-3% WEH in most equatorial to mid-latitude zones.

**Distribution of aqueous minerals:** The diversity of hydrous minerals that have been positively identified on Mars from orbit encompass phyllosilicates [9, 10], sulfates [20, 21], hydrated silica [22], halides [23] and iron oxy-hydroxides such as goethite [21, 24, 25]. These minerals are found in a variety of depositional environments on Mars.

**Table 1**

| Wt % $H_2O$ | Thickness of Altered Crust | Global Equivalent Layer of Water |
|---|---|---|
| 0.5% | 5 km | 15.5 m |
| | 10 km | 77.5 m |
| | 20 km | 155 m |
| 3% | 5 km | 93 m |
| | 10 km | 465 m |
| | 20 km | 930 m |

Orbital observations show hydrated minerals occur throughout Noachian-aged terrain [26, 12] and also in crustal materials excavated from beneath Hesperian ridges plains in the northern lowlands [11]. Hydrous minerals are rarely observed in Hesperian or younger terrains [e.g. 27, 28, 22]. Notable concentrations of aqueous minerals are observed in the very well exposed terrains in Nili Fossae [29, 30], Mawrth Valles, Meridiani [20] and Valles Marineris [20, 31, 32]. The detection of hydrous minerals in the crust is biased by exposure; dust and other surficial deposits can obscure the spectral signatures of the bedrock. Therefore, the

mapped occurrences of such deposits likely represent a lower limit.

**Depth of Alteration:** To what depth in the crust are hydrated minerals observed? Some of the thickest sections of crust exposed on Mars are the walls of Valles Marineris, and phyllosilicates have been observed in exposures of bedrock at the base of the walls of the canyon [36], up to 8 km below the plateaus. Impact craters also provide a means to explore the deeper crust of Mars and recent analyses show phyllosilicates exposed from depths of at least 7 km and up to 17 km [39]. Together, these observations suggest that at least the upper 10 km of crust contain hydrated minerals.

**Abundance of Aqueous Minerals:** Phyllosilicate abundances of various deposits have been estimated using radiative transfer modeling of OMEGA spectra by [35]. Except for Mawrth Vallis where more than 50% phyllosilicate is estimated, the modal mineralogy is dominated by primary non-altered minerals, with minor fractions of phyllosilicates. ChemMin analyses with the Curiosity Rover show phyllosilicate abundance of 20% with a further 20% amorphous component of uncertain hydration [Vaniman et al., 2014]. Combining estimates of $H_2O$ abundance with maps of aqueous mineral distributions, we conservatively estimate the abundance of hydrated minerals in Noachian crust to range from 1-10% when averaged over all Noachian terrains.

**Translating aqueous mineral abundance to water content:** The water content of phyllosilicate minerals typically averages 12-14% by weight. For the region with the highest phyllosilicate abundance (50% in Mawrth Valles) this would thus result in 7.8-9.1 % water assuming all the non-clay components are anhydrous. The $H_2O$ content of Mawrth Valles region was estimated by [20] to be 6-8%, consistent with the clay abudance estimates of water content. Another method to estimate the water content is from terrestrial analyses of altered crust. Altered oceanic crust that typically contains 10% hydrous minerals exhibits an average of 1-3% water [35].

**Size of the Hydrous Mineral Crust Reservoir:** Based on the presence of hydrated minerals throughout Noachian aged terrains and the depth to which they are observed, I estimate the size of the crustal reservoir for water in hydrous minerals (Table 1). I developed these estimates for two ranges. The lower conservative range is for an average water content 0.5% and the upper range for 3%. I then consider if the aqueous minerals are distributed over 5, 10, and 20 km of the martian crust. The minerals could be distributed over this range as a consequence of where the original hydrous minerals were formed, such as by alteration in the shallow crust [10], or they could have formed at or near the surface and have been redistributed by burial, impact processes, and/or other sedimentary transport processes [15]. These calculations result in GEL of water from a low of <20 m to ≈1 km for the upper range.

When and by what processes the aqueous alteration occurred are significant unknowns about this hydrated mineral water reservoir. Three hypotheses have been proposed: low grade metamorphism in the shallow crust [10], surface weathering and alteration mixed into the crust through impact processes [15] and alteration by supercritical fluids during accretion and formation of the first atmosphere [40, 41]. When and how alteration occurred would have had some effect on the evolution of aqueous activity on the surface and in the shallow subsurface. For example, the model proposed by [40] to explain the transition from a hypothesized warmer and wetter early Mars to a cold and arid Hesperian Mars required loss of water from the surface and near surface reservoirs of on the order of 60 m GEL.

**References:** [1] Carr, M. H., and J. W. Head. GRL 42.3 (2015): 726-732. [2] Baker, V. R. (2001) *Nature, 412*, 228-236. [3] Lunine, et al. (2003) *Icarus, 165*, 1-8. [4] Lammar et al., 2013. [5] Lasue et al. 2012. [6] Feldman, W. C., et al. (2004) *JGR Planets, 109, E09006,*doi: 10.1029/200 3JE002160. [7] Mellon et. al. 2004. [8] Clifford, S. M., et al., (2010), *JGR* , **115**, E07001, doi:10.1029/2009JE003462. [9] Ehlmann BL, Edwards CS. Ann. Rev. of EPS. 2014;42:291-315. [10] Ehlmann, BL et al., Nature, 2011. [11] Tarnas, J. et al., 2017. [12] Jakosky, B. M., et al, (2017). Science, 355(6332) [15] Carter, J., et al. (2013) *JGR 118.4.* [16] Ehlmann, B. L., et al. (2011) *Clays and Clay Min., 59, 4*, 359-377. [18] Sinton W.M. (1967) *Icarus,6***,** 222-228. [19] Milliken, R. E. and Mustard, J. F. (2005) *JGR Planets, 110, E12001*, doi: 10.1029/2005 JE002534. [20] Milliken, R. E. and Mustard, J. F. (2007a) *Icarus, 189, 2*, 574-588. [21] Milliken, R. E., et al. (2007b) *JGR Planets, 112, E08S07*, doi: 10.1029/2006 JE002853. [22] Jouglet, D., et al. (2007) *JGR Planets, 112*. [24] Leshin, L. A. and Vicenzi, E. (2006) *Elements, 2*, 157-162. [25] Gendrin, A., et al. (2005) *Science, 307*, 1587-1591. [26] Squyres, S. W., et al. (2004) *Science, 306*, 1709-1714. [27] Milliken, R. E., et al. (2008) *Geology, 36, 11*, 847-850. [28] Osterloo, M. M., et al. (2008) *Science, 319, 5870*, 1651-1654. [29] Christensen, P. R., et al. (2000) *JGR, 105, E4*, 9623-9642. [30] Bibring, J. -P., et al. (2007) *Science, 317, 5842*, 1206-1210. [31] Bibring, J. –P., et al. (2006) *Science, 312, 5772*, 400-404. [32] Mangold, N., et al. (2010) *Icarus, 207, 1*, 265-276. [33] Skok, J. R., et al. (2010) *Nature Geo.,* doi:10.1038/ngeo990. [34] Mangold, N., et al. (2007) *JGR Planets, 112, E08S04*, doi:10.1029/2006 JE002835. [35] Carlson, R. L. (2003) *GRL, 30, 22*, 2142-2145. [36] Roach, L. H., et al. (2010) *Icarus, 206, 1*, 253-268. [37] Murchie, S. L., et al. (2009) *JGR, 114, E00D06*, doi: 10.1029/2009JE003342. [38] Flahaut, J., et al. (2011) *Icarus, in press*. [39] Sun, V. and Milliken, RE, *JGR* 2015. [40] Elkins-Tanton LT. EPSL. 2008; 271(1):181-91. [41] Cannon, K. M., S. W. Parman, and J. F. Mustard. "Primordial Clays on Mars Formed Beneath a Steam or Supercritical Atmosphere." *Lunar and Planetary Science Conference*. Vol. 48. 2017. [42] Andrews-Hanna, J. C. and Lewis, K. W. (2011) *JGR, 116, E02007*, doi: 10.1029/2010JE003709.

**THE ROLE OF METEORITE IMPACTS IN CREATING A HABITABLE EARLY MARS.** G. R. Osinski[1,2], C. Caudill[1], C. S. Cockell[3], A. Pontefract[4], H. M. Sapers[5,6,7], S. Simpson[1], M. Svensson[1], and L. L. Tornabene[1], [1]Centre for Planetary Science and Exploration & Dept. of Earth Sciences, University of Western Ontario, Canada, [2]Dept. of Physics & Astronomy, University of Western Ontario, Canada, [3]Sch. of Physics and Astronomy, University of Edinburgh, UK, [4]Earth, Atmospheric & Planetary Sciences, Massachusetts Institute of Technology, USA, [5]Dept. of Earth Sciences, University of Southern California, USA, [6]Div. of Geological & Planetary Sciences, California Institute of Technology, USA, [7]NASA Jet Propulsion Laboratory, USA (gosinski@uwo.ca)

**Introduction:** Impact cratering is the most ubiquitous geological process throughout the Solar System, affecting all planetary objects with rocky or icy solid surfaces. On objects such as the Moon that retain large portions of their earliest crust, impact craters are the dominant geological feature. Despite being more geologically active than the Moon, impact craters are the most common geological landforms on Mars [1] and there are numerous proposals for giant impacts in the first 100 Myr. of Mars' history (e.g., [2–5]).

Meteorite impacts are generally viewed as agents of destruction that would have led to the "frustration" or "annihilation" of life on early Earth and Mars [6, 7]. There is also strong evidence that impacts have affected the "recent" biological evolution of the Earth as evidenced by the link between the Chicxulub impact structure, Mexico, and the Cretaceous–Paleogene mass extinction event 66 Myr. ago [8] that resulted in the disappearance, or species-level extinction, of several major animal, plant and protist groups. However, while speculative, it is likely that the other two domains of life (i.e., Bacteria and Archaea) consisting entirely of microscopic single-celled organisms, would have been largely unaffected by the Chicxulub impact on a global or even regional scale.

While we do not dispute the fact that impact events are immediate agents of destruction, we contend that impact cratering has not only had a profound effect on the geological evolution of Mars and Earth [9], but also on their biological evolution – in a *positive* way. We hypothesize that impact craters would have provided conditions suitable for the emergence of life on Mars through the production of substrates for prebiotic chemistry and through the production of habitats for the emergence and subsequent survival of microbial life. In this contribution, we provide observations from studies of several terrestrial impact craters and draw on key relevant literature to support this hypothesis.

We propose that studies of impact craters on Earth should be ramped up to prepare for the next generation of Mars life-detection and sample return missions and that Martian impact craters should be viewed as prime astrobiological landing sites – not for the *secondary* sedimentary record they contain (primarily the case for Gale and Gusev), but for the *primary* potential habitats and substrates that they comprise.

**Substrates for prebiotic chemistry:** It is becoming increasingly clear that mineral substrates likely played an important role in the origin of life (e.g., [10]). Specifically, it has been proposed that minerals may have played a role in both the formation of organic molecules ranging from formaldehyde to RNA, through reactions mediated by minerals. Clay minerals, and in particular montmorillonite, have been shown to catalyze a variety of organic reactions, in particular the formation of RNA [11, 12].

Studies of craters on Earth have shown that clays are typically the most common secondary mineral phases, forming through impact-generated hydrothermal alteration [13, 14] and through the devitrification of hydrous impact melt products [15]. Recent studies of melt-bearing breccias at the Ries impact structure, Germany, suggest complex, localized post-impact hydrothermal environments which have thus far been underappreciated both temporally and spatially. Mineralogical and $\delta$18 O isotopic data from both surface-exposed and core samples of the melt-bearing breccia suggests that hydrothermal activity outside the inner ring extensively altered impact melt clasts, yet was temporally restricted or lower temperature as compared to the pervasive intermediate argillic alteration and zeolitization of the crater-fill units [16, 17].

Clays and other hydrated minerals have been widely documented on Mars with the general view being that these phases formed by aqueous alteration in a wetter climate early in the planet's history [18]. Previous studies have shown that hydrated silicates (particularly clay minerals, zeolites, and hydrated silicate glass) are preferentially associated with the heavily cratered highlands of Mars although some lowland exposures, exclusively in impact craters, have also been found [19]. Clays within martian impact craters may have a pre-impact (i.e., the excavate pre-existing crustal clays), syn-impact (i.e., impact-generated), or post-impact (i.e., in impact crater lakes) [20]. However, as noted above, studies of craters on Earth show that clays formed as a direct result of the impact process are widespread. Thus, it seems clear that clays are likely to be a common – if not ubiquitous – product of impacts into $H_2O$-bearing planetary crusts

**Habitats for emergence and subsequent evolution of life:** For Earth, one of the most widespread

theories remains the emergence of life originated in hot, aqueous environments, in the form of hydrothermal systems [21]. Volcanic heat sources drive all the active hydrothermal systems on Earth today; however, it has also been shown that most large impact events on Mars likely generated hydrothermal systems [14, 22], which based on numerical modeling may have persisted for hundreds of thousands of years [23]. Thus, hydrothermal systems generated through the impact process may have provided habitats for the emergence of life on Mars. This is consistent with recent studies that have demonstrated the colonization of impact-generated hydrothermal systems in craters on Earth [24, 25]. Importantly, our work on studies of various impact craters on Earth provides a template as to where to predict occurrences of hydrothermal deposits within martian impact craters (Fig. 1). Furthermore, it is important to highlight continuous impact ejecta deposits as they can be distributed up to ~5 crater radii from the point of impact. On early Mars, where large the formation of large basin-size impacts (100s to 1000s km in diameter) would have been commonplace, this would have resulted in the distribution of substrates and the creation of habitats over large portions of the martian crust.

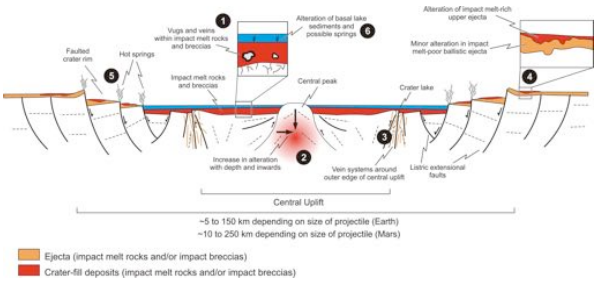


**Fig. 1.** Schematic representation of the distribution of hydrothermal deposits within impact craters (from [14]). 1) crater-fill impact melt rocks and melt-bearing breccias; 2) interior of central uplifts; 3) outer margin of central uplifts; 4) impact ejecta deposits; 5) crater rim region; and 6) post-impact crater lake sediments.

In addition to potential hydrothermal habitats, it has also been shown that impact events produce several habitats that are highly conducive to life and that were not present before the impact event:

- Impact-processed crystalline rocks, which have increased porosity and translucence compared to unshocked materials, improving microbial colonization [26, 27];
- Impact glasses, which, similar to volcanic glasses, provide an excellent readily available source of bioessential elements [28];
- Impact crater lakes, which form protected sedimentary basins with various niches and that increase the preservation potential of fossils and organic material [29].

How widespread these impact crater habitats are on Mars remains to be determined and requires parallel studies of impact craters on Earth and Mars.

**Impact craters as landing sites for future missions:** Impact craters have featured prominently in the surface exploration of Mars, where they have typically been viewed as sites offering unique bedrock exposure (e.g., Eagle, Endurance, Victoria Craters during the MER Opportunity's expeditions) or as sedimentary basins providing unique climate records (e.g., Gale and Gusev craters). We hope that this contribution stimulates interest and new studies of impact craters as prime exploration targets in the search for evidence of life on the Red Planet.

**Acknowledgements:** GRO thanks the following agencies for support for this work: Natural Sciences and Engineering Research Council of Canada, MDA, Canadian Space Agency.

**References:** [1] Strom, R.G. et al. (1992) *MARS*. H.H. Kieffer et al., eds. University of Arizona Press. 383–423. [2] Marinova, M.M. et al. (2008) *Nature*, *453*, 1216–1219. [3] Golabek, G.J. et al. (2011) *Icarus*, *215*, 1, 346–357. [4] Brasser, R. and Mojzsis, S.J. (2017) *GRL*, *44*, 12, 5978–5985. [5] Roberts, J.H. et al. (2009) *JGR Planets*, *114*. [6] Sleep, N.H. et al. (1989) *Nature*, *342*, 139–142. [7] Maher, K.A. and Stevenson, D.J. (1988) *Nature*, *331*, 612–614. [8] Schulte, P. et al. (2010) *Science*, *327*, 1214–1218. [9] Grieve, R.A.F. (2017) *Geoscience Canada doi:10.12789/geocanj.2017.44.113*. [10] Schoonen, M. et al. (2004) *AMBIO: 33*, 539–551. [11] Ferris, J.P. and Ertem, G. (1993) *J. Am.Chem. Soc.*, *115*, 26, 12270–12275. [12] Fraser, D.G. et al. (2011) *Phys. Chem. Chem. Phys.*, *13*, 3, 825–830. [13] Naumov, M. V (2005) *Geofluids*, *5*, 165–184. [14] Osinski, G.R. et al. (2013) *Icarus*, *224*, 347–363. [15] Osinski, G.R. et al. (2004) *Meteor. Planet. Sci.*, *39*, 10, 1655–1684. [16] Sapers, H.M. et al. (2017) *Meteor. Planet. Sci.*, *52*, 2. [17] Caudill, C.M. et al. (2017) *Fourth International Conference on Early Mars*, this conf. [18] Ehlmann, B.L. et al. (2011) *Nature*, *479*, 7371, 53–60. [19] Carter, J. et al. (2013) *JGR: Planets*, 1–29. [20] Tornabene, L.L. et al. (2013) *JGR: Planets*, *118*, 5, 994–1012. [21] Farmer, J.D. (2000) *GSA Today*, *10*, 7, 1–9. [22] Newsom, H.E. (1980) *Icarus*, *44*, 207–216. [23] Abramov, O. and Kring, D.A. (2005) *JGR: Planets*, *110*, doi:10.1029/2005JE002453. [24] Simpson, S.L. et al. (2017) EPSL 460:192–200. [25] Parnell, J. et al. (2010) *Geology*, *38*, 3, 271–274. [26] Cockell, C.S. et al. (2005) *Meteor. Planet. Sci.*, *40*, 1901–1914. [27] Pontefract, A. et al. (2014) *Astrobiology*, *14*, 522–533. [28] Sapers, H.M. et al. (2014) *Geology*, *42*, 471–474. [29] Cabrol, N.A. et al. (2001) *Icarus*, *154*, 98–112.

**THE MINERALOGIC ALTERATION HISTORY OF EARLY MARS: THE ROLE OF LARGE CRATERS AND BASINS IN TRANSIENT REGIONAL HIGH-TEMPERATURE ALTERATION.** A. M. Palumbo[1] and J. W. Head[1], [1]Department of Earth, Environmental and Planetary Sciences, Brown University, Providence, RI 02818 USA (Ashley_Palumbo@Brown.edu)

**Introduction:** The ~1500 km diameter Isidis basin is the third largest impact structure on Mars. Regions surrounding Isidis, including Nili Fossae and NE Syrtis, provide insight into the mineralogical and climatological history of Mars. The formation, alteration, and erosion of features in the cirum-Isidis region are well-constrained with time, beginning in the early Noachian after the Isidis-forming event, and ending in the Hesperian before the Syrtis Major lava flows embayed the area. Throughout the region, there are distinct stratigraphic layers with correspondingly distinct alteration products, suggesting multiple different aqueous alteration regimes [1]. The stratigraphically lowest layers are the (1) basement unit, characterized by low-Ca pyroxene and rich in Fe/Mg smectites, which contains megabreccia blocks and kaolinite patches; (2) overlying olivine-rich unit, which is variably altered to Mg-carbonate; and (3) spectrally flat and crater preserving capping unit [1–3]. Above these layers, emplaced later, is a sulfate-rich unit and a unit of Syrtis Major lava flows. In the past, it has been assumed that the different aqueous alteration regimes, related to the alteration of the different stratigraphic layers, were temporally separated [*e.g.* 1]. We suggest that this is not entirely the case, and that the three lowest units were formed and altered contemporaneously with the Isidis event, following the description of the Impact Cratering Atmospheric and Surface Effects (ICASE) model [4–6].

**Previous Interpretations:** *Basement unit.* The Fe/Mg smectites within the basement unit may represent deep hydrothermal alteration in the subsurface [7] that was exhumed by the Isidis event [8]. Terrestrial analogs suggest that formation of the smectites through this mechanism would take thousands of years and require temperatures up to ~873 K [1,8]. This interpretation of the basement unit is consistent with the presence of megabreccia blocks within the unit that were likely excavated during the impact event. Following emplacement, the unit experienced aqueous alteration (Fig. 1c), producing kaolinite patches. The kaolinite-bearing unit is tens of meters thick [1] and does not exhibit bedding, suggesting that the alteration was *in-situ*, and leading to formation hypotheses [*e.g.* 1]: (1) top-down leaching of the Fe/Mg smectite-rich basement unit, and (2) hydrothermal alteration in the subsurface and subsequent excavation. Large impact events could have caused regional high-temperature surface alteration, leading us to explore the former hypothesis further in the context of the Isidis basin event.

*Olivine-rich and capping units.* Overlying the basement unit is the olivine-rich unit (Fig. 1c). Leading formation hypotheses include (1) post-Isidis lava flows [9,10] and (2) the Isidis impact melt sheet [8,11]. The unit ranges in thickness from 5 m [3] to 160 m [2] and drapes underlying topography [2]. Aqueous activity has variably altered the unit to Mg-carbonate [1]. The spectral signature of Mg-carbonate is more uniform and pervasive in NE Syrtis than Nili Fossae, suggesting that aqueous alteration was more extensive in NE Syrtis [3], closer to the basin interior. Additionally, the olivine-rich unit has a high thermal inertia when compared to the other stratigraphic units [3], suggesting that it is more coherent. Overlying this layer in NE Syrtis is a ~10 m thick, spectrally flat, silica-rich capping unit [3].

*Summary.* The observed stratigraphy and mineralogy require at least three episodes of aqueous activity [1]: (1) formation of the Fe/Mg smectites, (2) alteration of the basement and olivine-rich units, and (3) a later episode involving less water-rock interaction that erodes the units. The episodes are canonically interpreted to be temporally distinct [1], possibly spanning 250 Myr [3].

**Applying ICASE to the Isidis Basin Event and Associated Mineralogy:** We explore the possibility that the emplacement and alteration of the basement, olivine-rich and capping units are essentially contemporaneous and related to the Isidis event and post-impact effects.

Basin-scale impacts vaporize significant volumes of target and projectile material [*e.g.* 12]. The vaporized material expands away from the impact site as a vapor plume composed of vaporized silicate material and water. The vapor plume cools through radiation and expansion. When the plume cools to condensation temperature for the silicate material, the silicate material will condense and fall out as molten spherules. We hypothesize that the fallout of silicate condensate material [4] corresponds to the emplacement of the olivine-rich unit. The olivine-rich unit drapes underlying topography [1,3], consistent with silicate condensate layer (SCL) emplacement. The average thickness of the Isidis SCL is estimated to be ~20 m [11], similar to the thickness of the observed olivine-

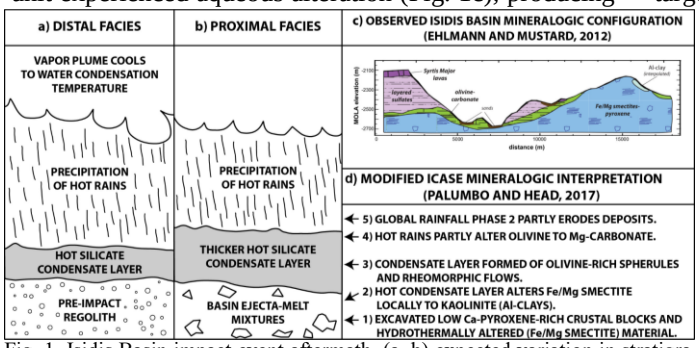

Fig. 1. Isidis Basin impact event aftermath. (a, b) expected variation in stratigraphy with distance. (c) observed mineralogic configuration, from [2]. (d) our interpretation for formation of the layers, highlighting the ICASE-related steps [6].

rich unit. Silicate condensate material preferentially deposits at the impact site, suggesting a thicker layer in the Isidis region, relative to more distal locations (Fig. 1). Proximal to the basin, the very high temperatures of the SCL (~1600 K) [*e.g.* 4] could encourage rheomorphic flow off of topographic highs and ponding in topographic lows, leading to local variations in thickness and exposure of the underlying basement unit. For these reasons, the Isidis SCL is a candidate for the observed structure and distribution of the olivine-rich unit (Fig. 1c,d).

This unit has a stronger olivine spectral signature than surrounding regions and stratigraphic layers [2,11] and is the strongest olivine signature detected on Mars [2]. Explanations for this observation in the context of ICASE [4–6] are (1) Noachian volcanic crustal compositions that were richer in olivine than later extrusives [8], (2) an olivine-rich projectile that contributed a significant olivine component to the vapor plume, or (3) early crystallization of olivine and quenching in the plume.

The olivine-rich unit is emplaced on top of the basement unit and thermal interaction and hydrothermal alteration between the units could account for some of the observed alteration products. Following the condensation and fallout of the silicate material, the vapor plume continues cooling and eventually reaches the condensation temperature for water vapor. The water rains out and reaches the surface at temperatures close to condensation temperature (~373 K). The rainfall (1) acts to cool the SCL, causing the water to cycle through the layer and atmosphere for hundreds of years, a phase characterized by rainfall rates of ~2 m/a [5]; (2) hydrothermally alters the upper portions of all exposed layers; and (3) quenches the upper-most parts of the SCL, producing spectrally flat, silica-rich glass (capping unit).

The high temperatures of the substrate and aqueous medium (rainfall) suggest that the upper portions of the olivine-rich unit and exposed areas of the basement unit could be altered to clays on timescales of tens of years [13]. Due to differences in parent rock composition, alteration of the olivine-rich unit is predicted to produce Mg-carbonates [2], and alteration of the basement unit is predicted to produce Al-phyllosilicates. Spectral analyses of the region show both variable alteration to carbonate and patchy distributions of kaolinite [1]; the alteration of both units is partial, with products (altered) and reactants (initial) remaining [2]. The ICASE model [4–6] could help account for this observation; the aqueous alteration related to impact-induced rainfall is intense but geologically short-lived, suggesting that the parent rock will undergo only partial alteration.

To summarize, our interpretation of several of the stratigraphic units follows: Low-Ca pyroxene-rich crustal blocks and hydrothermally altered Fe/Mg smectites are excavated and emplaced during the Isidis event (Fig. 1 d1). The vapor plume cools to silicate condensation temperature and precipitates the olivine-rich SCL (Fig. 1b, 1 d3); the SCL may aid in thermally altering the basement unit locally to produce Al-phyllosilicates (Fig. 1 d2). The silicate condensate material with the coolest temperatures will be emplaced last, producing the capping unit. Soon thereafter, the vapor plume cools to the water condensation temperature and precipitates abundant hot rainfall (Fig. 1b); the ensuing hot rains (1) partly alter the olivine-rich unit to Mg-carbonates and exposed regions of the basement unit to Al-clays (Fig. 1 d4), and (2) quench the capping unit to produce silica-rich, spectrally flat, glass. Last, the final impact-related rainfall partly erodes the deposit (Fig. 1 d5). In summary, the emplacement of the lower-most three units and several of the key alteration phases associated with the Isidis basin stratigraphy may be related to the Isidis event and its aftermath (Fig. 1d), rather than to separate subsequent environmental phases or events.

**Conclusions:** Following [4–6], we have characterized the mineralogical influence of large cratering events on early Mars. Critical to this analysis is the prediction of a hot SCL ~10s m thick and subsequent intense impact-induced rainfall [4,5]. These impact cratering depositional and alteration effects will clearly influence the pre-existing substrate, a factor that has not been widely considered in the past. We propose that the circum-Isidis region offers an opportunity to assess the different aqueous environments and resulting mineralogical effects that characterize the area (Fig. 1) and may have occurred elsewhere in association with other large craters and basins.

The proposed explanation for the observed stratigraphy in the circum-Isidis region suggests that the emplacement of the lower-most three stratigraphic layers and subsequent aqueous alteration occurred over hundreds of years, in contrast to the previous estimate of hundreds of millions of years. This explanation does not require a global climate transition, instead it explains the geology and mineralogy through a climatic perturbation related to the Isidis event. It is possible that post-impact conditions are responsible for the observed stratigraphic sequence, suggesting that a continuous warm and wet Noachian climate [14] was not required for formation of these clays.

**References:** [1] Ehlmann, B. et al. (2009) *JGR Planets*, *114*, DOI 10.1029/2009JE003339. [2] Ehlmann, B., and Mustard, J. (2012) *GRL*, *39*, L11202. [3] Bramble, M. et al. (2017) *Icarus*, *293*, 66–93. [4] Segura, T. et al. (2008) *JGR Planets*, *113*, E11007. [5] Toon, O. et al. (2010) *Annu. Rev. Earth Planet. Sci.*, *38*, 303–322. [6] Palumbo, A., and Head, J. (In Revision) *MAPS*. [7] Ehlmann, B. et al. (2011) *Nature*, *479*, 53–60. [8] Mustard, J. et al. (2009) *JGR Planets*, *114*, E00D12. [9] Hamilton, V., and Christensen, P. (2005) *Geology*, *33*, 433–436. [10] Tornabene, L. et al. (2008) *JGR Planets*, *113*, E10001. [11] Mustard, J. et al. (2007) *JGR Planets*, *112*, E08S03. [12] Melosh, H. J., *Impact Cratering: A Geologic Process*, Oxford University Press (1989). [13] Browning, L. et al. (2003) *LPSC XXXIV*, Abstract 1708. [14] Craddock, R., and Howard, A. (2002) *JGR Planets*, *107*, 5111.

**LATE NOACHIAN ICY HIGHLANDS CLIMATE MODEL: EXPLORING THE POSSIBILITY OF TRANSIENT MELTING AND FLUVIAL/LACUSTRINE ACTIVITY THROUGH PEAK ANNUAL/SEASONAL TEMPERATURES.** A. M. Palumbo[1], J. W. Head[1], R. D. Wordsworth[2], [1]Department of Earth, Environmental and Planetary Sciences, Brown University, Providence, RI 02912 USA, [2]School of Engineering and Applied Sciences, Harvard University, Cambridge, MA 02138 USA (Ashley_Palumbo@Brown.edu)

**Introduction:** Climate models have suggested that under the influence of a younger and less luminous Sun [1,2], early Mars would be forced into a cold steady state with mean annual temperatures (MAT) consistently below the melting point of water [3,4]. In contrast, there is geological evidence for fluvial and lacustrine activity during the Late Noachian and Early Hesperian, including valley networks (VNs) [5] and lakes [6]. With current models unable to produce relatively continuous clement conditions (MAT >273 K) [3,4], we consider the possibility of a "cold and icy" planet (MAT<273 K) and address the question: is formation of fluvial/lacustrine features possible from shorter periods of punctuated heating and associated snowmelt and runoff?

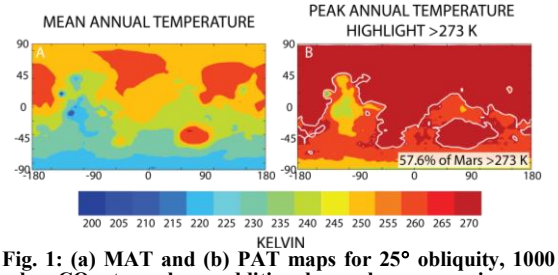


**Fig. 1: (a) MAT and (b) PAT maps for 25° obliquity, 1000 mbar $CO_2$ atmosphere, additional greenhouse warming.**

**Background:** General circulation models (GCMs) [3,4] show that when atmospheric pressure exceeds tens to hundreds of mbar, an altitude-dependent temperature effect is induced and $H_2O$ preferentially accumulates in the highlands, producing a "Late Noachian Icy Highlands" (LNIH) scenario [7]. The location of precipitation under a nominal "cold and icy" LNIH scenario versus a forced "warm and wet" scenario was examined by [8], who found that snow/ice accumulation under a cold climate is better correlated with the VN distribution than rainfall in a "warm and wet" climate.

The requirement remains, however, for melting of the ice and runoff to incise the VNs [9,10]. There are several end member options for transient atmospheric warming on early Mars including: (1) $SO_2$-induced warming from periods of intense volcanism [11], (2) impact cratering induced warming [12], and (3) transient melting from peak seasonal temperatures [*e.g.* 7]. Punctuated volcanism could lead to snowmelt and runoff from the increased $SO_2$ in the atmosphere, but rapid conversion of $SO_2$ to aerosols (cooling) would prevent heating from extending beyond decades to centuries [11]. Impact cratering induces high-temperature conditions and precipitation for a short duration (centuries) [12], but may produce global

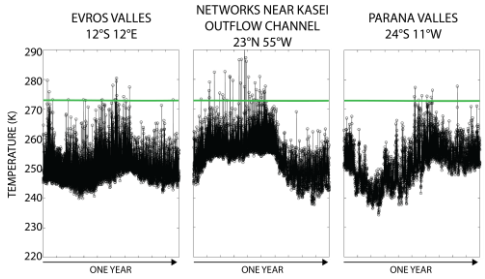


**Fig. 2: Temperature time-series at three VNs. Green line at 273 K.**

rain and too high rainfall rates to form the equatorially-concentrated VNs [13].

The focus of this work is to test hypothesis (3) by (1) assessing whether regions with peak annual temperatures (PAT) >273 K correlate with the predicted snow/ice distribution, producing meltwater, and (2) calculating annual meltwater volumes in order to place constraints on the cumulative duration required for this process to form the VNs. This work highlights the importance of considering seasonal and diurnal temperature variation in addition to MAT, and contributes an understanding of the climatic effects of modest greenhouse warming and varying eccentricity on early Mars.

**Methods:** In this analysis, we use the Laboratoire de Meteorologie Dynamique (LMD) GCM for early Mars and focus on a range of pressures (600, 800, and 1000 mbar) for a pure $CO_2$ atmosphere [*e.g.* 3], and a range of obliquities (25, 35, 45, and 55°) and eccentricities (0 and 0.17) for the Late Noachian [14]. We collect model data four times per model martian day (every six hours).

We also assess the addition of a small amount of greenhouse gas in order to assess atmospheres with slightly increased temperatures. Due to the uncertainty in sources and sinks for specific greenhouse gases, we account for the warming by adding gray gas, which absorbs evenly across the spectrum at a defined absorption coefficient. We choose a relatively small absorption coefficient, κ, to raise MAT by ~18 K, maintaining an overall "cold and icy" climate (κ=2.5e-5 kg $m^{-2}$).

*MAT and PAT maps:* Is transient melting and runoff a viable mechanism for VN formation? We assess which spin-axis orbital conditions and atmospheric pressures produced PAT >273 K in the locations where VNs are abundant and snow/ice is predicted to accumulate, producing meltwater (Fig. 1).

What percentage of the year >273 K would be required to cause melting and fluvial erosion? At Lake Hoare in the Antarctic McMurdo Dry Valleys (MDV) (MAT=~255 K), temperatures are >273 K for ~5-7% of the year, a duration sufficient to maintain the lake

through fluvial input. We hypothesize that a similar percentage of the year >273 K may be sufficient to form comparable features on early Mars. However, our analysis thus far (MAT and PAT maps) does not represent durations of conditions >273 K; each data point on the PAT map represents only the maximum annual temperature. Based on Fig. 1, we cannot conclude whether these conditions exist for more than a few hours yearly, a duration which is likely insufficient to cause the necessary scale of melting and erosion [9]. To reconcile this, we (1) determine the annual duration of melt conditions at three VNs and compare the duration with the observed ~5-7% of the year above freezing at Lake Hoare, and (2) use "positive degree day" (PDD) calculations to assess the annual amount of meltwater produced [9,15] and the number of years that this process must be active to produce sufficient meltwater for VN formation.

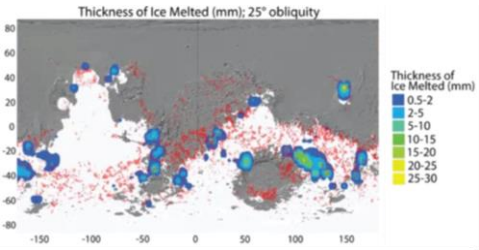

**Fig. 3: Results of PDD calculations and VNs (red).**

*VN study:* We examine Parana Valles, Evros Valles, and the Kasei networks, which are distributed near the edges of the predicted LNIH ice sheet at locations that require melting of ice and subsequent runoff to form in this climate. We produce temperature time-series for one martian year at each VN to determine the fraction of the year with temperatures >273 K (Fig. 2).

*PDD analysis:* Following the methods of [9], we determine the number of PDD at each model grid point (lat, lon; Fig. 3). Adopting the PDD conversion factor for Mars, 1.08 mm/PDD [9], we estimate the thickness of ice melted at all model grid points where PDD > 0 and LNIH snow/ice is present. Next, we integrate over the area of the ice sheet to determine the global volume of ice melted in one martian year. We then compare the annual amount of meltwater produced to the total volume required to form the VNs [10] to determine the number of years that this process must operate to carve the VNs.

**Results and Discussion:** We include a specific example from our study that represents optimal conditions for equatorial melting: 25° obliquity, 1000 mbar $CO_2$, circular orbit, and additional greenhouse warming (MAT=243 K). Lower obliquity concentrates maximum solar insolation near the equator and a thicker atmosphere increases the greenhouse effect. Thinner atmospheres prevent the studied VNs from experiencing melting conditions for $\geq 1$ day annually, a duration insufficient to form the VN. Although increased eccentricity contributes additional seasonal warming, the effect is minor and we do not highlight the results here.

Our models show that PAT can be >273 K in regions where both VNs are abundant and snow/ice accumulates (Fig. 1). Time-series at the three VNs show that each VN either approaches or exceeds 273 K for a few data points each year (Fig. 2). In this case, the VNs experience conditions above freezing for a fraction of the year comparable to the MDV, implying that these conditions might be sufficient to form the VNs if this process operates for a sufficiently long duration.

For these spin-axis/orbital conditions, a volume of $2.92 \times 10^{10}$ $m^3$ (~$2 \times 10^{-4}$ m GEL) meltwater is produced annually (Fig. 3). If 3-100 m GEL is required to form the VNs [10], this process must repeat for ~$1.5 \times 10^4$ to ~$5 \times 10^5$ years to produce enough meltwater. Previous analysis suggest that VN formation may have required a cumulative $10^5$-$10^7$ years of fluvial activity [16]. In concert with the predicted distribution of meltwater (Fig. 3), our results indicate that this mechanism could plausibly be responsible for VN formation.

Critically, runoff rates produced by this mechanism may be too low to produce the necessary erosion. At any grid point, the maximum thickness of ice melted annually is ~30 cm (Fig. 3). Unless all meltwater is produced and runs off within one day, runoff rates are lower than the rates required for VN formation [mm-cm/day; 15,16]. Thus, while significant meltwater is produced in our model, slightly warmer conditions may be required to generate the necessary higher runoff rates, a subject of ongoing work.

**Conclusions:** We highlight the importance of considering seasonal/diurnal temperature variations along with MAT to assess melting in "cold and icy" early Mars climate scenarios. We find that low obliquity and high atmospheric pressure are required to produce temperatures >273 K in the equatorial regions. PAT >273 K durations are not conducive to VN formation in the nominal MAT=225 K "cold and icy" climate and we suggest that additional heating is required, such as by impact cratering [12] or volcanism [11]. Under warmer conditions (MAT=243 K), however, transient melting of ice can occur during the warmest hours of the summer season. Under these conditions, a sufficient volume of meltwater can be produced to form the VNs, although runoff rates may be too low.

**References:** [1] Gough, D. (1981) *Sol. Phys.*, *74*, 21–34. [2] Sagan, C., and Mullen, G. (1972) *Science*, *177*, 52–56. [3] Forget, F. et al. (2013) *Icarus*, *222*, 81–99. [4] Wordsworth, R. et al. (2013) *Icarus*, *222*, 1–19. [5] Hynek, B. et al. (2010) *JGR Planets*, *115*, E09008. [6] Fassett, C., and Head, J. (2008) *Icarus*, *198*, 37–56. [7] Head, J., and Marchant, D. (2014) *Antarct. Sci.*, *26*, 774–800. [8] Wordsworth, R. et al. (2015) *JGR Planets*, *120*, 1201–1219. [9] Fastook, J., and Head, J. (2015) *PSS*, *106*, 82–98. [10] Rosenberg, E., and Head, J. (2015) *PSS*, *117*, 429–435. [11] Halevy, I., and Head, J. (2014) *Nat. Geosci.*, *7*, 865–868. [12] Segura, T. et al. (2008) *JGR Planets*, *113*, E11007. [13] Palumbo, A., and Head, J. (In Revision) *MAPS*. [14] Laskar, J. et al. (2004) *Icarus*, *170*, 343–364. [15] Scanlon, K. et al. (2016) *LPSC 47*, Abstract 1532. [16] Hoke, M. et al. (2011) *EPSL*, *312*, 1–12.

**THE CLIMATOLOGICAL AND GEOLOGICAL CASE FOR A WARMER AND WETTER EARLY MARS.** R. M. Ramirez[1] and R. A. Craddock[2], [1]Earth-Life Science Institute, email: ramsesny@gmail.com, [2]The Smithsonian Institution, email: craddockb@si.edu.

**Introduction:** The climate of early Mars has been a topic of intense debate for decades. Although most investigators believe that the geology, including the valley networks (Figure 1), indicates the presence of surface water, disagreement has persisted regarding how warm the surface must have been and how long such conditions may have existed. Climate models that only include $CO_2$ and $H_2O$ as greenhouse gases have been unable to generate warm surface conditions given the faint young Sun. Some models suggest that a continuously warm climate could have been possible by supplementing this $CO_2$-$H_2O$ warming with either secondary greenhouse gases or $CO_2$ clouds. Others posit that Mars' climate was cold most of the time, but underwent periodic episodes of transient warming caused by external events. Here, we argue that a predominantly icy early Mars cannot be reconciled with either the geologic record or climate modeling simulations. Mars may have had a warm and semi-arid climate instead (Fig. 1).

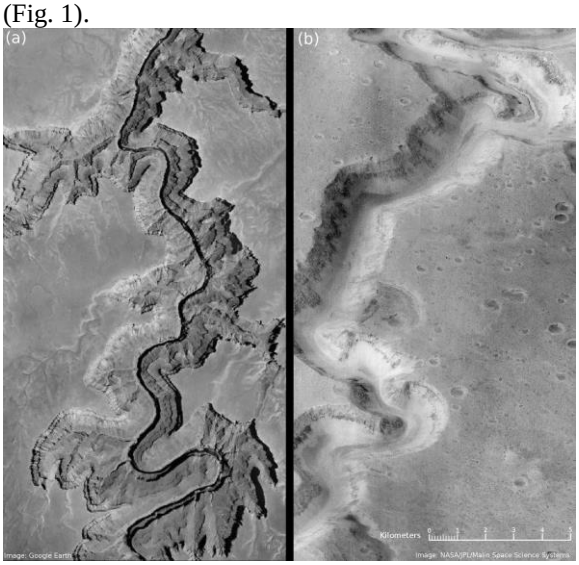


**Figure 1:** Split panel comparing (left) section of the Grand Canyon (Colorado River Canyon) against (right) a section of Mars' Nanedi Vallis. Nanedi Vallis is located in the Lunae Palus quadrangle (4.9 degrees N, 49 degrees W). The northern part of the Nanedi Vallis image shows a river had once cut through it, similar to the one flowing through the Colorado River Canyon. Nanedi Valles continues for over 500 km (not shown). Although this section of Nanedi Vallis is nearly 2.5 km in width, other portions (not shown) are at least twice as wide. Slight morphologic differences between the two canyons are attributable to the great age differences between the regions (Image Credit: Chester Harman)

**Methods**: We used a single-column radiative-convective climate model first developed by Kasting et al. [1] and updated in recent studies [2-4]. We assumed that the Sun remains fixed at a solar zenith angle of 60° as in previous works [2;5]. An average martian solar flux value of 439 W/m$^2$ was assumed for early Mars conditions ~3.8 Ga. Unless otherwise specified, most modeled atmospheres are cloud-free and are predominantly composed of $CO_2$ (80 – 95%) with varying amounts of (1-20%) $H_2$

**Results:** We show that warm and relatively non-glaciated early Mars require only ~1% $H_2$ and 3 bar $CO_2$ or ~20% $H_2$ and 0.55 bar $CO_2$ [6](Fig. 2). In contrast, the reflectivity of surface ice greatly increases the difficulty to transiently warm an initially frozen surface. Surface pressure thresholds required for warm conditions increase ~10 – 60% for transient warming models, depending on ice cover fraction. No warm solution is possible for ice cover fractions exceeding 40%, 70%, and 85% for mixed snow/ice and 25%, 35%, and 49% for fresher snow/ice at $H_2$ concentrations of 3%, 10%, and 20%, respectively (Fig. 3). If high temperatures (298 – 323 K) were required to produce the observed surface clay amounts on a transiently warm early Mars [7], we show that such temperatures would have required unrealistically high surface pressures (> 5 – 10 bar) for nearly all $H_2$ concentrations considered (1 – 20%).

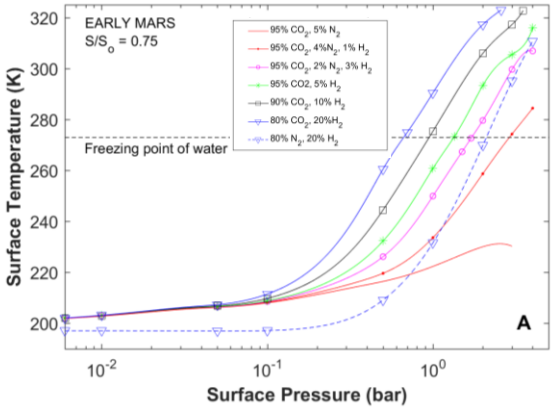


**Figure 2:** Surface temperature as a function of surface pressure for different fully-saturated atmospheric compositions. The assumed solar luminosity is 0.75 times present, appropriate for 3.8 Ga. The surface albedo is 0.216.

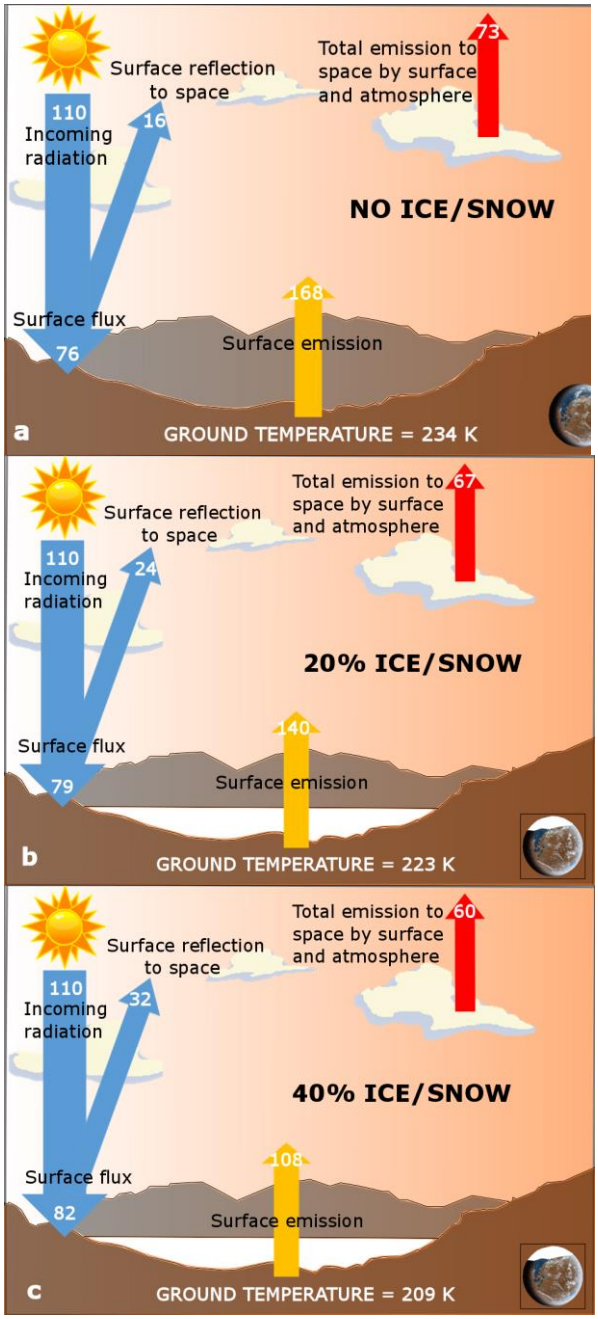


**Figure 3:** Simplified atmospheric model schematic diagrams using the model of Ramirez (2017) that compares the incoming and outgoing solar energy requirements (in W/m$^2$) to support various atmospheric and surface temperatures on a cold early Mars, assuming 0%, 20%, and 40% global coverage of " snow/ice mixtures (65% reflectivity) At lower surface temperatures, there is less surface and atmospheric emission available to heat the atmosphere. The addition of 20% (40%) surface ice reduces surface temperatures by 11 K (25 K). 3-D models with clouds also illustrate similar ice albedo problems [16] (From [17]).

**Discussion:** The geologic evidence does not support a heavily glaciated early Mars [8]. Glacial features, such as cirques, kames, and eskers, are noticeably absent in ancient terrains [9]. Furthermore, the geomorphology strongly suggests that a widespread process, most likely precipitation, was the major erosive agent on early Mars [8;10], countering the notion that localized sources of glacial melt from icy highland sheets [11;12] could have formed these fluvial features, including those in Arabia Terra [10]. Indeed, a recent analysis finds that a global water volume exceeding 5 km was necessary to carve the valley networks, suggesting a paleo-ocean and active hydrologic cycle did exist [13].

It is possible that early Mars was characterized by a warm semi-arid climate that produced enough precipitation (e.g. rainfall) to form the ancient valleys [8]. Such an interpretation is consistent with the observed lack of glaciation in ancient terrains [8;9], the water amounts necessary to form the older valleys [14], and the recent estimates for a smaller initial water inventory (< 200 m global equivalent)[15].

**References:**

[1] Kasting J.F. et al., (1993), Icarus, 101, 108-128. [2] Ramirez, R.M. et al. (2014) *NatGeo*., 7,59- 63 [3] Ramirez, R.M. & Kaltenegger, L. (2016) ApJ, 823, 6. [4] Ramirez, R.M. & Kaltenegger, L. (2017) ApJ, 837, L4 [5] Kasting, J.F., (1991). Icarus, 94, 1-13. [6] Ramirez, R.M. , (2017), Icarus, 297, 71-82. [7] Bishop et al., (2017), LPSC 48th abstract #1746.[8] Craddock, R.A. and Howard, A.D. (2002). JGR, 107, E11. [9] Wordsworth, R.D., (2016), *Annu. Rev. Earth Planet. Sci*, 44, 381 – 408. [10] Davis, J.M. et al., (2016), Geology, 44, 10, 847-850. [11] Wordsworth, R.D. et al., (2013) . Icarus 222, 1, 1-19. [12] Wordsworth, R.D. et al., (2015) . JGR 120,6, 1201 - 1219. [13] Luo et al.(2017), Nat.Commun.,8:157666doi:10.1038/ ncomms15766.[14] Hoke et al., (2011), EPSL, 312, 1, 1-12. [15] Villanueva et al., (2015), Science 348, 6231, 218-221[16]Forget et al., 2013), Icarus 222, 1, 81 – 99.[17] Ramirez and Craddock, (2017). NatGeo, in review

**STRATEGIES FOR INVESTIGATING EARLY MARS USING RETURNED SAMPLES.** Returned Sample Science Board (B. L. Carrier[1], D. W. Beaty[1], H. Y. McSween[2], A. D. Czaja[3], Y. S. Goreva[1], E. M. Hausrath[4], C. D. K. Herd[5], M. Humayun[6], F. M. McCubbin[7], S. M. McLennan[8], L. M. Pratt[9], M. A. Sephton[10], A. Steele[11], B. P. Weiss[12]
[1]Jet Propulsion Laboratory, California Institute of Technology, Pasadena, CA, [2]University of Tennessee, Knoxville, TN, [3]University of Cincinnati, Cincinnati, OH, [4]Universitiy of Nevada, Las Vegas, NV, [5]University of Alberta, Edmonton, Canada, [6]Florida State University, Tallahassee, FL, [7]NASA Johnson Space Center, Houston, TX, [8]Stony Brook University, Stony Brook, NY, [9]Indiana University, Bloomington, IN, [10]Imperial College, London, U.K., [11]Carnegie Institution, Washington, DC, [12]Massachusetts Institute of Technology, Cambridge, MA)

**Introduction:** The 2011 *Visions & Voyages* Planeary Science Decadal Survey identified making significant progress toward the return of samples from Mars as the highest priority goal for flagship missions in next decade[1]. Numerous scientific objectives have been identified that could be advanced through the potential return and analysis of martian rock, regolith, and atmospheric samples [2,3]. The analysis of returned martian samples would be particularly valuable in increasing our understanding of Early Mars.

There are many outstanding gaps in our knowledge about Early Mars in areas such as potential astrobiology, geochronology, planetary evolution (including the age, context, and processes of accretion, differentiation, magmatic, and magnetic history), the history of water at the martian surface, and the origin and evolution of the martian atmosphere. Here we will discuss scientific objectives that could be significantly advanced by Mars sample return.

**Early Mars Scientific Objectives:** There are several broad categories of study related to early Mars that could significantly benefit from the return and analysis of martian samples. For the purposes of this discussion, we have identified four such categories:

*1. Astrobiology/signs of ancient life:*

The question of whether life arose on Mars billions of years ago and for how long it persisted (or may still persist) has long been a driving factor in Mars exploration. Our current understanding of Mars and its history suggest that the planet was habitable for at least part of its history and parts of it may remain habitable today. The questions of whether the conditions were right for the emergence of life, and whether such emergence occurred, remain open. Several habitats on Mars are high-value targets including paleolacustrine sediments (especially those of Noachian age), hydrothermal deposits (sinters) and serpentinites. The investigation of samples from these types of habitats would significantly advance our understanding of both the history of water on Mars and its capability of supporting the emergence of life.

To develop a strategy for detection of Martian life, one must first identify a set of robust criteria for life detection that form a testable hypothesis. The simplest form of extraterrestrial life detection, with minimal assumptions on the nature of the organism or a potential "alien biochemistry" to be detected, is to understand the possible abiotic organic chemical reactions given the context of the samples, and to look for perturbations to that physiochemical system. Life assists in the detection process in that it is competition-driven to select a relatively small number of the many known organic chemicals produced by abiotic processes. Therefore, anomalous deviations from predicted abiological yields of organic chemicals under given conditions may be the easiest life detection protocol. The assumptions are minimal; life is carbon-based and it chooses only a subset of possible abiotic chemicals available. Therefore, knowing the abiotic reactions that are possible in a certain context provides a baseline value that can be compared to observations of natural Martian systems. If any anomalous concentrations of organics are observed, this anomaly may be a 'biosignature' [4].

The analysis of returned samples would allow for detailed replicate examination of abiotic and potentially biotic hypotheses for the origin of potential biosignatures, in an iterative fashion, ranging from microbial fossils and textures to possible biomolecules to isotopic and other geochemical signatures. The return of martian samples to Earth would allow for a much more comprehensive suite of analyses and at finer spatial scales than is possible through robotic *in situ* measurements, thus greatly enhancing our understanding of the the probability of determining whether life ever existed on Mars.

*2. Constraining martian geochronology:*

There are currently major sources of uncertainty in the absolute ages of different terrain units on Mars introduced by the use of crater size-frequency distribution models. Developing an accurate chronology requires determining absolute ages of crystallization or impact metamorphism of geological units with known crater frequencies. The precision of absolute age dating tehcniques that can currently be used *in situ* is limited and is insufficient to accurately calibrate crater counts.

*3. Planetary evolution (accretion, differentiation, magmatic and magnetic history):*

Most of what we know about the accretion and early differentiation of Mars comes from Martian meteorites. However, Martian meteorites provide coverage of limited periods of Martian history, are of unknown provenance, and have unknown original orientations on the

Martian surface. Apart from the 4.4 Ga NWA 7034 regolith breccia and the 4.1 Ga ALH 84001 orthopyroxenite, the other martian meteorites are either ~2.4 Ga, ~1.3 Ga or <0.6 Ga, such that igneous rocks from the Hesperian, reflecting an important phase of volcanic resurfacing of Mars, are missing from the collection. Igneous samples that span the Noachian-Hesperian boundary will assist in constraining the early global differentiation of Mars and the long-term history of silicate differentiation and magmatism, planetary heat loss, and the martian core dynamo.

Paleomagnetic studies of Martian meteorites have two major limitations: (a) the lack of ancient samples and (b) the meteorites' unknown orientations at the time they were magnetized. With respect to (a), the discoveries of magnetization in the Martian crust by the Mars Global Surveyor and in the ~4.16 billion year old meteorite ALH 84001 provide evidence for a dynamo active in at least the Early Noachian epoch [5,6]. However, it is unclear when the dynamo ended. Some studies suggest the end of the dynamo in the Early Noachian (~4.0-4.1 Ga) [7], while others suggest that it lasted into the Hesperian [8]. It has even been proposed that the dynamo originated only after 4.0 Ga [9]. The main obstacle to the resolution of this issue is that only a single Martian meteorite older than 1.3 Ga (ALH 84001) was successfully paleomagnetically analyzed [6]. Paleomagnetic measurements of a suite of returned samples spanning the Noachian to Hesperian would likely establish the lifetime of the dynamo.

With respect to (b), oriented, stratigraphically bound sample suites from known geologic locations could be used to characterize the temporal behavior of any dynamo to test the hypothesis that early Mars experienced plate tectonics and/or true polar wander.

*4. Martian atmosphere (origin and evolution):* The Martian atmosphere is expected to have been lost over time, so records of the isotopic compositions and/or partial pressures of its key components could be recovered from the analysis of returned samples. Particularly interesting are carbonate minerals, hydrated minerals, and other weathering products, especially phases that are amenable to radiometric age determination. There is also the possibility of analyzing atmospheric gasses, which have been trapped in impact melt or other inclusions. For example, the heavy isotopic compositions of H, Ar, and other species in the present-day relative to ancient reservoirs indicate that a substantial fraction of the atmosphere has been lost through time [10]. The loss of the atmosphere was likely caused by a combination of hydrodynamic escape, erosion by impacts, and possibly severe sputtering and pickup by the solar wind magnetic and electric fields following the death of an early dynamo [11] (see above).

In addition to studying the current Martian atmosphere and ancient trapped gasses in Martian sedimentary, igneous, and impact samples, there is considerable knowledge to be gained by examining the compositions of sedimentary rocks, regoliths, and secondary minerals that are especially sensitive to climatic influences such as obliquity-driven changes. For example, results from NASA's Curiosity Mars rover indicate that it is possible to obtain high resolution chemostratigraphic climate records from rhythmically bedded sedimentary rocks using in situ measurements – a capability that Mars 2020 is also expected to have (e.g., with SuperCam and PIXL). Analysis of selected returned samples from such *in situ* records would be extremely important in confirming and fully understanding such records. As another example, understanding the relationship between sedimentary rock, regolith and secondary mineral compositions and the contemporaneous atmosphere would also greatly expand our understanding of paleoclimatic conditions on Mars by revealing how the sedimentary record responds to such changes. Finally, there is growing capability of applying a variety of radiometric techniques to dating of the time of sedimentation. Obtaining such dates from climate-sensitive sedimentary sequences would greatly help to constrain the timescales of past climate changes.

**References:**

[1] Vision and Voyages for Planetary Science in the Decade 2013–2022. (2011) National Academies Press. [2]MEPAG E2E-iSAG (2011) Planning for Mars returned sample science: final report of the MSR End-to-End International Science Analysis Group (E2E-iSAG). *Astrobiology* 12:175-230 [3] MEPAG (2015), Mars Scientific Goals, Objectives, Investigations, and Priorities: 2015 at http://mepag.nasa.gov/reports.cfm. [4] A. Steele, F. M. McCubbin, M. D. Fries,. *Meteoritics & Planetary Science* (2016), doi:10.1111/maps.12670. [5] Acuña, M.H. et al. (2008) in *The Martian Surface: Composition, Mineralogy, and Physical Properties*, ed. by J.F. Bell (Cambridge University Press, Cambridge) 242–262. [6] Weiss, B.P. et al (2008) *Geophys. Res. Lett. 35(23)*. [7] Lillis, R.J. et al (2013) *J. Geophys. Res.: Planets 118(7),* 1488-1511. [8] Milbury, C. et al (2012) *J. Geophys. Res. :Planets 117*, E10. [9] Connerney, J.E.P. (2004) *Space Sci. Rev. 111,* 1-32. [10] Mahaffy, P.R. et al. (2015) *Science, 347*, 412-414. [11] Jakosky, B.M. & Phillips, R.J. (2001) *Nature, 412,* 237-244.

**DETECTING ASTROBIOLOGICALLY SIGNIFICANT OCEAN FLOOR SEDIMENTS IN THE TSUNAMI-BATTERED COASTS OF EARLY MARS.** J. A.P. Rodriguez[1], M. Zarroca[2], R. Linares[2], G. Komatsu[3], D. Oehler[1], A. Davila[4], V. Baker[5], D. Bernman[1], Hideaki Miyamoto[6], [1]Planetary Science Institute, Tucson, AZ; alexis@psi.edu; [2]Universitat Autònoma de Barcelona, Barcelona, Spain; [3]Università d'Annunzio, Pescara, Italy; [4]NASA Ames Research Center, Moffett Field, CA; [5]University of Arizona, Tucson, AZ; [6]University of Tokyo, Tokyo, Japan.

**Introduction:** Numerous investigations indicate that, approximately 3.4 Ga, an enormous ocean likely covered most of the Martian northern plains [1-2]. The geological record of sedimentary deposits laid down within this early Mars ocean could help decipher its characteristic types of submarine environments, thereby shedding light on its potential habitability. A major obstacle towards the remote-sensing detection of these purported ocean floor materials, however, is that detailed geologic maps position them within the northern plains buried stratigraphy, most likely beneath the Early Amazonian Vastitas Borealis Formation (VBF, Fig. 1 [3, 4]).

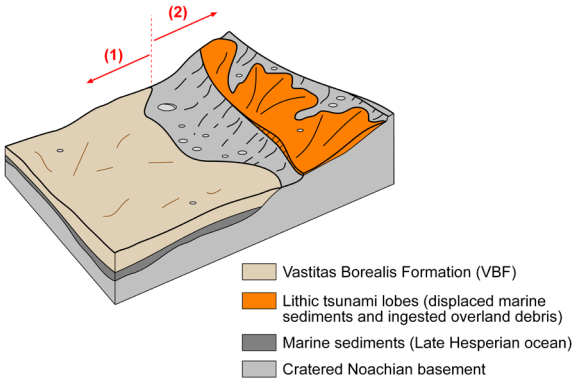


**Fig. 1** Schematic reconstruction of the northern plains (1) and adjoin boundary cratered regions in northwestern Arabia Terra (2). The VBF is depicted as overlying Late Hesperian marine sediments, which in turn lie on the cratered Noachian basement. The adjoinging tsunami debris fields are interpreted to be composed of displaced ocean floor strata intermixed with debris captured during overland flow. The lower boundary of the tsunami lobes represents the paleoshoreline location.

The VBF is thought to consist of an ice-rich geological unit [5, 6], which has been proposed to have initially formed during the ocean's freezing [7]. The unit could still retain some residual marine ice; however, its upper strata have been subject to intense resurfacing driven by numerous episodes of periglacial and aeolian processes [3,7], and thus the precise provenance of its surface lithological character and volatile content remain difficult to determine.

We propose that the recently discovered debris fields, interpreted to have been emplaced by tsunami waves that propagated enormous inland distances [8, 9] might allow access to shored-up ocean floor sediments (Fig. 1). On Earth long run-up tsunami deposits typically include significant lithological overprints generated by debris ingested during the overland propagation [10]. Tsunami deposits consisting exclusively of displaced submarine strata and biomass have been identified draping sizable ridges exposed above sea level [11]. Inspired by this analogy, we considered the Mars ocean paleo-geographic reconstructions developed by Rodriguez et al. [8], in which the paleoshoreline level is set at -3800 m. This analysis highlighted an area of potential tsunami sedimentation as particularly distinctive within the entire surveyed area: an extensive deposit draping over an ocean-facing cape on the outer margin of an enormous bay located in northwestern Arabia Terra (Fig. 2).

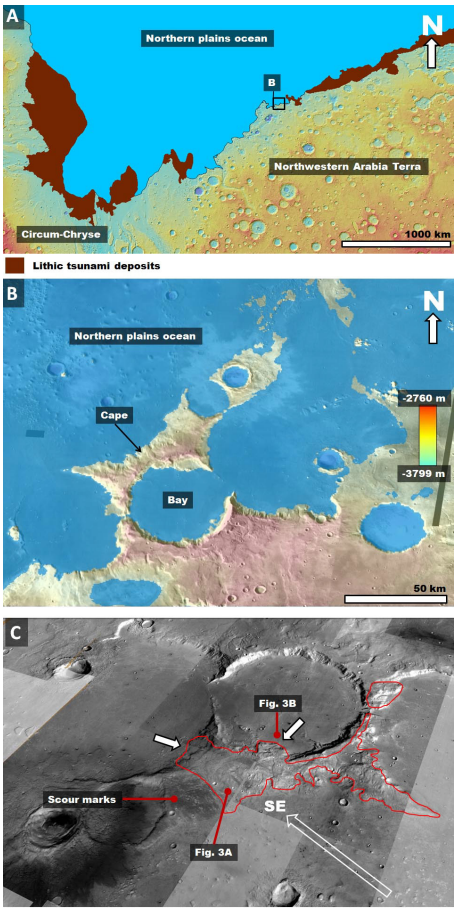

**Fig. 2 (A)** Distribution of lithic tsunami deposits extending from a paleo-shoreline high stand at -3800 m (light blue area) (modified from Rodriguez et al. [8]). **(B)** Paleo-shoreline reconstruction of an area in northwestern Arabia Terra, where we find that a bay would have secluded shallow coastal plains. The paleo-ocean is shown in light blue. **(C)** Perspective view of the bay facing south away from the paleo-ocean and towards the highlands. The red line outlines the extent of the proposed tsunami deposit. The white arrows identify two locations where the deposit overflowed devides and intruded into the bay's interior.

The cape's north-facing side comprises a broad ramp, which is overlain by extensive superposed sedimentary lobes with their frontal margins oriented in the upslope direction (Fig. 3A). The lithic composition of the lobes is indicated by a lack of evidence for ductile deformation, which for a glacial origin would result in flow elongation and topographic relaxation of superposed impact craters. Here, we propose that these sedimentary lobes consist of tsunami materials that were displaced from the ocean floor and deposited as pulses of density flows. The bay's interior floor is flanked by widespread benches that are cut into the interior crater walls as well as the frontal margins of the tsunami lobes (Fig. 3B), indicating that their formation must have post-dated the tsunami event.

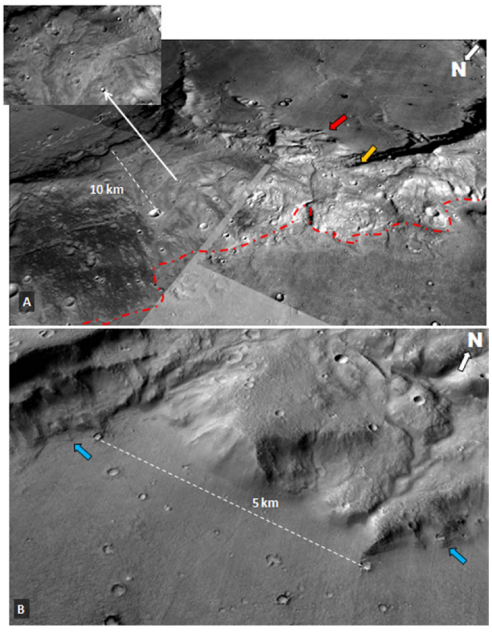


**Fig. 3 (A)** Highland-facing lobes, which locally overflow the crater rim (yellow) and into the bay's interior (red). The dashed red line represents an erosional contact along the deposit's ocean-facing margin, which we propose would have developed due to intense marine erosion following the deposit's emplacement. **(B)** View of an interior area of the bay, where an intruded tsunami flow and adjoining crater walls appear to be cut by terraces (blue arrows). Relative locations shown in Fig. 2C.

Characterizing the potential habitability of early Martian paleo-environments comprises a fundamental goal in ongoing and future space exploration. Here, we propose that interior plains of a bay in northwestern Arabia Terra constitute a landing site candidate of prime astrobiological significance. These plains offer in-situ accessibility to a potentially diverse tsunami-derived and non-tsunami-derived marine geologic record (Fig. 4), which, based on Earth analogues, might contain important, organic biosignatures [12].

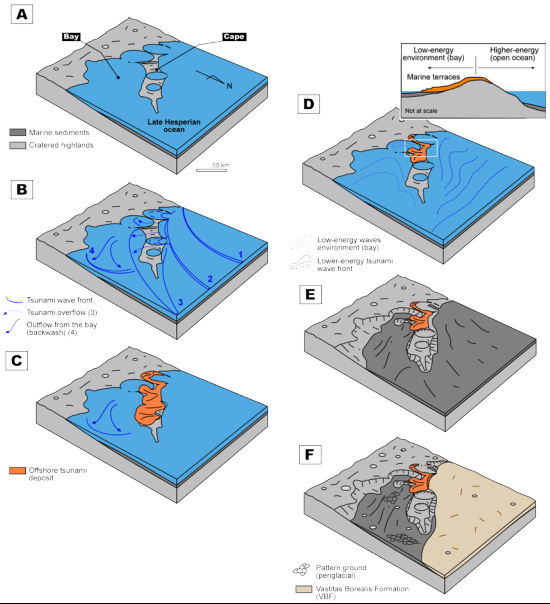


**Fig. 4** Sketches showing paleo-geographic reconstructions leading to the emplacement of the proposed tsunami deposit.

**References:** [1] Parker et al. (1989) Icarus, 82, 111-145. [2] Parker et al. (1993) JGR, 98, 11061-11078. [3] Tanaka et al. (2005) USGS SIM-2888. [4] Tanaka et al. (2014) USGS SIM-3292. [5] Tanaka (1997) JGR, 102, 4131-4149. [6] Mouginot et al. (2012) GRL, 39. [7] Kreslavsky and Head (2002) J. Geophys. Res. 107, 5121. [8] Rodriguez, J. A. P., et al. (2016), Nat. Sci. Rep., 6, 25106, doi:10.1038/srep25106. [9] Costard et al. (2017), J. Geophys. Res. Planets, 122, 633–649.[10] Goto et al. (2012) Marine Geology, 40, 887-890. [11] Ilayaraja and Krishnamurthy (2010). Jour. Coastal Conserv. v. 14 (3), 215-230. [12] Oehler and Allen (2012) SEPM (Society for Sedimentary Geology) Special Publication No. 102 (Sedimentary Geology of Mars), 183-194.

**PROPERTIES, ORIGINS, AND PRESERVATION OF ANCIENT OLIVINE-BEARING BEDROCK: IMPLICATIONS FOR NOACHIAN PROCESSES ON MARS,** A. D. Rogers[1], J. C. Cowart[1], J. W. Head[2], N. H. Warner[3], A. Palumbo[2], and M. P. Golombek[4], [1]Stony Brook University, Stony Brook, NY, USA (deanne.rogers@stonybrook.edu), [2]Brown University, Providence, RI, USA, [3]SUNY Geneseo, Geneseo, NY USA, [4]Jet Propulsion Laboratory, California Institute of Technology, Pasadena, CA, USA

**Introduction and significance:** Many intercrater plains and degraded impact craters in the Noachian highlands contain flat-lying, relatively high thermal inertia (TI) surfaces ("bedrock") that commonly show modest enrichments in olivine and/or pyroxene compared to surrounding materials (**Fig. 1**). These surfaces have maximum TI values above 500 J $m^{-2}$ $K^{-1}$ $s^{-1/2}$ in THEMIS images; some units exhibit TI values well above 900 J $m^{-2}$ $K^{-1}$ $s^{-1/2}$. These physicochemically distinctive units occur in dozens of isolated exposures ranging from ~$2x10^2$ to ~$3x10^4$ $km^2$ in area and exhibit morphologies indicating reduced/minimal sediment mantling. The units lack evidence of fine-scale layering in HiRISE imagery, and also lack evidence of aqueous alteration in spectral data [1-7].

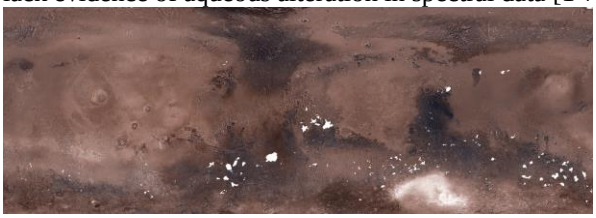

**Fig. 1.** Global distribution of high TI intercrater plains exposures (white) [7]. Surfaces with TES TI values > 325 J $m^{-2}$ $K^{-1}$ $s^{-1/2}$ were delineated using the qualitative THEMIS nighttime radiance mosaic. TI values quoted in text are derived from THEMIS nighttime imagery, from the warmest (least mantled) portions of the delineated bedrock unit.

The origin(s) of these units is uncertain. In past studies, an effusive volcanic origin was generally favored on the basis of the relatively high TI, distinctive composition, and the difficulty of spatially concentrating olivine over such large scales through sediment transport and sorting [1-6,8]. However, the lack of volcanic morphologies (e.g. flow lobes, source vents), as well as the degraded nature of these units and limited vertical exposure makes their origin(s) uncertain.

The widespread, distinctive nature of these units makes them significant; ascertaining their origins, preservation and early modification history is an important aspect of understanding the geological processes and environments that were occurring on early Mars. In this work we present a set of new observations that suggest that some of these Noachian bedrock units may have non-volcanic or non-effusive volcanic origins.

**Observations:** ***1. The bedrock units have not followed the same degradation and regolith development path as known volcanic plains.*** Hesperian volcanic plains have developed a thick regolith [9, 16] and have a notable lack of bedrock exposure compared to Noachian cratered terrains [10]. Even where Hesperian volcanic plains are in direct contact with older bedrock, a striking difference in TI and regolith cover is observed, such that Hesperian plains are more mantled than the older subjacent bedrock units [10] (**Fig. 2**). A candidate explanation for this is that the Noachian bedrock was rapidly buried and then recently exposed [10], however an alternative explanation is that the Noachian bedrock units are mechanically weak/fine-grained materials that break up into fine-grained materials [e.g. 11,12] that are more easily moved by wind. In contrast, competent Hesperian lavas would have comminuted into blocky/coarser-grained, less-mobile materials. Additional examples of high TI (less mantled) units subjacent to Hesperian lavas are observed in Gusev crater [13] and NE Syrtis (**Fig. 3**). In those locations, significantly mantled Hesperian lavas directly abut older, less mantled rock units. In Gusev crater, the older units may represent olivine-bearing basaltic tephras, similar to the Algonquin-class rocks investigated by the Spirit Rover [14]. At NE Syrtis, the older units contain sulfates and aqueously altered basaltic units [15]. Both of these rock types would likely be mechanically weak compared to unaltered basaltic lavas, such as those present in the Hesperian volcanic plains [e.g. 17].

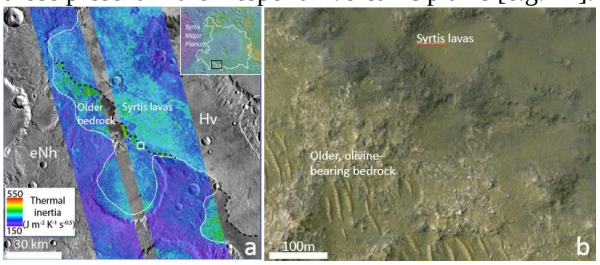


**Fig. 2**. Near the southern margin of Syrtis Major, light-toned toned, basaltic bedrock (higher TI) underlies darker toned basaltic lavas (lower TI). (a)THEMIS TI over THEMIS daytime radiance. (b)Portion of HiRISE image ESP_036579_1795. Light-toned bedrock contains isolated bedforms. Lows within darker-toned Syrtis lavas are covered by sediment.

***2. Quantitative analyses of bulk composition suggest that some olivine-bearing bedrock units are not significantly compositionally distinct from surrounding low TI units.*** Early work examining Noachian bedrock focused on eastern Noachis Terra, where bedrock units are most abundant and exhibit the highest TI values [2,4]. There, many bedrock surfaces are clearly compositionally distinct (more mafic bulk mineralogy) from the surrounding low TI plains, crater walls and ejecta, confirmed by spectral extraction and comparison for some of the regions. We have extended these analyses to bedrock

units in other highland locations, and find that some units are not spectrally distinct from surrounding materials (e.g. [7], **Fig. 4**).

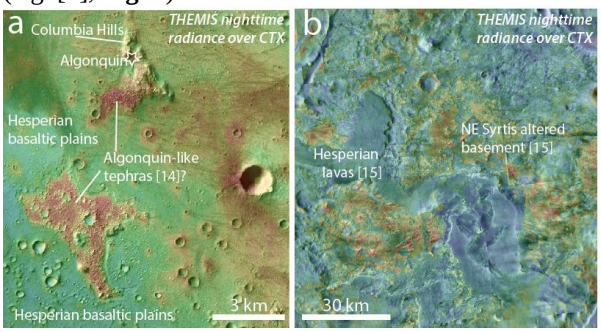


**Fig. 3**. Examples where Hesperian lavas abut older, likely mechanically weak materials (see text). (a) Gusev (b) NE Syrtis. The differences in surface TI expression may result from differences in friability.

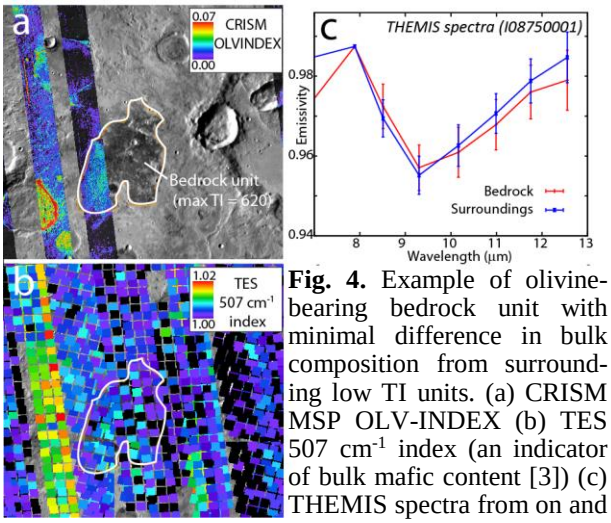


**Fig. 4.** Example of olivine-bearing bedrock unit with minimal difference in bulk composition from surrounding low TI units. (a) CRISM MSP OLV-INDEX (b) TES 507 $cm^{-1}$ index (an indicator of bulk mafic content [3]) (c) THEMIS spectra from on and off the bedrock unit.

**Discussion:** The observations discussed above indicate that *some* olivine-bearing bedrock units may represent mechanically weak materials, such as sedimentary or pyroclastic units. True thermal inertia values from these units would help to address this question; for example, Mini-TES derived thermal inertia values from individual blocks at Gusev crater showed that Adirondack class (Hesperian) basalts exhibited TI values of ~1200 J $m^{-2}$ $K^{-1}$ $s^{-1/2}$, whereas Columbia Hills rocks exhibited values around ~600 J $m^{-2}$ $K^{-1}$ $s^{-1/2}$ [18]. However, locating THEMIS pixels with fully unmantled exposures is a challenge. Detailed thermal modeling using THEMIS images spanning multiple times of day are underway to constrain underlying bedrock TI of these units [19].

Where the differences in bulk primary mineralogy between the bedrock and surrounding low TI materials is minimal, a sedimentary origin remains a strong explanation for these materials; however, lithification must have occurred with minimal amounts of water, as aqueous minerals are not observed in these units. Units significantly different in bulk composition from surroundings likely require a volcanic (effusive or pyroclastic) or other explanation. One such hypothesis is described below.

The influence of large Noachian-aged impact cratering events [20-21] has recently been revisited and the timeline of events and geological effects updated in order to understand the climatic implications for early Mars [22-23]. For basin-scale impact events, the vaporized silicate portion of the expanding vapor plume should be globally and homogeneously distributed and is predicted to condense out at very high temperatures and fall as hot spherules to the surface; the deposit will initially be sufficiently hot that it is likely to behave as rheomorphic flows, filling low-lying areas before final cooling and solidification. On the basis of this analysis, [22] suggest that an alternative interpretation to extrusive volcanism for Noachian-aged mafic silicate layers may be that of exposed remnants of silicate condensate layers of Noachian large craters and basins, with mineralogies representing crust and possible mantle contributions processed by the impact and vapor plume evolution, and subsequent silicate condensate layer emplacement [22-23]. We are currently further assessing this as one of our hypotheses for the origin of these high TI Noachian surfaces.

**Concluding remarks:** Intercrater plains bedrock units are variable in composition and morphology, and probably have different origins [e.g. 8,22,24]. The preservation and aeolian exposure history of these units is likely a key factor in their spatial distribution and in giving rise to their relatively high TI values compared to average values for low-dust regions. A close examination of the properties of each exposure is underway [7].

**Acknowledgments:** Thanks to Steve Ruff for useful discussions. This work was supported by NASA MDAP NNX14AM26G.

**References:** [1] Edwards et al., (2009), JGR 114, E11001 [2] Rogers et al. (2009) Icarus, 200 (2) 446-462 [3] Rogers and Fergason (2011), JGR 116(E8), 1–24 [4] Rogers and Nazarian (2013), JGR 118, 1-19. [5] Ody et al. (2012), JGR, 118, 1-29. [6] Edwards, C.S, et al. (2014), Icarus, 228, 149-166 [7] Cowart and Rogers (2017), 48th LPSC, Abs. 1547 [8] Rogers and Edwards (2016), GSA abstracts, doi: 10.1130/abs/2016AM-286571 [9] Warner et al., (2017) Space Sci Rev (2017). doi:10.1007/s11214-017-0352-x [10] Rogers and Head (2017), 48th LPSC, Abs. 1347 [11] Malin and Edgett (2000), Science, 290, 1927-1937 [12] Golombek et al. (2006), JGR, 111, E12S10 [13] Grant et al. (2006) GRL, 33, 2-7. [14] Ruff et al., (2014) Geology, 42, 359-362. [15] Ehlmann and Mustard (2012), GRL, 39, 1-7 [16] Golombek et al. (2006), JGR, 111, 1-27. [17] Thomson et al (2013), JGR, 118, 1233-1244 [18] Fergason et al. (2016), JGR, 111, E02S21 [19] Ahern et al. (2017), 48th LPSC, Abs. 2337 [20] Segura et al. (2002) Science, 298, 277-280 [21] Toon et al. (2010), Ann Revs., 38, 303-322 [22] Palumbo and Head (2017), Impact Cratering as a Cause of Climate Change, Surface Alteration, and Resurfacing During the Early History of Mars, M&PS, in revision [23] Palumbo and Head (2017), 8th Moscow SSS. [24] Salese et al. (2016), JGR: Planets, 121, 2239–2267

**WATER VOLUME REQUIERD TO CARVE THE MARTIAN VALLEY NETWORKS: UPDATED SEDIMENT VOLUME.** E. N. Rosenberg[1,2], J. W. Head[2], J. Cassanelli[2], A. Palumbo[2], and D. Weiss, [1]Department of Physics, Cornell University, Ithaca, NY 14850 (enr27@cornell.edu), [2]Department of Earth, Environmental and Planetary Science, Brown University, 324 Brook St., Providence, RI 02912 (james_head@brown.edu).

**Introduction:** The martian valley networks (VNs), the majority of which date to the late Noachian [1], demonstrate that the climate of Mars was once capable of supporting flowing liquid water. Some authors cite the VNs as evidence that the climate of Mars was once warm and earthlike, with regular rainfall and a vertically integrated hydrological system [e.g. 2,3]. However, climate models [e.g. 4,5] predict a cold and icy early Mars, in which water ice is preferentially deposited in the highlands, and the peak daytime temperatures remain below the melting point of water [6]. In this scenario, punctuated events, such as large impacts [7] or volcanic eruptions [8] are required to melt the ice [9] and form the VNs.

To distinguish between these climate scenarios, we estimate the cumulative volume of water that was required to erode the VNs. Specifically, we use the updated VN cavity volume measurement of [2] and the methods of [10] to convert this cavity volume to a water volume.

**Methods and Discussion:** Following [10], we estimate the volume of water required to carve the VNs as $V_w = V_s\, Q_f/Q_s$, where $V_s$ is the sediment volume and $Q_f/Q_s$ is the ratio of the fluid flux to the sediment flux in a flow carving the VNs. As in [10], we estimate $Q_f/Q_s$ from empirical measurements made on Earth [11] to be 30 – 1000. The sediment volume, in turn, is related to the volume of the observed VN cavities by $V_s = (1-\lambda)V_c$, where $\lambda$ is the porosity of the regolith that was eroded away to form the VNs and $V_c$ is the VN cavity volume. The porosity is constrained between ~ 0.2 – 0.4 [12,13], and, based on the mapping of [14], Luo et al. [2] use MOLA data to calculate the VN cavity volume to be $(1.74 \pm 0.8)\times10^{14}$ m$^3$, a factor of $7.3 \pm 3.3$ larger than the VN cavity volume used in [10] (the volume of the eight large VNs studied by [15]), but which agrees with the volume ($\sim1.52\times10^{14}$ m$^3$) obtained by multiplying the average transverse VN cross sectional area calculated from the MOLA measurements of [16] ($\sim1.88\times10^{5}$ m$^2$) by the total length of the VNs in the mapping of [14] (807,000 km). Using the cavity volume of [2], the fluid/sediment flux ratio of [10], and the full range of possible porosities (0.2 – 0.4), we estimate that at least 12 – 1800 m GEL of water was required to erode the VNs. This is a cumulative volume of recycled water and is not simply related to the global inventory of water. In particular, this volume of liquid water need not have existed on the surface of Mars at any one time.

*Minimum timescale of formation.* By assuming a VN channel width (not valley width) of ~280 m, Rosenberg and Head [10] calculate that cumulative fluid flux through the eight VNs studied by [15] is $4.4\times10^{4}$ m$^3$/s. Scaling this as $Q_{f,\text{total}} \approx Q_{f,8\text{ largest}} \frac{V_{c,\text{total}}}{V_{c,8\text{ largest}}}$, where $V_c$ refers to cavity volume, leads to a total fluid flux through the VNs of $(1.8-6.0)\times10^{5}$ m$^3$/s. Assuming a constant bankfull flux through the VNs, we estimate the minimum time to carve the VNs as $10^2 - 10^4$ Earth years. The acual time to form the VNs is likely much longer because of the intermittency of bankfull flow.

**Climatic Implications:** Previously, Luo et al. [2] estimated that at least ~5 km GEL of water were required to erode the VNs. However, our results indicate that the VNs could have been eroded with as little as 12 – 1800 m GEL of water. This overlaps with the estimation (3 – 100 m GEL) of [10]. The surface/near surface inventory of ice water in the Noachian is estimated to be ~24 m [17]. Thus, our results are consistent with the VNs being formed during punctuated melting events, each lasting a short geological timescale and causing a significant fraction of the planetary water inventory to flow through the VNs at bankfull width. However, our results cannot rule out a warm and wet early Mars.

**References:** [1] Fassett C. I. and Head J. W. (2008) *Icarus, 195*, 61–89. [2] Luo W. et al. (2017) *Nat. Commun., 8*, 15766. [3] Craddock R. A. and Howard A. D. (2002) *JGR-Planet., 107*, 21.1–21.36. [4] Wordsworth R. et al. (2013) *Icarus, 222*, 1–19. [5] Forget F. et al. (2013) *Icarus, 222*, 81–99. [6] Head J. W. and Marchant D. R. (2014) *Antarct. Sci., 26*, 774–800. [7] Segura T. L. et al. (2008) *JGR-Planet., 113*, E11007. [8] Halevy I. and Head J. W. (2014) *Nat. Geosci., 7*, 865–868. [9] Fastook J. L. and Head J. W. (2015) *Planet. Space Sci., 106*, 82–98. [10] Rosenberg E. N. and Head J. W. (2015) *Planet. Space Sci., 117*, 429–435. [11] Cleveland T. G. et al. (2013) Texas DOT Tech. Report. Project 0-6549. [12] Kleinhans M. G. (2005) *JGR-Planet., 110*, E12003. [13] Clifford S. M. (1993) *JGR-Planet.*, 10973–11016. [14] Luo W. et al. (2009) *JGR-Planet., 114*, E11010. [15] Hoke M. R. et al. (2011) *Earth Planet. Sc. Lett., 312*, 1–12. [16] Williams R. M. E. and Phillips R. J. (2001) *JGR-Planet., 106*, 23737–23751. [17] Carr M. H. and Head J. W. (2015) *JGR, 42*, 726–732.

**INVESTIGATING THE FLOOR OF PALEOLAKE JEZERO BY WAY OF GUSEV CRATER.** S. W. Ruff[1], [1]Arizona State University, School of Earth and Space Exploration, Tempe, AZ 85287-6305, steve.ruff@asu.edu.

**Introduction:** Gusev crater was selected as the landing site for the Spirit rover because of features indicative of an ancient lake, including the ~900 km long Ma'adim Vallis channel system entering the crater, and the landforms at its entry point originally thought to represent an eroded delta [e.g., 1]. On the floor of Gusev, Spirit encountered olivine-rich basaltic rubble, subsequently recognized as the remnants of low viscosity lava flows that spread across the floor ~3.65 billion years ago [2]. An earlier geologic history is preserved in higher-standing terrains that were embayed by the lava flows, including the Columbia Hills, which represent a kipuka or island of older terrain fully encircled by lava. The carbonate-rich outcrops there are perhaps the remnants of an evaporating lake in Gusev crater [3].

Jezero crater is the leading candidate site for the Mars 2020 rover mission because of evidence that it once hosted a lake, including an eroded fan deposit that is confidently interpreted as a fluvial delta [4]. Although the evidence for a lake is robust, much of the floor of Jezero displays basaltic mineralogy in terrain interpreted as a volcanic capping unit [5; 6]. This unit shares similarities with the basaltic floor of Gusev crater, but comparisons between the two have not been explored previously. Here I present observations from the two craters that highlight the similarities and differences of their respective volcanic floor units, with implications for the stratigraphy and geologic history of Jezero crater.

**Observations:** Lobate margins and kipukas are evident on the floor of both craters (Fig. 1), consistent with an interpretation of the volcanic floor unit (VF; [6]) in Jezero resulting from flowing lava. The kipukas at both sites include examples where the original higher-standing terrain is still present; is eroded below grade; or has been removed altogether. Where still present, such kipukas can show both an onlapping relationship with the embaying lava flows and a marginal depression or moat, the result of erosion of the higher-standing terrain after embayment. Such characteristics are displayed by the Columbia Hills, offering ground truth for comparisons elsewhere.

A small kipuka ~12 km from the Columbia Hills displays a prominent moat fully encircling higher-standing terrain of varying morphology . This kipuka is comparable in size to mounds on the floor of Jezero previously mapped as outliers of the delta deposits and described as "kipuka-like" [5] (Fig. 2). However, they lack a moat feature akin to that of the comparably-sized Gusev kipuka. An onlapping relationship is a possible explanation, but the lack of a prominent moat among any of these mounds implies that none has experienced erosion sufficient to open a gap between the mound sediments and the embaying volcanic unit. This could arise if the rate of erosion of the volcanic unit either keeps pace with or outpaces that of the mound sediments. Similarly, the contact between the VF and the main delta escarpment shows no prominent moat along its entire length, perhaps for the same reason.

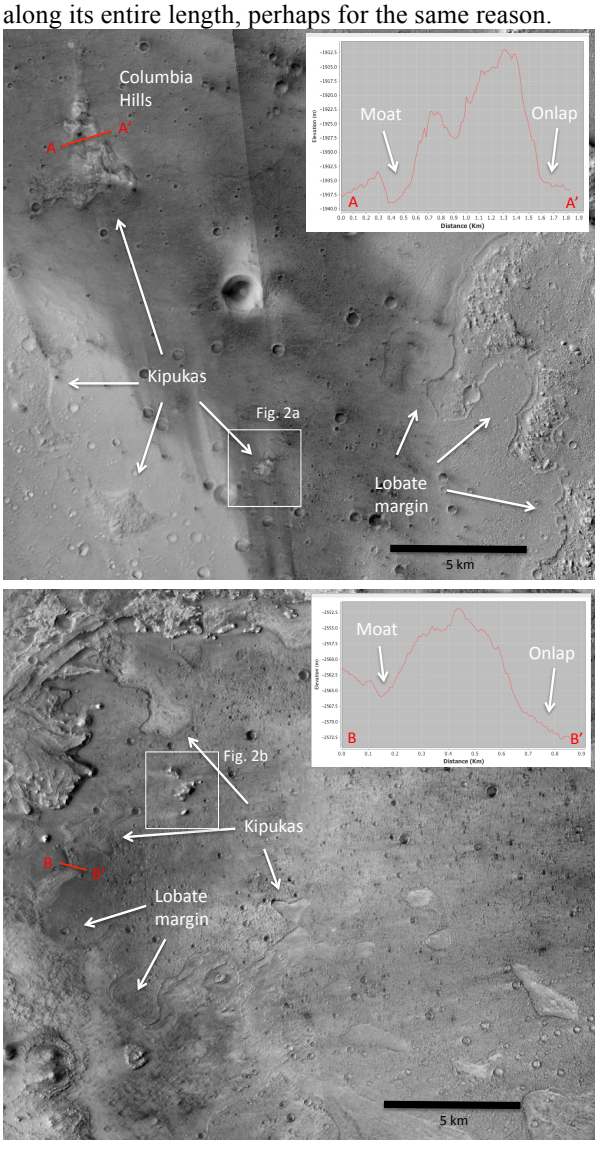


**Figure 1.** Comparison of common features on the floor of Gusev crater (top) and Jezero crater (bottom) shown in CTX mosaics. Insets show HiRISE DTM-based elevation profiles across a kipuka in both craters.

It is noteworthy that the only examples of kipukas in Jezero that display a prominent moat are associated with material described as the light-toned floor unit (LTF), which is highly fractured and shows spectral evidence for carbonate [6]. So the presence of prominent moats among kipukas of LTF and not the delta deposits may indicate that the former is more easily eroded.

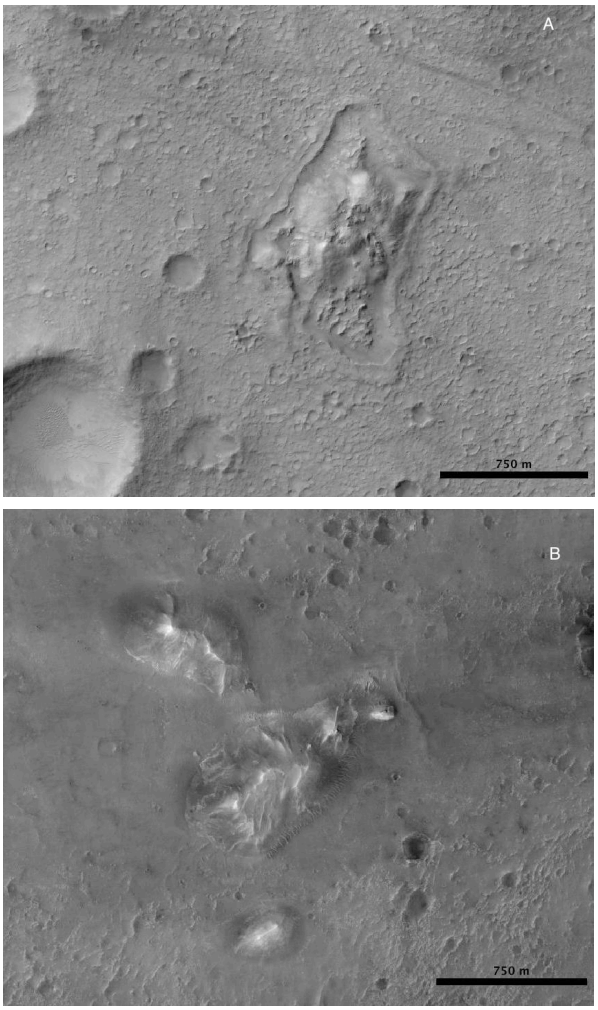


**Figure 2.** Comparison of a small kipuka in Gusev (A) and candidate kipukas of similar size in Jezero (B). The mounds in **B** lack a prominent moat like in **A**.

**An Alternative Hypothesis:** The lack of any prominent moats among the delta deposits contrasts with the style of embayment of LTF in Jezero as well as rock units in Gusev. This raises the possibility that the delta deposits are not actually embayed by VF but instead were deposited on top of it. In this scenario, the contacts between VF and delta deposits are erosional; the delta deposits are being stripped off of VF. This obviates the requirement that the delta sediments erode at the same rate or more slowly than VF in order to maintain the apparent topographic relationship.

**Conclusions:** The volcanic floor unit of Jezero crater displays features analogous to those on the floor of Gusev that resulted from emplacement of low viscosity basaltic lava flows. Unequivocal examples of kipukas in both craters attest to a history of emplacement and erosion of various rock units prior to embayment by lava. The embayment of the delta deposits by lava flows in Jezero is equivocal, demonstrating the need for further investigation.

**References:**

[1] Cabrol, N. A., et al. (2003), J. Geophys. Res., 108, E12, doi:10.1029/2002JE002026,
[2] Greeley, R., et al. (2005), J. Geophys. Res., 110, E05008, 10.1029/2005JE002401.
[3] Ruff, S. W., et al. (2014), Geology, 42, 4, 359-362, 10.1130/G35508.1.
[4] Goudge, T. A., et al. (2017), Earth Planet. Sci. Lett., 458, 357-365, 10.1016/j.epsl.2016.10.056.
[5] Schon, S. C., et al. (2012), Planet. Space Sci., 67, 28-45, 10.1016/j.pss.2012.02.003.
[6] Goudge, T. A., et al. (2015), J. Geophys. Res., 775-808, 10.1002/2014JE004782.

**GLACIAL MELTWATER AS A SOURCE OF AMORPHOUS SILICA ON EARLY MARS** A. M. Rutledge[1], B. Horgan[1], J. R. Havig[2], E. B. Rampe[3], N. A. Scudder[1], and T. L. Hamilton[4], [1]Dept. of Earth, Atmospheric and Planetary Sciences, Purdue University (alicia.rutledge@gmail.com), [2]Dept. of Earth Sciences, University of Minnesota, [3]NASA Johnson Space Center, [4]Dept. of Plant and Microbial Biology, University of Minnesota.

**Introduction:** New results show that cold-climate silica cycling is more efficient than previously reported, and is the dominant weathering process in glaciated mafic volcanics. Based on field work at glaciated volcanic sites, we hypothesize that this is due to a combination of high rates of silica dissolution from mafic bedrock and reprecipitation of silica in the form of opaline silica coatings and other poorly crystalline silicate alteration phases. Widespread evidence for past and present-day glaciation on Mars [1-4] means that this cycle must be investigated in order to better interpret silica deposits on the surface of Mars [5-9]. Amorphous silica in some settings on Mars could be interpreted as mineralogical evidence for alteration by glacial meltwater.

**Field study:** To investigate melt-driven silica cycling on mafic volcanic bedrock, water and rock samples were collected during June 2015 and July 2016 from glaciated volcanic bedrock in the Cascade Volcanic Arc: Mount Adams (46º9'N, 121º27'W), Mount Hood (45º21'N, 121º42'W), Middle Sister (44º9'N, 121º46'W) and North Sister (44º10'N, 121º47'W). Dominant bedrock compositions for each site are detailed in Table 1. Evidence for subglacial precipitation of poorly crystalline silica was found at North and Middle Sisters in the form of striated rock coatings with greasy lustre on recently deglaciated lava flows (Fig 1) [10] and in a silica-enriched poorly crystalline component of glacial flour from moraine deposits [11].

**Results:** Figure 1 shows a representative thermal infrared spectrum of a sampled rock coating. It exhibits similar absorptions to opaline silica and an Al-Si gel, indicating that it is composed primiarly of microcrystalline silica. Figure 2 details the mean glacial outwash stream silica concentrations, as measured from water samples. Within each field site, proglacial streams, springs, and lakes exhibit dissolved silica concentrations that are greater than observed in glacial snow/ice. The highest silica concentrations were measured in moraine-sourced springs.

*Silica cycling in terrestrial glacial systems* The high rate of bedrock comminution in subglacial environments results in high rates of both chemical and physical weathering, due to the increased reactive mineral surface area formed through glacial grinding. In most bedrock types, carbonate weathering is enhanced and silica fluxes are depressed in glacial outwash compared with global average riverine catchment runoff due to low temperatures and short residence times [12]. However, in mafic systems, higher dissolved $SiO_2$ concentrations have been observed [13-15]. Additionally, remote sensing has identified high-silica zones in proglacial outwash plains on mafic bedrock [16].

*Water composition.* The major difference between glacial alteration of volcanic bedrock and more typical continental terrains is the absence of significant dissolved carbonate in the former. In the absence of carbonate minerals which normally dominate dissolution processes at glacier beds [12], carbonation of feldspar can become the dominant weathering process [13]:

$$CaAl_2Si_2O_{8(anorthite)} + 2CO_{2(aq)} + 2H_2O_{(l)} \Leftrightarrow Ca^{2+}_{(aq)} + 2HCO_3^-{}_{(aq)} + H_2Al_2Si_2O_{8(s)weathered\ feldspar} \quad (1)$$

This reaction coupled with further alteration can result in a high proportion of dissolved silica fluxes in glacial outwash waters compared to the total cation flux. It is thought to be the dominant reaction in volcanic systems due to the lack of carbonate mineral dissolution, which would otherwise quickly saturate the aqueous system. Mafic volcanic rocks are particularly susceptible to silica mobility, due to the high concentration of soluble minerals (i.e. plagioclase) as compared to the high concentration of insoluble quartz found in felsic rocks [17].

*Subglacial deposits.* Silica concentrations are measured from glacial outwash samples, and thus reflect only the dissolved silica that is actively removed from the subglacial environment. Based on multiple observations of subglacially precipitated silica phases, we hypothesize that subglacial precipitation of silica-rich secondary minerals likely contributes to lowering silica fluxes in glacier outwash waters [18]. Subglacially-deposited silica coatings have been observed at mafic volcanic glacial margins [10,19], subglacially-sourced fluvial deposits in basaltic terrain in Iceland were found to have a poorly crystalline silica alteration component [20], and new analyses of mafic glacial flour appear to include a silica-rich poorly crystalline alteration phase [11,21]. Thus, dissolved silica concentrations in subglacial zones are most likely greater than measured in glacial outwash studies.

**Discussion:** This field study demonstrates that more mafic glaciovolcanic sites have, on average, higher concentrations of dissolved silica compared to more felsic glaciovolcanic sites (Figure 2). Though basalts have lower $SiO_2$ content than more felsic volcanic rocks, they are more susceptible to silica mobili-

ty due to their higher content of minerals such as olivine, pyroxene, and plagioclase, which are more soluble than quartz [17].

*Applications to early Mars* The significant effect of water and ice on the surface of Mars is well documented [1]. Chemical and mineralogical evidence strongly indicates aqueous alteration on Mars [5], and atmospheric modeling shows evidence of a "cold and icy" early Mars [3]. Some studies have proposed an early Mars dominated by widespread glaciation with transient melting [4]. Poorly crystalline phases should be a major product of snowpacks and localized wet margins of the ice sheet [22]. Additionally, silica is thought to be highly mobile on the surface of Mars [17]. Poorly crystalline silica deposits should thus not be interpreted as only hydrothermal; rather, morphology and context should be used to rule out an origin related to glaciers or alteration of glacial sediments.

Widespread poorly crystalline, high $SiO_2$ deposits have been modeled in Nothern Acidalia [5], consistent with low-T weathering of volcanic glass. Hydrated silica deposits have been identified in Valles Marineris [6], Nili Fossae [7], and Hellas Basin [8]. Additionally, poorly crystalline silicates have been identified as a major component of rock coatings in Gusev Crater [9]. We hypothesize that these phases may be indicators of a cold and/or rarely wet climate regime on early Mars such as one dominated by large regional ice sheets [3, 22]. So far, these detections correspond to Hesperian and Amazonian terrains, suggesting that poorly crystalline phases could be less common in Noachian terrains, especially compared to the large number of detections of crystalline clays [22]. The presence or absence of poorly crystalline phases in Noachian terrains could be tested *in situ* by the upcoming Mars 2020 rover.

**Conclusions:** Melt-driven silica cycling on low-carbonate, mafic rocks may be more important than previously thought, especially on early Mars. This cycle is most likely driven by the lack of immediately available carbonate minerals resulting in silicate-dominated weathering reactions, relatively high water-rock ratios, and/or long residence times.

**References:** [1] B.L. Ehlmann et al (2011) *Nature, 479*, 53-60. [2] J. Levy, J. (2014) *JGR, 119*, 2188-2196. [3] F. Forget et al. (2013) *Icarus, 222*, 81-99. [4] J.W. Head et al. (2014) *LPS XLV*, Abstract #1412. [5] E.B. Rampe et al. (2012) *Geology, 40*, 995-998. [6] R.E. Milliken et al. (2008) *Geology, 36*, 847-850. [7] B.H. Ehlmann et al. (2009) *JGR, 114*, E2. [8] J.L. Bandfield (2008) *GRL, 35*, 12. [9] S.W. Ruff & V.E. Hamilton (2013) *LPS XLIV*, Abstract #1753. [10] N.A. Scudder et al. (2016) *6th Mars Polar*, Abstract #6093. [11] R.J. Smith et al. *LPS XLVIII.* [12] S.P. Anderson et al. (1997) *Geology, 25*, 399-402. [13] J.C. Yde et al. (2005) [14] S. Gíslason et al. (1996) *Am. J. Sci, 296*, 837-907. [15] C.R. Cousins et al. (2013) *J. Volc. Geotherm. Res., 256*, 61-77. [16] A.M. Rutledge et al. (2016) *6th Mars Polar*, Abstract #6083. [17] S.M. McClennan (2003) *Geology, 31*, 315-318. [18] J.W. Crompton et al. (2015) *J. Glaciology, 61*, 1061-1078. [19] B. Hallet (1975) *Nature, 254*, 682-683. [20] C.R. Cousins (2015) *Life, 5*, 568-586. [21] Rampe et al. *LPS XLVIII*. [22] B. Horgan et al. (2017) *this meeting*. [23] W. Hildreth et al. (2012) *USGS Sci. Invstgs. Map* 3186

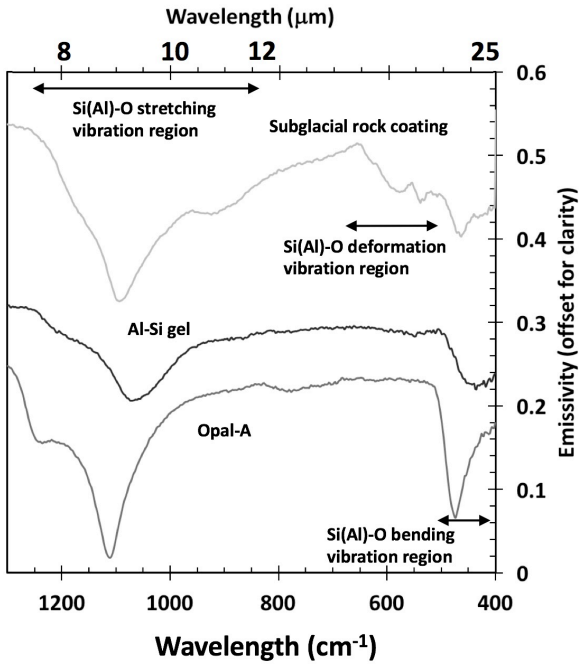


***Figure 1.*** *Rock sample measurement: representative TIR lab spectrum of subglacial rock coating exhibits similar absorptions to Al-Si gel and opaline silica.*

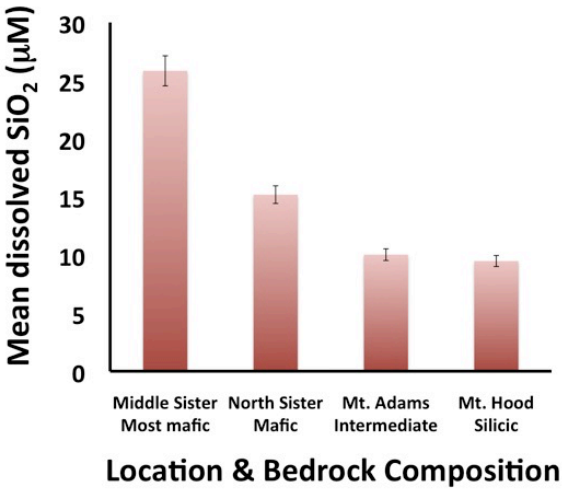


***Figure 2.*** *Bedrock composition vs. dissolved silica in meltwater at field sites. Data from [16, 22, 23].*

**Ion escape processes of Mars with a weak intrinsic magnetic field.** S. Sakai[1], K. Seki[1], N. Terada[2], H. Shinagawa[3], T. Tanaka[3,4], and Y. Ebihara[5]
[1]Graduate School of Science, University of Tokyo, [2]Graduate School of Science, Tohoku University, [3]National Institute of Information and Communications Technology, [4]International Center for Space Weather Science and Education, Kyushu University, [5]Research Institute for Sustainable Humanosphere, Kyoto University.

**Introduction:** Mars has a thin atmosphere consisting mainly of $CO_2$ and does not have liquid water on the surface in the present day. The latest space missions provided some evidences for existence of liquid water on ancient Mars, and suggested that Mars has experienced much atmospheric loss from the past through the present. One of the important mechanisms of the atmospheric loss is the ion escape from the ionosphere or the upper atmosphere. The ion escape is largely controlled by the solar conditions such as solar wind parameters and solar XUV (X-ray and extreme ultraviolet) irradiances, and magnetic-field configuration. A previous numerical simulation indicated that the ion escape rate was at most five orders of magnitude higher under the past active solar condition than under the present ones [1].

The planetary magnetic field is also an important factor in determining the ion escape rate. Present-day Mars does not have an intrinsic magnetic field, but it is leaving the magnetism in its crust, which is called as the crustal magnetic field. The existence of crustal magnetic field suggests that Mars had a global magnetic field of interior origin in the past and the escape mechanism was quite different from the present.

We present preliminary results of the ion escape process varying due to different strengths of the intrinsic magnetic field of Mars.

**Modeling:** A three-dimensional multi-species magnetohydrodynamics (MHD) modeling is applied to the simulation. This model was originally constructed for the modeling of an unmagnetized object [2], and afterwards improved for the Earth's magnetosphere and the planetary ionospheres [1][3][4]. The model solves a set of MHD equations for eight variables ($\rho$, $M_x$, $M_y$, $M_z$, $B_x$, $B_y$, $B_z$, and $e$), as well as additional continuity equations for ionospheric ion densities ($\rho_i$ and $i$ for up to fourteen ion species including $CO_2^+$, $O_2^+$, $O^+$, and $H^+$), where $\rho$ and $e$ are the mass and energy densities, and $M_{x,y,z}$ and $B_{x,y,z}$ are the momentum and magnetic field components, respectively. Input parameters are needed in order to solve the MHD equations. We use the neutral profiles based on the Viking observations, the solar wind (s/w) density of 3 $cm^{-3}$, s/w velocity of 450 km/s, and the Parker-spiral types of interplanetary magnetic field (IMF) of 2 nT as inputs [1]. The simulations are performed for the two different magnetic fields with (case 1) only the IMF and (case 2) the IMF and dipole field of 100 nT on the equatorial surface of the planet.

**Results:** The shape of the magnetosphere appears to be hybrid between the magnetosphere with strong dipole field such as Earth and the induced magnetosphere with no dipole field such as present-day Mars, when dipole field of 100 nT at the equatorial surface is considered. Figure 1 shows the simulation results of magnetic filed lines (white) and the IMF (right blue) in the case 2. The east-west component of magnetic field is predominant at the subsolar point due to the penetration of the IMF draped field into the ionosphere rather than the north-south component of the global dipole field. On the other hand, the dipole magnetic field dominates the tail region of the magnetosphere. Figure 2 shows the total flux of $O^+$ and $O_2^+$ on the $y$-$z$ plane at $x$ = -5 $R_M$ ($R_M$: Martian radii) of the Mars-centered Solar Orbital (MSO) coordinate system, and white dashed lines shows the magnetic neutral sheet of $B_x = 0$. The plasma sheet is on the $x$-$z$ plane in the case 1, while it is on the $x$-$y$ plane although it has a little inclinations in the $y$-$z$ plane in the case 2 (white dashed lines of Figure 2).

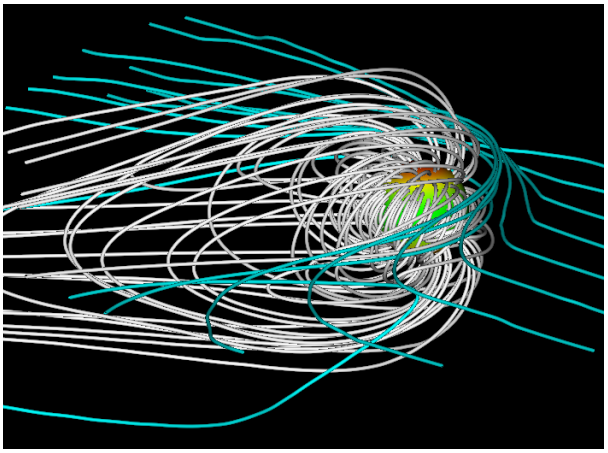

**Figure 1.** The magnetic field lines calculated under the dipole magnetic field of 100 nT at the surface of the planet (white) and the draped IMF (right blue).

The ion escape flux is obtained from the ion densities and velocities calculated. In the case 1, the flux has a peak near the center of the figure (Figure 2a). It suggests the ions created around Mars are flowing down to the tail. In contrast, in the case 2 the total flux has four peaks on the $y$-$z$ plane (Figure 2b). Two of them are located in the magnetic neutral sheet (a white dashed line of Figure 2b), and the others are in the higher latitudes. These results show that the difference of magnetic configuration significantly changes the ion escape flux and mechanism. The sunward flow is also found around the center in the case 2 (a black part of Figure 2b), but this only appears wihin 7 $R_M$.

**Discussion and Conclusion:** The four-peak structure of flux in the case 2 is brought by the magnetosphere, which is formed by the interaction between the assumed solar wind and global dipole field. The two peaks in the high latitude are associated with the cusp region. The

other two peaks are seen in the flank region of plasma sheet and yielded by the comprex reconnection between the dipole field and the IMF around the the magnetosheath. Inclined plasma sheet in the *y*-*z* plane is similar to that observed at Earth under existence of the positive IMF $B_y$ [5]. The return flow seen within 7 $R_M$ is driven by the viscous-cell like convection.

Comparisons between the two cases suggest that the ion tailward flux increases by the magnetization of the planet, and ions particularly escape through four channels in the magnetotail. This could result in the ion escape rate from the upper atmosphere enhanced. We will discuss formation mechanisms of the four escape channels in more details.

**References:** [1] Terada N. et al. (2009) *Astrobiology, 9,* 55–77. [2] Tanaka T. (1993) *JGR, 98,* 17251–17262. [3] Tanaka T. (1998), *EPS, 50,* 259-268. [4] Terada N. et al. (2009) *JGR, 114,* A09208. [5] Tsyganenko and Fairfield (2004) *JGR, 109*, A03218.

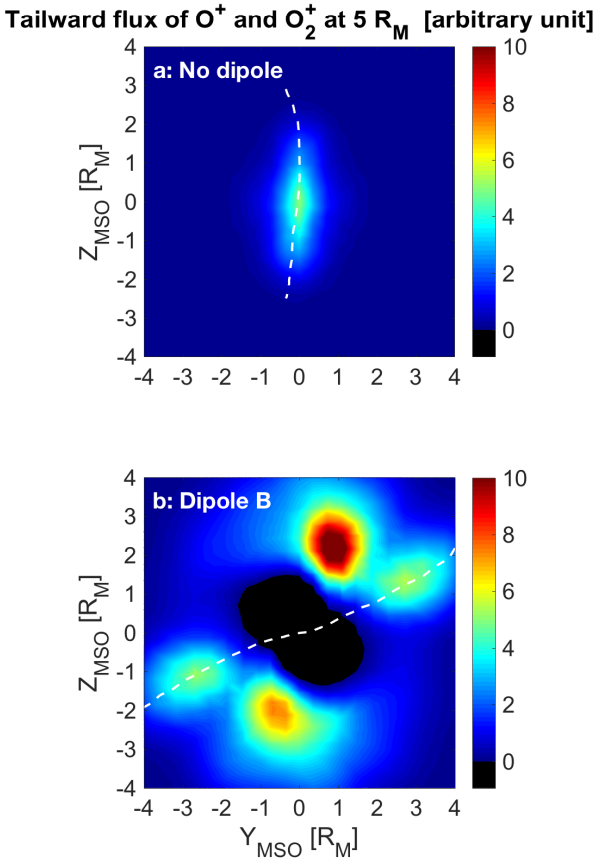


**Figure 2.** The total ion flux of $O^+$ and $O_2^+$ in the two different magnetic fields with (a) IMF and (b) IMF and dipole magnetic field of 100 nT on the equatorial surface on the *y*-*z* plane at $x$ = -5 $R_M$ of the MSO coordinate system. The white dashed line shows the magnetic neutral sheet of $B_x$ = 0.

**BULK MINERALOGY OF THE NORTHEAST SYRTIS AND JEZERO CRATER REGIONS OF MARS DERIVED THROUGH THERMAL INFRARED SPECTRAL ANALYSES.** M. Salvatore[1], T. Goudge[2], M. Bramble[3], C. Edwards[1], J. Bandfield[4], E. Amador[5], J. Mustard[3], and P. Christensen[6]. [1]Dept. of Physics & Astronomy, Northern Arizona University, mark.salvatore@nau.edu, [2]University of Texas at Austin, [3]Brown University, [4]Space Science Institute, [5]University of Washington, [6]Arizona State University.

**Introduction:** Jezero crater, its watershed, and the NE Syrtis region of Mars (hereby referred to as NW Isidis) are home to several candidate landing sites for future missions to Mars. Situated within the Nili Fossae troughs and between the Isidis impact basin and the basaltic flows from the Syrtis Major shield volcano, this region contains some of the most diverse and distinctive spectral signatures observed with visible/near-infrared (VNIR) orbital datasets [e.g., 1-6]. These investigations argue that the observed alteration phases, mapped stratigraphy, and geologic contexts are consistent with the proposed global environmental transition from an early near-neutral high water:rock conditions to more acidic and low water:rock conditions [7].

While the observed spectral diversity suggests a wide range of formation and alteration environments, the bulk mineralogy of NW Isidis has never been fully explored to investigate the mineralogic context of these VNIR identifications. In this investigation, bulk surface composition in previously mapped geologic units of NW Isidis is derived using hyperspectral thermal infrared (TIR) orbital data, while more local bulk mineralogical trends are studied using higher resolution multispectral TIR data. To derive bulk composition, we utilize an iterative spectral unmixing technique developed by [8], which makes it possible to statistically assess the necessity of different endmember phases in the unmixing models. Combined with the previous VNIR studies, our results provide critical constraints on the nature and extent of surface alteration throughout the NW Isidis region.

**Methods:** Both the Jezero crater and watershed [4] as well as the NE Syrtis [5] regions have been extensively studied and mapped using high resolution visible imagery and Compact Reconnaissance Imaging Spectrometer for Mars (CRISM) VNIR data. In our investigation, we obtained and processed all high-quality Thermal Emission Spectrometer (TES) spectra collected over these previously mapped units. Pixels were grouped by orbit and corrected for atmospheric effects using the NNLS minimization technique [9-10] before the derived surface emissivity spectra were averaged into a single spectrum for each geologic unit.

Averaged TES surface emissivity spectra were iteratively unmixed using a custom surface endmember library. In this method, up to ten endmember spectra are randomly removed from the endmember library, and each surface spectrum is linearly unmixed using the method of [11] to determine the best fit combination of mineral phases from the endmember library. This technique was iterated 60,000 times, randomly removing different endmembers as the algorithm progresses. The final result is an output table with the abundance of each endmember phase for each of the 60,000 runs for each previously mapped geologic unit. Endmembers were aggregated into endmember groups to simplify data interpretation. Using these data, it is possible to derive average surface compositions and model uncertainties, and to assess the distributions of modeled endmember abundances.

In addition to the relatively low spatial resolution of TES (~3 × 6 km/pix), higher resolution (~100 m/pix) multispectral TIR data from the Thermal Emission Imaging System (THEMIS) instrument were used to identify subtle changes in overall silica content across the landscape of NW Isidis. This is accomplished through mapping the Weighted Absorption Center (WAC) of the major TIR reststrahlen features [12-13]. Because more silicic and mafic lithologies trend towards shorter- and longer-wavelengh WAC values [14], we are able to assess relatively local variations in composition and to place these variations into the regional geologic framework.

**Results:** While VNIR data show a wide variety of alteration mineral phases indicative of a similarly wide variety of alteration environments, our TIR unmixing analyses indicate dominantly basaltic compositions with relatively minor mineralogical variability. All previously mapped geologic units are roughly composed of 15-25% plagioclase, 20-30% pyroxene, 15-30% phyllosilicates and amorphous components (PAC), and 15% sulfates, while other minor primary or secondary phases are present at or below ~10%. The modeled abundances of each endmember group in each geologic unit is shown in **Figure 1**, which also shows the relative distribution of model results.

The dominance of basaltic compositions in NW Isidis is confirmed by THEMIS WAC parameter values throughout the region, which suggest dominantly basaltic compositions with variable enrichments in olivine (**Figure 2**). The relationship between higher WAC values and increased olivine abundance is confirmed when comparing VNIR spectral signatures to the WAC parameter, where stronger olivine signatures in CRISM data are correlated to higher WAC values, as expected. Several small (< 1 $km^2$) exposures of very low WAC values were identified in the Jezero watershed, and are similar in appearance and distribution to those identified by [13] in the nearby Nili Fossae region. These exposures are predicted to contain

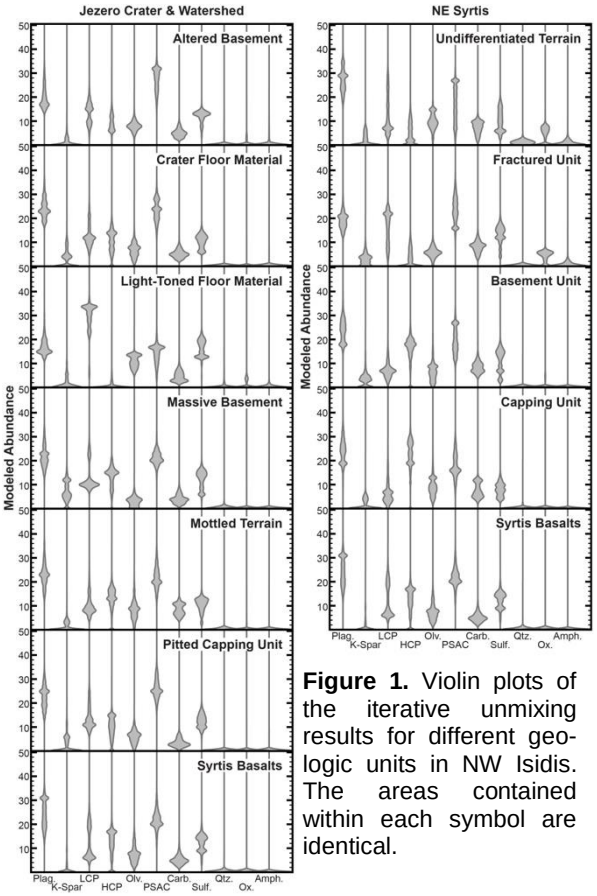


**Figure 1.** Violin plots of the iterative unmixing results for different geologic units in NW Isidis. The areas contained within each symbol are identical.

high-silica abundances, and comparisons to laboratory data suggest compositions consistent with monzonite.

Of particular interest throughout the NW Isidis region is the VNIR identification of carbonates associated with the Fractured Unit (FrU) of NE Syrtis [5] and the Mottled Terrain (MT) of the Jezero watershed [4]. The iterative unmixing suggests that these two units contain, on average, 8.8% and 9.1% carbonate, respectively, which are just below the traditionally accepted TES detection limit of ~10%. Iterative unmixing of each individual TES observation in the FrU of NE Syrtis reveals modeled carbonate abundances between 3.5% and 16.5%, suggesting significant spatial variability in the presence of carbonate. This observation is consistent with the VNIR observations of [5], who show that strong carbonate signatures are present largely in small bedrock exposures and are muted elsewhere due to limited exposure or mantling.

**Discussion & Conclusions:** TIR spectral analyses confirm that the NW Isidis region is dominated by basaltic compositions with variable amounts of alteration mineral phases. These results help to put the diverse alteration phases identified with CRISM data into geologic and compositional context. For example, aqueous alteration that occurred when these geologic units formed and altered was insufficient to thoroughly alter primary basaltic compositions, which still preserve mineral phases that are readily susceptible to chemical weathering (e.g., olivine).

Comparisons between different orbital and landed missions have shown that observed compositional diversity increases with improved spatial resolution. While CRISM observations of NW Isidis reveal the spectral dominance of many different mineral phases, mineralogical variations identified by lower resolution TIR datasets are far more muted. This suggests that future landed missions to NW Isidis would likely identify many diverse altered compositions and would be able to place these observations into better geologic and stratigraphic context. Fortunately, both Jezero crater and NE Syrtis are candidate landing sites for future missions to Mars.

Lastly, this demonstration of the iterative unmixing technique for regional-scale compositional analyses confirms its utility for critically evaluating unmixing model results and provides additional information on the distribution of model results and the robustness of endmember detections. Whether for investigating the presence of specific mineral groups [8] or bulk composition (this study), iterative unmixing is useful for assessing the performance of TIR unmixing models.

**References:** [1] Mangold et al. (2007), JGR 112, doi:10.1029/2006JE002835. [2] Ehlmann et al. (2009), JGR 114, doi:10.1029/2009JE003339. [3] Mustard et al. (2009), JGR 114, doi:10.1029/2009JE003349. [4] Goudge et al. (2015), JGR 120, doi:10.1002/2014JE004782. [5] Bramble et al. (2017), Icarus 293, doi:10.1016/j.icarus.2017.03.030. [6] Michalski et al. (2010), Icarus 206, doi:10.1016/j.icarus.2009.09.006. [7] Bibring et al. (2006), Science 312, doi:10.1126/science.1122659. [8] Goudge et al. (2015), Icarus 250, doi:10.1016/j.icarus.2014.11.034. [9] Lawson & Hanson (1974), 340 pp. [10] Rogers & Aharonson (2008), JGR 113, doi:10.1029/2007JE002995. [11] Ramsey & Christensen (1998), JGR 103, 577-596. [12] Smith et al. (2013), Icarus 223, doi:10.1016/j.icarus.2013.01.024. [13] Amador & Bandfield (2016), Icarus 276, doi:10.1016/j.icarus.2016.04.015. [14] Walter & Salisbury (1989), JGR 94, 9203-9213.

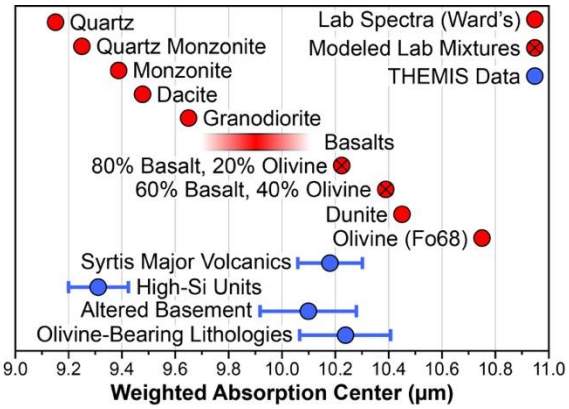


**Figure 2.** WAC values for laboratory (red) and orbitally derived spectra (blue). Bars surrounding average THEMIS measurements (circles) represent minimum and maximum recorded values.

**THE DORSA ARGENTEA FORMATION AND THE NOACHIAN-HESPERIAN TRANSITION: CLIMATE AND GLACIAL FLOW MODELING.** K. E. Scanlon,[1] J. W. Head,[1] J. L. Fastook,[2] and R. D. Wordsworth,[3] [1]Department of Earth, Environmental and Planetary Science, Brown University, Providence, RI, USA. [2]School of Computing & Information Science, University of Maine, Orono, ME, USA. [3]School of Engineering and Applied Sciences, Harvard University, Cambridge, MA, USA. <*kathleen_scanlon@brown.edu*>

**Introduction:** The Dorsa Argentea Formation (DAF), a set of geomorphologic units (Fig. 1) covering ~1.5 million square kilometers near the south pole of Mars [1-3], has been interpreted as the remnants of a large south polar ice sheet that formed near the Noachian-Hesperian boundary and receded in the early Hesperian [4,5]. Determining the extent and thermal regime of the DAF ice sheet, as well as the mechanism and timing of its recession, can therefore provide insight into the ancient martian climate and the timing of the transition from a comparatively thick $CO_2$ atmosphere to the present climate. We used early Mars global climate model (GCM) and glacial flow model simulations to constrain climates allowing (1) development of a south polar ice sheet of DAF-like size and shape, and (2) basal melting of this ice sheet in amounts and locations consistent with observed glaciofluvial landforms.

**Climate modeling:** To determine climate conditions that favor the growth of a DAF-like ice sheet, we ran the LMD GCM with a 64x48 horizontal grid and 25 vertical levels; a pure $CO_2$ atmosphere; 75% of present solar flux [6]; and modern topography. Simulations were conducted with atmospheric pressure ($P_{atm}$) of 600, 1000, and 1500 mb; the martian atmosphere is unstable to $CO_2$ condensation at the poles at $P_{atm}$ substantially higher than on modern Mars but lower than 600 mb [7; see 8 for similar results in another MGCM]. Since there is not yet a consensus on a gas that could warm early Mars sufficiently for "warm, wet" simulations, we added a grey gas, i.e. an artificial wavelength-independent absorption coefficient $\kappa = 5\times10^{-5}$ or $1\times10^{-4}$ [see 7].

Annual average surface temperature is nearly symmetric about the south pole on modern Mars [e.g. 9], reflecting the primary importance of insolation distribution on planets with thin atmospheres [e.g. 10]. In early Mars simulations, with a fainter sun and a thicker atmosphere, annual average surface temperature has a wavenumber-3 pattern about the south pole. Correlation between altitude and annual average temperature increases with $P_{atm}$, indicating that the south polar temperature pattern reflects both latitude-dependent insolation (important at low $P_{atm}$) and colder temperatures at higher altitude (important at high $P_{atm}$ [11, 12]). In GCM simulations with relatively low (15° or 25°) spin-axis obliquity and a thick (600 or 1000 mb) pure $CO_2$ atmosphere, an extensive region of ice stability (as indicated by a minimum in annual potential sublimation $S_{POT}$; cf. [7]) forms near the south pole, with DAF-like lobes along the 0°W and 90°W meridians. The asymmetric shape of the ice sheet is due to the regional topography of the southern polar regions and the dependence of surface temperature upon surface elevation in a thicker atmosphere. This indicates that the asymmetry of the DAF is therefore likely to reflect an asymmetric ice sheet rather than asymmetric erosion of the glacial deposits. In simulations without the Tharsis bulge, the south polar temperature and $S_{POT}$ minima lack the 90°W lobe, suggesting that the Tharsis bulge was at least partially present when the DAF formed.

Surface temperatures above 273 K in the DAF region are rare in GCM simulations warmed only by $CO_2$.

**Glacial modeling:** Since it does not simulate ice flow or basal ice temperature, the GCM alone cannot determine whether the extent of the south polar ice sheet in a given climate matches that of the DAF, or the amount and locations of basal melting. We used the University of Maine Ice Sheet Model (UMISM), adapted for Mars [5, 13, 14], to address these questions. We varied: (1) Atmosphere: 600 or 1000 mb $CO_2$, or 1000 mb $CO_2$ plus a grey gas; (2) global ice inventory: $2\times10^7 - 2\times10^8$ km$^3$; (3) geothermal heat flux: 45 – 65 mW m$^{-2}$ [15, 16].

In order to ensure that accumulation and ablation rates from the GCM reflected regions of long-term ice stability rather than short-term, transitional moisture transport patterns as the GCM surface ice adjusted from the artificial configuration imposed at the start of each simulation, we used GCM $S_{POT}$ for the UMISM annual ablation. Since the potential sublimation formulation assumes a uniformly infinite ice source at the surface and a uniformly dry atmosphere, we set a globally uniform ice accumulation rate. The value of the uniform accumulation was calculated for each climate scenario such that the sum of accumulation and ablation, integrated over the surface of the planet, is zero. However, since accumulation is always gradually reduced over the course of a supply-limited UMISM simulation to limit the total ice inventory to a set value chosen at the start of the simulation, results are not strongly sensitive to the value chosen for accumulation.

Like the GCM potential sublimation minimum, the modeled ice sheet is similar in shape to the DAF at low obliquity. Of scenarios studied here, the extent of the ice sheet is most similar to that of the DAF when global surface ice inventory is ~137 m GEL (Fig. 2). Widespread basal melting does not occur in any of our simulations with pure-$CO_2$ atmospheres, regardless of the value used for the late Noachian – early Hesperian geothermal heat flux, unless the global ice inventory is at least ~550 m GEL, in which case the extent of the ice sheet is much larger than the observed extent of the

DAF. Basal melting consistent with observed landforms does occur in simulations in which an idealized greenhouse gas provides additional warming beyond that from $CO_2$ alone, and the locations of maximum modeled basal melting (Fig. 3) are similar to the locations of observed glaciofluvial landforms (Fig. 1) in simulations with additional greenhouse warming.

**Conclusions:** In GCM simulations with a thick (i.e. ≥ 600 mb) pure $CO_2$ atmosphere, an extensive ice sheet forms near the south pole, with lobes near 0°W and 90°W. The asymmetry of the DAF therefore likely reflects emplacement by an asymmetric ice sheet, rather than asymmetric erosion. In UMISM simulations, the extent of the ice sheet is most similar to that of the DAF at low spin-axis obliquity (15°) and with global ice inventory is < $2\times10^7$ $km^3$ (≲ 137 m GEL). Widespread basal melting does not occur in the pure $CO_2$ atmospheres studied, but in scenarios with additional warming, melt maxima are located near observed glaciofluvial landforms. No eskers are observed where basal temperatures are warmest in the "cold and icy" climate endmember simulations, and few occur in association with glaciovolcanic features. We therefore conclude that the eskers in the DAF formed from a combination of surface melting and "top-down basal melting" [5] during warm intervals. Crater ages for the eskers [17] are consistent with this hypothesis and the hypothesis that they formed in the same era as the equatorial valley networks.

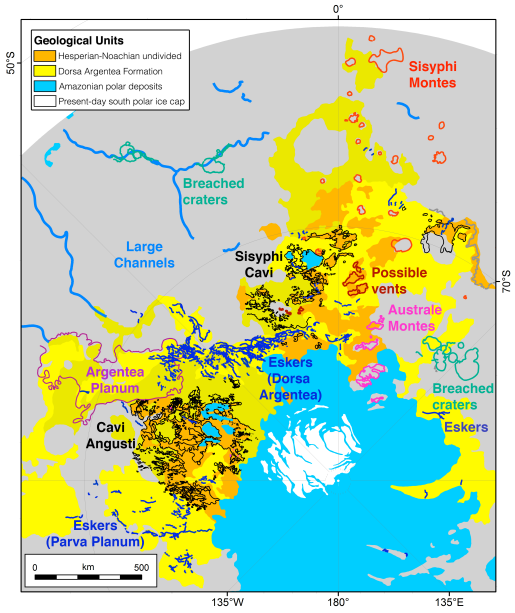


**Fig. 1.** The DAF: units as mapped by [1], with glaciofluvial and glaciovolcanic features outlined and labeled.

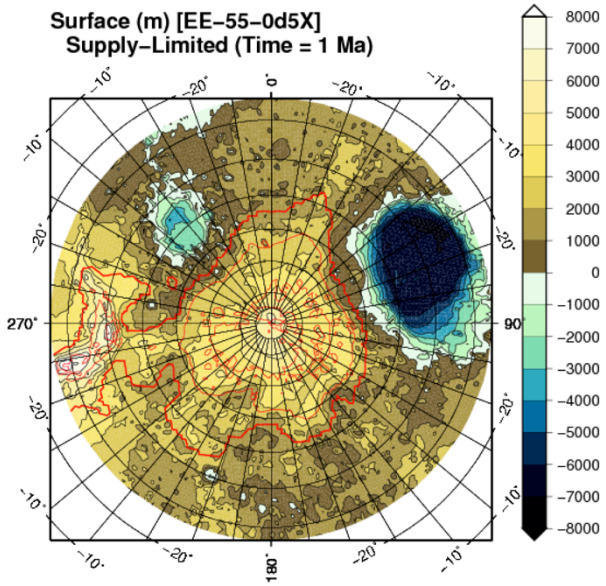


**Fig. 2.** UMISM south pole-centered ice surface in the 15° obliquity, 1000 mb $CO_2$, $\kappa = 0$ scenario. Ice thickness contour interval is 500 m.

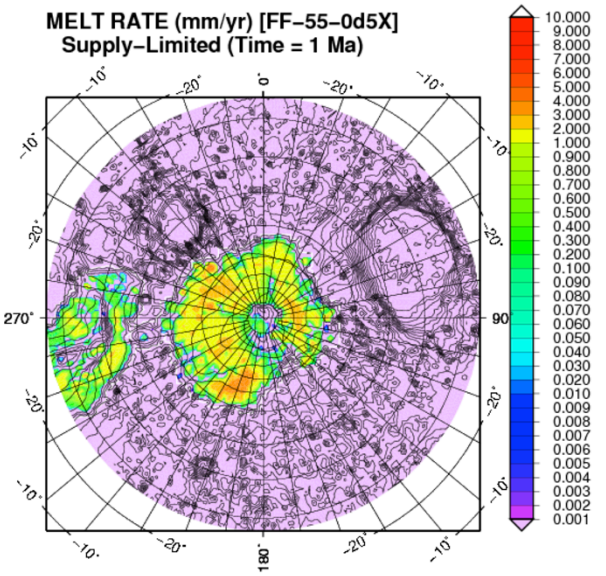


**Fig. 3.** Basal melting rate in the 15° obliquity, 1000 mb $CO_2$, $\kappa = 5\times10^{-5}$ scenario; shaded contour intervals are mm $yr^{-1}$.

**References:** [1] Tanaka, K.L., and D.H. Scott (1987), *USGS Map I–1802-C.* [2] Tanaka, K.L., and E.J. Kolb (2001), *Icarus, 154*, 3–21. [3] Tanaka, K. L. et al. (2014), *PSS, 95, 11–24*; [4] Head, J. W., and S. F. Pratt (2001), *JGR, 106,* 12275-12299; [5] Fastook, J.L., et al. (2012), *Icarus, 219,* 25-40. [6] Gough, D. O. (1981), *Physics of Solar Variations*, 21–34, Springer Netherlands; [7] Wordsworth, R. D., et al. (2015), *JGR: Planets, 120,* 1201–1219; [8] Soto, A., et al. (2015), *Icarus, 250,* 553-569; [9] Kieffer, H. H. (2013), *JGR: Planets*, *118*, 451-470. [10] Read, P. L., and S. R. Lewis (2004), *The martian climate revisited,* Springer Science & Business Media.; [11] Forget, F., et al. (2013), *Icarus, 222,* 81-99; [12] Wordsworth, R., et al. (2013), *Icarus, 222,* 1-19; [13] Fastook, J. L., et al. (2008), Icarus, 198, 305-317; [14] Fastook, J. L., and J. W. Head III (2015), *PSS, 106,* 82-98; [15] Montési, L. G. J., and M. T. Zuber (2003), *JGR: Planets, 108,* E6; [16] Solomon, S.C. et al. (2005), *Science, 307,* 1214–1220; [17] Kress, A. M., and J. W. Head (2015), *PSS, 109,* 1-20.

**FRACTIONATED NOBLE GASES IN MARTIAN METEORITE ALH84001 – AN INDICATOR FOR WATER-ROCK INTERACTION, OR A SAMPLE OF ANCIENT ATMOSPHERE?** S. P. Schwenzer[1,2,3],G. Bart[4,5], J. C. Bridges[6], S. A. Crowther[7], J. Filiberto[8,1], J. D. Gilmour[7], S. Herrmann[2], L. J. Hicks[6], S. P. Kelley[1,x], M. A. Miller[9], U. Ott[2,10], E. D. Steer[1,11], T. D. Swindle[5], and A. H. Treiman[3], [1]The Open University, Department of Environment, Earth and Ecosystems, Walton Hall, Milton Keynes MK7 5AA, UK; susanne.schwenzer@open.ac.uk. [2]Max-Planck Institute for Chemistry, Germany. [3]Lunar and Planetary Institute, USA. [4]University of Idaho, USA. [5]University of Arizona, USA. [6]University of Leicester, UK. [7]University of Manchester, Manchester, UK. [8]Southern Illinois University, Carbondale, IL 62901. [9]Southwest Research Institute, San Antonio, Texas 78228, USA. [10]MTA, ATOMKI, Debrecen, Hungary. [11]Nanoscale and MicroscaleResearch Centre (NMRC), University of Nottingham.

The composition of an atmosphere is the product of the processes which acted on it throughout its history. The Martian atmosphere today has a distinct noble gas isotopic fingerprint, mainly characterized by a high $^{129}Xe/^{132}Xe$ ratio of 2.6; the corresponding $^{84}Kr/^{132}Xe$ elemental ratio is 20.5 [1]. This was found by Viking [2] and confirmed by SAM on Curiosity [3]. Most importantly, the corresponding elemental and isotopic ratios have been measured in impact glasses in shergottite Martian meteorites [4,5]. In contrast, nakhlites and the unique ALH84001 Martian meteorite have lower $^{84}Kr/^{132}Xe$ ratios, which have presumably been caused by a range of processes from water-rock interaction to the existence of an ancient atmosphere.

**Meteorite evidence:** The relationships between the endmembers of Martian atmosphere, elementally fractionated Martian atmosphere, Martian interior and terrestrial air on the one hand, and the nakhlite and ALH84001 meteorites, on the other, in the $^{136}Xe/^{132}Xe$ vs. $^{84}Kr/^{132}Xe$ and $^{129}Xe/^{132}Xe$ vs. $^{84}Kr/^{132}Xe$ systems are illustrated in Fig. 1.

The plots show that both, the nakhlites and ALH84001 have a component of fractionated Martian atmosphere, which is clearly distinguishable from potential terrestrial contamination and – if extrapolated to a $^{129}Xe/^{132}Xe$ ratio of 2.6 – would have a $^{84}Kr/^{132}Xe$ ratio of about 8. Of course, the ancient Xe-isotope ratio could be lower, it has been estimated to be as low as ~2, e.g., in which case the corrensponding elemental ratio would be even lower about 5.

**Terrestrial evidence:** Terrestrial evidence for fractionation of noble gases is plentiful. Here we focus on observations of environments meteorites are found in most commonly: hot and cold deserts. Mohapatra et al. [21] investigated the effect of adsorbed terrestrial air contamination on the ability to measure the Mars interior component in hot desert finds, and concluded that elementally fractionated air (EFA) dominates the gas released at low temperatures.

Investigating a series of terrestrial samples from hot and cold deserts reveals that EFA is a ubiquituous occurrence (Fig. 2). Thus, a similar process could be expected to have acted on Mars, especially during a warm and wet period.

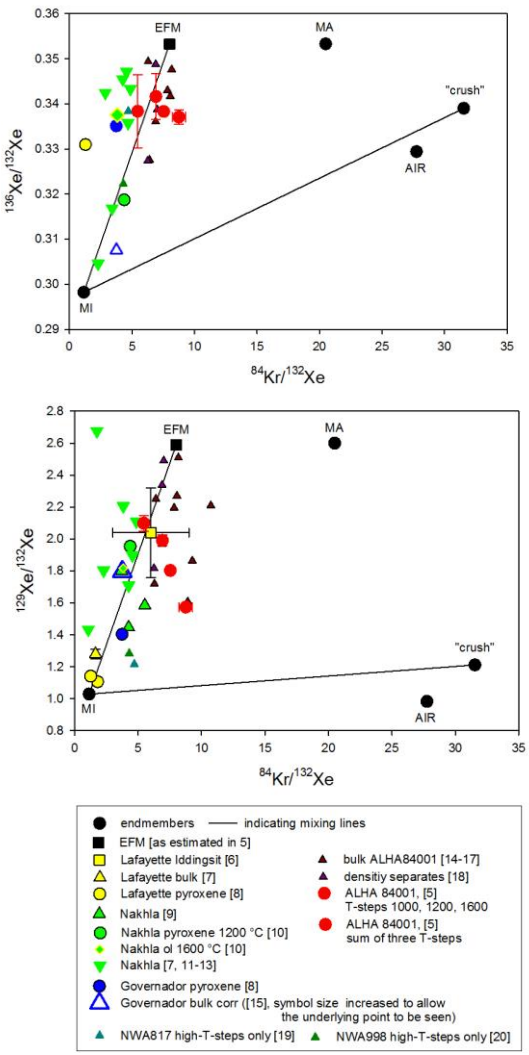


*Fig. 1 a (top). $^{136}Xe/^{132}Xe$ vs. $^{84}Kr/^{132}Xe$ ratios, and 1 b (bottom) $^{129}Xe/^{132}Xe$ vs. $^{84}Kr/^{132}Xe$ ratios. Endmembersin both panels: MA = Martian atmosphere [1], MI = Martian Interior [9], EFM = Elementally fractionated Martian atmosphere [5], Air = terrestrial atmosphere [1], and 'crush' = gases released upon crusing instead of heating [13]. Data corrected for terrestrial atmosphere, see [5].*

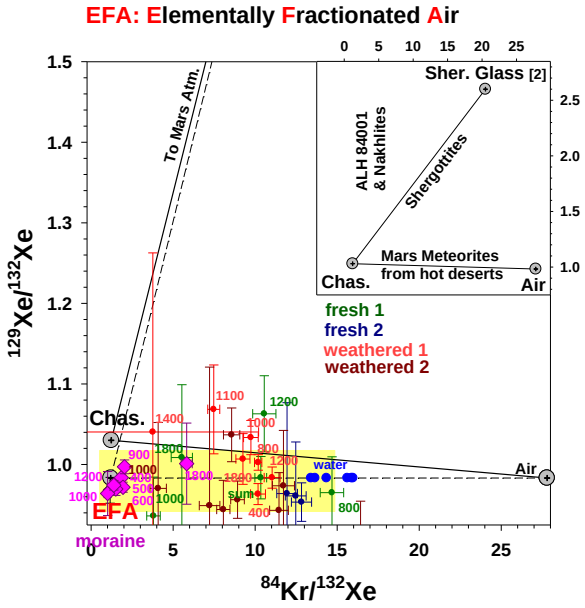


*Fig. 2. Plot of four different samples of Antarctic dolerite samples: 'fresh' (green and blue symbols) denominates subsamples from a large boulder with fresh appearance (see [22]), weathered 1 and 2 (red symbols) are oxidized rim subsamples from small boulders from the same dolerite and the pink symbols indicate samples from a moraine, freeze-thaw environement. All numbers are degassing T-steps, the yellow box outlines the $^{84}Kr/^{132}Xe$ variation found in samples from terrestrial hot deserts. Noble gas data from [23,24]. Endmembers shown on Fig. 1.*

**Experimental evidence:** It has long been recognized through experiments done on Apollo samples [25,26] that sample preparation, especially grinding, introduces heavy noble gases. More recently, similar observations have been made on Martian meteorites [27]. Thus, 'mechanical stress', but also exposing fresh surfaces to air [27], is well known to introduce heavy noble gases with a signature elementally fractionated in favour of the heavier element against the gas reservoir composition. Similarly, dissolution of air in water is known to result in elemental fractionation of Ar/Kr/Xe favouring the heavier element in solution [28]. Consequently, exposure of minerals to fluids and the resulting alteration, introduces a noble gas signature fractionated against the original gas reservoir.

We are currently undertaking experiments [29,30] to expose Mars relevant minerals (olivine, pyroxene, plagioclase, olivine glass, nakhlite composition glass, and mixtures thereof) to a simulated Mars atmosphere. Initial results point towards fractionation of the noble gas signature within the altered mineral surfaces. Ongoing measurements and modeling of the process is expected to give insights into the two step process of dissolution and incorporation of noble gases from a fluid phase, as well as potential changes to incorporation of noble gases due to differences in the chemistry of the alteration process (e.g., clay formation vs. oxide formation).

**Concluding remarks:** While it is well known that alteration of the mineral surface by mechanical stress or alteration processes can introduce elementally fractionated noble gases into minerals, details are yet to be explored. However, it is those details which will allow us to decide, which of the various processes brought forward in the literature (references see Fig. 1) can explain the incorporation of elementally fractionated Martian atmosphere into the nakhlites and ALH84001, and thus is the cause for the observed signatures. For the topic of this conference, ALH84001 is especially interesting, because it has been stated that the signature could be ancient Martian atmosphere [31] – or caused by water-rock interaction.

**References:** [1] Swindle T. D. (2002) *Rev. Min. Geochem., 47*, 171-190. [2] Owen, T. et al. (1977) *JGR, 82*, 4635–4639. [3] Conrad, P. G. et al. (2016) *EPSL, 454*, 1-9. [4] Bogard, D. D., Johnson, P. (1983) *Science, 221*, 651-654. [5] Schwenzer, S. P., Ott, U. (2006) 37th LPSC, abstr. #1614. [6] Swindle, T. D. et al. (2000) *MAPS, 35*, 107–115. [7] Ott, U. et al. (1988) *Meteoritics, 23*, 295–296. [8] Schwenzer, S. P. et al. (2006) 37th LPSC, abstr. #1612. [9] Ott, U. (1988) *GCA, 52*, 1937–1948. [10] Schwenzer, S. P. et al. (2002) *MAPS 37*, A127. [11] Mathew, K. J. & Marti, K. (2002) *EPSL, 199*, 2–20. [12] Busemann, H., & Eugster, O. (2002) *LPS XXXIII*, Abstr. #1823. [13] Wiens, R. C. (1988) *EPSL 91*, 55–65. [14] Mathew, K. J. & Marti, K. (2001) *J. Geophys. Res., 106 (E1)*, 1401–1422. [15] Swindle, T. D. et al. (1989) *LPS, XX*, 1097–1098. [16] Swindle, T. D. et al. (1995) *GCA 59*, 793–801. [17] Miura, Y. N. et al. (1995) *GCA 59*, 2105–2113. [18] Murty, S. V. S. & Mohapatra, R. K. (1997) *GCA 61*, 5417–5428. [19] Mathew, K. J. et al. (2003) *EPSL, 214*, 27–42. [20] Mathew, K. J. & Marti, K. (2005) *JGR., 111*, E12S05. [21] Mohapatra, R. K. et al. (2009) *GCA, 73*, 1505-1522. [22] Steer, E. D. et al. (2013) *EPSC, 2013*, abstr. # EPSC2013-166. [23] Schwenzer, S. P. et al. (2007) *38th LPSC*, abstr. # 1150. [24] Schwenzer, S. P. et al. (2007) *38th LPSC*, abstr. # 1143. [25] Niedermann, S. &, Eugster, O. (1992) *GCA, 56*, 493–509. [26] Niedermeier & S., Leich, D.A. (1976) *Proc. 7th Lunar Sciene Conf., GCA, Suppl. 7*, 587–597. [27] Schwenzer, S. P. et al. (2012) *MAPS, 47*, 1049–1061. [28] Ozima & M., Podosek, F. A. (2002): Noble Gas Geochemistry. [29] Schwenzer, S. P. et al. (2016) *47th LPSC*, abstr.# 1889. [30] Schwenzer, S. P. et al. (2017) *48th LPSC*, abstr.# 1531. [31] Gilmour, J. D. et al. (1998) GCA, 62, 2555-2571.

**Acknowledgement:** SPS, SH and UO thank Deutsche Forschungsgemeinschaft for funding between 2001 and 2007, SPS, MAM, AHT, JCB, SPK, and JF acknowledge NASA MFRP funding. EDS was supported by an STFC PhD studentship. JCB and SPS thank UKSA for support for the MSL work.

**ATMOSPHERIC ARGON ISOTOPE EVOLUTION INFORMED BY MAVEN RESULTS.** M. Slipski[1], B. M. Jakosky[1], M. Benna[2], P. Mahaffy[2], M. K. Elrod[2] [1]LASP, University of Colorado Boulder, Boulder, CO (marek.slipski@colorado.edu), [2]NASA/Goddard Space Flight Center, Greenbelt, MD.

**Introduction:** The MAVEN (Mars Atmosphere and Volatile Evolution MissioN) spacecraft has been in orbit for 2.5 years and has enabled detailed estimates of current atmospheric loss processes. Calculating the cumulative loss throughout Mars' history will require extrapolating all escape rates back in time through changing solar and atmospheric conditions. One method to estimate total loss is through the observed enrichment in heavy isotopes relative to light isotopes of species in the atmosphere (D/H, $^{15}N/^{14}N$, $^{13}C/^{12}C$, $^{38}Ar/^{36}Ar$); light isotopes are preferentially removed from the top of the atmosphere, leaving the remaining gas enriched in the heavier isotope.

$^{38}Ar$ is enriched relative to $^{36}Ar$ in Mars' bulk atmosphere compared to Earth's bulk atmosphere [1, 2]. Earth's atmospheric $^{36}Ar/^{38}Ar$ ratio is thought to be the result of efficient outgassing of juvenile gases from the interior and lack of significant loss because it is nearly equal to $^{36}Ar/^{38}Ar$ in the solar wind, chondrites, and Jupiter's atmosphere. If Mars' atmosphere formed with the same primitive ratio, then it has since been fractionated. Ar is unlikely to react chemically with the surface in significant amounts, so the observed enrichment must be a consequence of loss to space.

Ar is primarily removed by sputtering, where some ionized oxygen atoms that are picked up in the exosphere by the interplanetary magnetic field reimpact the upper atmosphere with sufficient energy to eject other particles into space. $^{36}Ar$ has a larger scale height than $^{38}Ar$ so it is relatively more abundant at the exobase. While sputtering itself does not prefer a particular mass, the greater abundance of $^{36}Ar$ at high altitudes causes those lighter isotopes to be removed more readily. The ratio of $^{36}Ar/^{38}Ar$ at the exobase today is not constant in time or space [3]. Furthermore, the distribution of reimpacting pickup ions is not globally uniform [4].

The Ar isotope evolution model presented by Slipski and Jakosky [5] includes time-variable rates of outgassing, sputtering, and impact supply and erosion. It has been updated to allow for variations in $^{36}Ar/^{38}Ar$ at the exobase observed by MAVEN [3]. Here, we provide a detailed explanation of the model simulations leading to the results in Jakosky et al. [3]. Because sputtering may not be uniform globally, we also investigate how its distribution affects our estimates of total atmospheric loss.

**Box Model:** The model we use [5] has three reservoirs for Ar: the mantle, crust, and atmosphere. We begin at 4.4 Gyr ago with no Ar in the atmosphere and march through time in intervals of 1 Myr. Several processes that affect the abundances in each reservoir occur at each time step. These include radioactive decay of $^{40}K$ into $^{40}Ar$ in the mantle and crust, volcanic outgassing of all Ar isotopes into the atmosphere proportional to their ratios in the mantle, and loss to space of Ar isotopes via sputtering. The rates of outgassing and crustal production are based on photogeologic analyses as well as thermochemical evolution models of the interior. To determine how much Ar is sputtered we scale to estimates of $CO_2$ sputtering [6, 7, 8]. Each isotope is sputtered in proportion to its expected yield [9] and its ratio at the exobase. The latter is determined according to the diffusive separation above the homopause, $\sim\exp(-\Delta z/H)$ where $\Delta z$ is the separation between the homopause and exobase and H is the mass-dependent scale height.

The outgassing and sputtering rates over time have significant uncertainty, so we use a multiplicative factor for each process that allows us to run many simulations and compare the results. In addition, because sputtering depends on the ratio of $Ar/CO_2$, we treat the initial $CO_2$ pressure and subsequent evolution in the same way. Exchange of $CO_2$ between the reservoirs in our model is much more complex, so we instead treat its evolution as a model parameter that can be varied. We show how changes in all of these model parameters affect the evolution of atmospheric $^{36}Ar$, $^{38}Ar$, and $^{40}Ar$. Then, we compare the abundances and ratios of those isotopes in the simulations at present-day to measurements of the lower atmosphere by Curiosity. From those runs where the present-day abundances are reproduced we can determine the range of total atmospheric Ar loss the measurements are consistent with.

**Upper atmospheric structure:** The model of [5] found that 48-63% of $^{36}Ar$ ever put into the atmosphere would have been removed by sputtering. However, they considered only a single value for the ratio of $\Delta z/H$, derived pre-MAVEN, which determines the relative amounts of sputtered isotopes as described above. Jakosky et al. [3] used homopause altitudes, exobase altitudes, and Ar scale heights derived from NGIMS (Neutral Gas and Ion Mass Spectrometer) density measurements taken over more than a year of MAVEN orbits. In Fig. 1, $\Delta z$ and H calculated from each orbit are shown as points, colored by the solar zenith angle where the measurement was taken. Choosing values of $\Delta z/H$ over that range and using them in the model provides different results for the total fraction of $^{36}Ar$ lost to space. The loss percentages

corresponding to a given Δz/H are shown by the dashed lines in Fig. 1. (These are averages, as we have varied the other model parameters discussed above as well). For the average Δz/H, we found an expected loss of ~66% of any $^{36}$Ar ever introduced into the atmosphere.

The variations in scale heights and homopause and exobase altitudes seen in Fig. 1 are products of local time, latitude, and seasonal changes. Where Δz/H is low, less fractionation of the isotopes occurs between the lower and upper atmosphere requiring more atmosphere to be removed to reproduce the present-day ratios. Measurements of precipitating particle fluxes suggest that sputtering is not a globally uniform process [4]. Thus, the Δz/H at the locations where strong precipitation occurs may be the most important for removing Ar; a global average of Δz/H may not truly represent how Ar isotopes fractionate from sputtering. So, we compare how measurements of precipitating ions and upper atmospheric structure change over time. Then, we update the model to take these variations into account and compare the new results with those obtained in [3].

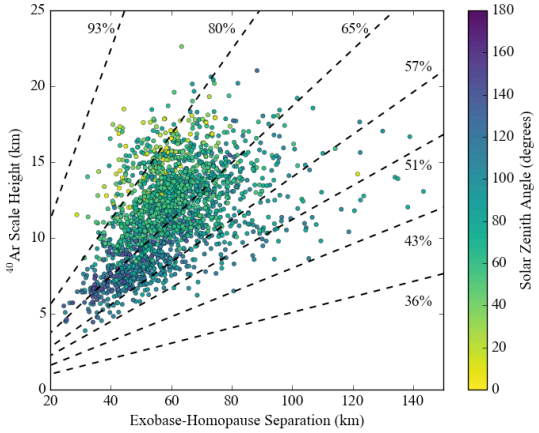


Figure 1: (from [3]) Calculations of the $^{40}$Ar scale height and distance between the homopause and exobase from a few thousand orbits of NGIMS data. Colors show the solar zenith angle of periapse of each orbit. Dashed lines show model results of total $^{36}$Ar loss for several examples of Δz/H.

**References:** [1] Webster C. R. et al. (2013), *Sci., 341,* 260-263. [2] Mahaffy P.R. et al. (2013), *Sci., 341,* 263-266. [5] Slipski M. and Jakosky B. M. (2016) *Icarus, 272,* 212-227. [3] Jakosky B. M. et al (2017) *Sci., 355,* 1408-1410. [4] Leblanc F. et al. (2017)., *ICMA* Abstract. [6] Luhmann J. G. et al. (1992) *GRL, 19,* 2151-2154. [7] Chassefiere E. et al. (2007) *Planet Sp. Sci., 55,* 343-357. [8] Chassefiere E. (2011) *Planet Sp. Sci., 59*, 207-217. [9] Jakosky, B. M. et al. (1994), *Icarus, 111,* 271-288.

**CONSTRAINING THE DURATION OF LATE HESPERIAN-AMAZONIAN HABITABILITY VIA CRATER INTERBEDDING WITH ALLUVIAL FANS.** J. W. Sneed[1*], E. S. Kite[1], D. P. Mayer[1,2], S. A. Wilson[3] [1]University of Chicago (sneedjw@uchicago.edu), [2]United States Geological Survey Astrogeology Science Center, [3]Smithsonian Institution.

**Introduction:** Alluvial fan deposits on the Martian surface record one or more episodes of liquid-water climate conditions [1,2,3]. This climate supported precipitation-sourced runoff volumes of greater than 0.1 mm/hr, feeding river discharge of more than 100 m/s [4]. The larger (>10 km$^2$) fans with ~2° slopes were deposited in a relatively late epoch [5], suggesting that habitable conditions may have existed on Mars as recently as the early Amazonian. We focus on the time of formation for these fans, in order to better constrain the duration of Hesperian and Amazonian liquid-water climate phases.

Previous work on alluvial fan depositional timeframes [e.g. 6,7] has relied on sedimentological methods that require assumptions about flow intermittency or sediment-to-water ratios, which remain poorly understood in these paleoflows. Correspondingly, these estimates provide very brief lower limits on alluvial fan formation time. Another approach has been to use crater density on different fans, using the spread of crater retention between fans as a proxy for the spread of fan formation times. However, at surface areas <$10^3$ km$^2$ , this method fails to distinguish age differences as large as 500 Ma [8]. Thus, our analysis (previously published as [9]), addresses an open problem.

**Embedded Crater Analysis:** We use the embedded-crater method of analysis [10,11]. On a stable planetary surface, crater density is proportional to exposure duration- the basis of traditional crater count dating methods. If, on the other hand, that surface were experiencing sedimentary accumulation (either steady or intermittent), then the same number of impacts would be distributed throughout the three-dimensional rock volume accumulated during the same time period. The greater the volumetric density of craters, the more slowly the sediments must have accumulated.

Because active sedimentation may bury many of the craters completely after deposition, a direct count of all craters in the fan volume is not possible. However, impacts that occur near the end of active sedimentation will only be partially buried, and may be distinguishable from later surface impacts by interbedding with fluvial deposits. Smaller craters are buried readily, and craters with large rims may require considerable sediment volumes before they are fully obscured. The time neded to bury a given crater population is given by

$$\tau_{raw,D} = N_D / (f_D\, a)$$

where $\tau_{raw,D}$ is the minimum time required to build an observed population of visible craters with minimum diameter $D$, $N_D$ is the number of observed embedded craters, $f_D$ is the past crater flux (#/km$^2$/yr), and $a$ is the area counted (km$^2$). Note that this gives the age of the visible surface layers only, without accounting for deeply buried strata, and should be interpreted as a strict lower limit.

Under the assumption of steady accumulation throughout the volume, we can extrapolate surface data through the total fan thickness $Z$ to calculate formation duration $\tau_{steady}$

$$W_D \approx 1.33 D\varphi / \tau_D$$

$$\tau_{steady,D} = Z / W_D$$

where $\varphi$ is obliteration depth as a fraction of diameter. 1.33 is a factor applied in order to correct for the fact that the median diameter observed in any crater population will exceed the minimum diameter; without correction, $D\varphi$ underestimates the true obliteration depth. Interestingly, postfluvial erosion of fans does not affect the validity of this measure. Just as with partial burial, a randomly oriented cut through the fan is biased towards the exposure of larger craters, and proportional to volumetric crater density. Thus, the accumulation time of an alluvial fan may be estimated from surface counts of interbedded craters, regardless of whether that surface is pristine or deeply eroded.

**Methods:** We examined $1.7\times10^4$ km$^2$ of previously catalogued fans, most of the surface area of exposed large alluvial fans on Mars, using 6m-per-pixel CTX satellite imagery. Candidate embedded craters were flagged for review by three of the authors (J.W.S, E.S.K, D.P.M.) for final classification. When possible, this classification was supplemented with 25 cm-per-pixel HiRISE imagery and CTX digital terrain models. 25 embedded craters were identified in this way.

In a supplemental HiRISE-only search (570 km$^2$), 13 embedded craters were found. In the diameter range 0.8-0.16 km, embedded crader densities are similar (within Poisson error); it is unlikely that a more detailed search of the total area would change our results significantly.

False positives in the data are likely rare. Although some marine Earth processes are known to produce concentric deposits [12], this mechanism is unlikely on Martian alluvial fan surfaces. In many cases, embedded craters are isolated rather than space-filling, and still show preserved rims. However, there are certainly false negatives; re-surveys found several embedded craters with scores ≤3. Further, impacts that occurred during active fluvial deposition may not be visibly interbedded at existing limits of orbital photography. Therefore, this count of embedded craters functions as a lower limit.

**Duration of Fluvial Activity:** The typical error estimate in this case would be calculated using Poisson statistics [14]. These can be seen as blue error bars in Fig. 1 & 2. However, this does not account for uncertainties in true crater flux, target strength, atmospheric filtering, obliteration depth, and fan formation time. Therefore, we adoped conservative estimates of each of these factors and incorporated each into a Monte Carlo simulation of $10^3$ trials (with Poisson error calculated analytically in each case).

Under the most conservative assumptions, we find that the best fit across all bin sizes for the shortest active window is ~44 Ma. This corresponds to the end member in which zero craters are completely entombed within buried strata, and the surface population of embedded craters is a complete population. Such a distributions relies on a process in which the bulk of fan material is deposited very rapidly, quiescent for > 44 Ma, and is then briefly reactivated in order to supply the necessary interbedding.

Under assumptions of steady accumulation, a more realistic case, the best-fit case corresponds to a lower limit of 125-250 Ma.

**Conclusions:**

| Permitted | Disfavored | Excluded |
|---|---|---|
| • Long-lived habitable environment (snowmelt or rainfall)<br>• Chaos trigger (Baker et al. 1991)<br>• Obliquity-shift control (Kite et al. 2013b) | • Methane bursts<br>• Fluvial sediment transport every year for >20 Myr | • Any explanation that produces a single burst of <20 Myr duration<br>• Triggering by the thermal pulse caused by the impacts that formed the large craters which host the alluvial fans |

**Table 1:** Scenarios permitted and excluded

**References:** [1] Moore J. M. and Howard A. D. (2005) *JGR, 110.E4* [2] Grant J. A. and Wilson S. A. (2012) *Planetary and Space Science 72.1, 44-52* [3] Kite E. S. et. al. (2015) *EPSL 420, 55-65* [4] Morgan A. M. et. al. (2014) *Icarus 229, 131-156* [5] Grant J. A. and Wilson S. A. (2011) *GRL 38.8* [6] Armitage J. J. (2011) *GRL 38.17* [7] Palucis M. C. et. al. (2014) *JGR 119.4, 705-728* [8] Warner N. H. et. al. (2015) *Icarus 245 198-240* [9] Kite E. S. et. al. (2017) *GRL 44.9, 3991-3999* [10] Hartmann W. K. (1974) *JGR 79, 3951-3957* [11] Kite E. S. et. al. (2013) *Icarus 225 850-855* [12] Tewksebury B. J. et al. (2014) *Geology 42.6, 479-482*

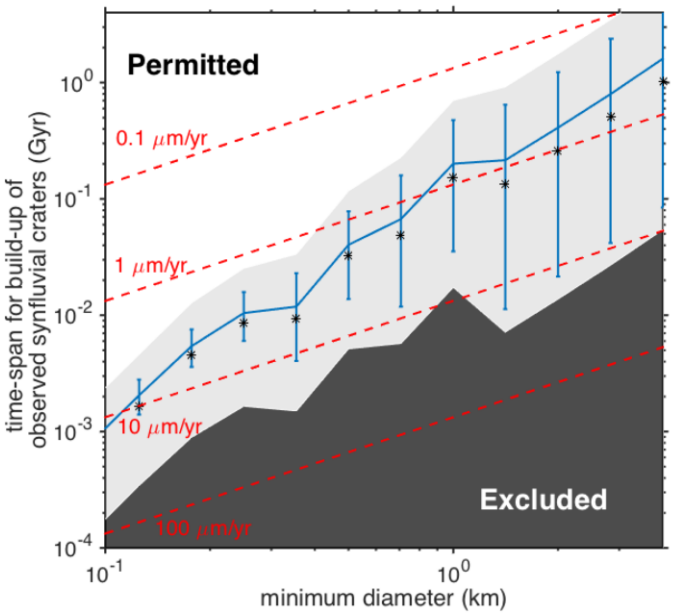


**Figure 1:** Minimum sedimentation timespan. Blue error bars are Poisson uncertainty, grey band corresponds to full Monte Carlo fit. Black and white zones are excluded and included with 95% confidence respectively.

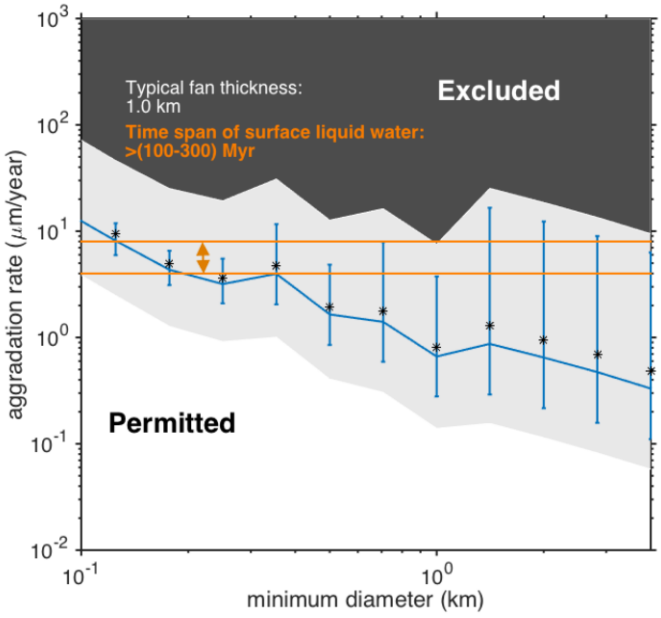


**Figure 2:** Minimum aggradation rate.

**SEARCHING FOR INDICATIONS OF SNOWMELT-DRIVEN EROSION ON EARLY MARS**

J. W. Sneed[1*], E. S. Kite[1], D. P. Mayer[1,2] [1]University of Chicago (sneedjw@uchicago.edu), [2]United States Geological Survey Astrogeology Science Center

**Introduction:** Despite clear evidence of ancient fluvial sedimentary processes, decades of Mars research have struggled to account for the presence of warm conditions that could support liquid water on the planetary surface [1][2]. Here, we examine new evidence that seasonal extremes may have allowed for transient periods of snowmelt production on slopes with prolonged exposure to direct sunlight [3][4][5][6].

If direct sunlight can act as a control on erosion rates by regulating liquid water availability, then anisotropy in slope orientation might be observed in response. In the case of younger, mid-to-high latitude modern processes, findings suggest that pole-facing slopes are systematically gentler than equator-facing slopes [7]. However, it has not yet been established whether a similar process was active in the surface evolution of ancient Mars.

When deeply incised by alluvial fan source regions despite a limited drainage area, circular crater walls provide a natural testing bed for this hypothesis, because their modern degraded state may be readily compared to a well-understood initial configuration and because their ring-like shape provides a full range of exposure angles. Therefore, we undertake a broad survey of the erosional patterns in such craters in order to look for signs of insolation angle as a major determinant of liquid water availability.

**Methods:** We examine ten low-latitude crater systems associated with large alluvial fans, as well as either partial or full coverage by 6m-per-pixel CTX orthopairs. These include, e.g., Harris, Ostrov, and Holden craters. Using the NASA Ames stereo pipeline [8], 24m-per-pixel DEM images are extracted and smoothed using a 5-pixel radius gaussian filter to reduce noise and small gaps in coverage. For each pixel in the crater wall elevation model (excluding secondary impact craters with a radius larger than 1 km), we calculate a slope, aspect, and angle with respect to the crater's center. Pixels with slope < 20° are excluded from this study.

Each pixel value is binned in ten-degree arcs with respect to their angle from the crater center, effectively creating a weighted average of crater wall aspects according to the radial position of each point. Using a Monte Carlo simulation with $10^3$ passes, we sample $10^3$ points from each bin per pass.

We will present an analysis of this dataset that includes comparison to equatorial craters with few alluvial fans, as a control set.

**Preliminary Results:** An early survey of 8 craters shows a clear preponderance of north- and south-facing slopes relative to those facing east and west (Fig. 1). In a sample of 36,000 points drawn evenly from each cardinal direction, differences between the most overrepresented and most underrepresented aspect populations exceeded a factor of 1.5.

Furthermore, this difference appears to be driven almost entirely by high variance in the aspects meas-

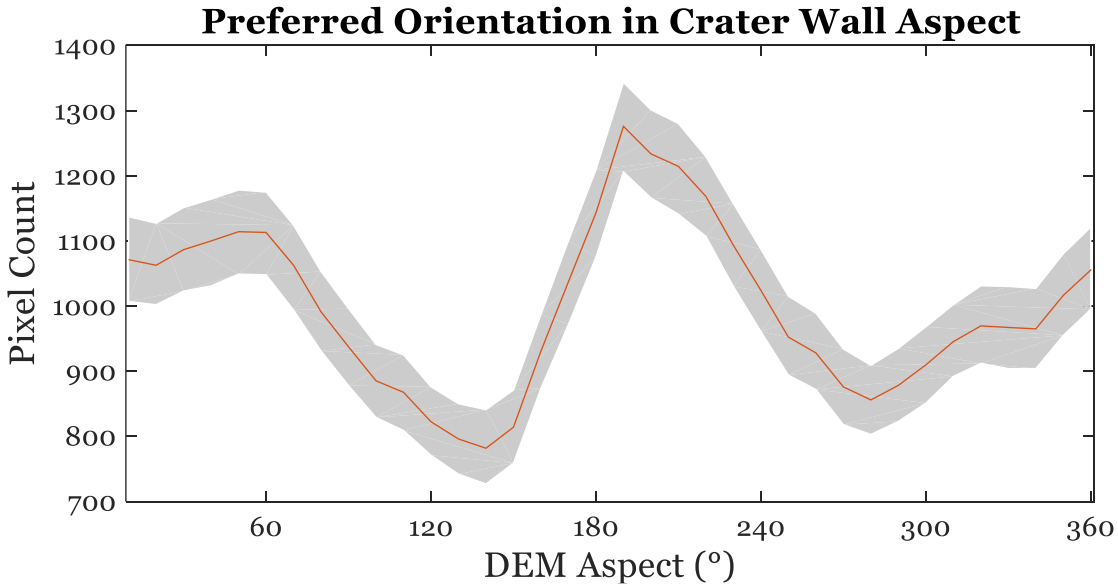


**Figure 1:** A disproportionately large number of north (0°) and south (180°)-facing slopes emerge in Monte Carlo simulations, after normalization by radial position around crater centers. Aspect values are grouped in 10° bins. Gray bar represents the 95% scatter in Monte Carlo trials.

ured on the east and west slopes of each crater relative to those in the north and south.

**Interpretation:** In addition to anisotropy between north/south versus east/west orientations, we observe significant asymmetry between north and south crater walls; this may be a product of later glacial smoothing, with southern walls being more prone to glaciation than northern walls [9]. Our presentation will further explore the relationship between the observed erosional anisotropy and trends in the local geometry of alluvial fan source alcoves. Are alcoves on the northern edge of craters more likely to be broad and shallow, with east and west edges producing smaller, box-like alcoves? Or are alcoves on east and west edges of a crater more likely to be deep channel-like structures incising away from the crater center, in comparison to shallow alcoves on the north and south walls?

These results, while preliminary, are consistent with obliquity-driven snowmelt patterns that bias local erosion patterns towards the production of slopes that experience direct sunlight. This bias towards pole- and equator-facing aspects on all sides of crater walls suggests that the pronounced seasonal variations of high-obliquity periods in Martian history may have left an enduring signal in planetary-scale erosional patterns.

**Acknowledgments:** We are grateful for financial support from the U.S. taxpayer via NASA grants NNX16AG55G and NNX15AM49G.

**References:** [1] Sagan C. and Mullen G. (1972) *Science 177.4043, 52-56* [2] Kasting J. F. (1991) *Icarus 94.1, 1-13* [3] Lasker J. et. al. (2004) *Icarus 170.2, 343-364* [4] Kite et. al. (2013) *Icarus 223, 181-210* [5] Hecht M. H. (2002) *Icarus 156.2, 373-386* [6] Costard F. et. al. (2002) *Science 295.5552, 110-113* [7] Kreslavsky M. A. and Head J. W. (2003) *GRL 30.15* [8] Mayer D. P. and Kite E. S. (2016) *LPS XLVII* Abstract #1241 [9] Conway S. J. and Mangold N. (2013) *Icarus 225.1, 413-423*

**REVISITING THE IMPACT HEATING HYPOTHESIS FOR EARLY MARS WITH A 3D GCM.** K. E. Steakley[1], M. A. Kahre[2], J. R. Murphy[1], R. M. Haberle[2], and A. Kling[2,3], [1]Astronomy Department, New Mexico State University, Las Cruces NM (steakley@nmsu.edu), [2]NASA Ames Research Center, Moffett Field CA, [3]Bay Area Environmental Research Institute, Petaluma CA.

**Introduction:** Comet and asteroid impacts have been investigated as a potential heating mechanism for early Mars [1,2,3,4]. Capable of injecting significant amounts of energy and water vapor into the atmosphere, it has been suggested that they could induce greenhouse warming to produce warmer surface temperatures and rainfall [1,2,3,4]. These potential climate effects have been studied with 1D models and suggest that impacts ranging from 30-100 km in size are capable of producing above-freezing temperatures for ~95 days to 6 years and between ~39.6 cm and 17.9 m of total rainfall not considering the radiative effects of water clouds [1]. A few cases in Segura et al. [1] that included radiatively active clouds resulted in either longer warm periods and increased rainfall or in shorter warm periods and decreased rainfall depending on the cloud particle size chosen. The Segura et al. [1] scenarios do not include a $CO_2$ cycle. Urata and Toon [5] explored the potential of a water cloud greenhouse effect to produce a warmer, wetter early Mars with a 3D GCM with mixed results. They found that the GCM's hydrological cycle was extremely sensitive to initial conditions, cloud particle sizes, and polar cap albedo and that warm and wet or cold and dry climates could be reproduced depending on these factors.

More recently, in depth GCM modeling has prompted a new potential paradigm for early Mars called the icy highlands hypothesis in which adiabatic cooling within a more massive ancient atmosphere results in significant water ice deposits in the southern highlands [6]. In this scenario, periodic warming from volcanism or impacts could cause snowmelt and runoff in the southern highlands to form valley networks [6]. Whether the geologic evidence supports this hypothesis is the subject of debate. In contrast to the idea of a transiently warm early Mars, it was suggested in Segura et al. [3] that it might be possible for impacts to induce a hot runaway climate that was stable in the long term. The role that impacts might have played in the early Mars climate is not understood, especially in the context of the greater debate about its nature and valley network formation.

In order to improve our understanding of the potential climate effects of impacts, we revisit the Segura et al. [1] cases using the NASA Ames Mars Global Climate Model (MGCM) with updated physics to better represent early Mars.

**The Ames MGCM for early Mars:** We have made several adjustments to the Ames MGCM to represent early Mars conditions. Solar luminosity is reduced to 75% of its current value and surface pressure is increased with cases at 150 mbar, 1 bar, and 2 bar (as per [1]). The microphysics package has been simplified to include three tracers for $CO_2$ clouds, water vapor, and water clouds that could be liquid or ice similar to [6]. Although $CO_2$ cloud capabilities are being developed (see Kahre et al., this conference), the $CO_2$ cycle is not included in these simulations, nor is it in Segura et al. [1]. The dust cycle is also not included at this time but a full water cycle is. Water clouds condense or evaporate in a grid box when it becomes supersaturated or subsaturated respectively accounting for the exchange of latent heat [7]. Precipitation occurs when clouds exceed a mass mixing ratio of 0.001 kg of water per kg of $CO_2$ [6] after which excess mass is put directly on the ground as precipitation. Water cloud particles undergo size-dependent gravitational sedimentation. We find that most of the water transferred from the atmosphere to the surface in these simulations comes from sedimentation as opposed to precipitation. Our water cloud, sedimentation, and precipitation scheme differs from Segura et al. [1] where precipitation occurs when clouds form near the surface, at which point water from the column is transferred to the ground. We have incorporated the radiative effects of water clouds, which are distinguished as liquid or ice clouds for radiative purposes only. A mie code was used to calculate optical quantities Qext, Qscat, and g for liquid and ice clouds based on indices of refraction from Hale and Querry [8] and Downing and Williams [9]. Cloud particle sizes are calculated based on the total mass in a grid box and a constant number of cloud condensation nuclei of $10^5$ particles per kg of $CO_2$ [6]. We find that the inclusion of radiatively active water clouds significantly affects surface temperatures in early Mars scenarios. Segura et al. [1] include a few cases with radiatively active clouds in which particle sizes are constant at 100 microns or 1 mm. We choose to include our updated water cloud physics package, which is similar to other GCMs [6], rather than introduce the physics from Segura et al. [1] into the MGCM. A moist convection scheme based on Manabe et al. [7] and Manabe and Wetherald [10] has also been incorporated. In this scheme, the code checks for instabilities against moist convection and adjusts mixing ratios and

temperatures accounting for latent heat exchange until the atmosphere is saturated and follows a moist adiabat. Moist convection is not included in Segura et al. [1] but we choose to include it here because it will affect temperature profiles and cloud formation. We have also updated the correlated-k radiative transfer scheme to include $CO_2$ far line absorption [11] and $CO_2$ collisionally induced absorption [12] as well as extend the temperature range of the radiation code up to 800K.

**Initial conditions for impact scenarios:** We revisit the Segura et al. [1] impact scenarios matching the described initial conditions as closely as possible using the early Mars Ames MGCM with the updated physics. The main cases in Segura et al. [1] represent 30-km, 50-km, and 100-km diameter impactors in a 150-mbar atmosphere; 50-km and 100-km impactors in a 1 bar atmosphere; and a 50-km impactor in a 2 bar atmosphere. These three impact sizes of 30-km, 50-km, and 100-km inject global equivalent layers of water that are 0.1534, 0.3563, and 1.75 m in depth respectively. This water is distributed globally as vapor. Segura et al. [1] describe their initial temperature profiles as starting with a near-surface temperature (600K for 30- and 50- km and 700K for 100-km) and following a moist adiabat until reaching the stratosphere above which temperatures are isothermal at 200K. They do not mention adjusting initial temperature profiles for different atmospheric surface pressure scenarios. We find that moist adiabats in a 150-mbar or 1-bar atmosphere with surface temperatures of 600K or 700K would contain significantly more water than even the 100-km impactor case and initial atmospheric temperatures would exceed 200K throughout our vertical pressure grid. Thus, we opt to follow a dry adiabat still using the same initial surface temperatures as Segura et al. [1]. We also incorporate the thick, hot debris layer in our subsurface model which has a temperature of 1600K and depths of 0.0696, 0.277, and 2.23 m as per Segura et al. [1].

**Expected results:** We present preliminary results of various impact scenarios from Segura et al. [1] which included 30-, 50-, and 100-km impactors in 150-mbar, 1-bar, and 1-bar surface pressure conditions. We will include results with and without the radiative effects of water clouds using our simplified early Mars MGCM physics package. Initial runs indicate that the radiative effects of clouds are significant in these early Mars scenarios. We will explore how the inclusion of global atmospheric dynamics affect the total precipitation volumes and time with surface temperatures above freezing that were originally reported in Segura et al. [1].

**References:**

[1] Segura, T. L., Toon, O. B., & Colaprete, A. (2008) *Journal of Geophysical Research (Planets), 113*, E11007. [2] Segura, T. L., Toon, O. B., Colaprete, A., & Zahnle, K. (2002) *Science*, *298*, 1977. [3] Segura, T. L., McKay, C. P., & Toon, O. B. (2012) *Icarus, 220*, 144. [4] Turbet, M., Forget, F., Svetsov, V. et al. (2017) The Mars Atmosphere: Modelling and observation, Abstract #4304. [5] Urata, R. A. and Toon, O. B. (2013) *Icarus*, *226*, 229. [6] Wordsworth, R., Forget, F., Millour, E., Head, J. W., Madeleine, J.-B., & Charnay, B. (2013) *Icarus*, *222*, 1. [7] Manabe, S., Smagorinsky, J., & Strickler, R. F. (1965) *Monthly Weather Review, 93*, 769. [8] Hale, G. M. and Querry, M. R. (1973) *Applied Optics*, *12*, 555. [9] Downing and Williams (1975) JGR, 80, 1656. [10] Manabe, S., & Wetherald, R. T. (1967) *Journal of Atmospheric Sciences, 24*, 241. [11] Perrin and Harmann (1989) JSRT, 42, 311-317. [12] Wordsworth et al. (2010) Icarus, 210, 992-997.

**WIND EROSION OF LAYERED SEDIMENTS ON MARS, AND THE ROLE OF TERRAIN.** Liam J. Steele[1], Edwin S. Kite[1] and Timothy I. Michaels[2], [1]University of Chicago, Chicago, Illinois, USA (liamsteele@uchicago.edu), [2]SETI Institute, Mountain View, California, USA.

**Introduction:** Most of the known sedimentary rocks on Mars take the form of mounds in craters and canyons [1] (e.g. Mount Sharp in Gale crater), but the mechanisms responsible for mound formation and evolution are uncertain. Wind erosion was an important process on early Mars [2-3]. One hypothesis for the mounds is that they are the result of the erosion of initially sediment-filled craters [4-5], while another is that mounds form in place by aeolian deposition [6].

Wind erosion occurs on Mars today, as evidenced by dune field activity [7-8]. Estimated erosion rates are 0.01–50 μm $yr^{-1}$, with the higher rates corresponding to vertical rock faces [9-11]. Over geological time, this allows for many km of cumulative erosion [12]. As mounds contain sedimentary deposits, wind erosion has implications for the preservation of organic matter. Areas recently and rapidly exhumed are the most promising candidates for future investigation [13].

The circulation within craters in the present-day is dominated by slope winds [14]. These winds will play an important role in the erosion of the sedimentary deposits, as well as the transport of sediment within or away from the craters. Thus, in order to identify the physical mechanisms involved in sedimentary mound formation and evolution, it is vital to obtain an understanding of (i) the diurnal variation of slope winds, (ii) the feedback between terrain and slope wind erosion, and (iii) changes to crater circulation and erosion with changing atmospheric pressure.

**Methods:** To investigate the role of terrain in wind erosion, we combine mesoscale model output with a landscape evolution model.

*Mesoscale model.* We use the Mars Regional Atmospheric Modeling System (MRAMS) [15] to investigate crater circulation. To isolate only the circulation related to crater topography, the simulations have the Coriolis force and thermal tides removed, and are initialized without large-scale winds.

Simulations are performed for a range of crater morphologies, with the diameter, depth, wall angle and rim height all varied. We also perform simulations of craters containing mounds, with the mound widths and heights varied (craters are axisymmetric). The surrounding topography is flat, and constant albedo and thermal inertia are used. The results show how the different crater morphologies impact the thermal and dynamical structure of the atmosphere surrounding the craters, and how these impact the erosion patterns.

*Landscape evolution model.* Results from the mesoscale simulations can be used as a lookup table for a landscape evolution model to investigate how crater topography changes with time. We have developed a Proof Of Concept Evolution of MOunds with erosioN (POCEMON) model, which can simulate detachment-limited erosion (where only the magnitude of the wind matters) as well as transport-limited erosion (where wind vectors are required for determining sediment transport). A power-law relationship between wind stress and mass flux is assumed [16].

**Results:** Mesoscale simulations were performed for a variety of crater morphologies, to study the effect of topography on circulation and erosion patterns. We simulated craters with diameters of 80, 160 and 320 km, depths ranging from completely infilled to 7 km deep, wall angles ranging from 5–15°, and the presence or absence of rims. Mound diameters ranged from 30–70% of the crater diameter, and mound heights ranged from 25–100% of the crater depth. Examples of the circulation for three craters with different mound shapes are shown in Fig. 1.

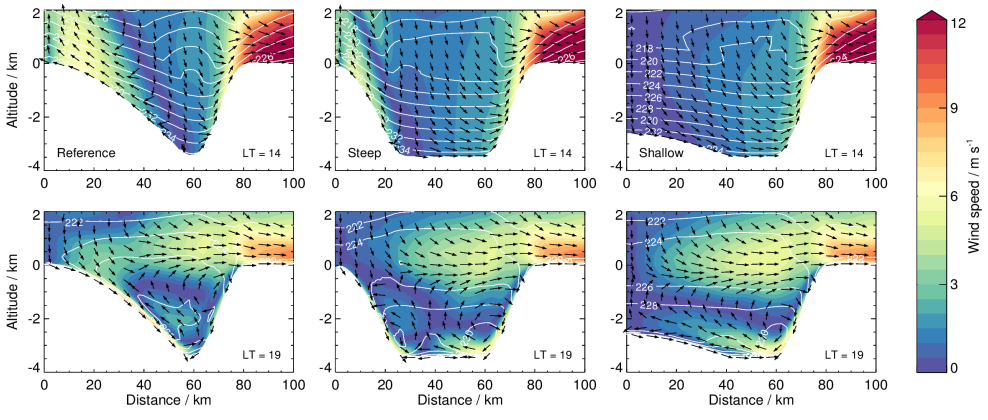


**Fig. 1**. Wind speeds (shading), directions (arrows) and temperature (contours) for three different crater morphologies. Anabatic (top) and katabatic (bottom) winds are shown at 2pm and 7pm local time (LT).

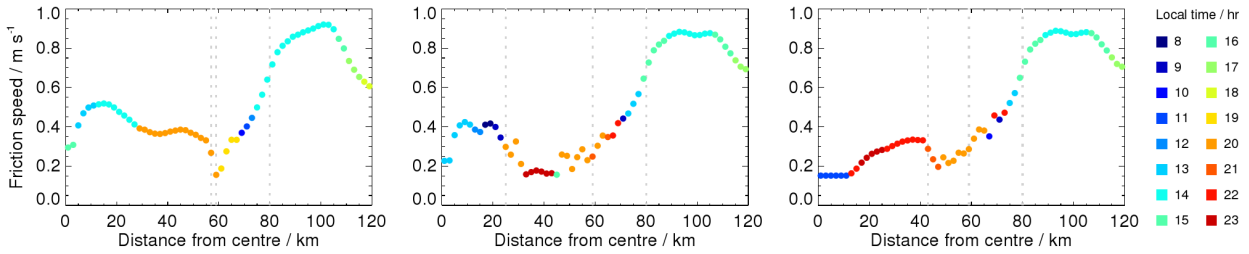


**Fig. 2.** Maximum daily friction speeds, as a function of distance from the crater center, color coded with the time of day they occur (in hours; see key). Grey lines mark the base of the mound and the start and end of the crater wall (see Fig. 1).

As can be seen in Fig. 1, while the circulation on the crater walls is similar, different mounds result in different circulation patterns. During the daytime (top panels) the anabatic winds on the mounds are stronger on the reference mound, while for the shallow mound the winds are weaker and downslope. During the night (lower panels) the reference mound has stronger katabatic winds than the other mound shapes. The mound size also affects katabatic winds on the crater walls, with stronger winds for the shallow mound case.

As well as mounds affecting the circulation, crater morphologies also play a role. For example, smaller diameter craters have stronger downwelling in the interior of the crater during the day, and the warming of the descending air makes the crater interior warmer, affecting circulation. Similarly, craters with shallow wall angles experience increased flux away from the crater during the day, which results in stronger downwelling in the interior of the crater during the day, and warmer temperatures compared to steeper wall angles.

For erosion, it is the friction speed that is important. Fig. 2. shows the maximum friction speeds for the three craters in Fig. 1, color coded by the time of day they occur. The strongest winds tend to occur on the tops of crater walls and mounds during the day, and towards the base of the crater at night. For detachment-limited erosion, only the magnitude of the wind speed (e.g. Fig. 2) is important. For transport-limited erosion, the direction of the circulation is important, as this determines where the sediment is transported.

Initial results using the landscape evolution model confirm that slope winds can sculpt a moat and mound from an initially flat crater infill. The results shown in Fig. 3 assume detachment-limited erosion. We will present results for other scenarios, including transport-limited erosion, at the conference.

**Future work:** To complement the studies of Mars' present atmosphere, we will investigate how circulation and erosion patterns change as the atmospheric density increases to values expected to have occurred on Mars billions of years ago, allowing us to trace erosion over time.

**References:** [1] Hynek B. M. et al. (2003) JGR, 108, 5111. [2] Zabrusky, K. et al. (2012) Icarus, 220, 311-330. [3] Kite, E. S. et al. (2016) JGR, 121, 2282-2324. [4] Malin, M. C. and Edgett, K. S. (2000) Science, 290, 1927-1937. [5] Day, M. et al. (2016) GRL, 43, 2473-2479. [6] Kite, E. S. et al. (2013) Geology, 41(5), 543-546. [7] Silvestro, S. et al. (2010) GRL, 37, L20203. [8] Chojnacki, M. et al. (2011) JGR, 116, E00F19. [9] Bridges, N. T. et al. (2012) Nature, 485(7398), 339–342. [10] Golombek, M. P. et al. (2014) JGR, 119, 2522-2547. [11] Kite, E. S. and Mayer D. P. (2017) Icarus, 286, 212-222. [12] Armstrong, J. C. and Leovy, C. B. (2005) Icarus, 176, 57-74. [13] Grotzinger, J. P. (2014) Science, 343, 386-387. [14] Tyler, D. and Barnes, J. R. (2015) GRL, 42, 7343-7350. [15] Rafkin, S. C. R. et al. (2001) Icarus, 151, 228–256. [16] Martin, R. L. and Kok, J. F. (2017) Sci. Advances, 3, 6.

**Acknowledgements:** This work was funded by NASA grant NNX15AH998G. We thank Jasper Kok, for discussions of saltation on Mars, and Daniel Tyler and Jeffrey Barnes for providing their simulation results for benchmarking our model.

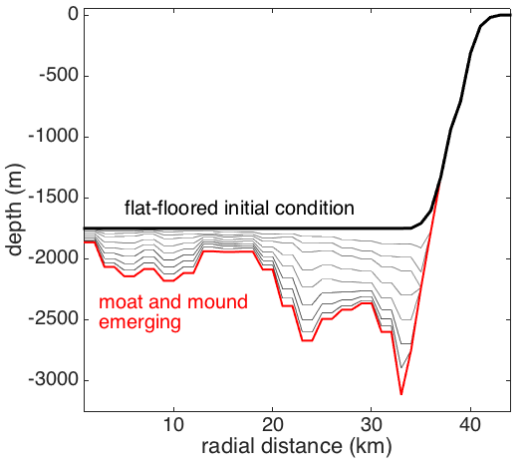


**Fig. 3.** A snapshot of moat-and-mound landscape evolution for detachment-limited wind erosion, assuming erosion flux is proportional to the time-average of the square of the wind stress. Erosion is only permitted for within-crater sediments.

**UNDERSTANDING HYDROLOGICAL AND CLIMATE CONDITIONS ON EARLY MARS THROUGH SULFATE CYCLING AND MICROBIAL ACTIVITY IN TERRESTRIAL VOLCANIC SYSTEMS.** A. Szynkiewicz[1], J. Mikucki[1], and D. Vaniman[2]. [1]University of Tennessee, 1621 Cumberland Ave., Knoxville, TN 37996 (aszynkie@utk.edu), [2]Planetary Science Institute, Tuscon, AZ.

**Introduction & Goals:** Sulfur (S)-bearing compounds are common on the Martian surface as sulfate minerals which are believed to be formed from water and volcanic/hydrothermal activity during the Noachian and/or Hesperian [1, 2]. However, it is unclear what type of hydrological and climate conditions (e.g., wet vs. dry) prevailed that led to elevated sulfate fluxes from oxidation of volcanic S-rich gases on early Mars. Therefore, our primary goal was to determine how changing wet and dry conditions of the seasonal hydrological cycle affect oxidation of volcanic S gases and sulfate fluxes into surface water and groundwater of a modern volcano, Valles Caldera in northern New Mexico, with active hydrothermal and acidic systems. Additionaly, we have investigated to what extent the acidic streams of this volcano can support diverse microbial communities capable of S transformation through oxidation and reduction (i.e. redox) reactions.

Our study is a type of Earth-based investigation in a Mars-analog environment that allows for quantitative S measurements coupled to understanding of multiple processes involved in aqueous-volcanic-microbial S cycling (e.g., hydrological, climatic, biogeochemical) that cannot be easily done under current, dry conditions on Mars and/or using the rock record alone. In particular, the aqueous $SO_4$ budget and hydrological transport of $SO_4$ can be studied and compared to the wetter conditions on early Mars. However, this study cannot be used to understand the $SO_4$ depositional environment because the study site represents an open system, without a depositional environment (e.g., lake), in which $SO_4$ is constantly transported away by active hydrological system.

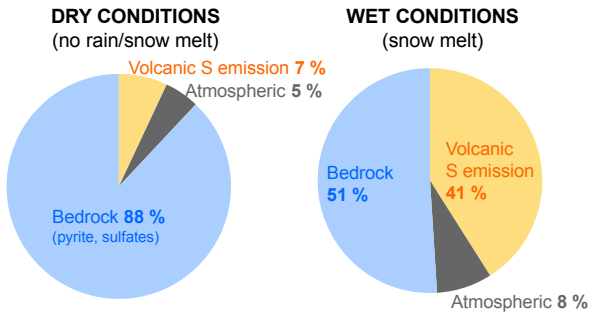


**Figure 1.** Total aqueous $SO_4$ budget in the hydrological system of Valles Caldera volcano. Blue, yellow and grey colors show % contributions of $SO_4$ from the bedrock (neutral pH streams), $H_2S$ emission (acidic streams) and atmospheric wet deposition, respectively.

**Analogue Setting:** The 22 km-wide Valles Caldera of northern New Mexico (USA) has hosted volcanic and geothermal activity since the last caldera-forming eruption at 1.25 Ma [3, 4]. The presence of active $H_2S$-rich fumaroles, volcanic sulfide/sulfate mineralization in the bedrock, the high elevation (2,600 to 3,400 m asl), snow cover during the winter, low annual temperatures (average ~8°C), and numerous streams make the Valles Caldera an useful hydrological and geochemical analogue for early Mars. The circular shape of the watershed, with the Jemez River draining a network of primary acidic and neutral pH streams, makes this site ideal for quantifying the relative contributions of $SO_4^{2-}$ from volcanogenic, bedrock and atmospheric sources in relation to climate, hydrology and elevated $H_2S$ gas emission.

**Methods:** Between 2012 and 2014, the amount of $SO_4$ transported in the surface hydrological system during one wet (snowmelt) and two dry (no rain/snow) seasons was determined by calculating the $SO_4$ flux in acidic and neuatral streams of Valles Caldera watershed. The stream $SO_4$ flux was determined by multiplying the stream-water $SO_4$ concentrations by the volumetric flow (stream discharge) rates. This flux corresponds to the mass of dissolved $SO_4$ ions that flow out of the caldera per unit time (e.g., kg $SO_4$ per day). Additionally, respresentative volcanic bedrock samples were collected for XRD analysis by a TERA instrument to determine quantities and types of sulfide/sulfate mineralization from earlier volcanic/hydrothermal activities. To link microbial metabolic potential with elevated volcanic S-rich gas emission in acidic streams, we examined both the diversity of the 16S rRNA gene and the presence of adenosine-5-phosphosulfate (APS) reductase, a key gene involved in both dissimilatory (i.e. energy yielding) sulfate reduction and S oxidation reactions.

**Results & Discussion:** Our initial results imply three major $SO_4$ sources in the studied aqueous volcanic system of Valles Caldera (Fig. 1): *i*) chemical weathering of older hydrothermal S-rich minerals, *ii*) modern oxidation of fumarolic $H_2S$ in surface environments), and *iii*) atmospheric deposition. Hydrothermal pyrite, gypsum and alunite are major S-bearing minerals in the bedrock and $H_2S$ contributes locally ~2% of total fumarole gas emission. The concentrations of $SO_4$ in the water column of the studied acidic springs were always significantly higher (500-1,200 mg/L) compared to $H_2S$

(<0.11 mg/L), which suggests that the majority of volcanic $H_2S$ is likely oxidized to $SO_4$ within the streambed and/or in shallow groundwater.

In the investigated seasons, contributions of $SO_4$ from volcanic $H_2S$ emission and oxidation varied seasonally (Figs. 1, 2), with highest inputs (41%) during snowmelt (wet conditions) when compared to bedrock (51%) and atmospheric (8%) sources. Under dry conditions (no rain/snowmelt, reduced stream discharges), the volcanic contributions were significantly smaller (7%) when compared to the bedrock (88%) and atmospheric (5%) inputs. This implies that wet conditions lead to more $H_2S$ oxidation to $SO_4$ in the surface environment. In contrast, during dry conditions more $H_2S$ is likely to be emitted and diluted in the atmosphere.

In the acidic springs samples where $H_2S$ gas emission and $SO_4$ concentrations were eleveated, DNA extraction and amplification were challenging due to low organic content. However, >50% of the 16S rRNA amplicons detected were related to groups known to oxidize reduced S compounds. APS reductase was also detected in these samples suggesting the potential for biological S-oxidation in the acidic springs. We were unable to confirm whether their APS reductase is operating in an oxidizing or reducing manner based on phylogenetic distance. Both S oxidizing and reducing 16S rRNA gene sequences were detected in our samples, although S-reducing sequenes were much less abundant. Our findings are in line with a previous molecular survey [5] that detected 16S rRNA sequences related to S-oxidizing acidophiles of the genus *Desulfurella* and *Thiobacillus*. Collectively our results add further support to a biological component to the S signal in the acidic streams of Valles Caldera.

**Conclusions:** Despite important quantitative differences in aqueous $SO_4$ contributions from direct oxidation of volcanic $H_2S$ and bedrock weathering (Fig. 1), both wet and dry conditions appear to support hydrological $SO_4$ transport in surface water and groundwater. This suggests that when an active hydrological cycle prevails at a particular time and the S reservoir (volcanic gas, hydrothermal minerals) is available for water interaction, $SO_4$ is actively formed and incorporated into this cycle. Therefore, even with limited water activity on early Mars the oxidation of volcanic S-rich gases/bedrock would lead to formation of aqueous $SO_4$.

The DNA content (molecular biosignatures) was relatively low and challenging to extract from S-rich sediments collected in the acidic streams with highest $H_2S$ gas emission. Therefore, similar molecular biosignatures on Mars might be difficult to detect if not returned to Earth. Nevertheless, current orbital instruments such as HiRISE and CRISM could be used to detect potential hydrological drainage sites associated with hydrothermal S-rich activity and habitable conditions, to guide the Mars 2020 rover for sample return. For example, streams and hot springs with elevated hydrothermal $H_2S$ emissions typicaly show high contents of elemental S and sulfate minerals [5 and this study].

**References:** [1] McLennan (2012) *Meteoritics & Planet. Sci., 32,* A74. [2] McCollom T.M. & Hynek B.M. (2005) *Nature 438*, 1129-1131 [3] Goff F. et al. (2007) *NMGS 58th Field Conf.*, 354-366. [4] Szynkiewicz et al. (2012) *EPSL, 321-322,* 1-13. [5] Rzonca & Schulze-Makuch (2003) *J. Hydrol. 280, 272-284*.

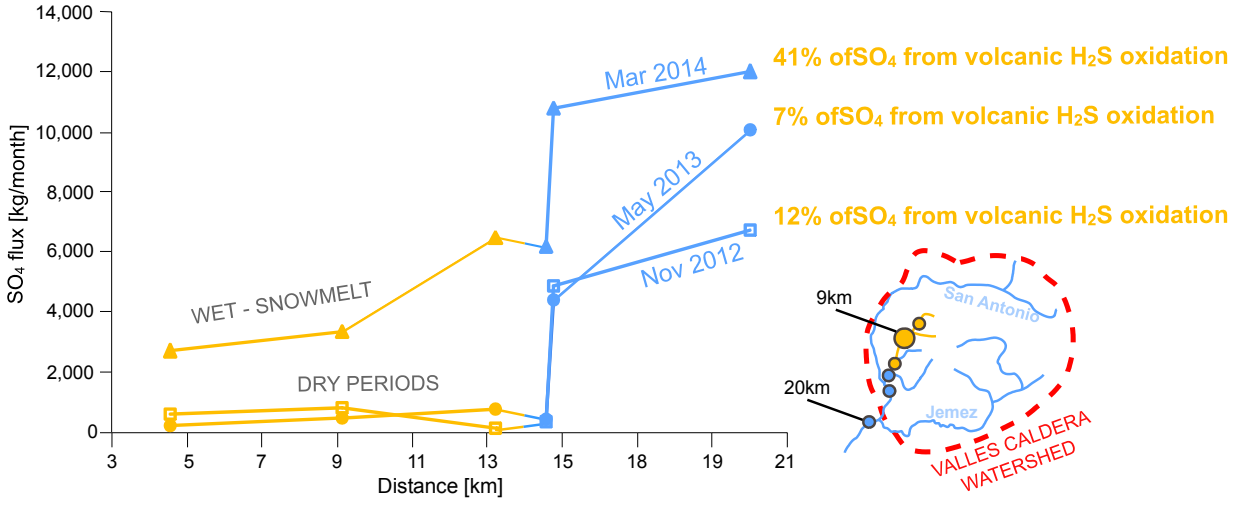


**Figure 2.** Seasonal changes of aqueous $SO_4$ fluxes in the acidic (yellow) and neutral pH (blue) streams of Valles Caldera volcano. On the right, a simplified sketch of major stream drainage system is presented for comparison with the plot on the left, showing $SO_4$ fluxes relative to distance.

**Acknowledgements:** This study was supported by NASA award No. NNX14AB63G.

**RADIOLYTIC $H_2$ PRODUCTION ON NOACHIAN MARS: IMPLICATIONS FOR SUBSURFACE HABITABILITY.** J. D. Tarnas[1], J. F. Mustard[1], B. Sherwood Lollar[2], M. S. Bramble[1], K. M. Cannon[3], A. M. Palumbo[1], [1]Brown University, Providence, RI, USA (jesse_tarnas@brown.edu), [2]University of Toronto, Toronto, ON, Canada, [3]University of Central Florida, Orlando, FL, USA.

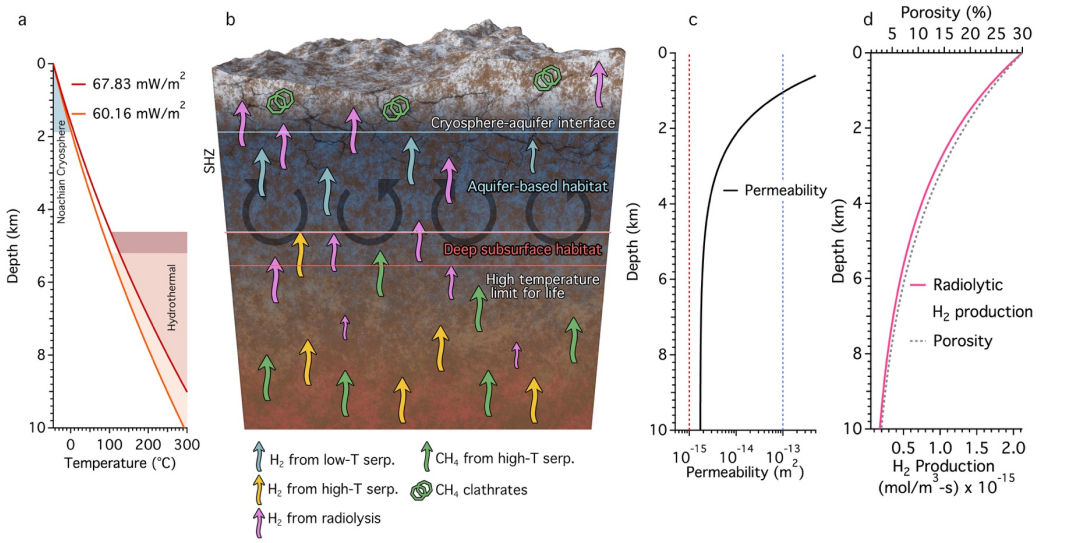


**Figure 1 | Noachian subsurface habitability model.** After [2]. **a)** Temperature increase with depth given a surface temperature of -45 °C [12] and two possible heat fluxes [13, 14] from initial mantle temperatures of 1650 K (60.16 mW/m$^2$) and 1850 K (67.83 mW/m$^2$). **b)** Cross-section of Noachian crust displaying the cryosphere, $H_2$ from radiolysis and serpentinization, $CH_4$ from serpentinization/carbonation, $CH_4$ clathrates, groundwater circulation (which contains dissolved $H_2$), and two distinct subsurface habitats –one aquifer-based within the subcryospheric highly-fractured zone (SHZ), and one between the depth that hydrothermal processes begin [2] (100 °C, 4.8 km) and the depth that the currently known upper temperature limit for life [26] is reached (122 °C, 5.6 km). **c)** Permeability decrease with depth based on the model from [16], but assuming a rock density of basalt rather than granite. The blue dotted line indicates the minimum surface permeability for basaltic aquifers in the Oregon Cascades ($10^{-13}$), while the maximum surface permeability is $10^{-9}$ m$^2$ ([16] and sources therein). The red dotted line indicates the maximum permeability at 10 km depth for basaltic aquifers in the Oregon Cascades ($10^{-15}$), while the minimum permeability at this depth is $10^{-18}$ m$^2$ ([16] and sources therein). **d)** Radiolytic $H_2$ production calculated using our model and porosity decay [11] with depth.

**Introduction:** The subsurface of Mars may have been the planet's longest-lived continually habitable environment [1,2]. Requirements for subsurface life include above-freezing temperatures, the elements CHNOPS for cell construction, and sufficient concentrations of reducing and oxidizing compounds to drive metabolisms of microbes through biologically facilitated redox reactions that sustain abundant subsurface microbial communities on Earth. $H_2$ produced through water-rock alteration reactions including radiolysis [3-5] and serpentinization [6, 7] is considered one of the most important reducing compounds feeding such ecosystems on Earth [8]. Here we model $H_2$ production on Noachian Mars via radiolysis of pore water by $\alpha$, $\beta$, and $\gamma$ radiation produced through decay of K, Th, and U in the martian crust. We find that the quantity of $H_2$ is sufficient to have sustained subsurface microbial ecosystems on Mars for hundreds of millions of years during the Noachian. Furthermore, we use geophysical arguments to constrain the probable location of this subsurface habitat, as shown in Figure 1. Biosignature-hosting material from this habitat, termed the subcryospheric highly-fractured zone (SHZ), can be excavated in megabreccia blocks ejected from later impacts that penetrate beneath the depth of the Noachian cryosphere, making this hypothesis testable through future robotic and human exploration of Mars.

**Methods:** Using the model described by [5] and [9], radiolytic $H_2$ production during the Noachian is calculated by extrapolating Odyssey's Gamma Ray Spectrometer (GRS) K and Th elemental maps [10] to Noachian concentrations, obtaining U abundances by assuming a Th/U ratio of 3.6, modeling the spatially resolved cryosphere depth [11] based on Noachian surface temperature [12] and heat flux [13, 14] models, and modeling Mars crustal porosity [11] using parameter values derived from GRAIL [15] scaled to martian gravity. Radiolytic $H_2$ produced beneath the cryosphere base is biologically useful, as illustrated in Figure 1. Following [16] we model crustal permeability, which we use as a proxy for groundwater activity, indicating the degree to which serpentinization would occur in ultramafic zones of the crust.

**Results:** For water-filled porosity and an initial mantle temperature of 1650 K (corresponding to the thickest cryosphere produced in our models, shown in Figure 2), the global $H_2$ production at 4 Ga is [0.72-2.40] $\times$ $10^{10}$ moles $H_2$ yr$^{-1}$ in the cryosphere, [2.63-6.23] $\times$ $10^{10}$ moles $H_2$ yr$^{-1}$ in the subcryosphere, with [0.35-1.13] $\times$ $10^{10}$ moles $H_2$ yr$^{-1}$ generated in the SHZ, assuming a 3 km depth SHZ base and including the estimates for both 10% and 30% surface porosity. These results represent the minimum biologically useful $H_2$ production under the boundary conditions of this study.

These radiolytic $H_2$ production rates for Noachian Mars are all approximately equal to the $H_2$ production rate in Earth's Precambrian crust ([1.6-4.7] $\times$ $10^{10}$ moles $H_2$ yr$^{-1}$) [3], which covers a similar surface area to the total surface area of Mars ($1.06 \times 10^8$ km$^2$ and $1.44 \times 10^8$ km$^2$,

respectively) and has been shown to support abundant chemolithotrophic microbial life in the terrestrial subsurface [3, 17]. Therefore, we propose radiolytic $H_2$ production during the Noachian was sufficient to support microbial life in the martian subsurface, especially when coupled with additional $H_2$ generated by serpentinization. Serpentinization has been estimated to produce approximately $6.83 \times 10^{10}$ moles $H_2$ $yr^{-1}$ at 4 Ga in the top 12 km of crust [18, 19], which lies within our estimated range of radiolytic $H_2$ production at 4 Ga in the top 10 km of crust ($[3.35\text{-}8.63] \times 10^{10}$ moles $H_2$ $yr^{-1}$). Both radiolysis and serpentinization would therefore supply chemical energy to subsurface martian microbial ecosystems during the Noachian in roughly equal amounts, though the majority of $H_2$ from serpentinization would be produced in the lower, hotter crust, and may be transported to the SHZ by circulating groundwater.

Radiolysis produces $H_2$ at approximately 0.1-1.3% the rate it was lost to space during the Noachian [20]. In order to have a significant climatic effect, this $H_2$ would need to be locked in $H_2$ clathrates, which are stable at the base of the Noachian cryosphere [21], and released during catastrophic events that perturb the cryosphere. Future investigation will determine whether enough $H_2$ could be stored in the cryosphere to have a significant climatic effect, such as increasing mean annual temperatures above the melting point of $H_2O$.

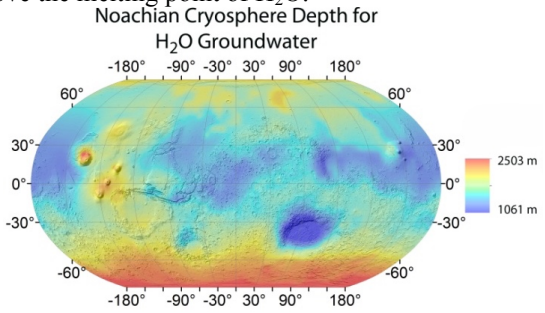


**Figure 2 | Noachian cryosphere depth.** Modeled depth of an $H_2O$ cryosphere 4.1 Ga based on modeled surface temperature [12] (1 bar $CO_2$ atmosphere, 25° obliquity) and heat flux [13, 14] (initial mantle temperature = 1650 K).

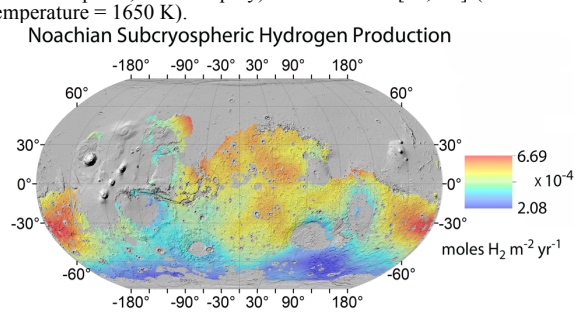


**Figure 3 | Radiolytic $H_2$ production maps.** Modeled $H_2$ production via radiolysis in the Noachian subcryosphere assuming 30% surface porosity, $H_2O$ groundwater, and 1650 K (1377 °C) initial mantle temperature.

**Discussion:** By integrating geophysical and geochemical models, we quantify the depth range of the most habitable section of the martian crust during the Noachian –the SHZ. Here, microbial ecosystems could have been sustained for hundreds of millions of years by $H_2$ derived from radiolysis and low temperature serpentinization, combined with $H_2$ and $CH_4$ derived from high temperature serpentinization and transported via groundwater circulation and gas diffusion, as shown in Figure 1.

Later impacts on Noachian or Early Hesperian age terrain that penetrate beneath the depth of the Noachian cryosphere can excavate material from the SHZ, exposing it in ejecta or interior crater deposits. These units are thus compelling targets for astrobiological exploration of the possible ancient subsurface martian biosphere. Megabreccia blocks on Mars commonly contain hydrated minerals such as phyllosilicates formed by hydrothermal alteration [22-24], either in the subsurface before impact [25] or from hydrothermal systems generated by impacts [20]. These units could contain biosignatures from both the SHZ and younger, transient, impact-induced hydrothermal environments [22]. Many megabreccias also contain unaltered megaclasts with their original mafic or ultramafic composition [22-24], revealing the $H_2$ production potential from serpentinization of this precursor material, as this is controlled by composition. Megabreccia that contain both altered and unaltered facies are thus potentially valuable astrobiological targets, as they may contain morphological, organic, and chemical biosignatures from both the SHZ, the longest lived habitable environment on Mars, and possible impact-induced transient hydrothermal habitats.

**Conclusions:** Using models of subsurface energy availability, crustal temperature profiles, and permeability, we quantify the probable location of the longest lived subsurface habitat on Mars, termed the SHZ. Later impacts into Noachian to Early Hesperian age terrain that penetrate beneath the depth of the Noachian cryosphere can excavate material from the SHZ that would contain morphological, organic, and chemical biosignatures if subsurface life did exist on ancient Mars. We postulate that the most valuable astrobiological targets on the martian surface are megabreccia blocks from such impacts that contain both their original unaltered mafic lithologies as well as altered phyllosilicate lithologies generated by both pre-impact subsurface hydrothermal alteration and post-impact hydrothermal alteration, as the former would contain biosignatures from the SHZ and the latter would contain biosignatures from impact-induced transient hydrothermal habitats, if either of these habitats did host life on Noachian Mars. This should be considered in the context of Mars 2020, ExoMars, and future robotic and human exploration of the Red Planet.

**References:** [1] Ehlmann B.L. et al. (2011) *Nat.*, *479*, 53-60. [2] Michalski J.R. et al. (2013) *Nat. Geo.*, *6*, 133-138. [3] Sherwood Lollar B. et al. (2014) *Nat.*, *516*, 379-382. [4] Lin L.-H. et al. (2005) *$G^3$*, *6*, Q07003. [5] Lin L.-H. et al. (2005) *GCA*, *69*, 893-903. [6] Kelley D.S. et al. (2005) *Sci.*, *307*, 1428-1434. [7] Sleep N.H. et al. (2004) *PNAS*, *101*, 12818-12823. [8] Boston P.J. (1992) *Icar.*, *95*, 300-308. [9] Onstott T.C. et al. (2006) *Astrobio.*, *6*, 377-395. [10] Boynton W.V. et al. (2007) *JGR*, *112*, E12S99. [11] Clifford S.M. et al. (2010) *JGR*, *115*, E07001. [12] Palumbo A.M. & Head J.W. (2017) *LPSC XLVIII*, *2107*. [13] Plesa A.-C. et al. (2016) *JGR*, *121*, 2386-2403. [14] Plesa A.-C., pers. comm. [15] Besserer F.B. et al. (2014), *GRL*, *41*, 5771-5777. [16] Hanna J.C. & Phillips R.J. (2005) *JGR*, *110*, E01004. [17] Lin L.-H. et al. (2006) *Sci.*, *314*, 479-482. [18] Vance S.D. et al. (2007) *Astrobio.*, *7*, 987-1005. [19] Vance S.D. et al. (2016) *GRL*, *43*, 4871-4879. [20] Wordsworth et al. (2016) *GRL*, *44*, 665-671. [21] Patchkovskii & Tse (2003) *PNAS*, *100*, 14645-14650. [22] Osinski G.R. et al. (2013) *Icar.*, *224*, 347-363. [23] Tornabene L.L. et al. (2009) *LPSC XL*, *1766*. [24] Tornabene L.L. et al. (2013) *JGR*, *118*, 994-1012. [25] Ehlmann, B.L. et al. (2011) *Nat.*, *479*, 53-60. [26] McKay, C.P. (2014) *PNAS*, *111*, 12628-12633.

**MAGNETITE AUTHIGENESIS AND THE ANCIENT MARTIAN ATMOSPHERE.** N. J. Tosca[1*], I. A. Ahmed[1], A. Ashpitel[1], J. A. Hurowitz[2] [1]Department of Earth Sciences, University of Oxford, Oxford, OX1 3AN, UK; [2]Department of Geosciences, Stony Brook University, Stony Brook, NY 11794-2100. *nick.tosca@earth.ox.ac.uk

**Introduction:** In 2013, NASA's Mars Science Laboratory *Curiosity* rover discovered an ancient fluvio-lacustrine environment in Gale Crater, Mars. Sedimentological, stratigraphic, and geochemical relationships document standing bodies of dilute water that persisted for hundreds to thousands of years [1].

Yet, how liquid water became physically stable at Gale Crater is unknown. Although the early Martian atmosphere is thought to have been dominated by $CO_2$ [2, 3], the *Curiosity* rover has provided only ambiguous detections of carbonate minerals at abundances significantly less than 1 wt. % [4, 5], and climate models indicate that in the absence of additional components, multi-bar $CO_2$ atmospheres could not have maintained surface temperatures above freezing [3, 6]. At relatively low abundance, $H_2$ and its reaction products (i.e., $CH_4$), could have warmed the surface in the presence of elevated $CO_2$ [7, 8], but a compelling generation and delivery mechanism for these species has yet to be identified. Volcanic sources have been identified as a potential source of $H_2$ [7], but these require reducing mantle conditions that may have limited $CO_2$ release and atmospheric $CO_2$ concentration [9].

**Experimental constraints:** Sedimentary rocks offer constraints on atmospheric composition if authigenic mineral formation pathways can be constrained. However, for Gale Crater mudstones, a poor understanding of Fe(II)-mineral precipitation kinetics precludes atmospheric reconstruction, in particular as the $CO_2$-dependence of these reactions is poorly known.

We addressed these uncertainties with two experimental approaches. First, to investigate the nucleation and growth kinetics of authigenic Fe(II)-minerals in Gale Crater mudstones, we conducted precipitation experiments using synthetic $Fe^{2+}$, $Mg^{2+}$, and $SiO_2(aq)$-bearing waters, modeled after those expected to form from reactions between water and basalt. As these anoxic waters experience pH increases above ~8.0, $Fe(OH)_2$ nucleation is triggered (**Fig. 1**). Once precipitated, ageing of $Fe(OH)_2$ renders it unstable, even under strictly anoxic conditions; in minutes, $Fe(OH)_2$ transforms to green rust, a structurally related Fe(II)-Fe(III)-hydroxide. As pH and anoxic conditions are maintained, green rust transforms to magnetite in days.

Electrochemical and dissolved gas analyses show that the anoxic decomposition of $Fe(OH)_2$ produces abundant $H_2$. Once $Fe(OH)_2$ is fully transformed to green rust as electrons as shuttled to $H_2O$, $H_2$ production ceases and ORP recovers to pre-experiment values as $H_2$ exsolves to the reactor headspace (**Fig. 1**).

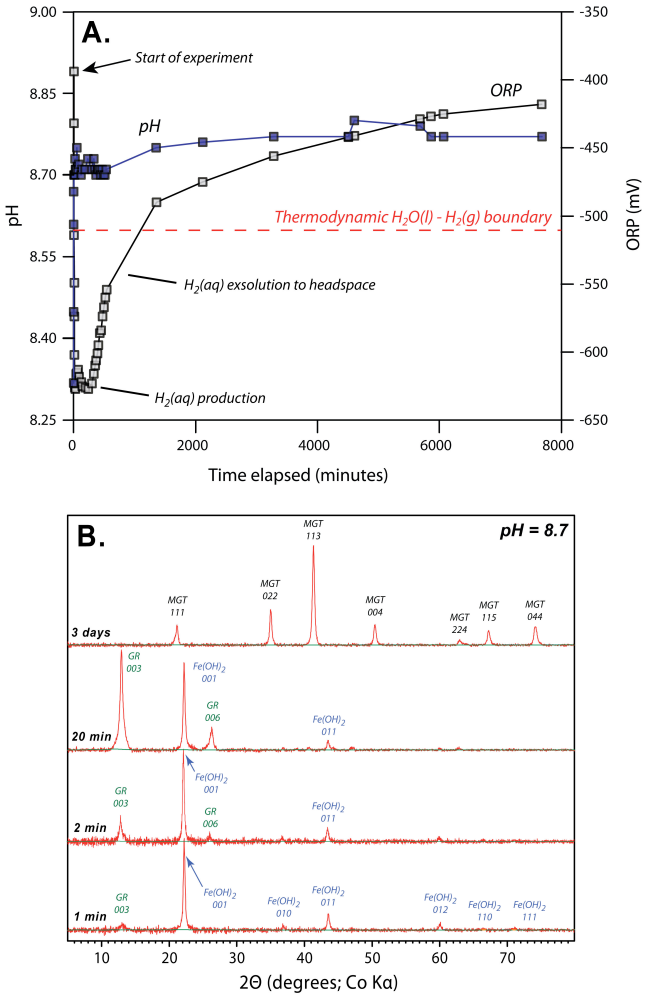


***Fig 1. (A.)*** *As pH is increased oxidation-reduction potential (ORP) falls below the thermodynamic stability of $H_2O(l)$ as $H_2(aq)$ is generated* ***(B.)*** *Under strictly anoxic conditions, pH increases precipitate $Fe(OH)_2$ which converts to green rust, in turn reducing $H_2O(l)$ and forming $H_2(g)$. Metastable green rust transforms to magnetite in days.*

To investigate the influence of dissolved $CO_2$, we conducted nucleation experiments in the $Fe^{2+}$-$Mg^{2+}$-$SiO_2(aq)$ system as a function of pH and $CO_2$, again under strictly anoxic conditions. As above, when its solubility is exceeded, $Fe(OH)_2$ precipitates and transforms to green rust (**Fig. 2**). Fe(II)-carbonates also nucleate, but at supersaturations well above those predicted by equilibrium siderite solubility (**Fig. 2**). In fact, our experiments delineate a critical supersaturation ($K_{crit}$) corresponding to the solubility of amorphous Fe(II)-carbonate (AFC), which, in solution, ages to siderite or chukanovite ($Fe^{II}_2(CO_3)(OH)_2$, metastable with respect to siderite [10]).

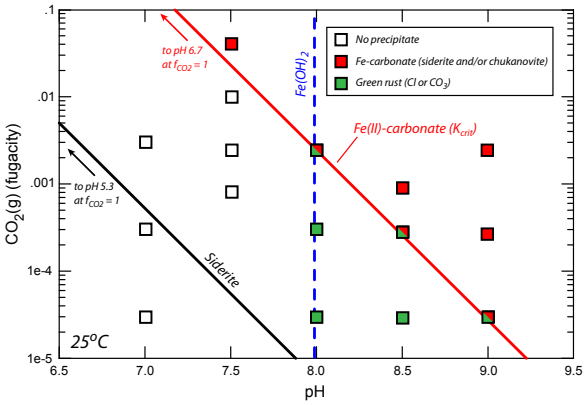


***Fig. 2.*** *Water compositions initially supersaturated with respect to $Fe(OH)_2$ (to the right of the blue line) generate green rust through the transformation shown in Figure 1. Compositions initially supersaturated with respect to siderite (above the black line) do not generate Fe(II)-carbonate unless a critical supersaturation value (red line) is crossed.*

**Magnetite authigenesis in Gale Crater mudstones:** Our experimental observations imply that Gale Crater lakes could have been in equilibrium with atmospheric $CO_2$ pressures up to 1 bar. High atmospheric $CO_2$ and low silicate dissolution rates sustain chemical conditions in the lake bodies far below the nucleation threshold for Fe(II)-carbonate or $Fe(OH)_2$ (i.e., pH ~5-6) for hundreds to thousands of years.

However, geochemical and mineralogical data indicate that $Fe(OH)_2$ solubility must have been exceeded in sediments that preserve authigenic magnetite. The topographic depression in which the lakes were situated resides at the lowest elevation for thousands of kilometers in any direction [1], implying that physical stabilization of a water body at this location involved a significant groundwater component [1].

To evaluate the role of groundwater infiltration on authigenesis in Gale Crater mudstones, we incorporated new experimental data for Fe(II)-mineral precipitation into a geochemical mixing model. These calculations show that as groundwater infiltrated lacustrine sediments at Gale Crater, Fe(II)-carbonate saturation was never reached, and $Fe(OH)_2$ precipitated instead. This scenario is consistent with data from the Sheepbed member mudstones at the base of the stratigraphic section, and deep-water mudstones of the stratigraphically higher Murray formation, both of which contain abundant authigenic magnetite [4, 11, 12].

**Implications for the ancient martian atmosphere:** More broadly, low temperature $H_2$ production may have provided a globally significant but transient feedback for stabilizing liquid water on early Mars. Although $CO_2$-rich atmospheres could not have stabilized liquid water, climate models predict that adiabatic cooling would have transferred water ice to high altitude equatorial and southern regions [13, 14]. Episodic melting events would have delivered melt water to topographic lows. As melt water infiltrated surface and subsurface reservoirs, pulses of magnetite authigenesis could have focused $H_2$ at their interface. Percent levels of $H_2$ in $CO_2$-dominated atmospheres leads to collision-induced absorption that could have maintained the surface of Mars above the freezing point of water; this would be further enhanced if $H_2$ reacted to form $CH_4$ [7, 8]. The timescales of $H_2$-induced warming would have been limited by $H_2$ escape and $CH_4$ photo-dissociation, restoring paleo-climates to cold steady-state conditions through adiabatic cooling after 100,000 years or more [8].

Geological observations made to date by the Curiosity rover are consistent with both estimated timescales and climatic shifts associated with transient $H_2$-induced warming. Bulk rock geochemistry of the Sheepbed member mudstone indicates exceedingly low chemical index of alteration (CIA) values, consistent with sediment production under cold or arid climates [1, 15]. Overlying stratigraphy at Gale documents shifts to higher CIA values in the Murray Formation, consistent with a climatic shift to conditions supporting more effective chemical denudation [11].

Finally, low temperature $H_2$ production implies that a wide range of biologically relevant chemical reactions may have been operative on early Mars. $H_2$ is a principal feedstock in the synthesis of both atmospheric $CH_4$ and prebiotic organic compounds [16, 17], and is a potent fuel for several autotrophic metabolisms. In fact, the exergonic reaction between $H_2$ and $CO_2$, both accumulating at the interface between lake bottom and groundwater on early Mars, lies at the core of the acetyl-CoA pathway, which is considered one of the earliest bio-energetic metabolisms on Earth [18, 19]. Gale Crater sediments provide a crucial missing piece to the Martian climate puzzle, and re-define the biological habitability of early Martian surface environments in unprecedented chemical detail.

**References:** [1] J. Grotzinger *et al*. (2015) *Science* **350**, 13. [2] J. Pollack, et al. (1987) *Icarus* **71**, 203-24. [3] J. Kasting, (1991) *Icarus* **94**, 1-13. [4] D. Vaniman *et al.*, (2014) *Science* **343**, 8. [5] D. Ming, *et al.*, (2014) *Science* **343**, 1245267. [6] F. Forget, *et al.* (2013) *Icarus* **222**, 81-99. [7] R. Ramirez, *et al.* (2013) *Nat. Geo.* **7**, 59-63. [8] R. Wordsworth, *et al.* (2017) *GRL* **44**, 665-71. [9] M. Hirschmann, *et al.* (2008) *EPSL* **270**, 147-55. [10] K. Dideriksen, *et al.* (2015) *GCA* **164**, 94-109. [11] J. Hurowitz, *et al.* (2017) *Science* **356**, 922. [12] E. Rampe, *et al.* (2017) *EPSL*, 471, 172 [13] R. Wordsworth, *et al.* (2013) *Icarus* **222**, 1-19 (2013). [14] R. Wordsworth, *et al.* (2015) *JGR Planets* **120**, 1201-19. [15] S. McLennan, *et al.* (2014) *Science*, **343**, [16] P. Abelson (1966) *PNAS* **55**, 1365-72. [17] S. Miller (1953) *Science* **117**, 528-9. [18] S. Ragsdale & E. Pierce (2008) *Biochim. Biophys. Acta* **1784**, 1873-98. [19] R. Braakman & E. Smith (2012) *PLoS Comput. Biol.* **8**, e1002455.

**THE ENVIRONMENTAL EFFECT OF METEORITIC IMPACTS ON EARLY MARS WITH A VERSATILE 3-D GLOBAL CLIMATE MODEL.**

M. Turbet[1], F. Forget[1], V. Svetsov[2], H. Tran[1], J-M Hartmann[1], Ozgur Karatekin[3], C. Gillmann[3], O. Popova[2], & J. Head[4]. Laboratoire de Météorologie Dynamique, IPSL, UPMC (martin.turbet@lmd.jussieu.fr), [2] Institute for Dynamics of Geospheres, Russian Academy of Sciences, Leninskiy Prospekt 38-1, Moscow 119334, Russia, [3] Royal Observatory of Belgium, Avenue Circulaire 3, 1180 Uccle, Belgium. [4] Brown University, Providence, RI 02912, USA.

**Introduction:** There are now numerous evidences that liquid water flowed on early Mars: high erosion rates, sedimentary deposits, hydrated minerals and geomorphological clues including dry river beds and lakes [1-14]. Sophisticated climate modelling under ancient Mars conditions assuming a faint young Sun and $CO_2$-dominated atmospheres have not been able yet to produce liquid water or significant precipitations anywhere on the planet [15,16], unless incorporating additional reduced greenhouse gases, e.g. $CH_4$ and/or $H_2$ [17-19]. For more information, we refer you the the review presented by Forget et al., this issue.

Meanwhile, it has been suggested that warm & wet conditions required to explain the formation of the aforementioned geological evidences could have been transient and produced in response to meteoritic impacts [16,20-23]. This scenario is seducing because the formation of the valley networks may be contemporaneous with the Late Heavy Bombardment that took place 3.8 Gya.

We model here the environmental effect of meteoritic impacts with a 3-D Global Climate Model, to explore if they could trigger the warm conditions and the precipitation rates required to explain the formation of the valley networks.

**Method:** This study was performed with the versatile 3-Dimensions LMD Generic Global Climate Model (GCM). The model works with a sophisticated water cycle that includes the formation of $H_2O$ and $CO_2$ ice clouds [15,16,24], and for various atmospheres made of $CO_2$/$N_2$/$H_2O$. Simulations were performed with resolution grids of 3°x3°x40 levels (in latitude x longitude x altitude). We used both the present-day MOLA and ancient Mars topographies [24-26], when appropriate. More details on the model can be found in [15,16,24,26,27].

Compared to previous studies [16,20-24,26], here we carefully incorporated the radiative effect of spectroscopic features (line widths at half-maximum, far line absorptions and Collision Induced Absorptions) typical of $CO_2$-$H_2O$ rich [28-30] post-impact atmospheres. As an illustration, far-line IR opacities can be increased by 1-2 orders of magnitude, when broadening properly $H_2O$ lines by $CO_2$ instead of air. For more information on these new spectroscopic refinements, we refer the reader to the poster presented by Martin Turbet (this issue).

**Effect of large impact events:** We simulated the climatic impact of large meteoritic impactors ($D_{impactor}$>100km, $N_{events}$ ~ 10) hitting the surface of Mars at velocities ~10km/s, by forcing initially the atmosphere/surface/subsurface at temperatures up to 600 Kelvins, and vaporizing up to several bars of water vapor.

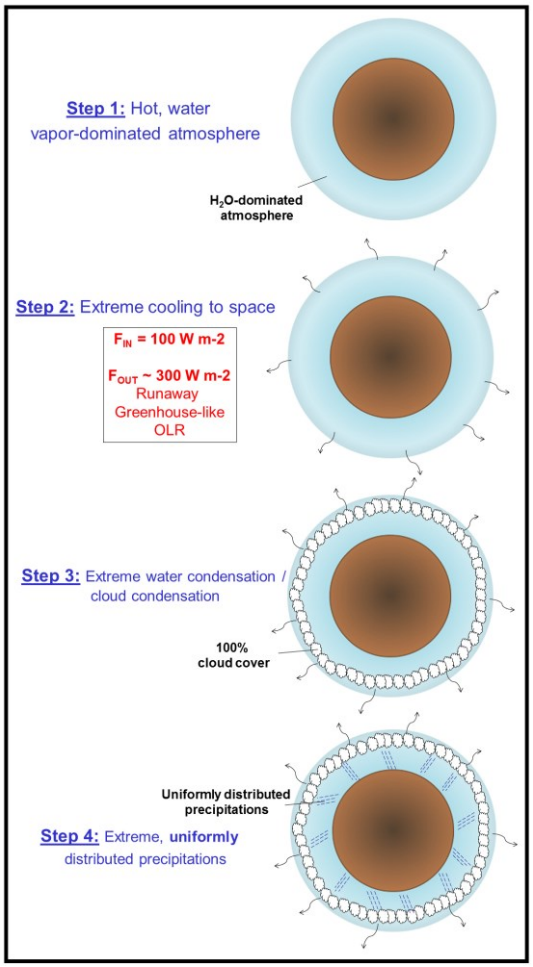


**Figure 1:** Sketches of the physical processes occuring after a post-impact hot, steam atmosphere forms on Early Mars.

Our main result is that, *whatever the initial impact-induced temperatures and water vapor content injected, warm climates cannot be stable and are in fact short-lived* (lifetime of ~ 5-7 martian years per bar of water vapor injected). The results of Segura et al. 2012 [22], which would require extremely high supersaturation

levels of water vapor to work, are at odd with our findings. Note that we obtain minimum outgoing thermal radiation fluxes that are in good agreement with recent studies on the runaway greenhouse effect [31].

When a hot, steam atmosphere forms after a large meteoritic impactor hits early Mars, our 3-D climate simulations indicate that the IR thermal emission to space is roughly 200W/m² higher than the incoming stellar radiation (under Faint Young Sun), *everywhere on the planet*. At the altitude of IR emission to space, water vapor condenses, releasing ~ 200W/m² of latent heat, everywhere on the planet. Consequently, a 100%, thick cloud cover forms, producing precipitation (rainfall, here) uniformly distributed on the planet. This mechanism is summarized in Fig 1. Warm & wet conditions that follow the largest impact events recorded on Mars should not only have been short-lived, but should also have produced thick 100% cloud coverage, responsible for precipitation patterns uniformly distributed on the planet, and thus uncorrelated with the position of the valley networks.

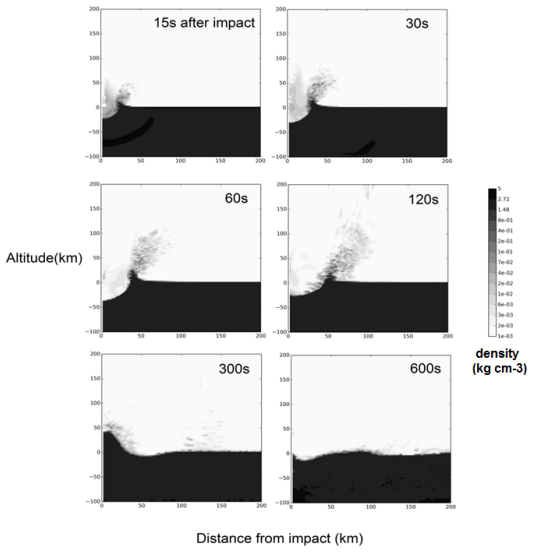


**Figure 2:** Time lapse of SOVA hydrocode simulations showing the volumetric density of materials following a ~15km diameter comet hitting the surface of Mars at 10km/s.

**Effect of middle-size impact events:** We estimate that moderate-size impact events (5km < $D_{impactor}$ < 50km, $N_{events}$ ~ $3x10^3$ [32]) being much more numerous, they are potentially the best candidates to be at the origin of the formation of the Noachian valley networks. They could in fact melt the ice that tends to accumulate preferentially in the regions where the rivers were sculpted ('Icy Highlands' scenario [16,25]). This scenario is particularly appealing because it would be an efficient mechanism of recharge of the valley network water sources between two impact-induced melting events.

To test this idea, we use the SOVA hydrocode [33] for short-term modelling of impact cratering. It provides us with post-impact temperature fields, injection of volatiles, ejecta and dust distribution (Fig 2) that serve as input for the LMD Generic Global Climate Model. Our goal is to derive from these simulations estimates of the amount of rainfall/snowmelt that could be expected after impact events depending on their size, composition, velocity, etc. We will present our preliminar results at the Fourth International Conference on Early Mars.

**References:** [1] Hynek et al. (2010), JGR. [2] Craddock & Howard (2002), JGR. [3] Mangold et al. (2012), JGR. [4] Grotzinger et al. (2015), Science. [5] Malin & Edget 2003, Science. [6] Moore et al. 2003, GRL. [7] Mangold & Ansan 2006, Icarus. [8] Poulet et al. 2005, Nature. [9] Bibring et al. 2006, Science. [10] Mustard et al. 2008, Nature. [11] Ehlmann et al. 2011, Nature. [12] Carter et al. 2013, JGR. [13] Carter et al. 2015, Icarus. [14] Haberle et al. 2017, Cambridge Univ. Press. [15] Forget et al. 2013, Icarus. [16] Wordsworth et al. 2013, Icarus. [17] Ramirez et al. 2014, Nature geoscience. [18] Batalha et al. 2015, Icarus. [19] Wordsworth et al. 2017, GRL. [20] Segura et al. 2002, Science. [21] Segura et al. 2008, JGR. [22] Segura et al. 2012, Icarus. [23] Toon et al. 2010, AREPS. [24] Turbet et al. 2017, Icarus. [25] Bouley et al. 2016, Nature. [26] Turbet et al. 2016, DPS. [27] Turbet et al. 2017, MAMO. [28] Ma & Tipping 1992, J. Chemn. Phys. [29] Pollack et al. 1993, Icarus. [30] Baranov 2016, JQSRT. [31] Kopparapu et al. 2013, ApJ. [32] Robbins & Hynek 2012, JGR. [33] Shuvalov 1999, Shock Waves.

**TOWARD A MORE ACCURATE SPECTROSCOPY OF $CO_2$/$H_2O$-RICH ATMOSPHERES: IMPLICATIONS FOR THE EARLY MARTIAN ATMOSPHERE.** M. Turbet[1], H. Tran[1], J-M. Hartmann[1] & F. Forget[1], [1]Laboratoire de Météorologie Dynamique, IPSL, UPMC (martin.turbet@lmd.jussieu.fr).

**Introduction:** Since the 1970s, there have been more and more evidences that liquid water had flowed on several occasions in the history of Mars [1-4]. Yet, the stability of significant amount of surface liquid water, necessary in particular to carve the 3.8 Gya valley networks, remains unexplained [4]. Climate models that consider only $CO_2$/$H_2O$ as greenhouse gases have been unable until now to produce warm climates suitable for liquid water on Early Mars [4-6], given the lowered solar luminosity at that time.

Alternatively, some studies have proposed that the warm conditions required to explain both the aqueous mineralogy and geology could have been transient and produced in response to meteoritic impacts [6-10]. In such conditions, it is expected that large amount of water (from water ice reservoirs or directly from the metorites) could be injected in the atmosphere, thus requiring an accurate radiative treatment of atmospheres made of large amounts of both $CO_2$ and $H_2O$ [11].

To this end, we constructed a state-of-the-art spectroscopy for $CO_2$/$H_2O$-rich atmospheres, by trawling through underrated scientifics papers and by conducting new calculations and measurements, when both needed and possible. We discuss in the next sections the several new improvements incorporated into this work.

**Width at half-maximum:** The HITRAN 2012 database [12] provides the air broadening coefficient at 296 K and its temperature dependence exponent for each line together with the self-broadening coefficient at 296 K. We incorporated here the half-width at half-maximum of $H_2O$ lines broadened by $CO_2$ ($\gamma^{H2O-CO2}$) and $CO_2$ lines broadened by $H_2O$ ($\gamma^{CO2-H2O}$). We also took into account the corresponding temperature dependence exponents ($n^{CO2-H2O}$ and $n^{H2O-CO2}$), based on references [13-16].

**Far line wings of $CO_2$:** Following Wordsworth et al. 2010 [17], we used the khi-factor approach - an empirical correction of the Lorentzian line shape adjusted to laboratory measurements - to model self-broadened $CO_2$ far line wings. We used the temperature dependent khi-factor of Perrin & Hartmann [18] (based on the 4.3µm / $\nu_3$ band measurements) extrapolated for all bands, except the $\nu_2$ band (at 15µm) where we used the parameterization derived from Tran et al. 2011 [19].

To compute $CO_2$ far line wings broadened by $H_2O$, we derived a khi-factor from both Baranov 2016 [20] and new laboratory experiments from Tran et al. 2017, in prep [21], based on measurements of the right wing of the $\nu_3$ band.

**Note on $CO_2$ line-mixing effects:** Collisional line mixing effects are due to the collisional transfers of rotational populations between closely-spaced absorption lines. Although such effects are in nature already taken into account in the khi-factor approach in the far wing regime, it has been recently claimed by Ozak et al. 2016 [22] that explicitely including the effect of collisional line mixing lead to $CO_2$ atmospheres that are more transparent to infrared radiation. This would in particular imply significantly colder surface temperatures (up to 15 K) for early Mars than estimated in previous studies [17]. However, these calculations were in fact biased due to a wrong choice of broadening species (air instead of $CO_2$). When choosing the correct collision partner ($CO_2$ here), Turbet & Tran 2017 [23] shows that calculations made with a collisional line mixing model [19,24] and with sub-Lorentzian line shapes [18] lead to a good agreement, with differences between early Mars surface temperatures smaller than 2 Kelvins only.

**Far line wings of $H_2O$:** We use the last version (3.0) of the MT_CKD continuum model for $H_2O$ self-broadening (from http://rtweb.aer.com/), as widely done in models of planetary atmospheres [25]. This continuum is calibrated for $H_2O$ lines cut at 25cm$^{-1}$. Note that the pedestal must be removed at ±25cm$^{-1}$ from the line center. Furthermore, we take this opportunity to discourage the use of both the BPS [26] and CAVIAR [27] database, since they are based on Fourier Transform Spectroscopy (FTS) measurements that are thought to be biased either by the presence of water droplets, or by a wrong calibration [28-30].

To compute $H_2O$ far line wings broadened by $CO_2$, we performed calculations using the line shape functions of Ma & Tipping 1992 [31], using the HITRAN 2012 database [12], and extended to wavenumber as high as 20,000cm$^{-1}$. The temperature dependence of the continua was derived empirically from Pollack et al. 1993 [32].

Note that these continua are shown on Fig 1.

**Collision Induced Absorptions:** Following Wordsworth et al. 2010 [17], we included the effect of $CO_2$-$CO_2$ Collision Induced Absorptions (CIA) in the 0-250cm$^{-1}$ region [33] and CIA and dimer absorption in the 1200-1600cm$^{-1}$ region [34]. We extrapolated the continua with a constant slope outside the wavenumber range validity as done in references [17] and [23]. We also added the $CO_2$-$CO_2$

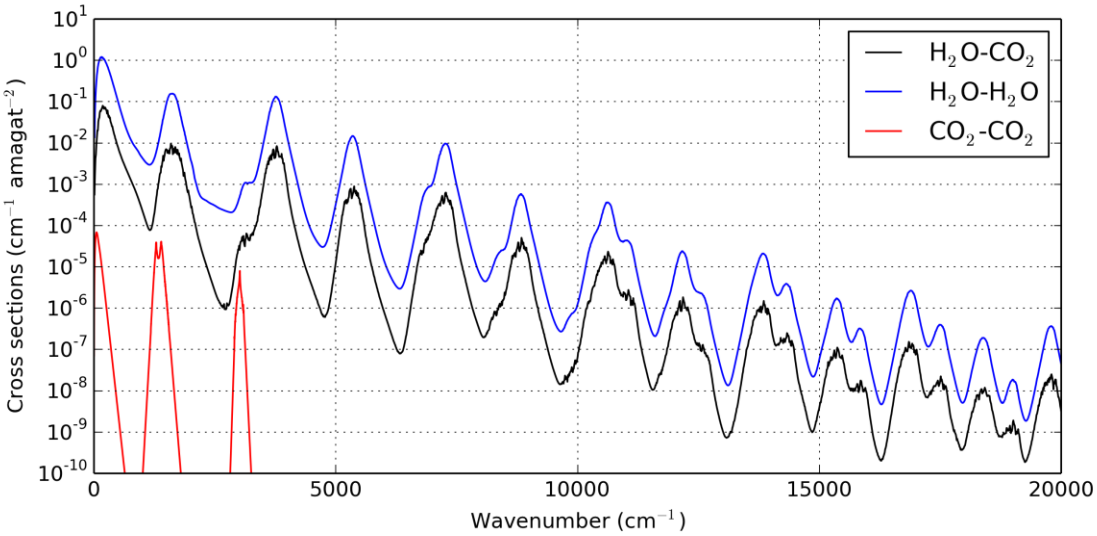


**Figure 1:** Cross-sections (in cm$^{-1}$ amagat$^{-2}$) of various continua at T=296K: In blue, the $H_2O$ self-broadening from the MT_CKD 3.0 (from http://rtweb.aer.com/). In black, the $H_2O$ far-lines (>25cm$^{-1}$ from line centers) broadened by $CO_2$ [31,32]. In red, the $CO_2$-$CO_2$ Collision induced absorptions (CIA) [33,34,35].

CIA measured in the 2900-3100cm-1 region by Stefani et al. 2013 [35], with the corresponding temperature dependence. These CIA and the dimer absorption are shown on Fig 1.

Eventually, we are currently running molecular dynamics simulations [36] to derive quantitative estimates of the $H_2O$-$CO_2$ and $CO_2$-$H_2O$ hybrid CIA.

**Conclusions and Perspectives:** We performed calculations, measurements and gathered existing data to construct a state-of-the-art spectroscopy for $CO_2$/$H_2O$-rich atmospheres. This new spectroscopy has been incorporated and tested in the LMD 3-D Global Climate Model to model the atmosphere of early Mars (for more information, see the presentation by Martin Turbet at the Fourth International Conference on Early Mars).

More generally, our goal is to provide the community with high resolution spectra and correlated-k absorption coefficients for $CO_2$/$H_2O$-rich atmospheres, as accurate as possible, and for a wide range of temperatures and $CO_2$/$H_2O$ partial pressures. Such effort is critical in our understanding of the early Martian atmosphere and its response to extreme events of various nature. Meanwhile, any feedback from the community is very welcome.

**References:** [1] Hynek et al. (2010), JGR. [2] Grotzinger et al. (2015), Science. [3] Bibring et al. 2006, Science. [4] Haberle et al. 2017, Cambridge Univ. Press. [5] Forget et al. 2013, Icarus. [6] Wordsworth et al. 2013, Icarus. [7] Segura et al. 2002, Science. [8] Segura et al. 2008, JGR. [9] Segura et al. 2012, Icarus. [10] Toon et al. 2010, AREPS. [11] Turbet et al. 2017, Icarus. [12] Rothman et al. 2013, JQSRT. [13] Brown et al. 2007, J Mol Spectrosc. [14] Gamache et al. 2016, J Mol Spectrosc. [15] Sung et al. 2009, Can J Phys. [16] Delahaye et al. 2016, J Mol Spectrosc. [17] Wordsworth et al. 2010, Icarus. [18] Perrin & Hartmann 1989, JQSRT. [19] Tran et al. 2011, JQSRT. [20] Baranov 2016, JQSRT. [21] Tran et al. 2017, in prep. [22] Ozak et al. 2016, JGR-Planet. [23] Turbet & Tran, submitted to JGR-Planet. [24] Kassi et al. 2015, JQSRT. [25] Yang et al. 2016, apJ. [26] Paynter & Ramaswamy 2012, JGR-Atmospheres. [27] Ptashnik et al. 2011, JGR-Atmospheres. [28] Mondelain et al. 2014, JGR-Atmospheres. [29] Mondelain et al. 2015, PCCP. [30] Campargue et al. 2016, JGR-Atmospheres. [31] Ma & Tipping 1992, Journal of Chemical Physics. [32] Pollack et al. 1993, Icarus. [33] Gruszka & Borysow 1997, Icarus. [34] Baranov et al. 2004, Journal of Molecular Spectroscopy. [35] Stefani et al. 2013, Journal of Quantitative Spectroscopy and Radiative Transfer. [36] Hartmann et al. 2011, Journal of Chemical Physics.

**KINETIC MODELING OF MINERAL SEQUENCES ON EARLY MARS USING FULLY OPEN SYSTEMS.** E. R. Uceda[1], A. G. Fairén[2,3], C. Gil-Lozano[2], E. Losa-Adams[4], L. Gago-Duport[4]. [1]Facultad de Ciencias, Universidad Autónoma de Madrid, Cantoblanco, 28049 Madrid, Spain. [2]Centro de Astrobiología (CSIC-INTA), Madrid 28850, Spain. [3]Department of Astronomy, Cornell University, Ithaca, NY 14853, USA. [4]Departamento de Geociencias Marinas, Universidad de Vigo, Lagoas Marcosende, 36200-Vigo, Spain.

**Introduction:** We have applied a reactive-transport approach to model the formation of mineral sequences known to exist on Mars, as described from lander and orbiter data [1-5], considering open system conditions both at the atmosphere-water and water-rock interfaces, and implementing a kinetic approach for the dissolution and precipitation of solid phases. We present a suite of models representing aqueous environments in systems under an early Mars atmosphere, to analyze the role of: (i) the reactive surface area of primary minerals, and (ii) the reactive transport processes through the basalt interface.

**Kinetic model:** We model the space-time variations of the conditions inside a basalt sediment column, where the surface water is in contact with an acidic-oxidative atmosphere at the upper interface ($CO_2$, $SO_2$, $Cl_2$) (as on early Mars, see [6]), and subject to a continuous loss of water by evaporation. We assume a continuous flux of gases derived from volcanic outgassing through the upper water layer, as these volatiles are the most obvious source of anions which can gradually change Eh and pH conditions. The model represents a 1-D kinetic system of evaporation + diffusion + reaction (precipitation/dissolution of mineral phases).

Oxidation is mainly driven by chlorine, through transient oxygen reactive species formed at the low pH-values induced by the $CO_2$ and $SO_2$ gases [6,7]. When the upper acidic and oxidant solution starts to diffuse and mix with the interstitial alkaline water, the pH rapidly decreases with depth. The extent of pH lowering toward acidic values and increase in oxidation potential, on both time and depth, is a function of the rate of diffusion and the buffering capacity of the interstitial pore water which, in turns, depends again on the dissolution rate of the basalt forming minerals. Therefore, this model considers the two different possibilities regarding the reactive surface area of the basaltic minerals, as follows.

First, when the solution is in contact with basaltic sediments of greater size, the total amount of reactive surface area is low and, therefore, the dissolution of the basalt proceeds relatively slowly. In this case, it is expected that the input of volatiles from the atmosphere and the loss of water from evaporation are the main factors inducing variations in pe-pH conditions, and in ionic strength. In this situation the system evolves towards an evaporitic scenario, characterized by extremely acidic and oxidizing conditions. The consequence is the formation of sulfates (i.e., alunite, gypsum), more abundantly in the upper part of the sediment column, while the distribution of clays tends to follow an opposite trend in the column (Figure 1).

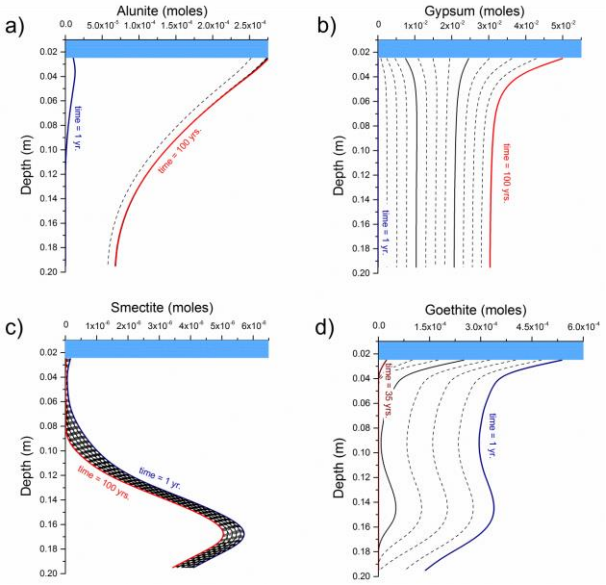


**Figure 1:** Depth profiles of the secondary mineral phases formed during aqueous reaction of a basalt column considering gases input from the atmosphere and low reactive surface area of primary minerals (cubes, L = 54 mm; $S_{reactive}$ = 0.11 $m^2$/kgw). Beidellite-Ca and gibbsite also precipitate. Both phases showed the maximum accumulation at the subsurface. Model approaches: flux of gases input: 0.1 mol/yr of $CO_2$(g) and 0.01 mol/yr of $SO_2$(g) and $Cl_2$(g); length of the sediment column = 20 cm; Dw = $1x10^{-9}$, $\phi$ = 0.4; simulation time = 100 yrs.; linear evaporation rate =0.1 mol/yr; secondary minerals considered in the model: clays (smectite, kaolinite, beidellite and chlorite), evaporites (jarosite, alunite, gypsum, and calcite), and hydroxides (goethite and gibbsite).

And second, when the reactive surface area of the basalt increases because the basalt minerals are pervasively fractured, the dissolution of basalt occurs faster, resulting in the rapid evolution of the solution towards very alkaline values. In this scenario, sulfates do not

form, and clays are the major precipitation product in the surface layer (Figure 2a, b and c). The alkaline pH also favors the precipitation of goethite. Goethite's precipitation front is gradually shifted towards the middle point of the column, due to the competition for ferric iron with clay minerals (i.e., nontronite) (Figure 2d).

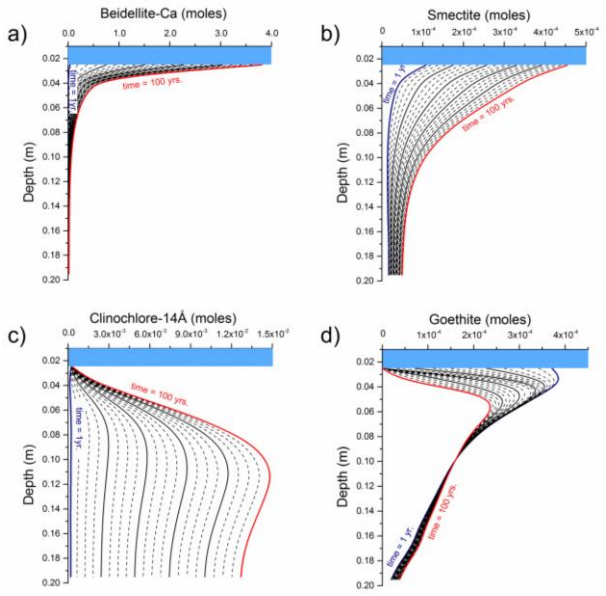


**Figure 2:** Depth profiles of the secondary phases formed during aqueous reaction of a basalt column under the same boundary conditions described in Figure 1 but assuming high reactive surface area of primary minerals (cubes, L = 5.5 μm; Sreactive = 1096 $m^2/kgw$). Calcite and gibbsite are also formed showing the maximum accumulation at surface and subsurface layers, respectively.

**Conclusions:** Our results are consistent with the stratigraphic sequence of Noachian phyllosilicates observed in certain locations on Mars: Fe/Mg clays (e.g., nontronite) in the lower layers, and Al-rich clays (e.g., beidellite) in the upper layers [8]. Taken together, these results highlight the importance of considering open kinetic models to reproduce the geochemical conditions on the surface of Mars. Cation removal by diffusion, together with the input of volatiles and the influence of the reactive surface area of the basalt, could play a central role in the time-evolution of the mineral sequences formed on aqueous environments on early Mars.

**References:** [1] Bandfield, J. L., et al. (2000). A global view of martian surface compositions from MGS-TES, Science, 287, 1626-1630. [2] Mustard J. F., et al. (2008). Hydrated silicate minerals on Mars observed by the Mars Reconnaissance Orbiter CRISM instrument, Nature, 454, 305-309. [3] McSween, H. Y., et al. (2009), Elemental composition of the martian crust, Science, 324(5928), 736-739. [4] Ehlmann, B. L., et al. (2011), Subsurface water and clay mineral formation during the early history of Mars, Nature, 479(7371), 53-60. [5] Vaniman, D. T. et al. (2014), Mineralogy of a mudstone at Yellowknife Bay, Gale crater, Mars, Science 343(6169), 1243480. [6] Fairén, A. G., et al. (2004), Inhibition of carbonate synthesis in acidic oceans on early Mars, Nature, 431(7007), 423-426. [7] Zelenski, M., and Y. Taran (2012), Volcanic emissions of molecular chlorine, Geochim. Cosmochim. Ac., 87, 210-226. [8] McKeown, N. K., et al. (2009), Characterization of phyllosilicates observed in the central Mawrth Vallis region, Mars, their potential formational processes, and implications for past climate, J. Geophys. Res., 114, E00D10, doi:10.1029/2008JE003301.

**Acknowledgements:** The research leading to these results is a contribution from the Project "icyMARS", funded by the European Research Council, Starting Grant no 307496. L.G.D. was supported by the Spanish Ministry of Science and Innovation in the Framework of the MICINN-FEDER Project CGL2011-30079. E.L.A. was supported by the UVIGO/CETMAR Marine Research Center and the Galician Regional Government through the EU Operative Program ERDF Gal-2014-2020/A Way of Making Europe.

**WHERE SHOULD SEARCH TRACES OF LIFE, WHICH COULD APPEAR ON MARS IN THE FIRST 300 MILLION YEARS.** A. P. Vidmachenko, Main astronomical observatory of NAS of Ukraine, Str. Ak. Zabolotnoho, 27, Kyiv, 03143. vida@mao.kiev.ua.

Mars rovers and orbital modules received a huge amount of information about Mars. The data collected by them allowed to reconstruct possible stages of the development of events on the planet [14, 16, 23]. About 4.5 billion years ago, the first geological era, the Phyllocian, began. It lasted ~ 500-700 million years. It is believed that Mars was then a humid planet. In this case, proceed from the fact, that the minerals belonging to this era subjected to significant water erosion. These rocks contain clay minerals – phyllosilicates. To form them, a lot of water, the temperature is above 273 K and low acidity is needed [18]. But such a wet period in the history of the planet was very short for so that the possibility of development of the modern terrestrial type of life [13, 21]. In its early years, Mars was like the ancient Earth. And the conditions on the planet were the same as on the then Earth. It had a dense atmosphere with a pressure of 0.4 bar, a water ocean on the surface, and there was much warmer than it is now. That is, the planet was once much more suitable for the existence of life than it is today. It was in those years that simple forms of life arose on the Earth. So, in Canada traces of vital activity of the most ancient bacteria on the Earth are found. They show that life on Earth existed almost 4.3 billion years ago; only 200 million years after the formation of the earth's crust. It is possible that the same could happen on Mars. So, recently on Mars, traces of methane and formaldehyde were detected. They can talk about a possible proof of the presence of life on the planet [6, 9]. The embryos of a possible life on the surface of the planet could have been brought down by fragments of comet nuclei (panspermia) [1-3, 24]. Somewhat later, the collision of the planet with planetesimals could lead to the formation of huge impact craters. As a result of such processes, the newly formed life could be conserved under powerful soil emissions [11, 17, 19]. Evidence of impacts of large bodies of Mars is the Hellas Planitia, located near the southern polar region. Now it is a plain with a diameter of more than 4000 km. At the bottom it narrows to 1500 km, and is surrounded by rock outbursts. Its depth in some places reaches 9 km. Five giant craters Argyr, Hellas, Isis, Tavmasia and Utopia lie on an arc of a great circle.

The close age and peculiarities of their mutual arrangement suggest that these craters could have formed simultaneously, as a result of a single cataclysm caused by the fall of fragments of a very large asteroid [22, 23]. In this case, the location of the surface details and even the shape of Mars could quickly and strongly change. Before that, ice caps lay on the poles, the planet was enveloped by a dense gas atmosphere, and the water filled the lakes and seas. It is assumed that the atmosphere and water were lost after such a powerful one-shot bombardment. Existing impact craters, and a large amount of magnetic sand (maghemite) on the surface indicate a possible bombardment. It is formed only during oxidation of magnetite with simultaneous strong heating.

(A similar substance occurs only on the territory of Yakutia on the Earth. It is believed that 35 million years ago, fragments of an asteroid 8-10 km in diameter fell there [11, 22]).

Emissions of millions of tons of soil on thousands of kilometers, covered a significant part of the surface of Mars. In the same place, the forms of life that began to form could be hidden. Now in many places on the surface of the planet thousands of sites with scattered are contained in a young volcanic soil. After the global climate change, probably caused by volcanic activity after the fall of a large asteroid, a new era – Theiikian – began. It lasted from 4 to 3.5 (3.3) billion years ago [12, 15, 17, 19]. Then, due to powerful volcanic emissions, a large amount of sulfur was supplied to the atmosphere, the environment became very acidic, and water reacted with sulfur compounds and formed sulphates. Evidence of this is the presence of gypsum and gray hematite in rocks belonging to the corresponding age. And the situation began to change. The planet began to cool slowly; The activity of volcanoes decreased and the release of gases into the atmosphere decreased. About 3.3-3.5 billion years ago, the third Siderikan era began. It was at this time that a large-scale formation of non-hydratable iron oxides began, which could give the planet a reddish color [20]. Now Mars is geologically almost dead [21, 23]. Mars has virtually no magnetosphere and there is a very subtle atmosphere. This is clearly not enough to protect a possible life from bombardment by solar wind and hard ultraviolet (UV). But there is a chance, that if life on Mars once appeared, it did not disappear without a trace. It could move from the surface of the planet to its interior, can be stored there either in fossils, and possibly in some simple forms. Therefore, it tracks should be sought at a depth

below the soil. But what kinds of life forms can there be conserved, and/or survive?

If life on Mars today there is, then, certainly, it is microbial. But even in this – we are not sure until we find and study them. However, we can make some assumptions about the nature of Martian life. For this, it is necessary to investigate some special biological aspects on Earth. The convincing evidence that liquid water periodically flows on the surface of Mars is the spectroscopic detection of hydrated perchlorate salt in streams on the walls of Martian craters. Perchlorate salts are composed of chlorine and oxygen, which are associated with various other elements. Some perchlorates do not allow freezing of the liquid at temperatures below -70 ° C. The most famous saline basin on Earth with calcium chloride is Don Juan Pond in Antarctica. But, perhaps, the Martian salt solution is even more salty. Also, a wide spectrum of halophilic (salt-loving) and psychrophilic (cold-loving) microbes was found on the Earth. Recently, found "lovers" of cold salt (psychrophalophiles) [5, 10]. They live in salt Antarctic lakes, or in veined glacial ice. The temperature limit for cell division is -12ºC, and for maintenance of the basic metabolic functions is -20ºC. Some of the microbes even produce antifreeze proteins that help limit the growth of ice crystals in their cells. Adaptations of psychrophalophiles on the Earth hint at possible life strategies of Martian microbes. But there are a few more problems that have to be overcome by any form of life on Mars. First, Mars is devoid of the ozone layer, and all day its surface is sterilized by UV radiation. One way to avoid radiation is to live under the surface. Usually perchlorates are highly toxic compounds for most organisms on Earth [5, 7]. But in one of the driest and most exposed to the radiation of the Atacama Desert on Earth, microbes are found that live in thin films of liquid water on the surface of salt crystals [7, 8]. That is, life on Earth repeatedly demonstrated an amazing ability to adapt to toxic environments. There are microbes that live in acid mines and in lakes with arsenic. Registered arctic microbes that have adapted to high levels of mercury contamination. In addition, on Earth, there are bacterial enzymes that can destroy perchlorate. A promising habitat is the thin water films that the polar landing gear "Mars Phoenix" observed in the soil on its own landing area.

The proof of the presence of liquid water on Mars does not mean that there is life on Mars. But this gives some hope.

**References:** [1] Churyumov K.I. et al. (2014) book:CAMMAC. 98-108. [2] Churyumov K.I. et al. (2014) AstSR, 10(1), 37-42. [3] Churyumov K.I. et al. (2013) 8Meteoroids-2013. 077. [4] De Maayer P. et al. (2014). EMBO Repots. 15(5), 508-517. [5] Hecht M.H. et al. (2009) Science. 325(5936), 64-67. [6] Krasnopolsky V.A. et al. (2004) Icarus. 72(2), 537-547. [7] Ojha L. et al. (2015) Nature Geoscience. 8(11), 829-832. [8] Parro V. et al. (2011) Astrobiology. 11(10), 969-996. [9] Peplow M. (2005) Nature. 436(7048), 158-159. [10] Polyextremophiles: (2013) Ed. by J. Seckbach et al., Springer. 27, -481. [11] Schultz P.H., et al. (2014) Geology. 42(6), 515-518. [12] Vidmachenko A.P. (2016) 5Int.Sc.Conf. Ed. by A. Mozhovyi, 43-48. [13] Vidmachenko A.P. (2012) AstSR. 8(2),136-148. [14] Vidmachenko A.P. (2009) AstSR. 6(1-2), 27-43. [15] Vidmachenko A.P. (2016) 18YSConf., 16-17. [16] Vidmachenko A.P. (2009) AstSR. 6(2), 131-137. [17] Vidmachenko A.P. (2016) 18YSConf., 14-16. [18] Vidmachenko A.P. (2009) AsAl. 56, 225-249. [19] Vidmachenko A.P. (2016) LPICo1912.2002. [20] Vidmachenko A.P. et al. (1981) SSRes. 14(4), 157-159. [21] Vidmachenko A.P. and Morozhenko A.V. (2012) AsAl. 59, 221-243. [22] Vidmachenko A.P. and Morozhenko O.V. (2014) pcse.book MAO, NULES, -388. [23] Vidmachenko A.P. and Morozhenko O.V. (2014) AstSR. 10(1), 6-19. [24] Vidmachenko A.P. and Steklov A.F. (2013) AstSR. 9(2), 146-148.

**INTERCOMPARISON OF MARTIAN CARBONATE-BEARING DEPOSITS.** S. M. Wiseman[1] and K. Robertson.[1], [1]Brown University Dept of Earth, Environmental and Planetery Sciences (sandra_wiseman@brown.edu).

**Introduction:** The detection of carbonate-bearing deposits within coherent stratigraphic units on the surface of Mars [e.g., 1-7] is significant because carbonate phases are important mineralogic indicators of neutral to alkaline aqueous geochemical conditions and may be indicators of past habitable environmental conditions on Mars. Identification of specific carbonate mineral phases combined with accompanying mineral asseblages can provide more refined information on past environmental conditions. Carbonate chemistry places constraints on fluid geochemistry at the time of fomation because carbonate major cation composition varies systematically with fluid chemistry and can be an indicator of $pCO_2$ whereas the accompanying mineral assemblages serve as important indicators of temperature. For example, an association of cabonate with chlorite and prehnite would indicate higher temperature conditions than an association with Fe/Mg-smectite [8; 9-12]. Similarly, an association with serpentine would indicate more alkaline conditions than with silica. The presence of serpentine is a particularly important indicator of past habitability due to the potential for microbial iron oxidation/$H_2$ production [13].

A range of formation conditions have been proposed for carbonate-bearing deposits on Mars, with favored hypotheses depending on mineralogy inferred largely from visible to near-infrared (VNIR) Mars Reconnaissance Orbiter CRISM [14] spectra, and geologic context. Carbonates in the Comanche outcrop in the Columbia Hills at Gusev crater are interpreted to have formed via hydrothermal alteration of olivine-rich ultramafic rocks under neutral pH conditions based on MER Spirit rover Mossbauer, APXS, and Mini-TES measurements [2]. These Columbia Hills carbonate-bearing deposits are relatively small and produce only shallow absorption features in orbital CRISM VNIR spectra [5]. However, carbonate-bearing deposits associated with olivine occur throughout eastern Nili Fossae [1] as well as neighboring Libya Montes [7] and exhibit distinctive carbonate and phyllosilicate signatures in CRISM VNIR spectra. [1] and [15] favor olivine carbonation at either low temperature, near surface conditions or hydrothermal conditions, similar to those proposed by [2]. These authors note that although serpentinization is possible, the lack of definitive detection of serpentine associated with the carbonates in CRISM data is problematic. [16,17] interpret CRISM spectral signatures previously identified as Fe/Mg smectites as being consistent with talc spectra and therefore favor carbonation of serpentine to produce talc and carbonate. Carbonates associated with Leighton crater central peak and Huygens basin are hypothesized to have originated as buried carbonate-bearing sediments that were metamorphosed and subsequently re-exposed via the impact process or may have formed in the subsurface [3,4]. Carbonates in McLaughlin crater near Marwth Vallis were posited to have formed in an alkaline lacustrine system fed by upwelling groundwater [7].

Diagnostic carbonate-related absorption features occur near 2300, 2500, 3400, and 3900nm and shift depending on the major cation in the carbonate [18-19]. Although CRISM spectra identified as carbonate-bearing exhibit bands near 2300 and 2500 nm (and sometimes 3400 and 3900 nm), the spectra are not entirely similar to any one terrestrial carbonate spectrum because other alteration phases are mixed with the carbonate. Detailed determination of specific carbonate mineral chemistry on Mars using CRISM spectra is complicated [e.g., 20] because the carbonate minerals are always mixed with other alteration phases (e.g., phyllosilicates) that have absorption features that overlap with and obscure diagnostic carbonate bands. For example, Nili Fossae carbonate spectra are at a minimum a mixture of magnesite, nontronite, and olivine [1,20] and possibly talc [16].

Multiple alteration phases have been identified in association with carbonates [e.g., 1-7]. However, the extents of individual phases have not been mapped because it is difficult to distinguish among phases with similar spectral features (e.g., chlorite and smectite) using simple parameter images and combinations of parameter images. We have found that it is feasible to map each CRISM pixel in terms of spectral classes using a small number of scene-derived image endmembers as inputs into a Hapke unmixing model [21].

This work aims to identify and map the extent of specific carbonate mineral assemblage phases using Hapke radiative transfer modeling of Discrete Ordinate Radiative Transfer (DISORT) [22-24] atmospherically-corrected CRISM spectra. We present intial results from mapping CRISM pixels within each carbonate-bearing site as a combination of the minimum number of scene derived endmembers and laboratory components needed to explain spectral variation.

**Mineral Assembelage Modeling:** In order to identify the extent of alteration phases associated with each carbonate-bearing deposit, CRISM images are modeled as a combination of the minimum number of scene derived endmembers needed to explain variation from 1000 to 2600nm. Each CRISM pixel can be represented as a mixture of scene- and laboratory-derived endmembers using Hapke modeling.

A Nili Fossae carbonate-bearing spectrum is shown in black in Figure 1. It was modeled as a combination of initial scene derived spectral classes (Figure 1, upper) and one laboratory carbonate endmember (Figure 1, lower). This simple example shows that candidate laboratory spectra can be identified via Hapke modeling of scene-derived components and laboratory endmembers. Error is minimized with inclusion of the magnesite component rather than the calcite component. The blue spectrum in Figure 1 (lower) illustrates that the combination of phyllosilicate and carbonate alters the position of the absorption feature at 2300nm to occur at a shorter wavelength than pure magnesite and highlights the difficulty of identifying spectral components by direct comparison of band centers to laboratory spectra for the case of mineral mixtures.

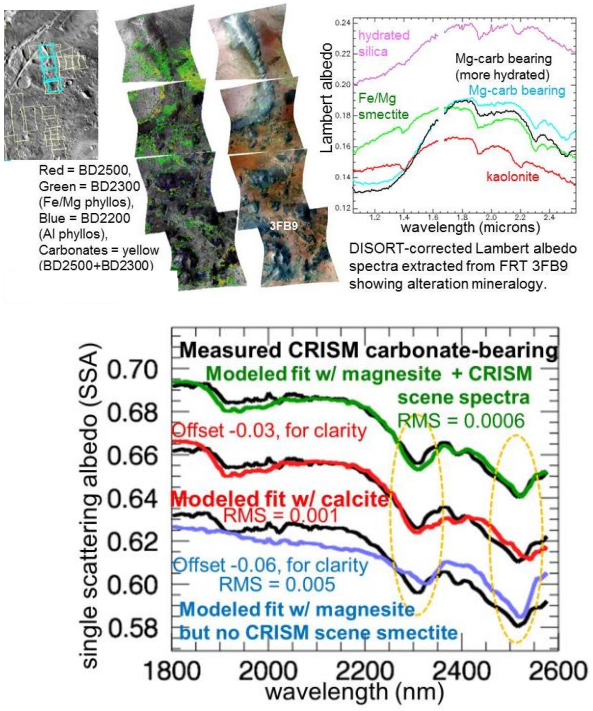


*Figure 1.* Example showing CRISM Nili Fossae carbonate-bearing spectrum and Hapke unmixing model fits. The green fit uses scene derived spectral endmembers plus magnesite, red uses scene spectra plus calcite, blue is the same as green but with no scene phyllosilicate. Results show that magnesite is necessary to model the CRISM 2500 nm band and phyllosilicate is also needed to model the 2300nm band.

**Discussion:** Carbonate chemistry places constraints on fluid geochemistry at the time of formation because carbonate major cation composition varies systematically with fluid chemistry and can be an indicator of $pCO_2$. Additionally, associated mineral assemblages can be used to constrain temperature. As discussed in [11], in Nili Fosse, an olivine-rich unit appears to be variably altered to Mg carbonate with occasional serpentine. In some locations, there are mixed pixels of carbonate and Fe/Mg smectite (and possibly talc [16-17]). That serpentine exists in these terrains confirms the existence of hydrothermal, reducing alteration of ultramafic rocks during the Noachian epoch. However, serpentine and carbonate are only identified in spatial association in a few locations. This is partly because serpentine can be difficult to distinguish from Fe/Mg smectite if it lacks a subtle, diagnostic 2100 nm feature (which has been observed to vary in strength with cation and grain size [25-27]). We aim to use relative abundance maps of serpentine, smectite, carbonate, etc, to assess the amount of serpentine that is associated with each carbonate-bearing deposit on Mars. The presence of serpentine is a particularly important indicator of past habitability and astrobiological potential due to the potential for microbial iron oxidation/$H_2$ production [13].

The lack of serpentine associated with most carbonate-bearinng deposits could suggest that olivine may have altered directly to Mg carbonate at cold temperatures [11]. Alternatively, Mg carbonate is commonly found on Earth in association with seprentinized terrains where alteration is at elevated temperatures. Mg-carbonate precipitation occurs diffusely in fractures as waters infiltrate an ultramafic rock; once waters participate in serpentinization in the subsurface, they are Mg-poor and Ca-rich, leading to precipitation of Ca-carbonates at discrete spring outflows as these waters become saturated with $CO_2$ [e.g., see discussion in 11]. In the Leighton and Huygens deposits we will look for evidence for the presence of residual Mg-carbonate which might indicate a surface or near surface origin for these deposits and support burial rather than deep subsurface formation.

**References:** [1] Ehlmann et al. (2008) *Science*, 322. [2] Morris et al. (2010) *Science*, 329. [3] Michalski and Niles (2010) *Nature Geo*. [4] Wray et al. (2011) *LPSC*. [5] Carter and Poulet (2012) *Icarus*. [6] Bishop et al. (2013) *JGR*, 119. [7] Michalski et al. (2013) *Nature Geo*. [8] Frey & Robinson, 1999. [9] Ehlmann et al. (2009) *JGR*, 114. [10] Ehlmann et al. (2011) *Nature*. [11] Ehlmann et al. (2010) *JGR*. [12] Evans (2004). [13] Schulte et al. (2006). [14] Murchie et al. (2007) *JGR*. [15] Edwards and Ehlmann (2015) *Geology*, 43. [16] Brown et al. (2010). [17] Viviano et al. (2013) *JGR*. [18] Hunt and Salisbury, (1971) *Mod. Geol*. 2, 195-205. [19] Gaffey (1986) *Amer. Min.*, 71, 151-162. [20] Bishop et al (2013) *LPSC*. [21] Hapke, 1993. [22] Stamnes et al., (1988) *Appl. Opt.*, *27*, 2502-2509. [23] K. Stamnes, (2002) *Radiative transfer in the atmosphere and ocean*, Cambridge University Press. [24] Wolff et al. (2009), *JGR*. [25] King Clark, (1989) *JGR*, 94. [26] Calvin and King (1997). [27] Bishop et al., (2008) *Clay Minieralogy*., *43*, 35-54.

**EARLY MARS VS. LHS1140b AND TRAPPIST-1f: HOW COMPARATIVE PLANETOLOGY CAN HELP ADDRESS LONG-STANDING QUESTIONS IN MARTIAN CLIMATE EVOLUTION** R. Wordsworth[1,2], J. Head III[3] and H. Wang[1]. [1]School of Engineering and Applied Sciences, Harvard University, Cambridge, USA (rwordsworth@seas.harvard.edu), [2]Department of Earth and Planetary Sciences, Harvard University, Cambridge, USA, [3]Department of Geological Sciences, Brown University, Providence, USA.

**Introduction:** The question of why Mars has so much evidence for surface liquid water in its distant past has motivated scientists since the 1960s [1]. Significant progress has been made over the last decade or so as a result of new advances in orbital observations of the surface geology, rover missions and paleoclimate modeling. However, major questions remain. Here we analyse the ways in which a new possibility, exoplanet comparative planetology, may allow us to tackle long-standing puzzles in Mars' evolution and climate history in the near to medium-term future.

**Knowns and unknowns in early Mars climate:** The evidence for liquid water on early Mars is irrefutable but the nature, frequency and duration of warming episodes remains subject to intense debate. We have previously shown the importance of adiabatic cooling to understanding the early martian water cycle [2-4], and proposed a scenario where the 'top-down' supply of water from the southern highlands and Tharsis leads to episodic melting events in a normally cold early climate. Possible warming mechanisms of relatively short duration include $SO_2$ volcanism [5] and meteorite impacts [6]. We have also recently shown that episodic release of $CH_4$ and $H_2$ from crustal alteration and/or clathrate destabilization provides a viable explanation for longer-term warming events to explain dendritic valley network formation [7]. More extreme solutions involving a greatly enhanced early solar flux [8] have been proposed but have not so far received widespread acceptance [9]. Crucial to answering the problem of Mars' early climate is understanding whether its history is in some way unusual, or similar to that of other rocky planets near the outer edge of the nominal 'habitable zone' [10].

**Size Matters:** Mars' mass is low compared to Earth's (0.107 $M_E$), and it is extremely likely that this difference has had a profound effect on its evolution. Knock-on effects of low planetary mass include an early shutdown of plate tectonics and the magnetic dynamo, enhanced atmospheric loss, and larger differences in surface elevation [11]. It has previously been suggested that an Earth-mass planet at Mars' orbit would remain habitable today [10,9]. The exoplanets LHS1140b [12] and TRAPPIST-1f [13] are particularly interesting in this context, because they currently receive a similar stellar flux to Mars, but at 6.65 $M_E$ and 0.68 $M_E$, respectively, are both more massive. They also transit stars that are only a few tens of light years from the Sun, and hence are amenable to atmospheric characterization in the near future. For the first time in planetary science, we therefore have the exciting possibility that Mars' climate evolution can be compared with that of other cool, rocky planets on a systematic basis.

**Red dwarf, yellow dwarf**: Besides mass, the most important difference between Mars, LHS1140b and TRAPPIST-1f is the host star type. The Sun is a yellow dwarf star (G-class) with equilibrium temperature of 5800 K, while LHS1140 is a red dwarf (M-class) with temperature around 3100 K. TRAPPIST-1, at 2550 K, is so small and cool that it is close to the brown dwarf limit. M-dwarfs have a significantly higher proportion of their flux as XUV and more flaring events than G-dwarfs early on, which likely enhances atmospheric escape. In addition, the red-shifted stellar spectrum leads to lower planetary albedos and enhanced near-IR atmospheric absorption, and volatile delivery during planet formation may differ from what occurred in our own solar system. These additional differences are vital to take into account when comparing martian and exoplanet climate evolution.

**The path forward:** Here we present calculations of the range of possible climate evolution scenarios for LHS1140b and TRAPPIST-1f and compare them with our current understanding of martian climate history. We also discuss the clues that we already have as to the compositions of these planets from existing observations. We then analyse the observations that will be possible with the James Webb Space Telescope and the ground-based observatories such as the GMT and E-ELT that are currently under construction. While the data available from exoplanets is always going to be more limited than what we have for the solar system, we will argue here that a systematic program of intercomparison, with close links betwen theory and observations, is likely to lead to rich new insights into Mars' fascinating climate history and habitability.

**References:** [1] Haberle, R., et al., 2017. *Cambridge University Press*. [2] Wordsworth, R., Forget, F., et al., 2013. *Icarus*, 222:1–19. [3] Forget, F., Wordsworth, R., et al., 2013. *Icarus*, 222, 81– 89. [4] Head and Marchant, 2014, Ant. Sci. 26, 774. [5] Halevy, I. and Head, J., 2014. *Nat Geosci*, *7*(12), p. 865. [6] Toon, O. B., et al., 2010. *AREPS*, *38*, p. 303-322. [7] Wordsworth, R., et al. 2017. *GRL*, *44*(2), p. 665-671. [8] Minton, D. and Malhotra, R., 2007. *ApJ*, *660*(2), p. 1700. [9] Wordsworth, R., 2016. *AREPS*, 44:381–408. [10] Kasting, J., Whitmire, D. et al., 1993. *Icarus*, *101*(1), p. 108-128. [11] Lammer, H., et al., 2013. *Space Science Reviews*, *174*(1-4), p. 113-154. [12] Dittmann, J., et al., 2017. *Nature*. [13] Gillon, M., et al. 2017. *Nature*, *542*(7642), p. 456-460.